FOOD ENGINEERING SERIES

José Miguel Aguilera
Peter J. Lillford
Editors

Food Materials Science

Principles and Practice

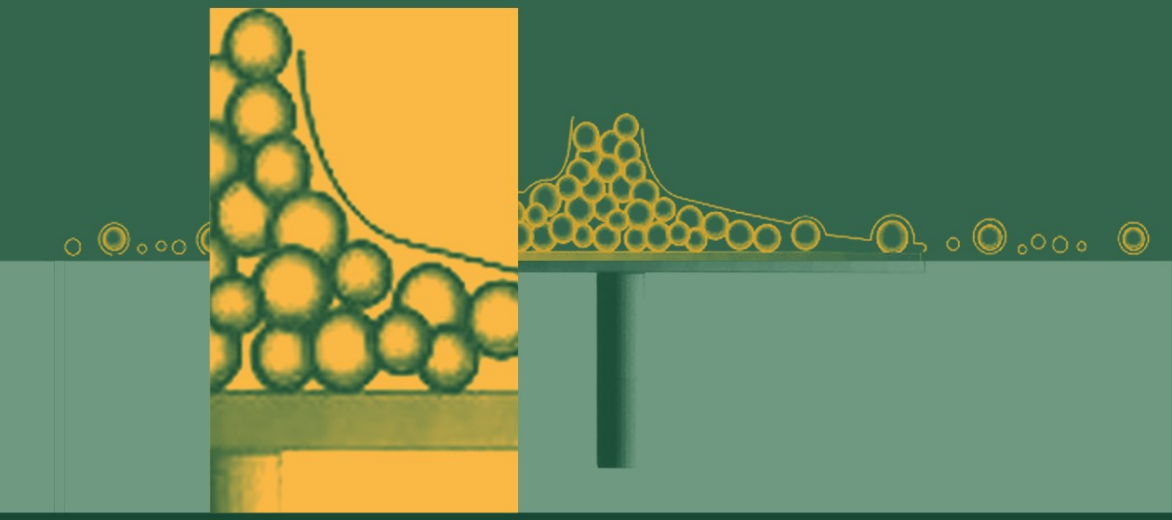

Springer

FOOD MATERIALS SCIENCE

Principles and Practice

FOOD ENGINEERING SERIES

Series Editor

Gustavo V. Barbosa-Cánovas, Washington State University

Advisory Board

José Miguel Aguilera, Pontifica Universidad Catolica de Chile
Xiao Dong Chen, Monash University
J. Peter Clark, Clark Consulting
Richard W. Hartel, University of Wisconsin
Albert Ibarz, University of Lleida
Jozef Kokini, Rutgers University
Michèle Marcotte, Agriculture & Agri-Food Canada
Michael McCarthy, University of California at Davis
K. Niranjan, University of Reading
Micha Peleg, University of Massachusetts
Shafiur Rahman, Sultan Qaboos University
M. Anandha Rao, Cornell University
Yrjö Roos, University College Cork
Walter L. Spiess, Bundesforschungsanstalt
Jorge Welti-Chanes, Universidad de las Américas-Puebla

Titles

José M. Aguilera and Peter J. Lillford, *Food Materials Science* (2008)
José M. Aguilera and David W. Stanley, *Microstructural Principles of Food Processing and Engineering*, Second Edition (1999)
Stella M. Alzamora, María S. Tapia, and Aurelio López-Malo, *Minimally Processed Fruits and Vegetables: Fundamental Aspects and Applications* (2000)
Gustavo Barbosa-Cánovas, Enrique Ortega-Rivas, Pablo Juliano, and Hong Yan, *Food Powders: Physical Properties, Processing, and Functionality* (2005)
Richard W. Hartel, *Crystallization in Foods* (2001)
Marc E.G. Hendrickx and Dietrich Knorr, *Ultra High Pressure Treatments of Food* (2002)
S.D. Holdsworth and R. Simpson, *Thermal Processing of Packaged Foods, Second Edition* (2007)
Lothar Leistner and Grahame Gould, *Hurdle Technologies: Combination Treatments for Food Stability, Safety, and Quality* (2002)
Michael J. Lewis and Neil J. Heppell, *Continuous Thermal Processing of Foods: Pasteurization and UHT Sterilization* (2000)
Jorge E. Lozano, *Fruit Manufacturing* (2006)
Rosana G. Moreira, M. Elena Castell-Perez, and Maria A. Barrufet, *Deep-Fat Frying: Fundamentals and Applications* (1999)
Rosana G. Moreira, *Automatic Control for Food Processing Systems* (2001)
M. Anandha Rao, *Rheology of Fluid and Semisolid Foods: Principles and Applications, Second Edition* (2007)
Javier Raso Pueyo and Volker Heinz, *Pulsed Electric Field Technology for the Food Industry: Fundamentals and Applications* (2006)
George D. Saravacos and Athanasios E. Kostaropoulos, *Handbook of Food Processing Equipment* (2002)

FOOD MATERIALS SCIENCE

Principles and Practice

Edited by

José Miguel Aguilera
Pontificia Universidad Católica de Chile
Vicuña Mackenna, Santiago, Chile

Peter J. Lillford
University of York
Heslington, UK

Springer

Editors:
José Miguel Aguilera
Dept. de Ingeniería Química y Bioprocesos
Pontificia Universidad Católica de Chile
4860 Vicuña Mackenna
Santiago
Chile
jmaguile@ing.puc.cl

Peter J. Lillford
Department of Biology
University of York
Heslington, York YO1 5DD
Heslington
UK
PL8@york.sc.uk

Series Editors:
Gustavo V. Barbosa-Cánovas
Dept. Biological Systems Engineering
Washington State University
220 L.J. Smith Hall
Pullman, WA
USA
barbosa@wsu.edu

ISBN 978-0-387-71946-7 e-ISBN 978-0-387-71947-4

Library of Congress Control Number: 2007926246

Printed on acid-free paper.

9 8 7 6 5 4 3 2 1

springer.com

PREFACE

Most people do not think of foods as engineering materials, and specialized books make almost no reference to them. Somehow, foodstuffs have been set apart from other materials—textiles, wood, clay, metals—used by mankind since prehistoric times and more recently, ceramics and plastics. Perhaps, it is because for many old cultures foods were a gift of the gods and it would appear demeaning now to consider them as mere substances.

Why then should we compile a book about the science of food materials? Reasons abound. The Merriam-Webster Dictionary defines food as "*material* consisting essentially of protein, carbohydrate, and fat used in the body of an organism to sustain growth, repair, and vital processes and to furnish energy." People describe the process of eating in terms typical of the mechanics and flow of materials (e.g., tough, soft, thick, thin). Modern food processing can be defined as a controlled effort to transform and create microstructures that are palatable. Even the amateur scientist realizes that foods do not escape the principles of physics and chemistry. Rising bubbles in champagne, dunking biscuits and the sound emitted by potato chips during mastication are the result of physical phenomena, and the flavors delivered by many foods originate from both molecular reactions and the collapse of physical structure.

Often, foods must be treated as engineering materials. Heat has to be transported so that the components become "cooked" or harmful microorganisms and toxins become inactivated. Even in the kitchen, mixing involves the mass transfer of liquids and solids to form metastable structures, which are "fixed" by subsequent treatment by heat or cooling. Heat transfer properties are crucial in the formation of ice crystals in ice cream and fat crystals in chocolate products. Food materials have been used as a source of industrial components: soybean proteins to manufacture auto parts in the 1940s, casein to make buttons and knitting pins, and starches in adhesives and thickeners.

Foods are unique among materials of our daily life in that they are ingested and become part of our body. This immediately adds several extra dimensions to their intrinsic properties: foods have to be appealing, tasty, nutritious and safe. Unlike the case of engineering materials food properties have no single value but they depend largely on consumers' characteristics (e.g., age, physiological state, etc.) and judgment. The biological origin of foods makes them prone to degradation, adding a temporal dimension to their desirable attributes not found in ordinary materials. Moreover, because natural edible materials play a biological role in plants, animals and fish they have a structure (usually assembled hierarchically) imposed by the functional role. Typical of foods is the presence of multiple chemical components adding complexity to their study. Foods are such easily recognised materials that many reputable scientists, including Nobel laureates, chose them to illustrate their

findings to the laymen. At the other extreme, innovative chefs are using the properties of food as materials to create dishes that astound their customers and provide exquisite sensations. This *mélange* of science and gastronomy is becoming an autonomous discipline: molecular gastronomy.

The body of scientific knowledge behind food fabrication started to accumulate less than 50 years ago. It has been in the last 20 years that the study of foods as materials has become a field in its own. It has been fostered by advances in related areas, most notably polymer science, mesoscopic physics, microscopy, and other advanced physical techniques. Progress in separations science has led to economically feasible processes that make available refined and functional food ingredients that replace or complement traditional raw materials. New technologies, most notably the use of membranes and microdevices, promise to bring the scale of fabrication closer to that of microstructural elements in dispersed phases (droplets, bubbles).

On the demand side, increasing evidence of links between diet and some nontransmissible diseases (obesity, cardiovascular diseases, and some cancers) has opened new opportunities to tailor-made products with reduced caloric content or increased levels of beneficial nutrients that may help prevent or ameliorate the effects of these diseases. In coming years, structuring foods for the brain (pleasure) and the gut (health) will become increasingly important as new knowledge emerges on neurophysiology and the fate of nutrients in the digestive tract, respectively. Discoveries in materials nanotechnology may be adapted to improve food quality and traceability. Lastly, the technology of genetic engineering provides the opportunity to harness cellular processes to fabricate the complex food molecules that we require. We can now alter the amount and properties of materials directly in the natural source. With this power to control the synthesis of biomolecules comes enormous responsibility, but the future seems bright and full of opportunities for food materials science.

This book describes the science and practice behind the materials in foods that impart their desirable properties. The first part of the book describes those physicochemical aspects that intervene in the organization of food components from the molecular level to actual products and methods used to probe into foods at different length scales. The second part explains how food structures are assembled during processing in order to achieve desirable and recognizable properties. Processed foods are mostly metastable structures in which water, air, and lipids are immobilized as dispersed phases within a polymeric matrix of proteins, polysaccharides, or a fat crystal network. The last section of the book presents specific examples of how structures of familiar products are obtained by processing and describe some new developments.

Combining breadth and depth was our ambitious goal for this book. This was only possible by bringing together the talent and knowledge of many scientists. Our first thanks go to the authors for contributing chapters. We were fortunate to gather a highly authoritative group of scientists that have made major contributions to what is presently the science of food materials. It has been a pleasure to work with them. We appreciate the enthusiasm and support provided by the publisher, in particular, by Susan Safren. We owe many thanks to our graduate students and colleagues for their critical comments and suggestions. Any errors that remain are, of course, entirely our own.

In these times of dwindling funding for science, the support of the Nestlé Research Centre (Lausanne), the Alexander von Humboldt Foundation, and recently, the Marcel Loncin Fund of IFT is appreciated by JMA. PJL wishes to thank Heather McGown without whom no texts would ever have been completed. He acknowledges all his former colleagues in Unilever Research for their stimulating challenges, and thanks CSIRO for a recent series of Fellowships which has given access to new co-workers, and an opportunity to develop the practice of food materials science.

Our families also deserve our gratitude, once again, for their forbearance. However, we warn them that acting as editors of this book does not mean we have the answers to the secrets of the kitchen. Hopefully, our responses will provide insight into the operating principles encountered every day by millions of food providers.

Santiago, Chile — José Miguel Aguilera
Heslington, York, UK — Peter Lillford

Contents

FUNDAMENTALS

Chapter 1

Why Food Materials Science?

Peter J. Lillford,[1] Heribert Watzke,[2] and José M. Aguilera[3]

[1]University of York, Department of Biology, PO Box 373, York, YO10 5YW, UK, PL8@york.ac.uk
[2]Nestle Research Center, Vers-chez-les-Blanc, CH-1000, Switzerland, heribert.watzke@rdls.nestle.com
[3]Universidad Católica de Chile, Department of Chemical and Bioprocess Engineering, Vicuña Mackenna 4860, Santiago, Chile, jmaguile@ing.puc.cl

1.1 Introduction

For centuries, mankind has hunted and farmed its food supply. For an equal amount of time, someone has had to convert these raw materials to an edible state, most of which required processing, since apart from fruits and nuts, most biological materials are not easily eaten and digested by *Homo sapiens*. In the hands of an expert, such as a the Cordon Bleu chef, this processing has been developed into an art form, using the intrinsic properties of the raw materials to create colours, textures and flavours for our delectation and nutrition. Furthermore, the methods and materials have been codified into millions of recipes, which are available to everyone.

So what more do we need to know about food materials and their processing?

Chefs, and indeed all cooks, operate batch processes on selected materials. Originally all food was prepared this way, and the resultant quality related to the individual's skill in selecting raw materials and operating subsequent processes. As civilization advanced and societies became urbanized, mass food preparation became necessary, with the concomitant problems of scaling up the operations and of sourcing raw materials of at least reasonable quality. By these criteria, the food manufacturing industry is highly successful. As a percentage of earned income, food is now cheaper in the developed world than it has ever been. However, it is still the case that product quality and utilisation of materials is inadequate because of:

1. *Irreproducibility*: Even in the hands of the best chefs results are variable, either because the raw materials are not completely specified or the processes are "interpretable" in terms of energy input and time. In a way, recipes are like patents: they tend to conceal "secrets" rather than reveal details.

2. *Cost*: The "best" materials are not always available. Agricultural products are conditioned by their biological source (genetics) and the action of abiotic stresses (the environment). All of the resultant raw materials should be used, to avoid waste and to maximise conversion efficiency, yet not all of them can be ideal for a given process or product type.
3. *Scale*: In our modern society most processing is not done locally by the producer but in large-scale factory conditions. The processes described in most recipes relate to a small scale, and are not directly transferable to large-scale, continuous processing.

The net effect is that food products are not easily standardised, and by the necessarily subjective measurement of quality by the consumer, not everyone is satisfied all of the time. Faults can occur for two major reasons. Either the product was not what was intended (problems in fabrication to an exact specification); or the product did not meet the performance expectation of the user (problems in performance and expectation).

The food industry is like any other manufacturing industry; Commercial practice is competitive, and the manufacturer who is best able to make the most acceptable product most often, from the most appropriate raw materials and at the right cost will be successful. The ability to innovate products, processes and interchange raw materials is necessary for financial survival, and so the science of food materials is necessary to deliver consistent quality and novelty of product to very demanding customers.

1.2 What is Quality?

Unlike other manufacturing industries, where the product can be accurately specified in terms of its performance, food is measured by individuals, and its qualities of appearance, texture and flavour are measured subjectively against a set of criteria established by experience. We know what we like, and it is very dependent on our own cultural background and lifestyle. As consumers, we detect some qualities instantly with our eyes, nose and mouth, all of which have multiple sensors with stimulus/response behaviour that is not completely understood. We have to recognise that these qualities are defined subjectively, and are described in words that have, as yet, no clear numerical definition. There are other qualities such as the effect of food on our longer-term health and well-being that as individuals we are not well equipped to measure. We cannot easily detect the effect of salt on our blood pressure or antioxidants on our cancer resistance. The development of biomarkers for health is outside the scope of this volume.

Returning to qualities that we *can* recognize during purchase and eating, we must understand that subjectively measured quality, and its relationship to perceived preference or liking, is the real criteria of success in food manufacture. Throughout this volume, reference will be made to how finished product structures relate to these

subjective assessments. Fortunately, even though individual preferences change, there are certain textural parameters such as toughness, crispness, smoothness, and so on, that are universally recognised, and we can attempt to understand their origin. Also, despite the fact that there are an enormous number of food types available, they all have to be chewed and swallowed, and the equipment we have to deal with them (teeth, tongue, saliva) are common to most consumers. We must recognise therefore, that quality is measured throughout the mastication process and is not just a simple property of the manufactured structure.

Quality control or quality assurance tests are already common throughout the industry. Many of these tests are physical measurements that have been derived empirically. Rather than relating to the fundamental physical properties of foods, they are designed to detect deviation from a standard sample already defined to be of acceptable quality. While useful, they should not be confused with the measurements necessary to understand how components interact with each other to form the complex composite structure required in most foods.

Apart from producing convenient food that is pleasant to eat, the food manufacturing industries face a further major challenge. International supply chains now offer the developed world a surfeit of food calories, so that our natural tendency to enjoy eating means that obesity, not malnutrition, is a major health risk (even in the less-developed world). Now consumers would like to continue to enjoy eating, but without the risk to their health in terms of chronic ailments such as diabetes, cardiovascular disease and cancer. These qualities of long-term health benefit are not directly measurable by the consumer, but consumers and legislators now demand both information and delivery of foods that will protect, or at least not cause a decline in, long-term health.

The boundaries between food science, nutrition and medicine are beginning to blur, and molecular nutrition, or "Nutrigenomics," is in vogue. While these topics are in the area of biological rather than material sciences, the findings will have to be translated into edible foodstuffs. Even if we knew the exact genomic regulation of every individual on the planet, and even if nutritionists might specify their exact daily requirements of macro- and micronutrients, unless the food was available, attractive and pleasant to eat, there would be little impact on human health.

Someone will have to develop and make the new foods and deliver them to the right markets at the right time. This will require continuous innovation in ingredients and processes. A greater depth of understanding of the relation between components of food, the effect of processes upon them, the net effect on the "architecture" of the composite structure, and the subsequent appearance, organoleptic and nutritional performance, will be required. Neither is this science required solely to fulfill the demands of the idle rich. If we are to feed the increasing world population, the need to use agricultural produce as efficiently as possible is mandatory, so a growth in knowledge of food materials behaviour is equally necessary. This is further justification of the approach we call "food materials science."

Ideally, the science of food materials should approach and provide answers to two fundamental questions:

1. What are the causal relations between the structure of a food and its performance when assessed visually, organoleptically and in the delivery of its components to the human digestive tract?
2. How do we control (predictively) the effect of processes on components to form the required product structure?

When both questions are answered, we can begin to develop "design rules" for food products, comparable to those available in assembled products from bridges and buildings to machinery and composites. When phrased in this way, it is obvious that food can be related to these other manufacturing industries, such as construction, ceramics, polymer products, and so on, and wherever possible we should borrow approaches and methodologies from them.

1.3 What Are the Materials?

The words "materials," "components" and "structures" have been used thus far with little regard to their definition. Without being too pedantic, we need to be clear about their use, and to do this the scale of the observation needs to be considered. Food materials and structures are similar to other well-known objects in this regard. For example, taking the analogy of the construction industry, we can equate a finished food to a building. This is obviously a structure made from components such as doors, windows, roofs, and so on, and materials such as bricks, mortar, timber, plastic, and so on. While we can see that components such as windows and doors are obviously structures in their own right, a little help with a hand lens shows that brick, timber, and mortar are themselves structures comprised of particles, fibres, and crystals. Likewise, at a higher level of magnification, the particles, fibres and crystals are structures formed from molecular assemblies, the properties of which are determined not only by the molecular species present but also by the conditions under which they were formed. The structural (mechanical) requirements of a building are that it should not fall down and remain stable for as long as possible. This requires appropriate organization at all hierarchical levels.

We can perform a similar analysis on a loaf of bread, a sausage or a tomato. Our components are starch granules, gluten networks, muscle, plant cells, and so on. But our assembly processes simultaneously modify the structure of components, colloidal assemblies and molecular configurations. The structural requirements for the lifetime of products are a little different, but stability is required during transportation and storage. Food materials scientists have a further, even greater challenge: Under incompletely specified conditions in the mouth and gastrointestinal tract, the structure must collapse in a fashion recognizable to the consumer and appropriate to the unique processes of mouth action and digestion. No wonder we do not yet have a handbook of food design!

Fortunately, we are not entirely alone in studying the architecture of biological structures. Nature itself provides many sophisticated solutions to mechanical problems faced by living organisms, using the same materials and components found in foods. For those wishing to explore this topic of biomechanics further, the now classic texts of Wainwright et al. (1976) and Vincent and Currey (1980) are recommended reading; these sources can be followed by the inspirational works of Gordon (1976, 1978).

We note from all this prior work that structure at the macro, micro, nano and molecular levels of organisation will all be important. Secondly, the properties of the composite food product will not be related simply to a list of its components (the recipe), since different structural forms can be assembled from the same components by different processes. Emphasis on structure and its origin discriminates food materials science from the former descriptive approach of formulation/process empiricism embodied in most recipes.

There is enough published microscopy of foods (Aguilera and Stanley, 1999) to indicate that their structures are enormously variable and complex. The physical property of appearance is derived from the structure itself, and texture, flavour, taste, and subsequent bioavailability of nutrients are derived from the manner in which the structure collapses or breaks down. Simple theories of composite solids tell us that the spatial organisation of components and materials, their own physical properties and the interfacial interactions between them will determine overall properties. The components and materials themselves consist of molecular assemblies. This hierarchy of structure suggests we will need measurement at all length scales from molecular to macrostructure and over timescales relevant to processing (milliseconds to hours) and product stability (minutes to months).

1.3.1 Fundamentals

In the first section of this volume we examine the fundamentals of structure at the level of the overall composite, as well as the properties of its components. The starting materials of food derive from living biological systems, whose mechanical properties have been studied in their own right. Vincent explores the extent to which biological composites can be related to other natural and manmade composites, and emphasises the difference between the properties of components (fibres and matrix) and the structure itself. This engineering approach to biological structures, whether natural or fabricated, shows the fundamental difference in the materials science approach, compared with the former recipe approach to food manufacture.

In subsequent chapters we examine the physical forms and properties of products and components. These are shown schematically in Figure 1.1.

It is important to recognise the ubiquitous presence of water in all foods. Every chapter will mention the particular impact of water as a solute, diluent and plasticiser, often converting one physical state to another and also promoting mixing or segregation of one component molecular species from another.

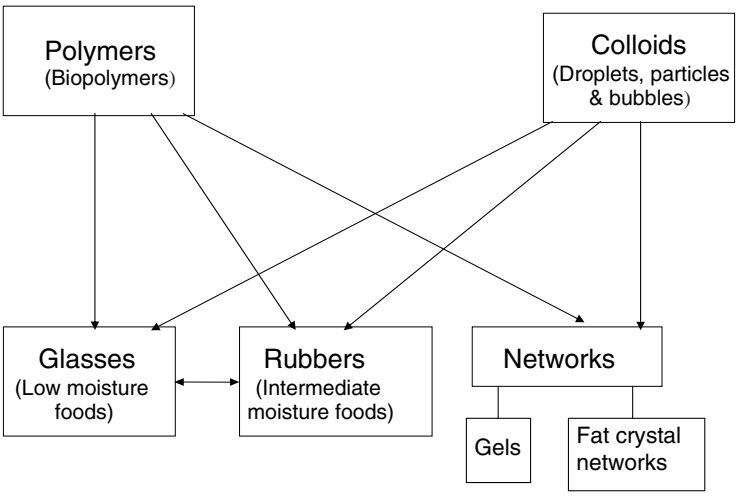

Figure 1.1. Physical forms of food components in processed products.

Most of the contributions in this section refer to principles derived by study of other polymer and colloidal assemblies of nonfood origin. We would be foolish to ignore approaches from other industries, but throughout this work the peculiar and particular properties and behaviour of biopolymers and small molecules will be emphasised.

For example: The behaviour of compatible and incompatible polymers leads to various forms of self-assembly that can be manipulated by processing. Crystals form a vital solid component of foods, but the architecture, morphology, form and habit can be varied by accident or design. The fact that food components can also exhibit glassy states (i.e., solid forms of amorphous assemblies) has been investigated more recently. Its significance in small molecule and biopolymer systems is now well recognised, but we still lack much of the detailed data that allows predictive rather than post-rationalised explanations of processing and storage performance. In particular, since biopolymers themselves are usually heterologous in a monomer sequence, they can simultaneously exhibit crystalline, glassy or rubberlike behaviour within their molecular structure, and at a macroscopic level. We would be unwise to believe that all the behaviour observed with entangled networks of synthetic polymers can be directly imposed on interacting assemblies of globular native and denatured proteins.

State diagrams describing overall properties have proved extremely valuable in describing the principles of process and product performance, but the practicality of optimized processing requires detailed knowledge of the particular materials in use. Such information is lacking in many cases, and is the subject of painstaking measurement, which is rarely recognized for its technological importance.

We also examine the cheapest ingredient of all, air, which is incorporated into our food by both natural and manufacturing processes. This chapter shows the principles by which materials that otherwise would be inedibly hard and strong can become structures amenable to fracture in the mouth.

Finally, while it is evident that even traditional processes operate on structures at the nano- and mesoscales, new measurement methods and manipulation techniques will allow us to consider more systematic control at these levels in the future. While this is an absorbing playground for materials scientists, and may well provide routes to controlled delivery of high-value ingredients, we are fortunate that the consumer is also inquisitive. The novel sensory impressions these sophisticated new structures can provide may also result in real commercial value.

1.3.2 Structuring Operations

This section examines the critical "unit operations" used throughout food manufacture in terms of the engineering equipment and, whenever possible, its impact on the materials themselves. What we observe throughout is that because of the metastability of most biological materials within the window of applied heat, shear and mass transfer imposed by many of these process events, the operation are far from simple in terms of what happens at the molecular level. Frequently, molecules are transformed in terms of their own organisation and their interaction with other molecular species. This creates new structural organization at all levels, up to the macroscopic.

As far as most molecular species are concerned, the processes are not unitary but multiple. We see that alternative equipment provides various sequences of molecular change and different dynamic rates. It becomes immediately clear that optimization with respect to the choice of processing equipment and its operation has no absolute value. Rather, it needs to be identified and performed with respect to the subsequent function of the ingredients or structural components it produces. Within that context, the key physico-chemical phenomena within each process are identified, and the obvious connection between operations at scale and the principles outlined in the first section are provided. Each chapter provides further evidence of the need to identify the cascade of structural events beginning with molecular reorganisation and the macroscopic properties of the subsequent assembly

The empirically developed processes of gelation, foaming, emulsification, drying and crystallization are teased apart and described in relation to the role and fate of molecular species. Each also examines novel forms of process equipment, offering alternatives to more traditional equipment that may provide the future option of different metastable structures. Many of these engineering options have been developed elsewhere, and it remains to be seen how they will fit into future large-scale food processing. As is often the case, we can anticipate that value will be developed empirically, by cost and energy savings or by the production of novel stability of products and components. Understanding the materials science should accelerate this process.

We still lack the details of behaviour at relevant length scales for many food materials and the subsequent manufactured food structures. However, identifying the problem is the best start towards applying relevant new techniques to measurement at all length and time scales. Elegant new information is emerging. which is given a special mention in this section.

1.3.3 Food Products

In this section, we look at what we have learned about the links between molecular behaviour and structural levels in traditional food types. We notice that that dairy, cereals and meat products and processing have been identified with, and driven by, the unique properties of the components of agricultural raw materials. However, in every case we can begin to relate performance with the principles identified in the first section and the events described in the second. Complete foods are derived from a combination of many of these principles and events. Our sensory impression of texture can now be described in terms of what mechanical events take place and are detected in the mouth, allowing us to design at the correct levels in the hierarchical structure. But complete interchange of materials to construct the same product type is not yet possible. For example, we can make simulated meats, but the particular properties of wheat gluten during processing still make it unique for bread structures.

Lastly we examine attempts to design structures for particular functions, namely, films that act as barriers and capsules that contain bioactive substances. In the future, we will need to create novelty in the long-term stability of products and delivery of specific molecules for a health benefit. These technologies are attracting attention not only from the food industry but also for nonfood use. Sustainable and environmentally friendly attributes of biomaterials are increasingly discussed, compared to petrochemically derived, synthetic polymers and plastics. For once, food materials scientists can teach other industries the "rules of the game."

1.4 Conclusions

Thorough readers will notice some repetition of theory and analysis across chapters. In a volume such as this we believe this is inevitable and serves to connect concept to reality. We believe each chapter provides a good review of its topic, and we thank all authors who have independently surveyed what is known and related this knowledge to the contributions of others.

1.5 References

Aguilera J.M. and Stanley, D.W. (1999). *Microstructural Principles of Food Processing and Engineering,* Aspen Publishers Inc., Gaithersburg, MD.

Gordon, J.E. (1976). *The New Science of Strong Materials,* 2nd ed., Princeton University Press, Princeton, NJ.

Gordon, J.E. (1978). *Structures: Or Why Things Don't Fall Down,* Penguin Books, Harmondsworth.

Vincent, J.F.V. and Currey, J.D. (1980). *The Mechanical Properties of Biological Materials,* Cambridge University Press, UK.

Wainwright, S.A., Briggs, W.D., Currey, J.D. and Gosline, J.M. (1976). *Mechanical Design in Organisms,* Edward Arnold, London.

Chapter 2

The Composite Structure of Biological Tissue Used for Food

Julian F.V. Vincent

Centre for Biomimetic and Natural Technologies, Department of Mechanical Engineering, The University, Bath, UK BA2 7AY

2.1 Introduction

Natural materials are all hierarchical composites composed of a relatively small number of basic materials. Commonly, the composite will be based on fibres that can support tensile loads (a fibre is defined as at least 100 times longer than wide) in a matrix that holds the fibres together and passes force, by shear, between the fibres. The fibres can be arranged parallel (the "preferred" orientation) or helically around a cylinder, or semi-randomly or random like a felt. This fibre-matrix composite is arranged in a series of structures of cascading size and complexity, giving a wide range of properties to the final structure, since at each level in the hierarchy the various components can be structured in different ways and stabilized to different degrees. This is the basic framework that nature has given us. At various stages in the chain of preparation of food both the materials and the structures can be modified to make their texture, flavour and nutritional characteristics more acceptable. This involves selection and breeding of the organisms, and preparation and cooking of what they yield. Wider considerations will require the selection and breeding to have minimal environmental impact ("sustainability") and the products to be entirely used or recycled.

2.2 Animals and Plants

In order to understand the materials and structures in any detail, it is necessary to know a little of the phylogenetic relationships and constructional principles of organisms. Most of the things that we eat are from eukaryotes—organisms with a membrane-bound nucleus—which have a very similar basic biochemistry across both the phylogeny and the size range. The cell is the main building unit; it can be independent or a subunit of a larger organism.

Plants and fungi generate their mechanical properties with a fibrous capsule around each cell (the cell wall). Fibres can carry loads in tension depending on their material properties but cannot carry loads in compression. Unless they are well stabilized by a surrounding matrix, they will bend and buckle out of the way. In the absence of such a matrix (provided, e.g., by the lignins in wood) the cells of plants and fungi prestress the fibres by generating an internal (turgor) pressure of about 10 bar, which is then greater than most of the external loads comprising, for instance, wind or snow-loads and the weight of the organism itself. Any external load has to overcome the internally generated prestress before it can do much damage. The fibrous component (mostly cellulose) has bonds with high energy that are difficult to break down and so is very stiff (about 130 GPa). The cells are glued together to make a tissue, organ or organism, and the whole structure is further stabilized by a fibrous outer layer (epidermis). The main function of an average plant cell is therefore to provide osmolar effectors that can generate turgor. Differences in turgor prestress are the prime generator of movement in plants and fungi.

Animal cells do not have a cell wall. Single cells rely variously on an internal support system, an external pellicle that supports other structures, or a stiff (mineralized or dehydrated) skeleton. The mechanical support and integrity of a larger animal are provided variously, for instance, by a low-pressure turgor (about 0.5 bar) reacting against an external collagenous membrane (collagen fibres are much less stiff than cellulose—about 1.5 GPa), which can be supplemented by an external skeleton, essentially tensile, as in soft-bodied insects and some worms.

In mammals, 25% of the protein in the body is collagen: it provides the scaffold that holds the entire body together. Movement is provided almost entirely by interactions of actin with myosin (making muscle) or of kinesin/dynein with microtubules (see also Chapter 21). Few animal materials have the chemical stability of cellulose; probably only chitin (primarily in arthropods and fungi, but also part of the metabolic pathway of other animals including man) and elastin.

Sponges, most molluscs, and vertebrates have a mineralized skeleton that may be internal or external. Arthropods and many molluscs have an external skeleton, commonly mineralized, stiff and chemically stable (i.e., indigestible). Culinary classification tends to cut across these boundaries, so that “shellfish” can be any aquatic organism with external mineralization, including molluscs and crustacea, but not insects or land molluscs.

2.3 Fibrous Composites

The many textures of the foods that result are due to only two basic polymers: proteins (fibrous ones are collagen, actin, myosin, keratin; there are very few matrix proteins) and polysaccharides (fibrous ones are cellulose and its subsets of short-chains such as hemicelluloses). There are also many materials that are a mixture of these two polymers, such as glycoseaminoglycans, which can have a variety of side groups—charged and uncharged—which then can also form stable gels binding significant amounts of water, providing bulk at low metabolic cost. They are commonly present as matrices between the fibres. There are a few materials that contribute to a composite

food structure only after processing. The obvious ones are the matrix-formers, starch and gluten from flour, which have little or no mechanical importance in their native state in the wheat grain. Since a fibre is of lower entropy than a matrix, it is statistically unlikely that a novel fibre will arise during or after processing unless orientation is provided by an external force.

These few materials have to account for the variety of textures and mechanical properties found in foods. Composite materials have a large amount of intrinsic variability. The fibres can be present in different amounts or volume fraction, and have different orientations in all three planes. Water plasticizes the matrix, decreasing its stiffness and increasing the extension possible before irreversible damage sets in. However, if the fibres are limiting the expansion of the matrix, either by containing it or being tightly bonded to it, the composite can become stiffer due to prestrain since an external compressive force will have to pay off the tension before the fibres buckle, and may well cause fibres elsewhere in the system to stretch further. When the matrix is especially soft the composite can become more like a textile. The fibres (which because of their tighter molecular bonding are more difficult to plasticise) become more mechanically differentiated from the matrix and more difficult to break since sufficient force cannot be fed into them via the matrix. The material will then become tougher and able to accommodate more damage before total failure. Decreasing amounts of water will cause the matrix to become stiffer, which reduces the mechanical difference between matrix and fibre and may render the material as a whole more brittle (see also Chapters 5 and 10).

The plant cell wall is a composite of cellulose (the main fibre) plus shorter lengths (hemicellulose) that help bind the fibre, plus pectin (the main matrix adhesive) and some proteins. There are fruits that have a soft melting texture when ripe (e.g., avocado and blackberry) in which the cell wall swells noticeably. This swelling is related to the degree of solubilisation of the pectin (Redgwell et al. 1997) which can be removed *in vitro* using enzymes or other chemicals.

When kiwifruit was treated with such enzymes, the results suggested that water moves into voids left in the cellulose-hemicellulose network of the cell wall by the solubilised pectin. This plasticizes the cell wall. Something like this happens when a fruit becomes over-ripe and the texture becomes "mealy," as in nectarines and apples, amongst others. Apple cells are about 100 μm in diameter with fairly thin (1–2 μm) cell walls, but the cell walls break in a brittle manner (Hiller et al. 1996), suggesting that the cell wall components are stuck together well. Although apple cells have air spaces between them (Reeve 1953; Vincent 1989), in general they are also stuck together well with insoluble pectins that transfer displacements (and hence forces) from one cell to the next. The balance is then whether the intercellular adhesion is stronger than the cell wall. If it is, the cell wall will break preferentially, releasing the cell contents as juice.

However, as an apple ripens the pectins become more soluble, absorb water, swell and lose their strength and adhesive properties. The cells then become spherical rather than polygonal as the constraint of neighbouring cells is removed, and the apple expands, often splitting the skin in the process, indicating that the cells are still capable of exerting significant turgor force, and the cells separate and can be removed individually. It then becomes difficult or impossible to transfer enough force

into the cell wall and it will not break. Thus no juice is released and the fracture on eating the apple is dry, with separated cells giving a rough, sandy, texture. It thus appears that the pectin in the apple cell walls is not affected by maturation in the same way as the intercellular pectins. Interestingly, early apples (which have been growing for only a few weeks and contain about 50% air space) may soften only a few days after picking, while late season apples (which have been growing for up to 6 months and have hardly any air spaces at all) seem not to over-ripen (Khan and Vincent 1993).

Sometimes, as in collagenous tissues, the "fibre" is itself composite, and in other materials (notably silks and mammalian keratins) matrix and fibre are different conformations of the same molecule. Both proteins and polysaccharides can have charged groups attached which bind water or ions with varying degrees of firmness. Other molecules can become involved, such as phenolic compounds (common in plants) increasing hydrophobicity snd thus encouraging the formation of secondary hydrogen bonds (Charlton et al. 2002), and sometimes providing extra covalent cross-links. As an animal ages its collagen tends to be more cross-linked, which does not affect the stiffness very much but greatly affects solubility and ease of denaturation with heat and other methods with insufficient energy to destabilize the bonds. In meat this is another way to generate stringy toughness, although this characteristic is not very well defined (Purslow 2005).

2.4 Hierarchy

All these structures are involved at a lower level of hierarchy, no more than a few micrometers and usually less. At larger sizes, and higher levels within the hierarchy, the composites form sheets or cells that confine or partition the other materials. Notably in plants, the cells—with walls that are a composite of cellulose fibres in a matrix of smaller polysaccharides—form larger structures which are themselves further stabilized with fibres. So the structure is a composite at a higher level, with cellular parenchyma appearing as a relatively homogeneous matrix with fibres (collenchyma and sclerenchyma) providing another level of complexity. This results in a "stringy" texture found in some wilted or cooked plant stems (e.g.. the basal part of asparagus shoots) and in some ripe fruits such as mango. Stringy texture can also be generated if the matrix is brittle by comparison with the fibre; in plants this would be typified by overage petioles of celery where the collenchyma fibres, which are not lignified and so are extensible, do not break at the low strains at which the fully-turgid parenchyma breaks (Esau 1936). In terms of fracture mechanics of composites this has not been investigated in food plants, although in grass leaves the longitudinal stiffness and transverse fracture properties are governed by the sclerenchyma (Vincent 1991a; Vincent 1991b).

Similar descriptions apply to animal tissues, except that the cellular materials can themselves be fibrous (as in muscle) within a fibrous network of connecting collagen. This complexity is far greater than is found in engineering materials for which the mathematical understanding of composite materials has been developed. Worse, biological materials deform by large amounts (more than 1%) and are nonlinear, both

characteristics that are not typical of engineering composites and for which the mathematics is not readily suitable. In muscles the perimysium is a bag around the muscle formed of crossed-helical fibres (Purslow 1989) which are eventually attached to the tendons at each end of the muscle. At the structural level this is a further complexity since the fibres move in concert and generate a mechanism with definable relationship between the enclosed volume, the angle between the fibres and the strain in the fibres. This is a ubiquitous mechanism in animals (Clark 1964; de Groot and van Leeuwen 2004).

Some collagens are present as a feltwork, most familiarly in mammalian skin. Animals that have no solid skeleton against which muscles can react can have complex arrangements of collagen. Examples are the squid, *Loligo*, and the cuttlefish, *Sepia*, whose mantle (a muscular membrane surrounding most of the body thus defining a cavity between it and the body) has to expand in order to draw water into the cavity, which is then jetted out in the escape response. This expansion is achieved by making the mantle thinner, the muscles acting via short collagen fibres (Gosline and Shadwick 1983; Macgillivray, et al. 1999) and generating a Poisson ratio effect.

2.5 Processing

Fibrous composites are of use in engineering and structural materials precisely because they do not break easily. So any consideration of fibrous composites for food has to include the fracture and failure modes. Some have been hinted at already. In general, in a technical composite the fibre is chosen to be stronger and stiffer than the matrix and the matrix is chosen to adhere moderately strongly to the fibre. When the material breaks the fibres fracture, but not all in the same plane as the main fracture and have to be pulled out of the matrix in order for the fracture to propagate, dissipating energy through friction as they do so.

A technical composite can be made tougher by increasing the fibre-matrix surface area, by making the primary fibres of smaller diameter or by making the fibres hierarchical or by making them longer, or all three. The crack can also be diverted at the interface between the fibre and the matrix and be blunted (Cook and Gordon 1964), which reduces the stress-concentrating effect and dissipates the force required required to break bonds. Unfortunately for the food scientist, most biological composites display all these and more characteristics, are remarkably tough, and are regarded as iconic by materials scientists. Collagen, especially in skin, can be reorientated by the displacements that occur around a notch or cut so that the fibres are arranged across the path of the cut and hinder its propagation (Purslow et al. 1984). Additionally, the stress-strain curve of collagen, typically J-shaped, provides an extra toughening effect, since the effect of increasing the length of a notch decreases fracture stress more than fracture strain; therefore the material has to be strained more in order to reach the fracture stress (Purslow 1991).

Over the millennia, food plants and animals have been selected and bred to reduce their intrinsic toughness; animals have developed strategies for coping with foods that are difficult to harvest and chew. For instance, the parallel sclerenchyma

fibres in grass sit in a relatively soft parenchyma that isolates the fibres mechanically and so prevents a crack from propagating across the leaf (Vincent 1991a). Cows break grass by brute force in tension; insects cut through it with scissorlike mandibles. Muscle is remarkably similar in texture, but at more levels of hierarchy, with parallel fibres and bundles of fibres that do not adhere laterally (Purslow 2005). Carnivores have developed scissorlike carnassial teeth. Man reduces the aspect ratio of the fibres by chopping small, such as cutting meat "across the grain," grinding, flaking, macerating, and so on. In general, however, the fibres need to be destroyed, softened, restrained by the matrix or given the same properties as the matrix in order that the food item can be chewed small.

To be chewable, food has to come within a proscribed range of properties in order for the mouth to be able to cope. In general, the important dimension for consideration of mechanical properties for chewing is somewhere between 1 mm and 2–5 cm. The available forces and displacements are limited by the muscles and morphology of the mouth and jaw (Heath 1991). For instance, fish and chicken tend to have shorter muscle fibres and so are easier for a small mouth, or a weak one, to process and so are favoured by children and invalids. Cooked meat is generally tougher and stronger than raw meat but breaks with less displacement. Teeth direct the forces; more especially, the incisors can generate a stress concentration for fracture in mode I (crack opening) which is useful for eating a nonfibrous material with relatively low work to fracture or for propagating a crack between fibres.

Size is also important in considering at what level of hierarchy the material is to be broken. Thus, although cellulose is very strong, it is rarely necessary to break open a single plant cell to reduce it to a size suitable for swallowing (about 1 mm^3) since plant cells are rarely more than 100 μm across. So the strength of the cellulose in plant cell walls is not particularly relevant, although the adhesion between cells may well be important. If the adhesive is stronger than the cell walls then the strength of the cell walls *will* be relevant. Cooking commonly dissolves pectic substances in plant structures, so the cells tend to separate. The material is no longer a fibrous composite.

The most common method of transforming food in preparation for eating it is to use heat. Since the bonds that stabilize biological composites cover a range of energies, such that lower-energy bonds are destabilized at lower temperatures, it is clear that cooking at different temperatures (or for different times, since we are concerned with the energy input) will have different results in terms of the bonds destabilized.

For instance, heating squid mantle at 100°C for a minute or so gelatinizes the collagen, thus destroying the fibres of the composite structure. Cooking for longer tends to dry the tissue (Collignan and Montet 1998). The rubbery texture that frequently characterizes cooked molluscs (squid, snails, scallops, etc) is presumably due at least in part to the conversion of the fibrous collagen into the randomly coiled gel phase which, with reduced water content, will yield an entropic rubber. Some cross-link sites are required to produce this rubbery behaviour, which could be provided by interactions of a fraction of the collagen remaining fibrous, or by interactions of the denatured collagen with the muscle fibres (see also Chapter 6). However, the crystalline elastoidin fibres of shark fins, which are made of particularly well aligned and interacting collagen (Woodhead-Galloway and Knight 1977) are presumably not

covalently cross-linked and so can be dissolved. Another unusual example is the edible sea cucumber, Stichopus japonicus, whose body wall collagen is largely (70%) highly insoluble. Its unique textural properties when cooked (i.e., rather tough with lumps in it) seem to be due to thermal denaturation of these insoluble collagen fibers (Saito et al. 2002).

Marinading can also transform texture. In animal tissues, dilute acid (e.g., acetic or citric) or salt solution destroys collagen–collagen interactions and so softens the fibres. Presumably in plant material, for which this treatment is also effective, it is the pectins that are altered, since the cellulose crystallites are too tightly bonded to be affected.

It is also possible to nullify the mechanical performance of a composite material by making the matrix and the fibre more or less identical in their properties. It is then relatively easy to propagate a crack through the material, since the fibres will not deform differently from the matrix and so will not distribute the forces throughout a large volume. An example is the generation of crisp texture by dehydration and the generation of glassy textures (see also Chapter 5). In potatoes this is easily done by heating thin (about 1 mm) slices in fat at 180°C, when the starch melts and then dehydrates becoming glassy (Thiewes and Steeneken 1997). Other vegetables and fruit can be given similar treatment but, presumably because they contain less starch, or it is of a lower molecular weight, or the material is more cellular (i.e., less stiff because there is less material present) the resulting texture is not so crisp.

2.6 Biting and Chewing

The processing before and during cooking leads ideally to a set of mechanical properties that fall within the range with which the mouth and teeth can cope. Although there have been studies on the forces that can be generated in the mouth, these are not particularly relevant since the requirements for fracture are that there is sufficient stress concentration to start a crack (which will be supplied by a force applied to a small area by the teeth) and sufficient energy to propagate the crack (which will be supplied by the jaw muscles, both directly from contraction and indirectly from the stored strain energy of the working muscle).

In fruits and vegetables the critical stress concentration required to start a crack, K_{IC}, commonly called toughness, appears to be directly equatable with hardness or crunchiness (Vincent et al. 2002). This psychophysical result was confirmed with a more rigorous theoretical approach, which predicted that the resistance of foods with an essentially linear elastic response to an initial bite in which the crack is initiated by the lower incisors would depend on the square root of the product of the Young's modulus and the surface energy, both of them parameters (i.e., typical of) the food material in question and therefore measurable in a mechanical testing machine (Agrawal and Lucas 2003). The analysis required the independent estimation, in the mouth, of the stress required to start the crack and the depth of the incisors at that moment:

$$\sigma_F \sqrt{a} = C\sqrt{ER}$$

Since K_{IC} is proportional to the left-hand side of this relationship, and the right-hand side is related to the work of fracture, a linear relationship between the two sides both confirms the psychophysical approach and provides a new parameter, C, which is inversely proportional to the efficiency of the lower incisors and so can be used to characterize the ease or lack of ease when biting into a food product. This exercise has yet to be performed. It would provide a very effective bridge between the measured mechanical properties of fibrous foods and their properties as measured by a taste panel.

2.7 Making Composites

We are so used to food that has a fibrous texture that when it is homogeneous fibres have to be added. An example is Quorn™, a mycoprotein produced from *Fusarium*, a mycelial fungus. The threads or hyphae are about 5 μm in diameter and very thin-walled. So they hardly register as giving texture. Since they can be given a variety of flavours, it makes sense to complete the illusion with texture. One way is to align the hyphae in a shear field, add some egg albumen and fix the structure with heat. Although this does not produce a hierarchical structure, and so is more similar to chicken or fish than mammalian muscle, it is nonetheless very acceptable.

Another technique—pressure-shift freezing—also shows promise. In this technique the material is subjected to high pressure (200 MPa) and cooled to –15°C. Under these conditions the water does not freeze. However, when the pressure is released suddenly, many small ice crystals form. This has two results: the small ice crystals do not rupture any structures present, but by dehydrating the unfrozen material the remaining structure is aggregated and stiffened by the introduction of secondary cross-links. At low concentration of solids there are too few interconnecting chains for there to be a load-bearing continuum, and the material tends to flocculate and settle out.

At higher concentrations the network becomes stiffer and stronger. Strain energy can now be transmitted through the material which, in the absence of fibres, becomes brittle (Kalichevsky-Dong et al. 2000). The Japanese have been exploiting the effect of freezing and thawing on the microstructure of foods for hundreds of years in the production of kori-tofu. Freezing and thawing produces a much stronger and more cohesive product than the original tofu, and extends the shelf life.

2.8 Likely Trends

My father was a gaucho in Argentina and, as was the custom, had a diet of meat and *maté* tea. He used to tell me stories about cows specially bred so that one could cut "9 slices off their bums, 9 times a day." Something like this thinking occurred to Douglas Adams when he wrote the "End of the Universe" scene in *The Hitchhiker's Guide to the Galaxy* (Adams 1986).

While this way of changing from batch to continuous production may be over-fanciful with the production of animals, it is more possible with plants. Scenarios of

future cities have high-rise farms producing food under artificial conditions. Hydroponics and related soilless culture techniques can provide the necessary nutrition, and are currently used for specialist growing, for provision of nutrition in space (NASA) and exploration in severe climates. The Aztecs used "floating gardens." Under these circumstances, with total control over the internal forces that plants have to produce in order to grow in the wind, support their own weight or create space in the soil for roots and tubers, it seems likely that production will be increased by reducing mechanical stresses and thus removing a large part of the need to generate fibrous materials. With the total control over pests that will be necessary under such growing conditions, the necessity for protective structures will also disappear and fruit skins and shells can be bred to be strong enough only to withstand handling and packaging. With control over light and temperature, plants will be grown all year round, agricultural seasons will disappear, and cropping will be continuous. Currently this is really possible only with mushrooms and with crops that are produced in fermenters such as *Fusarium*.

2.9 Sources of Further Information

One of the problems that food scientists have if they are to use the techniques of engineering materials science is that there are very few food materials that are remotely like engineering materials. Since on the whole engineers have a much better grasp of material properties and their proper measurement than do food scientists, and since food is, on the whole, much more complex than engineering materials or structures, this leaves the food materials scientist at a disadvantage, since there is very little with which to compare properties and structures. As an example, although it is not quite germane to this chapter, recent work on the fracture of potato crisps (Rojo and Vincent 2007) gave a stress intensity factor of about 4 $MPa.m^{0.5}$, which is about the same as a technical ceramic, and a work to fracture of about 45 Jm^{-2}, which is far higher than a technical ceramic. This apparent imbalance of properties becomes quite logical when we realise that potato crisps are cellular and therefore of low stiffness for a glassy material. There are no cellular glassy technical ceramics. The message is that the exploration of the mechanical properties of foods may be as much of an adventure for the materials scientist as it is for the food scientist.

2.10 References

Adams, D. (1986). *The Hitchhiker's Guide to the Galaxy*. Heinemann, London.

Agrawal, K.R. and Lucas, P.W. (2003). The mechanics of the first bite. *Proc. R. Soc*., B 270, 1277–1282.

Charlton, A.J., Baxter, N.J., Khan, M.L., Moir, A.J.G., Haslam, E., Davies, A.P., and Williamson, M.P. (2002). Polyphenol/peptide binding and precipitation. *J. Agricultural Food Chem.*, 50, 1593–1601.

Clark, R.B. (1964). *Dynamics in Metazoan Evolution: The Origin of the Coelom and Segments.* Clarendon Press, Oxford.

Collignan, A. and Montet, D. (1998). Tenderizing squid mantle by marination at different pH and temperature levels. *Lebensm.-Wiss. u.-Technol.*, 31, 673–679.

Cook, J. and Gordon, J.E. (1964). A mechanism for the control of crack propagation in all-brittle systems. *Proc. R. Soc.*, *A* 282, 508–520.

de Groot, J.H. and van Leeuwen, J.L. (2004). Evidence for an elastic projection mechanism in the chameleon tongue. *Proc. R. Soc.*, *B* 271, 761–770.

Esau, K. (1936). Ontogeny and structure of collenchyma and of vascular tissues in celery petioles. *Hilgardia,* 11, 431–467.

Gosline, J.M. and Shadwick, R.E. (1983). Molluscan collagen and its mechanical organisation in squid mantle. In: V. Fretter and A. Graham (Eds.), *The Mollusca*, pp. 371−398.

Heath, M.R. (1991). The basic mechanics of mastication: man's adaptive success. In: J.F.V. Vincent and P.J. Lillford (Eds.), *Feeding and the Texture of Food.* The University Press, Cambridge, UK, pp. 143–166.

Hiller, S., Bruce, D.M., and Jeronimidis, G. (1996). A micro-penetration technique for mechanical testing of plant cell walls. *J. Texture Stud.*, 27, 559–587.

Kalichevsky-Dong, T., Ablett, S., Lillford, P.J., and Knorr, D. (2000). Effects of pressure-shift freezing and conventional freezing on model food gels. *Int. J. Food Sci. Tech.*, 35, 163–172.

Khan, A.A. and Vincent, J.F.V. (1993). Compressive stiffness and fracture properties of apple and potato parenchyma. *J. Texture Stud.*, 24, 423–435.

Macgillivray, P.S., Anderson, E.J., Wright, G.M., and Demont, M.E. (1999). Structure and mechanics of the squid mantle. *J. Exp. Biol.*, 202, 683–695.

Purslow, P.P. (1989). Strain-induced reorientation of an intramuscular connective tissue network: implications for passive muscle elasticity. *J. Biomech.*, 22, 21–31.

Purslow, P.P. (1991). Notch-sensitivity of non-linear materials. *J. Mater. Sci.*, 26, 4468–4476.

Purslow, P.P. (2005). Intramuscular connective tissue and its role in meat quality. *Meat Sci.*, 70, 435–447.

Purslow, P.P., Bigi, A., Ripamonte, A., and Roveri, N. (1984). Collagen fibre reorientation around a crack in biaxially stretched aortic media. *Int. J. Biol. Macromo.*, 6, 21–25.

Redgwell, R.J., MacRae, E., Hallett, I., Fischer, M., Perry, J., and Harker, R. (1997). In vivo and in vitro swelling of cell walls during fruit ripening. *Planta*, 203, 162–173.

Reeve, R.M. (1953). Histological investigations of texture in apples II structure and intercellular spaces. *Food Res. Intl.*, 18, 604–617.

Rojo, F.J. and Vincent, J.F.V. (2007). Fracture properties of potato crisps. *Int. J. Food Sci. Tech*., (in Press).

Saito, M., Kunisaki, N., Urano, N., and Kimura, S. (2002). Collagen as the major edible component of sea cucumber (*Stichopus japonicus*). *J. Food Sci.*, 87, 1319–1322.

Thiewes, H.J., and Steeneken, P.A.M. (1997). The glass transition and the sub-T endotherm of amorphous and native potato starch at low moisture content. *Carb. Polym.*, 32, 123–130.

Vincent, J.F.V. (1989). The relation between density and stiffness of apple flesh. *J. Sci. Food. Agric.*, 47, 446–432.

Vincent, J.F.V. (1991a). Strength and fracture of grasses. *J. Mater. Sci.*, 26, 1947–1950.

Vincent, J.F.V. (1991b). Texture of plants and fruits. In: J.F.V. Vincent and P.J. Lillford (Eds.), *Feeding and the Texture of Food.* The University Press, Cambridge, pp. 19–33.

Vincent, J.F.V., Saunders, D.E.J., and Beyts, P. (2002). The use of stress intensity factor to quantify "hardness" and "crunchiness" objectively. *J. Texture Stud.*, 33, 149–159.

Woodhead-Galloway, J. and Knight, D.P. (1977). Some observations on the fine structure of elastoidin. *Proc. R. Soc.*, *B* 195, 355–364.

Chapter 3

Food Polymers

Vladimir Tolstoguzov

Tolstoguzov Consulting, 47 Route de Vevey, 1009 Pully, Switzerland. tolstoguzov.v@bluewin.ch

3.1 Introduction

This chapter discusses food biopolymers, their mixtures and the origins of their functionality. These subjects are of fundamental importance for a number of reasons. Most food polymers are functional components of living organisms and are consumed as either living organisms or ingredients from former living organisms. Structure–function relationships of biopolymers are essential to create life. Only the emergence of life implied the emergence of a demand for food. It is also of interest to discuss behavioural differences of biopolymers in biological and food systems and between biopolymers and synthetic polymers. The origins of biopolymer functionality are therefore of interest for application in the food industry (Tolstoguzov 2000, 2002).

Food polymers and the behaviour of their mixtures are mainly responsible for the structure–properties relationship in both food and chyme. The two basic features of food are that its biopolymers, proteins and polysaccharides are its main construction materials and water is the main medium, solvent and plasticizer. In other words, three components—protein, polysaccharide and water—are the main elements of food structure that are principally responsible for quality of foods (see also Chapter 13).

Foods are always a multicomponent physical system, so interactions between components are more significant than the chemical and physical properties of components. Food structures are mainly arranged by noncovalent, nonspecific interactions of proteins and polysaccharides in an aqueous medium. For instance, the most studied structural food macromolecules are soybean proteins, gluten, milk proteins, and starch. But despite detailed knowledge about individual components, the control of dough and milk system functionality remains empirical (but see Chapters 19 and 20).

Finally, food processing implies the conversion of biological systems based on specific interactions of components into foods with nonspecific interactions between components. For this reason the thermodynamic approach is especially applicable for studying the role of food polymers and water in structure–property relations. The logical starting point is therefore to consider mixed aqueous solutions of biopolymers.

3.2 Interactions of Food Biopolymers in Molecular and Colloidal Dispersions

Figure 3.1 illustrates the phase behaviour of mixed biopolymer solutions (Tolstoguzov 1997). On mixing solutions of a protein and a polysaccharide, four kinds of mixed solutions can be obtained. Figure 3.1 shows that two single-phase systems (1 and 3) and two-types of biphase systems (2 and 4) can be produced. The two-phase liquid systems 2 and 4 differ in the distribution of biopolymers between the co-existing phases. The biopolymers are concentrated either in the concentrated phase of system 2 because of interbiopolymer complexing, or within separated phases of system 4 because of incompatibility of the biopolymers. The term "biopolymer compatibility" implies miscibility of different biopolymers on a molecular level. The terms "incompatibility" or "limited thermodynamic compatibility" cover both limited miscibility or limited cosolubility of biopolymers (i.e., system 2) and demixing or phase separation

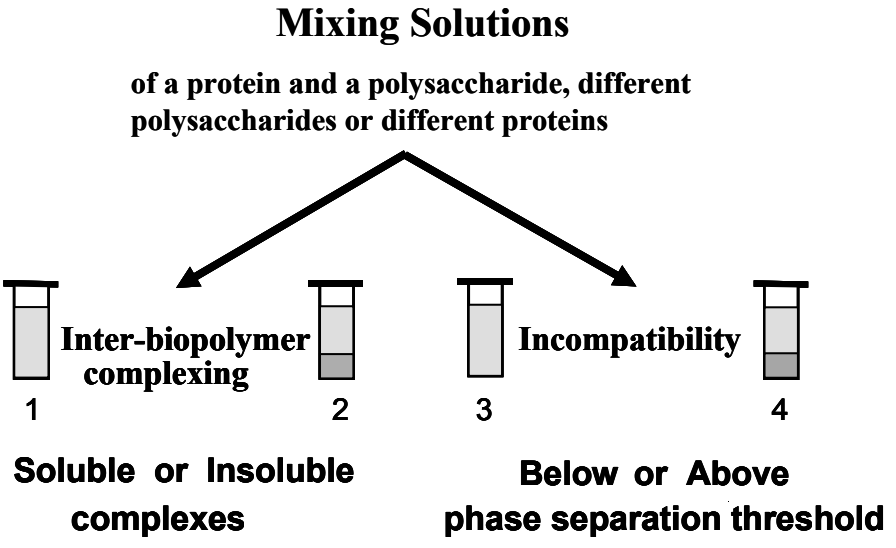

Figure 3.1. Main trends in the behaviour of mixed biopolymer solutions. Schematic representation of the four possible results obtained by mixing solutions of biopolymers: a protein and a polysaccharide; a protein and another protein; a polysaccharide and another polysaccharide.

of mixed solutions (system 4). In other words, unlike interbiopolymer complexing, phase separation caused by biopolymer incompatibility leads to a concentration of the biopolymers in the different phases. All four systems are very different in structure and properties. Consequently, functional properties of the biopolymers are also largely different in these systems (Tolstoguzov 1988, 1991, 1997, 1998).

Interbiopolymer complexes are formed in aqueous media between oppositely charged biopolymers, when the attractive forces between non-identical macromolecules are larger than between macromolecules of the same type. Interbiopolymer complexes can be both soluble (system 1) and insoluble (system 2). It has been shown that nonspecific interpolymer interactions can be reversible and non-reversible and cooperative and noncooperative in nature (Tolstoguzov et al. 1985).

Biopolymer incompatibility is a general phenomenon typical of all polymers. Biopolymer incompatibility occurs even when their monomers would be miscible in all proportions. For instance, sucrose, glucose and other sugars are normally co-soluble in the common solvent, water, while different polysaccharides usually are not miscible. The transition from a mixed solution of monomers to polymers corresponds to the transition from good to limited miscibility. Normally, a slight difference in composition and/or structure is sufficient for incompatibility of macromolecules in common solvent (Tolstoguzov 1991, 2002). Compatibility or miscibility of unlike biopolymers in aqueous solutions has only been exhibited by a few biopolymer pairs (Tolstoguzov 1991).

Investigations of protein–polysaccharide interactions were started more than 100 years ago. The first study on the phase behaviour of mixed biopolymer solutions was published in 1896 (Beijerinck 1896, 1910). He found that gelatin, starch and agar are not miscible in their common solvent, water. On mixing, these aqueous solutions formed a two-phase liquid system. On cooling, due to gelation of both phases, the emulsion structure solidified. Figure 3.2 shows another example. A mixed skimmed milk–apple pectin solution was broken down into a liquid biphasic system. This emulsion settled into two liquid layers. One of the layers was the transparent pectin solution containing milk whey proteins, while the other layer contained casein and a small amount of pectin and milk whey proteins. The general term "water-in-water" (W/W) emulsion for such systems was introduced later (Tolstoguzov 1986, 1988) to distinguish them from oil-in-water and water-in-oil emulsions.

The first study on the formation of complexes by oppositely charged biopolymers was carried out by F.W. Tiebackx about 85 years ago (Tiebackx 1911). He found that addition of acid to a mixed solution of gelatin and gum arabic separates it into two phases. The ratio of macromolecular reactants determined the yield of highly concentrated precipitate that contains both biopolymers. The pioneer in systematic investigations of the interaction between gelatin and gum arabic was Bungenberg de Jong and his colleagues (Bungenberg de Jong 1936, 1952). He found that mixing aqueous solutions of gelatin and gum arabic under different conditions results in two kinds of biphase systems. The gelatin and gum arabic are concentrated either in the same single bottom phase or in different phases of a two-phase system. These two phenomena of phase separation have been termed as complex and single coacervation, respectively.

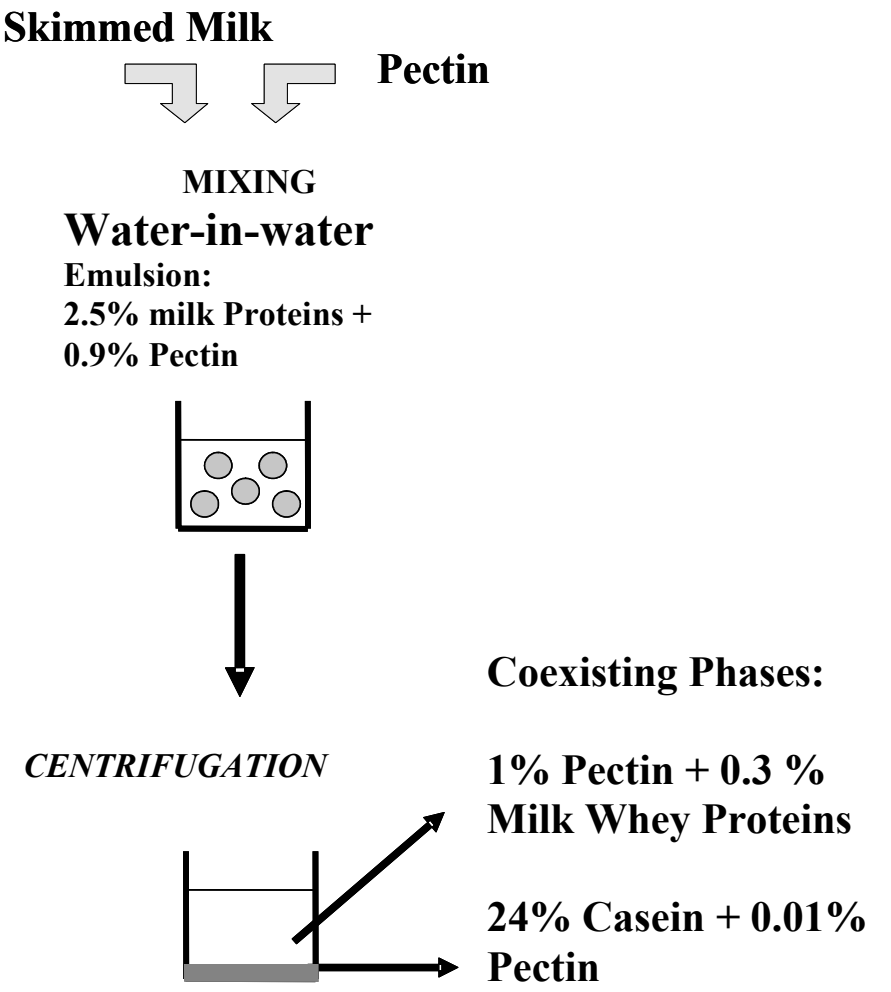

Figure 3.2. The mixture of skimmed milk and an apple pectin solution breaks down into the two liquid phases that on mixing form a "water-in-water" (*W*/*W*) emulsion where droplets of concentrated casein solution are dispersed in the continuous phase containing pectin and milk whey proteins. This emulsion settled into two liquid layers differing in composition.

Dobry and Boyer-Kawenoki (1948) showed that phase separation occurs in mixed solutions of many water-soluble polymers such as gelatin, serum albumin, gum arabic, glycogen, polyvinyl alcohol, polyvinylpyrrolidone, methylcellulose, polyacrylic acid, and so on. They have shown that immiscibility or limited co-solubility is typical of all polymers. The theory of the thermodynamic incompatibility of polymers was devel-

oped by Flory (Flory 1953). In the 1950s and 1960s, Albertsson carried out the first systematic investigation of the incompatibility of polysaccharides and water-soluble polymers including cellulose esters used in the food industry. He showed that aqueous two-phase polymer systems are of great importance for separation of biopolymers under mild conditions (Albertsson 1958, 1972, 1995). Later, phase behaviour of mixtures of gelatin with polysaccharides was studied by Grinberg and Tolstoguzov (1972, 1997), Tolstoguzov et al. (1985), Tolstoguzov (1991, 1992), and Clewlow et al. (1995).

Phase behaviour has mainly been studied with two system types, namely, in salt solutions of proteins and in mixed biopolymer solutions. Pioneering investigations on protein-saltwater systems were carried out on lactoglobulin and seed storage globulins (including arachin and soybean globulins) by Tombs in the 1960s–1970s (Tombs 1970, 1985; Tombs et al. 1974) and then on lens crystallins by Benedek et al. (Asherie et al. 1996; Liu et al. 1995; Broide et al. 1991). Phase separation in salt solutions of seed storage globulins was systematically studied in several other laboratories (Popello et al. 1990, 1991, 1992; Suchkov et al. 1990, 1997; Tolstoguzov, 1988, 1991). The formation of highly concentrated noncrystalline phases is of significance for both lens crystallins and seed storage globulins. Protein–saltwater systems show a reversible transition of salt–globulin solutions from the single-phase to the two-phase state on diluting with water, cooling, and shearing. The protein concentration in the bottom phase can exceed 40%, while in the top phase it may be below 0.4%. Systems containing native individual 11S and 7S seed globulins and their mixtures have upper critical points with the same critical protein concentration of 18%.

It has been assumed (Tolstoguzov 1988a, 1991, 1992) that phase separation occurs between associated and nonassociated forms of the same protein. This means that associated (micellelike) and nonassociated forms of the same proteins cannot recognize each other as being the same. It has been also suggested that the main factors determining the association of protein molecules and phase separation are the high excluded volumes of oligomeric seed storage proteins and the dipole–dipole interaction between their molecules. The attraction of large-sized micellelike associated protein particles suspended in aqueous solution of incompatible biopolymer probably arises from depletion flocculation (Tolstoguzov 1988, 1991, 1997).

During the 1970s and 1980s, experimental studies have shown that limited thermodynamic compatibility (or briefly, incompatibility) of biopolymers is a general phenomenon. Basic information concerning thermodynamic incompatibility of the main classes of food proteins and polysaccharides has been obtained and reviewed by Grinberg and Tolstoguzov (1997), Ledward (1993), Polyakov et al. (1997), Samant et al. (1993), Tolstoguzov et al. (1985) and Tolstoguzov (1988a, 1991, 1997a, 1998, 2002). Among more than 200 biopolymer pairs studied, only a few biopolymer pairs displayed compatibility in aqueous solutions (Tolstoguzov 1991).

Experimental studies (Antonov et al. 1975, 1979, 1982; Grinberg et al. 1972, 1997; Polyakov et al. 1997; Tolstoguzov 1991, 1997, 1998, 2002) have shown that incompatibility occurs in the following biopolymer mixtures: (i) proteins and polysaccharides; (ii) proteins belonging to different classes according to Osborne's classification (i.e., albumins, globulins, glutelines and prolamines); (iii) native and

denatured proteins; (iv) aggregated and nonaggregated forms of the same protein; and (v) structurally dissimilar polysaccharides.

For instance, denaturation and partial hydrolysis of proteins oppositely influence their incompatibility with other biopolymers (Tolstoguzov 1991). Most biopolymers are polyelectrolytes. Factors such as pH and salt concentration affect their interactions with one another, with the solvent and their compatibility. For instance, when the pH is shifted to their isoelectric point (IEP), the thermodynamic incompatibility of proteins is usually enhanced by self-association of the protein molecules. Generally, protein-neutral polysaccharide mixtures separate into two phases when the salt concentration exceeds 0.15 M.

Proteins and carboxyl-containing polysaccharides have a limited compatibility when either the pH exceeds the protein's IEP (at any ionic strength) or the pH is equal to or less than the protein's IEP and the ionic strength exceeds 0.2 M. With sulphated polysaccharides, globular proteins are usually incompatible at ionic strengths above 0.3 M, irrespective of the pH (Antonov et al. 1975, 1979; Grinberg and Tolstoguzov 1972, 1997; Tolstoguzov et al. 1985; Tolstoguzov 1988, 1997, 1997a). Phase separation usually takes place at biopolymer concentrations exceeding 2–20% (depending on the size and shape of the macromolecules). On the contrary, since attraction between dissimilar macromolecules leads to formation of inter-biopolymer complexes, insoluble complexes can form even when very dilute biopolymer solutions (bulk concentration less than 0.01%) are mixed.

3.3 Interbiopolymer Complexes

Carboxyl-containing polysaccharides behave as polyanions at mild acidic and neutral pH values, which are typical of most foods. Electrostatic complexing between proteins and anionic polysaccharides generally occurs in the pH range between the pK value of the anionic groups (carboxyl groups) on the polysaccharide and the protein's IEP. Sulphated polysaccharides are capable of forming soluble complexes at pH values above the protein's IEP.

Protein molecules have a net positive charge and behave as polycations at pH values below the IEP and as polyanions at pH values above it. The IEPs of most food proteins are between 4 and 7. However, there are some proteins and subunits of oligomeric proteins whose IEPs are in the basic pH range. For instance, lysozyme from egg white, soybean trypsin inhibitors, protamines and histones. When the pH is between the IEPs of two proteins, the proteins will be oppositely charged and they will form an electrostatic protein–protein complex. (Poole et al. 1984; Tolstoguzov 1986, 1990, 1997, 1998). Proteins and polysaccharides possess a large number of ionisable and other functional side groups with different pK values. The size and stability of junction zones are of importance for the stability and functional properties of interbiopolymer complexes. The formation of electrostatic interbiopolymer complexes is usually a reversible process depending on such variables as pH and ionic strength. Generally, electrostatic complexes dissociate when the ionic strength exceeds 0.2–0.3, or when the pH value is above the protein's IEP. Interbiopolymer complexes can

be regarded as a new type of food biopolymer whose functional properties differ strongly from those of the reactants.

Formation of electrostatic complexes means mutual neutralisation of the macromolecular reactant. This mutual neutralization of opposite charges and formation of the concentrated complex coacervate phase, minimizes the electrostatic free energy and reduces both the hydrophilicity and the solubility of the resultant complex. The loss of entropy on complexing may be compensated by the enthalpy contribution from interactions between macro-ions and by liberation of counter-ions and water molecules.

Another result is a decrease in the IEP of the complex compared to that of the initial protein. Therefore, the higher the relative content of polysaccharide, the lower the pH at which the complex precipitates. A maximum yield of insoluble complex is produced when the ratio of polyacid and polybase is equivalent, that is, when the net charge ratio of biopolymer reactants is close to unity. For instance, the composition of an insoluble complex formed between gelatin and sodium alginate depends on the pH of the system, but not on the ratio of their initial concentrations. At a given pH, the ratio of weight fraction of gelatin to anionic polysaccharide in an insoluble complex is equal to the ratio of their charges.

After the precipitation of an insoluble complex of a constant composition, an excess of one of the polymer components remains in solution. When the pH is decreased below the protein's IEP, the net charge of the protein increases while that of an anionic polysaccharide macro-ions decreases. As a result, the insoluble complex is enriched with a polysaccharide. Dispersed particles of an insoluble complex are aggregated, precipitated and form a dispersed phase of complex coacervate. Aggregation of individual complex particles is mainly due to hydrogen bond formation, hydrophobic interactions, as well as dipole-to-dipole and charge-to-dipole interactions. Junction zone formation is a time-consuming process since it requires mutual conformational adjustment of macro-ions. For instance, the aging of gelatin–alginate (or gelatin-low methoxy pectin) complex gels is accompanied by the formation of electrostatically stabilized junction zones and the conversion of these thermoreversible gelatinlike gels into thermally irreversible gels. Nonelectrostatic macromolecular interactions can lead to formation of an irreversible more stable complex, can cause nonequilibrium effects in the complexes, and affect gel-forming conditions. Non-electrostatic interactions play an important role in composition–property relationships of complex coacervates (Tolstoguzov 1990).

Unlike insoluble interbiopolymer complexes whose composition tends to satisfy the condition of electrical neutrality, the composition of soluble complexes depends on the initial ratio of reactants. Soluble complexes are formed when the ratio of biopolymer reactants is sufficiently far from equivalent. For instance, soluble complexes are formed in mixed gelatin solutions containing an excess of anionic polysaccharide. However, globular proteins more often form charged insoluble complexes with anionic polysaccharides. Normally, soluble electrostatic complexes can be regarded as metastable. They trend to aggregate with time and/or an increase in concentration. The aggregation of soluble complexes can be induced by the addition of a small amount of salt (Tolstoguzov et al. 1985; Tolstoguzov 1991).

The properties of protein–polysaccharide complexes formed near the protein IEP are independent of the way in which their have been produced. This indicates an equilibrium nature of complexing under conditions of weak protein–polysaccharide interaction.

When solutions of oppositely charged biopolymers are mixed at pH values below the protein IEP, that is, under conditions of strong interbiopolymer interaction, aggregated insoluble mixing-complexes are obtained. On the contrary, when the interaction between micro-ions gradually increases by a slow titration of their mixed solution from neutral to acid pH values around the protein IEP, the titration-complexes obtained are dispersible in water. This means that composition and properties of an electrostatic interbiopolymer complex can depend on the preparation method, that is, on the succession of mixing the system components, namely, the protein, polysaccharide and acid solutions. Nonequilibrium complexes are especially typical of polyelectrolytes with a high charge density. This means that strong electrostatic interaction of macromolecules is mainly responsible for nonequilibrium complexing (Tolstoguzov et al. 1985).

In the pH range close to the protein's IEP an interesting phenomenon of nonuniform redistribution of protein molecules among polysaccharide chains occurs (Tolstoguzov et al. 1985). The reason is that in the vicinity of the protein IEP the hydrophobic protein–protein and electrostatic protein–polysaccharide interactions can be energetically comparable with each other. Protein–protein association on the anionic polysaccharide matrix (or self-association of proteins), which is mainly due to hydrophobic interactions, is usually enhanced when the pH approaches the protein IEP. Accordingly, under conditions of a relatively weak protein–polysaccharide interaction, each free site situated near the site on the polysaccharide chain already occupied by a protein molecule becomes thermodynamically preferable for further binding of protein molecules. This leads to cooperative protein adsorption on an anionic polysaccharide. Some parts of polysaccharide chains tend to be completely covered by protein molecules (as in a virus) while other parts are completely free of protein.

3.4 Functional Properties of Electrostatic Complexes

The formation of complexes affects both particle–solvent and particle–particle interactions. The solubility of proteins may be increased by their electrostatic complexing with anionic polysaccharides. Formation of titration-complexes may increase protein solubility and inhibit protein precipitation at the IEP. Anionic polysaccharides can act as protective hydrocolloids inhibiting aggregation and precipitation of like-charged dispersed protein particles, for example, of denatured proteins. This protective action also can increase the stability of protein suspensions and oil-in-water emulsions stabilized by soluble protein-anionic polysaccharide complexes.

The difference between IEP and the net charge at a given pH of different proteins are the main factors enabling selective protein precipitation by anionic polysaccharides. This technique has been applied to the fractionation of milk and yeast proteins. At pH values below the IEP, anionic polysaccharides can also act as flocculants for

the precipitation of protein suspensions or emulsions stabilized by a protein. Complexing with dispersed protein particles decreases interparticle repulsive forces, crosslinks and flocculates by bridging flocculation. This approach can be used to recover protein from dilute dispersions, including different effluents and waste streams produced by the food industry and for clarification of different liquid food systems. (Tolstoguzov et al. 1985; Tolstoguzov 1997, 1998, 2002).

It is known that protein-stabilized foams and emulsions are more stable at the protein's IEP, where the electrostatic repulsive forces between protein molecules are minimized. The principle reasons for using protein–polysaccharide complexes as emulsion stabilizers are their high surface activity, their ability to increase viscosity of the dispersion medium and their ability to form gel-like charged and thick adsorbed layers. The mechanical strength of the adsorption layer as well as the electrostatic and steric effects are the most important factors contributing to higher kinetic stability of oil-in-water emulsions (Tolstoguzov et al. 1985; Tolstoguzov 1997, 2002). Negatively charged thick gel-like shells around colloid particles may be obtained either by directly using protein-anionic polysaccharide complexes to stabilize emulsions or by adding an anionic polysaccharide to a protein-stabilized emulsion. Interbiopolymer complexes can also be used to encapsulate liquid and solid materials. Generally, for encapsulation, mixtures of protein (usually gelatin) and anionic polysaccharide solution at a pH above the protein's IEP are used. The pH is readjusted to below the protein's IEP, which causes coating of each dispersed particle by a layer of the complex phase formed.

Now, we consider some features of biopolymers in terms of the incompatibility phenomenon.

3.5 Incompatibility of Biopolymers

Normally, sufficiently concentrated solutions of biopolymers differing in chemical composition, conformation and affinity for a solvent are immiscible. Biopolymers are usually incompatible at a sufficiently high ionic strength and at pH values above the protein's IEP, where the biopolymers are charged macro-ions. These conditions are typical of most food systems. When the bulk concentration of the biopolymers is below the cosolubility threshold (or the phase separation threshold) the mixed solution of the biopolymers is stable. However, when the bulk biopolymer concentration is increased above this critical level, the mixed solution breaks down into two liquid phases.

According to the Flory-Huggins theory of polymer solutions, polymers form single-phase mixed solutions only when changes in Gibbs free energy ($\Delta G = \Delta H - T.\Delta S$) is negative. (Flory 1953; Tanford 1961) Such a situation is rarely encountered (Krause 1978; Kwei and Wang 1978). On the contrary, thermodynamic incompatibility of biopolymers takes place when the Gibbs free energy of mixing is positive.

The mixing process can only give rise to complete compatibility when the entropy difference ($T . \Delta S$) between the two-phase and single-phase state is larger than the mixing enthalpy (ΔH). The entropy of mixing is the driving force for mixing two liquids to give an ideal solution. The entropy of mixing is positive and the enthalpy

of mixing is zero when the molecules spread throughout the bulk of the mixture and there are the same molecular interactions in the mixture and in the initial liquids. This is true for low molecular weight compounds, but not for polymers. The mixing entropy strongly decreases with transition from monomers to biopolymers.

Because of the large size and rigidity of biopolymer macromolecules, biopolymer solutions contain fewer independently moving particles. Since the mixing entropy is a function of the number of individual particles being mixed, the value of the entropy of mixing (ΔS) of biopolymers is several orders of magnitude smaller than that of monomers. Accordingly, molecularly homogeneous mixtures of biopolymers can be prepared if ΔH is negative, that is, the attractive forces between different macromolecules are equal to or larger than those between the same type of macromolecules (Flory 1953; Tanford 1961; Tolstoguzov 1991, 2002). This in turn means that biopolymer compatibility corresponds to formation of soluble interbiopolymer complexes. Consequently, the incompatibility of biopolymers occurs under conditions that inhibit interactions between macromolecules of different types (i.e., when interbiopolymer complexing is inhibited) and promote association between macromolecules of the same type.

3.6 The Space Occupancy Concept: Excluded Volume

The incompatibility phenomenon relates to both the occupation of a volume of the solution by macromolecules and the weak repulsion between unlike macromolecules. Phase separation in mixed solutions of a large number of biopolymers studied is sensitive to entropy factors given by the excluded volume of the macromolecules. Phase behaviour strongly depends, therefore, on the molecular weight and the conformation of the macromolecules. The excluded volume effect that depends on the size and shape of the macromolecules determines the phase separation threshold, water partition between the phases of *W*/*W* emulsions and biopolymer activity in mixed solution (Tolstoguzov 1986, 1991, 1992).

Figure 3.3 illustrates the idea of excluded volume. It shows two protein molecules as two adjacent spheres of the same radius *R*. Because molecules are not penetrable by each other, the volume of a solution occupied by a macromolecule is not accessible to other macromolecules. A minimal distance between two adjacent spherical molecules of a globular protein equals the sum of their radii, or the diameter of one of them. This means that around each protein molecule there is an excluded volume (*U*), which is 8–fold larger than that of protein molecule itself and is not accessible for centres of other protein molecules. The excluded volume is still larger for non-spherical macromolecules and depends on the flexibility of the macromolecular chain, and its configurational, rotational, vibrational properties and hydration (Tanford 1961).

The phase separation threshold is lower for systems containing a branched polysaccharide than for systems containing a linear polysaccharide of the same molecular weight. It is higher for globular proteins compared to proteins of unfolded structure. An increase in excluded volume means a decrease in the free volume of the solution accessible for biopolymers. Thus, the excluded volume of biopolymer molecules implies that water in real foods can be nonsolvent water relative to macromolecules,

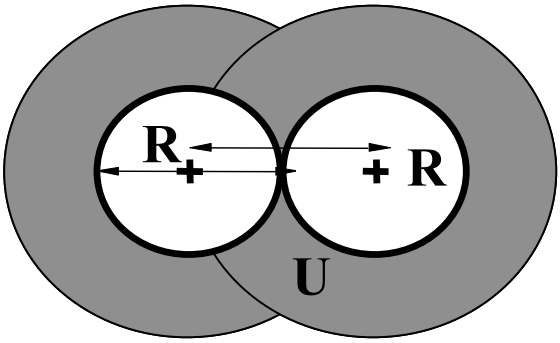

Figure 3.3. Schematic representation of the excluded volume (U) of globular protein molecules. The minimal distance between two adjacent protein molecules of the same radius R equals the diameter of the molecules. The volume U is eightfold larger than that of the protein molecule itself.

that is, inaccessible for macromolecular solutes, the main structure forming food components (Tolstoguzov 1999).

Excluded volume determines space occupancy in biopolymer solutions. Competition between macromolecules for space in a mixed solution determines the phase separation threshold. In a dilute solution of biopolymers, macromolecules hardly interact with one another, individual macromolecules are independent of one another, and biopolymers are cosoluble. The effects of spatial limitations are enhanced by the transition from a dilute mixed solution, to a semi-dilute biopolymer solution where molecules come into contact with one another, interact, compete for the same space, and do not mix in all proportions.

Figure 3.4 shows the simplest model to illustrate competition for solution space between macromolecules in continuous thermal motion. This model may be compared with the traffic on an overloaded motorway. Overloading of a motorway by vehicles greatly differing in weight, power, acceleration, braking distance and in the age and skill of drivers causes discomfort to all participants. How can traffic efficiency be improved? How can "unfavourable interactions" be reduced? Two opposite measures can make traffic more fluid: the collective movement of vehicles by car-transporters and "phase separation" of vehicles differing in size and performance between motorway lanes. The former model corresponds to biopolymer association and interbiopolymer complexing, the latter to phase separated systems. Unfavourable interactions of nonidentical macromolecules in a mixed solution give the same result: each macromolecule shows a preference to be surrounded by its own type. This model displays some other features of phase-separated systems, for example, the presence of interfacial (depletion) layers of decreased density between both those motorway lanes and the phases. Between the lanes will be regions of "clear" road—equivalent to the regions of nearly pure solvent between the phases.

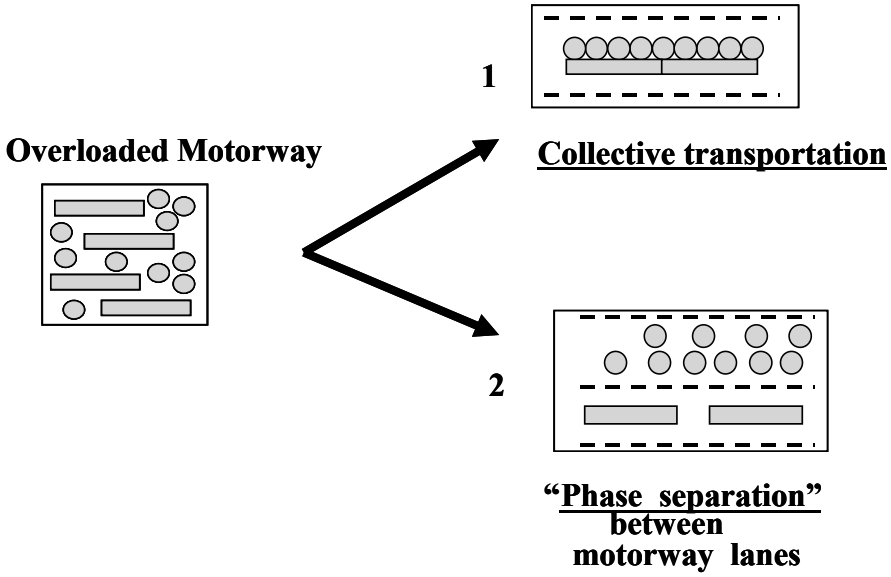

Figure 3.4. The traffic on an overloaded motorway represents the simplest mechanical model of competition for solution space between macromolecules in continuous thermal motion.

The phase behaviour of biopolymer mixtures can be predicted from the excluded volume of the macromolecules (Tolstoguzov 1991, 1992). Normally, phase separation occurs at about 1–2% for mixtures of rigid, rodlike polysaccharides; about 2–4% for mixtures of linear polysaccharides with proteins of unfolded structure, such as gelatin or casein; about 4% or higher for globular protein–polysaccharide mixtures; and exceeds 10% for mixtures of globular proteins. Most food systems are not dilute aqueous biopolymer solutions and contain a higher amount of biopolymers. The concentration of macromolecular components in a food usually exceeds their phase separation threshold. As a result, foods and chyme are normally phase-separated and highly volume-occupied systems.

3.7 Phase Diagrams: Phase Behaviour of Biopolymer-1–Biopolymer-2 Water Systems

The phase behaviour of a mixed biopolymer solution is quantitatively characterized by a phase diagram, which graphically describes the boundary conditions of phase separation, the partitioning of the components between the phases and the effects of different variables (temperature, pH, salt concentration, etc.) on the phase behaviour of biopolymers. Conventionally, phase diagrams of three-component (ternary) systems are presented in triangular coordinates. However, an excess of solvent water

(compared to biopolymers), which is typical for biological and food systems, makes the use of phase diagrams in rectangular coordinates more practicable and also simplifies plotting the effects of different variables (Tolstoguzov et al. 1985).

Figure 3.5 shows the phase diagram typical of protein–polysaccharide mixed solutions in rectangular coordinates. Normally, the concentrations of biopolymers are plotted on the axis in weight percent; the rest is assumed to be water. Every point in a phase diagram corresponds to a system composition. The bold curve is a binodal. The binodal curve separates the two regions of the single- and two-phase states of biopolymer mixtures. Biopolymers are fully miscible with one another in the concentration region under the binodal. The region lying above the binodal represents two-phase systems. The tie-lines connect the compositions of the co-existing phases. Biopolymer mixed solutions whose compositions correspond to the same tie-line will break down into two phases of the same composition.

The binodal branches do not coincide with the phase diagram axes. This means that the biopolymers are limitedly cosoluble. For instance, on mixing a protein solution A and a polysaccharide solution B a mixture of composition C can be obtained. This mixed solution spontaneously breaks down into two liquid phases, phase D and phase E. Phase D is rich in protein and E is rich in polysaccharide. These two liquid phases form a water-in-water (*W*/*W*) emulsion. The phase volume ratio is estimated by the inverse lever rule. The phase D/phase E volume ratio equals the ratio of the tie-line segments: EC/CD. Point F represents the phase separation threshold, that is, the minimal critical concentration of biopolymers required for phase separation to occur.

The position of phase separation threshold F geometrically corresponds to the point of contact between the binodal curve and the straight line cutting segments of the same length on the concentration axis of the biopolymers. The rectilinear diameter passes through the mid-tie-lines and the critical point G where both coexisting phases have the same composition. The rectilinear diameter gives the system compositions splitting into phases of the same volume. In the vicinity of the rectilinear diameter phase inversion can occur. Lower values of the critical point G indicate lower cosolubility of the biopolymers and greater incompatibility. On centrifugation the protein-rich phase usually forms the lower liquid layer while the polysaccharide-rich phase forms the upper liquid layer. The composition of the more concentrated and denser bottom phase is usually plotted as the abscissa while the less dense top phase is presented as the ordinate. The two-dimensional phase diagram corresponding to a certain constant temperature, pH, and ionic strength becomes three-dimensional when an additional variable, such as pH, salt concentration, or temperature is included (Tolstoguzov et al. 1985).

Competition between macromolecules for space also determines the water partition between the system phases, that is, the phase diagram asymmetry. The greater the difference in excluded volume (molecular weight) of the biopolymers, the greater the shift of the binodal towards the concentration axis of the biopolymer of lower excluded volume and the greater the shift of the phase separation threshold from the coordinate angle bisector in the same direction. Figure 3.5 shows that on mixing solutions of two incompatible biopolymers, one of them is usually diluted and the other is concentrated. For instance, protein concentration in phase D is higher than in

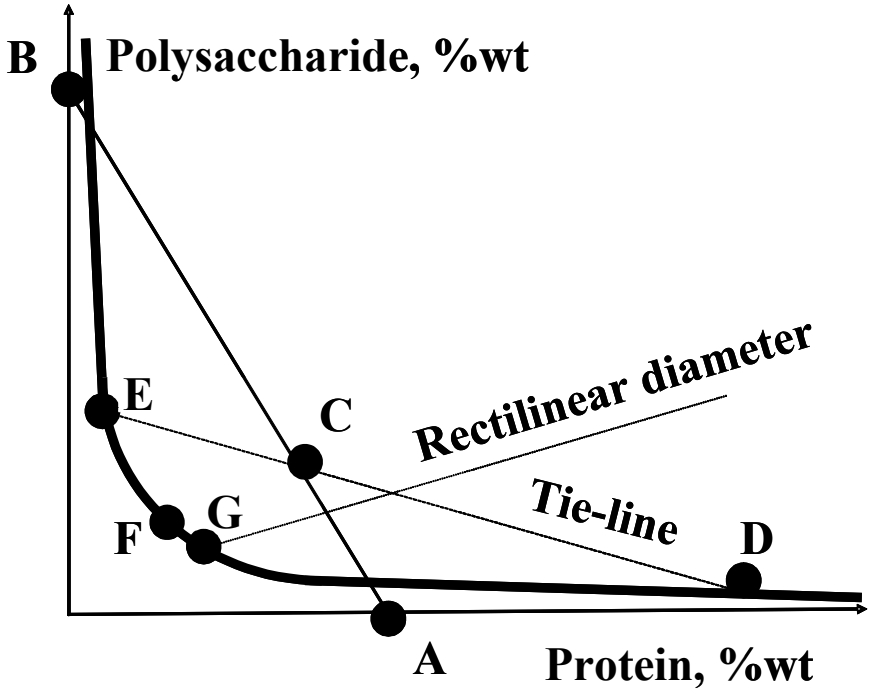

Figure 3.5. Phase diagram typical of mixtures of biopolymers in aqueous media. A-B compositions of protein (A) – polysaccharide (B) mixtures. D and E are the compositions of coexisting phases. EFGD – bimodal; DE – tie-line; G – critical point and F – phase separation threshold.

the initial protein solution A and the mixed solution C. Accordingly, the initial polysaccharide solution B is diluted to the point E. This process determining the water partition between phases of foods is called "membraneless osmosis" (Tolstoguzov 1988, 1991, 2002).

Phase diagram asymmetry can be evaluated by: (i) the ratio of the biopolymer concentrations at a critical point, (ii) the angle made by the tie-lines with the concentration axis of one of the biopolymers and (iii) the length of the segment of a binodal curve between the critical point and the phase separation threshold. Association of macromolecules usually changes both their excluded volume and the affinity for the solvent water. This results in nonparallel tie-lines on the phase diagram. Normally, the tie-lines can be nonparallel since an increase in concentration of biopolymers is usually accompanied by their self-association. Equilibrium between the phases is not achievable when phase separation is accompanied by gelation.

Gelation of one or both phases interrupts partitioning of water and large size dispersed particles between the phases. This illustrates the nonequilibrium nature of real foods that usually contain both gel-like and liquid aqueous phases (Tolstoguzov 1997a, 2000b). On a phase diagram this corresponds to convergence of the tie-lines

to a point representing the composition of the gelled phase. Accessibility of the gel phase volume to water is limited due to the elasticity back pressure of the gel compensating the osmotic pressure and stopping water transfer from the liquid phase to the coexisting gel phase.

Construction of phase diagrams usually starts with the preparation of series of mixed solutions sufficiently differing in bulk biopolymer concentration. Some of them can be single-phase solutions, others biphasic systems. A true equilibrium between the phases is experimentally obtained by mixing or shaking the water-in-water emulsions under different time-temperature conditions. Separation of the phases by centrifuge provides information about both the number and the volume ratio of the system phases. The closer a system composition is to the critical point, the smaller the difference in density is between the phases and the more difficult their separation is by centrifugation. The amount of each biopolymer in each phase can be quantified by various techniques. Estimation of protein concentration by UV absorbance at 280 nm is widely used because of its simplicity and sensitivity.

The disadvantage of the method is a strong contribution from nucleic acids at the same wavelength. Another method is binding of the anionic dye Coomassie blue to protein with an absorbance maximum at 590 nm. The Biuret reaction and the Lowry method where the Folin reagent is additionally included are not so widely applied because of strong interference from sugars, nucleic acids and buffers. Kjeldahl's method is especially applicable for measuring the percentage of proteins. The concentration of the polysaccharide is usually determined at 490 nm by the phenol-sulphuric method (Dubois et al. 1956). Alternative methods for analysis of the phases are optical activity, far-UV spectroscopy (190–220 nm), Fourier transform infrared spectroscopy, sedimentation, electrophoresis, HPLC and other chromatographic and radiometric (radio-labelled biopolymer) techniques (Albertsson 1972; Grinberg and Tolstoguzov 1972; Polyakov et al. 1980; Durani et al. 1993; Medin and Janson 1993). The phase volume ratio method was developed for determination of phase diagrams without chemical analysis (Polyakov et al. 1980; Antonov et al. 1987).

3.8 Colloidal Particles

Food systems usually contain a complex mixture of protein and polysaccharide macromolecules and their associates, aggregates and complexes differing in size, chemical and physical nature, degrees of denaturation, and aggregation. The transition from macromolecular to colloidal and coarser dispersions makes the effect of both interbiopolymer complexing and incompatibility even more pronounced. Unlike biopolymer solutions, colloidal dispersions are thermodynamically unstable because of an inherent excess surface free energy. Normally, the critical concentration of a polysaccharide that is required to precipitate a protein is significantly lower for protein suspensions and emulsions stabilized by proteins compared to that for protein solutions. For instance, phase separation of a protein–polysaccharide mixed solution usually takes place at a total biopolymer concentration exceeding 4%, while depletion flocculation can occur at concentrations of less than 1%. Under interbiopolymer

complexing conditions, an anionic polysaccharide can act either as a flocculating agent (bridging flocculation) or as a protective colloid. Protein–polysaccharide incompatibility in a solution may result in depletion flocculation of a protein suspension or an emulsion (Tolstoguzov 1991, 1997, 1998, 2000b). This phenomenon is similar to the phenomenon of limited thermodynamic incompatibility of biopolymers in mixed macromolecular solutions. Unlike biopolymer incompatibility phenomenon, depletion flocculation has a nonequilibrium nature. Depletion flocculation can also be treated as a particular case of flocculation and coagulation of colloidal particles in a nonwettable medium.

3.9 Water-in-Water Emulsions

We now turn to excluded volume effects on the general functional properties of *W*/*W* emulsions and their phases. Since foods are highly volume-occupied systems, excluded volume interactions obviously influence the formation of food structures. We can apply Le Chatelier's principle, which states that a system at equilibrium, when subjected to a perturbation, responds in a way that tends to minimise the effect of this perturbation. This means that an increase in biopolymer concentration favours processes reducing the excluded volume. Several physical-chemical processes can do this due to a decrease in the amount, volume and mobility of space-filling particles. These processes are: self-association of macromolecules and their segments, their adsorption at the interfaces, formation of interbiopolymer complexes (including enzyme–substrate complexes), crystallisation, and gelation. Excluded volume effects do not influence the thermal denaturation of proteins, since thermal denaturation does not substantially increase the volume of molecules. On the contrary, denaturation greatly increases aggregation and incompatibility of proteins. Thus, excluded volume effects do not affect conformational stability of proteins but favour aggregation, crystallisation and gelation of biopolymers and their adsorption at oil/water interfaces (Tolstoguzov 1991, 1997, 2002).

Physical–chemical features of *W*/*W* emulsions compared to oil-in-water (*O*/*W*) and water-in-oil (*W*/*O*) emulsions are: low interfacial tension, interfacial layers of low biopolymer concentration, interfacial adsorption of lipids and high deformability of aqueous dispersed particles. Low interfacial tension in *W*/*W* emulsions reflects similar compositions of coexisting phases, where water and the biopolymers are partially cosoluble. The low-density interfacial layer is due to a trend of incompatible biopolymers to have surroundings of the same type. One more feature of *W*/*W* emulsions is a great difference in concentration between coexisting phases. This is due to the competition between the biopolymers for space in solution. The competition can be characterized (Figure 3.5) by the angle made by the tie-line with one of the concentration axes.

3.10 Biopolymers in Biological and Food Systems

Since both biological and food systems generally contain the same proportions of macromolecular components, information about phase behaviour of foods must be of

great interest for understanding cytoplasm, and the particular properties of biopolymers that influenced and facilitated its formation and evolution. Some ideas are presented here, which show the commonality of foods and living systems.

Phase separation probably occurs more often in food than in biological systems. The reason seems to be that the biological systems are mainly based on specific interactions (mainly attraction) of biopolymers, while food is based on nonspecific interactions (both attraction and repulsion) of macromolecular compounds, native, denatured, partially hydrolysed aggregated and dissociated. Denaturation of proteins during food processing decreases their solubility and cosolubility of proteins with one another and with polysaccharides, and induces phase separation of the system. Since formulated foods usually contain denatured proteins, incompatibility of biopolymers is one of the most common features of foods. The advantages of native proteins as food components are maximal cosolubility with other ingredients and a minimal contribution to the system viscosity (Tolstoguzov 1999, 2000, 2000a, 2002, 2004a,b,c).

3.11 Molecular Mimicry and Symbiosis

Globular proteins are macromolecular compounds, but they do not exhibit typical behaviour. Among polymers, globular proteins can overcome the thermodynamic prohibition of polymer miscibility. Cosolubility of native globular proteins is surprisingly high, at least more than tenfold higher than that typical of classical polymers which tend to be completely separated between coexisting phases. High co-solubility is absolutely necessary for functioning enzymes.

It has been assumed that high cosolubility of globular proteins results from the phenomenon called *molecular mimicry* (Tolstoguzov 1999, 2002). The folding of polypeptide chain hides its chemical features inside the globule. The result of the hidden hydrophobic side-chains results in a chemical similarity of globular protein surfaces. Formation of compact globules diminishes the excluded volume. Both the similarity of the globular surfaces and the reduced excluded volume of globules increase the cosolubility of proteins with one another and with other biopolymers. This phenomenon is obviously of key importance for enzymatic activity. Due to molecular mimicry, globular proteins usually have quite similar physical–chemical properties such as viscosity, surface activity, conformational stability, and gelation. Mimicry induces similarity of proteins, but at the same time it impoverishes a set of physical properties of protein mixtures. For instance, properties of mixed protein solutions become difficult to control by changing their composition.

An additional thermodynamic tool that acts in the direction opposite to mimicry has been named molecular symbiosis (Tolstoguzov 1999, 2002, 2003). High excluded volume of long rigid macromolecules underlies this phenomenon. Their presence in a mixed solution concentrates other cosolutes including globular proteins. For instance, molecular symbiosis, for example, due to addition of polysaccharides, can increase concentration of an enzyme without need for additional synthesis.

3.12 Future Trends

More detailed discussion of food polymers and their functionality in food is now difficult because of the lack of the information available on thermodynamic properties of biopolymer mixtures. So far, the phase behaviour of many important model systems remains unstudied. This particularly relates to systems containing: (i) more than two biopolymers, (ii) mixtures containing denatured proteins, (iii) partially hydrolyzed proteins, (iv) soluble electrostatic protein–polysaccharide complexes and conjugates, (v) enzymes (proteolytic and amylolytic) and their partition coefficient between the phases of protein–polysaccharide mixtures, (vi) phase behaviour of hydrolytic enzyme–exopolysaccharide mixtures, exopolysaccharide–cell wall polysaccharide mixtures and exopolysaccharide–exudative polysaccharide mixtures, (vii) biopolymer solutes in the gel networks of one or several of them, (viii) enzymes in the gel of their substrates, (ix) virus–exopolysaccharide, virus–mucopolysaccharides and virus–exudative gum mixtures, and so on.

At the moment, there is no data concerning the compatibility of exocellular proteolytic, amylolytic enzymes and exopolysaccharides and amylopectin, and between exopolysaccharides of different intestinal bacteria species and exopolysaccharides and mucopolysaccharides covering gut wall villae.

There is also no information about the partition coefficient of different enzymes between chyme phases and the effects of mucopolysaccharides and exopolysaccharides on the efficiency of enzymes.

The influence of other food components (especially of low molecular weight, such as lipids, sugars and polyvalent metal ions) and operating conditions, such as high shear forces, high pressure and sufficiently high temperature (e.g., pasteurization and sterilization), on phase behaviour of protein–polysaccharide mixtures remains only partially studied.

Further basic studies on the nature of interactions among biopolymers and on the phase behaviour and physical properties of their mixtures will undoubtedly provide a sound scientific basis to improve conventional food technologies and design new food formulations and manufacturing processes.

3.12.1 Biopolymers as Nutrients

Normally, food and chyme are phase-separated systems, but only the first steps have been taken towards understanding the phase behaviour of food polymers in food processing and practically nothing in food digestion. The effects of thermodynamic compatibility of mucopolysaccharides, food fibers and exopolysaccharides of different bacteria species on selection of microflora in the intestine and colon have not been studied yet. The mechanisms of bacterial colonization of the intestine and peristaltic transportation of chyme also remain unstudied.

Our knowledge about nonspecific immunity and human nutrition, including the mechanisms of food digestion and absorption, remains extremely poor. Viruses and microorganisms that can be consumed with food, the properties of their surfaces and

the thermodynamic compatibility of their protein and polysaccharide coverage materials with mucopolysaccharides, dietary fibers and hydrolyzing enzymes have not been investigated yet. Among biopolymers, polysaccharides and polysaccharide-containing conjugates are mainly responsible for ecological contacts of living entities mainly for nonspecific immunity and, together with proteins (enzymes), for digestion of food. Information about thermodynamic properties and structure–property relationship in polysaccharides and their conjugates, especially acting as adaptogens and food vaccines is extremely limited (Tolstoguzov 1998, 2000a, 2002, 2002a, 2003a, 2007).

3.12.2 Physical Properties and Flavouring of Food

An important requirement for food flavouring is a universal and reversible binding of different flavours to biopolymers. Only a recoverability of adsorbed flavours can provide a characteristic flavour profile. Protein molecules can adsorb a surprisingly high amount of flavours. Information concerning the effects of structural organisations (formed in food processing) of biopolymers in melts, gels, emulsions, foams, dispersed (swollen gel) particles, and solutions on food system flavouring is also limited. Adsorption of flavours and other hydrophobic ligands change the thermodynamic properties of biopolymers, their phase behaviour and the surface activity. However, physical properties of flavour and their complexes with biopolymers remain unstudied. It is also related to the effects of biopolymer composition, structural and physical features of solid food systems (Tolstogustov 1999, 2000b, 2002).

3.12.3 Functional Properties of Food Systems

Since food systems usually contain a heterogeneous mixture of proteins and polysaccharides differing in chemical nature, conformation, chain rigidity, size, and shape of molecules, degrees of hydrolysis, denaturation, dissociation and aggregation, information on model systems containing two biopolymers is not sufficient to interpret phase behaviour and functionality of real dispersed food systems.

Unfortunately, information on the phase behaviour of some food–polymer mixtures and several studied native biopolymer blends is not sufficient for understanding the functional properties of proteins and polysaccharides in real processed food. So far the phase separation conditions and coexisting phase compositions can only be found experimentally, making the prediction of food system functionality a poorly developed area of science. Chemical modification of food polymers during food processing—for instance, the formation of conjugates, polyphenolic compounds and different interbiopolymer complexes—remains practically unstudied and results in unpredictable phase behaviour and functionality of real food systems. The effects of basic food processing operations, such as thermal and mechanical treatments, on the phase behaviour of food components remains little studied, so that the prediction and control of processed food quality remains inaccurate. (Tolstoguzov 1988, 1988a, 1991, 1992, 1995, 1997a, 1998a, 2002, 2003, 2003a).

3.13 Effects of Incompatibility on Structure–Texture Relationship in Food

The texture of traditional and novel formulated foods, its formation, modification, and/or preservation during processing (frying, cooking, freezing, etc.) and storage is one of the key quality aspects. Food texture, therefore, is important for the success of a food both in the marketplace and for consumption.

The most common food processing operations, both thermal and mechanical treatments, affect the phase state and texture of foods. The phase separation threshold for food–biopolymer mixtures is usually below the concentrations characteristically found in food. Phase-separation underpins texturisation processes during food processing and subsequent breakdown during digestion. The distribution of water between the phases, the adsorption of lipids between the phases, the deformation of dispersed particles in flowing water-in-water emulsions and the gelation of the phases result in the specific morphology and texture of food. A historical experience in texturisation includes the development of cooked food and texturized vegetable analogues of animal foods. The interfacial (or depletion) layer with low-biopolymer concentration determines some features of *W*/*W* emulsions: (i) easy coalescence of dispersed particles (by depletion flocculation), (ii) their easy deformability in flow, and (iii) adsorption of lipid particles between the phases. The effects of phase state of foods and beverages on their drying and rehydration is not clear yet (Tolstoguzov 1998a, 2002, 2006a).

3.14 Biological incompatibility aspects

Progress in the field of specific and nonspecific interbiopolymer complexing (of nucleic acids, nucleic acid–proteins, enzyme–substrates, etc.) is incomparably more significant than that of biopolymer incompatibility. Attention was mainly centred on the limited compatibility of the main classes of proteins and various polysaccharides and on the effects of variables such as pH, ionic strength, temperature, and shear forces on the phase state, equilibrium, and structure of these two-phase liquid systems. The general nature of the phenomenon of thermodynamic incompatibility of biopolymers accounts for its importance in structure formation in cytoplasm, in immunity defence and nutrition of cells, in the mechanisms of food digestion and apoptosis of cell (Tolstogustov 1999a, 2000, 2002, 2004, 2004a–c, 2006, 2007).

3.15 Conclusion

Very varied functionality is typical of biopolymers as main materials of life and of food. Functional roles in foods cover such applications as water binding, solubility and viscosity, catalysis, lipid and flavour adsorption, emulsion and foam stabilization, gel and film forming. Additionally, they provide biodegradable ingredients and materials, nutrients, vaccines, adaptogens, carriers and delivery of micro- and macronutrients, and so on.

The chapter has considered some specific features of food biopolymer mixtures related to the formation of food structures. We are still near the starting point in the understanding of nonspecific interactions of biopolymers in solutions and dispersions. The conditions of immiscibility and phase equilibrium have been only studied in a quite limited number of biopolymer mixtures: (i) gelatin and polysaccharide, (ii) a globular protein and a polysaccharide, (iii) a protein and another protein, (iv) native and thermally denatured proteins, (v) a native globular protein and its partial hydrolysate.

It should be noted that this chapter has been limited to physical–chemical interactions between food macromolecules in model systems. The main reason is that in food systems, chemical protein–polysaccharide and protein–polyphenols interactions have not yet been sufficiently studied. A new trend in this area is covalent protein–polysaccharide hybrids (conjugates natural and synthetic) that are of great interest as functional additives and food ingredients

Most food biopolymers have limited miscibility on a molecular level and form multicomponent, heterophase and nonequilibrium dispersed systems. A thermodynamic approach is applicable for studying structure–property relationships in formulated foods since their structures are based on nonspecific interactions between components and such thermodynamically based operations as mixing of components, changing temperature and/or pH, underlies processing conditions.

Biopolymer incompatibility seems to provide phase-separated liquid and gel-like aqueous systems. In highly volume-occupied food systems aggregation, crystallisation and gelation of biopolymers and their adsorption at oil/water interfaces favour an increase in the free volume, which is accessible for other macromolecules. Denaturation of proteins during food processing decreases their solubility and co-solubility of proteins with one another and with polysaccharides and induces phase separation of the system.

3.16 References

Albertsson, P.-A. (1995). Aqueous polymer phase systems: properties and applications in bioseparation. In: S.E. Harding, S.E. Hill, and J.R. Mitchell, (Eds.), *Biopolymer Mixtures,* Nottingham University Press. Nottingham, UK, pp. 1–12.

Albertsson, P.-A. (1972). *Partition of Cell Particles and Macromolecules*, Wiley-Interscience, New York.

Albertsson, P.-A. (1958). Partition of proteins in liquid polymer-polymer two-phase systems. *Nature,* 177, 709–711.

Antonov, Yu.A., Grinberg, V.Ya., Zhuravskaya, N.A., and Tolstoguzov, V.B. (1982). Concentration of protein skimmed milk by the method of membraneless isobaric osmosis. *Carbohydrate Polymers*, 2, 81–90.

Antonov, Yu.A., Grinberg, V.Ya., and Tolstoguzov, V.B. (1979). Thermodynamische Aspekte der Vertraeglichkeit von Eiweissen und Polysacchariden in waessrigen Medien. *Nahrung* 23, 207–214, 597–610.

Antonov, Yu.A., Grinberg, V.Ya., and Tolstoguzov, V.B. (1975). Phasengleichgewichte in Wasser/Eiweiss/Polysaccharid Systemen, *Starke*, 27, 424–431.

Asherie, N., Lomakin, A., and Benedek, G. (1996). Phase diagram of colloidal solutions. *Phys. Rev. Lett.*, 77, 4832–4835.

Beijerinck, M.W. (1910). Ueber Emulsionsbildung bei der Vermischung wässeriger lösungen gewisser gelatinierender kolloide. *Koll. Z.*, 7, 16–20.

Beijerinck, M.W. (1896). Ueber eine eigentümlichkeit der löslichen stärke, Centralblatt für Bakteriologie, Parasitenkunde und Infektionskrankheiten 2, 697–699

Broide, M.L., Berland, C.R., Pande, J., Ogun, O., and Benedek, G.B. (1991). Binary-liquid phase separation of lens protein solution. *Proc. Natl. Acad. Sci. USA*, 88, 5660–5664.

Bungenberg de Jong, H.G. (1952). In: H.R. Kruyt (Ed.), *Colloid Science*. Elsevier, New York, pp. 355–364.

Bungenberg de Jong, H.G. (1936). La coaceruation, les coacervates et leur importance en biologie, Hermann et Cie, Paris.

Burova, T.V., Grinberg, N.V., Grinberg, V.Ya., Leontiev, A.L., and Tolstoguzov, V.B. (1992). Effects of polysaccharides upon the functional properties of 11S globulin from broad beans. *Carbohydrate Polym*, 18, 101–108.

Clewlow, A.C., Rowe, A.J., and Tombs, M.P. (1995). Pectin–gelatin phase separation: the influence of polydispersity. In: S.E. Harding, S.E. Hill, and J.R. Mitchell (Eds.), *Biopolymer Mixtures*, Nottingham University Press, Nottingham, UK, pp. 173–191.

Dobry, A. and Boyer-Kawenoki, F. (1948). Sur l'incompatibilité des macromolécules en solution aqueuse, *Bull. Soc. Chim. Belges*, 57, 280–285.

Dubois M., Gilles, K.A., Hamilton, J.K., Rebers, P.A., and Smith, F. (1956). Colorimetric method for determination of sugars and related substances. *Anal.Chem.*, 28, 350–356.

Durrani, C.M., Prystupa, D.A., Donald, A.M., and Clark, A.H. (1993). Phase diagram of mixtures of polymers in aqueous solution using Fourier transform infrared spectroscopy, *Macromolecules*, 26, 981–987.

Flory, P.J. (1953). *Principles of Polymer Chemistry*, Cornell University Press, Ithaca, NY.

Grinberg, V.Ya. and Tolstoguzov, V.B. (1997). Thermodynamic incompatibility of proteins and polysaccharides in solutions. *Food Hydrocolloids*, 11, 145–158.

Grinberg, V.Ya. and Tolstoguzov, V.B. (1972). Thermodynamic compatibility of gelatin and some D-glucans in aqueous media. *Carbohydrate Res.*, 25, 313–320.

Krause, S. (1978). Polymer–polymer compatibility. In: D.R. Paul and S. Newman (Eds.), *Polymer Blends*, Vol. 1, Academic Press, San Diego, pp. 16–113.

Kwei, T.K. and Wang, T.T. (1978). Phase separation behaviour of polymer–polymer mixtures. In: D.R. Paul and S. Newman (Eds.), *Polymer Blends*, Vol. 1, Academic Press, San Diego, pp. 141–184.

Ledward, D.A. (1993). Creating textures from mixed biopolymer systems. *Trends Food Sci. Tech.*, 4, 402–405.

Liu, C., Lomakin, A., Thurston, G.M., Hayden, D., Pande, A., Pande, J., Ogun, O., Asherie, N., and Benedek, G.B. (1995). Phase separation in multicomponent aqueous-protein solutions. *J. Phys. Chem.*, 99, 454–461.

Medin, A.S. and Janson, J-Ch. (1993). Studies on aqueous polymer two-phase systems containing agarose, *Carbohydrate Polym.*, 22, 127–136.

Polyakov, V.I., Grinberg, V.Ya., and Tolstoguzov, V.B. (1997). Thermodynamic incompatibility of proteins. *Food Hydrocolloids*, 11, 171–180.

Poole, S., West, S.I., and Walters, C.L. (1984). Protein–protein interactions: their importance in the foaming of heterogeneous protein systems. *J. Sci. Food Agric.*, 35, 701–711.

Popello, I.A., Suchkov, V.V., Grinberg, V.Ya., and Tolstoguzov, V.B. (1992). Effects of pH upon the liquid-liquid phase equilibria in solutions of legumins and vicilins from broad beans and peas. *Food Hydrocolloids*, 6, 147–152.

Popello, I.A., Suchkov, V.V., Grinberg, V.Ya., and Tolstoguzov, V.B. (1991). Liquid/liquid phase equilibrium in globulin/salt/water systems. Vicilin. *J. Sci. Food Agric.*, 54, 239–244.

Popello, I.A., Suchkov, V.V., Grinberg, V.Ya., and Tolstoguzov, V.B. (1990). Liquid/liquid phase equilibrium in globulin/salt/water systems. Legumin. *J. Sci. Food Agric.*, 51, 345–353.

Samant, S.K., Singhal, R.S., Kulkarni, P.R., and Rege, D.V. (1993). Protein–polysaccharide interactions: a new approach in food formulations, *Int. J. Food Sci. and Technol*, 28, 547–562.

Suchkov, V.V., Popello, I.A., Grinberg, V.Ya., and Tolstoguzov, V.B. (1997). Shear effects on phase behaviour of the legumin-salt-water system. Modelling protein recovery. *Food Hydrocolloids*, 11, 135–144.

Suchkov, V.V., Popello, I.A., Grinberg, V.Ya., and Tolstoguzov, V.B. (1990). Isolation and purification of 7S globulin and 11S globulin from broad beans and peas. *J. Agric. Food Chem.*, 38, 92–95.

Tanford, C. (1961). *Physical Chemistry of Macromolecules*. John Wiley & Sons, New York, pp. 192–202.

Tiebackx, F.W. (1911). Gleichzeitige ausflockung zweier kolloide, Zeitschrift fur Chemie und Industrie der Kolloide, 8, 198–201.

Tolstoguzov, V.B. (2007). *The Origin of Polysaccharide Functionality*. In: P. Tomasik, V.P. Yuryev, E. Bertoft (Eds.), *Starch. Progress in basic and applied science*. Published by Polish Food Technologists' Society, Małopolska Branch, Cracow. pp. 79–93.

Tolstoguzov, V.B. (2006). Phase behaviour in mixed polysaccharide systems In: A.M. Stephen, G.O. Phillips, P.A. Williams and B.A. Lewis (Eds.), *Food Polysaccharides*, Ch 17., 2nd Ed. Marcel Dekker, New York, pp. 587–625.

Tolstoguzov, V.B. (2006a). Texturising by phase separation. *Biotechnology Advances*, 24, 626–628.

Tolstoguzov, V.B. (2004). Thermodynamic considerations on polysaccharide functions. Polysaccharides came first. *Carbohydrate Polym.*, 54(3), 371–380.

Tolstoguzov, V.B. (2004a). Why are polysaccharides necessary? *Food Hydrocolloids*, 86(5), 873–877.

Tolstoguzov, V.B. (2004b). Why were polysaccharides necessary? *Orig. Life Evol. Biosph.*, 34(6), 571–597.

Tolstoguzov, V.B. (2004c). Thermodynamic considerations on polysaccharide functionality. In: V. Yuryev, P. Tomasik, H. Ruck (Eds.), *Starch: From Polysaccharides to Granules, Simple and Mixture Gels*. New York: NOVA Science Publishers, Inc., pp. 3–18.

Tolstoguzov, V.B. (2003). Some thermodynamic considerations of starch functionality. *Carbohydrate Polym.*, 51, 99–111.

Tolstoguzov, V.B. (2003a). Some thermodynamic considerations in food formulation, *Food Hydrocolloids*, 17, 1–23.

Tolstoguzov, V.B. (2002). Thermodynamic aspects of biopolymer functionality in biological systems, foods and beverages, *Crit. Rev. Biotech.*, 22(2), 89–174.

Tolstoguzov, V. (2002a). Thermodynamic considerations of starch functionality in foods. In: V. Yuryev, A. Cesaro, W. Bergthaller (Eds.), *Starch and Starch Containing Origins: Structure*, *Properties and New Technologies*. NOVA Science Publishers, New York, pp. 227–267.

Tolstoguzov, V.B. (2000). Compositions and phase diagrams for aqueous systems based on proteins and polysaccharides. In: H. Walter, D.E. Brooks, and P.A. Srere (Eds.), *Microcompartmentation and Phase Separation in Cytoplasm*: *A Survey of Cell Biology*. International Review of Cytology, Vol. 192. Academic Press, San Diego, pp. 3–31.

Tolstoguzov, V.B. (2000a). Phase behaviour of macromolecular components in biological and food systems, *Nahrung*, 44, 5, 299–308.

Tolstoguzov, V.B. (2000b). Foods as dispersed systems. Thermodynamic aspects of composition-property relationship in formulated food. *J. Thermal Anal. Calorimetry*, 61, 397–409.
Tolstoguzov, V.B. (1999). The role of water in intermolecular interactions in food. In: Y.H. Roos, R.B. Leslie and P.J. Lillford (Eds.), *Water Management in the Design and Distribution of Quality Foods*. (Proceedings ISOPOW 7 Symposium), Technomic Publishing Company, Lancaster, PA, pp. 199–233.
Tolstoguzov, V.B. (1999a). Origins of globular structure in proteins. *Hypo. FEBS Lett.*, 444, 145–148.
Tolstoguzov, V.B. (1998). Functional properties of protein–polysaccharide mixtures. In: J.R. Mitchell, D.A. Ledward and S. Hill (Eds.), *Functional Properties of Food Macromolecules*. Blackie Academic & Professional, London, pp. 252–277.
Tolstoguzov, V.B. (1997). Protein–polysaccharide interactions. In: S. Damodaran and A. Paraf (Eds.), *Food Proteins and Their Applications in Foods*, Marcel Dekker, Inc., New York, pp. 171–198.
Tolstoguzov, V.B. (1997a). Thermodynamic aspects of dough formation and functionality. *Food Hydrocolloids*, 11(2), 181–193.
Tolstoguzov, V.B. (1995). Some physical–chemical aspects of protein processing in foods. Multicomponent gels. *Food Hydrocolloids*, 9, 317–332.
Tolstoguzov, V.B. (1992). The functional properties of food proteins. In: G.O. Phillips, P.A. Williams, and D.J. Wedlock (Eds.), *Gums and Stabilisers for the Food Industry:* 6, IRL Press, Oxford, pp. 241–266.
Tolstoguzov, V.B. (1991). Functional properties of food proteins and role of protein–polysaccharide interaction. *Food Hydrocolloids*, 4, 429–468.
Tolstoguzov, V.B. (1990). Interactions of gelatin with polysaccharides. In: G.O. Phillips, P.A. Williams, and D.J. Wedlock (Eds.), *Gums and Stabilisers for the Food Industry:* 5, IRL Press, Oxford, pp. 157–175.
Tolstoguzov, V.B. (1988). Creation of fibrous structure by spinneretless spinning, In: J.M.V. Blanshard and J.R. Mitchell (Eds.), *Food Structure: Its Creation and Evaluation*, pp. 181–196. Butterworths, London.
Tolstoguzov, V.B. (1988a). Some physical-chemical aspects of protein processing into foodstuffs. *Food Hydrocolloids*, 2, 339–370.
Tolstoguzov, V.B. (1986). Functional properties of protein–polysaccharides mixtures, In: J.R. Mitchell, J.R., and D.A. Ledward (Eds.), *Functional Properties of Food Macromolecules*, Elsevier Applied Sciences, London, pp. 385–415.
Tolstoguzov, V.B., Grinberg, V.Ya., and Gurov, A.N. (1985). Some physicalchemical approaches to the problem of protein texturization. *J. Agric. Food Chem.*, 33, 151–159.
Tombs, M.P. (1985). Phase separation in protein: water systems and the formation of structure. In: D. Simatos, and J.L. Multon (Eds.), *Properties of Water in Foods*, pp. 25–36. Martinus Nijhoff Publ., Dordrecht.
Tombs, M.P., Newsom, B.G., and Wilding, P. (1974). Protein solubility: phase separation in arachin-salt-water systems. *Int. J. Peptide Protein Res.*, 6, 253–277.
Tombs, M.P. (1970) Protein products. German Patent 1 940 561; (1972) Brit. Patent 1.265.661; (1975) Aqueous protein composition. US Patent 3870 801.

Chapter 4

The Crystalline State

Richard W. Hartel

University of Wisconsin, Department of Food Science, 1605 Linden Drive Madison, WI 53706 USA, rwhartel@wisc.edu

4.1 Introduction

From the snap, gloss and texture of chocolate to the shelf life of frozen foods, crystalline microstructure plays a very important role in the texture, appearance, shelf life and overall quality of many foods. The total amount of crystalline phase in a food, as well as the size distribution and shape of the crystals within the food, can affect the physical properties of the product. Furthermore, some materials in food can crystallize in different polymorphic forms so that control of polymorphic transformations may also be necessary.

Probably the most important components in foods that crystallize are water, sugars (and sugar alcohols) and fats. However, salts, organic acids, starch, emulsifiers, and even proteins may be found in crystalline form in certain foods.

Water is converted into ice in frozen foods either to extend storage time (as in frozen meats, vegetables and fruits) or to enhance the eating experience (as in ice cream). Freezing foods for extended shelf life requires that the ice crystals impart minimal damage to the structures (cell walls, air cells, emulsions, etc.) to maintain freshlike properties. The freezing rate is probably the most important parameter in freezing, since rapid freezing leads to formation of numerous small crystals that have the least impact on product qualities. Foods frozen for consumption have similar concerns for small crystals—the largest crystals should still be less than the threshold detection size. The cooling effect during consumption of a smooth, creamy ice cream comes from the numerous small ice crystals that were formed during freezing in a scraped surface freezer. In contrast, the rough texture of a popsicle comes from freezing under quiescent conditions to produce larger, needle-shaped crystals.

Numerous foods contain sugar crystals, including examples in the confectionery (fondant, grained caramels and fudge, and grained nougat) and cereal (frosted cereals) industries. In confections, the presence of small crystals leads to a "short" texture, where the chewy, stretchy strands of carbohydrates and/or proteins are broken up by the crystalline structure. The difference between a chewy caramel (no crystals) and a grained caramel is quite apparent upon consumption. Taken further, more and larger crystals lead to the soft, sometimes crumbly texture of fudge. In cereals, crystals are needed primarily to provide the desired appearance. The frostiness of some cereals is due exclusively to control of sugar crystallization during processing.

Probably the most difficult food components in terms of controlling crystallization are lipids, due to the extremely wide range of chemical composition. Most natural fats are made of numerous molecules, primarily triacylglycerols, which are all structurally similar except with slight differences in chain length and degree of saturation. These molecules, because of their close similarities, often cocrystallize into mixed crystals, with crystal composition depending on processing conditions such as the cooling rate and agitation. To make things even more difficult, lipids exhibit complex polymorphism. Thus, choice of processing conditions must account for polymorphic transformations. For example, tempering of chocolate is the controlled crystallization of cocoa butter into the proper crystal number, size and polymorph. If done correctly, a well-tempered chocolate is easily removed from the mold (proper contraction during crystallization), has a glossy surface, and is shelf stable for years as long as proper storage conditions are maintained.

In some cases, crystallization occurs during the manufacturing process so that phase equilibrium is nearly reached by the time the food is packaged. However, in many food processes, crystallization is initiated during manufacturing and phase equilibration only occurs in the package within days or even weeks in some cases. Conditions during both processing and storage can have huge impact on crystalline microstructure and thus on product quality.

Even after phase equilibration is reached in a product during storage, changes in storage conditions often lead to subsequent changes in the crystalline phase. For example, temperature cycles or moisture changes during storage can lead to changes in the amount of crystalline phase volume, the size distribution of crystals, shape and surface characteristics, and internal perfection, including polymorphic transformations. For the most part, changes in crystalline microstructure during storage cause degradation in product quality. Ice recrystallization in frozen desserts and fat bloom formation on chocolates are examples of such negative changes that occur during storage.

4.2 Crystallization and Nucleation

Controlling the formation, growth and perfection of crystals during processing and storage requires knowledge of both thermodynamic and kinetic parameters that affect crystallization. The interplay between the thermodynamic driving force and kinetic constraints on crystal formation generally govern the nature of the crystalline microstructure developed in a food.

4.2.1 Thermodynamic Driving Force

Most foods are complex mixtures of ingredients, many of which can influence crystallization behavior during processing and storage. To define the driving force for crystallization of any individual ingredient, it is necessary to its phase behavior in the complex food system. Phase diagrams define the thermodynamic equilibrium conditions for a given system. For a pure system, the phase diagram shows which phase is thermodynamically predicted at any temperature and pressure. For a binary system, like sugar and water, the phase diagram shows what phase is expected at equilibrium at any temperature and composition. The phase behavior of ternary systems, shown on triangle diagrams, document the expected phase at equilibrium for any combination of the three components, but only at a single temperature. A higher number of components in a system requires even more complex analysis and are rarely used in food analysis. The complexity of many foods has led to simplified approaches to understanding crystallization driving force.

4.2.1.1 Phase Behavior

For a pure material, the melting temperature defines the equilibrium point between crystal and liquid. Above that temperature, the material is liquid, whereas below that temperature the material will eventually become crystalline (governed by kinetic considerations). In foods, freezing and melting of ice is probably the simplest example of a melt system despite the fact that other ingredients in foods (e.g., salts, sugars, etc.) can influence the melting point of ice through the colligative effect.

The driving force, ϕ, for crystallization in a pure system can be given as

$$\phi = \left(\Delta H_f\right) \frac{\left(T_f - T\right)}{T_f} = \left(\Delta H_f\right) \frac{\left(\Delta T\right)}{T_f} \tag{4.1}$$

where T is absolute temperature of the system, T_f is the melting point temperature and ΔH_f is the latent heat of fusion.

Often, the driving force for crystallization in melt systems is given simply by the temperature difference, ΔT, with the melting point temperature. In general, the lower the temperature of a system, the greater the rate of crystallization until reduced mass transfer limits nucleation at very low temperatures.

In binary crystallizing systems, sometimes called solution systems, a solvent (usually water) dissolves a solute that eventually crystallizes either during processing or storage. Conditions in the manufacturing process are generally set so that the solute becomes supersaturated in the solvent, after which crystal formation, growth and ripening are controlled to give the desired microstructure. Examples of solution behavior in foods include sugar crystallization in confections, cereal frostings, and milk powders, and salt crystallization during storage of cheese (e.g., cheddar cheese).

Phase behavior of solution systems depends on the nature of the interactions between the two components. Although numerous types of phase diagrams can be found in nature (and foods), many systems of importance in foods exhibit eutectic

phase behavior, where the melting temperature of a mixture falls below the melting points of either of the two individual components. Figure 4.1 shows a generic eutectic phase diagram for a binary system. Above the melting line (solvent) or solubility line (solute), all molecules are in liquid form. At temperatures below or concentrations above the equilibrium phase boundaries, either solvent or solute may form crystals. The eutectic temperature, represented as the point where the solute and solvent equilibrium curves intersect, defines the point below which a eutectic solid should form. Nominally, a solid with a defined composition (based on the composition at the eutectic point) will be formed at temperatures below the eutectic temperature. However, in many food systems, because the solvent is water, with a molecular weight often much less than the solute molecules, it is common for no eutectic solid to form at all. In fact, it is common to find the solute, water, continuing to freeze independently even at temperatures well below the eutectic point. The solute does not crystallize simply due to kinetic constraints of limited molecular mobility.

One of the most important uses of phase diagrams in food applications is prediction of crystalline yield for a given system. For example, if a sucrose solution of certain concentration is allowed to crystallize to equilibrium, the amount of crystalline solid (yield) can be predicted based on the phase diagram. As will be seen later, crystalline phase volume is one of the most important determinants of food material properties.

In solution systems, the driving force for crystallization is the difference in chemical potential between molecules in the liquid state and those in the crystalline state. Therefore, the supersaturation driving force, ϕ, for crystallization of a solute from solution is given by

$$\phi = RT \ln\left(\frac{a}{a_{eq}}\right) = RT \ln\left(\frac{\gamma X}{\gamma_S X_S}\right) \approx RT \ln\left(\frac{C}{C_S}\right) \tag{4.2}$$

where a is the activity of the solute in the solution, a_{eq} is the activity of the solute at equilibrium, γ is the activity coefficient of the solution, γ_s is the activity coefficient of the saturated solution, X is the mole fraction of the solute in the solution, X_s is the mole fraction of the solute in the solution at saturation, C is the concentration of the solute in the solution, and C_s is the concentration of the solute at saturation.

Since activity and the activity coefficient are not easily measured, most food applications simply define the supersaturation driving force in a solution system, s, by the ratio of concentration to the saturation concentration.

$$s = \frac{C}{C_S} \tag{4.3}$$

In general, larger supersaturation driving forces lead to more rapid crystallization. However, in systems that exhibit glass transitions, very high driving forces lead to limited molecular mobility, which effectively blocks nucleation.

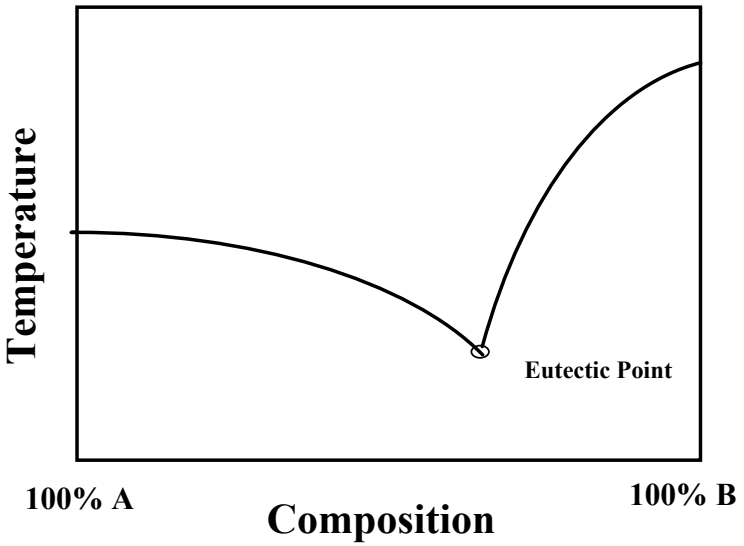

Figure 4.1. Eutectic phase diagram.

To take into account the effects of other ingredients in foods on crystallization behavior, more complex phase diagrams are needed. As noted previously, sometimes the phase behavior of complex systems can be modeled using ternary diagrams with solvent, solute and impurity on the three points of the triangle phase diagram. In sucrose refining, for example, a ternary diagram expressing the phase relationships among water, sucrose and dissolved impurities may be used to help understand crystallization in practical systems (Mathlouthi and Reiser 1995). Alternatively, sometimes it is sufficient to simply show the effects of one component in a food system on the solubility of the crystallizing component. For example, the effect of corn syrup on depressing sucrose solubility in water is often indicated on a binary-type phase diagram, where a new solubility line is drawn to indicate the new solubility of sucrose in the mixed system. However, in this approach, the meaning of the composition axis of a binary phase diagram is no longer simple since it is a mixed composition of sucrose and corn syrup.

The phase behavior of lipid systems is often quite complex, yet critical to controlling material properties of fat-based foods. In natural fats, mixtures of triacylglycerols (TAGs) with different melting points are quite common. Some TAGs have a high melting point, notably those with long-chain, saturated fatty acids. TAGs that contain shorter-chain and/or unsaturated fatty acids typically have lower melting point temperatures, and even may be liquid oils at food product temperatures. Thus, in complex natural fats, some TAGs are crystalline and some are likely to still be liquid. Recently, Wesdorp et al. (2005) outlined the steps necessary to thermodynamically model the phase behavior of complex mixed lipid systems. This approach also distinguished between the different polymorphs that can form in lipid crystals.

Because of the complexities of many food systems, numerous simplifications of phase diagrams have been developed over the years. In lipid systems, diagrams that show lines of constant solid fat content at different temperatures and composition are often used to indicate phase mixing behavior of two fats (Timms 2003). These may be best called pseudo-phase diagrams since, although they represent phase mixing behavior between the two fats, they are not true phase diagrams.

4.2.1.2 State Diagrams

Phase diagrams document the phase behavior expected at equilibrium (see Chapter 7). They can be used to predict crystalline phase volume and which crystalline form (polymorph, hydrate, etc.) is expected in a food that has reached phase equilibrium. However, in foods that never attain equilibrium, the phase diagram by itself is of limited value. In recent years, certain aspects of nonequilibrium have been characterized using the state diagram approach (Slade and Levine 1991).

The state diagram approach generally overlays the phase diagram for a system with the glass transition curve, as shown in Figure 4.2 for the sucrose–water system. The equilibrium phase boundary for solvent (water) crystallization is seen as the freezing point depression curve, and that for the solute (sucrose) is seen as the solubility curve. Overlaid on top of the standard binary phase diagram is the glass transition curve, which documents the conditions where this sucrose system may be expected to become a glass under certain nonequilibrium conditions.

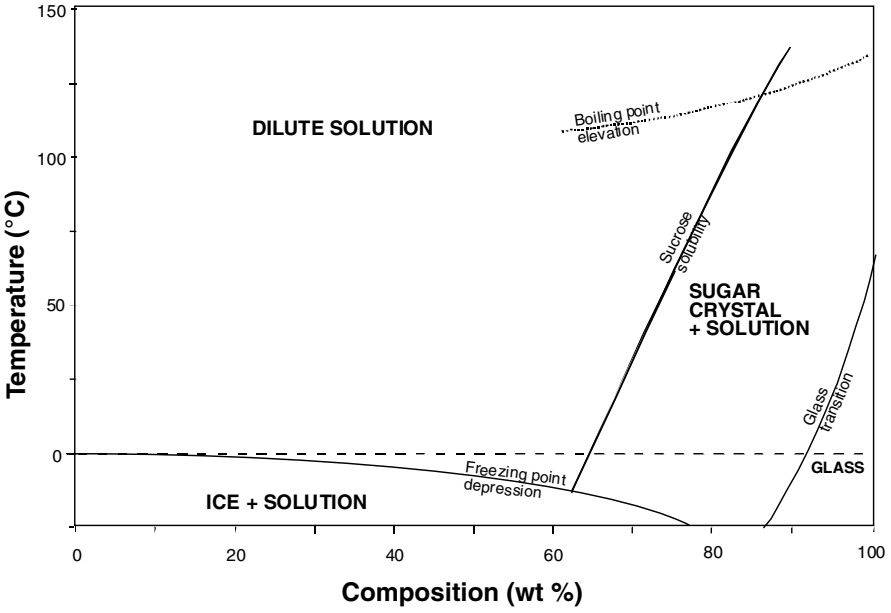

Figure 4.2. State diagram for sucrose–water (from Hartel 2001, with permission).

In Figure 4.2, crystallization of sucrose can only occur at conditions of temperature and composition that fall between the solubility and glass transition temperature lines. On either side of this crystallization envelope, there is either no thermodynamic driving force (dilute system) for crystallization or nucleation is constrained by kinetic effects due to limited molecular mobility. Thus, processing conditions must be controlled so that the system falls within the crystallization envelope to ensure crystallization. Furthermore, the point within the crystallization envelope at which crystallization occurs can significantly affect the nature of the crystalline phase in the food, and thus affect the material properties.

4.2.2 Nucleation

For crystals to form from a liquid state, the molecules of the crystallizing species must come together in sufficient number (form a cluster) to overcome the energy cost of forming a surface. Once this energy barrier is overcome, the latent heat associated with crystallization is released, and further nucleation is strongly promoted. Thus, there often is a metastable zone where a supersaturated or subcooled system may not nucleate for a very long time.

Furthermore, molecules in solution may be associated with one another (and with other molecules) in a manner quite dissimilar to the ordering of molecules in the crystal lattice. That is, molecular associations (whether hydrogen bonding or some other form of interaction) in the liquid state—particularly as solutions become more concentrated or melt systems become more subcooled—may actually impede ordering of the molecules into a crystal lattice.

Thus, nucleation is often considered to be a two-step process. The first step is the dissociation of liquid molecules from their native liquid state. This may be dissociation of two molecules of the crystallizing species, but may also be dissociation of molecules of the crystallizing species with other molecules in the system, even the solvent. For example, sugar molecules in solution are hydrated with up to 4 to 5 molecules of water (under dilute conditions). At higher concentrations of sucrose, fewer water molecules surround each sucrose molecule, allowing interaction among sucrose molecules, eventually leading to nucleation.

When the molecules of the crystallizing species become sufficiently dissociated, they begin to organize among themselves until eventually they form clusters of sufficient size to form a surface and organize into a crystal lattice. The driving force for cluster formation and nucleation is supersaturation in solution systems and subcooling in melt systems. In general, a higher driving force, meaning either higher supersaturation or greater subcooling, leads to more rapid nucleation.

Two parameters are necessary to fully describe nucleation kinetics: the induction time and the rate of nucleation. The moment a driving force is created, whether a supersaturation in solution systems or a subcooling in melt systems, the molecules begin to organize into crystallite clusters. The time at any given driving force required for the first nuclei to form is called the induction time. Unfortunately, the true induction time is difficult to measure since the exact point when nuclei are first formed is nearly impossible to measure. Nuclei are probably only nanometers in size, too small to be detected with any methods developed to date. Thus, measurement of

induction time usually contains some element of growth to detectable size. Induction times have been measured by visual inspection often aided by a microscope, light scattering (turbidity), image analysis, and calorimetry, among other techniques.

The nucleation rate gives the number of nuclei that are formed per unit volume over a specified time increment. The rate of nuclei formation depends on the mechanism by which nucleation occurs and the processing conditions during crystallization.

4.2.2.1 Nucleation Mechanisms

Although the general description of nucleation from the liquid state provided above applies in all cases, several different categories of nucleation can be distinguished. In homogeneous nucleation, molecules of the crystallizing species come together to form nuclei, whereas in heterogeneous nucleation, a foreign surface provides a portion of the energy for nuclei formation. Another special case of nucleation is when crystals form from the amorphous state, since molecular mobility is the limiting factor for nuclei formation in this case.

Homogeneous Nucleation

The classical form of nucleation involves molecules of the crystallizing species forming crystals through self-association. No external surface is needed or used for nucleation in this case. The rate of classical homogeneous nucleation, J [1/mL-min], of solution systems is often described by the following equation, derived by comparing the energy terms for surface formation (proportional to size squared) and energy release upon phase change (proportional to size cubed) (Mullin 1993).

$$J = A \exp\left\{ -\frac{16\pi\gamma^3 \upsilon^2}{3k^3 T^3 \left(\ln S\right)^2} \right\} \tag{4.4}$$

where A is an exponential factor, γ surface tension, and ν is molecular volume.

Equation (4.4) clearly shows the relative effects of various properties on the rate of nuclei formation. Temperature and supersaturation are the two parameters that can be adjusted to affect nucleation rate. Since most soluble systems exhibit some temperature dependence of the saturation concentration (phase boundary), these two parameters are not always independent. For example, raising temperature enhances nucleation kinetics (3rd power), but usually causes a decrease in supersaturation (square of logarithm power). Thus, the effects of temperature on nucleation are not always easy to predict since they depend on the relative changes of these two terms.

A similar expression is found for nucleation rate from melt systems, except the driving force is written in terms of the subcooling, as seen in Equation (4.5).

$$J = A \exp\left\{ -\frac{16\pi\gamma^3 T_f^2}{3kT\left(\Delta H_f\right)^2 \left(T_f - T\right)^2} \right\} \tag{4.5}$$

In both cases, the nucleation rate is a very strong function of the driving force. Essentially, the rate of nucleation is very low until some critical value of the driving force is reached. At this critical point, massive nucleation is then observed. This very sharp delineation in nucleation at some critical driving force leads to observation of a metastable zone, and is often related to the energy barrier that must be overcome for nucleation to occur.

Heterogeneous Nucleation

In virtually all food systems, there are numerous small particulates (dust, etc.) or surfaces (vessel walls, etc.) that catalyze formation of nuclei by providing a portion of the energy needed to form the interface. Thus, in most situations relevant to food manufacturing, homogeneous nucleation does not occur and nucleation based on a heterogeneous mechanism dominates.

The ability of a surface to catalyze formation of a crystal is thought to depend on several factors, but ultimately comes from its capacity to order the molecules of the crystallizing species in a form similar to that found in its crystal lattice. This ordering generally requires a matching of the lattice structures of the solid particle surface with the crystal lattice of the nucleating species, although other factors (surface energies, charges, etc.) are thought to influence the ability of a foreign surface to catalyze nucleation.

Furthermore, it seems that the ability of a surface to catalyze nucleation changes with time in some unknown manner. For example, studies where a sample is repeatedly heated and cooled to mark a crystallization temperature clearly show a variation that is difficult to explain mechanistically. Liquid metal systems and ice have both been studied, and although the range of crystallizing temperatures observed depends on the system, both systems exhibit a relatively wide range of temperatures over which nucleation occurred. The only explanation for this behavior is that the nucleating ability of the heterogeneous nucleation sites in the solution change over time with temperature cycling.

Due to this unexplained behavior, heterogeneous nucleation is often treated empirically, by simply utilizing a nucleation factor in the exponential in Equation (4.4). It is this variability, often uncontrolled, that leads to problems in controlling nucleation in food systems. Even in relatively pure systems, like carefully controlled supersaturated sugar systems, nucleation may occur over a very wide time span. For example, van Hook and Frulla (1952) found that identical supersaturated sucrose samples held at the same temperature nucleated over a very wide time span, with some crystallizing as quickly as 3 hours while other samples took over a day to nucleate.

Nucleation from the Amorphous State

Unlike the mobile liquid state, crystals that nucleate from the viscous amorphous state are less governed by thermodynamics than by kinetic constraints. To describe nucleation behavior in kinetically constrained systems, a modification of Equation (4.4), often attributed to Tamman, is used (Turnbull and Fisher 1949).

$$J = A \exp\left\{-\frac{16\pi\gamma^3 u^2}{3k^3T^3\left(\ln S\right)^2}\right\}\exp\left\{\frac{\Delta G'_v}{kT}\right\} \tag{4.6}$$

Here, $\Delta G'_v$ is the free energy associated with diffusion or molecular mobility.

The second term in Equation (4.6) describes the mobility of molecules of the crystallizing species, which in extremely viscous systems can completely dominate nucleation behavior despite an incredibly high supersaturation. In fact, in glassy systems, like often found in hard candies and spray-dried sugar powders, supersaturations are sufficiently high that nucleation should occur instantaneously if governed by thermodynamic considerations. However, the ability of molecules in the glass to diffuse and rotate to organize into a crystal lattice is severely restricted so that nucleation rates while a system is in the glassy state are effectively zero.

An alternative approach to describe nucleation from the amorphous state utilizes the glass transition temperature (T_g) concept (Williams et al. 1955; Slade and Levine 1991). Based on this approach, molecular mobility below T_g is sufficiently limited to kinetically impede nucleation for very long times. Amorphous systems, at temperatures above T_g, nucleate at a rate depending on the temperature difference above T_g. Williams et al. (1955) suggested that the rate of nucleation increases rapidly at temperatures just above T_g according to a kinetic expression given by the WLF (Williams-Landel-Ferry) equation.

$$\log\left(a_T\right) = \frac{-C_1\left(T - T_s\right)}{C_2 + \left(T - T_s\right)} \tag{4.7}$$

Here, a_T is relative nucleation rate compared at reference temperature (T_s), and C_1 and C_2 are constants.

Levenson and Hartel (2005) studied nucleation of amorphous sugar systems (sucrose and corn syrup mixtures) at temperatures above T_g, and compared Equation (4.6) with the WLF kinetic expression (Equation (4.7)). Because of the wide variability in the nucleation measurements, they were unable to distinguish which kinetic model better described the data, with both models fitting reasonably well. Interestingly, the first term, the thermodynamic term, in the Tamman equation (Equation (4.6)), had negligible effect in predicting the experimental data, verifying that in this case kinetic constraints dominate nucleation from the amorphous state despite the very large thermodynamic driving force.

4.2.2.2 Factors Affecting Nucleation

Although numerous factors affect nucleation in food systems, probably the most important for the glass-forming systems commonly found in foods is that of molecular mobility and the thermodynamic driving force. At low levels of driving force (ΔT or S), nucleation increases with increasing driving force—either decreasing temperature or increasing supersaturation. However, once concentration gets too high or temperature too low, the molecular mobility term decreases and nucleation rate decreases again. Figure 4.3 schematically shows the change in induction time for a supersaturated solution cooled to different temperatures prior to beating to promote

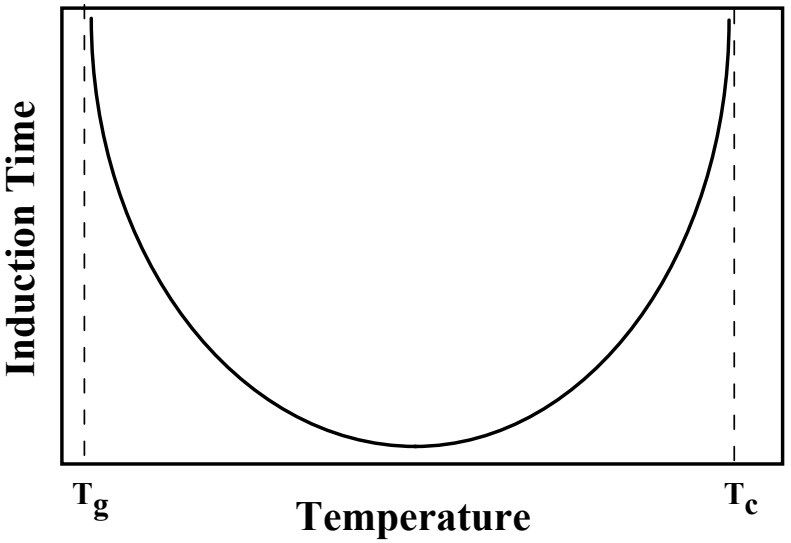

Figure 4.3. Schematic representation of induction time for a solution with given concentration cooled to different temperatures (T_g is glass transition temperature; T_c is temperature at which the solution is at saturation).

nucleation. The induction time is high at high temperatures because the supersaturation driving force is still low. At very low temperatures, the molecular mobility decreases and the induction time increases again. In this system, an optimal temperature exists where the fastest nucleation occurs based on the offsetting nature of decreased molecular mobility and increasing driving force. Ultimately, if molecular mobility effectively goes to zero, as might occur below the glass transition temperature, no nucleation would be expected.

In systems as described above, the rate of cooling must be significantly faster than the rate of nucleation in order for a glass to be formed. Effectively, the system must be cooled rapidly through the crystallization zone of the state diagram bounded by the solubility curve and the glass transition curve. Systems that crystallize more rapidly than they can be cooled will not form glasses.

Another important processing parameter of importance in crystallization in foods is agitation. A general rule of thumb is that agitation promotes nucleation. When a system is expected/desired to crystallize, then high-intensity mixing or shearing can help promote nucleation. However, when a labile system (one prone to nucleation, but held in a metastable state) must be prevented from nucleating, the least possible amount of shear or agitation should be exerted.

Each of the parameters discussed so far (temperature, cooling rate, shear rate) has been shown to influence crystallization and polymorphism of lipids (Garti and Sato 1988; Garti and Sato 2001). Lipids are generally not glass-forming systems in that even under very rapid cooling conditions they exhibit some crystallinity (organized

scattering of x-rays). However, the cooling rate and agitation profile affect which polymorphic crystal forms and how rapidly it forms. Since lipids exhibit monotropic polymorphism, less stable polymorphs nucleate preferentially over more stable forms, but then transform to the more stable forms over time at a rate that depends on process conditions.

In most food systems, a wide variety of ingredients are used to provide the desired textural and sensory characteristics. Thus, crystallization nearly always occurs in complex systems where phase behavior may be difficult to ascertain accurately. Furthermore, the specific interactions among ingredients can lead to significant inhibition of nucleation. Because of these often complex interactions, it is frequently difficult to predict nucleation behavior.

In fact, in some food applications, specific components are added because of their effect on crystallization. It is common in confections to add corn syrup or invert sugar as doctoring agents to control crystallization of sugar and modify the material properties of the product. For example, the inhibitory effect of corn syrup on sucrose crystallization allows the commercial manufacture of hard candy, a sugar glass. Large-scale commercial hard candy cookers have sufficient shear and mechanical energy input that approximately 30% corn syrup is needed to inhibit sucrose nucleation sufficiently to allow formation of a sugar glass.

4.2.3 Crystal Growth

Nuclei can increase in size through a number of different mechanisms. Molecular deposition, where molecules from the bulk liquid phase become incorporated into the existing crystal lattice, results in a decrease in crystallization driving force until growth ceases when the driving force is depleted. Alternatively, small crystals can agglomerate into larger crystals, resulting in polycrystalline aggregates, even when no residual crystallization driving force exists. A third mechanism by which crystals can grow larger is recrystallization, which is typically based on the mechanisms of ripening (crystal size effect on solubility). Since this most often occurs during storage, this latter mechanism will be covered in the section on changes during storage.

After a nucleus has formed, crystal growth will continue until phase equilibrium is attained. For crystal growth to occur, several steps are necessary. Molecules of the crystallizing species must diffuse through the bulk solution to the surface of the growing crystal, at which point they must organize into the appropriate configuration to fit into the existing lattice. This may mean losing water molecules (solvation) or organizing with other molecules to form a growth unit. The growth unit then migrates along the surface of the crystal until it finds a site for incorporation into the lattice. Once the molecules incorporate into the lattice, the latent heat associated with the phase change from liquid to crystal is released and must be removed from the system. If heat is not removed from the local environment around the growing crystal, the local temperature increases. A generalized diagram showing the transition from liquid to crystalline state is shown in Figure 4.4.

To simplify analysis of crystal growth, several distinct mechanisms may be postulated, any of which can become the rate-limiting step for growth. The three major contributors include (1) bulk diffusion (of crystallizing species to the surface

and of impurities away from the surface), (2) surface integration or incorporation of growth units into the lattice, and (3) removal of latent heat of crystallization.

Each of these different steps occurs in every case; however, in different crystallizing systems, the relative contributions of these three mechanisms may be quite different. For example, in sucrose crystal growth, bulk diffusion and surface integration are much more important than heat removal, although the relative influence of diffusion and surface integration depends on temperature. At higher temperatures (above about 40°C), bulk diffusion becomes more limiting, whereas at lower temperatures, the rate of surface integration is more limiting. In ice, however, counter-diffusion of impurities and rate of latent heat removal are the two most important steps limiting crystal growth.

The first step for crystal growth by molecular deposition is that the molecules of the crystallizing species must diffuse through the matrix to reach the surface of the growing crystal. Counter-diffusion of noncrystallizing molecules away from the growing surface must also be considered.

The driving force for mass transfer growth in solution systems is generally given as the difference in concentration between the bulk fluid, C_b, and the interfacial concentration, C_i, often taken as the concentration of solute molecules at the edge of the adsorbed layer (Figure 4.4). The mass transfer rate for solute molecules diffusing to the surface of a growing crystal is

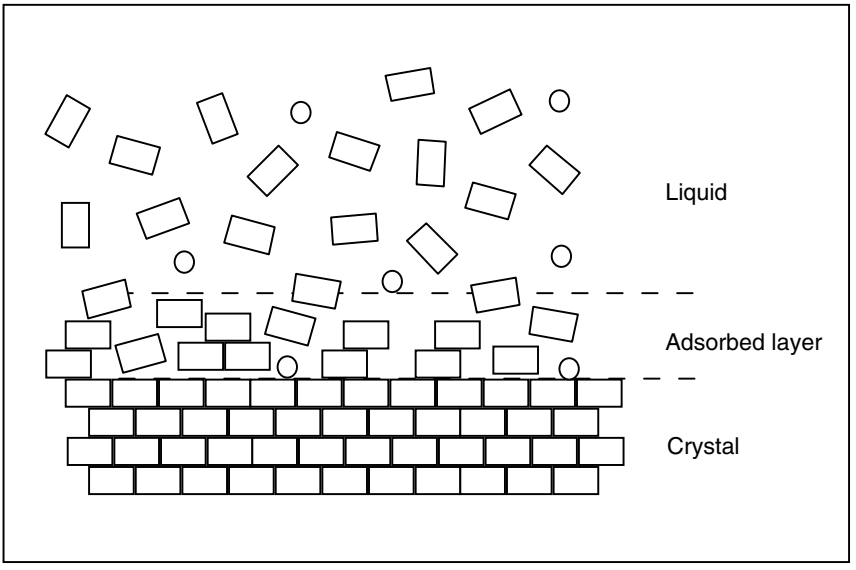

Figure 4.4. Schematic representation of a growing crystal surface. Rectangles represent growth units of crystallizing species and circles represent adsorbing impurity (from Hartel 2001 with permission).

$$\dot{m} = k_d\left(C_b - C_i\right) \tag{4.8}$$

where, $\dot{m}$ is mass flux of solute, and k_d is a mass transfer coefficient.

When mass transfer limits crystal growth, the interfacial concentration is often taken to be the saturation concentration, C_s, at the growth temperature and a linear growth rate G may be defined as

$$G = k_g\left(C_b - C_s\right) \tag{4.9}$$

where k_g is a growth rate constant that is actually a function of numerous operating parameters. It is influenced by temperature, agitation rate and impurities, among other factors. From Equation (4.9), mass transfer-limited growth rate typically has a linear dependence on supersaturation driving force based on the concentration difference.

When mass transfer is rapid, often the limiting mechanism for crystal growth is how fast the molecule becomes incorporated into the lattice. Typically, surface integration models also take into account the diffusion of molecules or growth units along the surface of the crystal prior to integration into the lattice. One model, called the birth and spread model, accounts for two-dimensional nucleation occuring on the growing crystal surface followed by spread of growth units to fill out the surface (Mullin 1993).

Another common surface incorporation model is based on regeneration of spiral dislocations in the lattice at the crystal surface. Such spirals have been clearly identified in many growing crystal systems and make an attractive incorporation site for growth units. The spiral growth model developed by Burton et al. (1951) predicts a second-order dependence of growth rate on supersaturation at low levels of supersaturation, but a linear dependence at higher supersaturations (Mullin 1993).

In systems with high latent heat of fusion, the amount of heat produced at the growing surface may be quite considerable. When sufficient heat is released during crystal growth to raise the temperature in the environment of the growing crystal to the equilibrium temperature, growth will cease. In this case, the rate at which heat is transported away from the growing crystal may limit how fast that face can grow. This is often found to be the limiting step for growth of ice.

Heat built up at a growing crystal surface can be dissipated either through the crystal itself (by conduction) or into the solution (by convection) or by some combination of the two mechanisms. In most food applications that involve freezing, it is likely that the majority of heat transfer is through the solution to the refrigerant. Thus, the convective heat transfer coefficient between the solution and crystal is usually the limiting factor for ice crystal growth. When fruits, vegetables, meats and other solid or solidlike foods are frozen, only natural convective transport removes the heat of fusion, meaning that the rate of heat transfer is generally tied to the thermal diffusivity of the material being frozen. Although thermal diffusivity generally increases due to ice formation, the main process parameters that influence crystal growth of ice during freezing of solid foods is the temperature difference with the

refrigerant, the surface area exposed to that refrigerant and the heat transfer mode between the food and the refrigerant.

4.2.3.1 Factors Affecting Crystal Growth

Crystal growth in many foods follows a similar pattern as that of nucleation, with the growth rate increasing as the driving force increases until molecular mobility limits the ability of molecules to form into the lattice. At low supersaturations (solution systems) or subcoolings (melt systems), crystal growth is slow, with the rate of growth increasing with increasing driving force. However, in glass-forming systems, limited molecular mobility at very high concentrations and/or very low temperatures results in a decrease in crystal growth rate. When the system surpasses the glass transition point, whether by reduction of water content or decrease in temperature, crystal growth is effectively stopped. In this case, crystals are surrounded by a glassy matrix that is stable for a very long time.

An increase in agitation rate (or velocity across the growing surface) results in an increase in growth rate, but only to a certain amount. Once any heat or mass transfer limitations to growth have been overcome through agitation, growth rate is controlled by the rate of surface incorporation. Any further increases in agitation do not lead to further increases in growth rate

The presence of the various components of a complex food can affect the speed of crystal growth in a manner similar to that seen in nucleation. Some components in a formulation may even be added as specific growth inhibitors. For example, certain bacteria are known to completely stop the growth of ice crystals, and these so-called ice-structuring bacteria are used to inhibit growth of ice crystals in frozen foods and desserts. The cell walls of these bacteria contain proteins that adsorb so tightly on the growing ice crystal surface that any further addition of water molecules is blocked, thereby stopping any further ice crystal growth.

4.2.4 Recrystallization

After crystals have formed and reached phase equilibrium with their surroundings, changes in the state of dispersion can still occur. These changes are generally called recrystallization, or sometimes ripening, although there are several different mechanisms that can drive these changes. The primary driving forces for recrystallization during storage are minimization of either surface or internal energy.

Changes in crystal dispersion due to surface effects are typically based on the Gibbs–Thomson equation (sometimes called the Ostwald–Freundlich equation), which describes the effects of particle size on equilibrium conditions (Hartel 2001). For solution systems, the equation is given as

$$\ln\left(\frac{C_r}{C_s}\right) = \frac{2(MW)\gamma}{\rho RTr} \tag{4.10}$$

and for melt systems, it is written as

$$\left(T_\infty - T_r\right) = \frac{2\gamma T_\infty}{\rho\left(\Delta H_f\right) r} \tag{4.11}$$

Here, C_r is the saturation concentration for a crystal of radius r; C_s is the saturation concentration for a large, flat crystal; MW is molecular weight crystallizing species; γ is interfacial tension at the crystal surface; ρ is crystal density; R is the ideal gas constant; T_∞ is the equilibrium melting temperature (for a large, flat crystal); and T_r is melting temperature for crystal of radius r.

Equations (4.10) and (4.11) show that the equilibrium condition, whether melting temperature or solubility concentration, changes with crystal size. Crystals that are very small, less than about a micron, have slightly lower solubility or melting temperature than larger crystals, and this difference, over extended storage times, is enough to cause changes in the particle dispersion.

Since small crystals are less stable than larger crystals, during extended storage, small crystals will disappear while larger crystals grow even larger, with no net change in the crystalline phase volume. This phenomenon is called Ostwald ripening, a thermodynamically driven change in the crystal size distribution simply due to the differences in equilibrium conditions for very small crystals. Even though the driving forces are quite small, less than 0.1°C for 1 μm ice crystals (Hartel 2001), over extended storage times, these differences can lead to large changes. However, Ostwald ripening by itself is probably not a major mechanism in recrystallization in most foods since storage conditions are rarely if ever constant.

Conditions during storage are critical to controlling recrystallization. Changes in temperature and/or moisture content lead to changes in crystalline microstructure, as the system attempts to follow the new equilibrium conditions. When temperature or moisture content increases, there is a decrease in the crystal phase volume as governed by the phase diagram. Crystals either melt or dissolve as a new equilibrium is approached at the new temperature and/or moisture content. When temperature or moisture content decreases, an increase in phase volume occurs for the same reason. Fluctuations in temperature and/or moisture content can cause significant changes in crystalline dispersion. If small crystals dissolve or melt completely away during a high-temperature cycle, for example, the entire mass of that crystal must reform onto another crystal when temperature cycles back down. In general, no new nuclei are formed during storage and the end result is a decrease in total numbers of crystals along with an increase in mean size. This melt–refreeze phenomenon is one of the most important in determining the shelf life of frozen desserts due to coarsening of the ice crystal size distribution.

4.3 Controlling Crystallization to Control Material Properties

Depending on conditions during processing and storage, a crystalline microstructure develops in many foods that can significantly impact food properties. Some important characteristics of the crystalline dispersion include the crystalline phase volume, mean size and size distribution of crystals, shape and surface characteristics of the particles, polymorphic characteristics, and any network structure that forms between

crystals. Furthermore, interactions between crystals and other structural elements (air cells, fat globules, etc.) may also impact food properties. These properties can be controlled through careful choice of formulation and process conditions.

4.3.1 Crystal Phase Volume

In a food product that contains a dispersed phase of crystalline material, the phase volume of crystals has a huge impact on material properties. Some foods are highly crystalline, such as chocolate and grained mints, whereas others have merely a few percent of crystalline phase volume. Given that everything about a system is the same, including parameters like the size of crystals and the nature of the continuous phase, a higher crystalline phase volume gives a harder material. This is easily seen, for example, in something like spreadable fats (de Man and de Man 2002). Butter, at refrigeration temperature, contains about 50% solid fat and is quite hard. Margarine, on the other hand, has much lower solid fat, 20–35% depending on the type of product, and is much softer (and more easily spread).

Another good example of where differences in phase volume lead to distinct difference in hardness of a product is fondant. This highly crystallized sugar confection owes its firmness to the large number of small sugar crystals, which are held together by a saturated sugar solution. Differences in phase volume are usually controlled by addition of crystallization inhibitors such as corn syrup and invert sugar. Although these products also impart some functional properties to the continuous phase, their main mode of action is to reduce the amount of crystalline sugar in the fondant. Thus, a fondant made with higher content of corn syrup or invert sugar has less crystalline sucrose and is softer.

Another good example of the effects of crystal phase volume on texture is in caramels. Caramels vary from completely ungrained to highly grained fudges. Ungrained caramels are extremely chewy, stretching widely when pulled between the fingers before breaking. However, a small amount of crystalline material (whether sucrose of lactose) gives a distinct “short” texture. A strand of caramel with perhaps 10% crystalline phase volume breaks almost immediately upon stretching because the sugar crystals break the strands of protein and carbohydrate. When crystalline phase volume reaches 30–40%, as found in some fudges, the product is almost crumbly.

To control the crystalline phase volume in a food, an understanding of the phase diagram is necessary. Ultimately, a food product will come to phase equilibrium either during processing or storage unless kinetic constraints are sufficient to maintain the product in a metastable state for its entire shelf life. If phase equilibration occurs, the product will lie along one of the equilibrium lines—freezing point depression curve in freezing or solubility curve in solute crystallization. In solution systems, the initial solute concentration and the solubility concentration at phase equilibrium can be used to calculate the amount of solute that crystallized.

4.3.2 Crystal Size Distribution

Crystalline phase volume by itself is generally not sufficient to determine material properties; some measure of the dispersion of that crystalline material is also needed. A product that contained all the mass in a few large crystals would have completely different material properties than the same product containing a dispersion of numerous small crystals. Hardness is related to the size of crystals in a system, with more numerous small crystals typically giving a harder product. The product with numerous small crystals has many more interparticle contacts under applied force than a product with the same crystalline phase volume but fewer larger crystals.

Furthermore, the crystal size distribution affects the viscosity of fluid dispersions. In this case, many small particles typically give higher viscosity and higher yield stress than a similar system with fewer larger crystals. The number of interparticle contacts during shearing would be significantly higher with numerous small crystals. For example, the number of submicron sugar crystals found in chocolate as a result of refining (particle breakdown) has a significant effect on chocolate viscosity. Small sugar crystals in melted chocolate are hydrophilic particles in liquid oil, so they tend to orient together. In a shear field, the small sugar crystals orient and aggregate, resulting in high viscosity. The function of lecithin as an emulsifier in chocolate is to coat the surface of the sugar crystals and allow them to flow more easily under shear. As little as 0.3% lecithin reduces chocolate viscosity equivalent to addition of 2–3% more cocoa butter.

Sensory properties are also influenced by particle size. Each crystalline material in a food has a critical threshold detection size, where above that critical size the particles are detected in the mouth and the food has a coarse texture. The critical threshold detection size depends on the properties of the crystals, namely, how rapidly they melt or dissolve in the mouth. Crystals that melt rapidly in a viscous carrier matrix, such as ice crystals in a frozen dessert, can be up to 50 μm in size before sensory detection. In contrast, crystals that are hard and dissolve slowly in the mouth, like lactose crystals in sandy ice cream, can be no larger than about 15 μm before they are detected. A fine chocolate will have the majority of particles smaller than 20 μm to avoid sensory coarseness.

To control crystal size distribution in a food containing crystalline material, it is necessary to control the relative rates of nucleation and growth during manufacturing. Controlling crystallization in fondant makes an especially good example (formation of ice crystals in ice cream is another excellent example of these principles). In fondant manufacture, a sugar syrup is concentrated quickly to the appropriate water content for the final product, after which it is cooled quickly to an optimal beating temperature. The optimal beating temperature in this case is the temperature where induction time is at a minimum and nucleation rate is at the optimum (Figure 4.3). This point falls somewhere between the solubility curve and the glass transition curve on the state diagram (Figure 4.2). The goal in fondant manufacture is to initiate nucleation all at once in the beating tube at high supersaturation. The intensive mechanical energy input in the beating tube promotes the maximal rate of nucleation over a very short time. Almost the entire supersaturation is relieved within minutes and primarily through nucleation with as little crystal growth as possible. In this way,

numerous small crystals are formed to provide the creamy texture desired in fondant. If nucleation were not as well controlled, the result would be larger crystals that that would lead to a coarser texture.

4.3.3 Shape and Surface Characteristics

The interface between crystals and the rest of the food matrix is another important concern in governing food properties. As noted in the previous section, the hydrophilic nature of sugar crystals in melted chocolate dramatically impacts fluid viscosity, as does the effect of modifying that interface through addition of an emulsifier.

The crystal shape may also impact material properties. The packing arrangement of particles in a food matrix depends to some extent on their size and shape. Furthermore, the distribution of forces applied to a food matrix depends on the arrangement of the particles within the structure. For example, spherical particles in a fluid shear field will roll across each other more easily than irregularly shaped particles, resulting in higher viscosity and yield stress for the system with irregularly shaped particles.

Sensory attributes of crystalline structures are also influenced by crystal shape. Compare the different textures of popsicles and ice cream, where the crystals have quite different shape. Ice crystals in ice cream are small (generally less than 50 μm), smooth, and disc-shaped, whereas in popsicles, ice crystals are long (over 300–400 μm) and irregular needle-shaped (Hartel 2001). The texture of these two products is quite different, primarily because of the differences in size and shape of the crystals.

4.3.4 Polymorphism

In foods containing crystalline lipids, control of polymorphism is important for making products with desirable material properties and shelf stability. Conditions during processing govern the polymorphic behavior of fat. The process of tempering of chocolate nicely demonstrates these principles.

Chocolate typically contains between 30% and 40% cocoa butter, about 75% of which is crystallized during chocolate solidification. However, it is imperative that the proper polymorph be formed during tempering to ensure the desired material properties of surface gloss, contraction from the mold, stability to recrystallization (bloom) and hardness or snap. Tempering of chocolate involves first cooling below the crystallization point of unstable polymorphs (which form more readily) and then raising the temperature to a point above the melting point of the less stable polymorph but still below the melting point of the desired polymorph. The result is a tempered chocolate containing a few percent crystalline seeds, with numerous small cocoa butter crystals in the desired polymorph. Under proper cooling conditions, these seeds catalyze crystallization of the rest of the cocoa butter mass into the proper polymorphic form to produce chocolate with the desired material properties.

4.3.5 Network Structures

In some foods, the crystalline microstructure forms networks between individual crystals. These network structures may also interact with other elements of the food matrix, including emulsion droplets and air cells. The nature and strength of these

network interactions may dominate the material properties of the food, affecting such textural characteristics as hardness, meltability and spreadability.

Although much has been written about fat crystal networks (Marangoni 2005), formation of interactive structures is also important in other foods as well. For example, during storage, particularly under conditions of temperature fluctuations, ice crystals in frozen desserts fuse together to form a network. This network of ice crystals changes the material properties of stored ice cream so that it no longer melts properly and has a distinctly different texture. As can be imagined, there is a difference in how applied forces are dispersed when individual ice crystals come into contact, compared to a network of ice crystals. This network structuring during long-term storage is one of the many indicators of the end of shelf life for these products.

4.4 Future Trends

From a materials science standpoint, several future developments stand out for controlling crystallization in foods. Control of crystalline structure formation provides enhanced control of food texture, shelf life and quality.

The complex nature of many foods has led to a largely empirical approach to controlling crystallization. Since foods are often composed of mixtures of components that impact phase behavior, the thermodynamic factors affecting crystallization of various components of foods are still often not understood very well. Further studies are needed to characterize the thermodynamic driving forces that govern crystallization. In other foods, for example, where crystallization occurs during storage from the amorphous state, the kinetic aspects that govern crystallization are not very well understood; further work is needed in these areas as well.

As crystallization proceeds during processing and/or storage, molecular organization at the nanoscale eventually leads to the microscopic (and sometimes macroscopic) structures that impact food texture. Further work to understand the effects of compositional and processing parameters on molecular structuring during crystallization would allow better control of food texture, shelf life and quality. Application of fundamental computer crystal modeling tools would be useful, although the complexity of most food systems has limited this approach up till now.

The next area of future development is microstructure analysis. Although numerous attempts have been made to connect crystal structure to food texture, a long road still remains ahead before it can be said that a certain type of structure leads definitively to certain mechanical properties. Development of methodologies for structure analysis and further developments in analytical modeling of crystalline microstructure are needed. Further, the connection between these microstructural models and food properties related to the crystalline microstructure are important.

Finally, the crystalline microstructure in many foods is not the only microstructural element of interest. Often crystal dispersions are found alongside other structures, such as air cells, fat globules, protein micelles, liquid crystals, and others. The interactions among these structural elements will be the focus of future studies in complex foods.

4.5 References

Burton, W.K., Cabrera, N., and Frank, N.C. (1951). The growth of crystals and the equilibrium structure of their surfaces. *Philos Trans R Soc Lond*, *A* 243, 299–358.

deMan, J.M. and deMan, L. (2002). Texture of fats. In: A.G. Marangoni and S.S. Narine (Eds.), *Physical Properties of Lipids*. Marcel Dekker, New York, pp. 191–217.

Garti, N. and Sato, K. (Eds.) (1988). *Crystallization and Polymorphism of Fats and Fatty Acids*, Marcel Dekker, New York.

Garti, N. and Sato, K. (Eds.) (2001). *Crystallization Processes in Fats and Lipid Systems*. Marcel Dekker, New York.

Hartel, R.W. (2001). *Crystallization in Foods*. Aspen, New York.

Levenson, D. and Hartel, R.W. (2005), Nucleation of amorphous sucrose–corn syrup mixtures, *J Food Eng* 69, 9–15.

Marangoni, A.G. (2005). *Fat Crystal Networks*. Marcel Dekker, New York.

Mathlouthi, M. and Reiser P. (Eds.) (1995). *Sucrose: Properties and Applications*. Blackie, London.

Mullin, J.W. (1993). *Crystallization*. 3rd Ed. Butterworth-Heinemann, Oxford.

Slade, L. and Levine, H. (1991). Beyond water activity: recent advances based on an alternative approach to the assessment of food quality and safety. *Crit Rev Food Sci Nutr* 30, 115–360.

Timms, R.E. (2003). *Confectionery Fats Handbook*. The Oily Press, Bridgewater, England.

Turnbull, D. and Fisher, J.C. (1949). Rate of nucleation in condensed systems. *J Chem Phys* 17(1): 71–73.

Van Hook, A. and Frulla, F. (1952). Nucleation in sucrose solutions. *Ind Eng Chem* 44, 1305–1308.

Wesdorp, L.H., van Meeteren, J.A., de Jong, S., v.d. Giessen, R., Overbosch, P., Grootscholten, P.A.M., Struik, M., Royers, E., Don, A., de Loos, T., Peters, C., and Gandasasmita, I. (2005). Liquid-multiple solid phase equilibria in fats: Theory and experiments. In: A.G. Marangoni (Ed), *Fat Crystal Networks*. Marcel Dekker, New York, pp. 481–709.

Williams, M.L., Landel, R.F., and Ferry, J.D. (1955). The temperature dependence of relaxation mechanisms in the liquid and glassy states. *J Am Chem Soc* 77, 3701–3707.

Chapter 5

The Glassy State

Yrjö H. Roos

University College Cork, Department of Food and Nutritional Sciences, Cork, Ireland, yrjo.roos@ucc.ie

5.1 Introduction

The physical state of materials is often defined by their thermodynamic properties and equilibrium. Simple one-component systems may exist as crystalline solids, liquids or gases, and these equilibrium states are controlled by pressure and temperature. In most food and other biological systems, water content is high and the physical state of water often defines whether the systems are frozen or liquid. In food materials science and characterization of food systems, it is essential to understand the physical state of food solids and their interactions with water. Equilibrium states are not typical of foods, and food systems need to be understood as nonequilibrium systems with time-dependent characteristics.

The glassy state of materials refers to a nonequilibrium, solid state, such as is typical of inorganic glasses, synthetic noncrystalline polymers and food components. Characteristics of the glassy state include transparency, solid appearance and brittleness (White and Cakebread 1966; Sperling 1992). In such systems, molecules have no ordered structure and the volume of the system is larger than that of crystalline systems with the same composition. These systems are often referred to as amorphous (i.e., disordered) solids (e.g., glass) or supercooled liquids (e.g., rubber, leather, syrup) (Slade and Levine 1991; Roos 1995; Slade and Levine 1995).

Understanding the physical state of food materials requires that food composition and properties of individual food components and their interactions with each other are well known. The physical characterization of a food system needs to consider all components within the system, the molecular environment of the components and all micro- and nanostructural aspects of factors contributing to the properties of the material. The first studies referring to glass formation by food components were those on dairy powders (Supplee 1926) and glucose (Parks and Thomas 1934). These

and later studies have recognized that sugars form solid, noncrystalline structures (glasses) and that the noncrystalline properties of lactose in dairy powders and ice cream are often responsible for dramatic changes in quality.

These examples showed that solid, dehydrated food systems as well as frozen systems contain noncrystalline (i.e., amorphous) components, and the physical state of the components control product stability. For example, water can be removed from milk by dehydration or freezing. The process may retain component molecules in a disordered manner retained from a dissolved or dispersed state in milk. The solvent water is removed from the system in dehydration and subsequently dissolved components (e.g., lactose, hydrophilic components) form a solid, continuous phase of the dehydrated, glassy material with dispersed particles (e.g., protein aggregates, fat globules). The physical appearance of the material is solid or a free-flowing powder composed of individual, solid particles. The characterization of this solid state needs to consider the colloid structure of milk and changes resulting from water removal at a molecular and individual component level. Macroscopic observation of the material suggests that dehydration leads to glass formation but a systematic material science approach is required for full characterization of the glass formation and its properties, including stability of these glassy, dehydrated food system.

Carbohydrates and proteins are typical hydrophilic components of concentrated food systems. These components tend to form amorphous, noncrystalline structures at low water contents (White et al. 1966; Slade et al. 1991; Roos 1995). Well-known food processes resulting in glass formation by amorphous or partially amorphous food components include baking, extrusion, dehydration and freezing (Roos 1995). In these processes, removal of water as part of the manufacturing process results in the formation of a noncrystalline, amorphous state, which is extremely sensitive to water and may show various time-dependent changes causing loss of quality and reduced shelf life.

When their thermal, mechanical and dielectric behaviour is studied, amorphous food systems exhibit relaxations and transformations typical of noncrystalline synthetic polymers (Sperling 1992; Roos, 1995; Roudaut et al. 2004). The most important property of amorphous materials is their glass transition and relaxations associated with increased molecular mobility in the vicinity of the glass transition. The glass transition describes a temperature range over which a change of a solid glass to a softened material with the concomitant appearance of vibrational and translational mobility of component molecules takes place. Hence, various thermal analytical techniques are crucial in obtaining information of glass transitions and their related transformations in food systems.

There are several glass transition-related changes in foods that affect their properties and stability. These include stickiness and caking of powders and sugar containing products, collapse in freeze-drying and collapse of dehydrated structures, crispness of snack foods and breakfast cereals, crystallization of amorphous sugars, recrystallization of gelatinised starch, ice formation and recrystallization in frozen foods and to some extent nonenzymatic browning and enzymatic reactions (Roos 1995; Slade et al. 1995; Roudaut et al. 2004)). The state transitions and properties of amorphous food systems are discussed in the present chapter.

5.2 Glass transition

5.2.1 Thermodynamic Considerations

Phase transitions indicate changes in the equilibrium state of materials and can be described and classified according to changes in thermodynamic properties resulting in a change in phase (Roos 1995). The main requirement for any phase to coexist with another phase is that the Gibbs energy of two or more phases at the transition pressure and temperature is the same. Classification of phase transitions define first-order transitions as those at which the first derivatives of the thermodynamic functions suffer discontinuity, that is, at a first-order transition temperature there is a discontinuity in heat capacity and thermal expansion coefficient (Roos 1995). Such discontinuity occurs in melting/crystallization and boiling/condensation temperatures. A second-order phase transition shows a step change in properties, that is, the material exhibits a change in heat capacity and thermal expansion coefficient at the second-order transition pressure and temperature.

The classification of phase transitions into first-, second- and higher-order transitions is important in thermodynamic characterization of highly supercooled liquids (where the material temperature is well below its equilibrium melting temperature) and noncrystalline solids. These materials are amorphous as they exhibit no definite molecular order, and they also have a thermodynamic driving force towards the equilibrium crystalline state. Hence, such materials exist in a nonequilibrium state and their properties cannot be described with thermodynamic terms assuming equilibrium. It is well known that a glass transition (i.e., the solid–liquid transformation of an amorphous, noncrystalline material) involves a step change in heat capacity and, therefore, is often referred to as a transition with some characteristics of a second-order phase transition (Roos 1995). Because glass transitions occur in a nonequilibrium system, they do not involve a change in phase but a change in state of an amorphous material. It should be emphasized that the amorphous state is a nonequilibrium state and its properties are time-dependent. For example, molecules within an amorphous state can have an infinite number of arrangements and any observed arrangement occurs only at the time of observation. Hence, changes in amorphous materials can be observed as a function of time and the rate of change is likely to depend on the rates of molecular relaxations and diffusion.

Supercooled liquids and solids can be formed by a number of routes, such as quench cooling of a liquid (melt), rapid condensation of vapor, rapid removal of solvent from solution and removal of crystallized solvent (Slade et al. 1991; Roos and Karel 1991a; Sperling 1992). Depending on the rate of solvent (water) removal or cooling into the solid state, glasses with different characteristics can be obtained. Reorganization of molecular arrangements and relaxations in heating over the glass transition coincides with development of rapid translational mobility in supercooled systems.

5.2.2 Glass Transition and Relaxations

The glass transition is a change in state associated with a considerable change in molecular mobility and relaxation times in amorphous systems. The glass transition is also a solid–liquid transformation as translational mobility of molecules appears and molecules frozen in a solid, glassy system begin to move, resulting in flow (Sperling 1992). Molecular mobility is time-dependent, and no exact glass transition temperatures can be measured or defined. Observed changes in heat capacity, which are characteristic of a glass transition, occur over a temperature range. The glass transition temperature is often taken from the onset temperature of the glass transition temperature range (onset T_g) or as a temperature corresponding to a 50% change in heat capacity occurring over the transition (midpoint T_g) in a differential scanning calorimetric (DSC) measurement (Figure 5.1).

The glass transition is a property of concentrated, amorphous, nonequilibrium food solids which may be present in low-moisture, dehydrated or frozen foods in which a concentrated solute phase is noncrystalline. Pure food components, such as amorphous sugars, often show a single, clear glass transition that can be observed using dielectric, mechanical and thermal analytical or various spectroscopic techniques (Kalichevsky et al. 1992; Söderholm et al. 1999; Talja and Roos 2001; Ludescher et al. 2001; Roudaut et al. 2004). These techniques may observe the change in heat capacity associated with a glass transition; or the increased heat capacity required by the supercooled liquid when heated to temperatures above the glass transition (DSC); or changes in molecular mobility resulting in dielectric or mechanical relaxations. The temperature range of glass transitions, the changes around glass transitions and material properties above the glass transition are all highly dependent on food composition and molecular weight of component compounds. Low molecular weight components, for example, water and simple sugars,

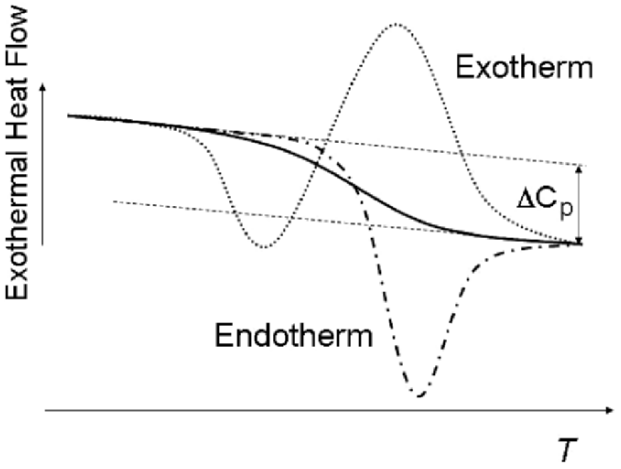

Figure 5.1. Schematic representation of typical differential scanning calorimetry curves showing a glass transition and possible exothermal and endothermal relaxations.

show a glass transition over a relatively narrow temperature range followed by very rapidly increasing flow above it (Roos 1993). High molecular weight food components, such as proteins and starch, as well as heterogeneous food systems, show a glass transition over a broad temperature range and slowly developing plasticization above the glass transition (Roos 1995; Roudaut et al. 2004).

The glass transition of systems with two or more components depends on component properties and their miscibility. Solvents, such as water in foods, often have a low molecular weight and they are fully miscible with their glass-forming solutes. The glass transition temperature of a solute is highly dependent on the presence and concentration of solvents. Even very small amounts of solvent may substantially decrease the observed glass transition temperature. It has been found that an increasing amount of water decreases both the glass transition temperature and its temperature range and increases the change in heat capacity of the transition (Roos and Karel 1991b). Other mixtures of miscible components, for example, sugars, also show composition-dependent glass transition temperatures, and they are often substantially affected by the lower molecular weight components (Roos 1995; Bhandari and Roos 2003). In food systems, several components (e.g., starch, proteins) can exist in partially amorphous states and many of them exhibit only partial miscibility or remain immiscible, forming single or several phases within food microstructure (Kalichevsky and Blanshard 1993; Vega et al. 2005).

The glass transition occurs in both cooling and heating and also during removal or sorption of water. As a state transition and because of the nonquilibrium nature of the amorphous state, the glass transition is time-dependent and may have varying temperature values at different experimental time scales (e.g., frequency). Furthermore, depending on the rate of glass formation and possible changes with time in the glassy state (ageing), various relaxations may be associated with an observed glass transition (Figure 5.1).

5.2.3 Methodology

Changes in physical state may be observed from changes in thermodynamic quantities, which can be measured by calorimetric techniques, dilatometry, and thermal analysis. Spectroscopic methods are also available for the determination of changes in molecular mobility around transition temperatures. In addition to the changes in thermodynamic quantities and molecular mobility, a glass transition has significant effects on mechanical and dielectric properties.

Natural food systems are complex mixtures of carbohydrates, proteins, lipids, a variety of minor components and water. Traditionally, differential thermal analysis (DTA) and differential scanning calorimetry (DSC) are the most common techniques for determination of glass transitions in inorganic, organic, polymeric and food materials. DTA measures the temperature of a sample and a reference in a dynamic heating or cooling process. DSC uses the same principle, but the temperature difference between the sample and the reference is used to derive the difference in the energy supplied. An alternating/modulated/oscillating DSC uses a varying-temperature programme during heating and cooling of samples. First-order phase transitions produce peaks, while a step change in heat flow occurs at second-order transitions. Hence,

the glass transition of amorphous systems can be detected from the heat capacity change occurring over the glass transition temperature range (Figure 5.1).

Dynamic mechanical analysis (DMA/DMTA) and dielectric analysis (DEA/DETA) together with (DSC) are the most common thermal analytical methods in the characterisation of amorphous food systems (Kalichevsky et al. 1992; Talja and Roos, 2001; Roudaut et al. 2004). In general, amorphous structures are fairly stable in the solid, glassy state (Sperling 1992; Slade and Levine 1995). At temperatures around and above the transition, the solid state is transformed to a supercooled liquid state with more rapid time-dependent flow (White et al. 1966; Roos 1995; Roudaut et al. 2004). This change in mechanical properties is observed by DMA and detected as a change in the complex moduli of the material. These changes are referred to as alpha relaxations, which also appear as analogous changes in dielectric properties in a DEA analysis (Figure 5.2). For example, dehydrated, glassy foods have a solid and brittle behavior while the materials may flow or become soggy above the glass transition (e.g., freeze-dried foods). This change is associated with a decreasing modulus appearing in a DMA analysis.

Mechanical and dielectric properties detect glass transition in foods by their sensitivity to relaxations and changes in modulus and dielectric properties (Kalichevsky et al. 1992; Sperling 1992; Roos and Talja 2001). The transitions are observed from storage modulus, E' or G', loss modulus, E'' or G'', dielectric constant, ε', dielectric loss constant, ε, and mechanical and dielectric loss, tan d. The observed relaxation temperatures are highly dependent on the frequency, f, of the applied stress or voltage, which clearly indicate the time-dependent character of material response to disturbance. Arrhenius plots showing log f against $1/T$ for alpha relaxations of food polymers have suggested that the apparent activation energy is 200 to 400 kJ/mol

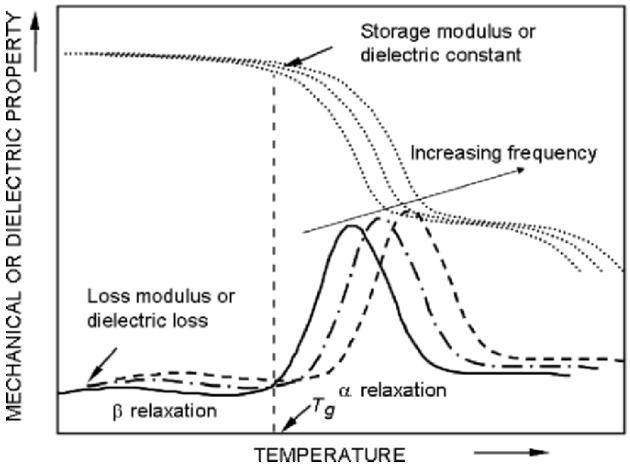

Figure 5.2. A schematic representation of typical alpha and beta relaxations observed from mechanical and dielectric properties. The observed relaxation temperatures increase with increasing frequency.

(Kalichevsky et al. 1993). The loss modulus and tan *d* show a pronounced peak at the transition temperature.

DMA and mechanical spectroscopy have been applied in the analysis polysaccharides (Kalichevsky et al. 1993), proteins (Kokini et al. 1994), sugars (Roos et al. 1991b) and frozen dough (Laaksonen). In DEA measurements, the dielectric constant, ε', dielectric loss constant, ε'', and tan δ can be detected by placing a sample between parallel plate capacitors and alternating the electrical field. Polar groups in the sample respond to the alternating electrical field and an absorption maximum is obtained at the frequency that is correlated with molecular motions. DEA has been used in the analysis of some food-related materials, such as amorphous sugars and polyols (Noel et al. 1992; Talja and Roos 2000), amylopectin (Kalichevsky et al. 1992) and frozen dough (Laaksonen et al. 2002). A number of researchers have used frequences around 1 Hz in DMA and DEA measurements. However, it appears that frequencies showing relaxations at calorimetric glass transition temperatures appear at much lower frequencies (Talja et al. 2001).

Spectroscopic methods, such as FT-infrared (FTIR) and Raman spectroscopy detect changes in molecular vibrational characteristics in noncrystalline solid and supercooled liquid states. Various nuclear magnetic resonance (NMR) techniques and electron spin resonance (ESR) spectroscopy, however, are more commonly used, detecting transition-related changes in molecular rotation and diffusion (Champion et al. 2000). These methods have been used for studies of the amorphous state of a number of sugars in dehydrated and freeze-concentrated systems (Roudaut et al. 2004).

5.3 Water Plasticization

Water plasticization refers to the presence and interaction of water molecules within food solids resulting in changes in amorphous structure and depression of the glass transition to a lower temperature. Water has a primary interaction with carbohydrate and protein, while lipids are relatively little affected by water, that is, the latter components exist in separate phases and show little interactions with hydrophilic components and functional groups of food polymers (Roos 1995). However, glass-forming food components can be of great importance in encapsulation of dispersed phases in food colloids (Vega and Roos 2006). Examples of such systems include solid dispersions obtained by dehydration of emulsions, including milk, and extrusion, which are typical processes in production of food ingredients and flavorings.

5.3.1 Water Plasticization of Food Components

The glass transition in food systems is a property of noncrystalline, amorphous solids and occurs at about 100–150°C below their equilibrium melting temperature (Figure 5.3). This behaviour is typical of glass-forming synthetic polymers and it seems to apply to most mono- and disaccharides (Roos 1993). Experimental data of melting properties of proteins are not available, but it is likely that a similar extent of supercooling is a requirement for formation of a solid structure in general. In fully amorphous carbohydrates and proteins, water acts as a plasticizer and solvent, that is, the free volume of the materials increases with increasing water content resulting in

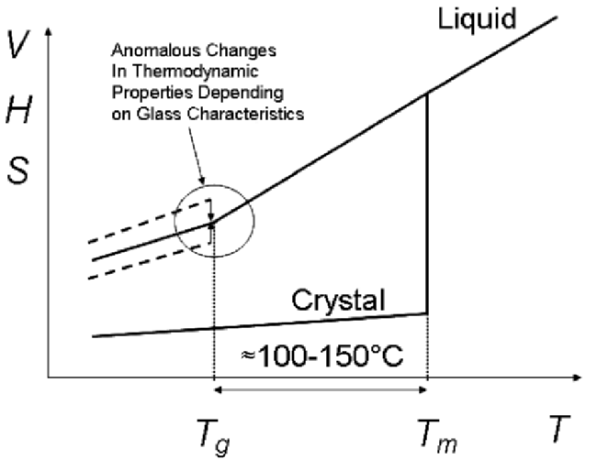

Figure 5.3. Changes in volume, *V*, enthalpy, *H*, and entropy, *S*, around glass transition and melting. Amorphous materials can have an infinite number of "glassy states" which result in relaxations around glass transition.

enhanced molecular mobility and a concomitant decrease in the glass transition temperature. Therefore, changes in properties of amorphous food systems may result either from a glass transition occurring because of increasing temperature (i.e., thermal plasticization) or increasing water content (i.e., water plasticization) or both.

The transition temperatures of carbohydrates and proteins are significantly affected by water. It is often reported that an increase in water content results in a substantial decrease in transition temperatures (Slade and Levine 1995). For example, the glass transition of dehydrated food solids decreases as a result of water sorption (i.e., water uptake from its surroundings) and their properties may change from those of the glassy solid to viscous liquids or syrup (e.g., sugar systems) or leathery material (e.g., protein systems) in an isothermal process.

The glass transition of amorphous sugars occurs over a temperature range of 10–20°C while the glass transition of food polymers may extend over a temperature range of more than 50°C (Hoseney et al. 1986; Roos 1995; Roudaut 2004). The change in heat capacity (ΔC_p) of sugar glasses around their glass transition is around 0.5–1.0 J/g°C while the ΔC_p of proteins and starch occurs over a broad temperature and is only measurable with a relatively large level of water plasticization (Roos 1995). There is a possibility that single foods exhibit numerous glass transitions depending on composition and extent of phase separation (i.e., miscibility). Some anhydrous food components have glass transitions below room temperature and many polymeric food components above 200°C, close to their decomposition temperatures. Multiple glass transitions, however, have not been routinely measured for foods probably because of decomposition of polymers, broad transitions and lack of sensitivity of measurements. A common problem in observing glass transitions in food systems at intermediate water contents is that liquid–crystalline transitions of lipids often overlap the glass transition of hydrophilic food solids.

5.3.2 Frozen Systems

Freezing of water in food systems occurs at temperatures below the equilibrium melting temperature of water, T_m. The equilibrium melting temperature refers to the temperature where last ice crystals melt during heating of a frozen material and it is dependent on dissolved food components and their concentration. Below T_m, freezing of water may continue until a maximum amount of ice has formed (Roos and Karel 1991c; Roos 1995). Eutectic behavior of solutes in foods is not common and ice formation ceases at solute-dependent temperatures as a result of increasing viscosity and vitrification of solutes with some unfrozen water (Slade and Levine 1991; Roos et al. 1991c).

A maximally freeze-concentrated system shows an initial solute concentration independent glass transition temperature, T'_g with an onset of ice melting during heating at an initial concentration independent temperature, T'_m. This behavior has been well established for a number of common sugars and carbohydrates (Goff 1995; Roos 1995; Slade and Levine 1995). Typically, the solute concentration of a glassy unfrozen solute phase dispersing the maximum amount of ice formed in a frozen system is around 80% (w/w) (Slade et al. 1991; Roos 1993; Talja et al. 2001). These transitions can be described by state diagrams (Figure 5.4).

Phase and state transitions of maximally freeze-concentrated materials are complex. However, the same thermal analytical techniques as well as ESR and NMR techniques provide information of transitions of freeze-concentrated solids and ice melting (Slade et al. 1995; Roos, 1995; Laaksonen et al. 2002; Roudaut et al. 2004). Low molecular weight components, such as sugars, often exhibit clearly observable

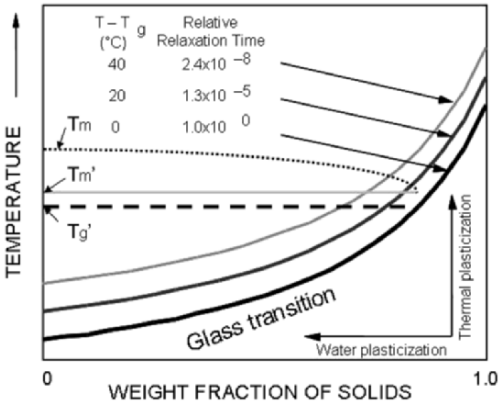

Figure 5.4. A schematic state diagram showing water plasticization at increasing water weight fraction towards glass transition of water at –135°C. Relaxation times decrease rapidly above the glass transition as a result of thermal or water plasticization. Maximally freeze-concentrated solutes show glass transition at T_g' and onset of ice melting at T_m'. Equilibrium melting is described by the T_m curve.

and separate transitions (Roos et al. 1991b,c). In DSC measurements, the glass transition temperature of the maximally freeze-concentrate solute, T_g', can be taken from the onset temperature of the transition temperature range but no midpoint or endpoint can be defined as ice melting often occurs before completion of the transition (Roos 1995; Roos 2002). Melting of ice gives a relatively sharp endothermic peak and its onset temperature can be taken as the onset of ice melting, T_m', for ice within the maximally freeze-concentrated system (Roos et al. 1991c). Freezing to this maximally freeze-concentrated state requires substantial thermal treatment (i.e., annealing) at a temperature favoring maximum ice formation (Roos et al. 1991c; Singh and Roos 2005).

5.3.3 State Diagrams

A state diagram can be derived from phase and state transition data to describe material states at various temperatures and levels of water plasticization (Roos et al. 1991a). A typical state diagram shows the glass transition temperature against water content with T_g', T_m' and T_m data (Figure 5.5). The effect of water on the glass transition can be predicted, for example, using the Gordon–Taylor equation (Roos 1995). We have combined water sorption and glass transition data to establish diagrams showing critical values for water content and water activity that correspond to glass transition at storage temperatures (Figure 5.6). Such diagrams can be established using, for example, the Gordon–Taylor equation to model water plasticization and the Guggenheim–Anderson–De Boer (GAB) equation to model water sorption (Roos 1995). The critical water content and water activity diagrams together with State Diagrams are important tools in explaining changes in time-dependent mechanical and flow properties which are related to glass transition and water plasticisation (Slade et al. 1991; Kokini et al. 1994; Roos 1995; Rahman 2006).

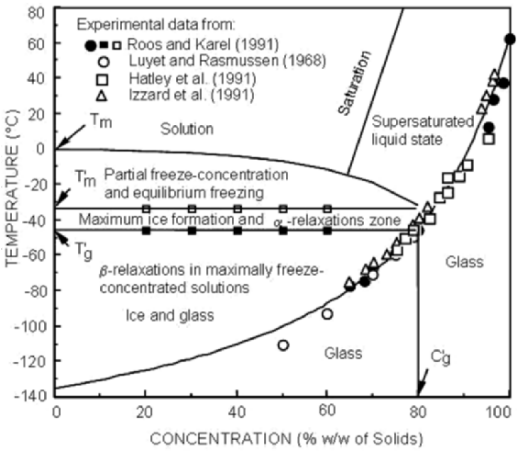

Figure 5.5. State diagram of sucrose with typical experimental data at high concentrations and in the maximally freeze-concentrated state. Dynamic mechanical and dielectric measurements show glass transition–related relaxations.

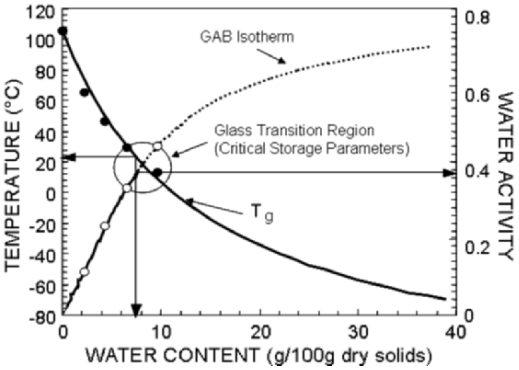

Figure 5.6. Water plasticization and sorption behavior typical of dairy powder showing critical water content and water activity resulting in glass transition at a typical room temperature.

5.4 Glass Formation in Food Systems

Glass formation in food systems is based on solidification of hydrophilic components with some water. Rapid cooling of concentrated sugar melts and plasticized mixtures of carbohydrate polymers and proteins are typical of candy and confectionery manufacturing and extrusion, respectively (White et al. 1966; Slade et al. 1991; Roos 1995). Freeze-drying is a process used to remove crystallized solvent from a maximally freeze-concentrated material and spray drying is an example of rapid removal of solvent and resultant vitrification of solutes (Roos 2004). These processes will be discussed as examples of glass formation in food manufacturing processes.

5.4.1 Concentrated and Extruded Systems

Evaporation of water leads to formation of highly concentrated systems that can be cooled to form a glassy structure, such as hard sugar candies (White et al. 1966). Such melt processing of foods often requires the presence of water as a plasticizer. The presence of water allows the use of lower processing temperatures and enhances formation of a homogeneous, viscous mass. This is also typical of extrusion which, at a high pressure and temperature, favors gelatinization of starch (Roos et al. 1996).

The physical state of starch during extrusion can be considered to change from a partially crystalline polymer to a polymer melt which is homogenized by shear. Extrusion may also decrease the molecular size of starch components, which is observed from decreased melt viscosity (Lai and Kokini 1991), and obviously a decreased molecular size results in a decreased glass transition temperature of the extrudate. The dramatic decrease of pressure that occurs as a viscous, plasticized melt exits the die may allow an extremely rapid loss of water, expansion of the melt and cooling to an amorphous solid state.

Rheological properties of melts and the structures of extruded foods are affected by several factors and particularly by processing and storage pressure and temperature. Rheological properties of the resultant glassy materials are in large part governed by

the molecular weight and the extent of thermal and water plasticization. One of the main desired characteristics of extruded snacks and breakfast cereals is a crispy texture. These properties are typical of glassy materials and crispness may be considered to be a property of glassy membranes produced in expansion at the die as the extruded, plasticized melt expands and cools rapidly (Roos 1995).

5.4.2 Frozen and Freeze-Dried Systems

The freezing step in freeze-drying is extremely important in defining ice crystal size and the extent of ice formation. Ice crystal size depends mainly on nucleation, although material properties often have an effect on ice crystal formation at various freezing conditions, and particularly on ice recrystallization during storage (Slade et al. 1991; Goff 1995; Roos 1995). The extent of freezing at given conditions is significantly affected by the nature of solids and dissolved substances, but some water in food systems always remains unfrozen (Slade et al. 1991; Roos et al. 1991c; Roos, 1995; Singh et al. 2005).

The T'_g and T'_m temperatures of biological materials are extremely important determinants of appropriate operation parameters in freeze-drying (Roos 2004). Freeze-drying requires that dissolved substances are freeze-concentrated to an almost solid state and that the highly viscous state is retained throughout the dehydration process, that is, the material should consist of solid ice and a freeze-concentrated, solid, glassy, unfrozen phase. Ice melting above T'_m has a dramatic plasticization effect in a freeze-concentrated system and results in flow. Accordingly, the highest allowable pressure (or ice temperature) in freeze-drying is defined by the initial melting temperature of ice in the system. At conditions allowing melting, flow may occur and some dehydration occurs from the liquid state and the process no longer can be referred to as freeze-drying.

Collapse in freeze-drying occurs above a critical temperature, which allows viscous flow of freeze-concentrated amorphous solutes (Bellows and King 1973) as they are plasticized by unfrozen water (Roos 2004). The onset temperature of ice melting, T'_m, can be used as a critical reference temperature for production of properly freeze-dried materials.

5.4.3 Spray Dried Systems

Spray drying is an efficient dehydration method for a large variety of liquid materials and slurries that can be converted to small liquid droplets using rotating discs or pressure nozzle atomizers. The tiny droplets can be dehydrated in hot air within seconds, which allows continuous production of free-flowing powders. Although, the principle of the process is relatively simple, phase and state transitions of food solids have a significant impact on whether the materials can be spray dried successfully or if the powders have free-flowing properties in handling, packaging stages, storage and use. Studies of Bhandari (Bhandari and Howes, 1999) have suggested that formation of the glassy state of carbohydrates has a correlation with spray drying behavior of sugars and fruit juices.

Several sugar-containing materials, such as fruit juices, are extremely difficult to dehydrate as the solids stick on drier surfaces and cake inside processing equipment. Stickiness is probably the most important property in establishing criteria for the suitability of food materials to spray drying. Studies of glass transitions of dehydrated sugars and high-sugar products have confirmed that stickiness is related to the glass transition of amorphous powders (Roos and Karel 1990). Based on the knowledge of phase and state transitions in dehydration of liquids with dissolved substances, it may be assumed that the rapid removal of water causes vitrification of the liquid droplets within a short time and formation of a solid particle surface (Roos 2004). Glass transition of solids at the surface is a key parameter in defining stickiness of the particles and formation of liquid bridges as a result of rapid decrease in surface viscosity above the glass transition. Materials with an anhydrous glass transition below room temperature cannot be spray dried.

Roos and Karel (1991d) showed that glass transitions of mixtures of sucrose and maltodextrins were a function of the molecular weight and DE of the maltodextrins. The results suggested that large amounts of low DE maltodextrins need to be mixed to carbohydrate materials with low glass transition temperatures to improve their dehydration characteristics. It is obvious that materials with low glass transition temperatures, such as solutions of monosaccharides and fruit juices, cannot be successfully dehydrated by spray drying due to their low glass transition temperatures and particle stickiness (Roos 2004). The glass transition temperature of some sugar-containing products, however, can be increased by adding miscible components, such as higher glass transition maltodextrins. Such materials improve dehydration properties and storage stability of powders.

5.5 Future Trends

The amorphous state of food components and its impact on properties of foods at low water contents and in frozen systems has been well documented. Thermal analytical and spectroscopic techniques have become available to characterize food components and relate observed transitions to food properties and stability. There is a continuing need to measure and understand state transitions of mixtures of food components as well as their miscibility and functions in dispersions and other colloid systems. A number of carbohydrate–protein systems are responsible for structure formation and protection of sensitive functional food components. New techniques and detailed knowledge will be needed to manipulate food characteristics to improve sensory properties and overall quality, particularly those of dehydrated and frozen foods. The same approach may be taken to improve production and availability of new food ingredients with enhanced functional properties and storage stability. Understanding of the glassy state and state transition behavior of such food systems is one of the key aspects of future developments in food engineering and technology. Their relevance is ubiquitous in many food processes and product systems. Frequent reference was made throughout this volume (see for example Chapters 7, 10, 14, 16, 18, 20 and 24).

5.6 References

Bellows, R.J. and King, C.J. (1973). Product collapse during freeze drying of liquid foods. *AIChE Symp. Ser.*, 69(132), 33–41.

Bhandari, B.R. and Howes, T. (1999). Implication of glass transition for the drying and stability of dried foods. *J. Food Eng.*, 40, 71–79.

Bhandari, B.R. and Roos, Y.H. (2003). Dissolution of sucrose crystals in the anhydrous sorbitol melt. *Carbohydr. Res.*, 338, 361–367.

Champion, D., Le Meste, M., and Simatos, D. (2000). Towards an improved understanding of glass transition and relaxations in foods: molecular mobility in the glass transition range. *Trends Food Sci. Technol.*, 11, 41–55.

Goff, H.D. (1995). The use of thermal analysis in the development of a better understanding of frozen food stability. *Pure Appl. Chem.*, 67, 1801–1808.

Hoseney, R.C., Zeleznak, K., and Lai, C.S. (1986). Wheat gluten: A glassy polymer. *Cereal Chem.*, 63, 285–286.

Kalichevsky, M.T. and Blanshard, J.M.V. (1993). The effect of fructose and water on the glass transition of amylopectin. *Carbohydr. Polym.*, 20, 107–113.

Kalichevsky, M.T., Jaroszkiewicz, E.M., Ablett, S., Blanshard, J.M.V., and Lillford, P.J. (1992). The glass transition of amylopectin measured by DSC, DMTA and NMR. *Carbohydr. Polym.*, 18, 77–88.

Kokini, J.L., Cocero, A.M., Madeka, H., and de Graaf, E. (1994). The development of state diagrams for cereal proteins. *Trends Food Sci. Technol.*, 5, 281–288.

Laaksonen, T.J., Kuuva, T., Jouppila, K., and Roos, Y.H. (2002). Effects of arabinoxylans on thermal behavior of frozen wheat doughs as measured by DSC, DMA, and DEA. *J. Food Sci.*, 67, 223–230.

Lai, L.S. and Kokini, J.L. (1991). Physicochemical changes and rheological properties of starch during extrusion. *Biotechnol. Prog.*, 7, 251–266.

Ludescher, R.D., Shah, N.K., McCaul, C.P., and Simon, K.V. (2001). Beyond Tg: optical luminescence measurements of molecular mobility in amorphous solid foods. *Food Hydrocolloids*, 15, 331–339.

Parks, G.S. and Thomas, S.B. (1934). The heat capacities of crystalline, glassy and undercooled liquid glucose. *J. Am. Chem. Soc.*, 56, 1423.

Rahman, M.S. (2006). State diagram of foods: Its potential use in food processing and product stability. *Trends Food Sci. Technol.*, 17, 129–141.

Roos, Y. (1993). Melting and glass transitions of low molecular weight carbohydrates. *Carbohydr. Res.*, 238, 39–48.

Roos, Y.H. (1995). *Phase Transitions in Foods*. Academic Press, San Diego.

Roos, Y.H. (2002). Thermal analysis, state transitions and food quality. *J. Thermal Anal. Calor.*, 71, 197–203.

Roos, Y.H. (2004). Phase and state transitions in dehydration of biomaterials and foods. In: A.S. Mujumdar (Ed.), *Dehydration of Products of Biological Origin*, Science Publishers, Enfield, pp. 3–22.

Roos, Y. and Karel, M. (1990). Differential scanning calorimetry study of phase transitions affecting the quality of dehydrated materials. *Biotechnol. Progr.*, 6, 159–163.

Roos, Y. and Karel, M. (1991a). Applying state diagrams to food processing and development. *Food Technol.*, 45, 66, 68–71, 107.

Roos, Y. and Karel, M. (1991b). Nonequilibrium ice formation in carbohydrate solutions. *Cryo-Letters*, 12, 367–376.

Roos, Y. and Karel, M. (1991c). Amorphous state and delayed ice formation in sucrose solutions. *Int. J. Food Sci. Technol.*, 26, 553–566.

Roos, Y. and Karel, M. (1991d). Phase transitions of mixtures of amorphous polysaccharides and sugars. *Biotechnol. Progr.*, 7, 49–53.

Roos, Y.H., Karel, M., and Kokini, J.L. (1996). Glass transitions in low moisture and frozen foods: effects on shelf life and quality. *Food Technol.*, 50(11), 95–108.

Roudaut, G., Simatos, D., Champion, D., Contreras-Lopez, E., and Le Meste, M. (2004). Molecular mobility around the glass transition temperature: a mini review. *Innov. Food Sci. Emerging Technol.*, 5, 127–134.

Singh, K.J. and Roos, Y.H. (2005). Frozen state transitions of sucrose–protein–cornstarch mixtures. *J. Food Sci.*, 70(3), E198–E204.

Slade, L. and Levine, H. (1991). Beyond water activity: recent advances based on an alternative approach to the assessment of food quality and safety. *Crit. Rev. Food Sci. Nutr.*, 30, 115–360.

Slade, L. and Levine, H. (1995). Glass transitions and water-food structure interactions. *Adv. Food Nutr. Res.*, 38, 103–269.

Söderholm, S., Roos, Y.H., Meinander, N., and Hotokka, M. (1999). Raman spectra of fructose and glucose in the amorphous and crystalline states. *J. Raman Spectroscopy*, 30, 1009–1018.

Sperling, L.H. (1992). *Introduction to Physical Polymer Science*, 2nd ed., John Wiley & Sons, New York.

Supplee, G.C. (1926). Humidity equilibria of milk powders. *J. Dairy Sci.*, 9, 50–61.

Talja, R.A. and Roos, Y.H. (2001). Phase and state transition effects on dielectric, mechanical, and thermal properties of polyols. *Thermochim. Acta*, 380, 109–121.

Vega, C. and Roos, Y.H. (2006). Spray-dried dairy and dairy like emulsions – compositional considerations. *J. Dairy Sci.*, 89, 383–401.

Vega, C., Kim, E.H.J., Chen, X.D., and Roos, Y.H. (2005). Solid-state characterization of spray-dried ice cream mixes. *Coll. Surf. B: Biointerfaces*, 45, 66–75.

White, G.W. and Cakebread, S.H. (1966). The glassy state in certain sugar-containing food products. *J. Food Technol.*, 1, 73–82.

Chapter 6

Rubber Elasticity and Wheat Gluten Proteins

A.S. Tatham[1] and P.R. Shewry[2]

[1] Department of Applied Life Sciences, University of Wales Institute Cardiff, Llandaff Campus, Cardiff, CF5 2YB, UK. atatham@uwic.ac.uk
[2] Rothamsted Research, Harpenden, Herts., AL5 2JQ, UK. peter.shewry@bbsrc.ac.uk

6.1 Introduction

Many materials exhibit elastic behaviour when a stress is applied, the material returning to its original dimensions after the stress has been removed. In crystalline and glasslike solids the elastic limits rarely exceed 1%. In contrast, true elastomers are able to undergo large elastic deformations, that is, to stretch and return to their original state in a reversible way and without breaking. Such elastomeric materials are polymers consisting of long flexible chainlike molecules These chains are capable of undergoing considerable molecular motion, unlike in crystalline solids where only limited atomic movement is permitted. The energy involved in the deformation of elastomers is stored and on removal of the stress this energy is recovered. This latter stage is therefore passive in that it does not require energy input. The degree to which an elastomer is "ideal" is determined by how much of the stored energy is recovered, with some systems being more efficient than others.

Whereas solids exhibit elastic behaviour, fluids generally exhibit viscosity, which may be either Newtonian where the shear stress is linearly proportional to the shear rate, or non-Newtonian where the viscosity changes with the applied shear force. Liquids deform on application of stress, but cannot return to their original dimensions when the stress is removed. Some foods exhibit both viscous and elastic properties and are known as viscoelastic materials, a typical example being wheat gluten. Cream, cheese and most gelled products are also viscoelastic materials (see also Chapters 13, 19 and 21). The balance between elasticity and viscosity has impacts on the functional qualities of a number of foods and the example of wheat flour dough and gluten is discussed in this chapter, and also in Chapters 10, 14, 18 and 20.

6.2 Rubberlike Elasticity

6.2.1 Criteria for Rubberlike Elasticity

The ability of materials to exhibit rubberlike elasticity relates to their polymer structure. Rubberlike materials must satisfy a number of criteria:

1. Individual monomers must be flexible, amorphous and conformationally free, so that they can stretch rapidly when a force is applied.
2. The individual monomers must be cross-linked to form a network. These cross-links act to constrain the system.
3. The materials must retract rapidly and recover their original dimensions on the removal of the applied stress.

The first requirement for material to exhibit rubberlike elasticity is that it consists of long flexible chainlike molecules, able to undergo rapid rotation about the bonds in the backbone, enabling the molecule to respond quickly to an applied stress. In rubber the backbone is composed of carbon–carbon bonds. The torsion angles of these bonds change, allowing the conformation of the chain to vary from being highly coiled to linear. Such molecules change their conformation readily at room temperature and in the unstrained state adopt a random conformation. When stretched the molecules become oriented and their conformational freedom is restricted. Regularity in the structure of the chains may allow them to pack together to form a regular crystalline lattice. If this occurs the polymer will become rigid to an extent determined by the degree of crystallinity; if this is high the material will exhibit plastic properties. Elastomeric materials must be above their glass transition (T_g) temperatures to allow high local segmental mobility, below their T_g the polymer chains will show little segmental mobility.

The second requirement for an elastomeric material is that the chains be cross-linked to form a loose three-dimensional intermolecular network. This cross-linking may be either by covalent chemical bonds or by strong non-covalent interactions such as hydrogen bonds or hydrophobic interactions. Cross-linking is essential for the restoring mechanism once the stress is removed from the material. If the material is not cross-linked, low stresses will straighten the polymer chains, but at higher stresses they will slip past each other and irreversibly deform.

In cross-linked materials such slippage is prevented from occurring by the cross-links, so that when the stress is removed the material returns to its original shape. The degree of cross-linking is also critical in modulating the properties of the elastomer, and the length of polymer chain between the cross-links needs to be long enough to allow conformational flexibility on application of the stress. At high cross-linking density the degree of extension of the material will be reduced and at very high densities the material will not be extensible. Within the polymer the cross-linked regions may form small crystalline domains (due to their restricted mobility) within an amorphous rubberlike structure. Sulphur is used to cross-link natural rubber (a process called vulcanization) and the degree of cross-linking determines the elastic properties of the material.

Thirdly, elastomeric materials must be able to recover their original dimensions rapidly and completely. If materials are repeatedly stressed and relaxed and do not recover their original dimensions after each cycle they will deteriorate rapidly. However, such deterioration is rarely observed, and when materials are stressed for long periods a small amount of flow or creep may result from separate molecules slipping past one another.

The position and nature of cross-links varies in biological elastomers, conferring specific properties that are required for their biological functions. In elastin and collagen lysyl–aldehyde cross-links are formed by reaction of ε-amino groups of lysine residues. These result in protein polymers, which are essentially insoluble in all reagents. Covalent disulphide bonds and noncovalent hydrogen bonding both contribute to the cross linking of wheat gluten proteins while in spider silks both hydrophobic and hydrogen bonds are important for functionality (Bailey 2003).

6.2.2 Ideal and Nonideal Elastomers

When a stress is applied to a cross-linked rubber it reaches a state of equilibrium almost immediately with the stress remaining constant for an indefinite time in a sample maintained at constant strain. Once at equilibrium the properties of the rubber can be described by thermodynamics. The elastomeric force, f, the force developed on stretching an elastomeric material, has two components, an entropic component f_s and an internal energy component, f_e, with

$$f = f_s + f_e$$

where f_e is attributed to strain in the bonds and f_s to a decrease in the number of conformations in the lowest energy state. The f_s originates from the reduction in entropy. Entropy is reduced as the chain is stretched from a high-entropy random coil conformation to a constrained conformation in which it can adopt a restricted number of conformations. The restoring force, which causes the polymer chain to return to its equilibrium or unstretched state once the applied stress has been removed, provides the drive to return to a high entropy random coil conformation. As bond strain can result in bond breakage an ideal elastomer is one in which $f_e = 0$, therefore $f = f_s$. For a predominantly entropic (ideal) elastomer the value of $f_e/f < 0.5$, with the value for natural rubber being 0.18 and for mammalian elastin 0.26.

Ideal elasticity is the property where the energy expended in the extension of an elastomer is completely recovered on removal of the extending force. Ideal elastomers exhibit perfectly reversible force-extension curves, that is, complete recovery of the energy expended in deformation. Rubber theory is founded on the idea of ideal elasticity, based on the observation that an increase in the temperature of the elastomer occurs due to stretching and that cooling occurs when the material is allowed to contract (Flory 1968). The release of heat on stretching correlates with the loss of motion, which is interpreted as a decrease in entropy on extension. This decrease in entropy provides the restoring force. However, there is also a nonentropic internal energy component to rubber elasticity. As the internal energy component increases the strain on bonds increases leading to the possibility of irreversible processes

occurring such as chain breakage. More durable elastomers have a predominantly entropic mechanism with little or no risk of bond breakage.

Indeed, a purely entropic mechanism is required for some biological elastomers. For example, the properties of extensibility and elastic recoil are important for the function of elastin in arterial blood vessels, as these tissues have to last the lifetime of the animal. In contrast, a purely entropic mechanism would not be appropriate for other biological elastomers. For example, the framework silks of spiders' webs are poor energy storage devices, with the web dissipating some of the energy of the impacting insect as heat. In this case a purely entropic mechanism would convert the energy of the impacting insect into recoil and catapult the insect out of the web! In spider silks the physical properties of the polymers are modulated by the size of the repetitive domains and degree of cross-linking, those with higher extensibility having longer repetitive domains and fewer cross-linking sites (Lewis 2003).

A number of different mechanisms have been proposed to account for the rubber-like properties of materials. In classical rubber theory these properties are attributed to a decrease in conformational entropy on deforming a network of kinetically free random polymer molecules. Stress orders the polymer chains and decreases their entropy by limiting their conformational freedom, thus providing the restoring force to the relaxed state. Such a theory was developed for elastin by Hoeve and Flory (1958) based on a random chain network with a Gaussian distribution of end-to-end chain lengths between cross-links. Weis-Fogh and Andersen (1970) developed an alternative mechanism of elastin elasticity based on a decrease in solvent entropy on extension. This suggested that the hydrophobic side-chains of the protein would be exposed to the solvent on extension and the change in solvent entropy would provide the entropic component of the elastomeric force. Urry et al. (1982), on the basis of structural studies and molecular dynamic calculations of elastin, repeats that the entropic component arose from a decrease in available configurational space on extension.

The tenet of classical rubber theory has been that the chains are in random networks and the networks comprise a Gaussian distribution of end-to-end chain lengths. However, the mechanisms and molecular bases for the elasticity of proteins are more complex than that of natural rubber. In biological systems elastomeric proteins consist of domains with blocks of repeated sequences that imply the formation of regular structures and domains where covalent or noncovalent cross-linking occurs. Although characterised elastomeric proteins differ considerably in their precise amino acid sequences they all contain elastomeric domains comprised of repeated sequences. It has also been suggested that several of these proteins contain β-turns as a structural motif (Tatham and Shewry 2000).

6.3 Gluten Viscoelasticity

Wheat is unique among the cereals in that doughs exhibit the properties of viscosity and elasticity, termed viscoelasticity, the balance of which determines their suitability for different end-uses. For breadmaking, "strong" (elastic) doughs are required, allowing the doughs to stretch and trap carbon dioxide gas bubbles produced during

fermentation, enabling the bread to rise. More extensible doughs are required for making cakes and biscuits: too elastic a dough will allow the biscuit "spring back" after moulding to give a smaller biscuit and too viscous a dough will allow flow after shaping.

As stated above, a viscoelastic material has both an elastic and a viscous component. The elastic component of a material acts to return the material to its original state (once the stress had been removed) without loss of heat. In contrast, the viscous component will allow continuous deformation until the stress is removed (but the material will not return to its original state) and result in the loss of heat. When stress is applied to a viscoelastic material the polymer chains can change position and slip past each other (termed creep), on removal of the stress the material does not fully recover its original dimensions.

The viscoelastic properties of wheat dough are primarily determined by the major seed storage proteins, which are termed prolamins. These proteins are present in the cells of the mature grain as a proteinaceous matrix and are brought together during dough mixing to form a continuous network called gluten. Gluten can be prepared from dough by washing out starch, fibre and water-soluble components. The resulting fraction comprises predominantly prolamins (about 70% dry wt.) with smaller amounts of other proteins, entrapped starch granules, and lipids. The proteins present in gluten have, therefore, been subject to extensive research to determine their structure and interactions and how these impact on end-use properties.

Gluten is a highly complex mixture of proteins, with at least 50 individual proteins being resolved by 2D IEF/SDS-PAGE gels (Shewry and Tatham 1990). In addition, there is considerable variability in the patterns of gluten proteins present in different genotypes.

The prolamins are defined as a protein group on the basis of their solubility in alcohol–water mixtures but this applies to only about half of the native gluten proteins. These are monomeric components called gliadins. The remaining proteins, called glutenins, are present as polymers stabilised by interchain disulphide bonds and are only soluble in alcohol–water mixtures if these bonds are reduced to release the individual subunits. The gliadins are further divided into the α-, β-, δ- and ω-gliadins on the basis of their sequences, with the α-, β-, δ-gliadins containing intramolecular disulphide bonds and the ω-gliadins no disulphide bonds. The polymeric glutenin subunits are divided into two groups on the basis of their sequences; these are called low molecular weight (LMW) and high molecular weight (HMW) subunits. Both the HMW and LMW subunits contain inter- and intramolecular disulphide bonds enabling them to form covalently bonded polymers.

The gliadins are considered to impart viscous properties to dough and the polymeric glutenins elastic properties. However, one group of glutenin proteins, the HMW subunits, has been shown to play a major role in determining dough elasticity.

6.3.1 The HMW Subunits and Gluten Elasticity

The HMW subunits are encoded by genes located on the group 1 chromosomes at loci designated Glu-A1, Glu-B1 and Glu-D1. Each Glu-1 locus comprises two tightly linked genes encoding proteins defined on the basis of their molecular weights and

sequences as *x*-type and *y*-type subunits. Hexaploid bread wheat therefore contains a total of six HMW subunit genes. However, the number of expressed subunit proteins ranges from three to five HMW, due to the specific silencing of one, two or three genes. This results in variation in the total amount of HMW subunit protein (Halford et al. 1992), which may relate to impacts on dough strength.

Although the HMW subunits only account for about 10–12% of the total gluten proteins (Halford et al. 1992), allelic variation in their composition has been reported to account for 45–70% of the variation in breadmaking performance of European wheats (Payne et al. 1987, 1988). A range of studies has shown that ther are major determinants of dough strength including the analysis of near-isogenic lines differing only in their HMW subunit composition (Popineau et al. 1994).

A large number of gene sequences are now available for HMW subunits, showing that they typically comprise between 630 and 820 amino acids, with M_r ranging from 67,500 to 88,000 (Shewry et al. 2003). Their sequences can be divided into three domains, an extensive central domain consists of repeated sequences based on two or three peptide motifs, hexapeptides (consensus Pro.Gly.Gln.Gly.Gln.Gln), nonapeptides (consensus Gly.Tyr.Tyr.Pro.Thr.Ser.Pro/Leu.Gln.Gln) and tripeptides (consensus Gly.Gln.Gln) which vary in length from 420 to 700 residues. These repetitive domains are flanked by shorter non-repetitive domains which vary in length between 81 to 104 residues at the *N*-terminus and 42 residues at the *C*-terminus. The non-repetitive *N*- and *C*-terminal domains contain most or all of the cysteine residues available for inter-chain covalent bonding.

The HMW subunits are only present in high M_r glutenin polymers, with masses extending above 1×10^6 (Wahlund et al. 1996), but little is known about their precise organisation in these polymers or their pattern of disulphide bond formation. However, it has been suggested based on the distribution of cysteine residues and limited amino acid sequencing of cross-linked peptides that they form mainly head-to-tail polymers (Tao et al. 1992) and that these polymers form the backbone of the glutenin polymers with the LMW subunits forming "branches" (Graveland et al. 1985). It is also probably that the ratio of LMW to HMW subunits in these polymers varies between genotypes and between polymers of different size classes and that this variation also contributes to effects on dough strength.

The HMW subunits therefore display the characteristics required of an elastomeric material. These are an extensive central repetitive domain that is unconstrained by covalent cross-links and can undergo structural changes on deformation and shorter *N*- and *C*-terminal domains in which cross-linking can occur.

The central repetitive domains have been proposed, on the basis of spectroscopic and modelling studies, to consist of β- and/or γ-turns which are organised to form spiral-like structures. Molecular modelling using energy minimization and molecular dynamics has yielded a range of such structures, comprising γ-, β- or both γ- and β-turns and with diameters between 1.7 and 2.4 nm (Parchment et al. 2001; Kasarda et al. 1994). It has been suggested that these structures may be intrinsically elastic and act as molecular "springs."

These structures are also consistent with the results of hydrodynamic and scanning probe microscopy (SPM) studies reviewed by Shewry et al. (2003). Hydrodynamic studies indicate that the HMW subunits have an extended rod-like structure in

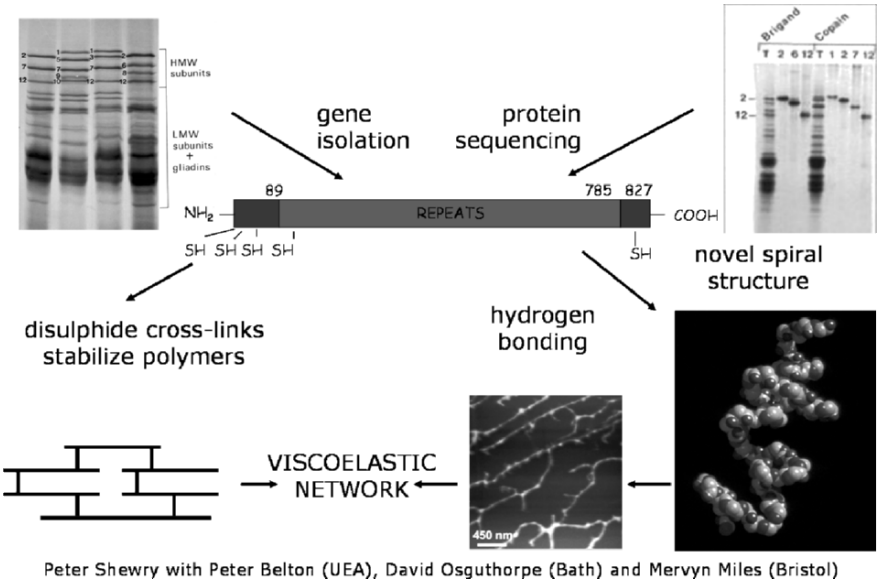

Figure 6.1. The role of HMW subunits in gluten structure and functionality. Amino acid sequences derived from direct analysis of purified proteins and the isolation and sequencing of corresponding genes show that the proteins have highly conserved structures, with repetitive domains flanked by shorter nonrepetitive domains containing cysteine residues (SH) available for formation of interchain disulphide bonds. Molecular modelling indicates that the individual repetitive domains form a loose spiral structure (bottom right) while SPM shows that they interact by noncovalent forces to form fibrils (centre right). Includes figures from Parchment et al. (2001) and Humphries et al. (2000).

solution, with diameters between 1.5 and 6.4 nm, and SPM images of subunits in the hydrated solid state show aligned rods (with diameters of about 1.8 nm) which may form filamentous fibre structures.

The information presented above is summarised in Figure 6.1.

6.3.2 The Mechanism of Gluten Viscoelasticity

The HMW subunits and other gluten proteins are present in dough in the hydrated solid state and changes in the proportions of β-turn and intermolecular β-sheet structures during hydration. Subsequent extension has been monitored using Fourier transform infrared spectroscopy. This indicates that the dry solid is probably disorganised in structure with hydration leading to the formation of mobile segments that are rich in β-turn structure. During extension (or dough mixing) the subunits become aligned, resulting in the formation of more rigid intermolecular β-sheet structures stabilised by interchain hydrogen bonds and corresponding decreases in β-turn structures. These mobile β-turn rich and rigid β-sheet rich regions have been termed "loops" and "trains," respectively (Belton et al. 1995, 1999), by analogy with the

interactions of polymers with surfaces (Dickinson 1992). In the latter the polymer makes many interactions with the surface. Although these individual interactions may be weak, it is statistically unlikely that all will be broken at one time and hence the polymer will not be washed off of the surface unless all of the interactions are broken. Gluten proteins are rich in glutamine residues which predominate in the repetitive peptide sequence motifs, accounting for approx. 35 mol% of the repetitive domains of the HMW subunits. Studies of gluten (Alberti et al. 2001) have shown that two different populations of glutamine residues are present and it is possible that one of these is associated with loops and the other with trains.

When the fully hydrated dough is at equilibrium the gluten proteins will form a ratio of loop-to-train structures that will depend on the precise structures of the HMW subunits and on the history of the dough (e.g., the degree of work input into dough mixing). When the dough is extended the loops will extend first, which requires little energy. Further extension will then start to pull apart the β-sheet structures, which requires more energy and allows the proteins to slide over each other, while even further extension may lead to breaking of the disulphide bonds. When the extending force is removed there will be a tendency for the system to relax back to an equilibrium between loops and trains. However, the precise ratio of loops to trains may differ from that in the initial dough if the extension results in the alignment of sequences that are able to form stable regions of β-sheet structure.

Hence a higher proportion of trains may be retained when the force is released and the ratio of to β-turn to β-sheet structures will increase with successive cycles of extension and relaxation (Wellner et al. 2005). This model explains the origins of gluten viscoelasticity as it provides an explanation for gluten extension and elastic recovery. It also provides an explanation for the increase in dough elasticity that occurs during dough mixing: the alignment during extension allows the HMW subunits to form more extensive and stable regions of β-sheet (i.e., trains). Although the HMW subunits are a relatively minor component of the gluten system they appear to be responsible for much of the gluten viscoelasticity: this disproportionate effect is not unusual in food systems where relatively minor components can radically alter the physical properties of systems.

Measurements of the elastomeric force of purified HMW subunits that had been cross-linked by radiation indicate that the mechanism of elastic recoil is different from that of other protein elastomers (Tatham et al. 2001). The mechanism of elastic recoil in elastin and natural rubber is predominantly entropic in origin, with f_e/f ratios below 0.5. However, the ratio determined for the HMW subunits of glutenin was 5.6, indicating that the mechanism of elasticity is not predominantly entropic in origin. As the ratio is greater than 1, other mechanisms may be contributing to the total elastomeric force. Tensile stress must be either entropic or energetic in origin, and the elastic recoil of the HMW subunits may be associated with extensive hydrogen bonding both within and between subunits in addition to entropic and energetic contributions.

The advantage of an entropic mechanism of elastomeric force is that it depends on the decrease in the number of accessible states on extension and can be considered ideal for a biological elastomer that is required to be durable, such as elastin. In contrast, the elastomeric properties of the HMW subunits and other gluten proteins

have no known biological significance, and hence there has been no evolutionary pressure to develop an elastic mechanism that is durable. The gluten proteins are storage proteins that provide a store of carbon, nitrogen and sulphur for the developing seedling. Their elastomeric properties may therefore have developed fortuitously as a consequence of their evolution by reiteration of the sequence repeats.

6.3.3 Allelic Variation in HMW Subunits and in Processing Quality

It is probable that the HMW subunits have both quantitative and qualitative effects on dough strength. Firstly, it is probable that differences in the total amount of HMW subunit protein resulting from differences in the number of expressed genes (Halford et al. 1992) or from the overexpression of individual subunits such as subunit 1B*x*7 (Vawser and Cornish, 2004) have impacts on dough strength, with more protein giving more elasticity. This may account for the good properties associated with an expressed 1A*x* subunit compared with the null (silent) allele (Halford et al. 1992).

However, there are also well-established qualitative differences between allelic subunits that are expressed at similar levels. In particular, one pair of HMW subunits encoded by the Glu-D1 locus (1D*x*5 + 1D*y*10) are associated with good breadmaking properties compared with other allelic pairs encoded by the same locus (1D*x*2 + 1D*y*12, 1D*x*3 + 1D*y*12). The repetitive domains of subunits 1D*y*10 and 1D*y*12 show minor differences in sequence which may affect the number of β-turns that form and hence the stability and interactions of the subunits. In contrast, the small differences between the sequences of HMW subunits 1D*x*2 and 1D*x*5 are not predicted to affect the proportions of β-turns (Shewry et al. 2003). However, subunit 1D*x*5 contains an additional cysteine residue compared with subunit 1D*x*2, which is located at one end of the repetitive domain. This cysteine may affect the pattern of covalent cross-links, forming more highly cross-linked polymers that are more elastic and less extensible than those formed by subunit 1D*x*2. Thus, cross-linking behaviour and non-covalent interactions may both contribute to the differential effects of allelic subunits on dough viscoelasticity.

6.3.4 Conclusions: Wheat Gluten Proteins and Dough Viscoelasticity

Despite a vast volume of research, our understanding of the molecular structure and mechanisms of viscoelasticity of wheat gluten and dough are at an early stage compared with other elastomeric materials such as spider silks and mammalian collagen and elastin. Quantitative and qualitative effects of HMW subunits on end-use quality have been demonstrated although the precise bases for these correlations are not known and we lack information on the higher-order structure and organisation of the glutenin polymers.

It is also important to remember that wheat gluten and dough are complex materials, consisting not only of protein and water, but also starch-, lipid-, water- and salt-soluble proteins and smaller carbohydrates, and so on. The properties of these materials and their interactions with the gluten proteins are poorly understood but can be expected to also influence the viscoelastic properties. The challenge therefore is to understand gluten structure at the molecular level and how this structure interacts

in complex materials such as dough. Understanding the molecular basis for gluten viscoelasticity should enable wheat to be used in a wider range of products than its traditional uses in food processing.

6.4 Future Trends

Wheat is being used to produce an increasing range of products, including baked products with enhanced nutritional properties (e.g., high-fibre and whole grain breads). The combination of these properties with traditional requirements for a light porous crumb structure may require specific improvements in the properties of the gluten proteins. Similarly, increased use of wheat gluten in other food applications can be expected, including the development of functional ingredients (such as foaming and emulsifying agents) based on partially hydrolysed or modified gluten proteins. A detailed knowledge of gluten protein structure and functionality will be required to support such developments.

6.5 Sources of Further Information

Rubber elasticity: physics and chemistry of natural and synthetic rubbers:

Treolar, L.R.G. (1975). *The Physics of Rubber Elasticity*. Oxford University Press, New York. 3rd Edition. 1975.

Review of the properties of the HMW subunits of wheat glutenin:

Shewry, P.R., Halford, N.G., Tatham, A.S., Popineau, Y., Lafiandra, D., and Belton, P.S. (2003). The high molecular weight subunits of wheat glutenin and their role in determining wheat processing properties. *Adv. Food Sci. Nutrition* 45:219–302.

Protein elasticity, mechanisms and biological roles:

Elastomeric Proteins: Structures, Biomechanical Properties and Biological Roles. (2003). Shewry, P.R., Tatham, A.S., and Bailey, A.J. eds. Cambridge University Press, Cambridge.

6.6 References

Alberti, E., Gilbert, S.M., Tatham, A.S., Shewry, P.R., Naito, A., Okuda, K., Saito, H., and Gil, A.M. (2001). Study of wheat HMW 1D*x*5 subunit by C and H solid-state NMR. II. Roles of nonrepetitive terminal domains and length of repetitive domains. *Biopolymers*, 65, 158–168.

Bailey, A.J. (2003). Restraining cross-links in elastomeric proteins. In: P.R. Shewry, A.S. Tatham, and A.J. Bailey (Eds.), *Elastomeric Proteins: Structures, Biomechanical Properties and Biological Roles*, Cambridge University Press, Cambridge. pp. 321–337.

Belton, P.S. (1999). On the elasticity of wheat gluten. *J. Cereal Sci.*, 29, 103–107.

Belton, P.S., Colquhoun, I.J., Grant, A., Wellner, N., Field, J.M., Shewry, P.R., and Tatham, A.S. (1995). FTIR and NMR studies on the hydration of a high M_r subunit of glutenin. *Int. J. Biol. Macromol.*, 17, 74–80.

Dickinson, E. (1992). *An Introduction to Food Colloids.* Oxford University Press, Oxford.

Flory, P.J. (1968). Molecular interpretation of rubber elasticity. *Rubber Chem. Tech.*, 41, G41–48.

Graveland, A., Bosveld, P., Lichtendonk, W.J., and Moonen, J.H.E. (1985). A model for the molecular structure of the glutenins from wheat flour. *J. Cereal Sci.*, 3, 1–16.

Halford, N.G., Field, J.M., Blair, H., Urwin, P., Moore, K., Robert, L., Thompson, R., Flavell, R.B., Tatham, A.S., and Shewry, P.R. (1992). Analysis of the HMW glutenin subunits encoded by chromosome 1A of bread wheat (T*riticum aestivum* L.) indicates quantitative effects on grain quality. *Theor. Appl. Genet.*, 83, 373–378.

Hoeve, C.A.J. and Flory, P.J. (1958). The elastic properties of elastin. *J. Am. Chem. Soc.*, 80, 6523–6526.

Humphries, A.D.L., McMaster, T.J., Miles, M.J., Shewry, P.R., and Tatham, A.S. (2000). An AFM study if the interactions of the HMW subunits of wheat glutenin. *Cereal Chem.*, 77, 107–110.

Kasarda, D.D., King, G., and Kumonsinski, T.F. (1994). Comparison of β-spiral structures in wheat high molecular weight glutenin subunits and elastin by molecular modelling. In: T.F. Kumonsinski and M. Liebman (Eds.), *Proceedings of the Symposium on Molecular Modelling*, ACS, Washington, DC. pp. 209–220.

Lewis, R. (2003). Sequences, structures and properties of spider silks. In: P.R. Shewry, A.S. Tatham and A.J. Bailey (Eds.), *Elastomeric Proteins: Structures, Biomechanical Properties and Biological Roles*, Cambridge University Press, Cambridge. pp. 136–151.

Parchment, O., Tatham A.S., Shewry, P.R., and Osguthorpe, D.J. (2001). Molecular modelling of the central repetitive domains of the high molecular weight subunits of wheat. *Cereal Chem.*, 49, 268–275.

Payne, P.I., Nightingale, M.A., Krattinger, A.F., and Holt, L.M. (1987). The relationship between HMW glutenin subunit composition and the bread-making quality of British grown wheat varieties. *J. Sci. Food Agric.*, 40, 51–65.

Payne, P.I., Holt, L.M., Krattinger, A.F., and Carillo, J.M. (1988). Relationship between seed quality characteristics and HMW glutenin subunit composition determined using wheats grown in Spain. *J. Cereal Sci.*, 7, 229–235.

Popineau, T., Cornec, M., Lefebvre, J., and Marchylo, B. (1994). Influence of high M_r glutenin subunits on on gluten polymers and rheological properties of gluten and gluten subfractions of near-isogenic lines of wheat Sicco. *J. Cereal Sci.*, 19, 231–241.

Shewry, P.R. and Tatham, A.S. (1990). The prolamins storage proteins of cereal seeds—structure and evolution. *Biochem. J.*, 267, 1–12.

Shewry, P.R., Halford, N.G., and Tatham, A.S. (2003). The high molecular subunits of wheat glutenin and their role in determining wheat processing properties. *Adv. Food Nut. Res.*, 45, 219–302.

Tao, H.P., Adalsteins, A.E., and Kasarda, D.D. (1992). Intermolecular disulfide bonds link specific high molecular weight glutenin subunits in wheat endosperm. *Biochim. Biophys. Acta*, 1159, 13–21.

Tatham, A.S., Hayes, L., Shewry, P.R. and Urry, D.W. (2001). Wheat seed proteins exhibit a complex mechanism of protein elasticity. *Biochim. Biophys. Acta*, 1584:187–193.

Tatham, A.S., and Shewry, P.R. (2000). Elastomeric proteins: Biological roles, structures and mechanisms. *Trends Biol. Sci.*, 299, 567–571.

Urry, D.W., Venkatachalam, C.M., Long, M.M., and Prasad, K.U. (1982). Dynamic β-spirals and a librational entropy mechanism of elasticity. In: R. Srinivasan and R.H. Sarma (Eds.), *Conformations in Biology*, Guilderland, NY: Adenine Press, pp. 11–27.

Vawser, M.J. and Cornish, G.B. (2004). Over-expression of HMW glutenin subunit *Glu-B1* 7*x* in hexaploid wheat varieties (*Triticum aestivum* L.). *Aust. J. Agric. Sci.*, 55, 577–588.

Wellner, K., Mills, E.N.C., Brownsea, G., Wilson, R.H., Brown, N., Freemam, J., Halford, N.G., Shewry, P.R., and Belton, P. (2005). Changes in protein secondary structure during

gluten deformation studied by dynamic Fourier transformed infrared spectroscopy. *Biomacromol*, 6, 255–261.

Wahlund, K.G., MacRitchie F., Nylander T., and Wannerberger, L. (1996). Size characterization of wheat proteins, particularly glutenin, by asymmetrical flow field flow fractionation. *J. Cereal Sci.*, 23, 113–119.

Weis-Fogh, T. and Andersen, S.O. (1970). New molecular model for the long-range elasticity of elastin. *Nature*, 227, 718–721.

Chapter 7

State Diagrams of Food Materials

Didem Z. Icoz and Jozef L. Kokini

Rutgers, The State University of New Jersey, Department of Food Science,
didemz@rci.rutgers.edu
kokini@aesop.rutgers.edu

7.1 Introduction

The physical/chemical states and the thermal transitions of food materials determine the process conditions, functionality, stability and overall quality, including the texture, of the final food products. Carbohydrates and proteins—two major biopolymers in various food products—can exist in an amorphous metastable state that is sensitive to moisture and temperature changes (Cocero and Kokini 1991; Madeka and Kokini 1994, 1996). The physical states of components in a biopolymer mixture determine the transport properties, such as viscosity, density, mass and thermal diffusivity, together with reactivity of the material.

Temperature, moisture content, pressure, concentration, shear, time, and so on, can alter the physical state of biopolymers (Roos 1995; Madeka and Kokini 1996). A phase–state diagram describes various states of a material as a function of various conditions and provides a predictive basis for developing novel products and quality improvements of the existing products. The relationship between the composition of a food product and its physical state, represented on a state diagram, enables understanding on the processing requirements and storage stability. The difference between a phase diagram and a state diagram is that a phase diagram contains information on equilibrium conditions, whereas a state diagram contains both equilibrium and nonequilibrium states including metastable equilibrium (Fennema 1996).

In food systems, phase transitions have significant importance, since transitions during processing, storage and consumption affect the quality, stability and in turn consumer acceptance of the final food products. State diagrams can predict the behavior of food biopolymers during baking, extrusion and storage (Levine and Slade 1990; Kokini et al. 1994a). Glass transition temperature as a function of moisture content or water activity forms the simplest state diagrams for food systems.

7.2 Simple State Diagrams Involving Food Solutes and Water

A simple state diagram for a binary system of water-soluble food component and water is shown in Figure 7.1. This basic diagram shows the stability in the glassy state and time-dependent changes in the rubbery state at constant pressure. As water content increases, glass transition temperature (T_g), which is the temperature at which the material passes from a rigid-glassy state into a rubbery state, decreases due to plasticization effect of water. C'_g is the solute concentration in the maximally freeze-concentrated solute and when initial solute concentrations are lower than C'_g, ice formation occurs (Figure 7.1). T'_g is the temperature for the onset of glass transition for the maximally freeze-concentrated solute matrix and T'_m is the temperature above which ice melting occurs.

According to Levine and Slade (1986), the difference between the total water content and the total amount of ice melting in the sample gives C'_g, assuming that the latent heat of melting ice in the food is equal to the latent heat of pure water and there is no solute crystallization. Experimental T_g versus solute concentrations provides the best C'_g values (Roos and Karel 1991a), which is determined to be around 80% (*W/W*) for various food components (Ablett et al. 1992; Roos 1993). A plot of the latent heat of ice melting in samples divided by weight of the solids versus various initial water contents gives a straight line that can be extrapolated to zero latent heat giving the amount of unfrozen water (Roos 1992).

It should be remembered that food materials are complex since most contain multiple ingredients/components. Therefore, it is not very easy to represent them on

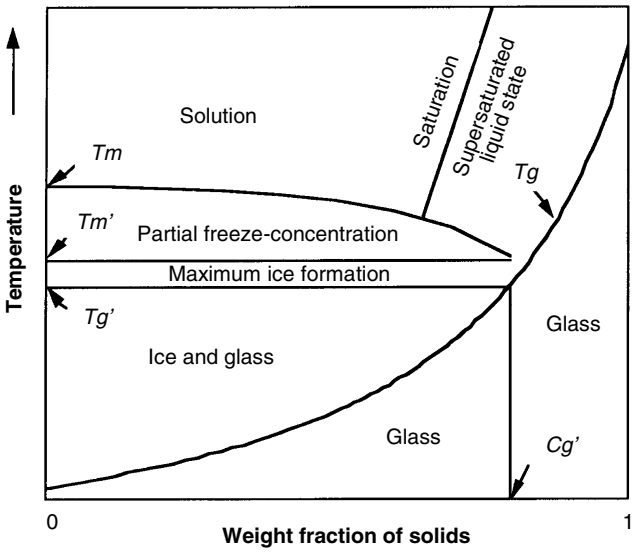

Figure 7.1. A schematic state diagram for food solutes and water (Reprinted from Phase Transitions in Foods, Roos, Chapter 4: Water and Phase Transitions, pp. 73–107, Copyright (1995), with permission from Elsevier.)

state diagrams, but estimates of the glass transition curve provide effective information for determination of food stability and quality. Examples of state diagrams of food materials, showing T_g as a function of water content; and the effect of ice formation on T_g and on ice melting temperature, T_m, are presented in the following sections.

7.3 State Diagrams of Carbohydrates

State diagrams for various carbohydrates are reported in the literature: starch (Van de Berg 1986; Roos and Karel 1991b); maltose and maltodextrins (Roos and Karel 1991b); lactose (Roos and Karel 1991c); sucrose (Roos and Karel 1991a, 1991c; Roos et al. 1996; Slade and Levine 1988); glucose and fructose (Slade and Levine 1988). For example, Figure 7.2 shows the glass transition temperature versus water activity relationship for lactose, sucrose and mixtures of sucrose–fructose and sucrose–Amioca, demonstrating that T_g decreases with increasing water activity (Roos and Karel 1991d).

Figure 7.3 is another example of a typical state diagram, developed for maltose. Maltose solutions are in glassy state below T_g curve. T'_g (onset of glass transition) and T'_m (onset of ice melting) show constant values for the maximally freeze concentrated solutions, where maximum ice formation occurs between T'_m and T_g; and T'_m is at the end point region of T'_g (Figure 7.3) (Roos and Karel 1991b). State diagram for sucrose (Figure 7.4) also shows similar characteristics (Roos and Karel 1991a).

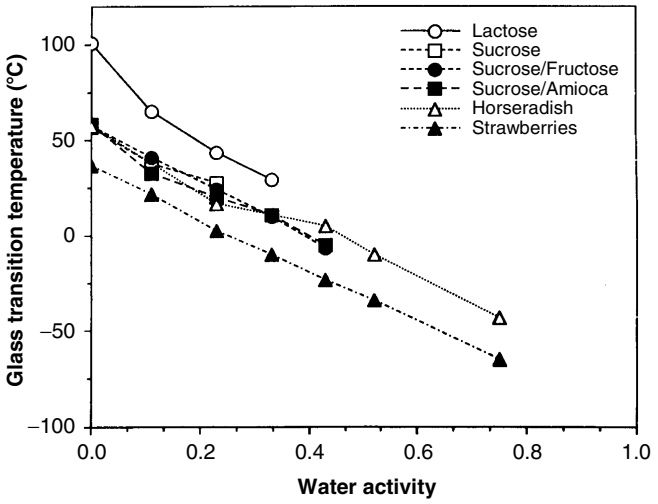

Figure 7.2. Glass transition of amorphous monosaccharides and some food materials as a function of water activity (Reproduced with permission from Roos and Karel, 1991d, Plasticizing effect of water on thermal behavior and crystallization of amorphous food models, J. Food Sci. 56, pp. 38–43, Institute of Food Technologists.)

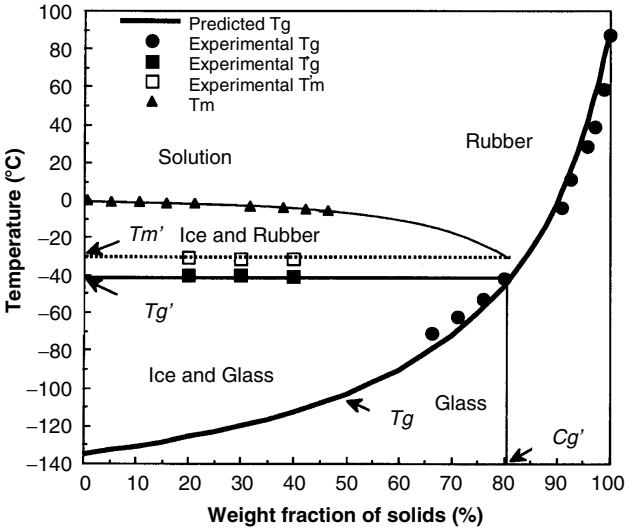

Figure 7.3. State diagram for maltose (Reproduced with permission from Roos and Karel, 1991b, Water and molecular effects on glass transitions in amorphous carbohydrates and carbohydrate solutions, J. Food Sci. 56, pp. 1676–1681, Institute of Food Technologists.)

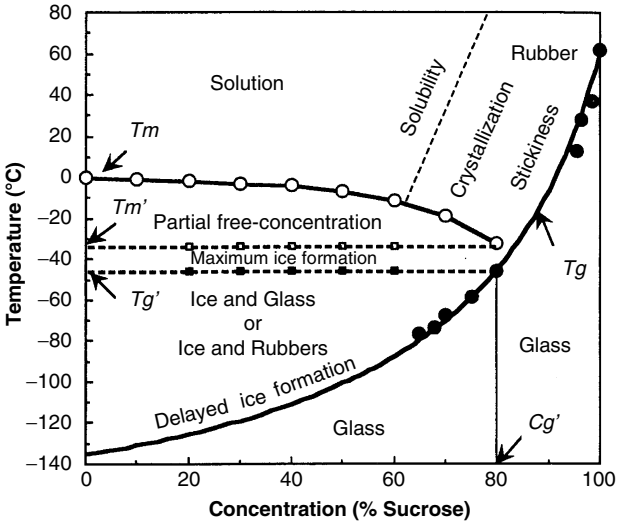

Figure 7.4. State diagram for sucrose (Reproduced with permission from Roos and Karel, 1991a, Amorphous state and delayed ice formation in sucrose solutions, Int. J. Food Sci. Tech. 26, pp. 553–566, Blackwell Publishing, Inc.)

The effect of water and molecular weight on the glass transition has been shown on the state diagram for maltodextrins (Figure 7.5). Although T'_g and T'_m are observed individually with maltose (Figure 7.3), the difference between T'_g and T'_m is

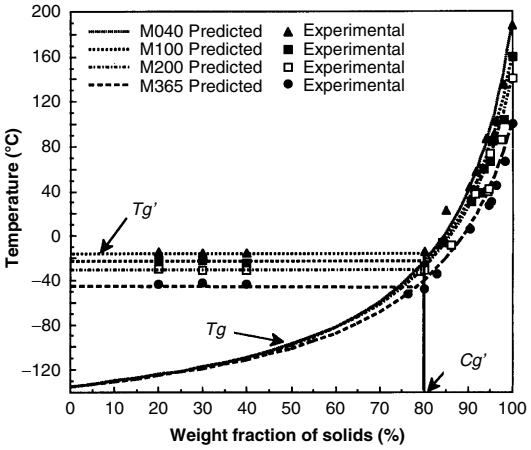

Figure 7.5. State diagram for maltodextrins (Reproduced with permission from Roos and Karel, 1991b, Water and molecular effects on glass transitions in amorphous carbohydrates and carbohydrate solutions, J. Food Sci. 56, pp. 1676–1681, Institute of Food Technologists.)

very low for maltodextrins (Figure 7.5). T_g increases with molecular weight and does not change significantly above 50% solid fractions. T'_g also increases as molecular weight increases, where it is predicted to become constant for high molecular weight maltodextrins (Figure 7.5) (Roos and Karel 1991b).

For linear polymers, the general relationship between molecular weight and glass transition temperature is described as (Fox and Flory 1950);

$$T_g = T_{g,\infty} - \frac{A}{M} \tag{7.1}$$

where $T_{g,\infty}$ is the glass transition temperature at infinite molecular weight; M is the molecular weight; and A is a polymer dependent constant. Equation (7.1) indicates that glass transition temperature increases with molecular weight (Aklonis and MacKnight 1983; Slade and Levine 1991a; Ruan et al. 1999; Sperling 2001; Gropper et al. 2002), which is a consequence of the decrease in free volume. This is caused by the increased number of connected monomer units in the system and decreased number of end groups with increasing molecular weight. (Aklonis and MacKnight 1983; Sperling 2001). At very high molecular weights, the concentration of chain ends is negligible, which results in the glass transition temperature being independent of the molecular size (Aklonis and MacKnight 1983; Slade and Levine 1991b).

The glass transition temperature versus $1/M_w$ of maltodextrins shows linearity (Figure 7.6) (Roos and Karel 1991e), as represented in Equation (7.1). Icoz et al. (2005) have suggested a logarithmic relationship between T_g and M_w of dextrans (Figure 7.7), showing that T_g increases sharply with M_w up to a critical molecular weight above which T_g is relatively independent of M_w. Similar behavior is also observed in other polymer systems (Cowie 1975; Gropper et al. 2002). The independence of T_g on M_w at high molecular weights has been attributed to entanglement coupling that occurred in high molecular weight polymers, essentially leading to an

infinite molecular weight bound network (Slade and Levine 1991b). Dextran molecules have been shown to attain their entanglement coupling around 23,000 < M_w < 30,000, which is also confirmed by steady shear rheological measurements where zero-shear viscosity versus M_w of dextrans at different polymer concentrations shows higher slope above M_w of approximately 22,000 (Figure 7.8), quite close to the critical M_w obtained from T_g versus M_w plots (Figure 7.7) (Icoz et al. 2005).

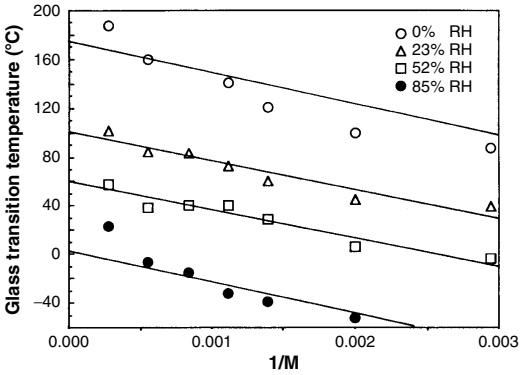

Figure 7.6. Effect of molecular weight on the glass transition temperature of maltodextrins (Reprinted with permission from Roos and Karel, Phase transitions of mixtures of amorphous polysaccharides and sugars, Biotechnol. Progr. 7, pp. 49–53. Copyright (1991) American Chemical Society.)

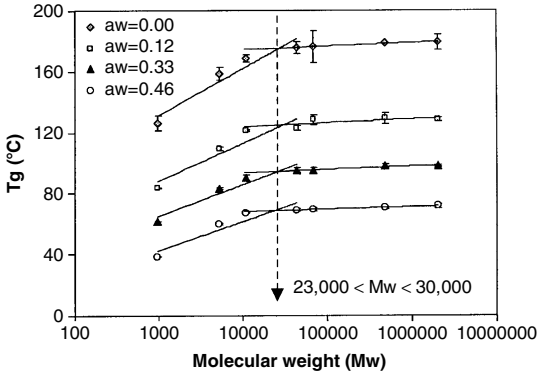

Figure 7.7. Effect of molecular weight on glass transition temperature of dextrans at various water activities (Reprinted from Carbohyd. Polym., 62, Icoz, Moraru, and Kokini, Polymer-polymer interactions in dextran systems using thermal analysis, pp. 120–129, Copyright (2005), with permission from Elsevier.)

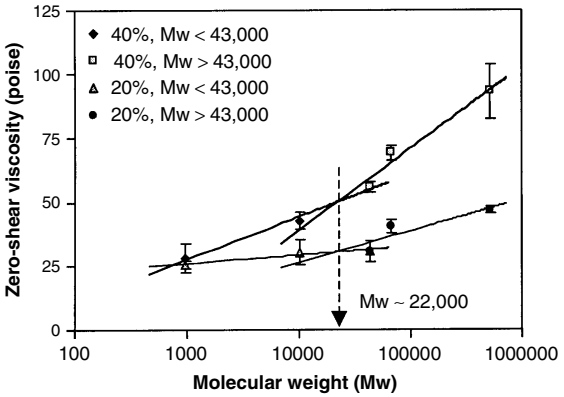

Figure 7.8. Zero-shear viscosity for dextrans with different molecular weights in 40% and 20% solutions (Reprinted from Carbohyd. Polym., 62, Icoz, Moraru, and Kokini, Polymer-polymer interactions in dextran systems using thermal analysis, pp. 120–129, Copyright (2005), with permission from Elsevier.)

Zimeri and Kokini (2003) have shown that water acts as a plasticizer for gelatinized waxy maize starch (WMS) identified by the decrease in T_g with increasing moisture content (Figure 7.9). At room temperature, the glass transition occurs at a moisture content around 28% corresponding to a water activity (a_w) value less than 0.93, showing that gelatinized WMS is in glassy state below a_w of 0.93 (Zimeri and Kokini 2003). Mizuno et al. (1998) reported similar values for potato and wheat starch. Similar phase behaviors showing the effect of water as a plasticizer on starch are also given by Van den Berg (1986); Zeleznak and Hoseney (1987); Blanshard (1988); and Bizot et al. (1997).

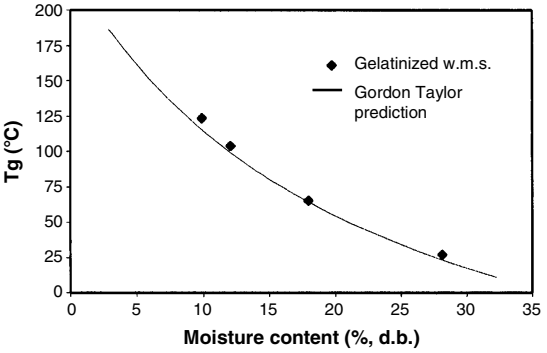

Figure 7.9. Glass transition temperature of gelatinized WMS as a function of moisture content compared to the Gordon–Taylor predictions (Reprinted from Carbohyd. Polym., 51, Zimeri and Kokini, Phase transitions of inulin-waxy maize starch systems in limited moisture environments, pp. 183–190, Copyright (2003), with permission from Elsevier.)

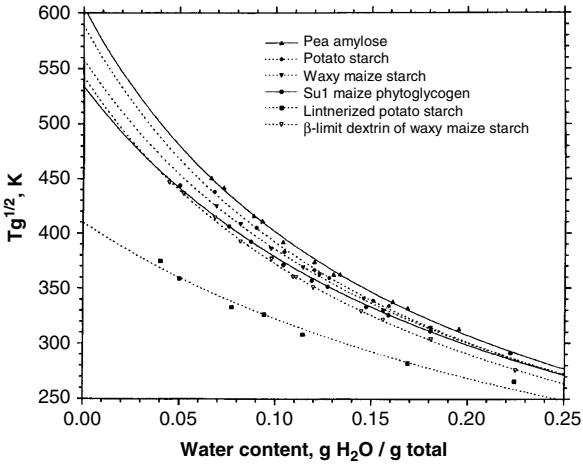

Figure 7.10. Glass transition temperature versus moisture content of starch subfractions measured by DSC with 3°C/min heating rate ($T_g^{1/2}$ represents the values at the midpoint of the transition in the second scans) (Reprinted from Carbohyd. Polym., 32, Bizot, Le Bail, Leroux, Davy, Roger, and Buleon, Calorimetric evaluation of the glass transition in hydrated, linear and branched polyanhydroglucose compounds, pp. 33–50, Copyright (1997), with permission from Elsevier.)

Bizot et al. (1997) compared the glass transition temperature of various starch subfractions as a function of water content (Figure 7.10). Amylose with its long linear chains has the highest T_g values, whereas waxy maize starch with 98% amylopectin has relatively lower T_g s. T_g values of potato starch with its 23% amylose and 77% amylopectin content lie in between the T_g s of amylose and waxy maize starch. Su-1 maize phytoglycogen, which is extracted from maize su-1 by aqueous dispersion and alcoholic precipitation, and β-limit dextrins of waxy maize starch have T_g values lower than waxy maize starch. Lintnerized potato starch, which is prepared by mild acid hydrolysis of potato starch and rich in 1–4 linkage, has shown the lowest T_g values (Figure 7.10) (Bizot et al. 1997).

Gelatinization and retrogradation are two important steps that determine the process and storage stability of starch-containing food products, such as bread. Amorphous but crystallizable starch in a kinetically metastable rubbery state, which is sensitive to the effect of water and temperature, can go through a nonequilibrium recrystallization process known as starch retrogradation (Levine and Slade 1988). When the moisture loss is prevented by adequate packaging, staling of bread occurs due to retrogradation or time-dependent recrystallization of amylopectin, which is the major component in most varieties of starch. Amylopectin recrystallizes from a completely amorphous state of a freshly baked product to the partially crystalline state of a stale product (Levine and Slade 1988, 1990).

It is suggested that softening of the glassy regions be a requirement for melting of crystalline regions of starch (Biliaderis et al. 1980; Maurice et al. 1985; Biliaderis et al. 1986; Levine and Slade 1988). In order to obtain the soft and rubbery texture of freshly baked product, a required amount of moisture is needed so that the crystalline regions can melt at the baking temperature. According to Levine and Slade (1988), a minimum of 27% of water is needed for recrystallization of wheat starch. Increasing water content in the range of 27–50% increases the ratio of recrystallized starch due

to the increased mobility of the macromolecular structure that allows the structural reorganization (Levine and Slade 1988).

The textural changes occurring in bread after baking but before retrogradation are suggested to be due to the cooling of the bread during which transformation through the rubbery state to the glassy state occurs (Blanshard 1986). The effective network T_g of stale bread is higher than the segmental T_g of fresh baked bread (Levine and Slade 1990). In order to decrease the effective T_g of stale bread and to obtain a sufficient temperature difference above T_g, a high moisture content is required for mobility and softness in the stale bread at room temperature. Addition of sugars to bread dough prevents starch retrogradation and consequently prevents bread staling due to increasing network glass transition, also called antiplasticization (Levine and Slade 1990). If a higher molecular weight sugar is used, a higher network glass transition will be obtained resulting in a better antistaling effect (Levine and Slade 1988, 1990).

7.4 Flow Characteristics in Glassy and Rubbery States of Proteins

Morales-Diaz and Kokini (1998) have used rheological models to describe the flow characteristics in glassy and rubbery state of 7S and 11S soy globulins. Glass transition temperatures of 7S fraction have shown values between 114°C and –67°C for moisture contents of 0–35%, and those of 11S fraction is determined between 160°C and –17°C at a moisture range of 0–40%, determined by differential scanning calorimetry (DSC) and mechanical spectroscopy (RMS) (Figure 7.11).

Temperature-induced reactions result from either formation of higher molecular weight products or from degradation of molecular structures. Formation of higher molecular weight products results in increase in the storage modulus (G') and loss

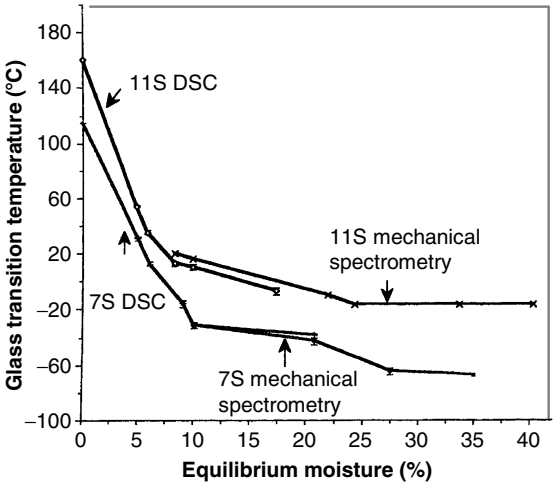

Figure 7.11. Glass transition temperature of the 7S and 11S soy globulins as a function of moisture content by DSC and RMS (Copyright 1998 from 'Understanding phase transitions and chemical complexing reactions in 7S and 11S soy protein fractions' by Morales-Diaz and Kokini (In: Phase/State Transitions in Foods, Rao and Hartel (Eds.)). Reproduced by permission of Routledge/Taylor & Francis Group, LLC.)

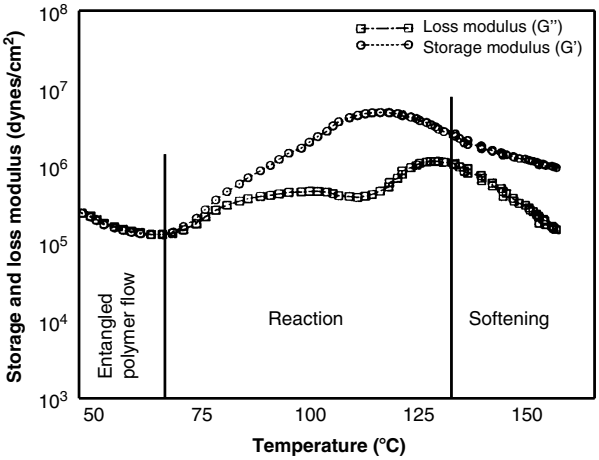

Figure 7.12. Temperature sweep of gliadin with 25% moisture (Reprinted from J. Food Eng., 22, Madeka and Kokini, Changes in rheological properties of gliadin as a function of temperature and moisture: Development of a state diagram, pp. 241–252, Copyright (1994), with permission from Elsevier.)

modulus (G'') during rheological analysis. For example, Figure 7.12 shows that G' increases approximately 100 times during heating throughout the reaction zone of gliadin due to the cross-link formation that joins gliadin molecules, which results in the formation of a three-dimensional network. As the network is formed, the increase in the G' is sharper than the increase in the G'' (G' and G'' represent solidlike and liquidlike properties, respectively). As the reaction is completed, a temperature-induced softening is observed that is identified by the decrease in G' and G'' (Figure 7.12) (Madeka and Kokini 1994; Kokini et al. 1994b).

Figure 7.13 demonstrates the temperature-induced transitions of soy globulins determined through pressure rheometry. At 20.8% moisture content, 7S enriched globulin fraction shows decreasing G' with increasing temperature up to 112°C, after which G' starts to increase, suggesting that the material starts to experience structure-forming reactions. The material experiences the entangled flow behavior, which turns into a reaction zone after the critical temperature (112°C) where the material cross-links. At 168°C, maximum structure formation occurs where G' shows a maximum. At higher temperatures, G' decreases suggesting the softening of the cross-linked network. Figure 7.13 also shows that G' has a clear shoulder before reaching its maximum at 168°C, corresponding to the reaction zone of 7S globulin with a lower denaturation temperature than 11S fraction that is a contaminant in the 7S fraction. The highest point of the shoulder forms the maximum 7S structure, whereas the second part of the G' increase corresponds to the reaction zone and maximum structure formation of 11S fraction with a much harder and elastic structure (Morales-Diaz and Kokini 1998).

At 30% and 40% moisture contents of 7S globulin, the entangled polymer flow region turns into the reaction zone at around 70°C (Figure 7.14). For samples with higher moisture content, the reaction zone is completed at lower temperatures (116°C and 104°C for 30% and 40% moisture contents, respectively). Because the

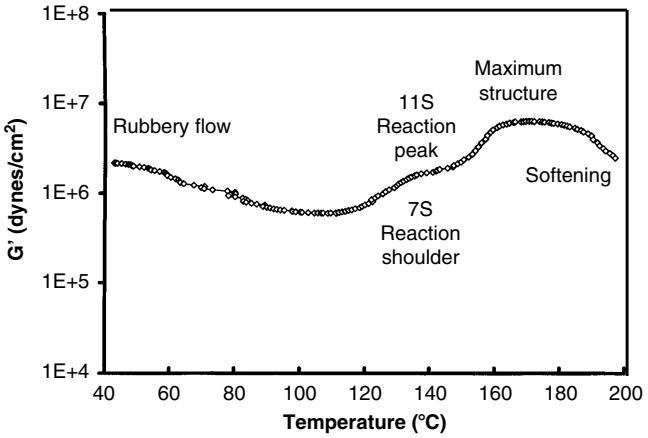

Figure 7.13. Storage modulus of 7S enriched globulin fraction with 20.8% moisture content as a function of temperature (Copyright 1998 from 'Understanding phase transitions and chemical complexing reactions in 7S and 11S soy protein fractions' by Morales-Diaz and Kokini (In: Phase/State Transitions in Foods, Rao and Hartel (Eds.)). Reproduced by permission of Routledge/Taylor & Francis Group, LLC.)

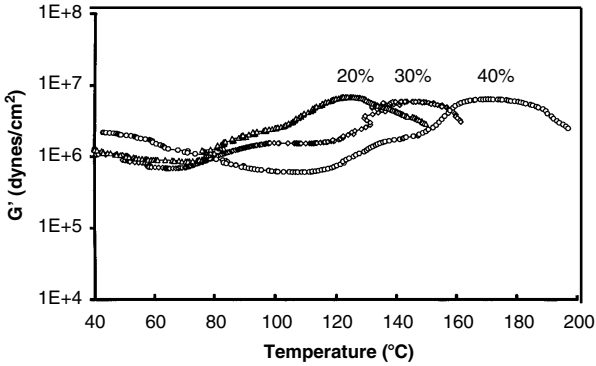

Figure 7.14. Storage modulus of 7S enriched globulin fraction with different moisture contents as a function of temperature (Copyright 1998 from 'Understanding phase transitions and chemical complexing reactions in 7S and 11S soy protein fractions' by Morales-Diaz and Kokini (In: Phase/State Transitions in Foods, Rao and Hartel (Eds.)). Reproduced by permission of Routledge/Taylor & Francis Group, LLC.)

mobility increases at higher water contents, the reactive molecules move closer to one another in order to react. The initiation of the structure formation, the length of G', and the initiation of the second part of increase in G' are moisture content dependent, indicating that additional water shifts the thermosetting reaction to lower temperatures (Figure 7.14). Similar behavior occurs in 11S globulin fractions (Figure 7.15). G' shoulder present in 7S fraction (Figure 7.13) is not present in the 11S fraction but still there is the initial structure forming reaction at 70°C (Figure 7.15) (Morales-Diaz and Kokini 1998).

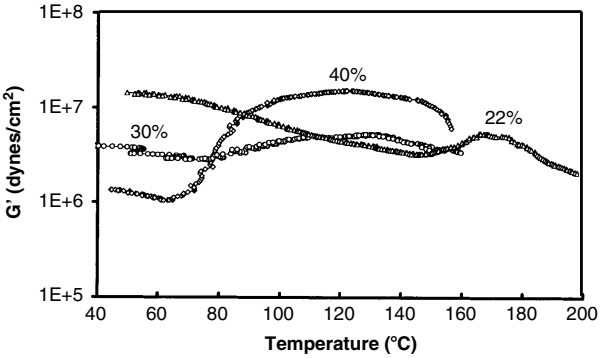

Figure 7.15. Storage modulus of 11S globulin fraction with different moisture contents as a function of temperature (Copyright 1998 from 'Understanding phase transitions and chemical complexing reactions in 7S and 11S soy protein fractions' by Morales-Diaz and Kokini (In: Phase/State Transitions in Foods, Rao and Hartel (Eds.)). Reproduced by permission of Routledge/Taylor & Francis Group, LLC.)

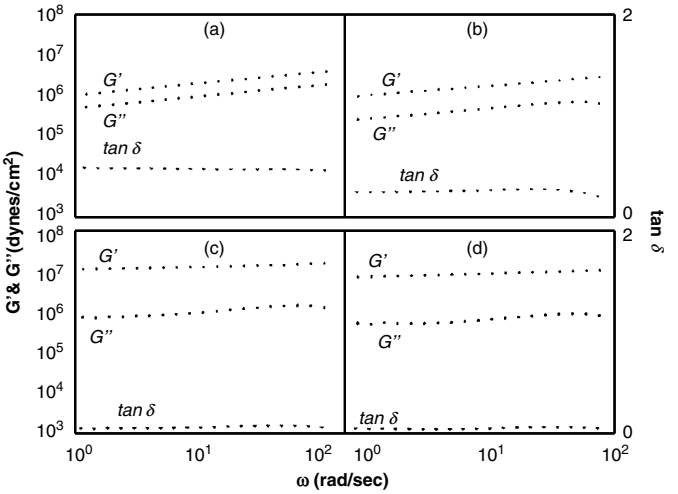

Figure 7.16. G', G'' and tanδ of 7S globulin fraction at 30% moisture content as a function of frequency: (a) 65°C, (b) 70°C, (c) 115°C, (d) 138°C (Copyright 1998 from 'Understanding phase transitions and chemical complexing reactions in 7S and 11S soy protein fractions' by Morales-Diaz and Kokini (In: Phase/State Transitions in Foods, Rao and Hartel (Eds.)). Reproduced by permission of Routledge/Taylor & Francis Group, LLC.)

The temperature-induced reactions of 7S and 11S soy globulins are also confirmed by looking into the frequency dependence of G', G'' and tanδ (Figure 7.16). G' and G'' have close values at 65°C, and both values increase with frequency at a slope of 0.30 (Figure 7.16a), suggesting the entangled polymer flow region. At 70°C, G' and G'' get apart from each other and the effect of frequency is less with a slope of 0.19. On the other hand, at the highest frequency, both G' and G'' are independent of frequency indicating a shorter range networking compared to the behavior at

65°C (Figure 7.16b). At 115°C, the values of G' and G'' almost do not depend on frequency with a slope of 0.07; G' and G'' get even further apart from each other; and the value of G' is almost eight times higher than that at 70°C (Figure 7.16c), indicating the formation of a cross-linked polymer. At 138°C, G' and G'' decreases (Figure 7.16d), due to possible depolymerization of the cross-linked network around this temperature. As networking occurs at higher temperatures, $\tan\delta$ decreases (Figure 7.16), confirming the individual behaviors of G' and G'' (Morales-Diaz and Kokini 1998).

Stress relaxation experiments of 7S and 11S globulin fractions at various temperatures—covering the range of glassy state, glass transition regions and rubbery state—is utilized to obtain stress-relaxation master curves as a function of time (Morales-Diaz and Kokini 1998). The Kohlrausch–Williams–Watts (KWW) equation is used to model 7S and 11S globulin fractions in the glassy state;

$$G(t) = G_0 . \exp\left[-\left(t / \lambda_G\right)^{\beta} \right] \tag{7.2}$$

where t is time; $G(t)$ is the relaxation modulus at t; λ_G is the characteristic relaxation time for the glassy material; G_0 is the zero time relaxation modulus; and β is an adjustable parameter related to the narrowness of the distribution ($\beta = 1$ shows single relaxation time). Figure 7.17 shows that the KWW equation fits the experimental relaxation modulus of both globulin fractions in their glassy state. The model predicts the relaxation modulus from very short time region up to $t \sim \lambda_G$ (at $t \sim \lambda_G$, $G \sim G_0/e$). β values for both fractions are close to 0.1 (Figure 7.17), suggesting the existence of a distribution of relaxation times (Morales-Diaz and Kokini 1998). The 11S fraction shows much higher relaxation time than 7S, partially due to structural differences between 7S and 11S fractions (Fukushima 1991a, 1991b), resulting in lower free volume (Matsuoka et al. 1978).

Morales-Diaz and Kokini (1998) have also shown that high stress is required to start deforming the samples of 7S and 11S soy globulin fractions using uniaxial extension experiments to obtain stress-strain curves (Figure 7.18). The 7S fraction is deformed more easily than 11S (at lower stress levels) due to its less cross-linked nature. After a certain strain (5% and 7.5% for 7S and 11S fractions, respectively), equilibrium stress values are obtained and the samples break at higher strains. Equation (7.3), from rubber elasticity theory, is used to model 7S and 11S globulin fractions in the rubbery state using the stress-strain data in Figure 7.18,

$$f = 2.\left[\lambda - \left(1 / \lambda^2\right) \right].\left[C_1 + C_2 / \lambda \right] \tag{7.3}$$

where λ is the extension ratio ($= L/L_0$); f is the force acting in the direction of strain; and C_1 and C_2 are the Mooney–Rivlin constants, where C_1 and C_2 are determined from the intercept and slope of $f / [\, 2.(\lambda - (1/\lambda^2))]$ versus $1/\lambda$ plots. According to Figure 7.19, both soy globulin fractions do not behave as Mooney–Rivlin materials (Morales-Diaz and Kokini 1998) as the plots do not follow a linear behavior (Sperling, 2001).

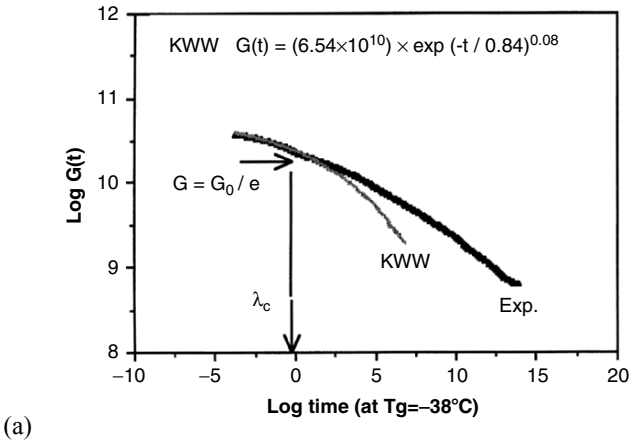

(a)

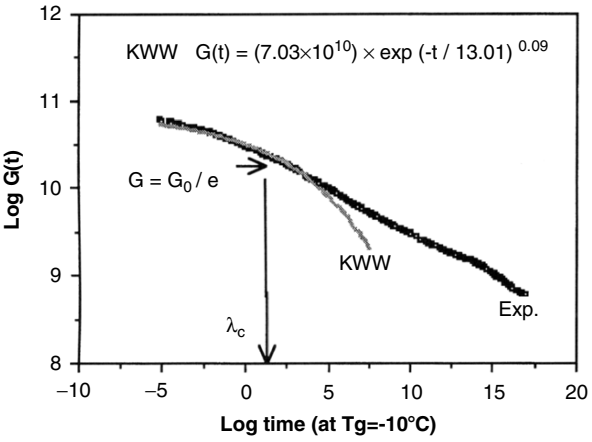

(b)

Figure 7.17. Stress relaxation master curve of; (a) 7S enriched globulin fraction; (b) 11S fraction; and the KWW equation in the glassy state (Copyright 1998 from 'Understanding phase transitions and chemical complexing reactions in 7S and 11S soy protein fractions' by Morales-Diaz and Kokini (In: Phase/State Transitions in Foods, Rao and Hartel (Eds.)). Reproduced by permission of Routledge/Taylor & Francis Group, LLC.)

7.5 State Diagrams of Proteins

Figures 7.20a-b show the physical/chemical states of soy globulins (7S and 11S soy globulins, respectively) as a function of moisture content and temperature. At low temperatures and at low moisture contents, the soy globulins are in the glassy state. Above the glass transition, a rubbery region is observed. Comparison of the glass transition behavior of 7S and 11S globulins shows that the transition of 11S globulin

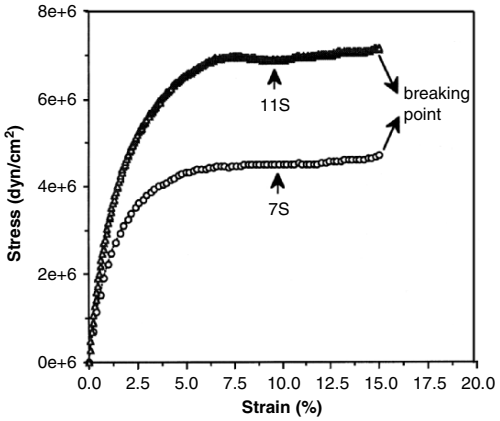

Figure 7.18. Stress-strain behavior of 7S and 11S soy fractions with 30% moisture content (Copyright 1998 from 'Understanding phase transitions and chemical complexing reactions in 7S and 11S soy protein fractions' by Morales-Diaz and Kokini (In: Phase/State Transitions in Foods, Rao and Hartel (Eds.)). Reproduced by permission of Routledge/Taylor & Francis Group, LLC.)

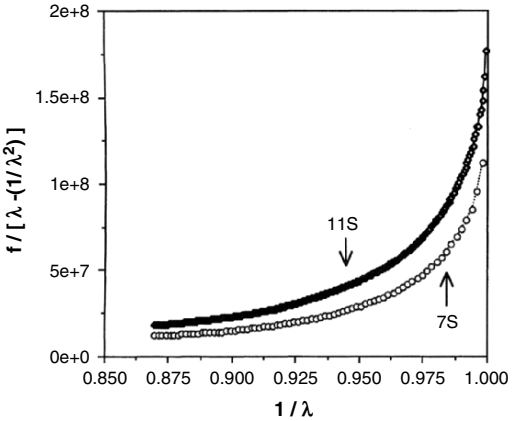

Figure 7.19. Mooney–Rivlin plot for 7S and 11S soy fractions at 30% moisture content (Copyright 1998 from 'Understanding phase transitions and chemical complexing reactions in 7S and 11S soy protein fractions' by Morales-Diaz and Kokini (In: Phase/State Transitions in Foods, Rao and Hartel (Eds.)). Reproduced by permission of Routledge/Taylor & Francis Group, LLC.)

occurs at higher temperatures than the transition of 7S globulin (Figure 7.20). The entangled rubbery phase polymer softens at higher temperatures, forming the entangled polymer flow region, which is given as a hypothetical transition located at 100°C above T_g. This is the region where it is expected that the viscosity of the material decreases with increased mobility. At much higher temperatures, the soy globulin molecules have enough mobility and energy to form aggregates and cross-links, which are identified as the reaction region in Figure 7.20. As the temperature increases, the elastomeric structure melts forming the softening regions. The horizontal line below the rubbery state in Figure 7.20 represents the glass transition temperature of maximally freeze-concentrated globulins (T'_g) (Morales-Diaz and Kokini 1998).

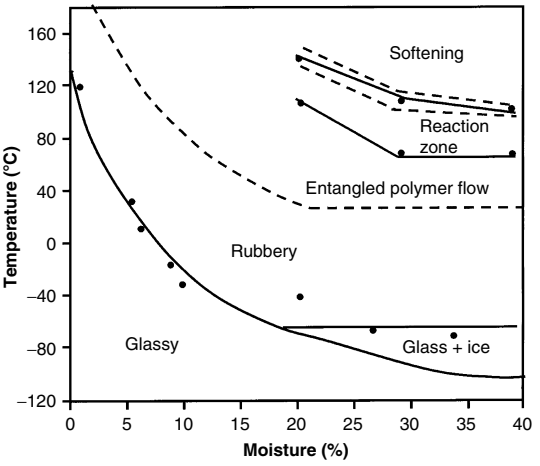

(a)

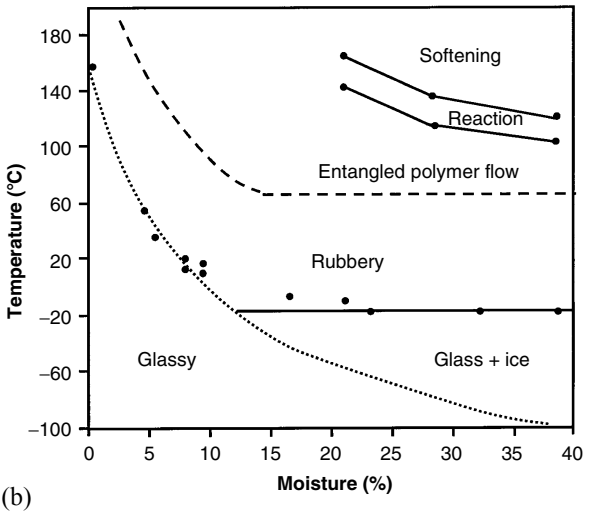

(b)

Figure 7.20. State diagram for; (a) 7S soy globulin and (b) 11S soy globulin (Copyright 1998 from 'Understanding phase transitions and chemical complexing reactions in 7S and 11S soy protein fractions' by Morales-Diaz and Kokini (In: Phase/State Transitions in Foods, Rao and Hartel (Eds.)). Reproduced by permission of Routledge/Taylor & Francis Group, LLC.)

Reaction rate constants (k) for cross-linking process of 7S and 11S soy globulin fractions have been obtained utilizing a first-order kinetics using Equation (7.4) (Morales-Diaz and Kokini 1998) as;

$$\ln \frac{M_c - M_e}{M_{c,0} - M_e} = -k.t \tag{7.4}$$

where M_c is the molecular weight between cross-links; $M_{c,0}$ is the initial molecular weight between cross-links during complexing reactions; and M_e is the molecular weight between cross-links at equilibrium (Figure 7.21). The temperature dependence of the cross-linking reaction rate constants shows Arrhenius-type behavior;

$$k = A_0 . e^{\left[-E_a/RT\right]} \tag{7.5}$$

where E_a is the activation energy; A_0 is the rate constant; T is absolute temperature; and R is the gas constant. Activation energies for 7S and 11S globulins are determined as 27,900 cal/mol and 39,460 cal/mol, respectively, supporting the fact that complexing reactions occur at higher temperatures for 11S globulins than for 7S globulins (Figure 7. 20).

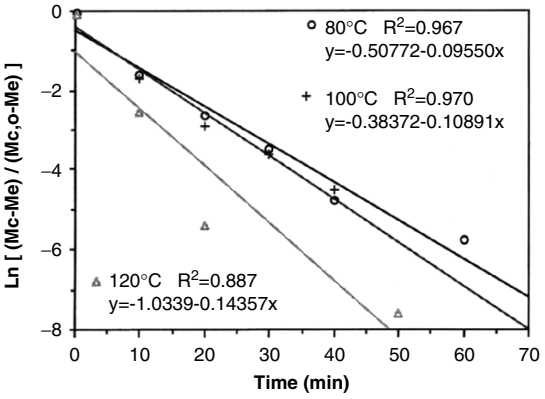

(a)

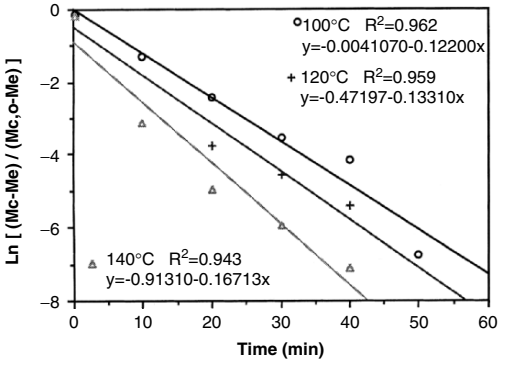

(b)

Figure 7.21. Cross-linking kinetics for; (a) 7S enriched globulin fraction, and (b) 11S globulin fraction (Copyright 1998 from 'Understanding phase transitions and chemical complexing reactions in 7S and 11S soy protein fractions' by Morales-Diaz and Kokini (In: Phase/State Transitions in Foods, Rao and Hartel (Eds.)). Reproduced by permission of Routledge/Taylor & Francis Group, LLC.)

State diagrams for other cereal proteins, such as gliadin (Madeka and Kokini 1994; Kokini et al. 1994a, 1994b) (Figure 7.22); glutenin (Kokini et al. 1994a, 1994b) (Figure 7.23); zein (Kokini et al. 1995; Madeka and Kokini 1996) (Figure 7.24) are also reported in literature. These state diagrams also show several order-disorder transitions and chemical reactions, including glassy regions, rubbery regions, entangled polymer flow region, networking reaction zone and softening regions.

Glutenin, gliadin and zein are glassy polymers at low moisture content and low temperatures determined using DSC and mechanical spectroscopy (Kokini et al. 1994a, 1994b). Water plasticizes these proteins through the hydrophilic amino acids in their structure (Figures 7.22–7.24).

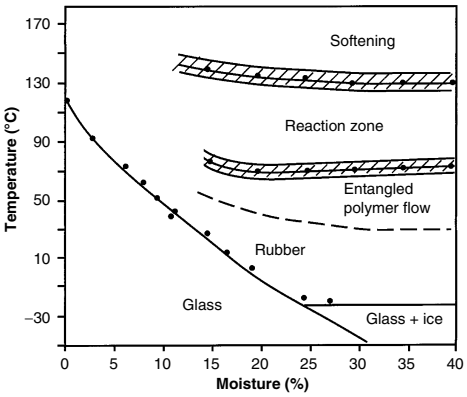

Figure 7.22. State diagram for gliadin (Reprinted from J. Food Eng., 22, Madeka and Kokini, Changes in rheological properties of gliadin as a function of temperature and moisture: Development of a state diagram, pp. 241-252, Copyright (1994), with permission from Elsevier.)

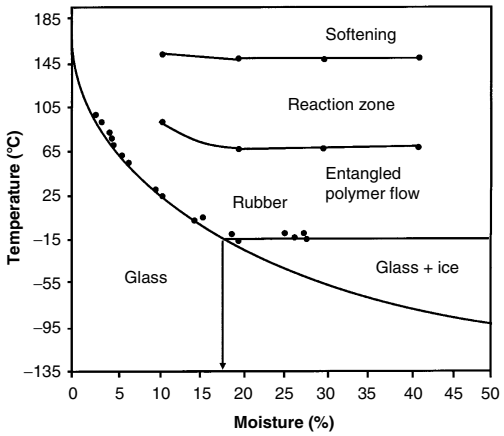

Figure 7.23. State diagram for glutenin (Reprinted from Trends Food Sci. Tech., 5, Kokini, Cocero, Madeka, and De Graaf, The development of state diagrams for cereal proteins, pp. 281-288, Copyright (1994), with permission from Elsevier.)

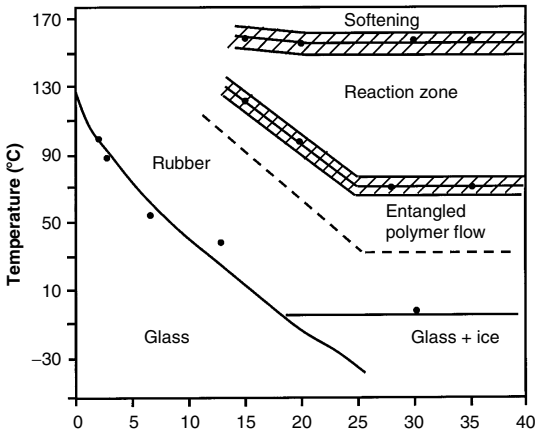

Figure 7.24. State diagram for zein (Reproduced with permission from Kokini, Cocero, and Madeka, 1995, State diagrams help predict rheology of cereal proteins, Food Technol. 49, pp. 74-81, Institute of Food Technologists.)

Kokini et al. (1994b) have shown that the storage modulus of glutenin fall only by a factor of 10^1dyn/cm^2 through the glass transition region using mechanical spectroscopy (Figure 7.25). This decrease is different from the usual 10^3dyn/cm^2 decrease common in synthetic polymers (Sperling 2001). For moisture contents between 0% and 28%, T_g of glutenin is reported to be between 141°C and –12°C (Kokini et al. 1994b); and T_g of gliadin in the same moisture content range is reported to be between 121°C and –25°C (Madeka and Kokini 1994). T_g of zein is in the range from 139°C to –14°C for moisture contents between 0% and 30% (Kokini et al. 1994a, 1994b; Madeka and Kokini 1996).

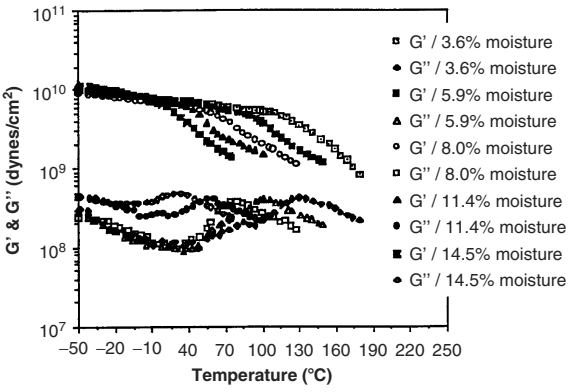

Figure 7.25. Storage modulus and loss modulus of glutenin at low moisture contents as a function of temperature (Reprinted from Trends Food Sci. Tech., 5, Kokini, Cocero, Madeka, and De Graaf, The development of state diagrams for cereal proteins, pp. 281-288, Copyright (1994), with permission from Elsevier.)

Glutenin, gliadin and zein are determined to be in the rubbery state at room temperature at moisture contents higher than 11%, 15%, 17%, respectively (Kokini et al. 1994a, 1994b; Madeka and Kokini 1994) (Figures 7.22–7.24). Pressure rheometry experiments are used to demonstrate the entangled polymer flow of glutenin, gliadin and zein (Kokini et al. 1994a, 1994b). Figure 7.25 shows the temperature sweep of glutenin where G′ has a decreasing characteristic through the entangled polymer flow region. The material becomes softer and the molecules become more mobile as their temperature is increased prior to network formation. The Bird–Carreau model is used to predict the shear properties of glutenin in entangled flow region (Kokini et al. 1994a). Wang and Kokini (1995) have shown predictions of steady shear and steady extensional flow properties of gluten using Wagner constitutive model.

Reactions of proteins result in either the formation of higher molecular weight products or in the degradation of molecular structure. Large increases in G' is the indication of complexing reactions, whereas a decrease in G' is the indication of degradation. For instance, at the maximum G', glutenin reaches the maximum structure formation. G'' shows a minimum at the similar temperature where G' has a maximum, which indicates that there is a solid protein network formed (Kokini et al. 1994b). Similar complexing reactions for gliadin and zein have also been shown (Madeka and Kokini 1994, 1996; Kokini et al. 1994b). At the end of the reaction region, softening of the material is observed due to the thermal effect of the material or due to depolymerization. Reaction and softening regions for glutenin, gliadin and zein are also strongly moisture dependent (Figures 7.22–7.24).

State diagram of gluten (Figure 7.26) shows the glassy and rubbery regions below and above glass the transition line, respectively (Toufeili et al. 2002). The temperature of maximally freeze-concentration (T'_g) of gluten is located at –20°C with the corresponding weight fraction of 76% (W'_g). An entangled polymer flow region occurs at 92–140°C at around 10% moisture content, after which a network structure is formed in the reaction zone. At higher levels of moisture content, gluten forms cross-links at lower temperatures; at 120°C with 20% moisture content, and at 93°C with 30–40% moisture levels. Softening of the cross-linked network occurs

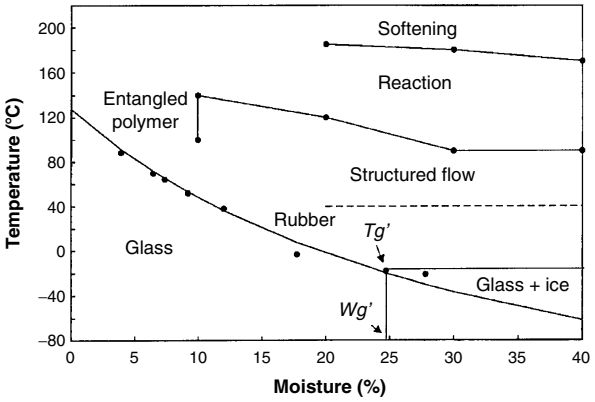

Figure 7.26. State diagram for gluten (Reproduced with permission from Toufeili, Lambert, and Kokini, 2002, Effect of glass transition and cross-linking on rheological properties of gluten: development of a preliminary state diagram, Cereal Chem. 79, pp. 138-142, American Association of Cereal Chemists.)

at moisture contents higher than 20%; and at lower temperatures as water content increases (Figure 7.26) (Toufeili et al. 2002).

7.6 The Use of State Diagrams During Food Processes

The physical properties of amorphous food materials can be related to their glass transition through state diagrams. State diagrams are important to monitor and predict the changes in food products during dehydration, freezing and heating/cooling (Figure 7.27). Typical processes that are affected by the time-dependent and viscosity-related structural transformations—including ice formation, stickiness, collapse and crystallization—are shown in Figure 7.28.

Dehydration represents rapid removal of water, where the remaining solutes are transformed into an amorphous state. Food products can undergo structural changes, such as collapse and stickiness, as the temperature or relative humidity changes (Figure 7.28). Near T_g, structural changes are kinetically postponed, whereas these changes occur above T_g due to the tendency of the rubbery state to minimize its volume (Roos and Karel 1991c). Crystallization occurs concurrently with the structural changes above T_g (Figure 7.28) and its rate increases as T-T_g increases. When crystallization occurs in foods, water is released. The released water is then absorbed by the amorphous portion of the food and results in lower T_g values (or higher T-T_g values) resulting in rapid crystallization. If there is moisture transfer available between the food material and its environment, then released water is lost, leaving the amorphous portion of the food approximately at constant moisture level and the rate of crystallization is determined through constant T-T_g (Roos and Karel 1991c). Before freezing, T_g of most foods are below their freezing point (Figure 7.28). Effective T_g increases with the freeze-concentration and the physical state can be

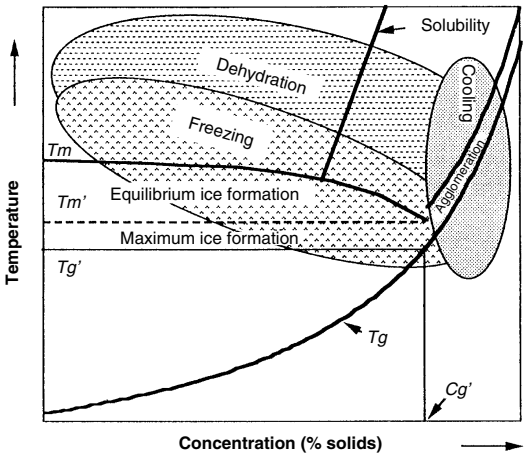

Figure 7.27. Location of various food processes, including freezing, dehydration, heating and cooling, on a state diagram (Reproduced with permission from 'Effects of glass transition on processing and storage' by Karel, Buera, and Roos (In: The Glassy State in Foods, Blanshard and Lillford (Eds.)), 1993, Nottingham University Press.)

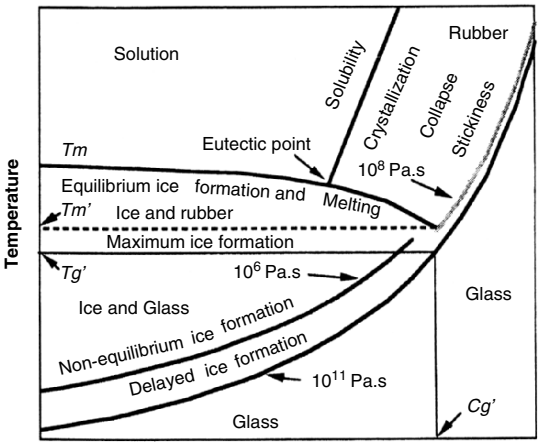

Figure 7.28. A state diagram showing stability and time-dependent changes in the rubbery state with typical processes (Reproduced with permission from Roos and Karel, 1991c, Applying state diagrams to food processing and development, Food Technol. 45, pp. 66, 68-71, 107, Institute of Food Technologists.)

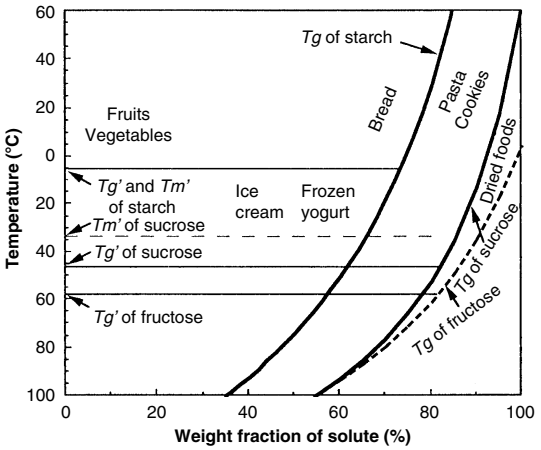

Figure 7.29. A state diagram representing the position of various food products (Reproduced with permission from 'Effects of glass transition on processing and storage' by Karel, Buera, and Roos (In: The Glassy State in Foods, Blanshard and Lillford (Eds.)), 1993, Nottingham University Press.)

predicted from the state diagram. Figure 7.29 shows approximate locations of various food products including pasta, cookies, bread, ice-cream, frozen yogurt and dried foods on a binary state diagram.

During processes such as baking and extrusion, prediction of material phases is critical to control the final food product quality. Therefore, state diagrams are of great importance for developing predictive capabilities for food materials as they

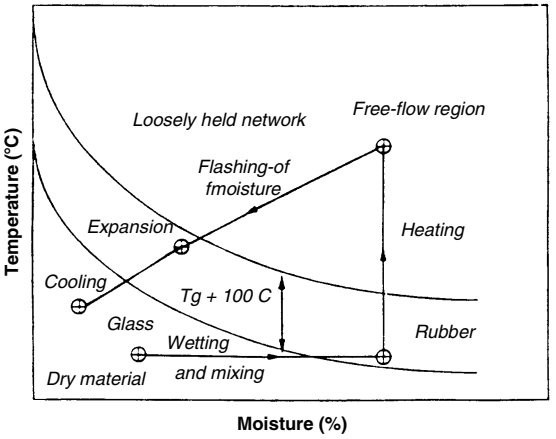

Figure 7.30. Hypothetical state diagram of cereal proteins during wetting, heating and cooling/drying stages of extrusion cooking (Reprinted from Trends Food Sci. Tech., 5, Kokini, Cocero, Madeka, and De Graaf, The development of state diagrams for cereal proteins, pp. 281-288, Copyright (1994), with permission from Elsevier.)

describe the temperature and moisture content region at which the material undergoes appropriate reactions. For instance, state diagrams for extrusion cooking and baking would describe the specific temperature and moisture contents where the proteins would form the cross-linking reactions that in turn form the crisp texture of an extruded product or the crumb of a baked product (Kokini et al. 1994b). Therefore, development of state diagrams during processing enables a predictive tool for product development. As an illustration, a hypothetical state diagram of cereal proteins during extrusion processing and storage is shown in Figure 7.30.

Moraru et al. (2002) have developed the state diagram for extruded meat–starch systems as a function of temperature and water activity (Figure 7.31), showing that the physical state of the product is controlled by the glass transition location of the protein. Direct examination of the meat–starch extruded samples has shown that the samples with water activity lower than 0.32 are brittle and glassy, whereas samples with water activity higher than 0.57 are rubbery and pliable, which are clearly shown in the state diagram (Figure 7.31). This observation is validated by the mechanical analysis results. At room temperature, samples with water activity lower than 0.32 are shown to have a storage modulus of order of magnitude of 10^{10}dyn/cm^2, which is typical for glassy polymers, where storage modulus decreases to 10^9dyn/cm^2 and 10^8dyn/cm^2 at higher water activities (Moraru et al. 2002).

Figure 7.32 shows the state diagram of sucrose–water systems on which location of lean (low sugar/fat ratio) and rich (high sugar/fat ratio) cracker dough, rich cookie dough, and final baked cookie and cracker products are positioned according to their process temperatures and typical sucrose–water content. T'_g is the intersection of liquidus (nonequilibrium extension) and glass curves, whereas T'_e (eutectic melting temperature) is the intersection of liquidus and solidus curves (Levine and Slade 1993).

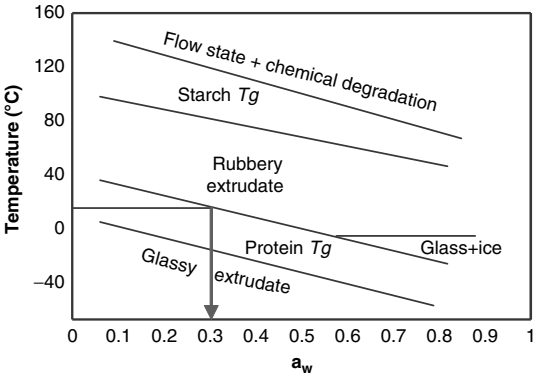

Figure 7.31. State diagram for the extruded meat–starch matrix. (The arrow indicates the water activity above which the extrudates become rubbery at room temperature) (Reproduced with permission from Moraru, Lee, Karwe, and Kokini, 2002, Phase behavior of a meat-starch extrudate illustrated on a state diagram, J. Food Sci. 67, pp. 3026-3032, Institute of Food Technologists.)

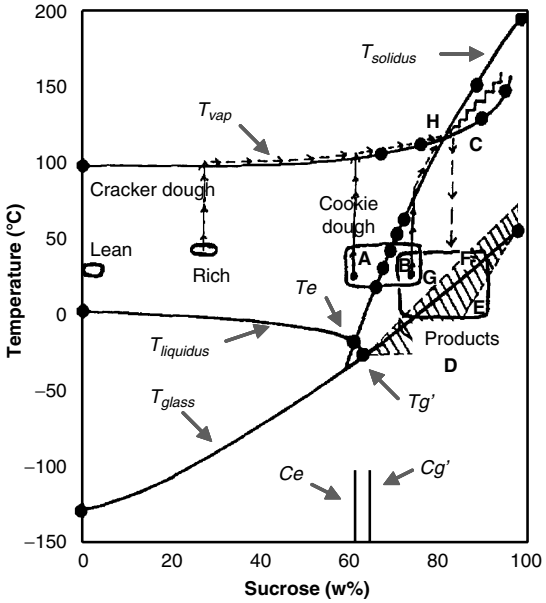

Figure 7.32. State diagram of a sucrose–water system showing the location of cracker and cookie dough together with the final cracker and cookie products (Reproduced with permission from 'The glassy state in applications for the food industry' by Levine and Slade (In: The Glassy State in Foods, Blanshard and Lillford (Eds.)), 1993, Nottingham University Press.)

Lean and rich cracker dough is located above the glass curve, showing that it is relatively easy to dry these products during baking. As the temperature of the cracker dough is increased above the vaporization temperature, the liquid water in dough becomes water vapor. This water vapor is removed more as baking continues, resulting

in increased concentration of dissolved sucrose. When the dough is baked and cooled to room temperature, the final baked crackers becomes glassy (Box D in Figure 7.32) (Levine and Slade 1993).

Cookie dough is more complex than cracker dough due to the additional presence of crystalline sugar dissolving during mixing. The cookie dough can be either in Box A or Box B in Figure 7.32 (Levine and Slade 1993). A temperature increase during baking results in either initial water evaporation and then sugar dissolving (path from A to H) or initial sugar dissolving and then water evaporation (path from B to H). There may be various routes for the other baked products as described in detail in Levine and Slade (1993). The important point that Figure 7.32 makes is that the glass transition curve on the state diagram of sucrose–water represents the behavior of the final baked products. The storage stability of the products depends on the temperature, time and possible moisture content changes during distribution, where high-quality products should be located in Box D in Figure 7.32 (Levine and Slade 1993).

7.7 Concluding Remarks

In this chapter, we have made an attempt to give a review of state diagrams of various carbohydrates and proteins. The flow characteristics of proteins in glassy and rubbery states that lead to formation of protein state diagrams are summarized. We hope that this chapter will serve as a useful reference to those who want to capture the key ideas behind development of state diagrams and the usage of these diagrams during food processing.

7.8 References

Ablett, A., Izzard, M.J., and Lillford, P.J. (1992). Differential scanning calorimetric study of frozen sucrose and glycerol solutions. *J. Chem. Soc. Faraday T*. 88, 789–794.

Aklonis, J.J. and MacKnight, W.J. (1983). *Introduction to Polymer Viscoelasticity*. John Wiley & Sons, New York.

Biliaderis, C.G., Maurice, T.J., and Vose, J.R. (1980). Starch gelatinization phenomena studied by DSC. *J. Food Sci.* 45, 1669–1680.

Biliaderis, C.G., Page, C.M., Maurice, T.J., and Juliano, B.O. (1986). Thermal characterization of rice starches: A polymeric approach to phase transitions of granular starch. *J. Agr. Food Chem*. 34, 6–14.

Bizot, H., Le Bail, P., Leroux, B., Davy, J., Roger, P., and Buleon, A. (1997). Calorimetric evaluation of the glass transition in hydrated, linear and branched polyanhydroglucose compounds. *Carbohyd. Polym*. 32(1), 33–50.

Blanshard, J.M.V. (1986). The significance of the structure and function of the starch granule in baked products. In: J.M.V. Blanshard, P.J. Frazier and T. Galliard (Eds.), *Chemistry and Physics of Baking*. Royal Society of Chemistry, London, pp. 1–13.

Blanshard, J.M.V. (1988). Elements of cereal product texture. In: J.R. Mitchell and J.M.V. Blanshard (Eds.), *Food Structure: Its Creation and Evaluation*. Butterworths, London, pp. 313–330.

Cocero, A.M. and Kokini, J.L. (1991). The study of the glass transition of glutenin using small amplitude oscillatory rheological measurements and differential scanning calorimetry. *J. Rheol.* 35(2), 257–269.

Cowie, J.M.G. (1975). Some general features of T_g-M relations for oligomers and amorphous polymers. *Eur. Polym. J*. 11, 297–300.

Fennema, O.R. (1996). Water and ice. In: O.R. Fennema (Ed.), *Food Chemistry*, 3rd Edition. Marcel Dekker, New York, pp. 17–94.

Fox, T.G. and Flory, P.J. (1950). Second-order transition temperatures and related properties of polystyrene. I. Influence of molecular weight. *J. Appl. Phys*. 21, 581–591.

Fukushima, D. (1991a). Recent progress of soybean protein foods: Chemistry, technology, and nutrition. *Food Rev. Int*. 7(3), 323–351.

Fukushima, D. (1991b). Structures of plant storage proteins and their functions. *Food Rev. Int*. 7(3), 351–381.

Gropper, M., Moraru, C.I., and Kokini, J.L. (2002). Effect of specific mechanical energy on properties of extruded protein–starch mixtures. *Cereal Chem*. 79(3), 429–433.

Icoz, D.Z., Moraru, C.I., and Kokini, J.L. (2005). Polymer–polymer interactions in dextran systems using thermal analysis. *Carbohyd. Polym*. 62(2), 120–129.

Karel, M., Buera, M.P., and Roos, Y. (1993). Effects of glass transition on processing and storage. In: J.M.V. Blanshard and P.J. Lillford (Eds.), *The Glassy State in Foods*. Nottingham University Press, Loughborough, UK, pp. 13–34.

Kokini, J.L., Cocero, A.M., Madeka, H., and De Graaf, E. (1994a). Order–disorder transitions and complexing reactions in cereal proteins and their effect on rheology. In: D.A. Siginer and Y.G. Yanovsky (Eds.), *Advances in Structured and Heterogenous Continua*. Allerton Press, New York, pp. 215–234.

Kokini, J.L., Cocero, A.M., Madeka, H., and De Graaf, E. (1994b). The development of state diagrams for cereal proteins. *Trends Food Sci. Tech*. 5, 281–288.

Kokini, J.L., Cocero, A.M., and Madeka, H. (1995). State diagrams help predict rheology of cereal proteins. *Food Technol*. 49(10), 74–81.

Levine, H. and Slade, L. (1986). A polymer physico-chemical approach to the study of commercial starch hydrolysis products (SHPs). *Carbohyd. Polym*. 6, 213–244.

Levine, H. and Slade, L. (1988). Water as a plasticizer: Physico-chemical aspects of low-moisture polymeric systems. In: F. Franks (Ed.), *Water Science Reviews* 3. Cambridge University Press, New York, pp. 79–186.

Levine, H. and Slade, L. (1990). Influences of the glassy and rubbery states on the thermal, mechanical, and structural properties of doughs and baked products. In: H. Faridi and J.M. Faubion (Eds.), *Dough Rheology and Baked Product Texture*. Van Nostrand Reinhold, New York, pp. 157–330.

Levine, H. and Slade, L. (1993). The glassy state in applications for the food industry. In: J.M.V. Blanshard and P.J. Lillford (Eds.), *The Glassy State in Foods*. Nottingham University Press, Loughborough, UK, pp. 333–373.

Madeka, H. and Kokini, J.L. (1994). Changes in rheological properties of gliadin as a function of temperature and moisture: Development of a state diagram. *J. Food Eng*. 22, 241–252.

Madeka, H. and Kokini, J.L. (1996). Effect of glass transition and aggregation on rheological properties of zein: Development of a preliminary state diagram. *Cereal Chem*. 73(4), 433–438.

Matsuoka, S., Blair, H.E., Bearder, S.S., Kern, H.E., and Ryan, J.T. (1978). Analysis of non-linear stress relaxation in polymeric glasses. *Polym. Eng. Sci*. 18(14), 1073–1080.

Maurice, T.J., Slade, L., Page, C., and Sirett, R. (1985). Polysaccharide–water interactions-Thermal behavior of starch. In: D. Simatos and J.L. Multon (Eds.), *Properties of Water in Foods*. Martinus Nijhoff, Dordrecht, pp. 211–227.

Mizuno, A., Mitsuiki, M., and Motoki, M. (1998). Effect of crystallinity on the glass transition temperature of starch. *J. Agr. Food Chem*. 46, 98–103.

Morales-Diaz, A.M. and Kokini, J.L. (1998). Understanding phase transitions and chemical complexing reactions in 7S and 11S soy protein fractions. In: M.A. Rao and R.W. Hartel (Eds.), *Phase/State Transitions in Foods*. Marcel Dekker, New York, pp. 273-311.

Moraru, C.I., Lee, T-C., Karwe, M.V., and Kokini, J.L. (2002). Phase behavior of a meat–starch extrudate illustrated on a state diagram. *J. Food Sci*. 67(8), 3026–3032.

Roos, Y.H. (1992). Phase transitions and transformations in food systems. In: D.R. Heldman and D.B. Lund (Eds.), *Handbook of Food Engineering*. Marcel Dekker, New York, pp. 145–197.

Roos, Y. (1993). Melting and glass transitions of low molecular weight carbohydrates. *Carbohyd. Res*. 238, 39–48.

Roos, Y.H. (1995). *Phase Transitions in Foods*. Academic Press, San Diego, CA.

Roos, Y.H. and Karel, M. (1991a). Amorphous state and delayed ice formation in sucrose solutions. *Int. J. Food Sci. Tech*. 26, 553–566.

Roos, Y.H. and Karel, M. (1991b). Water and molecular effects on glass transitions in amorphous carbohydrates and carbohydrate solutions. *J. Food Sci*. 56, 1676–1681.

Roos, Y.H. and Karel, M. (1991c). Applying state diagrams to food processing and development. *Food Technol*. 45, 66, 68–71, 107.

Roos, Y.H. and Karel, M. (1991d). Plasticizing effect of water on thermal behavior and crystallization of amorphous food models. *J. Food Sci*. 56, 38–43.

Roos, Y. and Karel, M. (1991e). Phase transitions of mixtures of amorphous polysaccharides and sugars. *Biotechnol. Progr*. 7, 49–53.

Roos, Y., Karel, M., and Kokini J.L. (1996). Glass transitions in low moisture and frozen foods: Effect on shelf life and quality. *Food Technol*. 50(11), 95–108.

Ruan, R., Long, Z., Chen, P., Huang, V. Almaer, S., and Taub, I. (1999). Pulse NMR study of glass transition in maltodextrin. *J. Food Sci*. 64(1), 6–9.

Slade, L. and Levine, H. (1988). Structural stability of intermediate moisture foods: A new understanding. In: J.M.V. Blanshard and J.R. Mitchell (Eds.), *Food Structure: Its Creation and Evaluation*. Butterworths, London, pp. 115–147.

Slade, L. and Levine, H. (1991a). Beyond water activity: Recent advances based on an alternative approach to the assessment of food quality and safety. CRC Cr. Rev. Food Sci. 30, 115–360.

Slade, L. and Levine, H. (1991b). A food polymer science approach to structure–property relationship in aqueous food systems: Nonequilibrium behavior of carbohydrate–water systems. In: H. Levine and L. Slade (Eds.), *Water Relationships in Food*. Plenum Press, New York, pp. 29–101.

Sperling, L.H. (2001). *Introduction to Physical Polymer Science*. 3rd Edition. John Wiley & Sons, New York.

Toufeili, I., Lambert, I.A., and Kokini, J.L. (2002). Effect of glass transition and cross-linking on rheological properties of gluten: Development of a preliminary state diagram. *Cereal Chem.* 79(1), 138–142.

Van de Berg, C. (1986). Water activity. In: D. MacCarthy (Ed.), *Concentration and Drying of Foods*. Elsevier Applied Science, London, pp. 11–36.

Wang, C.F. and Kokini, J.L. (1995). Simulation of the nonlinear rheological properties of gluten using the Wagner constitutive model. *J. Rheol*. 39(6), 1465–1482.

Zeleznak, K.J. and Hoseney, R.C. (1987). The glass transition in starch. *Cereal Chem*. 64(2), 121–124.

Zimeri, J.E. and Kokini, J.L. (2003). Phase transitions of inulin-waxy maize starch systems in limited moisture environments. *Carbohyd. Polym*. 51, 183–190.

Chapter 8

Nanotechnology in Food Materials Research

Jooyoung Lee, Xiaoyong Wang, Chada Ruengruglikit, Zafer Gezgin, and Qingrong Huang

Rutgers University, Department of Food Science, 65 Dudley Road, New Brunswick, New Jersey 08901. qhuang@aesop.rutgers.edu.

8.1 Introduction

Nanotechnology is an enabling science and technology that allow scientists and engineers to manipulate, measure, formulate, synthesize, and control nanostructured materials and devices so that novel properties and functions can be achieved. The term "nano" corresponds to dimensions in the order of 10^{-9}. Therefore, one nanometer (nm) means one-billionth meter. According to the U.S. National Nanotechnology Initiative (www.nano.gov), the length scale of nanotechnology is in the range of 1–100 nm. More importantly, nanotechnology implies (1) novel phenomena, properties, and functions at nanoscale; and (2) the ability to manipulate matter at the nanoscale in order to change those properties and functions.

Nanotechnology has recently become one of the most active research fields in the areas of solid-state physics, chemistry, materials science, cell biology, and biotechnology (Edvardsson et al. 2005; Niemeyer and Mirkin 2004). However, nanotechnology for food applications is still in its infancy. In Fall 2002, the U.S. Department of Agriculture (USDA) organized the first strategic roadmap planning workshop on nanoscale science and engineering for agriculture and food systems (www.nseafs.cornell.edu). Since then, several food nanotechnology-related initiatives have been launched by governments, universities, and industries around the world. For example, USDA initiated the funding opportunities in nanoscale science and engineering for agriculture and food systems for the first time in 2004 in its National Research Initiative Competitive Grants Program. According to a study by Helmut Kaiser Consultancy (http://www.hkc22.com/nanofood.html), the nanofood market is expected to surge from $2.6 billions in 2003 to $7.0 billions in 2006 and to $20.4 billions in 2010. Many companies (>200) around the world are actively involved in nanofood research, but only a handful nanofood products are available in the market right now. Several feature articles have been published to address the

potential of food nanotechnology in the areas of food quality, health promotion, and food safety/security (Baeumner 2004; Chen and Zhang 2006; Moraru et al. 2003).

The growing demand for functional foods has largely been driven by the increasing knowledge of the relationship between functional ingredients and food matrixes. Because of the complexity of modern multicomponent food systems, food materials physical properties, such as phase behaviors, mechanical properties, and intermolecular interactions between food components at different length scales (nano-, micro-, and macro-scales) must be understood. This chapter will briefly present the potential of nanotechnology as applied to foods, and some applications of nanotechnology in food materials research-related areas, such as nanoscale properties and interactions of food biopolymers. Recent development in functional foods research, such as nanoencapsulation of nutraceuticals, will also be discussed.

8.2 Food Nanotechnology: A New Frontier in Food Science and Engineering

Food nanotechnology is a promising approach for novel developments in the areas of food science and engineering, due to the fact that the nanoscale control over food molecules may lead to the modification of many macroscale characteristics, such as the texture, taste and other sensory attributes. Nanoencapsulation and controlled-release of active food ingredients are important applications in food science that can be attained with nanotechnological approaches. Fabrication of the nanostructures required to realize such purposes can be achieved either by a bottom-up or top-down approach, where the former necessitates an extensive control and understanding of building blocks, their interactions and dynamic properties (Zhang 2003). Self-assembly of proteins into nanotubes is an excellent example of the bottom-up approach.

Food Protein–Based Nanotubes. Protein nanotubes are open-ended hollow tubular structures formed through the self-assembly of polypeptide chains (Okamoto et al. 2001). Electronic and molecular properties of the proteins determine the characteristics of the final structure (Fukasaku et al. 1998). Some examples of these structures observed in nature are virus capsids, microtubules, actin filaments, and amyloid fibrils (Valery et al. 2004). They can be designed artificially by protonating cyclic polypeptides, which leads to the formation of nanotube structure with hundreds to thousands of nanometers in length and tens to hundreds of angstroms in the inner diameter (Ghadiri et al. 1993). Another recently proposed way to form protein nanotubes is to crosslink proteins with glutaraldehyde solution through layer-by-layer deposition, which provides control over the wall thickness (Hou et al. 2005).

Several proteins have been studied and reported to form nanotubes to date. However, the only food protein currently known to possess this ability is alpha-lactalbumin (Graveland-Bikker and de Kruif 2006). Alpha-lactalbumin is one of the key components in whey protein with an isoelectric point (pI) of 4–5. In addition, it's the main protein in breast milk (Lonnerdal and Lien 2003). Observed earlier as the micro-structured stiff gel by Ipsen et al. (Ipsen et al. 2001), self-assembly of alpha-lactalbumin into nanotubes is achieved by its incubation with a protease from *Bacillus licheniformis* (BLP) acting on the Glu-X and Asp-X bonds, in the presence of Ca^{2+}

(Graveland-Bikker et al. 2006a). The mechanism of this assembly is explained by the step-by-step cleavage of alpha-lactalbumin to a final fragment mass of 8.8 kDa, linked between 26–37 and 50–113 sequences via a disulphide bond, which is estimated to have generated additional hydrophobic surfaces and calcium binding sites, leading to the formation of ordered nanotubes (Otte et al. 2004). Figure 8.1 shows the proposed 3-D model of α-lactalbumin nanotubes (Graveland-Bikker 2006).

In addition to its basic functional properties in foods as a thickening and gelling agent due to its ordered structure, the 8 nm cavity inside the tubes and amphiphilic structure of the alpha-lactalbumin polypeptide chain can be utilized to encapsulate a variety of food molecules (Graveland-Bikker and de Kruif 2006). Mechanical strength studies of the nanotubes using AFM give a Young's modulus of 0.6 GPa, which is stiff compared with proteins of similar biological structures (Graveland-Bikker et al. 2006b). This feature is important in terms of the stability of encapsulated core materials. Furthermore, reversible assembly of the nanotubes with the variation in Ca^{2+} concentration of the medium can be used to control the release of the encapsulated material (Graveland-Bikker et al. 2004).

Fabrication of protein nanotubes has the potential to lead food science and engineering to new heights. However further studies need to be conducted to fulfill the promise in many potential food applications. Interactions of nanotubes with the materials to be encapsulated—their structures, characteristics and controlled release properties—should be studied using the model or actual food systems. Another important area of future research is the investigation of the self-assembly characteristics of other food proteins that can be used for similar purposes.

Nanocomposites. In recent years, considerable research has been devoted to organic/inorganic hybrid nanocomposites (Ray et al. 2006). Nanocomposites are defined as materials consisting of two or more components in which characteristic dimension of one constituent is between 1 and 100 nm. These materials have attracted intensive interest because of their applications in food packaging, low dielec-

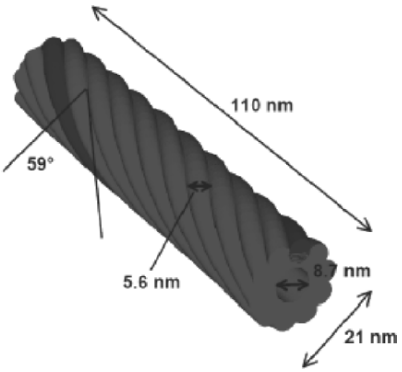

Figure 8.1. Model of α-lactalbumin nanotube as a 10-start right-handed helix with outer diameter 21 nm, cavity diameter 8.7 nm, pitch 110 nm, pitch angle 59°, and interstrand spacing 5.6 nm (Graveland-Bikker 2006).

tric constant films for the microelectronic industry, the preparation of high-surface-area substrates for chemical/biosensors, and in photonic materials. These nanocomposite materials have elicited interest because of their improved properties relative to the pure polymers, which are often achieved without the sacrifice in density, processability, or toughness that is often observed in conventional composite/blend approaches.

Nanocomposites formed by biopolymers and clay have been commonly used as novel food packaging materials due to their enhanced barrier, mechanical, and thermal properties (Ray et al. 2006). Protein-based "green" materials are of special interest because of their high performance, low cost, and eco-friendly characteristics (Chen et al. 2006). Chen and Zhang (2006) have successfully prepared the soy protein isolate (SPI)/Na^+-montmorillonite (MMT) nanocomposites with highly exfoliated and intercalated structures, and characterized their structure and properties using a combination of x-ray diffraction, TEM, and differential scanning calorimetry (DSC). Their results suggest that MMT content plays an important role in the structure of SPI/MMI nanocomposites, which may be affected by two types of interactions between SPI and MMT: (1) the electrostatic interaction between the positive-charge-rich domains of soy protein and the negatively charged MMT layers; and (2) the hydrogen bonding between the –NH and Si-O groups. "Smart" nanocomposites that integrate bioactive ingredients with controlled-release characteristics and radio frequency identification (RFID) system will be the future direction for novel food packaging materials.

8.3 Nanoscale Properties of Food Biopolymers

Polysaccharides and proteins are the two key components in both natural and processed foods (Tolstoguzov 1991). Polysaccharides and proteins have critical impacts on the structure and stability of food systems through their gelling, thickening, and surface-stabilizing functional properties (see Chapter 3). Proteins and polysaccharides are usually used in composites, especially when the creation of new products is required. Since both intrinsic functional properties of individual components and the interactions between two components determine the final structure, texture, and stability of the food materials, the knowledge of interactions between proteins and polysaccharides is of importance not only in making cost-efficient use of functional ingredients, but also in designing novel foods, controlling and improving the structures of food ingredients and textural properties of fabricated foods (Sanchez et al. 2002; Sanchez et al. 1997).

Interactions between protein and polysaccharide have attracted increasing interests in the past two decades also because of their implications in many biological processes such as the organization of living cells and the use in many industrial applications such as microencapsulation, protein separation and purification, and in processed foods (Berdick and Morawetz 1954; Burgess and Carless 1984; Dubin et al. 1994; Tolstoguzov 1991).

The interactions of proteins with polysaccharides in solution have been widely investigated using turbidimetric titration, static and dynamic light scattering, electro-

phoretic light scattering, confocal scanning laser microscopy, small-angle x-ray scattering, and small-angle neutron scattering (Kaibara et al. 2000; Wang et al. 2007b; Weinbreck et al. 2003). Protein molecules initially bind on polysaccharide chains to form primary soluble protein/polysaccharide complexes at the first critical pH (pH_c) even when protein molecules carry the same net charges as polysaccharide chains because of the heterogeneous distribution of charges in proteins (Kwok et al. 1997; Park et al. 1992; Xia and Dubin 1994).

At the second critical pH (pH_ϕ), which is usually below the protein isoelectric point, strong electrostatic interaction between positively charged protein molecules and anionic polysaccharide chains will cause soluble protein/polysaccharide complexes to aggregate into insoluble protein/polysaccharide complexes. For negatively charged weak acid-based (e.g., carboxylic acid) polysaccharides like pectin, with the decrease of pH below the pK_a of the polysaccharide, protein (e.g., bovine serum albumin (BSA))/polysaccharide (e.g., pectin) insoluble complexes may dissociate into soluble complexes, or even non-interacted protein molecules and polysaccharide chains, due to the low charges of polysaccharide chains as well as the repulsion between the positively charged proteins (Dickinson 1998).

Pectin is a natural polymer extracted from plant cell walls and is used broadly not only in the food industry but also in the field of cosmetics and pharmaceutical applications (Oakenfull 1991; Thakur et al. 1997). The major constituent common to pectin is a backbone chain structure of 1,4-linked α-D-galacturonic acid units interrupted by the 1,2-linked L-rhamnopyranosyl residues in adjacent or alternate positions. Because the complexes formed by protein molecules and oppositely charged polysaccharide chains are mainly driven by the long-range character of the electrostatic interaction, physicochemical parameters, such as pH, ionic strength, polysaccharide linear charge density, protein surface charge density, rigidity of the polysaccharide chain, and protein/polysaccharide ratio, have been demonstrated to strongly influence the protein/polysaccharide interaction in solution (Schmitt et al. 1998).

Although extensive investigations of interactions between protein and polysaccharide have been accomplished in solutions, such interactions on the surface have received little attention, which may be due to both the complexity of experimental design and the lack of highly sensitive techniques. In addition, the macroscopic properties of food biopolymers are determined to a great extent by the mechanical characteristics of individual components, including such aspects as entropic and enthalpic elasticity as well as their molecular conformations. However, the intermolecular interactions of each component also contribute to the mechanical characteristics of the bulk assembly. The properties and interactions of single polymer chains cannot be derived from conventional ensemble measurements. Therefore, the development of techniques to characterize food materials at the nanoscale is important and necessary. Recently, three powerful techniques, atomic force microscopy, quartz crystal microbalance with dissipation monitoring (QCM-D), and small-angle neutron scattering have been applied to investigate nanostructures and interfacial properties of protein and polysaccharide-based food systems.

Atomic force microscopy (AFM) is a powerful tool for probing intermolecular interactions (Binnig et al. 1987) because it can resolve forces with piconewton sensi-

tivity and has a spatial resolution of nanometer (Colton et al. 1998). These features enable AFM to produce nanometer to micron scale images of topography, adhesion, friction, and compliance, and thus make AFM an essential characterization technique for fields from materials science to food science (Abu-Lail and Camesano 2002; Bemis et al. 1999; Camesano and Wilkinson 2001; Fisher et al. 1999; Heymann and Grubmuller 2000; Hugel and Seitz 2001; Maurstad et al. 2003; Mazzola 1999; Smith et al. 1986). The interactions between proteins and polysaccharides can be carried out by AFM in the contact mode, which uses the piezoelectric drive tube to hold the sample and the tip at one *x*-*y* position relative to each other, and then ramp them up and down in the *z*-direction to create the force-distance curves. Any deflection of the tip is monitored using the split photodiode, and a plot of piezo displacement *z* versus photodiode voltage *v* may be generated. The force acting on the cantilever at any position can be obtained providing its spring constant *k* (separately measured) is known using Hooke's law (Hugel et al. 2001; Janshoff et al. 2000):

$$F = kd \tag{8.1}$$

where *d* is the tip deflection. Recently, with the development of pico-Newton sensitive instrumentation, AFM-based single-molecule force spectroscopy (SMFS) has been used to study cell adhesion (Benoit et al. 2000), desorption force (Cui et al. 2003), nano-mechanics of macromolecules (Zhang et al. 2000), and conformation transition of polysaccharides (Li et al. 1999; Xu et al. 2002).

One of the most commonly used applications of AFM is the topographical imaging of food biopolymer surfaces. Figure 8.2 shows the contact-mode height image (left) and friction force image (right) of a complex coacervate of pectin and bovine serum albumin (Lee and Huang, unpublished results). AFM results can provide an intuitive observation of coacervate phase, and help to better understand the mechanism of pH-induced complex coacervate formation on protein/polysaccharide mixtures.

AFM can also be used to probe local mechanical properties of thin films of food biopolymers, which are difficult to measure using traditional rheological methods. Several mechanical models have been developed to analyze the Young's modulus of food systems. One of the simplest models, the Hertz model, assumes that only the elastic deformation exists in a surface with spherical contacts, and the adhesion force can be neglected (Hugel and Seitz 2001). Equation (8.2) describes the relationship between the loading force, *F* and the penetration depth, *d*, where *a* is the radius of contact area, *R* the curvature of the tip radius, ν_1 and ν_2 the Poisson's ratios of the two contact materials that have Young's modulus, E_1 and E_2:

$$F = \frac{K a^3}{R} = K d^{\frac{3}{2}} R^{\frac{1}{2}} \tag{8.2}$$

where

$$d = \frac{a^2}{R}$$

and modified Young's modulus,

$$K^{-1} = \frac{3}{4}\left(\frac{1-\nu_1^{\ 2}}{E_1} + \frac{1-\nu_2^{\ 2}}{E_2}\right)$$

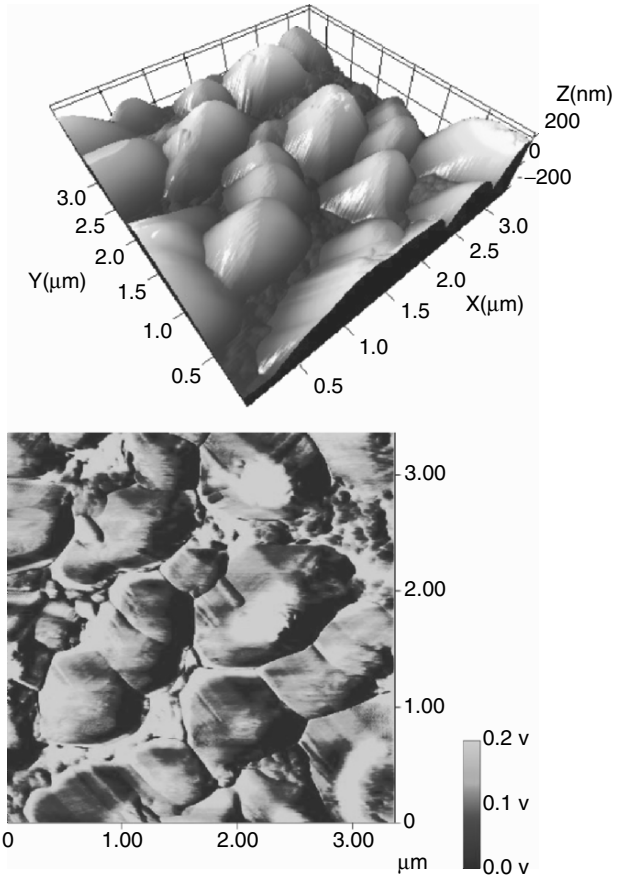

Figure 8.2. AFM contact mode height (left) and friction force (right) images of a complex coacervate formed by pectin and bovine serum albumi. (See Color Plate.)

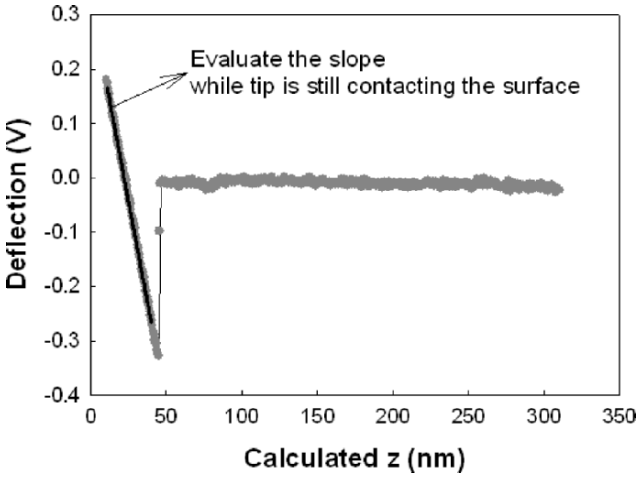

Figure 8.3. Typical force–distance curve of a κ-carrageenan film (Lee and Huang, unpublished).

Another approach is the model proposed by Johnson, Kendall, and Roberts (JKR), which considers the elastic deformation and takes into account of the adhesion contribution in contact mechanics (Hugel and Seitz 2001; Janshoff et al. 2000). This model considers the influence of van der Waals forces within the contact zone, and the diminished force of elastic repulsion caused by the attraction. A general equation relating contact area and load is described as follows:

$$F = \frac{K a^3}{R} - \sqrt{6\pi\sigma K a^3} \tag{8.3}$$

Here σ is the work of adhesion. In most cases, the JKR model is adequate to describe the experimental conditions found in analyzing soft and very adhesive materials.

Figure 8.3 shows the typical force–distance curve for a κ-carrageenan film. From the slope of the curve, where the AFM tip is in contact with the film surface, Young's modulus of the κ-carrageenan film can be estimated by using the Hertz model with the proper measurement of the AFM tip radius using scanning electron microscopy (SEM) and estimated value of Poisson's ratio based on the characteristics of film surface, which is around 1.4 MPa.

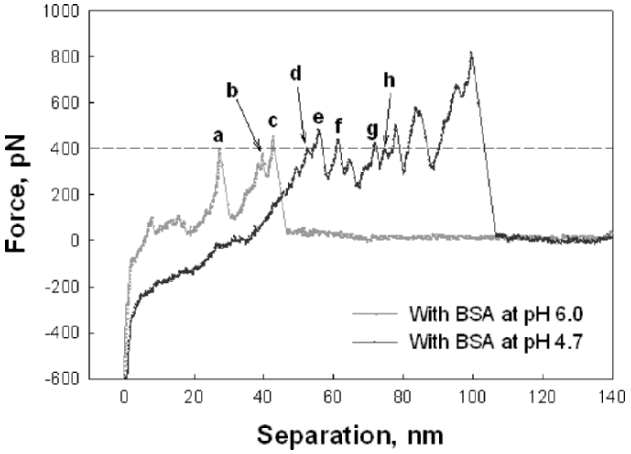

Figure 8.4. Typical normalized retracting force curves (force vs. separation *x*) measured between BSA-functionalized tip and κ-carrageenan in 0.1 M NaCl solution at pH 6.0 (left) and at pH 4.7 (right) (Lee and Huang, unpublished). (See Color Plate.)

Another AFM-based technique is chemical force microscopy (CFM) (Friedsam et al. 2004; Noy et al. 2003; Ortiz and Hadziioannou 1999), where the AFM tip is functionalized with specific chemicals of interest, such as proteins or other food biopolymers, and can be used to probe the intermolecular interactions between food components. CFM combines chemical discrimination with the high spatial resolution of AFM by exploiting the forces between chemically derivatized AFM tips and the surface. The key interactions involved in food components include fundamental interactions such as van der Waals force, hydrogen bonding, electrostatic force, and elastic force arising from conformation entropy, and so on. Other interactions such as chemical bonding, depletion potential, capillary force, hydration force, hydrophobic/hydrophobic force and osmotic pressure will also participate to affect the physical properties and phase behaviors of multicomponent food systems. Direct measurements of these inter- and intramolecular forces are of great interest because such forces dominate the behavior of different food systems.

Figure 8.4 shows the typical normalized retracting force curves (force vs. separation *x*) measured between a BSA-functionalized tip and κ-carrageenan in 0.1 M NaCl solution at pH 6.0 (left) and at pH 4.7 (right) (Lee and Huang, unpublished results). Around the rupture force of 400 pN (dashed line), a significant difference in extension distance appeared in Figure 8.4. At the same rupture force, the stretching length at pH 4.7 was significantly longer than at pH 6.0, suggesting that the stronger binding strength between κ-carrageenan and BSA at low pH causes carrageenan and BSA collectively to be extended longer. At pH below the isoelectric point (pI), the overall charges of BSA change from negative to positive. The lower the pH, the more positive charges exist in BSA, therefore the stronger electrostatic interaction exist between BSA and the negatively charged κ-carrageenan.

8.4 Interfacial Properties of Proteins and Polysaccharides

Recently, an effective and easy technique based on the piezoelectric effect, quartz crystal microbalance (QCM) has attracted increasing interest outside of its traditional development domain area of analytical chemistry and electroanalytical chemistry (Ebara and Okahata 1993; Guilbault 1983; Marx 2003; Okahata and Ebato 1992). QCM is well established as a very sensitive mass-measuring device in both gas and liquid phases. In QCM, an AC voltage is pulsed across an AT-cut piezoelectric quartz crystal, causing it to oscillate in shear mode at its resonant frequency. The resonance frequency of the QCM electrode decreases linearly with the increase in the mass of the electrode due to the adsorption of some compounds, and the sensitivity of QCM is at the nanogram level. A new extension of QCM called the quartz crystal microbalance with dissipation (QCM-D) monitoring, allows time-resolved simultaneous measurements of changes in frequency (*f*) and energy dissipation (*D*) (Galli Marxer et al. 2003; Höök et al. 1998). The measured energy dissipation factor (*D)* is related to changes in the viscoelastic properties of the surface-bound molecules. This additional capability has made QCM-D attractive to investigate various scientific problems, including monitoring of protein and lipid vesicle adsorption, interactions of specific antibodies and antigens, interactions of peptides and DNA, monitoring of cell adhesion and spreading, and investigation of changes in the rheological properties of polymer films (Edvardsson et al. 2005; Kößlinger et al. 1992; Muratsugu et al. 1993; Thompson et al. 1986).

Recently, we have used QCM-D to study the adsorption of pectin on BSA, a model globular protein with a well-known structure (Foster 1977; Peters 1996). The adsorption amount of pectin onto BSA surface and the thickness of adlayers at various polysaccharide concentrations have been determined by the Voigt model, which can also be used to obtain viscoelastic properties of pectin layers on the BSA surface.

Gold-coated quartz crystal is the basic substrate for QCM-D. Natively, this support can bind to biomolecules mostly through physical adsorption or covalent bonding between cystein groups of proteins and thiol linked on the gold surface. However, it is expected that a chemisorbed protein will be stable under physiological conditions due to the much higher bond energy between gold and the thiol group than hydrogen bonding and electrostatic interaction. BSA molecules are linked on gold surfaces through an alkanethiol molecule (11-MUA) linker, which can self-assemble to readily form a monolayer on the surface of the gold substrate.

Figure 8.5 shows the FTIR spectra corresponding to the changes of surface chemistry after the gold surface was treated with 11-MUA, activated with EDC/NHS solution, and then treated with BSA solution. A characteristic band at 1740 cm^{-1} corresponding to a C=O free carboxylic acid stretching mode, and a small shoulder at around 1720 cm^{-1} corresponding to a H-bonded carboxylic acid stretching mode suggested the presence of 11-MUA on the gold surface (Frey and Corn 1996). After the activation of 11-MUA with EDC/NHS solution, there were the bonds at 1818, 1719, and 1745 cm^{-1}, corresponding to the C=O carbonyl stretch of NHS ester of MUA, the C=O symmetric stretch of NHS carbonyl, and the C=O asymmetric stretch of the NHS carbonyl, respectively, while the bond at 1740 disappeared. The results led to the conclusion that the –COOH group was changed into an amide group when

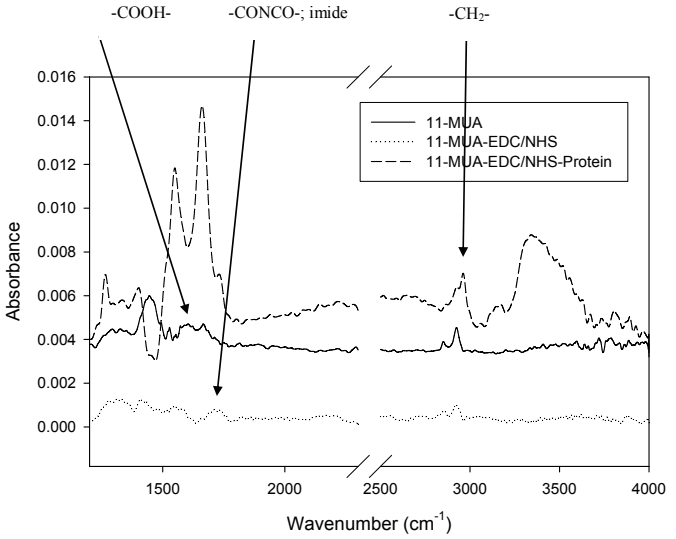

Figure 8.5. FTIR spectra of QCM-D quartz following surface treatment with chemicals and BSA.

EDC/NHS solution was applied. After surface immobilization with BSA, the bands at 1639 cm^{-1} (amide) and 1546 cm^{-1} (amide), corresponding to the C=O stretch and to the N-H bend coupled with the C-N stretching mode, respectively (Brynda et al. 1998; Frey and Corn 1996), suggested the success of BSA immobilization onto the gold surface.

Figure 8.6 displays typical *f* and *D* responses versus time for the third overtone upon the sequential addition of pectin onto the BSA surface. Prior to introducing pectin into the measurement chamber, a steady baseline was acquired with pH 4.0 acetate buffer. Then, sequential additions of pectin of increasing concentrations from 0.01 to 1 g/L were carried out. The jump in *f* and *D* after each pectin injection was sometimes observed, which was due to the disturbance of pressure or temperature from the pectin addition. After each right injection of pectin, there was often a rapid decrease in *f* and a marked increase in *D*, followed by a much more gradual change of *f* and *D*, after which a steady state was obtained. These changes in the frequency and dissipation indicated a net increase in mass as well as the formation of a viscoelastic layer on BSA surface owing to the sequential binding of pectin to BSA surface.

Provided that a mass added to electrode surfaces is (i) small compared to the weight of the crystal, (ii) rigidly adsorbed, and (iii) evenly distributed over the active area of the crystal, the Sauerbrey relationship has been classically used for quantitative determination of mass deposited on the sensor surface in terms of the following equation (Sauerbrey 1959).

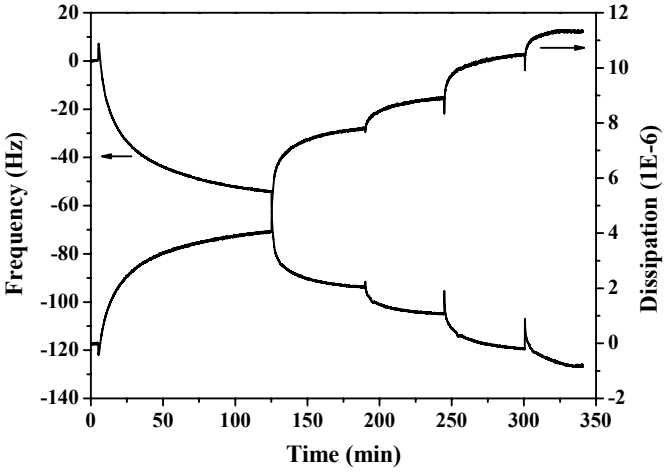

Figure 8.6. QCM-D *f* and *D* response to pectin addition at various pectin concentrations. Pectin additions of 0.01 g/L (5–125 min), 0.05 g/L (125–190 min), 0.1 g/L (190–245 min), 0.5 g/L (245–300 min), and 1 g/L (300–340 min).

$$\Delta m = -C\Delta f/n \tag{8.4}$$

where C is the mass sensitivity constant (C = 17.7 ng cm^{-2} Hz^{-1} for a 5 MHz crystal), and n is the overtone number (n = 1, 3, 5, . . .). For a rigid mass deposition, the frequency shift is expected to be proportional to the overtone number according to Sauerbrey equation. In our work, however, the values of $\Delta f/n$ at various overtones are generally not identical with one another. This violation of the conditions for the Sauerbrey equation is believed to originate from the viscoelastic properties of the pectin layer, since pectin and BSA are both soft materials. Viscoelastic changes in the deposited overlayer on the sensor surface, and entrapment of liquid in rough and porous interfacial structures create additional frequency shifts besides the ones due to the mass load on the electrode surface (Höök et al. 2001).

QCM-D measurements that include dissipation allow a more accurate estimate of mass changes through application of Voigt model that takes into account the viscoelastic properties of the system. Modeling software QTools supplied by Q-Sense uses the full thick layer expressions to model the response. Here, this program has been used to estimate the mass, thickness, viscosity, and shear elastic modulus of the adsorbed pectin layer on BSA surface, with a best fit between the experimental and model *f* and *D* values.

Figure 8.7 gives the changes of mass and thickness of a pectin layer during pectin adsorption on BSA surface. With the increasing pectin concentration, the mass and thickness of the pectin layer are seen to become larger. In Figure 8.8, the change of mass of pectin layer is further plotted against the pectin concentration, and results

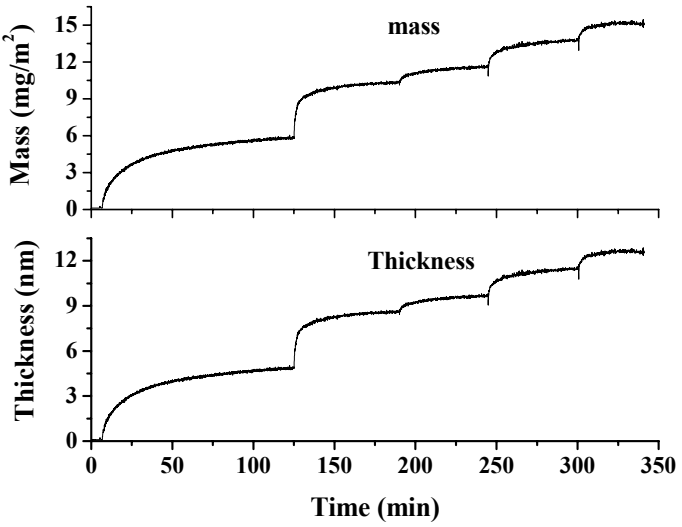

Figure 8.7. Changes of mass and thickness of pectin layer during pectin adsorption on the BSA surface. Pectin additions of 0.01 g/L (5–125 min), 0.05 g/L (125–190 min), 0.1 g/L (190–245 min), 0.5 g/L (245–300 min), and 1 g/L (300-340 min).

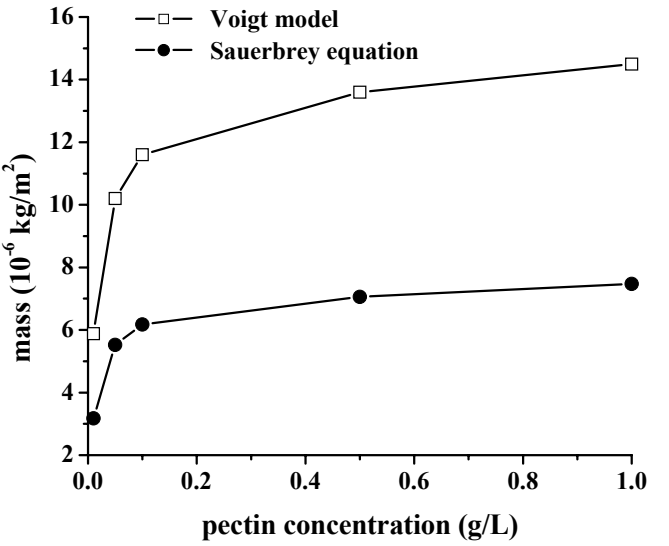

Figure 8.8. Comparison of mass of pectin layer with increasing pectin concentration estimated by the Voigt model and Sauerbrey equation.

from both the Voigt model and Sauerbrey equation are given for comparison. The adsorption amount of pectin is found to be higher from the Voigt model than from the Sauerbrey equation, similar to other researchers' results (Glasmastar et al. 2002). In both cases, the mass values increased nearly linearly with the pectin concentration up to about 0.1 g/L, and then tended to level off. Usually, the adsorption of biomolecules can be considered to be of Langmuir type when a monolayer structure is formed. But in our work, the change of thickness of adsorbed pectin with pectin concentration denies the formation of a pectin monolayer. It is easy to understand that the addition of increasing amounts of pectin will lead to more pectin molecules adsorbed onto the BSA surface and consequently a larger mass of pectin bound on the BSA surface. At lower pectin concentration, for example, 0.01 g/L, pectin molecules may bind onto BSA surface mainly from electrostatic interaction between pectin and BSA molecules. However, nonelectrostatic interaction of bound pectin molecules with unbound ones will play another function when pectin binding occurs at higher pectin concentration. The aggregation of pectin molecules will contribute for the thickness increase with further adsorption of pectin. Thus, the adsorbed pectin will generate a multilayer film on BSA surface, especially at high pectin concentrations.

One unique capability of the QCM-D technique is its successful extraction of quantitative information about a film's viscoelasticity. Figure 8.9 shows the variation of viscosity and shear elastic moduli of a pectin layer during pectin adsorption on the BSA surface from the Voigt model. It is noted that the shear elastic moduli is much

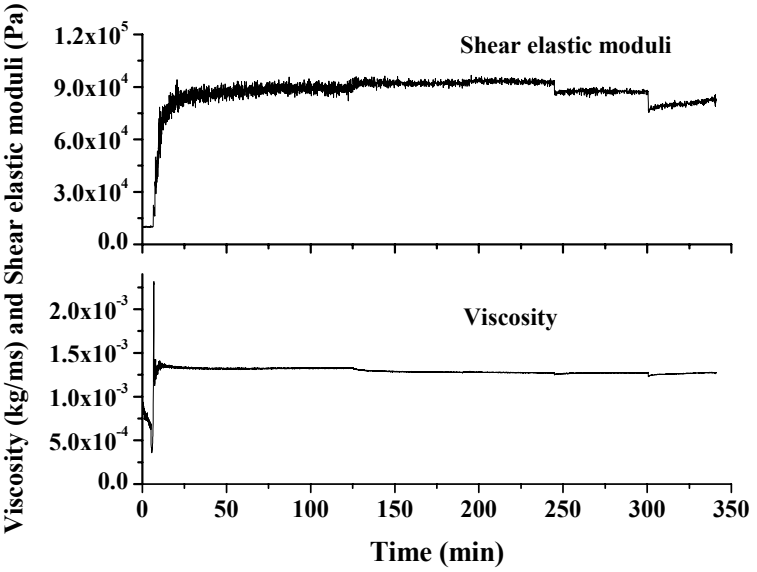

Figure 8.9. Changes of viscosity and shear elastic moduli of pectin layer during pectin adsorption on the BSA surface. Pectin additions of 0.01 g/L (5–125 min), 0.05 g/L (125–190 min), 0.1 g/L (190–245 min), 0.5 g/L (245–300 min), and 1 g/L (300-340 min).

higher than viscosity values of the pectin layer, where both modulus are almost independent of pectin concentration. In a previous dynamic rheology study of pectin/BSA coacervates (Lee et al., unpublished), we found that the storage modulus (G') of coacervates is significantly greater than the loss modulus (G''), which indicates that pectin/BSA coacervates have a highly interconnected gel-like network structure. Although the frequency range for QCM-D is higher than in rheology measurements, the similar elastic behavior of the pectin layer suggest a close structure of pectin layer with pectin/BSA coacervates. When pectin molecules bind on the BSA surface, the electrostatic attraction between pectin and BSA molecules will let pectin chains adsorb several BSA molecules, which will neutralize the charges of the pectin chains. The neutralized pectin chains tend to aggregate with other similar pectin chains to form a pectin network on the BSA surface. Further addition of pectin molecules will cause some pectin chains to bind with several BSA molecules, and then aggregate with other pectin chains, while some pectin chains will directly aggregate with adsorbed pectin chains. These two cases will enhance the formation of a network structure of the pectin layer on the BSA surface.

In summary, the QCM-D technique has successfully demonstrated the adsorption of pectin on the BSA surface as well as determined the viscoelastic properties of the pectin layer. As pectin concentrations increase, the adsorbed mass of pectin estimated from the Voigt model show higher values than those estimated from the Sauerbrey equation because the former takes into account the hydrated layer. But the similar increase of thickness of pectin suggests that the pectin chains form a multilayer structure. In agreement with our previous rheology results, the main elastic character of the pectin layer in terms of Q-tool software tells us the network structure of the pectin layer on the BSA surface. In summary, QCM-D cannot only help to better understand the polysaccharide/protein interactions at the interface, but also to gain information of the nanoscale structure of polysaccharide multilayers on protein surface.

8.5 Nanotechnology in Functional Food Research

Recently, driven by the increasing consumer demand for novel food products, as well as increased fortification with healthy food ingredients, the functional food market is expected to increase at an average growth rate of 13.3%, bringing the market value to $37.7 billion by 2007 (www.bccresearch.com). To enhance nutritional quality and stability of the functional foods, one option is to encapsulate the functional ingredients using food-grade materials that can exhibit controlled release (Wang et al. 2007a). Traditional encapsulation techniques, such as spray drying, spray chilling and cooling, coacervation, fluidized bed coating, liposome, liposome entrapment, rotational suspension separation, extrusion and inclusion complexation, have been developed and widely used in food or pharmaceutical industries (See Chapter 24). However, there are still limitations for these traditional encapsulation technologies. Many of the plant phenolic compounds in capsules and tablets, such as curcumin, green tea catechins, and black tea extracts etc., have poor oral

Table 8.1. The effects of oral administration of nanocurcumin emulsions on the growth of transplant human prostate cancer cell in male SCID mice.

	Tumor records	Vehicle control	Nano-curcumin emulsion	% Inhibition
1	First tumor appear time	15 days after tumor transplant	22 days after tumor transplant	—
2	Total numbers of tumors	5	3	40%
3	Tumor volume per tumor	212 ± 69	83 ± 38	61%
4	Total tumor volume	850 mm^3	333 mm^3	61%
5	Tumor incidence	100%	75%	25%

bioavailability. Therefore, novel delivery systems are necessary in order to enhance the bioavailability of these phytochemicals.

As an effective food delivery system, the delivery vehicle should be GRAS (generally recognized as safe) and able to transfer the active ingredients to the desired sites through the gastrointestinal tract. Nanoemulsions are particularly attractive because of their small sizes and high kinetic stability (Nakajima 1997). Nanoemulsions are a class of extremely small emulsion droplets that appear to be transparent or translucent with a bluish coloration (Nakajima 1997; Solans et al. 2005). Similar to normal emulsions, oil-in-water (*O/W*) and water-in-oil (*W/O*) nanoemulsions can be prepared by the dispersion or high-energy emulsification methods, such as the electrified coaxial liquid jets (Loscertales et al. 2002), high-shear homogenization, high-pressure homogenization, and ultrasonic homogenization (Solans et al. 2005). Other methods, such as phase inversion temperature method (Rang and Miller 1999), colloidosomes (Dinsmore et al. 2002), cubosomes (Spicer 2004), and microfluidic channels (Xu et al. 2005), can also be used to prepare nanoemulsions.

One example that can demonstrate the effectiveness and great promise of nanoencapsulation is the curcumin nanoemulsions. Curcumin is the major yellow pigment in turmeric (*Curcuma longa Linn*). In South and Southeast Asia, curcumin preparation or turmeric has been used extensively to treat inflammatory conditions and chronic diseases (Reddy and Rao 2003). Orally administered curcumin usually has low systemic bioavailability. Only trace amounts of curcumin (or its metabolites) appear in the blood, and most of ingested curcumin is excreted in the feces. One reason is that curcumin has low solubility and does not disperse for absorption. The absorbed curcumin is rapidly metabolized in the intestine and liver to several reduction products (di-, tetra-, and hexa-hydrocurcumin and hexahydrocurcuminol) and

their glucuronide or sulfate conjugates (Ireson et al. 2001; Lin et al. 2000; Pan et al. 1999). Recently, we have successfully prepared curcumin nanoemulsions with the droplet diameter of ~200 nm (Wang et al. 2007a). We have also studied the effects of oral administration of nanocurcumin emulsion on the growth of transplant human prostate cancer cell in male SCID mice. Four male SCID mice (7-8 weeks old; 8 mice) were subcutaneously injected with human prostate cancer PC-3 cells (2×10^6 cells) / 0.1 ml medium with metrigel on the back of each mouse, and then the mice were randomized into two groups (four mice per group). Starting on the second day after tumor transplantation, the mice in the first group were given nanoemulsions without curcumin as the sole source of drinking fluid (vehicle control). The mice in the second group were given 0.3% curcumin nanoemulsions in vehicle as their sole source of drinking fluid until the end of the experiment. Tumor sizes were measured and recorded at the end of five weeks of treatment. Table 8.1 shows that mice that drank 0.3% curcumin nanoemulsion as their sole source of drinking fluid had fewer tumors per mouse, smaller tumor volumes and less tumor incidence in comparison to mice that drank the vehicle nanoemulsion control.

8.6 Future Trends

To design novel functional food products, the structure and materials properties of functional foods must be taken into account. The performance of functional ingredients of foods is determined by the physical properties of functional ingredients, food matrix, and processing conditions of food components. Newly developed nanotools can help in delineating the nanostructures and nanoscale properties of food materials. The new knowledge obtained can significantly enhance our ability to design novel food products. The nanoemulsion-based delivery systems have shown great potential for improving the efficiency of delivery of phenolic compounds by significantly enhancing their bioavailability. Recently, nanoparticle-based delivery systems have also been developed. The idea is that the unstable or poorly bioavailable phytochemicals, such as conjugated linoleic acid or curcumin, respectively, will be conjugated to food polymers such as hydrocolloids. These hydrophobic phytochemicals will self-assemble to form cores, while the water-soluble polymers will form a surrounding shell. With the help of food polymers, the blood circulation time of phytochemicals inside the body increases; therefore, the desired pharmaco-kinetics (PK) of these phytochemicals may be achieved.

One of the most highlighted applications of nanobiotechnology is the use of semiconductor nanocrystal quantum dots (QDs) for biological labeling applications. Compared with organic dyes, II-VI semiconductor QDs have size-dependent and tunable photoluminescence (PL) with broad excitation spectra and narrow emission bandwidths, which allow simultaneous excitation of several particle sizes at a single wavelength. In addition, their high photobleaching threshold renders continuous or long-term monitoring of slow biological processes possible.

Very recently, a method to prepare water-soluble CdTe QDs with excellent chemical stability and quantum yields has been developed (Wang et al. 2006). By integrating these water-soluble with our nanoemulsion- or nanoparticle-based

delivery systems, it is possible to strengthen the power of these delivery systems with the addition of the traceable and targetable capabilities. All these developments suggest that the full potential of nanotechnology is still not fully revealed, and we believe that nanotechnology will become one of the most promising parts of food materials research in the years to come.

Acknowledgements. This work was supported by ACS-PRF (41333-G7) and in part by USDA-NRI.

8.7 References

Abu-Lail, N.I., and Camesano, T.A. (2002). Elasticity of *Pseudomonas putida* KT2442 surface polymers probed with single-molecule force microscopy. *Langmuir*, 18, 4071–4081.

Baeumner, A. (2004). Nanosensors identify pathogens in food. *Food Technol.* 58(8), 51–52, 54–55.

Bemis, J.E., Akhremitchev, B.B., and Walker, G.C. (1999). Single polymer chain elongation by atomic force microscopy. *Langmuir*, 15, 2799–2805.

Benoit, M., Gabriel, D., Gerisch, G.t., and Gaub, H.E. (2000). Discrete interactions in cell adhesion measured by single-molecule force spectroscopy. *Nat. Cell Biol.*, 2, 313–317.

Berdick, M., and Morawetz, H. (1954). The interaction of catalase with synthetic polyelectrolytes. *J. Biol. Chem.*, 206, 959–972.

Binnig, G., Gerber, C., Stoll, E., Albrecht, T.R., and Quate, C.F. (1987). Atomic resolution with atomic force microscope. *Europhys. Lett.*, 3(12): 1281–1286.

Brynda, E., Houska, M., Skvor, J., and Ramsden, J.J. (1998). Immobilisation of multilayer bioreceptor assemblies on solid substrates. *Biosens. Bioelectr.*, 13, 165–172.

Burgess, D.J., and Carless, J.E. (1984). Microelectrophoretic studies of gelatin and acacia gum for prediction of complex coacervation. *J. Colloid Interface Sci.* 88, 1–8.

Camesano, T.A., and Wilkinson, K.J. (2001). Single molecule study of xanthan conformation using atomic force microscopy. *Biomacromolecules*, 2, 1184–1191.

Chen, H., Weiss, J., and Shahidi, F. (2006). Nanotechnology in nutraceuticals and functional foods. *Food Technol.* 60(3), 30–36.

Chen, P., and Zhang, L. (2006). Interaction and properties of highly exfoliated soy protein/montmorillonite nanocomposites. *Biomacromolecules*, 7, 1700–1706.

Colton, R., Engel, A., Frommer, J., Gaub, H., Gewirth, A., Guckenberger, R., Heckl, W., Parkinson, B., and Rabe, J. (1998). *Procedures in Scanning Probe Microscopy*. John Wiley & Sons, New York, pp.672.

Cui, S., Liu, C., Zhang, W., Zhang, X., and Wu, C. (2003). Desorption force per polystyrene segment in water. *Macromolecules*, 36, 3779–3782.

Dickinson, E. (1998). Stability, and rheological implications of electrostatic milk protein–polysaccharide interactions. *Trends Food Sci.Technol.* 9, 347–354.

Dinsmore, D., Hsu, M.F. Nikolaides, M.G. Manuel Marquez, A.R. Bausch, and D.A. Weitz, Colloidosomes: Self-assembled, selectively permeable capsules composed of colloidal particles *Science* 298, 1006.

Dubin, P.L., Gao, J., and Mattison, K.W. (1994). Protein purification by selective phase separation with polyelectrolytes. *Sep. Purif. Methods*, 23, 1–16.

Ebara, Y., and Okahata, Y. (1993). In situ surface-detecting technique by using a quartz-crystal microbalance. Interaction behaviors of proteins onto a phospholipid monolayer at the air-water interface. *Langmuir* 9, 574–576.

Edvardsson, M., Rodahl, M., Kasemo, B., and Höök, F. (2005). A dual-frequency QCM-D setup operating at elevated oscillation amplitudes. *Anal. Chem.*, 77, 4918–4926.

Fisher, T.E., Marszalek, P.E., Oberhauser, A.F., Carrion-Vazquez, M., and Fernandez, J.M. (1999). The micro-mechanics of single molecules studied with atomic force microscopy. *J. Physiolo.*, 520, 5–14.

Foster, J.F. (1977). Some aspects of the structure and conformational properties of serum albumin. In: V.M. Rosenoer, M. Oratz and M.A. Rothschild (eds.), *Albumin: Structure, Function, and Uses.* Pergamon Press, New York, pp. 53–84.

Frey, B.L., and Corn, R.M. (1996). Covalent attachment and derivatization of poly(L-lysine) monolayers on gold surfaces as characterized by polarization-modulation FT-IR spectroscopy. *Anal. Chem.*, 68, 3187–3193.

Friedsam, C., Becares, A.D.C., Jonas, U., Gaub, H.E., and Seitz, M. (2004). Polymer functionalized AFM tips for long-term measurements in single-molecule force spectroscopy. *Chem. Phys. Chem*., 5, 388–393.

Fukasaku, K., Takeda, K., and Shiraishi, K. (1998). First-principles study on electronic structures of protein nanotubes. *J. Phys. Soc. Jpn.*, 67, 3751–3760.

Galli Marxer, C., Collaud Coen, M., and Schlapbach, L. (2003). Study of adsorption and viscoelastic properties of proteins with a quartz crystal microbalance by measuring the oscillation amplitude. *J. Colloid Interface Sci.*, 261, 291–298.

Ghadiri, M.R., Granja, J.R., Milligan, R.A., McRee, D.E., and Khazanovich, N. (1993). Self-assembling organic nanotubes based on a cyclic peptide architecture. *Nature*, 366(6453): 324.

Glasmastar, K., Larsson, C., Höök, F., and Kasemo, B. (2002). Protein adsorption on supported phospholipid bilayers. *J. Colloid Interface Sci.*, 246, 40–47.

Graveland-Bikker, J., and de Kruif, C. (2005). Self-assembly of hydrolysed alpha-lactalbumin into nanotubes, *FEBS J.* 272 (Suppl 1), 550.

Graveland-Bikker, J.F., and de Kruif, C.G. (2006). Unique milk protein–based nanotubes: Food and nanotechnology meet. *Trends in Food Science & Technology*, 17, 196–203.

Graveland-Bikker, J.F., Fritz, G., Glatter, O., and de Kruif, C.G. (2006a). Growth and structure of [alpha]-lactalbumin nanotubes. *J. Appl. Crystallogr.*, 39, 180–184.

Graveland-Bikker, J.F., Ipsen, R., Otte, J., and deKruif, C.G. (2004). Influence of calcium on the self-assembly of partially hydrolyzed α-lactalbumin. *Langmuir*, 20, 6841–6846.

Graveland-Bikker, J.F., Schaap, I.A.T., Schmidt, C.F., and deKruif, C.G. (2006b). Structural and mechanical study of a self-assembling protein nanotube. *Nano Lett.*, 6(4): 616–621.

Guilbault, G.G. (1983). Determination of formaldehyde with an enzyme-coated piezoelectric crystal detector. *Anal. Chem.*, 55(11): 1682–1684.

Heymann, B., and Grubmuller, H. (2000). Dynamic force spectroscopy of molecular adhesion bonds. *Phys. Rev. Lett.*, 84(26, Pt. 1): 6126–6129.

Hou, S., Wang, J., and Martin, C.R. (2005). Template-synthesized protein nanotubes. *Nano. Lett.* 5, 231–234.

Höök, F., Kasemo, B., Nylander, T., Fant, C., Sott, K., and Elwing, H. (2001). Variations in coupled water, viscoelastic properties, and film thickness of a Mefp-1 protein film during adsorption and cross-linking: A quartz crystal microbalance with dissipation monitoring, ellipsometry, and surface plasmon resonance study. *Anal. Chem.*, 73, 5796–5804.

Höök, F., Rodahl, M., Brzezinski, P., and Kasemo, B. (1998). Energy dissipation kinetics for protein and antibody–antigen adsorption under shear oscillation on a quartz crystal microbalance. *Langmuir* 14, 729–734.

Hugel, T., Grosholz, M., Clausen-Schaumann, H., Pfau, A., Gaub, H., and Seitz, M. (2001). Elasticity of single polyelectrolyte chains and their adsorption from solid supports studied by AFM based single molecule force spectroscopy. *Macromolecules*, 34, 1039–1047.

Hugel, T., and Seitz, M. (2001). The study of molecular interactions by AFM force spectroscopy. *Macromol. Rapid Commun.*, 22, 989–1016.

Ipsen, R., Otte, J., and B. Qvist, K. (2001). Molecular self-assembly of partially hydrolysed [alpha]-lactalbumin resulting in strong gels with a novel microstructure. *J. Dairy Res.* 68, 277.

Ireson, C., Orr, S., Jones, D.J., Verschoyle, R., Lim, C.K., Luo, J.L., Howells, L., Plummer, S., Jukes, R., Williams, M., Steward, W.P., and Gescher, A. (2001). Characterization of metabolites of the chemopreventive agent curcumin in human and rat hepatocytes and in the rat in vivo, and evaluation of their ability to inhibit phorbol ester-induced prostaglandin E2 *Production. Cancer Res.*, 61, 1058–1064.

Janshoff, A., Neitzert, M., Oberdorfer, Y., and Fuchs, H. (2000). Force spectroscopy of molecular systems-single molecule spectroscopy of polymers and biomolecules. *Angew. Chem. Int. Ed.*, 39, 3212–3237.

Kaibara, K., Okazaki, T., Bohidar, H.B., and Dubin, P.L. (2000). pH-Induced coacervation in complexes of bovine serum albumin and cationic polyelectrolytes. *Biomacromolecules*, 1, 100–107.

Kößlinger, C., Drost, S., Aberl, F., Wolf, H., Koch, S., and Woias, P. (1992). A quartz crystal biosensor for measurement in liquids. *Biosens. Bioelectr.*, 7, 397–404.

Kwok, D.Y., Gietzelt, T., Grundke, K., Jacobasch, H.J., and Neumann, A.W. (1997). Contact angle measurements and contact angle interpretation. 1. Contact angle measurements by axisymmetric drop shape analysis and a goniometer sessile drop technique. *Langmuir*, 13, 2880–2894.

Lee, J., Wang, X., Wang, Y., and Huang, Q. Rheological properties of BSA/pectin complex coacervates. (Manuscript ready for submission).

Li, H., Rief, M., Oesterhelt, F., Gaub, H.E., Zhang, X., and Shen, J. (1999). Single-molecule force spectroscopy on polysaccharides by AFM-nanomechanical fingerprint of a-(1,4)-linked polysaccharides. *Chem. Phys. Lett.*, 305, 197–201.

Lin, J.-K., Pan, M.-H., and Lin-Shiau, S.-Y. (2000). Recent studies on the biofunctions and biotransformations of curcumin. *BioFactors*, 13, 153–158.

Loscertales, I.G, Barrero, A., Guerrero, I. Cortijo, R. Marquez, M., and Gañán-Calvo, A.M. (2002). Micro/nano encapsulation via electrified coaxial liquid jets. *Science* 295, 1695–1698.

Lonnerdal, B., and Lien, E.L. (2003). Nutritional and physiologic significance of alpha-lactalbumin in infants. *Nutr. Rev.*, 61, 295–305.

Marx, K.A. (2003). Quartz crystal microbalance: A useful tool for studying thin polymer films and complex biomolecular systems at the solution-surface interface. *Biomacromolecules*, 4, 1099–1120.

Maurstad, G., Danielsen, S., and Stokke, B.T. (2003). Analysis of compacted semiflexible polyanions visualized by atomic force microscopy: Influence of chain stiffness on the morphologies of polyelectrolyte complexes. *J. Phys. Chem. B*, 107(32): 8172–8180.

Mazzola, L.T. (1999). Probing biomolecular recognition using atomic force microscopy. PhD Thesis, Stanford University, Stanford, CA, pp. 115.

Moraru, C.I., Panchapakesan, C.P., Huang, Q., Takhistov, P., Liu S., and Kokini, J.L. (2003). Nanotechnology: A new frontier in food science. *Food Technol.* 57(12), 24–29.

Muratsugu, M., Ohta, F., Miya, Y., Hosokawa, T., Kurosawa, S., Kamo, N., and Ikeda, H. (1993). Quartz crystal microbalance for the detection of microgram quantities of human serum albumin: relationship between the frequency change and the mass of protein adsorbed. *Anal. Chem.*, 65, 2933–2937.

Nakajima, H. (1997). Microemulsions in cosmetics. In: C. Solans and H. Kunieda (eds.), *Industrial Applications of Microemulsions*. Marcel Dekker, Inc., pp. 175–198.

Niemeyer, C.M., and Mirkin, C.A. (2004). *Nanobiotechnology: Concepts, Applications and Perspectives.* Wiley-VCH Verlag, Weinheim, Germany.

Noy, A., Zepeda, S., Orme, C.A., Yeh, Y., and De Yoreo, J.J. (2003). Entropic barriers in nanoscale adhesion studied by variable temperature chemical force microscopy. *J. Am. Chem. Soc.*, 125, 1356–1362.

Oakenfull, D.G. (1991). The chemistry of high-methoxyl pectins. In: R. Walter and S. Taylor (eds.), *The Chemistry and Technology of Pectin.* Academic Press, New York, pp. 88–108.

Okahata, Y., and Ebato, H. (1992). Detection of bioactive compounds using a lipid-coated quartz-crystal microbalance. *Trends Anal. Chem.*, 11, 344–354.

Okamoto, H., Takeda, K., and Shiraishi, K. (2001). First-principles study of the electronic and molecular structure of protein nanotubes. *Phys. Rev. B*, 64(11): 115425/1–115425/17.

Ortiz, C., and Hadziioannou, G. (1999). Entropic elasticity of single polymer chains of poly(methacrylic acid) measured by atomic force microscopy. *Macromolecules*, 32, 780–787.

Otte, J., Ipsen, R., Ladefoged, A.M., and Sorensen, J. (2004). Protease-induced aggregation of bovine [alpha]-lactalbumin: Identification of the primary associating fragment. *J. Dairy Res.* 71, 88–96.

Pan, M.-H., Huang, T.-M., and Lin, J.-K. (1999). Biotransformation of curcumin through reduction and glucuronidation in mice. *Drug Metab. Dispos.*, 27(4): 486–494.

Park, J.M., Muhoberac, B.B., Dubin, P.L., and Xia, J. (1992). Effects of protein charge heterogeneity in protein–polyelectrolyte complexation. *Macromolecules*, 25(1): 290–295.

Peters, T. (1996). *All about Albumin Biochemistry, Genetics, and Medical Applications.* Academic Press, San Diego, CA.

Rang, M.J., and Miller, C.A. (1999). Spontaneous emulsification of oils containing hydrocarbon, nonionic surfactant, and oleyl alcohol. *J. Colloid Interface Sci.*, 209, 179–192.

Ray, S., Quek, S.Y., Easteal, A., and Chen, X.D. (2006). The potential use of polymer-clay nanocomposites in food packaging. *Int. J. Food Eng.*, 2: No. 4, Article 5.

Reddy, B.S., and Rao, C.V. (2003). Chemoprevention of colon cancer by curcumin. In: M.S. Meskin, W.R. Bidlack, A.J. Davies, D.S. Lewis and R.K. Randolph (eds.), *Phytochemicals: Mechanisms of Action.* CRC Press, Boca Raton, FL, pp. 177–192.

Sanchez, C., Renard, D., Robert, P., Schmitt, C., and Lefebvre, J. (2002). Structure and rheological properties of acacia gum dispersions. *Food Hydrocolloids*, 16, 257–267.

Sanchez, C., Schmitt, C., Babak, V.G., and Hardy, J. (1997). Rheology of whey protein isolate-xanthan mixed solutions and gels. Effect of pH and xanthan concentration. *Nahrung*, 41, 363–343.

Sauerbrey, G. (1959). Verwendung von schwingquarzen zur wägung dünner schichten und zur mikrowägung (The use of quartz oscillators for weighing thin layers and for microweighing). *Z. Phys.*, 155, 206–222.

Schmitt, C., Sanchez, C., Desobry-Banon, S., and Hardy, J. (1998). Structure and technofunctional properties of protein-polysaccharide complexes: A review. *Crit. Rev. Food Sci. Nutr.*, 38(8): 689–753.

Smith, D.P.E., Binnig, G., and Quate, C.F. (1986). Atomic point-contact imaging. *Appl. Phys. Lett.*, 49, 1166–1168.

Solans, C., Izquierdo, P., Nolla, J., Azemar, N., and Garcia-Celma, M.J. (2005). Nano-emulsions. Curr. Opin. *Colloid Interface Sci.*, 10(3-4), 102–110.

Spicer, P. (2004). Cubosomes: Bicontinuous liquid crystalline nanoparticles. In: *Encyclopaedia of Nanoscience and Nanotechnology*, Marcel Dekker, New York, pp. 881–892.

Thakur, B.R., Singh, R.K., and Handa, A.K. (1997). Chemistry and uses of pectin: A review. *Crit. Rev. Food Sci. Nutr.*, 37, 47–73.

Thompson, M., Arthur, C.L., and Dhaliwal, G.K. (1986). Liquid-phase piezoelectric and acoustic transmission studies of interfacial immunochemistry. *Anal. Chem.*, 58, 1206–1209.

Tolstoguzov, V.B. (1991). Functional properties of food proteins and role of protein-polysaccharide interaction. *Food Hydrocolloids*, 4, 429–468.

Valery, C., Artzner, F., Robert, B., Gulick, T., Keller, G., Grabielle-Madelmont, C., Torres, M.-L., Cherif-Cheikh, R., and Paternostre, M. (2004). Self-association process of a peptide in solution: from β-sheet filaments to large embedded nanotubes. *Biophys. J.* 86, 2484–2501.

Wang, Q., Kuo, Y., Wang, Y., Shin, G., Ruengruglikit, C., and Huang, Q. (2006). Luminescent properties of water-soluble denatured BSA-coated CdTe quantum dots. *J. Phys. Chem. B*, 110, 16860–16866.

Wang, X., Jiang, Y., and Huang, Q.R. (2007a). Encapsulation technologies for preserving and controlled-release of enzymes and phytochemicals. In: J. Lakkis (ed.), *Encapsulation and Controlled Release Technologies: Practical Applications in Food Systems*. Blackwell Publishing, Ames, IA, 135–148, published on June 1, 2007.

Wang, X., Li, Y., Wang, Y., Lal, J., and Huang, Q. (2007b). Microstructure of β-lactoglobulin/pectin complex coacervates studied by small-angle neutron scattering. *J. Phys. Chem. B*, 111, 515–520.

Weinbreck, F., de Vries, R., Schrooyen, P., and de Kruif, C.G. (2003). Complex coacervation of whey proteins and gum arabic. *Biomacromolecules*, 4, 293–303.

Xia, J., and Dubin, P.L. (1994). Protein-polyelectrolyte complexes. In: P.L. Dubin, J. Bock, R.M. Davis, D.N. Schulz and C. Thies (eds.), *Macromolecular Complexes in Chemistry and Biology*. Springer-Verlag, Berlin, pp. 247–271.

Xu, Q., Zhang, W., and Zhang, X. (2002). Oxygen bridge inhibits conformational transition of 1,4-linked alpha-D-galactose detected by single-molecule atomic force microscopy. *Macromolecules*, 35, 871–876.

Xu, Q.Y., Nakajima, M., and Binks, B.P. (2005). Preparation of particle-stabilized oil-in-water emulsions with the microchannel emulsification method. *Colloids Surf. A, Physicochem., Eng. Aspects*, 262(1-3), 94–100.

Zhang, S. (2003). Fabrication of novel biomaterials through molecular self-assembly. *Nat Biotech*, 21, 1171–1178.

Zhang, W., Zou, S., Wang, C., and Zhang, X. (2000). Single polymer chain elongation of poly(*N*-isopropylacrylamide) and poly(acrylamide) by atomic force microscopy. *J. Phys. Chem. B*, 104, 10258–10264.

Chapter 9

Assembly of Structures in Foods

E. van der Linden

Wageningen University, Food Physics Group, Bomenweg 2, 6703 HD Wageningen, The Netherlands, erik.vanderlinden@wur.nl

9.1 From Foods to Molecules and Back

From a physical point of view, a natural way to describe a system is to define the macroscopic physical state it is in, that is, the solid, liquid or the gas state. These three states are differentiated from one another by the degree of order between the atoms or the molecules (a common denominator being constituents). The order is highest within a solid (where there exists a regular stacking) and lowest in a gas (where the probability of finding a neighbour of one constituent is only dependent, isotropically, on the density of the gas, which must be an average quantity) (de Gennes and Prost 1993). Systems composed of one type of atoms may even exhibit all three phases, depending on temperature and pressure. Another possible state is the liquid crystal state (de Gennes and Prost 1993), which, at least in one direction, exhibits liquidlike order and anisotropy.

Food systems are often not composed of one type of constituent but of a mixture thereof. Usually one does not operate at conditions where all constituents mix homogeneously, and even if that were the case, the formulation window turns out to be rather narrow (e.g., the case of Pastis, an anise-holding drink (Grillo 2003)). In most cases one finds that demixing occurs, leading to a situation of each constituent forming its own phase separated from the other phases by a so-called interface.

A well-known example is a mixture of oil in water, which shows demixing when put into contact with each other, resulting in an oil phase on top of a water phase, allowing a small quantity of oil solubilised in the water phase and vice versa. Upon vigorously shaking an oil–water mixture, droplets of one phase in the other are created, which, however, forms two separate macroscopic phases after a short while. Addition of so-called amphiphilic molecules, which tend to reside at the oil–water interface, leads to a slowing down of the separation into two macroscopic phases.

Depending on the energy involved while shaking or stirring, one can obtain micron-sized droplets of one liquid in the other. Such an emulsion system may retain its condition for quite a while, depending on the amphiphilic molecules used.

Emulsion systems as described above form one important class of food systems (see Chapter 15). If one replaces the liquid inside the droplets (the dispersed medium) by a gas, and retains the dispersing phase as a liquid, one obtains a foam, and when the gas is replaced by a solid (and retains the dispersing phase as a liquid), one refers to the resulting system as a dispersion. One may switch from a dispersion to an emulsion by increasing the temperature as is the case, for example, for a chocolate dispersion in water which becomes a chocolate emulsion at a higher temperature.

By tuning the interaction between dispersed droplets (of any sort of material) and adjusting the droplet concentration, systems can be created where the droplets themselves are situated with respect to one another in a regular array, such as molecules in a crystal lattice. One then obtains a so-called colloidal crystal. If the droplet interactions are strongly attractive the droplets will want to cluster together and form a concentrated droplet phase with a small fraction of fluid, in contact with a fluid phase with a small amount of droplets. This is analogous to some extent to the separation of oil and water, but now occurring at a colloidal scale. This clustered droplet phase contains a small fraction of fluid and consequently does not flow easily, in contrast to a fluid with a small fraction of droplets. After a concentrated droplet phase is brought into contact with an excess fluid, that is, diluting the droplet phase, there will be low diffusivity of the droplets into that liquid, that is, the dissolution often is slow. In that sense, such concentrated systems can be considered to be *gluey*. This glueyness is the origin of the name "colloid," stemming form the Greek word for glue (Djabourov 1988).

Apart from systems consisting of droplets glued together and embedded in a liquid, one may also imagine many molecules glued together covalently and embedded in a liquid. These systems may also exhibit gluey behaviour, that is, belonging to the colloid class, because the chains of molecules (polymers) are difficult to disentangle. Both the concentrated droplet phase and the polymer phase are not flowing easily. The droplets and the polymers actually form a network, that is, one is able to walk over the droplets or polymers from one side of the system to the other side. That is, there is connectivity macroscopically through the dispersed phase. Apart from that connectivity, there also exists connectivity within the dispersing phase. Furthermore, due to the interaction between the dispersed units, energy is involved to deform the network of these dispersed units, making it difficult to flow. Systems that exhibit such connectivity in both dispersed and dispersing phase, as well as the property that energy is needed for deformation of the system, and are composed of one component that is finely dispersed in a liquid, are called a gel according to a classification by Hermans (Djabourov 1988). Gels exhibit both solid-type and liquid-type behaviour. At this point the reader may want to refer to Chapters 13, 14 and 15 for a detailed treatment of gels, foams and emulsions.

Many foods may be categorised as either a gel, emulsion, dispersion or foam. However, many more foods are actually a combination of these four types. For example, one may consider bread as being a gel in which air is dispersed, that is, a foam where the liquid around the droplets is a gel instead of a fluid. In order to

accommodate for this multitude of possible combinations and to use a systematic method of deciding what type of category a food type belongs to, more detailed schemes have been introduced taking into account the different colloidal structures with their solid, gel, liquid crystalline, liquid or gas type of behaviour (This 2005).

In summary, for solid-type materials, molecules can form regular arrays leading to crystals, and this also may occur with colloidal-scale particles. For liquid-type materials, molecules may be dispersed on a molecular scale (i.e., dissolved) in a liquid, or they may cluster together into a separate and homogeneous phase (i.e., show phase separation). Colloidal-scale particles may also exist as separate particles in a liquid, but these particles may also cluster into a dense phase. Whether the size of the building blocks is molecular or colloidal, the phenomena of phase separation, clustering and structure formation show many similarities.

In the case of crystals, one usually encounters structures that are anisotropic on a molecular scale, due to anisotropic interactions between the molecules. Clusters formed by colloidal-scale particles often do not exhibit anisotropy due to the isotropic character of the interactions on that colloidal scale. One may introduce anisotropy in that case by applying an external field, for example, a flow field or electric–magenetic field, and subsequently freezing the morphology by, for example, gelation.

The above categorizations from a physical point of view contain information regarding the physical properties of the food. In order not to lose sight of the food point of view, it should be stressed that these physical properties are in turn relevant to the behaviour of the food during its production, storage and consumption. Coming back now to the categorisation, it is important to note that although information on a microscopic scale in principle contains more detailed structural information than information on a macroscopic scale, it does not necessarily mean that knowing the microscopic physical state implies having all the knowledge about the macroscopic physical state. For instance, a foam can be in a solid state or a liquid state; an example of a solid foam is a meringue, while an example of a liquid foam is a beer foam. Thus, the information on a microscopic scale may be more detailed from a structural point of view, but from this information on the microscopic scale one cannot deduce immediately the information relevant to a macroscopic scale. This can only be done, in principle, once the physical properties of the microstructural units and their mutual interaction are known.

In the example given, the meringue consists of proteins, sugar and a small amount of water. It is the small amount of water that brings the aqueous protein–sugar mix in a solid state. This surrounds the air bubbles in the meringue. It is this glassy state of the continuous phase within the foam that explains the solid character of the meringue. The continuous phase is the relevant microstructural unit. In the case of the beer foam, the microstructural unit is still the continuous phase, but this is now in a liquid state, which explains that the beer foam loses liquid as it drains downwards into the beer liquid below the foam head.

It has been outlined above how important it is to know the physical properties of microstructural units and their mutual interaction to predict the macroscopic physical properties of a food. Now, in turn, the properties of these microstructural units will depend on the molecules building them, in fact, the molecular ingredients of the food. Also, the interactions between the microstructural units will depend on the

molecules building them. Finally, the types of ingredients determine which type of microstructural units are being formed, that is, their size, number and form. It is because of the molecular scale properties of the available food molecules that one finds such a large variety in the types of microstructural units that can be formed from them, and this explains the rich variety of different types of food available.

Let us repeat the importance of the molecular-scale properties of the ingredients, and their relevance to foods. In fact, these properties are the very starting point for a food scientist who in general faces the following question: "Which ingredient do I have to put in, where, when and how, during the preparation of a product (new or already existing), and what do I have to assure during processing, storage and consumption in order to meet the criteria being put forward regarding safety, taste, stability (physical and chemical), health and convenience?"

In practice, in order to answer such a question, the type of food has to be specified first. This is because each product has its specific types of ingredients and for each product one has different consumer expectations. For instance, regarding the question of how a food has to be stored, ice cream is a frozen product and therefore needs to be stored in the freezer, while mayonnaise should not be frozen and therefore should not be stored in the freezer. Both products need to be stable, but under different storage conditions.

In order to systematically approach any specific food science question one thus needs to have a systematic way of ordering the types of products. Such a systematic categorization allows answering the question in an efficient manner. Many different categorizations have been put forward in the literature, but many boil down to more or less the same idea. Here given by McGee (McGee 2004) is adopted.

Milk and dairy products
Eggs/egg-based products
Meat
Fruits/vegetables and herbs
Grains and nuts
Bread and dough
Sauces
Chocolate, sweets, sugars
Alcoholic beverages (wine, beer, liquors)
Drinks, juices

The categorization in types of products *helps* to *specify* the questions posed to the food scientist, but the answers to the question still need to be sought. One also needs to specify which ingredients are in the product, and one has to have knowledge of the relationships between ingredient properties (down to a molecular scale) and consumer-relevant product properties (up to a macroscopic scale). Answering in terms of such specific relationships is important. Examples of consumer-relevant product properties are firmness, pourability, spreadibility, colour, thickness, crunchiness, and so on. Examples of physical and physico-chemical properties of ingredients are the shape of the molecule, chemical fine structure, and so on. The type of molecules to focus on in foods are proteins, carbohydrates and fat molecules, water molecules and

molecules in air, as these are the main components of foods. Besides these ingredients one also has other ingredients in foods, but these are present in relatively low amounts or play a minor role.

Two important aspects need to be considered in formulating physical and physico-chemical relationships between properties of molecules and consumer-relevant properties. First, there is a factor of billion difference in length scale between molecular scale and macroscopic scale (nanometers to meters). Second, foods are usually not homogeneous on a length scale of microns, since they exhibit microstructural units. Examples are bread, beer foam and margarine.

In order to formulate the desired relationships in a useful way, one needs to know about the intermediate inhomogeneous domain. This domain is referred to as the mesoscopic domain. Of particular relevance are domain sizes between 10 nanometers and millimeters, which are referred to as the colloidal domain. The physics that is relevant to this intermediate domain size is called mesoscopic physics, and science relevant to this length scale is classically referred to as colloid science. The physics and the physical chemistry regarding the mesoscopic domain acts as a bridge for formulating relationships between properties on a molecular scale and those at a macroscopic scale.

Ingredients can form a multitude of different structures on a colloidal scale. One can have platelets, spheres, long thin threads, and threads that form a coil-like structure. This is schematically summarized as different "microstructural units" below. The macroscopic properties depend on how the structures exhibit interaction, and on the properties of the colloidal structures themselves. The combination of product knowledge and generic knowledge can be used as a toolbox to solve aspects of the general question that was formulated above.

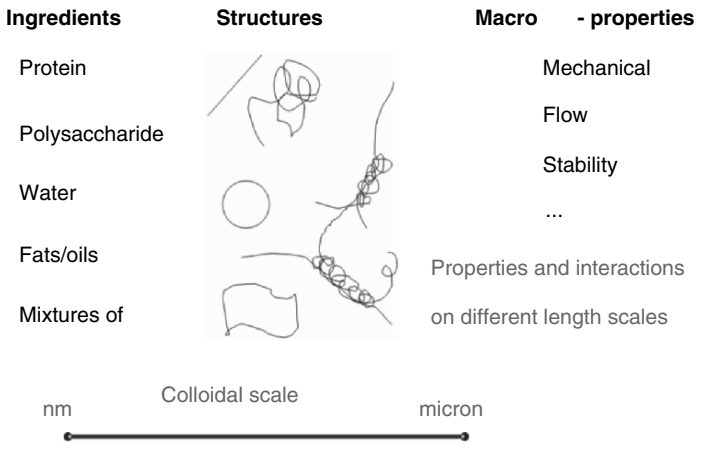

Figure 9.1. Generic physical knowledge relevant to food technology.

In summary, starting with any food, one may wonder about the origin of its physical properties, as a food scientist or as any curious individual. One realizes that the macroscopic physical properties depend on the properties and mutual interactions of the microstructural units that are present. These properties and mutual interactions, in turn, depend on the molecules that build up the units. Thus, foods have made us think about the macroscopic scale, and how properties on this scale can be related to properties on a molecular scale. The line of reasoning can also be reversed. In fact, food molecules yield a large variety of different possible structures. The knowledge of how food molecules build up microstructural units and determine their properties can be used to build microstructural units with specific properties, leading to desired properties of the food itself, being it from a taste or health perspective (see Chapter 12).

One important class of molecules abundant in foods is that of amphiphilic molecules (including fats, lipids and proteins), also known as surfactants. In the following sections some novel insights are presented into the formation of lamellar phases (colloidal structures with varying topologies depending on thermodynamic and flow conditions), and the formation of anisotropic colloidal protein structures is discussed.

9.2 Lamellar Phases in Foods

9.2.1 Background

Mesoscopic physics has developed rapidly over the last three decades. An example is the vast amount of work on microemulsions, both experimentally and theoretically, including simulations. Theoretical, simulated and experimental results are consistent with one another for key parameters of specific systems. Furthermore, certain key parameters such as the bending modulus have been determined experimentally for specific systems using a multitude of methods, also yielding consistent results. Because of the above, the area of mesoscopic physics is especially *now* suitable for application in the food technology area.

In subsequent sections we will discuss, by way of example, the use of mesoscopic physics to bridge the properties on both a molecular and macroscopic length scale for a specific system. First the choice of the system and its functional properties (i.e., suspendibility, viscosity) are addressed. Then shear-induced mesostructural changes, according rheological changes, and a key (mesoscopic) parameter, determining these rheological changes will be discussed. Subsequently, we address the mesoscopic determinants of this key parameter. Finally some methods to relate these determinants to molecular parameters will be outlined. In the subsequent section conclusions on the use of mesoscopic physics in food systems are presented.

9.2.2 The Liquid Crystalline Lamellar Phase and Its Relevance to Real Food Systems

Heertje et al. (1998) have reported on the use of liquid crystalline phases in the structuring of food systems. They mention as a practical example a fat-free margarine that

contains 30 mg monoglyceride per gram of product, in a so-called coagel state. This coagel state is formed from the liquid crystalline lamellar phase, via the so-called α-gel state. Thus, for this particular monoglyceride system, the α-gel state is not the final state. However, for other compounds, such as the lactic acid ester of monoglyceride (Heertje et al. 1998), the α-gel state is the final state.

Schematically, the structure of the α-gel state is given in Figure 9.2, which can be deduced from the photographs (Figures 9.7 and 9.8) in the reference of Heertje et al. (1998). The structure consists of a continuous phase of bilayers, which are stacked parallel to one another in regions with a specific domain size, and of droplets being embedded in this continuous phase. The droplets consist of bilayers that are stacked concentrically, like the layers in an onion, and are separated by water layers. For obvious reasons these droplets are sometimes denoted by the term *onions*.

The rheological (i.e., functional) properties of a product consisting of such a α-gel state depend on parameters such as the number of droplets, their size, the concentration of bilayers and whether bilayers have folded themselves around several droplets, thus forming entanglements. The question is whether, and how, such a parameter can be controlled. The first thing to notice is that optimal control of the structure will be when the bilayers are still in the liquid state. This phase is also the phase encountered during processing of products, thereby having practical relevance. Thus, the first step towards answering whether and how to control such parameters is to investigate what type of structural transitions are possible in a liquid crystalline phase, how to induce them and whether there would be a key parameter identifiable. This is discussed in Section 9.2.3.

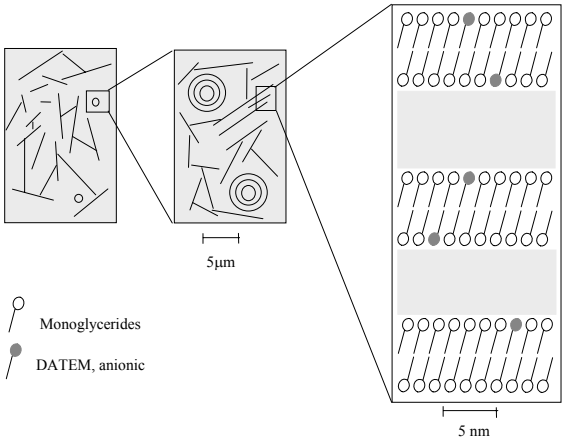

Figure 9.2. A schematic structure of a lamellar phase system.

9.2.3 Shear-Induced Mesostructural Changes and Rheology of the Liquid Crystalline Lamellar Phase

Various authors have investigated the effect of shear on the (meso)structure of a liquid crystalline lamellar phase (Bohlin and Fontell 1978; Bohlin 1979; Bergenholtz and Wagner 1996; Roux 1993; Van der Linden et al. 1996). Starting from a continuous lamellar phase in a simple shear cell, with the bilayers being stacked parallel to the cell boundaries, one finds in the low shear rate regime (up to about 0.1 s^{-1}) that the viscosity, η, decreases at increasing shear rate, $\dot{\gamma}$, according to $\eta\,\dot{\gamma}^{-0.5}$ (Van der Linden et al. 1996; Van der Linden and Droge 1993) (cf. Figure 9.3).

At certain shear rates, one finds a sudden increase in viscosity, related to a structural transition from a continuous lamellar phase to a phase consisting of onions embedded in a continuous lamellar phase. The sudden increase in viscosity amounts to a factor 100 or so. After the transition, the power law for viscosity versus shear rate remains $\eta \sim \dot{\gamma}^{-0.5}$; however, the zero shear viscosity is found to be two orders of magnitude higher than that of the initial continuous lamellar phase. This implies that the structural transition indeed relates to a functional property such as suspendability of the system.

The extent of the structural transition must depend on the amount of shear exerted on the system versus the deformability of the droplet and continuous lamellar phase. Furthermore, as mentioned above, the rheological (i.e., functional) properties of a system in the α-gel state depend on parameters such as the number of droplets, their size, and how many times bilayers have folded themselves around several droplets, thus forming entanglements. Among these parameters one can identify one key

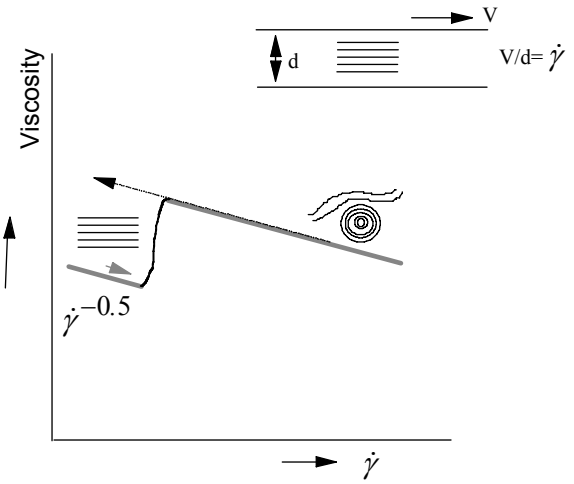

Figure 9.3. Mesostructural changes in a model lamellar phase induced by shear, and some rheological consequences

parameter—the onion size (directly related to deformability of the lamellar phase). In Section 9.2.4 we address what mesoscopic parameters this onion size depends on and how the size relates to the shear exerted on the system.

9.2.4 Mesoscopic Determinants of the Onion Size as a Function of Shear

In order to study the dependence of the onion size as a function of shear rate and determine its mesoscopic determinants, one needs a well-defined flow field. Using the set-up in Figure 9.3, one finds that starting from a continuous lamellar phase, a monodisperse droplet phase is obtained during shearing (Roux 1993). The onion size is found to directly relate to the shear rate (Roux 1993). In normal emulsions, the droplet size depends on a balance between shear stress and droplet surface stress, including a droplet break-up criterion. Lamellar phases are different, however, from normal emulsions in at least two respects. First, the droplets are structured internally. Second, the droplets only distinguish themselves from their surrounding by the fact that the curvature of the lamellar phase is different within and outside the droplets. For the rest, droplet and surrounding are equal. This is apparent from fact that these solutions are somewhat transparent.

Now we introduce a model to describe the size of the droplets. During shear, and thus during formation of the droplets, the difference in curvature must correlate to a surface stress, which should equal the (local) shear stress exerted on that same surface. The surface stress can be expressed in terms of a Laplace pressure, $4\sigma_{eff}/D$, where σ_{eff} denotes the so-called effective surface tension (Van der Linden and Droge 1993), and D the diameter of the droplet. This effective surface tension is defined here as the energy needed to deform a lamellar droplet, divided by the excess surface area needed to induce the specific deformation. The local shear stress stems from the stress exerted on the fluid by the moving boundaries and this stress penetrates into the lamellar phase over a characteristic distance, say L, where $L >> D$. If the gap width, G, of the sample holder, is smaller than L, penetration of the stress is ensured throughout the sample. In our experiments, 1 mm < D < 10 mm, L = (1–100) mm (Gennes 1974), and G = 1mm, satisfying $G < L$. Hence the local shear stress will equal the experimentally determined shear stress, as measured during preparation. According to this model (Van der Linden et al. 1996):

$$D = 4\sigma_{eff}/\text{shear stress} \tag{9.1}$$

The first test of this model is whether D is inversely proportional to the shear stress. This is indeed the case (Van der Linden et al. 1996). The second part of the test is to verify the proportionality constant, $4\sigma_{eff}$. This effective surface tension, σ_{eff} , has been calculated as follows (Van der Linden and Droge 1993). The effective surface tension is defined as "the energy needed to deform a lamellar droplet, divided by the excess surface area needed to induce that specific deformation." Hence, one first needs to calculate the deformation energy for a given deformation and secondly divide that by the concomitant excess surface area.

It turns out that σ_{eff} is a function of the flexibility of the bilayers and their mutual interaction (Van der Linden and Droge 1993). These two parameters are the mesosopic determinants. In a special case of AOT bilayers in brine, one can deduce from theory as well as from experiment (Nallet et al. 1989; Nallet 1991; Helfrich 1978), making use of the theoretical expression in Van der Linden and Droge 1993), that

$$\sigma_{eff} = 0.48\ \phi^2/(\delta/\text{Å})^2 \tag{9.2}$$

where ϕ denotes the volume fraction of bilayers and δ their thickness (in Å). Combining Equations. (9.1) and (9.2) leads to

$$D = 1.92\phi^2/\text{ shear stress}*(\delta/\text{Å})^2 \tag{9.3}$$

For AOT we found separately (Van der Linden et al. 1996) that "shear stress = 8 $(\gamma)^{1/2}$" and thus our model predicts

$$D = 0.24\phi^2\,(\gamma)^{-1/2}\,/(\delta/\text{Å})^2 \tag{9.4}$$

Diat et al. (1993) actually measured the scaling of the size with shear rate and with volume fraction. The scaling behaviour that they observed is in line with our model. We note that they used another system, which, however, should not affect the conclusions regarding the scaling behaviour. Quantitatively, our model would predict from Equation (9.4) that, for the system of Diat et al. (1993), taking a reasonable bilayer thickness of 40Å (Safinya et al. 1986), D is given by $D(\mu m) = 150\phi^2\ (\gamma)^{-1/2}$ where we *assume* that the relation "shear stress = 8 $(\gamma)^{1/2}$" as found for the AOT system also applies to the Roux system. They actually find experimentally $D(\mu m) = 100\phi^2\ (\gamma)^{-1/2}$ (Diat et al. 1993) which, taking into account the assumption, is in satisfactory agreement with our model.

Hence we conclude that a mesoscopic description for the size of an onion is quantitatively possible and that the mesoscopic determinants are bilayer flexibility and bilayer interaction.

9.2.5 Relation to Molecular Parameters

Having established that bilayer flexibility and bilayer interaction are the mesoscopic determinants, the next question is whether these determinants can be coupled to molecular parameters. In fact, this has been done to quite some extent. In general, bilayer flexibility can be shown (both experimentally as well as theoretically by simulation methods) to be directly related to bilayer thickness, lateral interaction between heads and tails of the surfactants, type of head group (ethoxylate, sugar, etc.), type of tail (saturated, unsaturated) and specific molecular mixes (e.g. SDS with or without pentanol). The bilayer interaction is known to be related to characteristics such as classical electrostatics, Van der Waals, Helfrich undulation forces (stemming from shape fluctuations), steric hindrance, number, density of bilayers, ionic strength, and type of salt. Two examples will be dicussed.

a. Bilayer interaction has been deduced, for example, from synchroton x-ray scattering experiments (Roux and Safinya 1988). For the system SDS/pentanol/water/with or without NaCl it was found (Roux and Safinya 1988) that zero salt yielded classical electrostatic interaction between two flat plates. High salt yielded an energy per surface area E/A scaling with $1/k\mathrm{d}^2$, where the bilayer flexibility, k, was found to be 0.5kT (Roux and Safinya 1988). This scaling behaviour had been predicted by Helfrich (Helfrich 1978). It is noted that recently the case of intermediate bilayer flexibility (k = 10kT) and low to intermediate salt levels has been calculated (Odijk 1992) and has been observed experimentally to lead to extreme swelling behaviour of lamellar phases (Odijk 1993).

b. Bilayer flexibilities have been determined experimentally for many systems now. Different methods gave consistent results for the same systems and are in line with simulation results and theoretical estimates. By way of example, one elegant way of determining the bilayer flexibility is to measure the deformation of the vesicle as a function of an applied electric field. The deformation is determined by a balance between an electrostatic force and a surface force, which is a function of the unknown flexibility (Kummrov and Helfrich 1992).

9.3 Protein Assemblies*

9.3.1 Introduction

The area of protein assembly and resulting phase behaviour has also received considerable attention. The main focus for many years has been on solubility, crystallisation, interfacial assembly, phase separation and gel formation, in terms of molecular properties of the protein or protein mixture. Since assemblies of proteins are abundant in food products, the exploration of their morphology, physico-chemical characteristics and mutual interactions is relevant for the engineering of food materials. It is only for the past few decades that the morphology of the assemblies has received more attention. This has been explored in terms of fractal aggregates. The type of protein assembly that is usually found in foods (in three dimensions) exhibits a morphology that has many branches per unit length. An extreme case is an infinitely stiff aggregate with zero branches per unit length, that is, a rod (fractal dimension equals 1). This fibrillar type has been the subject of intensive studies lately, in various science areas, ranging from material science, to food science, to medical sciences (beta-amyloid diseases). Apart from the fact that the rod morphology is relevant, as it is an extreme case of zero branches, it also has practical relevance, for example, because the fibrils act as a vehicle to form extremely low weight fraction gels. Another example of a protein aggregate is a hollow capsule (serving as a protection device of many viruses).

---

* This section was published originally in a chapter entitled: "Similarities in self-assembly of proteins and surfactants: An attempt to bridge the gap," by Erik van der Linden and Paul Venema, in *Food Colloids, Self-Assembly and Material Science*, Eds. E. Dickinson, and M.E. Leser, published by Royal Society of Chemistry, Cambridge, UK ISBN 9780854042715. Reproduced here with permission.

First, mesoscopic parameters relevant for describing the aggregate morphology, phase behaviour and topology of surfactant systems will be addressed. Secondly, a similar scheme will be presented for the use of relevant mesoscopic parameters in describing the morphology and topology of protein aggregates, ranging from fractal dimensions between 1 and 3. Influence of pH, salt concentration and salt type, and temperature will be considered. Nonequilibrium effects regarding the particular assembly of proteins into fibrils will also be addressed. Thirdly, the similarities and differences regarding surfactant versus protein assembly will be discussed.

9.3.2 Surfactant Assembly

The fluctuations in size of aggregates, exchange rate of surfactants between those in solution versus those in the aggregate, as well as the rate of aggregate formation, are all assumed to be fast in comparison with experimental time scales. The scheme as laid out by Israelachvili (1992) and Israelachvili et al. (1976) will be followed.

The first step in the scheme of any model is the distinction between monomers, dimers, trimers, and so on, in solution, all in equilibrium with one another. We denote an aggregate containing a number of n monomers as an aggregate with size n, or in short as an n-mer.

The second step is assume chemical equilibrium and hence equate the chemical potential of the surfactant as monomer with the chemical potential of the surfactant within an n-mer. This leads to the following expression for all aggregates of size N, $M > 1$ (Israelachvili 1992)

$$\mu_1 = \mu_1^0 + kT \ln X_1 = \mu_M = \mu_M^0 + 1/M\, kT \ln(X_M/M) = \mu_N = \mu_N^0 + 1/N\, kT \ln(X_N/N) \tag{9.5}$$

where μ_1 denotes the chemical potential of the surfactants as monomer, that is, the surfactant in solution, M and N denote different sizes of the aggregate, X_N the mole fraction of surfactants that are present in aggregates of size $n = N$, μ_N the chemical potential of a surfactant within an aggregate of size N, and μ_N^0 the self free energy of the surfactant within an aggregate of size N. Here one assumes a dilute solution so that the use of the term $kT \ln X_N$ is justified, and the factorization of $1/N$ ensures that the contribution of each surfactant molecule within an aggregate of size N is only counted once. We note that mass balance yields that $X_1 + X_2 + \ldots + X_N = X_{\text{total}}$, the total mole fraction of surfactant in solution. Equation (9.5) yields

$$X_N = N\{X_1 \exp[\mu_1^0 - \mu_N^0]/kT\}^N \tag{9.6}$$

As the total mole fraction cannot exceed one, there appears automatically an upper boundary for X_1, also known as a critical aggregation concentration, or critical micelle concentration, X_c which is given by

$$X_c = \exp - (\mu_1^0 - \mu_N^0)/kT \tag{9.7}$$

Until now we have not assumed anything about the type of surfactant nor about the morphology of the aggregate. For that matter, the above is equally valid for

proteins. If one wants to advance with the description above, one needs to include molecular information of the surfactant in order to calculate the interaction potential between surfactants within an aggregate of size n, to subsequently arrive at an expression for the chemical potential of a surfactant in that aggregate of size N, that is, μ_N^0.

Such an expression should in principle also contain information about the shape of the aggregate, as the aggregate shape also influences the distances between the hydrophilic and hydrophobic parts of the surfactants and thus their chemical potential. It should be realized at this point that the following complicating factor exists in general. If one wants to arrive at a size distribution of aggregates of a particular surfactant, on the basis of an equilibrium approach as above, one must include the shape of the aggregate in order to calculate the chemical potential. However, it is this shape itself that also should in principle be part of the minimisation scheme of the free energy of the overall system. In fact, one should minimise the free energy of the system on the basis of a size distribution and morphology of the system simultaneously. Setting aside for a moment this complication in the variational calculus, one may set an a priori shape at first and put forward hydrophilic and hydrophobic interactions within such an aggregate and determine, for example, the average size as a function of experimental parameters.

Israelachvili et al. (1976) argue that despite the intrinsic difficulties of incorporating all of the hydrophilic interaction contributions, the contribution to the chemical potential per surfactant within an aggregate of size N by the repulsive interaction can be assumed to adapt a simple form:

$$\mu_{N\,\text{hydrophillic}}^0 \sim \text{constant}\; D\, e^2/\varepsilon\, a \tag{9.8}$$

which is based on modelling the energy contribution as the energy of a capacitor with a charge per unit area of e/a, and separation D of the planes (resulting from the double layer of charge with thickness D), where the ε is the relative dielectric constant of the medium around the surfactant head group. Indeed, Tanford (1974) has shown that this $1/a$ dependence explains micelle sizes and critical micelle concentrations satisfactorily.

Including hydrophobic interactions leads to an overall chemical potential (Israelachvili 1992)

$$\mu_N^0 = \mu_{N\,\text{hydrophobic}}^0 + \mu_{N\,\text{hydrophillic}}^0 = \gamma\, a + c/a + g \tag{9.9}$$

where γ denotes the surface tension, a the area between hydrophobic groups versus water (a constant), and where the term g denotes constant surface area and/or bulk contributions (Israelachvili et al. 1972). Combining Equations (9.8) and (9.9) yields an optimum area, $a_0 = (c/\gamma)^{1/2}$, for which the free energy is a minimum. This relates to a specific number of surfactant molecules per aggregate. Having a larger number of surfactants per aggregate yields a smaller area per surfactant, and, vice versa, having a smaller number leads to a larger area. Both cases imply a higher free energy, leading to a size distribution of micelles.

The optimal area a_0 can be used as a practical criterion for the shape of the micelle versus the size of the head group and tail of the surfactant, assuming that the

chemical potential is not affected too much by the change of shape, that is, assuming that a_0 is not affected too much by the choice of aggregate shape. Considering a spherical micelle, with radius R, and denoting the volume of the hydrocarbon tail as v, and the surface area between hydrocarbon and water as a_0 then $R = 3\ v/a_0$. Realizing that there is an upper limit to the extension of the hydrocarbon chain given by the maximum tail length l_c, a spherical micelle will only be formed when $3\ v/a_0 < l_c$, leading to the condition for spherical micelle formation as $v/a_0 l_c < 1/3$ (Israelachvili et al. 1976) Similarly, one has for a cylinder the condition $v/a_0 l_c < 1/2$ and for planar objects $v/a_0 l_c < 1$.

One may investigate further, now assuming a certain shape, again following Israelachvili et al. (1976), the effect of the number of surfactants on the chemical potential. Suppose one has energy of binding between monomers when within an aggregate, of magnitude α. In the case of a rodlike structure, the endpoints are unbound, leading to (Israelachvili 1974)

$$N\,\mu_N^0 = -N\alpha\ kT + \alpha\ kT = -(N-1)\alpha\ kT \tag{9.10}$$

or

$$\mu_N^0 = \mu_\infty^0 + \alpha\ kT/N \tag{9.11}$$

where μ_∞^0 is the energy of the surfactant within an infinite aggregate. Similarly, taking always into account the number of endpoints of the aggregate one may derive for planar aggregates (Israelachvili 1976)

$$\mu_N^0 = \mu_\infty^0 + \alpha\ kT/N^{1/2} \tag{9.12}$$

and for spherical aggregates (Israelachvili et al. 1976)

$$\mu_N^0 = \mu_\infty^0 + \alpha\ kT/N^{1/3} \tag{9.13}$$

Now we know how the chemical potential depends on size, one may answer how the aggregate size depends on the value of α? Using Equations (9.11)–(9.13) one may rewrite Equation (9.6) as

$$X_N = N\{X_1 \exp[\alpha]\}^N . \exp(-\alpha) \tag{9.14}$$

for rod like structures, while for planar and spherical structures one has

$$X_N = N\{X_1 \exp[\alpha]\}^N . \exp(-\alpha N^p) \tag{9.15}$$

with p being 1/2 or 2/3 for discs and spheres, respectively. One can see from Equation (9.15) that when α is of the order of 1, X_N becomes negligible for larger N. Indeed, a separate phase is then formed consisting of infinitely large aggregates. This is the case for a constant α, and where μ_N^0 is a constantly decreasing function of N, that

is, the chemical potential is smaller the larger the aggregate. In other words, it favours infinite aggregates. It is only when μ_N^0 reaches a minimum value for finite N that one will end up with finite aggregates, and that one will have more of these aggregates as the concentration of surfactants increases. This miminum of the chemical potential can be addressed by Equation (9.9) from which an optimum head group area of the surfactant was deduced, and consequently an optimal number N per aggregate.

When the concentration becomes high enough to induce interaction between aggregates, thus influencing the chemical potential of the surfactants again, shape transitions may take place, as, for example, is the case of SDS exhibiting a spherical-to-rod transition at a certain concentration. The success of the model above can be attributed to an accurate enough description of the shape of the surfactant and the contributions to the chemical potential of the surfactant in various circumstances. When α is large, but $p = 1$, that is, referring to Equation (9.14), X_N does not decrease rapidly to zero, that is, one may have large aggregates of finite size provided that the structure is rodlike.

9.3.3 Spherical Protein Aggregates

A class of spherical protein aggregates that are in equilibrium with their monomeric constituents, and thus resemble micelles, are empty virus core shells, also called capsids (Kegel and Van der Schoot 2004; Bruinsma et al. 2003; Caspar 1980). Rather detailed experiments have been undertaken by Ceres and Zlotnick (2002), and these have been analysed in terms of micellisation by Kegel and Van der Schoot (2004). This analysis successfully explains the influence of salt and temperature on the micellization of the capsids. The expression for the chemical potential is based on the consideration that the hydrophobic patches account for a negative contribution to the chemical potential while the electrostatic charge distribution accounts for a positive contribution. The number of units building up the spherical assembly is set as a constant. Kegel and Van der Schoot arrive at an energy of binding for the assembly which we rewrite as

$$N\mu_N^0 = -N\gamma a_h + N a_C kT \sigma^2 \lambda_B \kappa^{-1} + \text{constant} \tag{9.16}$$

with γ the surface tension between the hydrophobic site of area a_h, which per protein particle is involved in assembly, a_c the area of interaction per protein involved in the Coulombic interaction, σ denoting the charge per surface area, λ_B the De Bjerrum length and κ^{-1} the electrostatic Debije screening length. In fact, the electrostatic contribution, the second term, is based on similar considerations as leading to Equation. (9.9). The end effects that are taken into account in Equation (9.9) on the basis of the surface area of hydrophobic molecular parts that are exposed to water is omitted in Equation (9.16). It is assumed that the main contribution to the chemical potential due to hydrophobicity arises from the efficient shielding of hydrophobic sites, giving rise to a negative term.

The expression can explain also effects of pH as observed with a closely related protein when using an expression for σ as originating in the Henderson–Hasselbalch equation (Stryer 1980) according to

$$\sigma = \sigma_b /(1 + 10^{\text{pH-pKb}}) - \sigma_a /(1 + 10^{\text{pKa-pH}}) \tag{9.17}$$

where pKb denotes an effective value for the basic groups of the protein sequence lumped together, and analogously for pKa.

9.3.4 Protein Assemblies of Arbitrary Morphology: A First Attempt

From a surfactant point of view, one may determine a packing criterion originating from minimising the sum of the two surface contributions to the chemical potential. The surfactant can be divided into a hydrophobic and a hydrophilic part, which are clearly separated. The bulk contribution to the chemical potential due to the replacement of water molecules around hydrocarbon chains by its own hydrocarbon chains is the driving force for assembly. The packing criterion and the consequent optimal number of surfactants in a micelle is determined by the minimization of the surface contribution at a finite N. The first step in testing the model of surfactant assembly is testing the size of spherical micelles as a function of experimental parameters like salt concentration and temperature.

Analogous to the surfactant approach, assembly of proteins into empty virus core shells has also been modelled in case of spherical assembly, as seen in Section 9.3. We propose as a first Ansatz a simple extension to Equation (9.15) in order to account for nonspherical and/or branched structures, and at the same time to take into account endpoint defects (i.e., the endpoints do not fully contribute to the chemical potential) here, compared to when an aggregate would be infinite, in the same manner as done in, for example, Equation (9.11) for rods, that is, aggregates of dimension 1. Taking into account an arbitrary shape, and/or degree of branching, the dimensionality may be denoted by its fractal dimension, D_f, defined by

$$\phi = (R/r)^D f \tag{9.18}$$

with ϕ the volume fraction of material within the aggregate, r the size of the constituents building up the aggregate, and R the size of the aggregate. In the case of surfactants, the dimensionality of a planar aggregate is 2; however, there exists in this case a particular arrangement due to the anisotropic nature of the surfactant. In the case of proteins, there is usually less structural anisotropy present per molecule. This means that in the case of proteins one expects arrangements that are exhibiting more isotropy. In principle, D_f may range form 1 to 3, 1 resembling rods, and 3 resembling a fully packed spherical assembly. The extent to which an aggregate exhibits linearity (and thus the less it exhibits branching) can be expressed in terms of how close D_f comes to being 1. The number of endpoints, defined as the outermost points, of a fractal aggregate, equals:

$$n_{\text{endpoints}} = \mathrm{D}_f N^{(D_f - 1)/D_f} \tag{9.19}$$

Taking into account also the endpoint contribution we find

$$\mu_N^0 = (-\alpha + \beta)kT + (\alpha - \beta)\, kT\, D/N^{1/D_f} \tag{9.20}$$

with $\alpha = \gamma a_h/kT$ and $\beta = a_C\ \sigma^2\ \lambda_B\ \kappa^{-1}$ and $(\alpha - \beta)kT$ denoting the energy of bonding per particle. Again one finds that if $(\alpha - \beta)$ is order 1 or larger, phase separation is expected for $N > 1$. If the bonding energy is higher than kT, only finite aggregates will be formed when $D = 1$, that is, rodlike structures.

The question remaining is whether one may expect equilibrium structures with a fractal dimension larger than 1. The idea of surfactant assembly was that also for $D_f > 1$ one would be able to have finite aggregates when the bonding energy was of order kT, since there is usually an optimum in surface area of the surfactant being exposed to the water phase. This optimum in the cases of surfactants is caused by two surface energy contributions per particle, which together can be minimised, yielding the optimal surface area per surfactant within the aggregate. Subsequently, one was able to deduce minimal packing constraints for the surfactants, thus defining the preferred shape of the aggregate. We propose to follow an analogous procedure now for proteins.

We assume a number, n_p, of hydrophobic patches with equal surface area, a_p (a patch may be (1–30) nm^2 in size (Lijnzaad et al. 1996). We assume a number of bonds per protein within the aggregate (i.e., neglecting the endpoints for the moment) of n_b. The exposed area of the protein surface to the surrounding solution then equals $a_{exp} = a - n_b a_p$, where a denotes the total surface area of the protein. There exist two contributions to the chemical potential that arise from the exposed area of the protein within the aggregate to water. The chemical potential for assembly can be written as

$$\gamma(n_p a_p - a) + \gamma a_{exp} + 4\pi\ (q)^2\ \lambda_B\ \kappa^{-1}\ kT/a_{exp} \tag{9.21}$$

with q the number of unit charges. Minimisation of Equation (9.21) with respect to a_{exp} leads to a minimal exposed surface area, a_{exp}^0 given by

$$a_{exp}^0 = |q|.(\ 4\pi\ \lambda_B\ \kappa^{-1}\ kT/\ \gamma)^{1/2} \tag{9.22}$$

or

$$a_{exp}^0/a = |\sigma|\ .(\ 4\pi\ \lambda_B\ \kappa^{-1}\ kT/\ \gamma)^{1/2} \tag{9.23}$$

where we have introduced the surface charge density σ. In terms of a minimal number of neighbours, n_b^0 we find

$$n_b^0 = (\ a - a^0_{exp})/a_p = a/a_p\ (1 - |\sigma|\ (4\pi\ \ \lambda_B\ \kappa^{-1}\ kT/\ \gamma)^{1/2}\ )) \tag{9.24}$$

Substituting $\lambda_B = 0.7$ nm, values for κ^{-1} ranging between 0.25 and 1.75 nm (experimentally existing window for a fibrillar beta-lactoglobulin assembly at pH 2), $kT = 4.10^{-21}$ J, $\gamma = 50$ mN/m, a $\sigma = 4.2.10^{17}$ (using 21 unit charges at pH2, and a radius of 4 nm of the protein) we arrive at a value for n_b^0 ranging between 0.4 a/a_p and 0.8 a/a_p for κ^{-1} ranging between 0.25 and 1.75 nm.

Experimentally it is known that in the above-mentioned regime fibrils are being formed, with almost no branches, that is, $n_b = 2$, implying that a/a_p is in the range 2.5–5, that is, 20–40% hydrophobic surface area per protein, a seemingly reasonable value. From Equation (9.17) it is clear that the charge density is also a strong function of pH, which in turn sharply affects the n_b^0 and thus the experimentally accessible n_b as is observed experimentally also (Hermansson et al. 1986; Veerman et al. 2003; Aymard et al. 1996; Aymard et al. 1999; Schokker et al. 2000). It is clear that the above equation needs further refinement, which will be deferred to a future publication. This first crude estimate is a first attempt to predict equilibrium aggregate forms of proteins in solution. It needs to be emphasised that the above description is meant to cover an equilibrium aggregate morphology. This approach may also have merit for the description of the behaviour within the so-called crystallisation slot (George and Wilson 1994) and beyond, as well as in describing effects of different salts by means of affecting γ (Hofmeister series).

One may take Equation (9.24)\further by realising that n_b^0 should not decrease below 1. If this should happen nonetheless, one may use Equation (9.24) as a packing criterion for formation of an aggregate where not the single protein is the building block of the aggregate, but instead dimmers or *n*-mers will start to form the building blocks of the aggregate, since *n*-mers effectively decrease the exposed surface area. Thus, Equation (9.24) may also be used to identify transitions from single-stranded fibrils to fibrils having more than one strand around one another, or fibrils with, for example, two strands that have a twist with respect to each other, tubules or other topologies.

9.3.5 Beta-Lactoglobulin Fibrils: Equilibrium Assembly or Not?

An example of a fibrillar protein assembly is beta-lactoglobulin assembling into fibrils of one or two monomers thick strands, when heating above 80°C, at pH 2, and low ionic strength (Hermansson et al. 1986; Veerman et al. 2003; Aymard et al. 1996; Aymard et al. 1999; Schokker et al. 2000). The length distribution of the mature fibrils is a polydisperse, single-peaked distribution with a smooth linear decrease to zero. The initial reversibility of the fibrillisation process becomes irreversible after some time, that is, the fibrils become stable under dilution (Veerman et al. 2003). It is not obvious from our own measurements that there exists a critical concentration below which no fibrils are formed. If such a concentration existed, it would need to be substantially lower than 0.5% (*W/W*), indicating a rather high bond energy between the proteins.

From electric birefringence measurements it was concluded that the proteins are ordered "head-to-tail" within the fibril, in a helical configuration (Rogers et al. 2005). The fact that one needs a minimal temperature in order to induce fibrillisation is directly related to the fact that at a certain elevated temperature the protein will partially unfold. Since we have also observed the formation of fibrils at 4°C, after having applied this (partial) denaturation step, the elevated temperature is not essential during assembly. However, at the lower temperature, the assembly was found to be much slower, indicating that temperature affects the kinetics of the assembly process. The relation between the fibrillar type of assembly and the partially unfolded state also has been found for other proteins (e.g., ovalbumin, hen egg white

lysozyme, bovine serum albumin) (Tani et al. 1995). In the latter case it was reported that upon partial unfolding, some hydrophobic regions become exposed to the solvent. A requirement for obtaining long fibrils with few branches is maintaining a low pH and low ionic strength. Moderate ionic strength yields more flexible fibrils, while even higher ionic strength and/or higher pH yields more condense spherical aggregates with a fractal dimension of around 2 (Aymard et al. 1996; Aymard et al. 1999; Schokker et al. 2000).

The length distribution for beta-lac fibrils is not a sharp-peaked Poisson distribution, in which case one would expect a "full-width half-height" of around 100 nm. In case of a reversible aggregation the equilibrium length distribution was predicted by several authors using Equation (9.14) (Israelachvili 1992) and yields a smooth and single-peaked distribution given by:

$$C_L = L \exp(-aL) \tag{9.25}$$

with the constant a being proportional to the chemical potential of the protein in the fibrils, and depending on concentration and temperature. The peak of the distribution is located at $1/a$. Despite the more complex nature of proteins compared to simple surfactants we do find a distribution with a shape that is at least similar to the theoretical prediction according to Equation (9.25)

One also has to take into account two kinetic mechanisms that play a role in reaching the equilibrium distribution of the fibrils: First, a nucleation event, followed by subsequent growth of the fibril and possible redistribution of proteins between the fibrils. It is a reasonable assumption, when no shear is applied, that every fibril is extended at the same rate independent of its length. With this in mind the resulting length distribution could never have developed if there was an instantaneous nucleation of all nuclei and if protein redistribution between the fibrils was absent. Secondly, we also have to consider the influence of the (apparent) long-term irreversibility of the assembly. The fact that the attachment of proteins to the fibril becomes irreversible after some time will have a pronounced influence on the fibril length distribution. In the early stages of the self-assembly, when the typical time the protein remains attached to the fibril's end is much longer than the time necessary to form a permanent bond, the fibril will grow and will be able to form irreversible bonds (beta-sheet structures). The proteins in the fibril are in a "trapped state" as a result of the high bond energy of the beta-sheet. This, together with the high charge density at low pH, and the strong hydrophobic interactions at elevated temperature, may explain that under these circumstances fibrils and not aggregates are obtained of fractal dimension much higher than 1.

The irreversibility does not in general apply for the proteins attached to both ends of the fibril. If this was the case, all proteins would eventually be incorporated into the fibrils, which is something contrary to our observations. At concentrations low enough, the typical time the average protein remains attached to the fibril's end is much shorter than the time necessary to form a permanent bond (a two-step mechanism where the protein first attaches to the fibrils and subsequently becomes incorporated in the beta-sheet of the fibril). Due to the partially irreversible assembly of most of the proteins in the fibril, only limited rearrangement of protein monomers

can occur. Therefore, we expect the final length distribution to be somewhat wider than a Poisson distribution but narrower as predicted by Equation (9.25).

After a mild denaturation step (elevated temperature, pH2) the protein partially unfolds leading to an effective attraction between the protein molecules. Since the proteins are in a head-to-tail arrangement within the fibril this suggests the attraction is of a dipolar nature. This dipolar attraction could very well be the sum of the different forces (electrostatic, hydrophobic) involved. In order to initiate the growth of the fibril a nucleation event is necessary. Initially, the assembly is reversible, but after some time (typically hours) the fibril is stabilized by a crossed beta-sheet structure, running perpendicular to the long axis of the fibril. As a result of this irreversibility, thermodynamic equilibrium theories can only be applied with caution. The system might be kinetically trapped in the later stages of the assembly and as such cannot reach its equilibrium by rearranging the proteins between different fibrils or even spherulites. It is unknown if the assembly is entropy driven or enthalpy driven. It remains to be further tested whether at short times the above suggested attempt for an equilibrium approach to protein assembly into fibrils can be applied, and whether the equilibrium approach can be extended to regions of higher salt concentration and/or different pH.

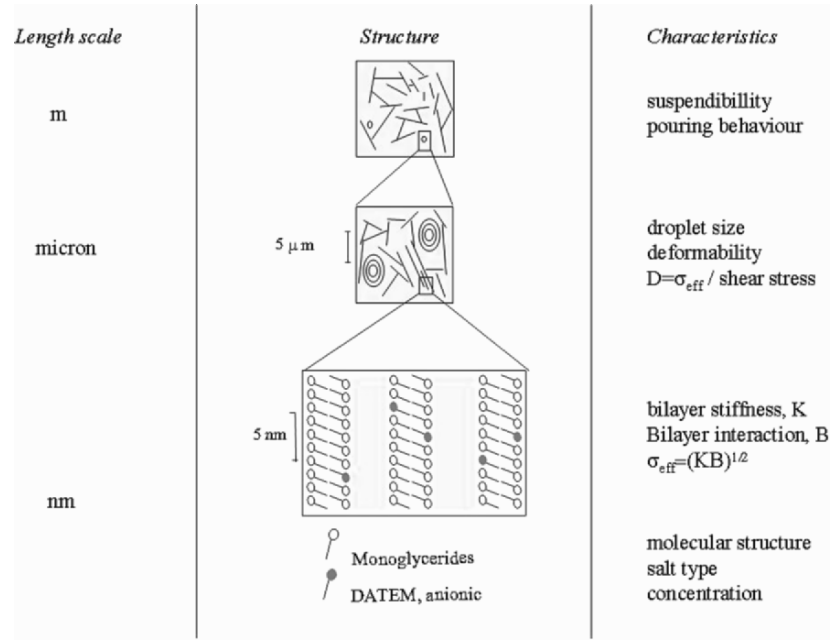

Figure 9.4. Scheme showing the relationship between structures and parameters at different length scales.

9.4 Conclusions

In the section on lamellar phases we have shown that macroscopic rheological properties of a lamellar structure, of relevance to real foods, can be related to the type of

mesoscopic structure, which in turn can be related to key mesoscopic variables such as lamellar droplet size and deformability. This size and deformability can be expressed in terms of flexibility of the bilayer building the lamellar phase, and the interaction between the bilayers, and was shown to be valid experimentally in a model system. See Figure 9.4 for a schematic picture of how various parameters on various length scales are related.

The lamellar phase exists by virtue of the fact that amphiphilic molecules assemble into such a phase under given circumstances. One challenge is to relate properties of such a mesophase to macroscopic relevant properties, which was addressed in Section 9.2. In Section 9.3 a scheme has been given that was introduced by Israelachvili, which is useful in describing why certain amphiphiles form certain mesophases. This scheme has been successfully applied to many amphiphilic systems. One of the challenges addressed in Section 9.3 is to see how that scheme may be also applied to the assembly of proteins, as another type of amphiphile, in particular how to explain recently observed phenomena of protein fibrillisation.

Acknowledgements. I thank John van de Pas, Hans Droge, Ies Heertje, Frank Kleinherenbrink, Edgar Blokhuis, Rob Groot, Marijn Warmoeskerken, Henk Lekkerkerker, Wim Hogervorst and Norman Wagner for discussions on various subjects treated in Section 9.2. I gratefully acknowledge permission for reproduction of Section 9.2, which originally appeared as part of the chapter "Mesoscopic Physics and Functional Properties of Foods," in: *Supramolecular and Colloidal Structures in Biomaterials and Biosubstrates* (2000), edited by M. Lal, P.J. Lillford, V.M. Naik, and V. Prakash, Imperial College Press, Singapore, ISBN 1-86094-236-9. I am also grateful for permission to reproduce Section 9.3, which was originally published as a chapter, entitled "Similarities in Self-Assembly of Proteins and Surfactants: An Attempt to Bridge the Gap," authored by Erik van der Linden and Paul Venema, in *Food Colloids: Self-Assembly and Material Science* (2007), edited by E. Dickinson and M.E. Leser, published by Royal Society of Chemistry, Cambridge, UK, ISBN 9780854042715. I thank Mrs. Els Jansen for help in editing the manuscript.

9.5 References

Aymard, P. et al. (1996). A comparison of the structure of beta-lactoglobulin aggregates formed at pH 7 and pH 2. *Int. J. Polym. Anal. Ch*. 2, 115–119.

Aymard, P., Nicolai, T., Durand, D., and Clark A. (1999). Static and dynamic light scattering of beta-lactoglobulin aggregates formed after heat-induced denaturation at pH 2. *Macromolecules* 32, 2542–2552.

Bergenholtz, J., and Wagner, N.J. (1996). Formation of AOT/brine multilamellar vesicles. *Langmuir* 12, 3122–3126.

Bohlin, L., and Fontell, K. (1978). Flow properties of lamellar liquid crystalline lipid–water systems. *J. Colloid Interf. Sci*. 67, 272–283.

Bohlin, L. (1979). Coordination of structural units from flow measurements. *J. Colloid Interf.* Sci. 69, 194–195.

Bruinsma, R.F., Gelbart, W.M., Reguera, D., Rudnick J., and Zandi, R. (2003). Viral self-assembly as a thermodynamic process. *Phys. Rev. Lett*. 90, 248101–248104.

Caspar, D.L. (1980) Movement and self-control in protein assemblies. Quasi-equivalence revisited. *Biophys. J.* 32, 103–138.
Ceres, P., and Zlotnick, A. (2002). Weak protein–protein interactions are sufficient to drive assembly of hepatitis B virus capsids. *Biochemistry* 41, 11525–11531.
De Gennes, P.G. (1974). *The Physics of Liquid Crystals*, Oxford University Press.
De Gennes, P.G., and Prost J. (1993). *The Physics of Liquid Crystals*, 2nd edition, Clarendon Press, Oxford
Diat, O., Roux, D., and Nallet, F. (1993). Effect of shear on a lyotropic lamellar phase *J. Phys.* II, 3, 1427.
Djabourov, M. (1988). Architecture of gelatine gels. *Contemp. Phys*. 29, 273–297.
George, A., and Wilson W.W. (1994). Predicting protein crystallisation forma dilute solution property, *Acta Cryst. D* 50, 361–365.
Grillo, I. (2003). Small angle neutronscattering study of a worldwide known emulsion: Le Pastis. *Colloid Surface A* 225, 153–160
Heertje, I., Roijers, E.C., and Hendrickx, H.A.C.M. (1998). Liquid crystalline phases in the structuring of food products. *Lebensm. Wiss. u. Technol*. 31, 387–396.
Helfrich, W. (1978). Steric interaction of fluid membranes in multilayer systems. *Z. Naturforsch.*, A33, 305–315.
Hermansson, A.M, Harbitz, O., and Langton, M. (1986). Formation of 2 types of gels from bovine myosine. *J. Sci. Food Agric*. 37, 69–84.
Israelachvili J.N., Mitchell, D.J., and Ninham, D.W. (1976). Theory of self-assembly of hydrocarbon amphiphiles into micelles and bilayers *J. Chem. Soc. Faraday Trans*. II 72, 1525–1568.
Israelachvili, J. (1992). *Intermolecular & Surface Forces*, 2nd edition, Academic Press, London.
Kegel, W.K., and Schoot, P. van der (2004). Competing hydrophobic and screened-Coulomb interactions in Hepatitis B virus capsid assembly. *Biophys. J.* 86, 3905–31913.
Kummrov, M., and Helfrich, W. (1991). Deformation of giant lipid vesicles by electric fields *Phys. Rev. A* 44, 8356–8360.
Lijnzaad, P., Berendsen, H.J.C., and Argos, P. (1996). A method for detecting hydrophobic patches protein. *Protein. Struct. Funct. Genet*. 26, 192–203.
Linden, E. van der, and Droge, J.H.M. (1993). Deformability of lamellar droplets. *Physica A*, 193, 439–447.
Linden, E. van der, Hogervorst, W.T., and Lekkerkerker, H.N.W. (1996). Relation between the size of lamellar droplets in onion phases and their effective surface tension. *Langmuir*, 12, 3127–3130.
McGee, H. (2004). *On Food and Cooking: The Science and Lore of the Kitchen*. Scribner, New York.
Nallet, F., Roux, D., and Prost, J. (1989). Dynamic light scattering study of dilute lamellar phases. *Phys. Rev. Lett.,* 62, 276–279.
Nallet, F. (1991). Membrane fluctuations in dilute lamellar phases. *Langmuir* 7, 1861–1863.
Odijk, T. (1992). Self-consistent theory of a charged multimembrane system. *Langmuir* 8, 1690–1691.
Odijk, T. (1993). Evidence for undulation-enhanced forces from the melting curves of a lamellar phase and a hexagonal polyelectrolyte gel. *Europhys. Lett*. 24, 177–182.
Rogers, S.S., Venema, P., Ploeg, J.P.M. van der, Sagis, L.M.C., Donald, A.M., and Linden, E. van der (2005). Electric birefringence study of an amyloid fibril system: The short end of the length distribution. *Eur.Phys. J. E.* 18, 207–217.
Roux, D., and Safinya, C.R. (1988). A synchrotron x-ray study of competing undulation and electrostatic interlayer interactions in fluid multimembrane lyotropic phases *J. Phys. France* 49, 307–318.
Roux, D. (1993). Rheology of lyotropic lamellar phases. *Europhys. Lett.*, 24, 53–58.

Safinya, C.R., Roux, D., Smith, G.S., Sinha, S.K., Dimon, P, Clark, N.A., and Bellocq, A.M. (1986). Steric interactions in a model multimembrane system: a synchrotron x-ray study. *Phys. Rev. Lett.* 57, 2718–2721.

Schokker, E.P., Singh, H., and Creamer, L.K. (2000). Heat-induced aggregation of beta-lactoglobulin AB at pH 2.5 as influenced by ionic strength and protein concentration. *Int. Dairy J*. 10, 233–240.

Stryer, L. (1980). *Biochemistry*, W.H. Freeman and Company, New York.

Tanford, C. (1974). Theory of micelle formation in aqueous solutions. *J. Phys. Chem.* 78, 2469–2479.

Tani, F., Murata, M., Higasa, T., Goto, M., Kitabatake, N., and Doi, E. (1995). Molten globule state of protein molecules in heat-induced transparent food gels. *J. Agric. Food Chem*. 43, 2325–2331.

This, H. (2005). Modelling dishes and exploring culinary "precisions": the two issues of molecular gastronomy, *Brit. J. Nutr. (Suppl.*) 1, 139–146.

Veerman, C., Baptist H.G.M., Sagis, L.M.C., and Van der Linden, E. (2003). A new multistep Ca^{2+}-induced cold gelation process for beta-lactoglobulin, *J. Agric. Food Chem*. 51, 3880–3885.

Chapter 10

Solid Food Foams

Maria G. Corradini and Micha Peleg

University of Massachusetts, Amherst, MA, Department of Food Science,
mariagcorradini@gmail.com, micha.peleg@foodsci.umass.edu

10.1 Introduction

The words "cell" and "cellular" came to English (via French) from the Latin *cella*, a store room or chamber. In modern usage, they have several very different meanings. The two that are pertinent to food structure and texture have to do with the cells in edible tissues of plants, fungi and animals or with the open spaces, filled with air or another gas, enclosed by a liquid or solid matrix that forms the cell walls.

Rheologically speaking, "solid" is a term that needs to be used with caution. An albumen foam and whipped cream, under most circumstances, do not flow under their own weight and are therefore solid in a certain sense. Yet, upon disintegration, they leave behind a liquid. This is in contrast with puffed cereals and snacks, pieces of freeze-dried vegetables or chicken, and agglomerated, spray dried or instant coffee particles. These, if ground, would leave a powder made of solid particles. But what about fresh bread, cakes, marshmallows and popcorn? We will consider them solids despite the fact that their cell wall material is plasticized.

There are different ways to classify cellular solid foods. Here are some:

a. *Structural:* Open and/or closed cells, thick vs. thin walls (relative to the cell's size), "solid" walls or walls that themselves have tiny bubbles, isotropic vs. directional structures, uniform vs. nonuniform bubble size distribution, single or layered array.
b. *Method of formation*: Fermentation and baking, extrusion and puffing, aeration or gas release (CO_2) followed by heat setting, agglomeration, freeze drying.
c. *Texture:* "Soft" (i.e., easily deformed) vs. brittle, (i.e., a material that shatters upon impact or compression), weak or strong (disintegrates easily or only under a considerable stress), elastic (springs back to its original shape) or plastic (maintains its deformed shape).
d. *Hygroscopicity:* Physically stable under normal humidity conditions or tend to absorb or lose moisture rapidly.

e. *Unit size scale*: Consumed or handled as individual units (a bread slice, snack) or as an assembly (puffed breakfast cereals, instant coffee).

None of the above categories is sharply defined and there can be other classifycations. One can easily contemplate solid cellular foods that can move between otherwise mutually exclusive groups—fresh or dried bread crumbs is a good example, and so is ice cream, although for very different reasons. Moreover, with the above classifications, the number of possible combinations must be enormous even without considering the food's chemical composition. Yet, most cellular solid foods share a small number of common features and hence can be discussed as belonging to two major categories—soft and brittle—keeping in mind that within the two categories, there may be numerous subclassifications. Examples are given in Table 10.1.

Table 10.1. Typical physical properties of cellular solid foods.

Food	Density ($g\ cm^{-3}$)	Wall density ($g\ cm^{-3}$)	Void Fraction (%)	Type
Popcorn	~0.07	~1.40	>95	Soft
Puffed rice	0.13–0.17	1.35–1.40	88–90	Brittle
Extruded products	0.10–0.33	1.25–1.40	75–90	Soft or brittle
Meringue	0.17–0.18	~1.55	88–90	Mixed
Baked bread loaf	0.20–0.35	~1.25	72–85	Soft
Sponge cake	0.25–0.35	~1.25	70–80	Soft

Adapted from Campbell and Mougeot (1999).

10.2 Mechanical Properties of "Soft" Cellular Foods

Pictures of bread slice specimens, intact and at three levels of compressive deformation, are presented in Figure 10.1 (top). When only slightly deformed, the open structure is characterized by bending of the cells' walls. At progressively higher compressive deformations the cell walls buckle—some may even rupture; see below—until much of the volume is occupied by the collapsed cell wall material. When this occurs, the deformation is to a large extent of the solid material itself. As might be expected, the dense compacted structure offers stronger resistance to deformation than the original open structure. Since the collapsed solid matrix primarily fills open spaces, the compressed specimen's cross-sectional area hardly changes, even under strains on the order of up to about 75%. This is in contrast to incompressible solids, such as cheese or ham (see Figure 10.1, bottom), the cross-sectional expansion of which is considerable. When the volume of a solid is preserved, or almost preserved, the product of its cross-sectional area multiplied by its height is constant, or approximately constant. Hence, any reduction in the specimen's height leads to a corresponding area expansion, a factor that needs to be taken into account in the interpretation of such materials' force–displacement or stress-strain relationships.

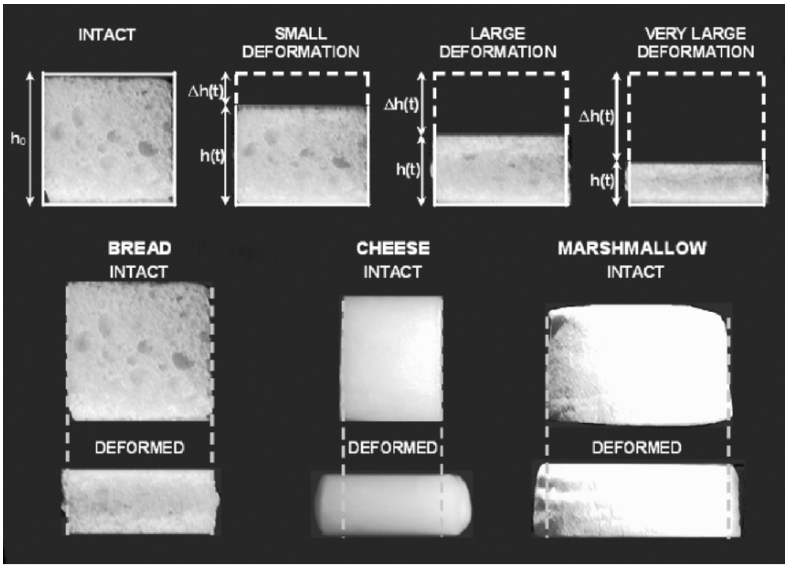

Figure 10.1. *Top*: The compressibility of bread crumbs. Notice the collapse of the cell walls. *Bottom*: Comparison of the compressibility of bread crumbs, cheese and marshmallows. Notice that the bread crumb collapses on itself, and hence the specimen does not expand laterally.

Soft Cellular solids with thick walls and very small air bubbles can exhibit a compressibility pattern similar to that of a dense solid; see the discussion of marshmallows bellow. Marshmallows are such an example. However structural collapse unaccompanied by significant lateral expansion is a characteristic of the majority of solid food foams, regardless of whether their cells are open or closed and whether their cell wall material is brittle or complying ("soft").

10.2.1 The Compressive Stress–Strain Relationships of "Typical" Cellular Solids

The mechanics of solid foams has been extensively studied, theoretically and experimentally. Many of the important and influential results can be found in the works of Ashby and in the by now classic book of Gibson and Ashby (1997), *Cellular Solids: Structure and Properties*. Briefly, the compressive force– deformation curves, when converted into a engineering stress–strain relationship, have the typical shape shown in Figure 10.2. [The engineering stress, σ_E, is the force divided by the specimen's original cross-sectional area, which, as stated, remains fairly constant as long as the deformed specimen still maintains a cellular structure.] The engineering strain, ε_E, is the absolute deformation (Δh) divided by the original specimen's height, (h_0); see Figure 10.1. The classic stress–strain curve, σ_E vs. ε_E, of cellular solids has three discernible regions. They correspond to the deformed specimen's states depicted in Figure 10.1 (top).

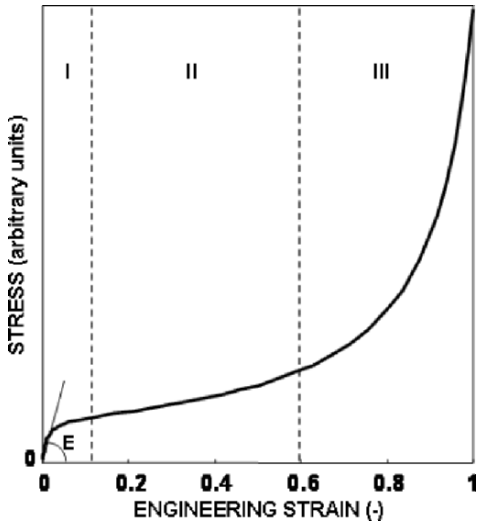

Figure 10.2. Schematic view of the three regions of the force–displacement curve of a typical cellular solid: I, small deformation of the intact structure; II, buckling and fracture of cell walls; and III, compaction of what is increasingly collapsed cell wall material.

At low strains, according to Ashby (1983), Gibson and Ashby (1997) and others, the specimen's deformability can be characterized by a modulus of elasticity, E, defined as the slope of the stress–strain curve, that is, the stress divided by strain. This modulus is related to the foam's density by the equation:

$$\frac{E}{E_s} = k\left(\frac{\rho}{\rho_s}\right)^n \tag{10.1}$$

where E_s is the cell wall material's modulus, ρ and ρ_s are the densities of the foam and of the cell wall material, respectively, and k and n are constants. The constants k and n, according to Ashby, are determined by the cellular structure, that is, by whether the cells are open or closed, the relative thickness of the wall (which determines the wall's tendency to buckle), and so on. This formula has been used to characterize cellular foods too (e.g., Aguilera and Stanley 1999) but it is still unclear whether all solid foods indeed exhibit true elasticity even under small strains. One of the implications of Equation (10.1) is that the plot of log E vs. log ρ is a straight line. Thus, in principle, if ρ_s and E are known, or can be measured or estimated, this straight line's slope and "intersect" (i.e., where $\rho/\rho_s = 1$) will yield the parameters k and n, from which the foam's structure characteristics would be inferred.

In practice, attempting to change a food's density, even when the ingredients' composition remains unchanged, may also induce structural changes that may complicate the interpretation of the E vs. ρ plot. Also, in contrast with theoretical models in which the cells are uniform and their geometry is well-defined, the bubbles of real solid food foams have varying cell wall thickness as well as a size distribution

that is not always known, let alone uniform. Moreover, in solid food foams, some of the cells can be open while others are closed, that is, they belong to groups that according to Equation (10.1) would have a different exponent, *n*. This is in contrast to synthetic solid foams such as the familiar polystyrene and polyurethane, the cells of which are either closed or open. Still, the equation can probably be used to characterize cellular foods if and when they exhibit distinct elastic response at low strains and conform to the theoretical classifications of Ashby (1983) and Gibson and Ashby (1997).

The central region of the stress–strain curve is typically characterized by a constant or almost constant low-stress level over a large range of strains; see Figure 10.1. This ability of solid foams to undergo considerable deformation while the stress remains low makes them ideal for cushioning sensitive items to protect them against mechanical damage. The presence of air bubbles also makes them excellent thermal insulators. This characteristic also influences the processing of cellular foods where heat transfer plays an important role.

In the third phase of the deformation (see Figure 10.2), there is a steep stress rise as the number of still uncollapsed cells rapidly diminishes and the compact's density approaches that of the cell wall's material.

The textural implications of the above characteristics of the stress–strain relationships are not always clear. When one examines a bread loaf or a roll with the fingers to evaluate its freshness, it seems obvious that the perceived mechanical stimulus is associated with the first region of the curve. Yet, in mastication, the compact's resistance to *tearing* probably plays a more significant role than the first and second stages of the compression. At the point where the bread crumb is torn, however, the specimen may have already been wetted by saliva so that the relationship between the stress–strain characteristics of the dry sponge and its perceived textural properties is usually obscured.

10.2.2 Mathematical Characterization of the Compressive Stress–Strain Relationship of Polymeric Foams, Breads and Cakes

Typical sigmoid compressive stress–strain relationships of both synthetic foams and bakery products can be expressed mathematically by a variety of empirical models among them (Swyngedau et al. 1991):

$$\sigma = \frac{C_1 \varepsilon}{(1 + C_2 \varepsilon)(C_3 - \varepsilon)} \tag{10.2}$$

$$\sigma = C_1 \varepsilon^{n_1} + C_2 \varepsilon^{n_2} \quad (n \leq 1 \text{ and } n > 1) \tag{10.3}$$

$$\sigma = C_1 \left(\frac{\varepsilon}{C_2 - \varepsilon} \right)^n \tag{10.4}$$

$$\sigma = \frac{\log_e \left(1 - \frac{\varepsilon}{C_1} \right)^{\frac{1}{n}}}{C_2} \tag{10.5}$$

where σ is the engineering stress, ε is either the engineering or Hencky's (natural) strain and the *C*'s and *n*'s are constants. Hencky's strain preserves the relative magnitude of the deformation by taking into account the continuously changing specimen's height. For this reason it is commonly used to describe systems where the deformations are large. Mathematically, the compressive Hencky's strain, ε_H, is defined by:

$$\varepsilon_H = \log_e\left(\frac{h_0}{h_0 - \Delta h}\right) \tag{10.6}$$

Obviously, the magnitude of the *C*'s and *n*'s in Equations (10.2)-(10.5) will not be the same if the strain is Hencky's, ε_H, or the engineering, ε_E. The fit of the four models is demonstrated in Figure 10.3.

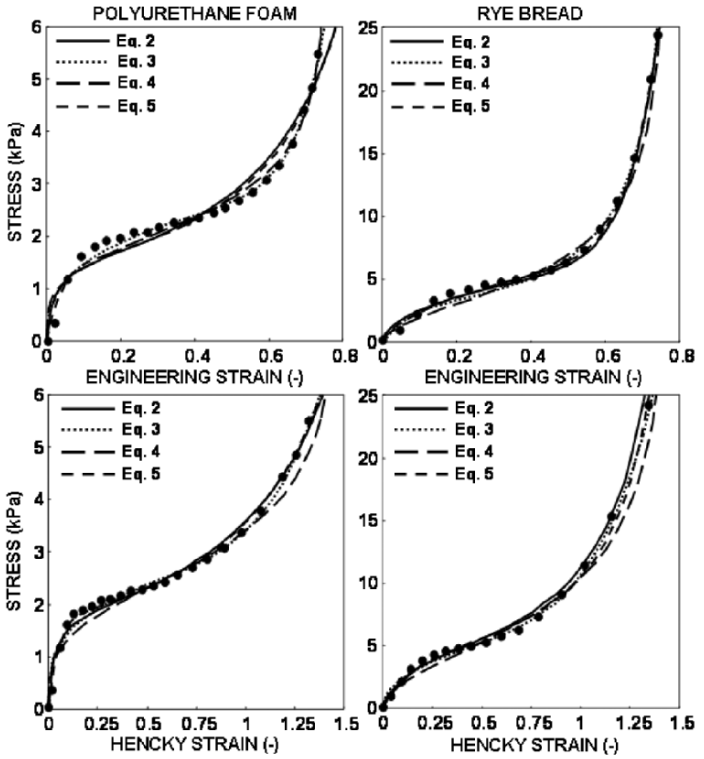

Figure 10.3. The stress–strain relationship of a polyurethane and bread crumb foams fitted with four empirical models (see text). From Swyngedau et al. (1991).

The advantage of Equation (10.2) as a model is that C_1, serves as a sort of a scale factor, C_2 as a measure of the flat region's (shoulder's) prominence (when $C_2 = 0$ the shoulder disappears altogether) and C_3 is a marker of the strain where the densification (stage three) becomes the dominant deformation mechanism (when $\varepsilon \rightarrow C_3$, $\sigma \rightarrow \infty$). The advantage of Equation (10.3) is that it identifies two compressive mechanisms, one dominated primarily by buckling with a scaling factor of less than one (downward concavity) and one by compaction with a scaling factor of more than one (upper concavity). The only advantage of Equations (10.4) and (10.5) is that they have an analytic inverse, that is, one can express ε as a function of σ algebraically. This characteristic can be exploited in the calculation of the mechanical properties of layered arrays; see below.

10.2.2.1 Breads

If all food sponges had been truly elastic over a large range of strains, repeated compression–decompression cycles would have produced identical stress–strain relationships, perhaps with a small hysteresis as shown schematically in Figure 10.4. Since the area under the stress–strain curves has energy per volume units, the area enclosed by the hysteresis loop would reflect the energy loss as a result of internal friction. In reality, though, successive compression–decompression cycles can produce stress–strain relationships that are *qualitatively different*. The stress–strain curves of a white bread crumb repeatedly compressed (Figure 10.5) is an example. Notice that the "shoulder," which was quite prominent in the first compression, totally disappears in all successive cycles. A possible interpretation of this observation is that the initial compression caused the burst of closed cells, turning the cellular crumb into an open "spongy" structure, whose deformability pattern was quite distinct (Peleg et al. 1989). Similar observations were recorded in other breads, so the phenomenon cannot be uncommon.

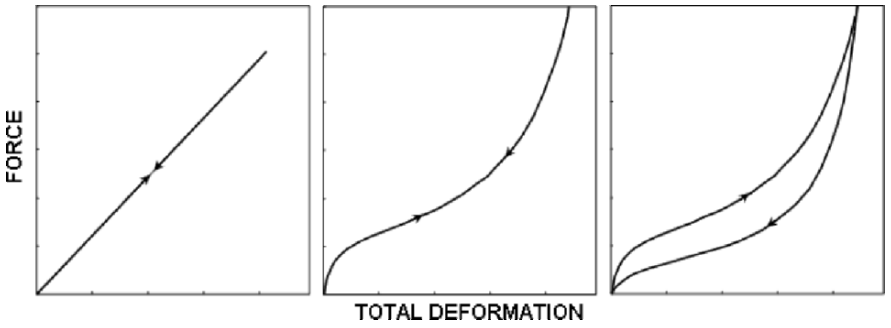

Figure 10.4. Schematic view of reversible and irreversible stress–strain relationships in a compression–decompression cycle. *Left*, ideal linear elasticity (small deformation); *center*, nonlinear elasticity; and *right*, a relationship showing a hysteresis loop.

Figure 10.5. The stress–strain relationships of a bread crumb in successive compression–decompression cycles. Notice the disappearance of the shoulder in the second and third cycles, which is probably an indication of closed cells rupture. After Peleg et al. (1989).

10.2.2.2 The Deformability of Marshmallows

Although marshmallows are cellular solids, they exhibit a deformability pattern that is atypical for cellular solids of the kinds classified by Ashby (1983). The marshmallow deformability is characterized by the *absence* of a prominent shoulder in the stress–strain relationships as shown schematically in Figure 10.6 (top).

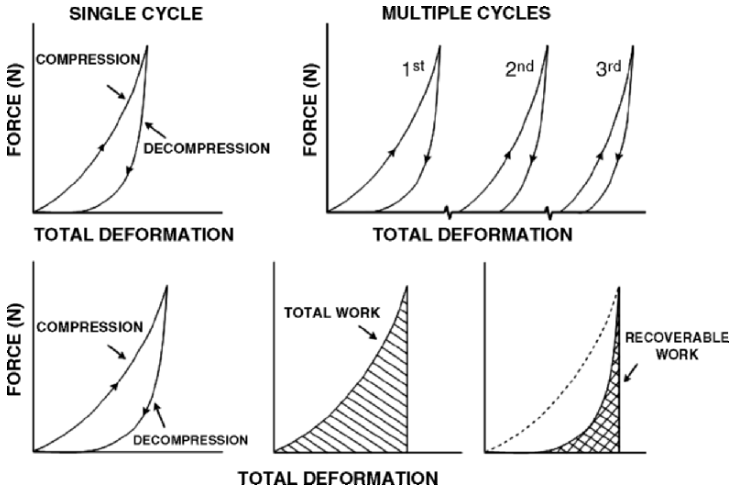

Figure 10.6. *Top*: Schematic view of the force–deformation relationships of marshmallows. Notice the absence of a shoulder. After Kaletunc et al. (1992). *Bottom*: Schematic view of how the degree of elasticity can be assessed from a compression–decompression curve. (Notice that the area under the stress–stress strain curve has work per unit volume units and that the degree of elasticity can be defined as the recoverable/total work ratio.)

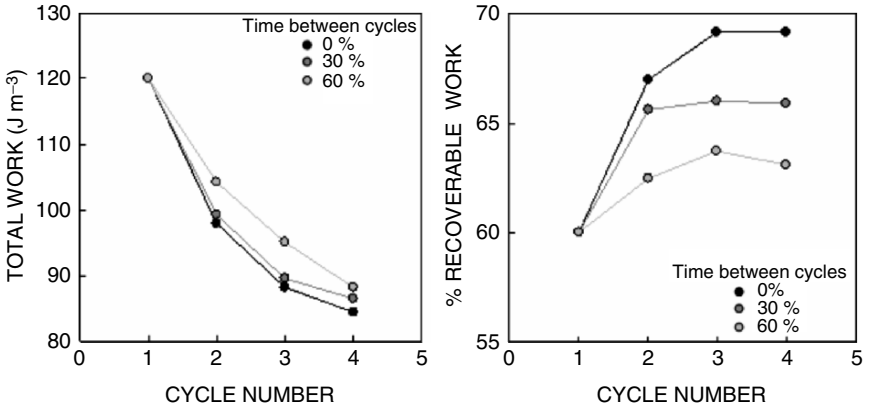

Figure 10.7. Degree of elasticity of marshmallows. From Kaletunc et al. (1992).

Apparently, because of the plasticized and relatively thick cell walls, buckling, let alone gross fracture and collapse, simply do not occur. But large deformation does affect the mechanical response of marshmallows. This becomes evident when they are subjected to repeated compression–decompression cycles. If their degree of elasticity can be assessed in terms of the relationship between the recoverable to total work (after reaching a given strain)—see Figure 10.6 (bottom)—then there is a clear loss of elasticity upon repeated deformation, as shown in Figure 10.7 (Kaletunc et al. 1991, 1992). The extent to which this loss of elasticity occurs is different in marshmallows of different brands, an observation supported by other measures obtained from stress relaxation tests (Kaletunc et al. 1992).

10.2.2.3 Popcorn

The force–displacement of stress–strain curves of puffed popcorn, compressed individually or in bulk, do not have a prominent shoulder (Nussinovitch et al. 1991). As in marshmallows, this can be explained by the plasticity and relative thickness of the cell walls. Support for this view comes from the comparison of their deformability pattern with that of synthetic "popcorn" (polystyrene), which is used for the cushioning of transported goods. The stress–strain curve of polystyrene foam particles not only shows evidence of at least a weak shoulder but it also indicates an overall stress level that is by far lower than that of natural popcorn, as shown in Figure 10.8. It ought to be remembered, though, that in both the natural and the synthetic products, the puffed particles morphology and orientation play an important role in shaping the force–displacement curve. This is regardless of whether they are tested individually or in bulk. Thus, although the cellular structure is still largely responsible for the cushioning properties of such particles, geometry is also an important factor.

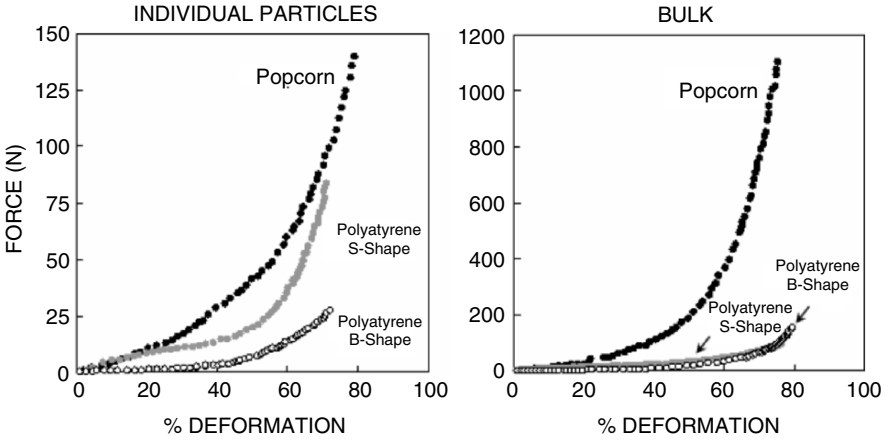

Figure 10.8. Comparison of the force–displacement curves of synthetic (polystyrene) and natural puffed popcorn, tested individually and in bulk. After Nussinovitch et al. (1991).

10.2.3 Layered Arrays

10.2.3.1 Arrays of Cellular Solids Only

A schematic view of a layered array of typical cellular solids is given in Figure 10.9 (left). When compressed uniaxially, the force in all the layers is the same and their deformations (displacements) are additive, as is also shown in the figure (right). Thus, the force–displacement curve of an array is constructed by adding the displacements of the individual layers that correspond to any given force. Since with few exceptions—such as the previously discussed marshmallows—the cross-sectional area of compressed solid foams does not expand to any significant extent, adjustment for the area is not needed here. It will be a factor to be reckoned with if one or more of the layers are incompressible or approximately incompressible; see below. The principle of equal force and added deformation pertains not only to arrays of cellular layers, each having a distinct structure and mechanical properties, but also to a single solid foam whose properties change gradually from top to bottom.

For an array of the kind depicted in Figure 10.9, the *stress* is assumed to be the same in all the layers, that is, $\sigma = \sigma_A = \sigma_B = \sigma_C = \ldots$ while the total *strain*, $\varepsilon_{\text{Total}}(\sigma)$, is constructed by adding the deformations, that is,

$$\varepsilon_{\text{Total}}(\sigma) = \frac{1}{h_{0\text{Total}}} \cdot \left[h_{0A}\varepsilon_A(\sigma) + h_{0B}\varepsilon_B(\sigma) + h_{0C}\,\varepsilon_C(\sigma) + \cdots\right] \tag{10.7}$$

where $h_{0\text{Total}}$ is the initial (combined) height (or thickness) of the array, that is, $h_{0\text{Total}} = h_{0A} + h_{0B} + h_{0C} + \cdots$, and $\varepsilon_A(\sigma)$, $\varepsilon_B(\sigma)$, $\varepsilon_C(\sigma)$, and so on, are *the strains* of the individual layers, which progressively change with the increasing stress.

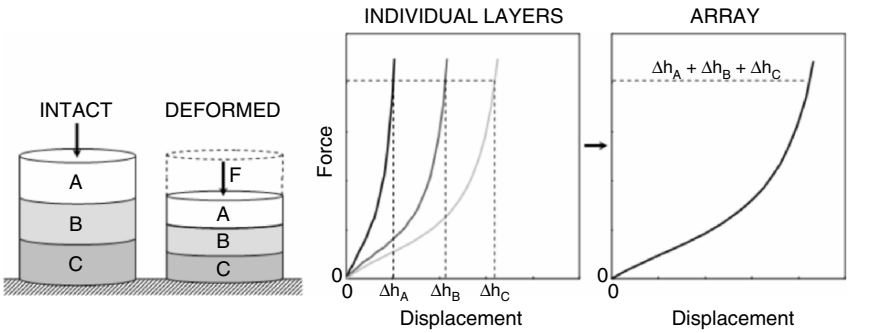

Figure 10.9. Schematic view of the construction of the force–displacement curve of a layered array of cellular (spongy) solids. Notice that the force in the layers is the same and that the deformations are additive.

The validity of this model and its ability to predict the deformability of layered baked foods and polymeric solid foams arrays have been demonstrated by Swyngedau et al. (1991), Swyngedau et al. (1991) and Swyngedau and Peleg (1992). When Hencky's strain is used to characterize the deformation, then (Peleg 1993a):

$$\varepsilon_{\mathrm{HTotal}}(\sigma) = \log_e h_{0\mathrm{total}} - \log_e \{h_{0A} \exp[-\varepsilon_{HA}(\sigma)]\} + h_{0B} \exp[-\varepsilon_{HB}(\sigma)] + h_{0C} \exp[-\varepsilon_{HC}(\sigma)] + \cdots\} \tag{10.8}$$

If the stress–strain relationships of all the individual layers can be described by Equations (10.4) or (10.5), the layered array's total strain can be calculated analytically (Swyngedau et al. 1991). Since the strain of the first layer can be expressed algebraically, that is,

$$\varepsilon_A(\sigma) = \frac{C_2\left(\dfrac{\sigma}{C_1}\right)^{\frac{1}{n}}}{1+\left(\dfrac{\sigma}{C_1}\right)^{\frac{1}{n}}} \tag{10.9}$$

or

$$\varepsilon_A(\sigma) = C_1[1-\exp(-C_2\sigma)]^{\frac{1}{n}} \tag{10.10}$$

and so all the other layers, the terms $\varepsilon_A(\sigma)$, $\varepsilon_B(\sigma)$, $\varepsilon_C(\sigma)$, … are all fully defined and can be inserted into Equations (10.7) or (10.8) with the corresponding layers' initial thickness (h_{0A}, h_{0B}, h_{0C}, etc.) These equations can then be used to construct the whole force–deformation or stress–strain relationships of the array. In cases where any or all the layers' deformabilities are characterized by Equations (10.2) or (10.3), the model can be solved numerically to produce the desired stress–strain relationships, again regardless of whether the layers have equal or different thickness.

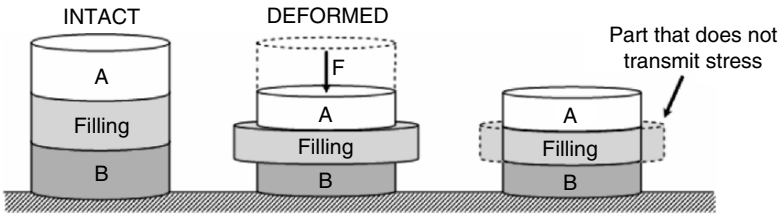

Figure 10.10. Schematic view of the compressibility of a mixed layered array of cellular (spongy) and a soft incompressible component.

10.2.3.2 Mixed Arrays

The described principle of equal force (stress) and added deformations (strains) equally applies to parallel layers of any kind, provided that their structure is isotropic. However, if any of the layers in the array is incompressible and softer than the rest, then it will expand laterally upon the force application. This is a familiar experience. When a sandwich or a layered cake is compressed, the filling sometimes leaks out from the sides, as shown schematically in Figure 10.10. For such a situation, Equations (10.7) or (10.8) will not be an appropriate model. However, because the cellular layers retain their cross-sectional area, and because the "free" part of the expanded filling does not transmit any stress (theoretically), the stress–strain relationship of the array can still be calculated by accounting for the exuded material.

The applicability of the method has been recently demonstrated by Barrett et al. (2005). They also showed that it can be used to monitor the moisture exchange between the filling and a model bread. In such a case, the *deviation from the model's predictions* will reveal that the mechanical properties of the layers have been altered. (The situation would be different, of course, if the liquid or semi-liquid filling was being absorbed into the neighboring cellular layers).

10.2.4 Tensile Properties of Cellular Solid Foods

Although never rigorously proven, the tensile or "tearing" strength of bread crumbs and most other soft cellular foods may be just as relevant to their perceived texture as their compressibility, if not more so. This is because the effort to tear the compacted structure is usually much bigger than that needed to cause the collapse of the open structure. (This does not mean that there is a universal relationship between the two and one ought to consider that the tearing, except for the initial bite into the food, might be of a compressed sponge already wetted by saliva). Regardless, the main technical problem with testing food sponges in tension is the grip. Preparation of a suitable specimen seems to be a lesser problem because a bread crumb or similar solid foam can be carved with an electric knife or punched out. A proper grip can be achieved by attaching an adhesive tape to the slightly compressed specimen's ends (Nussinovitch et al. 1990; Chen et al. 1994). When the tested specimen has a dog-bone shape, failure is almost guaranteed to occur in the middle rather than in the grip regions (which would have invalidated the test); see Figure 10.11.

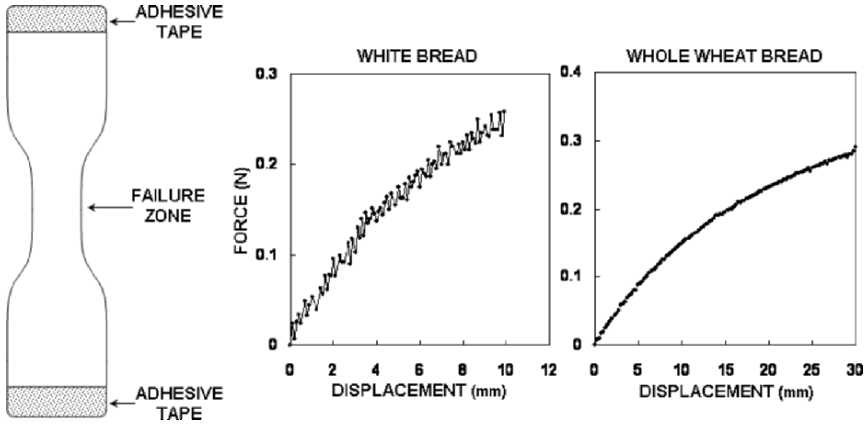

Figure 10.11. Schematic view of a bread crumb specimen ready for tensile testing and typical tensile force–deformation curves. Notice that the serrated curve is a record of successive tearing of cell walls.

The typical shapes of the tensile force–displacement curves of breads are also shown in Figure 10.11. They have a clear *downward concavity* caused by the simultaneous contraction of the cross-sectional area as the specimen stretches, and by that the same absolute deformation produces a progressively *decreasing strain* as the specimen is elongated. Since all the tests reported by Nussinovitch et al. (1990) and Chen et al. (1994) were performed at low deformation rates, viscoelastic effects most probably had not played a significant role. The reader should notice the serrated appearance of the white bread's force–displacement curves. The force oscillations are records of local failure events that preceded the gross failure of the specimen. Results of various breads testing indicated that neither the bread crumb's original density, nor its precompression, had a dramatic effect on the measured tensile strength (the tensile stress at failure) or on the ultimate strains that the specimen could sustain (Nussinovitch et al. 1990).

Moreover, the bread crumb's moisture loss during seven days of storage open to the air, also did not show a consistent dramatic effect on these two tensile parameters (Chen et al. 1994) as one would expect. The same can be said about the compression parameters, which too showed little correlation with the moisture loss, which was measurable, of course. These reported findings, if indeed representative of the three tested breads (white, Canadian and whole wheat), would suggest that the initial textural changes that accompany bread staling are quite subtle and hence cannot be always manifested in the described crude mechanical parameters. An alternative explanation is that the failure to find the expected trends was mainly due to the large scatter in the experimental results that masked the true trend, if it really existed.

10.3 Mechanical Characteristics of Brittle Cellular Foods

10.3.1 Interpretation of Jagged Compressive Force Displacement Curves

The most salient characteristic of brittle cellular foods, regardless of their composition and how they have been formed is that their force–displacement curves are irregular and irreproducible (Peleg 1997a). Examples are shown in Figure 10.12. Brittleness is the property of certain solids to fail or shatter after very small deformation. Glass is perhaps the most familiar brittle material. Brittleness and strength can be independent mechanical properties. A strong material like a candy drop is brittle while a soft cheese is not. Yet, some cellular foods are both brittle and fragile, that is, they break or shatter after being subjected to a low stress.

In the case of compressed cellular solid foods, brittleness causes fracture of cell wall material. Such a local fracture can propagate, triggering major failure, or remain a local event. The process can then repeat itself when more cell walls break down as the specimen is being further compressed. The successive failures of different magnitudes are manifested in corresponding force drops. The result is a force–displacement curve that has force oscillations of various amplitudes and frequencies. Cutting a brittle food like a puffed snack, a cereal particle or an instant coffee agglomerate can cause its disintegration. Therefore, it is better to test them intact. But since most such foods do not have parallel surfaces anywhere, meaningful calculation of stresses and strains is often impossible. The best one can do is to test specimens of more or less the same size and, if possible, in the same orientation. One can sometimes refer to the percent deformation, calculated by dividing the absolute displacement by the specimen's initial height, as a pseudo strain. But stresses are by far more difficult to calculate, even nominally, if the specimen's cross-sectional area is grossly nonuniform. The texture of brittle foods has been an active area of research and various methods to quantify their "crunchiness" or "crispiness" have been proposed; see Luyten et al. (2004), Vincent et al. (2002), Vincent (1998), Norton et al. (1998).

For what follows, consider the compressive force–deformation curve as a "mechanical signature." Now compare this signature of a brittle foam with any of those of the soft cellular foods discussed in the previous sections of this chapter. The obvious difference between the two is their degree of jaggedness. Quantifying a degree of jaggedness can be done in different ways (see Peleg 1997b and below). But before we address the various jaggedness measures, we should keep in mind that a jagged force–displacement curve has two elements:

a. A smooth "skeleton," which is a manifestation of the overall stiffness and toughness of the food in question. Obviously, there is a difference between a pretzel or crouton and a puffed cheese ball or a puffed breakfast cereal which has more to do with the effort to break them rather than with the brittleness that they all have; and
b. An irregular "noise" superimposed on the smooth "skeleton," whose amplitudes and frequencies are the record of the cascade of failure events that accompany the deformation.

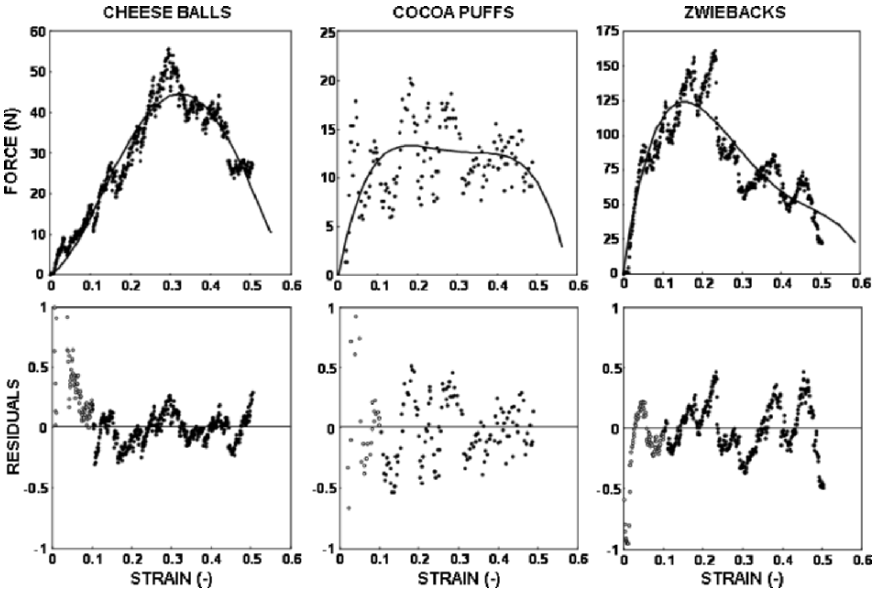

Figure 10.12. Typical compressive force–displacement curves of three brittle cellular foods fitted (smoothed) with a polynomial model. *Bottom*: The normalized signature composed of the residuals around the smoothed curve.

This is obviously an oversimplification of the deformation mechanism, which, as already explained, involves failure initiation and propagation. Nevertheless, this approach facilitates the extraction of useful information from irregular and irreproducible force–displacement curves that would otherwise be viewed as meaningless.

10.3.2 Jaggedness Assessment

An irregular signature's jaggedness can be assessed by using the complete record for the analysis. Alternatively, the record can be fitted with a polynomial or another model, a process called smoothing, followed by the analysis of the oscillations around the smooth curve separately. If the original record is in the form of $F(t)$ vs. t, and the fitted curve is $F^*(t)$ vs. t (see Figure 10.12), the normalized residuals (dimensionless), $y(t)$, will be calculated by:

$$y(t) = \frac{F(t) - F^*(t)}{F^*(t)} \tag{10.11}$$

Notice that $y(t)$ oscillates around the zero line as shown in the figure. Also, since at the beginning of the curve the force oscillations can be very large relative to the absolute magnitude of either the measured or fitted force, the division of the absolute residual $F(t) - F^*(t)$ by $F^*(t)$ can yield absurdly big numbers. Consequently this initial part of the normalized data, in our experience up to a displacement of about

10%, can be safely discarded. It is not representative of the textural properties and can be viewed as a mathematical artifact.

10.3.2.1 Statistical Measures of Jaggedness

A jaggedness index I_J can be formulated from the force oscillations' standard deviation, σ, which is not to be confused with the stress that has the same symbol, or the variance, σ^2. An example, see Tan et al. (1994), is:

$$I_J = 1 - \frac{1}{1+\sigma} \tag{10.12}$$

or

$$I_J = 1 - \frac{1}{1+\sigma^2} \tag{10.13}$$

When σ = 0 (smooth curve), I_J = 0 and when σ→ ∞, (extremely wide force fluctuations), $I_J \rightarrow 1$. This is a simple effective index. Its only drawback when applied to normalized records is its diminishing sensitivity as the standard deviation and variance become large.

A crude measure of jaggedness, promoted by the manufacturer of a popular mechanical testing instrument, is the force peaks counts. Probably, it is the simplest jaggedness measure, but it suffers from the uncertainty regarding what constitutes a true peak force (see section 10.3.2.4), and it does not discriminate between small and large force oscillations. The problem can be avoided by counting the force direction reversals of the signature (Corradini and Peleg 2006).

10.3.2.2 The Power Spectrum

An amplitude–time record can be converted into a power–frequency relationship by the Fourier transform. This conversion can be done almost instantaneously with modern software which employs the fast Fourier transform (FFT) algorithm. A jagged force–time record will have a Fourier transform "rich" in the high frequencies region. The curve's general shape will be primarily manifested in the low frequencies part, which can be filtered out. What remains provides a measure of the high frequencies' contribution, which is prominent in jagged signatures but almost nonexistent in smooth ones. (Recall that the raw information that a standard testing machine generates is in the form of voltage–time data that are converted into force–displacement relationship by taking into account the sensor's calibration and the crosshead's velocity. Thus, the reciprocals of the displacement are in fact representative of frequencies despite the fact that their units are length^{-1} and not time^{-1}.)

10.3.2.3 The Apparent Fractal Dimension

A smooth curve has a Euclidian dimension of a line, that is, D = 1. But imagine an extremely jagged curve so convoluted and dense that it almost occupies the whole plane on which it is drawn. We can say that the dimension of such a curve approaches the Euclidian dimension of a plane, that is, $D \rightarrow 2$. Curves having an intermediate

degree of jaggedness will have noninteger dimensions between 1.0 to 2.0. A curve or an object having a noninteger dimension is known as a fractal. Examples of such curves, generated with two different algorithms, are given in Figure 10.13. The figure demonstrates that the fractal dimension, D_F, is unaffected by the general shape of the curves and therefore can serve as a universal measure of a line's jaggedness. (The same is true for a surface's roughness, in which case D_F will be between 2.0 and 3.0.) However, for an object or signature to be truly fractal, that is, to have a noninteger dimension, it has to be self-similar. Self-similarity is manifested in that without the length scales being specified, the object's or curve's parts are indistinguishable from the whole (see figure).

In real physical objects, in contrast with purely mathematical creations, self-similarity can only exist over a limited range of length scales, but this is a technical rather than a conceptual limitation. A more serious difficulty arises in recorded mechanical or acoustic signatures, such as the force–displacement or sound intensity–time relationships of brittle cellular foods, where the force or sound intensity is logged

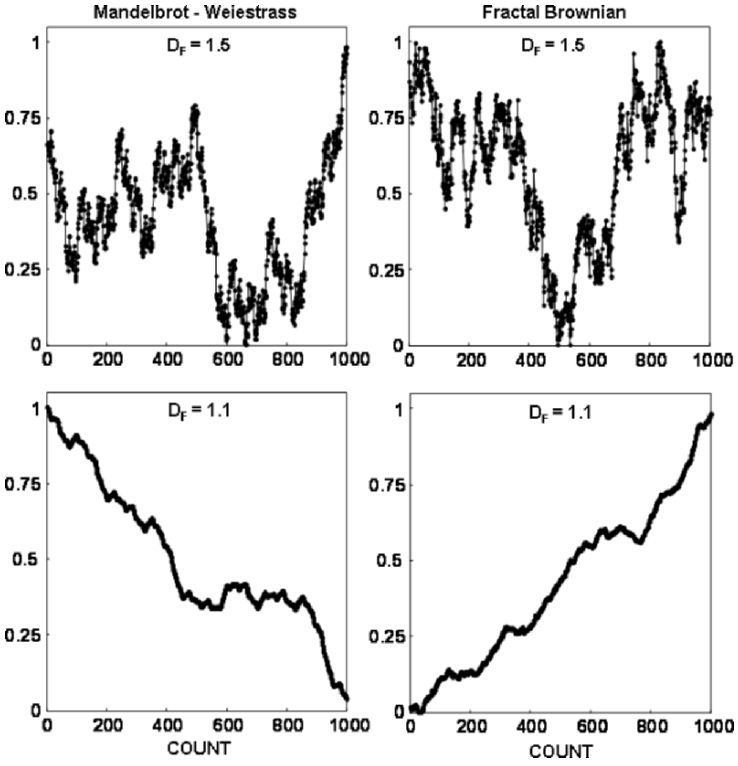

Figure 10.13. Jagged fractal curves generated with Russ's program (Russ, 1994). Notice that the degree of jaggedness is independent of the curve's general shape and the algorithm used for its generation.

at fixed time intervals. Such signatures, like the contour of a rugged mountain's chain, cannot have self-similarity in the *x*-axis direction and are hence called self-affine. Nevertheless, in the case of mechanical signatures, the two most often used methods to determine a fractal dimension of a jagged line, the Richardson plot and the Kolmogorov box-counting algorithm, can be used to determine their *apparent* fractal dimension. Moreover, either method is based on converting the data into a plot, whose slope is used to calculate the dimension and whose linearity indicates that the algorithm is appropriate.

In software like that offered by Russ (1994), this plot is produced automatically and is displayed together with the calculated dimension. When Russ's program is applied to the mechanical signatures of brittle cellular foods, other algorithms, more sensitive to the self-similarity requirement (such as Minkowski's or Korcak's) almost invariably produce a curved plot instead of a linear one, indicating that the calculated dimension is wrong or suspect (Borges and Peleg 1996). But even if the method to calculate the apparent fractal dimension works, it will still be advisable to verify the magnitude of the resulting apparent dimension by comparing it to the dimension calculated by another algorithm. For example, subjecting the force–displacement experimental data to both the Richardson and Kolmogorov analyses, or to another jaggedness measure, such as the one derived from the records' Fourier transform or the force oscillations statistical properties would strengthen any conclusion regarding the signature's degree of jaggedness.

10.3.2.4 The Role of the Sampling Rate and the Testing Machine's Resolution

The term *jaggedness* in the vernacular refers to a contour with sharp fluctuations. Yet the appearance of jaggedness can be attributed either to the fluctuations' amplitude, their frequency or both. Consequently, when the degree of jaggedness of a mechanical signature is expressed by a single number, regardless of the index used, its magnitude will depend simultaneously on the instrument's resolution and the chosen sampling rate. The former determines the smallest observable force oscillations and the latter, the highest frequency. Both, however, also depend on the testing machine's *time response*, which puts a physical limit to the signature's resolution. It can also affect the magnitude of the recorded forces, the rise and fall of which are in most cases very steep. Therefore, although the machine's software may allow the user to set the sampling rate at will, the result may be a distorted record, if the machine's and electronic system's response times are not taken into account. There are theoretical ways to estimate the true fractal dimension of a signature from data sets obtained at finite resolutions. Their practicality in routine testing, however, is highly questionable (Damrau et al. 1997; Peleg 1997b). Thus, when the jaggedness of different signatures is compared in terms of their apparent fractal dimension, an effort should be made so that they are obtained at the same resolution and sampling rate, and that they have a similar number of points for the comparison to be meaningful. The same applies to any jaggedness measure.

10.3.2.5 Reproducibility

The mechanical signatures of brittle cellular foods are not only jagged but also irreproducible, even when recorded under almost identical conditions. The irreproducibility is not an experimental artifact but *an inherent characteristic*, a manifestation of the haphazard nature of the failure mechanism. A minor crack or a particularly weak or thin cell wall can develop into a major structural failure expressed in a large force drop, but it does not have to. Consequently, and since the cellular structure is heterogeneous to start with, the actual failure pattern and the exact shape of the force–displacement curves are unpredictable *in principle*. However, if the tested specimens are of similar size, overall structure, composition and moisture contents, then their mechanical signature's *degree of jaggedness* can be remarkably reproducible. Although this is an empirical observation (see section 10.4) it is not totally unexpected. The *probability* that units having a similar structure and size will have a similar (but not identical) number of major and minor fracture events should be quite high. Thus, although each force–displacement relationship is unique, it still shares a certain general resemblance to other such relationships, even if not necessarily to all. And since the units of the same lot are expected to have a similar cell size and wall thickness distributions, the oscillations' frequencies and amplitudes are expected to have similar distributions too.

10.3.3 Stiffness and Toughness

Stiffness is the resistance of an object to deformation and is represented by a modulus (see section 10.2.1). The modulus is defined as stress per unit strain (which is dimensionless) and hence has stress units. Although even in the uniaxial compression of a homogeneous cylindrical or rectangular specimen the stresses distribution is far from being uniform, one can still use the *average stress*, the measured force divided by the specimen's cross-sectional area, for the modulus calculation.

Toughness, in materials science, is defined as the work (mechanical energy) that should be invested in order to reach a given strain, usually determined at and specified for the failure strain. It is represented by the area under the force–displacement curve, or the stress–strain curve, in which case the units are of work per unit volume, as already mentioned. All the above hardly applies if the force–displacement curve at hand is spiky or extremely jagged as is almost always the case with brittle cellular foods. The cross-sectional area, the strain and consequently the slope of the force–displacement curve are poorly defined, if at all, and so is the area under the curve. In such a case, the experimental or fitted force at a given deformation level, 15% or 25%, for example, can serve as a practical measure of the specimen's stiffness (e.g., Suwonsichon and Peleg 1997). Or alternatively, one can identify the heights of the increasingly larger peak forces, in which case a plot of their magnitude vs. the percent displacement would usually be a straight line, the slope of which will be a measure of the specimen's *minimal* stiffness (Peleg and Normand 1995); see Figure 10.14.

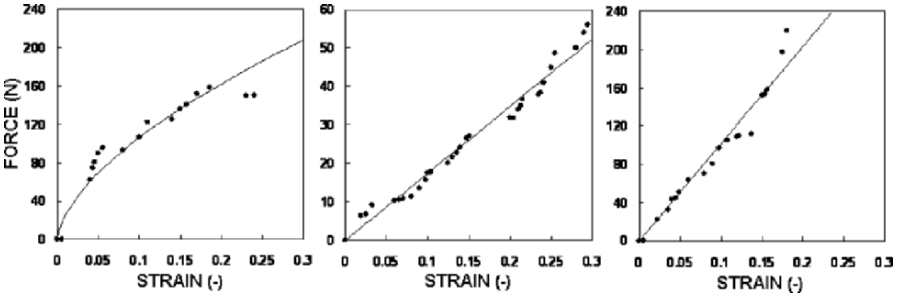

Figure 10.14. Assessing the stiffness of brittle cellular foods by connecting the increasing force peaks in their jagged force–displacement curves. After Peleg and Normand (1995).

All the above measures of stiffness are fairly reproducible (see below) despite the fact that the original data from which they are derived are not. The area under the original or fitted force–displacement curve can be a measure of the specimen's toughness as already stated. However, since there is a multitude of failures (in contrast with a single failure of most polymers and engineering materials), the percent deforation for the toughness determination must also be arbitrarily chosen. One can argue, though, that unless the force–displacement curves have very different shapes, the stiffness and toughness of specimens of the same food will rise and fall more or less in unison. In such a case, an increase or decrease of the specimen's stiffness will also be indicative of similar changes in its toughness.

10.3.3.1 Directionality

Puffed extrudates and other expanded foods can exhibit different mechanical properties if tested axially or transversally, that is, in the extrusion's direction or perpendicular to it. An example is shown in Figure 10.15. This is a manifestation of the oriented structure formed during the materials shear and expansion. Although the differences can be easily picked up by a testing machine, it is unclear whether they can also be perceived sensorily by humans.

10.3.3.2 Units Tested Individually and in Bulk

Most cellular solid foods (breakfast cereals and agglomerated or freeze dried instant coffee included) come in units that are large enough to be tested individually with machines that have a good crosshead speed and positioning control. Thus, if tested slowly enough, a sufficiently detailed force displacement curve can be obtained. Yet, in some cases it would be more convenient to test the particles in bulk, especially when the unit's size is extremely variable and so is their shape (see, e.g., Nuebel and Peleg 1993, and González-Martínez et al. 2003).

The relationship between the mechanical properties of individual cellular food particles and their assembly has been addressed in several publications from our

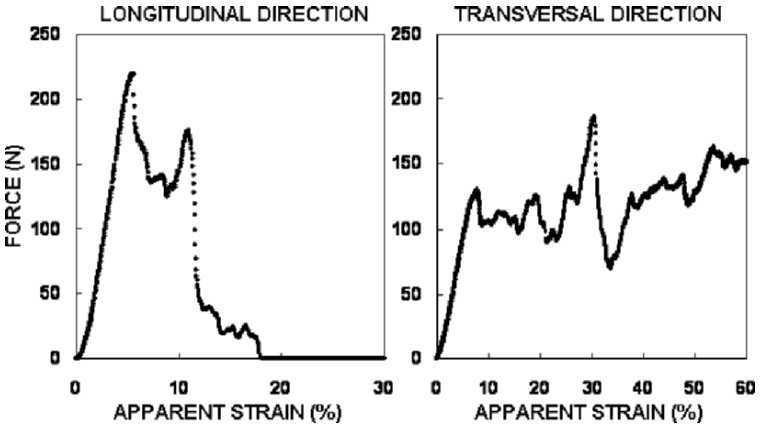

Figure 10.15. The expression of anisotropy in puffed extruded cellular solids. Notice the qualitative as well as the quantitative difference in the force–displacement curves when determined in the longitudinal and transversal directions.

laboratory (Nuebel and Peleg 1993; Nixon et al. 1994; Ulbricht et al. 1994; Ulbricht et al. 1995; Nixon and Peleg 1995; Suwonsichon and Peleg 1998; Gerhards et al. 1998). It has been demonstrated that, at least in the case of round puffed cereals particles, it is possible to reproduce the force–displacement curves of the individual particles from those of their assemblies.

When a single layer of such particles all have a similar size, a condition largely satisfied when it comes to commercial products, then the force of the assembly is simply the sum of the forces exerted by the individual particles. Consequently, the array's particles stiffness can be assessed by dividing the measured force by the number of particles. The latter is proportional to the cross-sectional area of the container in which the particles are held. Hence when particulates are tested in a container, the total force is expected to be proportional to the container's diameter squared. The jaggedness of the force–displacement curve of brittle particles, when compressed as a layer or in bulk, is always considerably smaller than that of a single particle. The reason is that local peak forces would most likely be offset by local minima and vice versa. The result would be a jagged record but with a *smaller* oscillations amplitude. If the "noise" in the force–displacement curve of the individual particles is or can be considered as random, the amplitude suppression would be proportional to the *square root* of the number of particles. Thus, one can estimate the force–displacement curve of an individual particle by dividing the layer's smoothed force readings by the number of particles and amplifying the noise around it by the square root of this number. As shown by Ulbricht et al. (1995), the principle can also be used to create averaged or typical signatures of puffed snacks and cereals, zwiebacks and the like; see Figures 10.16 and 10.17.

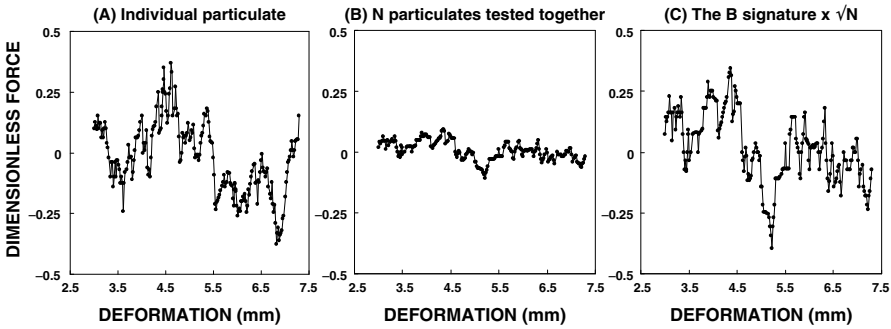

Figure 10.16. Demonstration of the averaging effect when brittle particulates are tested together. Notice that signatures *A* and *C* have the same degree of jaggedness. After Ulbricht et al. (1995).

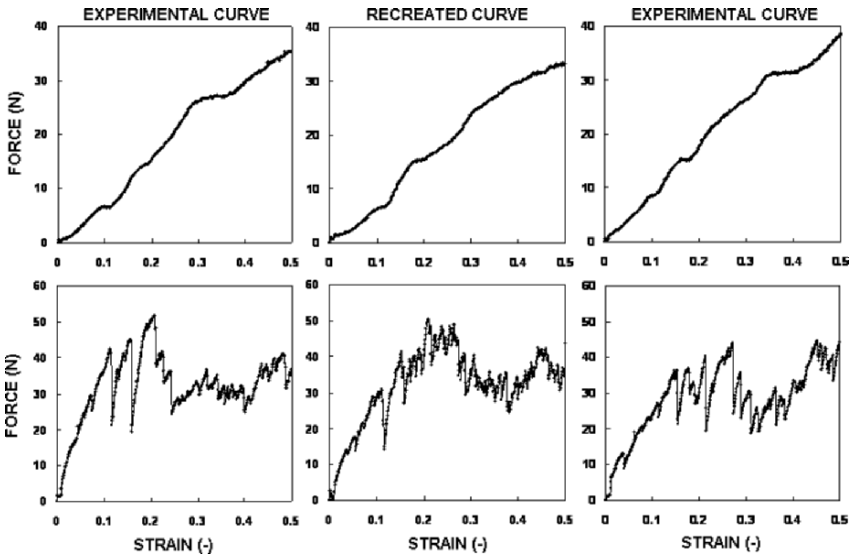

Figure 10.17. Typical smooth (*top*) and jagged (*bottom*) force–displacement curves created by averaging the forces of five curves and adding their oscillations multiple by √5. Notice that the recreated ("typical") curve is indistinguishable from the experimental ones. From Ulbricht et al. (1995).

If the particulates are compressed as a bed of significant depth, then it is still possible to estimate the properties of a single particulate. This requires a series of tests performed on beds of different width and height, which makes it an unattractive option for most particulated cellular foods. However, particulates that always have nonuniform size and shape, such as pork rind (*chicharrón*) (González-Martínez et al. 2003), and corn flakes for that matter (Nixon and Peleg 1995), are notable exceptions. It is much more convenient to test them as an assembly rather than individually.

10.4 Effect of Moisture

Moisture, absorbed or lost, invariably affects the mechanical properties of the cell walls material and consequently the texture of cellular solid foods. The plasticization or hardening of solid foods has been attributed to their *glass transition* through lowering or elevating their *glass transition temperature*, or T_g. Hence, a food that is glassy at a given moisture content will become rubbery when it absorbs more moisture by being above its T_g at the same temperature. Similarly, a rubbery food will become glassy, and therefore brittle, upon losing moisture, which will move it to below its T_g.

The concept of a glass transition temperature, or T_g, was originally proposed in order to characterize the softening or hardening of noncrystalline materials such as classic glasses (e.g., window glass) and synthetic polymers in what is known to be a second-order phase transition. In contrast with a first-order transition such as melting or boiling of a pure substance, the changes take place not at a point but over a temperature range that can be shifted by changing the heating or cooling rate. Also, over the temperature range of the transition, the mechanical properties of the polymeric material need not change in unison. Consequently, different calorimetric and mechanical methods to determine the glass transition temperature, or T_g, yield values that can differ by *tens of degrees Celsius*, sometimes by over a hundred degrees; see Syler (1994) and Donth (2001). At ambient temperature, most solid food materials, cellular included, are in or very close to the transition region. Thus, if the concept that being a few degrees above or below the T_g has a dramatic effect on a food's properties (especially mechanical) is accepted, then one could influence a food's physical stability by choosing the method to determine its T_g...

Moisture, no doubt, is an effective plasticizer. However, its exact effect on the mechanical properties of cellular solid foods, with the possible exception of the class of soluble low molecular materials (see below), cannot be predicted on the basis of their T_g even if there were an acceptable way to determine it. This is primarily because whenever the cell wall solid is mainly made of a high molecular weight polymer, such as starch and/or protein, moisture can affect its various mechanical properties differently and in a manner that must be determined experimentally.

10.4.1 Low Molecular Weight Matrices

Consider dry agglomerated or freeze dried coffee particles of approximately the same size. They have a considerable porosity and, as shown in Figure 10.18 (top), very jagged compressive force–displacement curves when dry. They are also rather stiff, as the level of the forces they can sustain indicates, but they are still fragile and crumbly. Their crumbliness is primarily due to failure propagation in various directions. The process produces daughter particles of various sizes, which themselves can subsequently disintegrate and produce even smaller particles. It is this failure at different levels that is responsible for the fractal appearance of the force–displacement curve; see the figure. Because of their moisture sorption pattern, instant coffees remain practically unchanged when their water activity is below about 0.5. At that point, they practically dissolve, in which case there is a *simultaneous* loss of brittleness and stiffness as shown in Figure 10.18 (bottom).

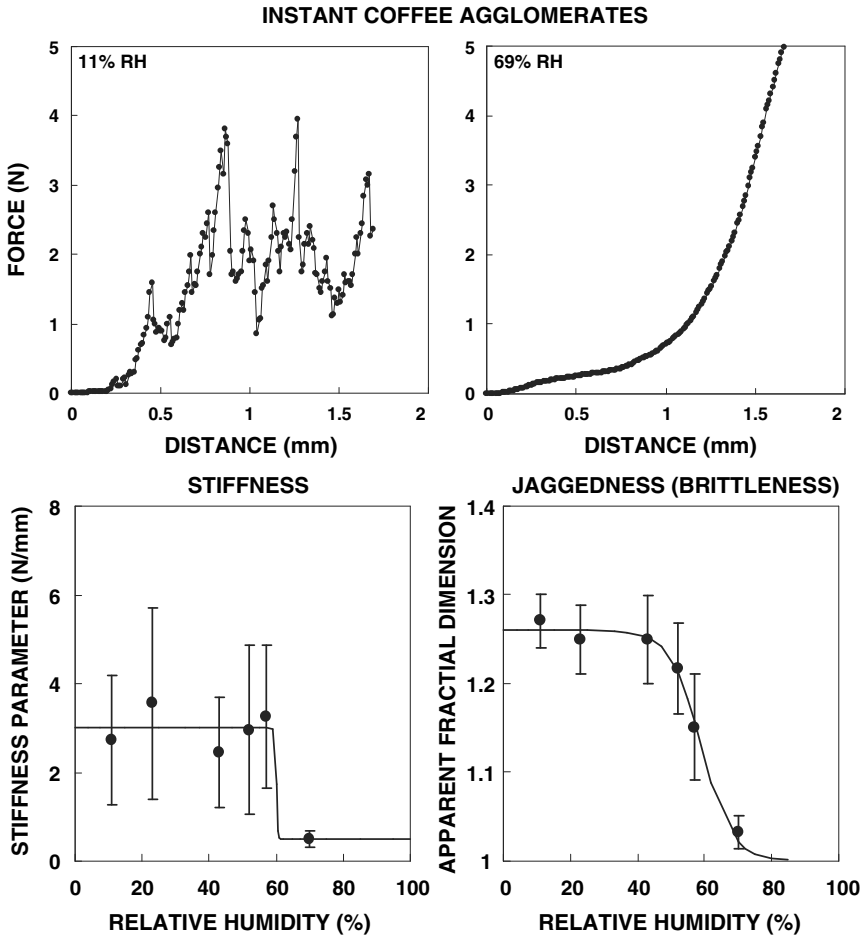

Figure 10.18. *Top*: Typical force–displacement curves of agglomerated instant coffee when dry and after moisture sorption. *Bottom*: The effect of water activity on the stiffness and brittleness of agglomerated instant coffee. Notice the sharp drop of both at about the same water activity. From Gerhard et al. (1998).

Such a dramatic change in both properties is clearly evident despite the large scatter in both the jaggedness and stiffness measures. Both indicate the occurrence of a sharp transition at almost the same water activity. (The shown large scatter in the mechanical tests results was inevitable because the agglomerates were tested intact. Although they had been gently sieved to obtain a uniform size, their shape was not the same. Therefore, much of the scatter can be attributed to the variability

in their morphology rather than to any substantial difference in their solid's mechanical properties). A similar moisture effect can be expected in other particulates largely composed of soluble low molecular weight compounds. Examples are instant (agglomerated) milk and dry beverages. Their sugars are in a crystalline form and hence have a critical moisture above which they readily dissolve.

10.4.2 Cereals and Snacks

The cell wall material of puffed cereals and snacks is largely starch or protein but it can also contain a considerable amount of sugar or salt as well as other materials, usually at a much lower concentration. When the solid matrix is primarily a biopolymer (starch and/or protein), the effect of moisture on their properties can be somewhat different from that exerted on soluble solids of lower molecular weight. The main difference, as has already been stated, is that their plasticization, that is, the transition from brittleness to ductility, takes place over a considerable range of moisture contents or water activities; (e.g., Attenburrow and Davies 1993; Roos 1995; Martínez-Navarrete et al. 2004; Lewicki 2004; Aguilera 2006), as shown in Figures 10.19-10.20. These figures demonstrate that regardless of whether the matrix is primarily starch–sugar (Cocoa Puffs®) or protein–salt (pork rinds), the transition has a considerable span. Thus, the concept that the material just crosses its T_g line is certainly inappropriate in this case. Any attempt to identify the beginning or middle of the drop as the crossover point will also be futile. It will tell nothing about the transition span, which can vary considerably among cereals and snacks. One must conclude, therefore, that any model of the brittleness loss in cereals and snacks must account for both the moisture or water activity level around which it occurs and the range over which the transition takes place. Or, stated differently, the brittleness loss at the transition region must be characterized by at least two parameters, one to identify the transition's location and the other its steepness or broadness. (For more on this point see Peleg (1993), for example.)

10.4.2.1 Moisture Toughening

A peculiar phenomenon quite common in cellular foods can be called *moisture toughening* (Harris and Peleg 1996; Wollny and Peleg 1994). Water, as everyone knows and as already has been repeatedly stated, is a perfect plasticizer. Therefore, intuitively, one would expect that upon moisture sorption, the loss of brittleness (monitored in terms of the apparent fractal dimension, for example, or any other measure of jaggedness) will be accompanied by a corresponding loss of stiffness and toughness. After all, a completely plasticized or soggy food has hardly any stiffness or toughness at all. Yet, as shown in Figures 10.19 and 10.22, this is not necessarily the case. At moderate levels of moisture absorption the particles' stiffness actually *increases*. Consequently, their toughness as represented by the area under the force–displacement curves (see Figure 10.21) also increases.

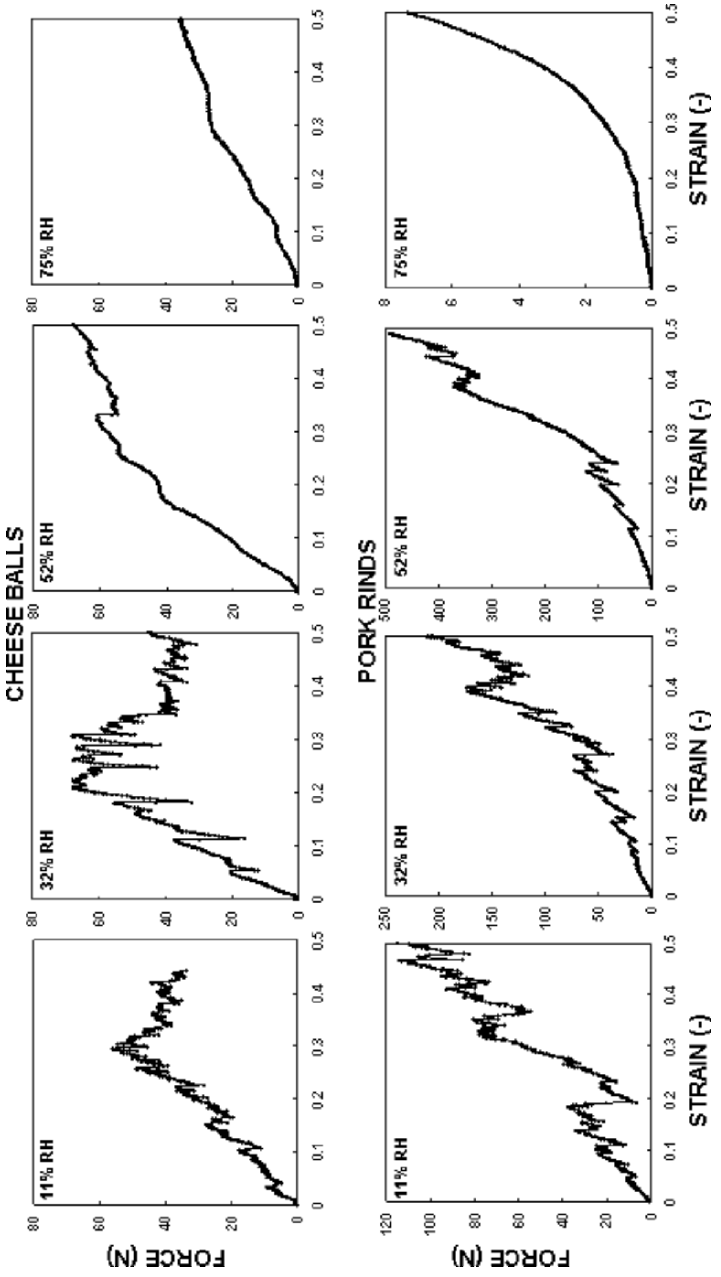

Figure 10.19. The effect of moisture on the force-displacement curves of two puffed snacks. Notice the jaggedness loss in the wet particles force-displacement curves and that they can be higher than those of the dry ones.

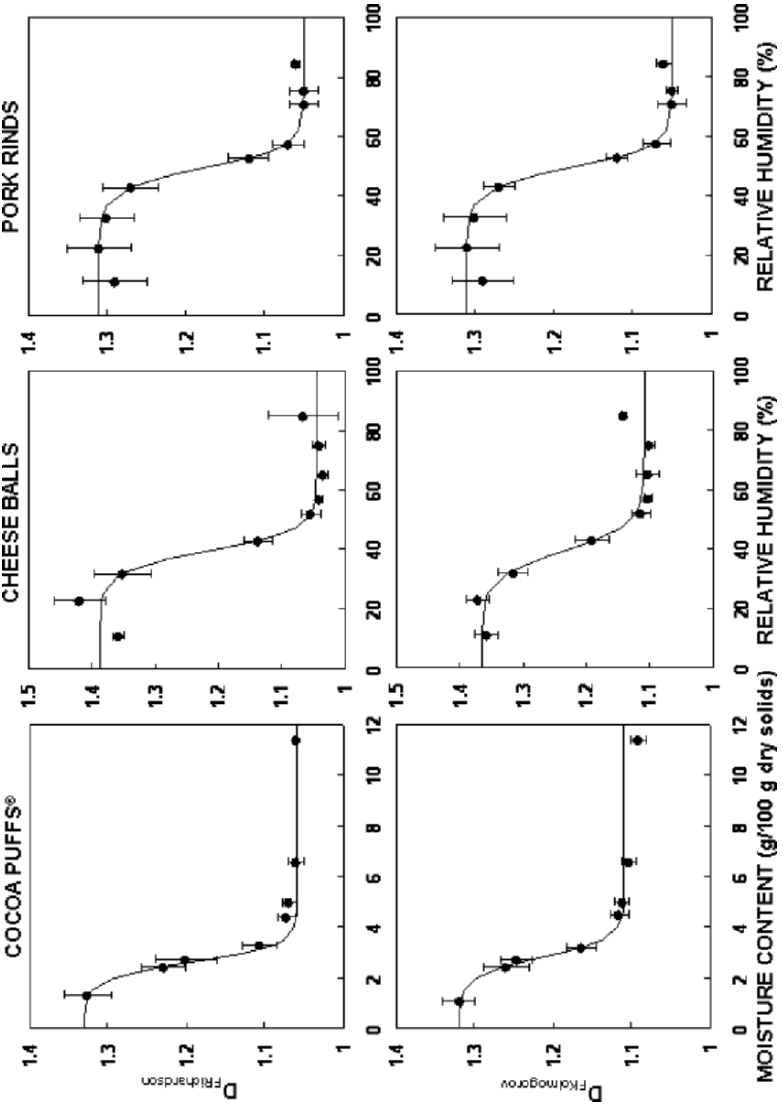

Figure 10.20. The effect of moisture on the brittleness of three snacks. Notice the fit of the Fermi model and that the drop had a considerable span.

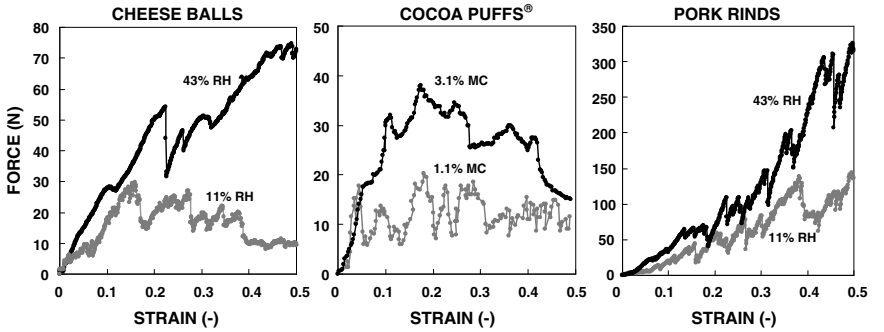

Figure 10.21. Moisture toughening in three snacks. Notice that the moderate moisture sorption can increase a snack's stiffness (and toughness, represented by the area under the force–displacement curve) by inhibiting the ability of the fracture to propagate. From Suwonsichon and Peleg (1998) and González-Martínez et al. (2003).

Moisture toughening has also been observed in other brittle foods (e.g., Attenburrow et al. 1989) and even in gluten films plasticized by water (Nicholls et al. 1995). Such observations cannot be predicted from the standard glass transition theories, according to which plasticization by crossing the T_g line should be manifested in a total textural collapse of the specimen. The phenomenon has a simple explanation. The partial plasticization of the solid matrix material, that is, its loss of brittleness, inhibits the ability of failure to propagate (Suwonsichon and Peleg 1998; Aguilera 2006). Consequently, the cellular structure, by retaining some of its integrity, can continue to resist the imposed deformation, which is manifested in the continued force increase. But once the *plasticization* reaches a certain level, ductility sets in and the semi-liquid cell walls can no longer offer any significant mechanical resistance. At this stage, the specimen's stiffness diminishes, and it may disappear altogether when the solid is fully plasticized.

10.4.2.2 Sensory Perception

The qualitative different effects of moisture absorption on the brittleness and stiffness of cereals and snacks may not be an academic matter. The difference can be perceived sensorily by humans as demonstrated in Figure 10.23. This means that the brittleness loss (perceived as a loss in crunchiness/crispiness) and the stiffness and toughness rise (perceived as an increase in hardness) can be sensed *simultaneously*, which may be of interest to those engaged in food products formulation. Because the sensation of crunchiness/crispiness is associated with acoustics, it can be added that the effect of moisture contents on the richness of the acoustic signal follows a very similar pattern to that of the mechanical signatures jaggedness (Figure 10.20) and of the sensory crunchiness/crispiness ratings (Figure 10.23).

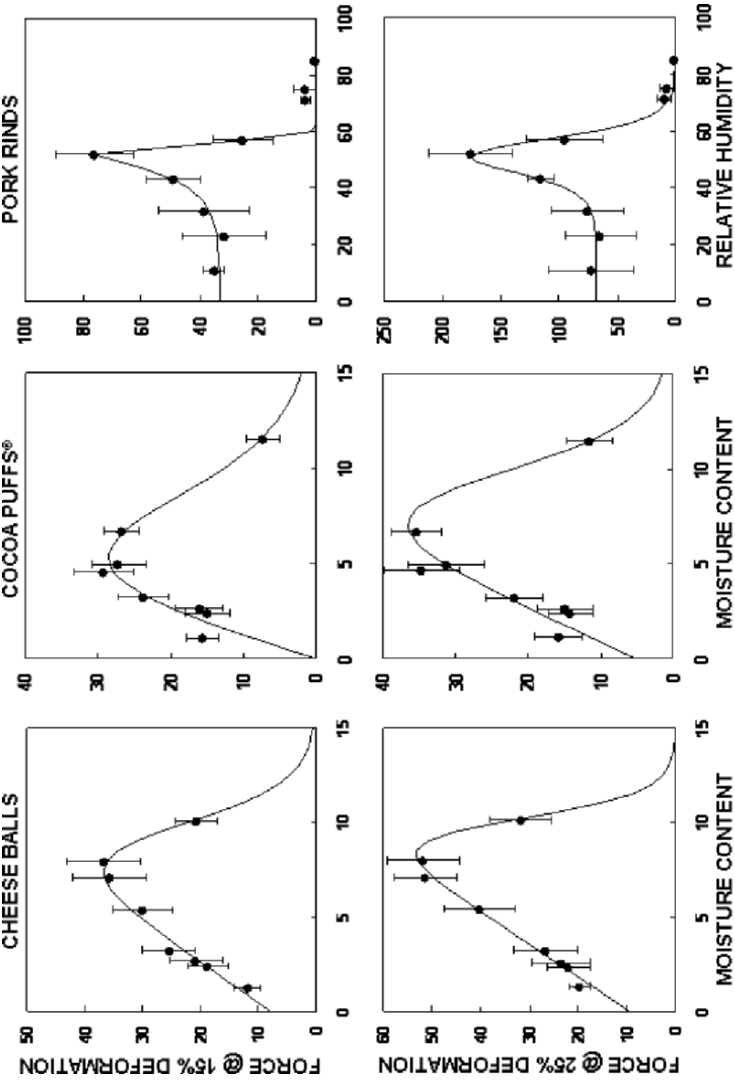

Figure 10.22. The effect of moisture on the stiffness of three snacks. From Suwonsichon and Peleg (1998) and González-Martínez et al. (2003).

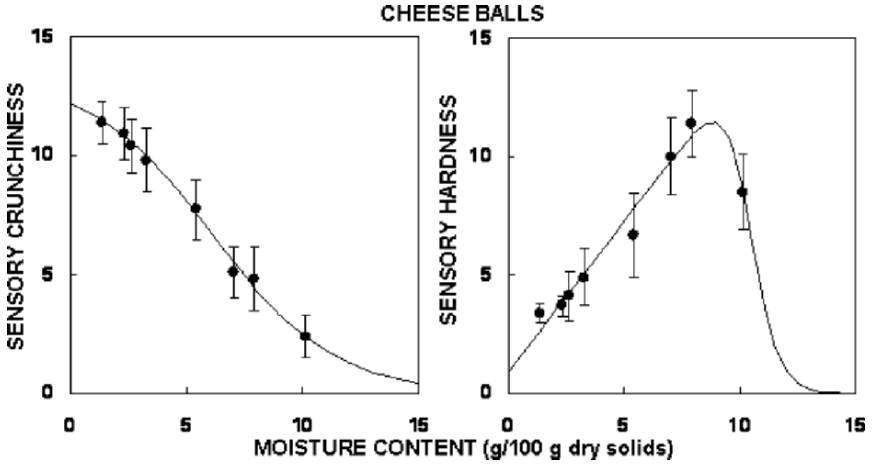

Figure 10.23. The effect of moisture on the perceived crunchiness and hardness rating of a puffed snack. Notice that the loss of brittleness and moisture toughening can be sensed simultaneously not only by machines (Figures 10.19–10.22) but also by humans.

This suggests that the same failure–fracture events that are responsible for the irregular force oscillations are also responsible for the sound emissions. If the richness of the mechanical and acoustic signatures is governed by similar rules, that is, those of several units compressed together are less jagged than that of one unit, then the perception of crunchiness or crispiness may be effected, to at least some extent, by the size and number of units consumed at the same time. However, a more systematic study will be required to establish that this indeed happens. The hypothesis that the jaggedness of the mechanical signature is associated with the sensory perception of crunchiness (or crispiness) has been demonstrated in the match of the apparent fractal dimension versus moisture relationship and that between the corresponding perceived crunchiness ratings (Suwonsichon and Peleg 1998). Nevertheless, the sensory scores indicated a significantly broader transition than that found instrumentally. This was probably a reflection of the lesser sensitivity of humans when it comes to the edges of the brittleness range. The issue of sensitivity to textural attributes needs more in-depth study, as has been pointed out elsewhere (Peleg 2006).

10.5 Concluding Remarks

The mechanics of a cellular solid is an excellent example of the role that *geometry* and *morphology* can play in the properties of materials. Buckling, for example, is a characteristic of all thin solid objects. Thus, the mechanical properties of cellular foods can be affected to a large extent not only by their composition and thermal history but also by their matrix's structural features. Understanding and eventually control of the texture of cellular solid food products requires knowledge not only of what affects the cell walls strength and flexibility but also of how the cells are organized in space.

Ashby's theoretical studies of the mechanical behavior of cellular solids, and those of his followers as well, serve as most useful guidelines. But one should always keep in mind that cellular foods do not have cells of uniform size and geometry. Closed and open cells can coexist at different ratios and the former can sometimes burst open upon compression, as has been demonstrated in breads. In the future, nondestructive imaging methods to determine 3-D structures will probably provide information that will clarify the relationship between the cellular architecture, the cells properties and texture.

In the past, many or perhaps most publications on cellular solids in the nonfood literature were the result of interest in their performance at relatively small deformations (strains). In contrast, during their mastication, foods are subjected to very large compressive strains and are then torn apart. Moreover, in engineering and biomechanics applications, the solid foam is expected to be rather inert. Or, if it does interact with the environment, this would be a slow process that takes place on a time scale of months or years. In contrast, cellular foods interact with moisture very rapidly and the resulting changes can be quite unique, depending on the amount of water soluble components in their cell walls.

A change in composition or a commercial food product's formulation is most likely to affect its cellular structure, especially if formed by extrusion or puffing. Thus, studying the effect of structure or composition in isolation may not be an easy task. However, there are ways to investigate their effects. For example, freezing at different rates usually produces ice crystals of different sizes, which upon dehydration can produce foams with almost identical composition but different cellular structure. Freeze-dried model foams, based on food gums with and without additives can be used to study the effect of the cell wall material in foams that have a similar structure (see, e.g., Nussinovitch et al. 2000, 2001). Whether this kind of study will generate wide interest, however, is uncertain.

The moisture and most probably temperature effects on cellular solid foods can have a large impact on several food producers, from the manufacturers of puffed cereals and snacks to the producers of instant coffee and agglomerated dry beverages. They also influence these products' fate once reaching the consumer. It appears though that the prevalent theories to explain the temperature or moisture effects on mechanical properties, originally developed for synthetic polymers and adapted for foods, notably those of glass transition, need a modification for successful application to cellular food products. Thus, how to combine the roles of second-order transitions and cellular solids mechanics might be an interesting area in food texture research. The results of such studies, no doubt, will have many practical implications in several food industries and probably in other industries as well.

Acknowledgements. Contribution of the Massachusetts Agricultural Experimental Station at Amherst. The authors thank Professor José Miguel Aguilera for many useful comments and suggestions.

10.6 References

Aguilera, J.M., and Stanley, D.W. (1999). *Microstructural Principles of Food Processing and Engineering*, 2nd ed. Aspen Publishers, Gaithersburg, MD, p. 432.

Aguilera, J.M. (2006). Structure–property relationships in low-moisture products. In M.P. Buera, J. Welti-Chanes, P. Lillford, and H. Corti (eds.), *Water Properties of Food Pharmaceutical and Biological Materials*. CRC/Taylor and Francis, Boca Raton, FL, pp. 126–127.

Ashby, M.F. (1983). The mechanical properties of cellular solids. *Metall. Trans. A*, 14, 1755–1769.

Attenburrow, G.E., Goodband, R.M., Taylor, L.J., and Lillford, P.J. (1989). Structure, mechanisms and texture of a food sponge. *J. Cereal Sci*., 9, 61–70.

Attenburrow, G., and Davies, A.P. (1993). The mechanical properties of cereal based foods in and around the glassy state. In J.M.V. Blanshard and P.J. Lillford (eds.), *The Glassy State in Foods*. Nottingham University Press, Loughborough, UK.

Barrett, A., Cardelo, A., Maguire, P., and Peleg, M. (2005). Moisture distribution and textural changes in stored model sandwiches. *J. Texture Stud*., 36, 569–589.

Borges, A., and Peleg, M. (1996). Determination of the apparent fractal dimension of the force–displacement curves of brittle snacks by four different algorithms. *J. Texture Stud*., 27, 243–255.

Campbell, G.M., and Mougeot, E. (1999). Creation and characterization of aerated food products. *Trends Food Sci. Tech*., 19, 283–296.

Chen, P., Whitney, L.F., and Peleg, M. (1994). Some tensile characteristics of bread crumb. *J. Texture Stud*., 25, 299–310.

Corradini, M.G., and Peleg, M. (2006). Direction reversals in the mechanical signature of cellular snacks: a measure of brittleness? *J. Texture Stud*., 37, 538–552.

Damrau, E., Normand, M.D., and Peleg, M. (1997). Effect of resolution on the apparent fractal dimension of jagged force–displacement relationships and other irregular signatures. *J. Food Eng.*, 31, 171–184.

Donth, E. (2001). *The Glass Transition: Relaxation Dynamics of Liquids and Disordered Materials*. Springer, New York.

Gerhards, C., Ulbricht, D., and Peleg, M. (1998). Mechanical characterization of individual instant coffee agglomerates. *J. Food Sci*., 63, 140–142.

Gibson, L.J., and Ashby, M.F. (1997). *Cellular Solids: Structure and Properties*. Cambridge University Press, Cambridge, MA.

González Martínez, C., Corradini, M.G., and Peleg, M. (2003). Effect of moisture on the mechanical properties of pork rind ("chicharrón"). *Food Sci. Technol. Int*., 9, 249–255.

Harris, M., and Peleg M. (1996). Patterns of textural changes in brittle cellular cereal foods caused by moisture sorption. *Cereal Chem*., 73, 225–231.

Kaletunc, G., Normand, M.D., Nussinovitch, A., and Peleg, M. (1991). Determination of elasticity of gels by successive compression–decompression cycles. *Food Hydrocolloids*., 5, 237–247.

Kaletunc, G., Normand, M.D., Johnson, E.A., and Peleg, M. (1991). Degree of elasticity determination in solid foods. *J. Food Sci*., 56, 950–953.

Kaletunc, G., Normand, M.D., Johnson, E.A., and Peleg, M. (1992). Instrumental determination of elasticity of marshmallow. *J. Texture Stud*., 23, 47–56.

Lewicki, P.P. (2004). Water as the determinant of food engineering properties: a review. *J. Food Eng.*, 61, 483–495.

Luyten, H., Plijter, J.J., and van Vliet, T. (2004), Crispy/crunchy crusts of cellular solid foods: a literature review with discussion. *J. Texture Stud*., 35, 445–492.

Martínez-Navarrete, N., Moraga, G., Talens, P., and Chiralt, A. (2004). Water sorption and the plasticization effect in wafers. *Int. J. Food Sci. Tech*., 39, 555–562.

Nicholls R.J., Appelquist J.A.M., Davies A.P., Ingman S.J., and Lillford P.J. (1995). Glass transition and the fracture behaviour of gluten and starches within glassy state. *J. Cereal Sci*., 21, 25–36.

Nixon, R., Ulbricht, D., Nuebel, C., Wollny, N., Normand, M.D., and Peleg, M. (1994). Mechanical characteristics of brittle crumbly particulates tested individually and in bulk. *Particle Technology Forum. Vol. 3*. American Institute of Chemical Engineers, New York. pp. 50–57.

Nixon, R., and Peleg, M. (1995). Effect of sample volume on the compressive force–deformation curves of corn flakes tested in bulk. *J. Texture Stud*., 26, 59–69.

Norton, C.R.T., Mitchell, J.R., and Blanshard, J.M.V. (1998). Fractal determination of crisp and crackly textures. *J. Texture Stud*., 29, 239–253.

Nuebel, C., and Peleg, M. (1993). Compressive stress–strain relationships of two puffed cereals in bulk. *J. Food Sci*., 58, 1356–1360, 1374.

Nussinovitch, A., Roy, I., and Peleg, M. (1990). Testing bread slices in tension. *Cereal Chem.* 61, 101–103.

Nussinovitch, A., Cohen, G., and Peleg, M. (1991). Comparison of the compressive characteristics of puffed popcorn and polystyrene foam particles. *J. Cell. Plast*., 27, 527–539.

Nussinovitch, A., Corradini, M.G., Normand, M.D., and Peleg, M. (2000). Effect of sucrose on the mechanical and acoustic properties of freeze-dried agar, kappa-carrageenan and gellan gels. *J. Texture Stud*., 31, 205–223.

Nussinovitch, A., Corradini, M.G., Normand, M.D., and Peleg, M. (2001). Effect of starch, sucrose and their combinations on the mechanical and acoustic properties of freeze-dried alginate gels. *Food Res. Int.*, 34, 871–874.

Peleg, M., Roy, I., Campanella, O.H., and Normand, M.D. (1989). Mathematical characterization of the compressive stress–strain relationships of spongy baked goods. *J. Food Sci.*, 54, 947–949.

Peleg, M. (1993a). Calculation of the compressive stress–strain relationships of layered arrays of cellular solids using equation solving computer software. *J. Cell. Plast*., 29, 285–293.

Peleg, M. (1993b). Mapping the stiffness–temperature–moisture relationship of solid biomaterials at and around their glass transition. *Rheol. Acta*, 32, 575–580.

Peleg, M., and Normand, M.D. (1995). Stiffness assessment from jagged force–deformation relationships. *J. Texture Stud*., 26, 353–370.

Peleg, M. (1997a). Mechanical properties of dry cellular solid foods. *Food Sci Technol. Int*., 3, 227–240.

Peleg, M. (1997b). Line jaggedness measures and their applications in textural evaluation of foods. *CRC Crit. Rev. Food Sci*., 37, 491–518.

Peleg, M. (2006). On fundamental issues in texture evaluation and texturization. *Food Hydrocolloids.*, 20, 405–414.

Roos, Y.H. (1995). *Phase Transitions in Foods*. Academic Press, San Diego, CA.

Russ, J.C. (1994). *Fractal Surfaces*. Plenum Press, New York.

Suwonsichon, T., Normand, M.D., and Peleg, M. (1997). Estimation of the mechanical properties of individual brittle particles from their bulk's compressibility. *J. Texture Stud.*, 28, 673–686.

Suwonsichon, T., and Peleg, M. (1998). Instrumental and sensory detection of simultaneous brittleness loss and moisture toughening in three puffed cereal products. *J. Texture Stud.*, 29, 255–274.

Swyngedau, S., Nussinovitch, A., Roy, I., Peleg, M., and Huang, V. (1991). Comparison of four models for the compressibility of breads and plastic foams. *J. Food Sci*., 56, 756–759.

Swyngedau, S., Nussinovitch, A., and Peleg, M. (1991). Models for the compressibility of layered polymeric sponges. *Polymer Eng. Sci*., 31, 140–144.

Swyngedau, S., and Peleg, M. (1992). Characterization and prediction of the stress–strain relationship of layered arrays of spongy baked goods. *Cereal Chem*., 69, 217–221.

Syler, R.G. (1994). *Assignment of the Glass Transition*. ASTM STP 1249. American Society of Testing Materials, Philadelphia, PA.

Tan, J., Gao, X., and Hsieh, F. (1994). Extrudate characterization by image processing. *J. Food Sci.*, 59, 1247–1250.

Ulbricht, D., Normand, M.D, Peleg, M., and Horowitz, J. (1994). Assessment of the crumbliness of individual fragile particulates from that of their assemblies. *Powder Technol.*, 81, 83–91.

Ulbricht, D., Normand, M.D., and Peleg, M. (1995). Creating typical jagged force–deformation relationships from the irregular and irreproducible compression data of crunchy foods. *J. Sci. Food Agri.*, 67, 453–459.

Vincent, J.F.V. (1998). The quantification of crispness. *J. Sci. Food Agri*., 78, 162–168.

Vincent, J.F.V., Saunders, D.E.J., and Beyts, P. (2002). The use of critical stress intensity factor to quantify "hardness" and "crunchiness" objectively. *J. Texture Stud*., 33, 149–159.

Wollny M., and Peleg M. (1994). A model of moisture-induced plasticization of crunchy snacks based on Fermi's distribution function. *J. Sci. Food Agri*., 64, 467–473.

Chapter 11

Probing Food Structure

Martin Michel and Laurent Sagalowicz

Nestlé Research Center Lausanne, Nestec Ltd., Vers-Chez-Les Blanc, CH-1000 Lausanne 26, Switzerland, Martin.Michel@rdls.nestle.com, Laurent.Sagalowicz@rdls.nestle.com

11.1 Importance of Food Structure

The relationship between a food's structure and its properties/functionalities is of fundamental interest in food materials science. The great expectation is to relate the functionality of a food material to the physico-chemical characteristics of its ingredients and their geometric arrangement (i.e., structure formation). Functionalities of interest are either of chemical (e.g., flavor release from a given matrix), physical/mechanical (e.g., shelf life, sensory) or biological nature (e.g., nutrient bioavailability). Currently we are far from being able on a routine basis to relate food structures to functionality, and only in rare cases is it possible to establish a direct relationship (Renard et al. 2006). Recent examples are ice crystal size and fat destabilization in ice cream and its effects on texture and melting properties (Muse and Hartel 2004) as well as sugar particle size in chocolate and its influence on the rheological properties of the chocolate mass (Servais et al. 2002).

Most foods are complex colloidal multiphase systems (Aguilera 2006), composed of different aggregation states such as liquid or solid, crystalline or glassy or even liquid crystalline. Structural elements of importance cover length scales from nano- to millimeters. Examples of structural entities in the nano length scale (e.g., nanostructures) are association colloids made of phospholipids or monoglycerides, forming structures such as micelles, liposomes, cubosomes, and hexosomes. Other nanoscale structures are the tertiary structure of polymers, soluble protein–polysaccharide complexes and physical entanglement structures in gel networks (Leser et al. 2003). Prominent structural entities in the micro length scale (called microstructures) are oil or water droplets in milk or margarine, gas bubbles in mousses and ice cream and fat, sugar or ice crystals in milk, chocolate or ice cream, respectively.

It is important to note that nano- and microstructures are not only different with respect to their size but also with respect to their thermodynamic properties.

Microstructures are frequently present in a kinetically trapped nonequilibrium state, and their structures depend on the components and colloidal interactions based on their different chemical and physical properties, as well as on the procedure by which these components have been assembled. These structures are thermodynamically unstable and tend to reduce their free energy (surface area) with time. On the contrary, self-assembly nanostructures are thermodynamically stable, unless the molecules react with the environment or degrade. Most food systems are based on an interplay of kinetically stabilized and thermodynamic equilibrium structures. Some typical examples of structures at different length scales found in food systems are shown in Figure 11.1.

A major challenge in food materials science is to understand the dynamics involved in structure formation during production (Aguilera 2006; Aguilera et al. 2000), structure changes occuring during shelf-life (Man 2004), structure breakdown during consumption (Lucas et al. 2002) and, finally, processes involved in digestion of a food product (Armand et al. 1996). Time-scales involved range from nanoseconds for enzymatic reactions (Agarwal 2006), up to years for nonenzymatic browning (Franzen et al. 1990). So far, much more progress has been made in understanding the length than the time-scale problems. This certainly shows the merit of advances in methodologies for structure analysis such as microscopy techniques (e.g., atomic force, electron and optical microscopy) which has enabled us to get an accurate picture of many food systems over a large range of spatial scales, although always averaged in time. Currently there is no single methodology that allows a thorough structure characterization over all length- and time-scales involved in food materials science. It is therefore necessary to make a choice of methodologies adapted to the problem to be investigated using concepts from physics and nonfood materials science, as recently reviewed by Mezzenga et al. (2005).

It is the objective of this chapter to give an overview of the state of the art of methodologies for food structure characterization, as well as to indicate currently existing gaps. The available techniques will be discussed and illustrated with practical examples, showing advantages and disadvantages with a special emphasis on accessible length and time-scales. We will use milk and its processed products as well as monoglyceride self-assembly structures in order to illustrate the complexity involved in food structure characterization and its typical scales. Milk is a complex nutritious product containing substances that are soluble (e.g., lactose, whey proteins, mineral salts), suspended (e.g., casein micelles) or emulsified (e.g., fat and fat-soluble vitamins). All these components are used as structural building blocks for designing various different foods such as milk powders, yogurts, cheese, dairy desserts, and so on.

Monoglycerides are widely used in the food industry, especially in bakeries where approximately 60% of all monoglycerides are used (Krog 1997). As with all amphiphiles of this nature, they show interesting self-assembly properties in the presence of oil and water (de Campo 2004; Larsson and Krog 1973; Soderberg and Ljusberg-Wahren 1990). These self-assembly structures can be emulsified, resulting in internally self-assembled emulsion droplets (Yaghmur 2005). Such structures are

Type of structure		Methods
Phospholipid bilayer in vesicle	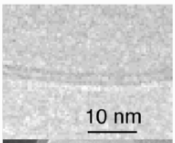	TEM SAXS Neutron scattering
Liquid crystalline phase particle	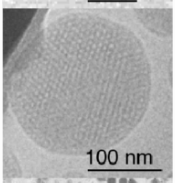	TEM SAXS Light scattering NMR
Emulsion droplet in milk stabilized by proteins	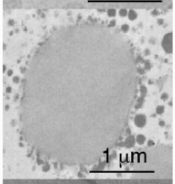	TEM, SEM Light scattering SAXS
Casein micelle	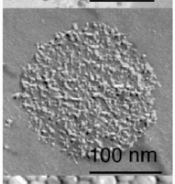	TEM, SEM Light scattering SAXS
Closely packed emulsion droplets in mayonnaise	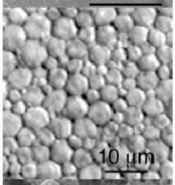	TEM, SEM Optical microscopy Light scattering Rheology
Casein micelle network in yogurt	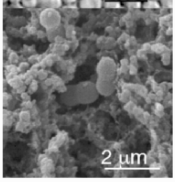	TEM, SEM Optical microscopy Light scattering Rheology

Figure 11.1. Different food structures as observed by microscopy and classical methods to characterize them; from top to bottom: cryo-transmission electron microscopy (TEM) image showing bilayer of a phospholipid vesicle with a membrane width of 3–4 nm, adapted from Sagalowicz et al. (2003); cryo-TEM of an inverse micellar cubic phase particle with an internal periodicity in the range of 10 nm., adapted from Sagalowicz et al. (2006b); TEM of milk fat droplet stabilized by milk proteins; freeze fracture of a casein micelle; light microscopy of fat droplets in a mayonnaise; scanning electron microscopy (SEM) micrograph of a yogurt gel formed by casein micelles. Copyright © 2006 Nestec Ltd.

of technological interest as delivery systems for liposoluble and amphiphilic bioactives (Sagalowicz et al. 2006a). In order to optimize their specific release functions of, for example, flavor molecules during eating or bioactives upon digestion we need to use appropriate state-of-the-art tools, getting structural insight at different length and time-scales.

Nowadays the target of many food developers is to provide food products with health benefits (Hardy 2000; Milner 1999; Milner 2000). This requires a thorough understanding of how food microstructure needs to be designed in order to maintain the desired health benefits throughout the entire life cycle of a food product, from the raw material to the effects in the body (Ward et al. 2004). Major challenges are the incorporation of health-beneficial bioactives within a complex food matrix without compromising organoleptic properties and getting the substance to the right target.

11.2 Lactose in Milk Processing

Lactose, besides water, is the major ingredient of milk and is rather small in size. Vuataz (2002) has elucidated the importance of lactose phase transitions on the quality of milk powders. Milk powder manufacture should preserve the emulsion functionality throughout the process and guarantee an appropriate powder reconstitution. In particular, fat globules need to be encapsulated in a fully amorphous matrix in order to optimally preserve the original milk emulsion structure. As an important step, lactose should be present in the glassy state and lactose crystallization, either during concentration, spray-drying or during shelf-life should be avoided (Pisecky 1997). Because amorphous lactose is metastable, water uptake or heat treatment can provoke lactose crystallization in a powder. Vuataz has shown that lactose may undergo two phase transitions depending on lactose concentration and temperature (Vuataz 2002). In supersaturated milk concentrates, nucleation of α-hydrate lactose occurs, whereas in a rubbery glassy milk powder β-anhydrous crystals are formed (Figure 11.2). However, in a rubbery, glassy skim milk powder, a mixture of anhydrous α and β crystals with a ratio 5:3 has been identified (Jouppila et al. 1997; Vuataz 2002). The crystalline type of lactose can be of technological importance, for example, managing water release for control of Maillard reaction products via crystallization of an amorphous matrix.

Essential techniques for establishing the phase behavior are differential scanning calorimetry (Kim et al. 2005; Fernandez et al. 2003), polarized light microscopy (Arellano et al. 2004; Mazzobre et al. 2003), wide angle x-ray diffraction (Haque and Roos 2005), near-infrared (NIR) and Raman spectroscopy (Norgaard et al. 2005). The state diagram concept in food has been pioneered by Roos and Karel (1991) and has become a very useful tool in process optimization (see the lactose state diagram in Figure 11.2), allowing also kinetic considerations of critical conditions, for example, for lactose crystallization in a time-scale range from seconds to years. Additional details on the concept can be found in a recent review article of Rahman (2006) as well as in an excellent book of Roos (1995).

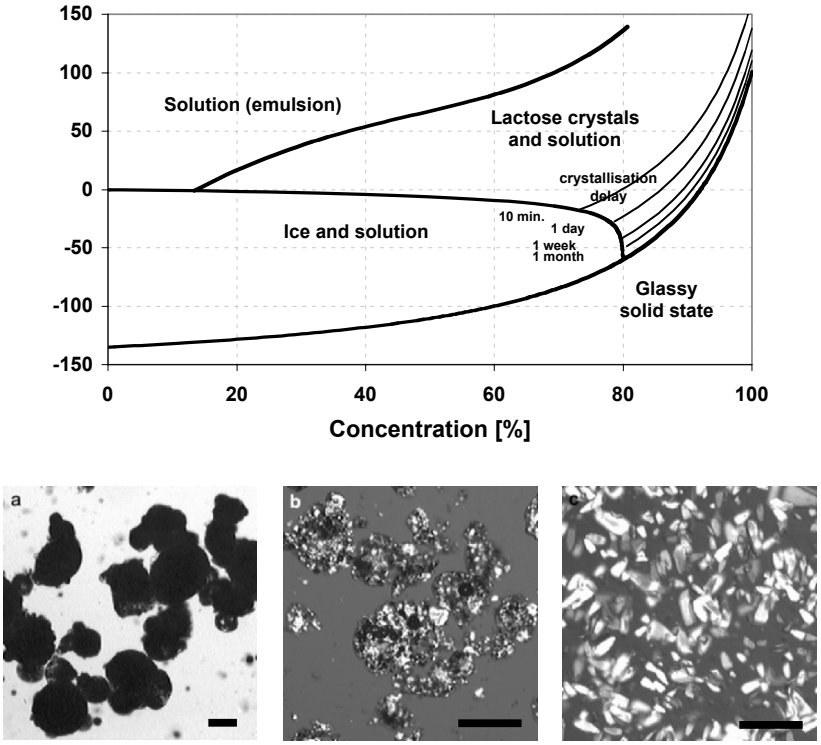

Figure 11.2. State diagram of lactose in whole milk (*upper part*). Polarized light microscope image showing (a) fully amorphous whole milk powder, (b) presence of anhydrous β-lactose crystals in a whole milk powder, and (c) α-hydrate lactose crystals in a skim milk concentrate. Scale bar represents 100 μm. Copyright © 2006 Nestec Ltd.

11.3 Milk Proteins

Milk proteins are either present in soluble form such as the globular whey proteins or dispersed in form of casein micelles. Casein micelles have been the object of intensive research activities, and despite the research efforts made so far, their structure is still a matter of debate as recently reviewed by Phadungath (2005) and Horne (2006). The casein micelle is a complex association colloid produced in the Golgi apparatus of the mammary gland (Boisgard et al. 2000; Farrell et al. 2006). Bovine casein micelles are built of the calcium insensitive κ-casein and the calcium sensitive α_{s1}, α_{s2} and the β-caseins, which are phosphorylated on specific serine residues. It is generally accepted that in unheated milk of physiological pH the majority of the κ-caseins are located on the casein micelle surface, resulting in a steric repulsion upon collision of two casein micelles (Tuinier and Kruif 2002). Casein micelles are polydisperse, showing a size distribution from approximately 50 to 600 nm in

diameter. Size distribution measurements of bovine casein micelles are rather tricky. Classical light scattering technology needs strong dilution of the casein suspension, and has to be done in serum in order to maintain the integrity of the micelles. Recent progress made in light scattering techniques based on 3-D cross-correlation light scattering allows analysis of particle sizes in turbid media such as milk (Urban and Schurtenberger 1998).

A main problem in structure characterization of the casein micelles is the irregular structure of the proteins involved. Horne describes the casein molecules as flexible block copolymers which self-assemble via hydrophobic and electrostatic interactions. Many different structure characterization techniques such as transmission (Hillbrick et al. 1999; Kalab et al. 1995) and scanning electron microscopy (Dalgleish et al. 2004), atomic force microscopy [(Uricanu et al. 2004), nuclear magnetic resonance (NMR) (Kolar et al. 2002; Thomsen et al. 1995; Rollema and Brinkhuis 1989; Kakalis et al. 1990), small angle x-ray, neutron and light scattering and combinations thereof (Alexander et al. 2002; Cross et al. 2005; Gebhardt et al. 2006; Holt et al. 2003; Schmidt et al. 1974)] have been applied in order to establish a structural description of the casein micelle architecture. As outlined by McMahon and McManus (1998), electron microscopy is prone to artifacts, and care has to be taken in interpretation of the obtained images.

11.4 Milk Fat

The major component in milk fat is triglycerides, which are composed of three fatty acids covalently bound to a glycerol molecule by ester bonds. Other lipidic fractions are diacylglycerols, cholesterol, phospholipids and free fatty acids. Fat in bovine milk is present as fat globules ranging from 0.2 to 15 μm in diameter. The fat globules in native milk are covered by a thin milk fat globule membrane helping to stabilize the fat globules in an emulsion within the aqueous environment of the milk (Lopez 2005). The native milk fat globule membrane consists of a complex mixture of proteins, glycoproteins, enzymes, phospholipids, cholesterol and other minor components (Evers 2004). Upon homogenization, droplet size is reduced, leading to an increase in surface area, and the milk fat globule membrane is partly replaced in its surface active role by proteins such as casein micelles or whey proteins (Ye 2002), providing physical stability.

At room temperature, milk fat triglycerides form periodic crystalline structures and they are in the solid state. The best way to study highly organized solid matter is wide angle x-ray diffraction (Lopez et al. 2002; Lopez et al. 2001; Lopez et al. 2001). The peaks observed correspond to distances between crystallographic planes and can be used to identify the crystallographic structure of a periodic arrangement. In theory, the complete organization of lipid crystals can be determined using position and intensity of the peaks. In reality, this determination is very often impossible for most food structures due to the limited order and the presence of crystallographic (structural) defects and molecular impurities affecting peak intensities. However, crystallographic structure can still be determined by comparing the position of the

peak, or equivalently the interplanar distance, with crystals obtained from purified fats or simulated x-ray diffraction spectra.

Differential scanning calorimetry (DSC) is another powerful technique to study phase transitions of oils and fats (Michalski et al. 2004; Kalnin et al. 2002). It enables analysis of the energy release (i.e., exothermic transformation) or energy intake (i.e., endothermic transformation) occurring during a phase change. DSC can be either done isothermally or by varying temperature. It is used to study fusion, crystallization and transformation from one fat polymorph to another one. The temperature and the energy associated with a given transformation allow us to determine the nature of the phases involved in phase transitions. Recently DSC and x-ray were used simultaneously to study the thermal and structural behavior of fat crystallization in a whipped emulsion made from inter-esterified palm oil (Kalnin et al. 2002).

Nuclear magnetic resonance (NMR) is also well suited to give insight into complex molecular arrangements. A simple method is low-resolution NMR, which allows the precise determination of the amount of solid fat present (Bertram et al. 2005; Granger et al. 2003). Polarized light microscopy is frequently used to study fat crystals (Marangoni and Narine 2002; Narine and Marangoni 1999a; Narine and Marangoni 1999b). Figure 11.3 shows a freeze fracture TEM micrograph of an oil in water emulsion where the fat constituting the droplets crystallized and the crystallites show straight faces typical of crystals.

Stabilization of the interfaces between oil and water is of great importance in emulsion technology. Interfaces are usually stabilized with the help of amphiphilic molecules such as low molecular weight surfactants and biopolymers. Interfaces are two-dimensional nanoscopic spaces where amphiphilic molecules accumulate and self-assemble. Time-scales are very important in emulsion technology, as the adsorption events at the newly created interface take place in the millisecond range and are governed by the diffusion properties of the surfactant molecules (Brosel and

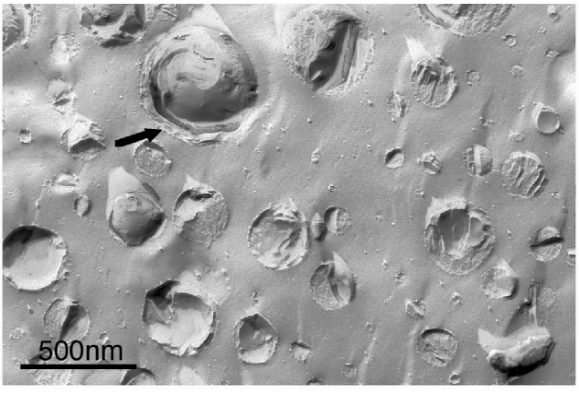

Figure 11.3. Freeze fracture image of an emulsion where the fat is crystallized. Notice the straight interface (arrowed) originating from crystalline fat, separating the fat droplets and the aqueous media. Copyright © 2006 Nestec Ltd.

Schubert 1999; Nilsson and Bergenstahl 2006; van der Graaf et al. 2004), whereas long-term stability can go up to years and is governed by processes such as oil droplet coalescence, Ostwald ripening and flocculation (Radford and Dickinson 2004; Dickinson et al. 2003; Dickinson 2003b; Dickinson 2001).

Methodologies to assess interface properties of amphiphiles are surface tension measurements (Phan et al. 2006; Golding and Sein 2004; Miller et al. 2004), ellipsometry (Dickinson 2003a; Murray 2002) and Brewster angle microscopy (Grigoriev et al. 2006; Rodrguez Patino et al. 2001). Both ^{13}C and ^{31}P NMR have been applied in order to study the conformation and dynamics of β-casein at the oil–water interface of emulsions (ter Beek et al. 1996). Their NMR results showed that the protein at the interface has mobile regions with little secondary structure in which the motions are rather slow.

11.5 Yogurt: A Particle Gel

Yogurt is a typical food particle gel formed by fractal aggregation of casein micelles and fat globules formed upon slow acidification of milk through lactic acid bacteria. After destabilized, the casein micelles (Figure 11.4) as well as the protein-stabilized fat globules start to aggregate and finally form a three-dimensional network entrapping the serum phase (Figure 11.5).

Understanding the relationships between the interparticle forces, structure formation and final mechanical properties of particle gels is a complex problem, as discussed by Dickinson (2000). The challenge is to control the aggregation dynamics

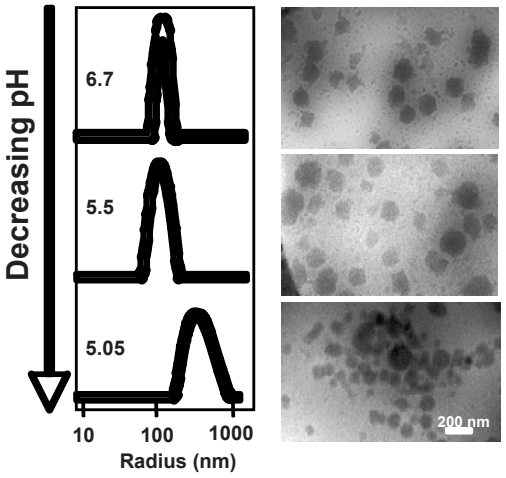

Figure 11.4. Aggregation of casein micelles acidification as observed by 3-D cross-correlation light scattering (*left column*) and cryo-TEM (*right column*). Copyright © 2006 Nestec Ltd.

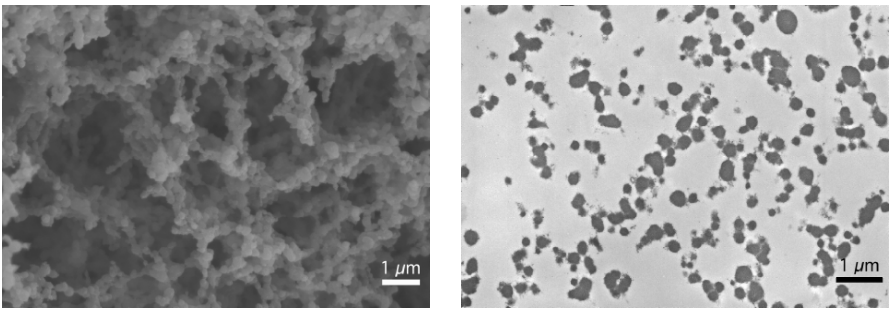

Figure 11.5. SEM and TEM micrographs of acidified skim milk. Copyright © 2006 Nestec Ltd.

driven by the involved interparticle interactions. Aichinger et al. (2003) showed, that the processing parameters and the destabilization mechanism (e.g., acidification, renneting with chymosin) can result in different gel structures and hence mechanical properties.

Gel formation in milk has been studied using a multitude of techniques. Methods such as oscillatory rheometry (Anema et al. 2004; Anema et al. 2004; Castillo et al. 2006; Lucey and Singh 1997; Lucey et al. 1998; Lucey et al. 2000; Lucey et al. 2001), diffusing-wave spectroscopy (Alexander et al. 2006; Alexander and Dalgleish 2004; Alexander and Dalgleish 2005; Alexander et al. 2002; Hemar et al. 2004; Hemar et al. 2004; Horne 1984; Horne 1991; Vasbinder et al. 2001) and ultrasonic spectroscopy (Meyer et al. 2006; Taifi et al. 2006; Challis et al. 2005; Dwyer et al. 2005; Dalgleish et al. 2004) have been used to investigate various aspects of the dynamics of gel formation. Electron microscopy (del Angel and Dalgleish 2006; Famelart et al. 2004; Sanchez et al. 2000; Roefs et al. 1990) and confocal laser scanning microscopy (Bhat et al. 2006; Durrenberger et al. 2001) have been applied to characterize milk gel structures.

Despite experimental progress, the mechanisms and kinetics of acid milk gelation are still not fully understood. Theoretical approaches such as the adhesive sphere, percolation or fractal model applied to acid-induced milk gel formation can successfully explain specific aspects of the process (Tuinier and Kruif 1999), but all fail in rationalizing its kinetics (Horne 1999).

Most food systems are of a colloidal as well as a polymeric nature. The presence of a nonadsorbing polymer in a skim milk dispersion induces an effective attraction between the casein particles, called depletion interaction, resulting in phase separation at sufficiently high polymer concentration. Tuinier et al. (2003) discussed the influence of colloid–polymer size ratio, polymer concentration regime, size, polydispersity and charges in colloid/biopolymer mixtures, demonstrating the challenging complexity of the subject.

The depletion mechanism can be of interest to create new food structures resulting in novel texture properties if one gets control of the dynamics and finds ways to kinetically trap the separation process (Aichinger 2005). For the study of such

complex systems, dynamic light microscopy such as time-resolved confocal microscopy is of great help (Loren et al. 1999). An example of this is seen in Figure 11.6, showing structure evolution in a xanthan–skim milk mixture. Using image analysis techniques allows extraction of quantitative data on structure characteristics as a function of formulation changes and process parameters (pH, temperature) allowing establishment of relationships between structure and the mechanical/texture characteristics of a gel (Aichinger et al. 2006).

Bhat et al. (2006) recently developed a new ultra small angle light scattering technique which allows following the phase separation behavior of casein micelles in the presence of xanthan in real time. Such new techniques will be of tremendous help for designing novel composite gels.

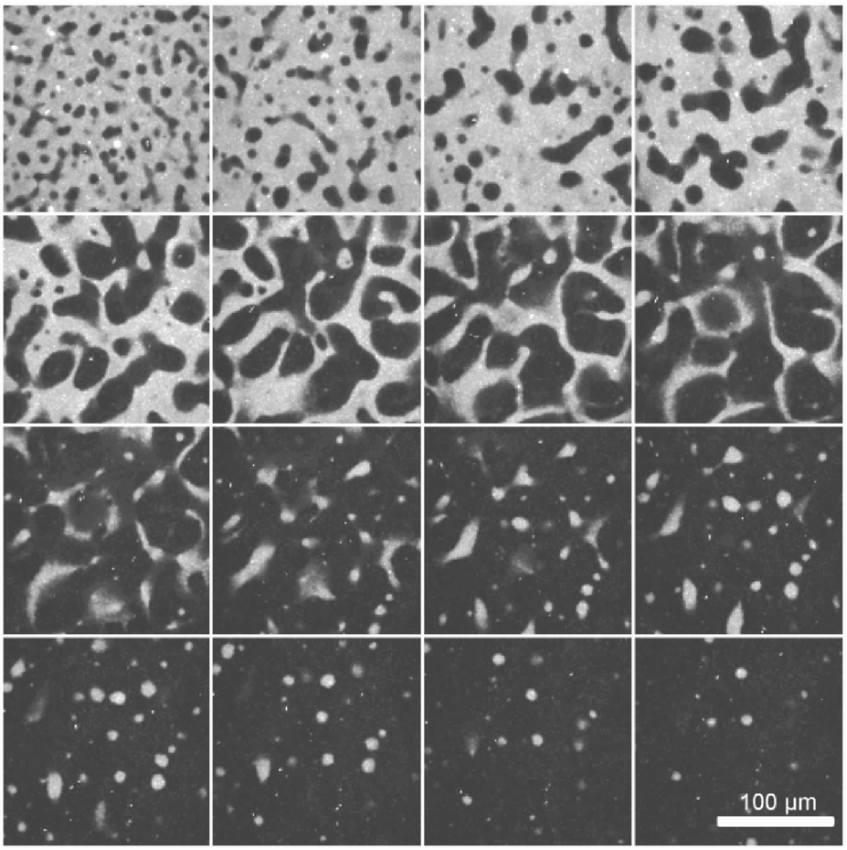

Figure 11.6. Dynamic imaging of a phase separating skim milk–xanthan mixture showing the structures formed due to depletion interactions. Copyright © 2006 Nestec Ltd.

11.6 Monoglyceride Self-Assembly Colloids

Emulsifiers such as monoglycerides and phospholipids are commonly used in foods to stabilize interfaces. Due to their amphiphilic character they form a multitude of self-assembly structures, such as lamellar, micellar, cubic or hexagonal mesophases. Because these molecules have a certain mobility within the self-assembly structure, monoglyceride and phospholipid self-assembly structures show a very different state from that of lipid crystals. This freedom to move is governed by hydrophobic and ionic interactions, resulting in a long-range order (of the order of several molecules) and the structure of some of these liquid crystalline phases can be therefore rather stiff. Distances of interest for liquid crystals and self-assembly structures are typically in the range of 10 nm, making small angle x-ray scattering (SAXS) and NMR the preferred methods for their analysis. (Caboi et al. 2002; Caboi et al. 2001). Figure 11.7 shows SAXS curves of different self-assembly structures that occur upon heating Dimodan U, a commercially available monoglyceride. At room temperature, the structure is liquid crystalline inverted bicontinuous cubic; at temperatures above 50°C, it is reversed hexagonal; and, finally, when heating above 90°C the liquid crystalline structure melts and we have an L_2 microemulsion, which is composed of nonordered reversed micelles. DSC can also be used to follow transitions between different phases; however, the transition enthalpy between two self-assembly structures is only about 1% of that between two crystals (or one crystal and a liquid) needing higher sensitivity as provided by a micro DSC equipment (Sagalowicz et al. 2006a). These techniques, together with polarized light microscopy, provide the information to construct phase diagrams as shown in Figure 11.7.

Electron microscopy is a very powerful technique for identifying the structure of self-assembly particles such as micelles exhibiting a typical size in the range of 5–20 nm or liposomes, which can be as large as several micrometers. However, it is a rather time-consuming technology, and care has to be taken for the interpretation of the results obtained. Compared to SAXS, electron microscopy allows analysis of much smaller volumes as well as visualizing structures of individual objects.

Freeze fracture techniques have been applied to study the space group of liquid crystalline phases. Delacroix et al. (1996), using this technique, showed that the space group of the micellar cubic structure was Fd3m and not Fd3, while SAXS was in this case inconclusive. One limitation of freeze fracture is that due to the relatively large thickness of the sample, the bulk phase may crystallize, leading to the formation of ice crystals, destroying the original self-assembly structure. Gulik-Krzywicki and Delacroix (1994) compared therefore their microscopy results with SAXS experiments performed at liquid nitrogen temperature, confirming that the bulk phase was vitrified. Another limitation of freeze fracture is that the fracture plane proceeds in an uncontrolled way through the sample, making it difficult to efficiently analyze the exact order in a liquid crystalline system.

A very powerful alternative to freeze fracture is cryo-TEM (Adrian et al. 1984), which only recently found its application in food structure characterization. Cryo-TEM methodology consists of depositing a small droplet of the sample to be analyzed onto a holey polymer film supported on a standard TEM grid. The excess of specimen solution

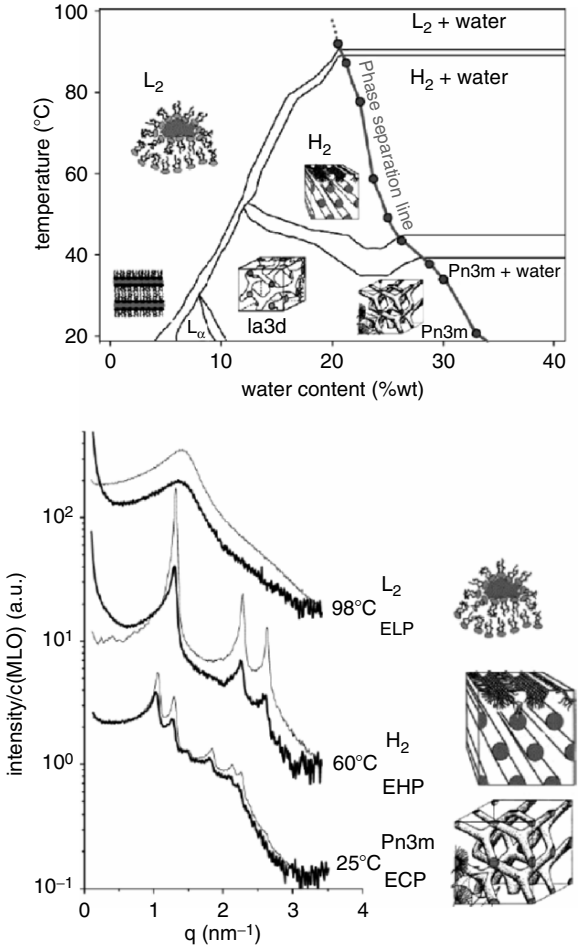

Figure 11.7. Phase diagram of monoglycerides (*upper part*). Structure characterization using small angle x-ray scattering (*lower part*). Adapted from de Campo et al. (2004). Copyright © 2006 Nestec Ltd.

is removed by filter paper(s) followed by plunging the grid into liquid ethane (Figure 11.8). Sample observation is done at liquid nitrogen temperature in a transmission electron microscope. Because the sample is rather thin (a layer of approximately 100 nm is frozen) vitrification is rather easy to achieve and can be verified by electron diffraction during sample analysis. In order to avoid evaporation effects that have an influence on the sample concentration, a controlled humidity and temperature chamber can be used where the humidity is fixed in most cases at 100% (Egelhaaf et al. 2000). Blotting may introduce size segregation of the dispersed particles as well as leading to shearing forces, resulting in artifacts such as vesicle to micelle changes.

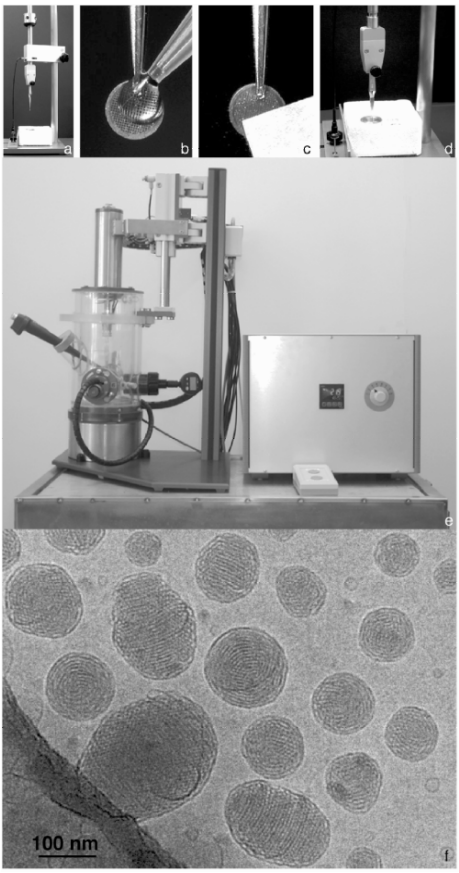

Figure 11.8. Illustration of sample preparation for cryo-TEM imaging. Parts (a)–(d) show specimen preparation for sample freezing; (e) shows plunge freezing apparatus with temperature and humidity control; and (f) a typical image obtained by cryo-TEM. Copyright © 2006 Nestec Ltd.

Despite this, cryo-TEM is considered to be safe, and comparison of the structures obtained by SAXS and cryo-TEM are generally in very good agreement (de Campo et al. 2004; Yaghmur et al. 2005). Imaging is done using appropriate defocus settings in the TEM.

Figure 11.9 shows that it is possible to image a phospholipid membrane bilayer structure with the dark lines corresponding to the polar phosphor head groups (Sagalowicz et al. 2003). The membrane thickness can be estimated as shown by the intensity line scan in Figure 11.9. Interpretation of the images needs an expert view since various artifacts such as beam damage and surface contamination can lead to misinterpretations (Won 2004).

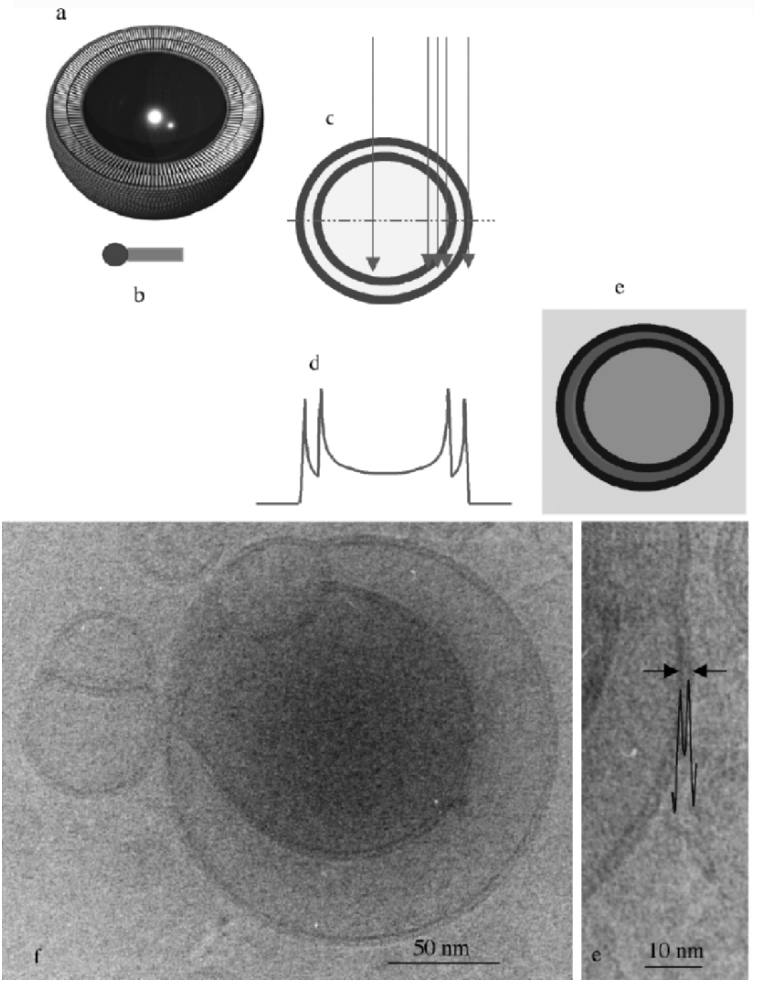

Figure 11.9. Contrast formation in cryo-TEM. (a) Schematic image of a vesicle formed with phospholipid molecules. (b) Schematic representation of a phospholipid molecule with polar headgroup and apolar tail. (c)(d) Projection of the polar head group, which is the strongest scattering center. (e) Calculated line scan considering the projection of the polar head groups. (d) Schematic image of a vesicle. (e)(f) Experimental images of vesicles where the double layer with a thickness of about 3.5 nm is clearly seen. Adapted from Sagalowicz et al. 2003.

Some recent examples of cryo-TEM in food research are imaging of milk fat globule membrane lipids (Waninge 2003) and α-lactalbumin self-assembly aggregates (Graveland-Bikker et al. 2006; Graveland-Bikker and de Kruif 2006). Cryo-TEM has become an indispensable tool to acquire high-resolution images of self-assembly nanostructures and dispersed liquid crystalline structures (Sagalowicz et al. 2006c; Talmon 1996).

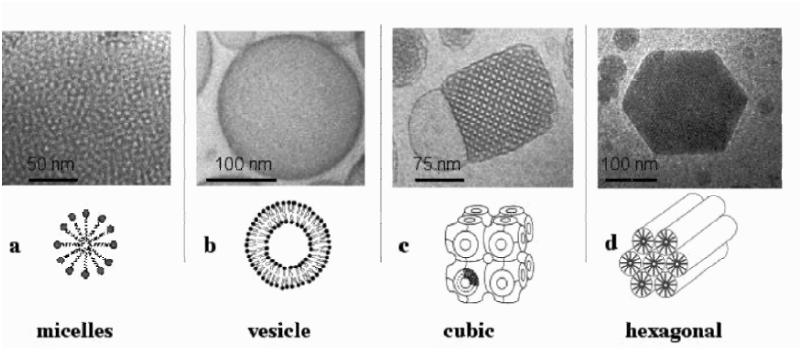

Figure 11.10. Structure of dispersed self-assembly particles. The original cryo-TEM image is shown at the top with schematic representation of the structure below the images. Particles shown are (a) micelles, (b) vesicle, (c) inverted bicontinuous cubic and (d) reverted hexagonal phase particle. Adapted from Sagalowicz et al. 2006a.

Figure 11.10 gives an overview of cryo-TEM pictures of various dispersed self-assembly structures such as micelles, vesicles, inverted bicontinuous cubic and reverted hexagonal phases. Time-resolved studies of dynamic events are possible, applying on the grid processing such as pH and temperature jumps (Siegel et al. 1989), spray mixing (Unwin 1995) or flow-induced deformation (Zheng et al. 2000).

In cryo-TEM the same particle can be observed in different directions by tilting the sample in the microscope, enabling a complete 3D-reconstruction of particles (Lucic et al. 2005). This allows imaging of completely different structure motifs, enabling an exact identification of the liquid crystalline phase type. Analysis is done using fast Fourier transform algorithms on image areas of interest, resulting in the calculation of average distances present in the sample reflecting interplanar distances of the liquid crystal structure (Sagalowicz et al. 2006c). Figure 11.11 shows, for example, how tilting can be used to discriminate between different space groups present in an inverse cubic liquid crystalline particle. Resolution is not as good as that obtained with SAXS, but a single particle can be analyzed, which is an advantage in diluted and inhomogeneous dispersions.

11.7 Food Structure and Nutrition

A major question to address in the future is how structure influences the dynamics of digestion and the signaling processes involved. Armand et al. (1996, 1999) investigated the digestion and lipid absorption from emulsions with different droplet sizes in humans. Healthy subjects received intragastrically a coarse (10 μm) and a fine (0.7 μm) lipid emulsion of identical composition in random order. Gastric and duodenal aspirates as well as triglyceride appearance in the blood were analyzed. They found an increase in droplet size in the stomach; however, the fine emulsion retained droplets

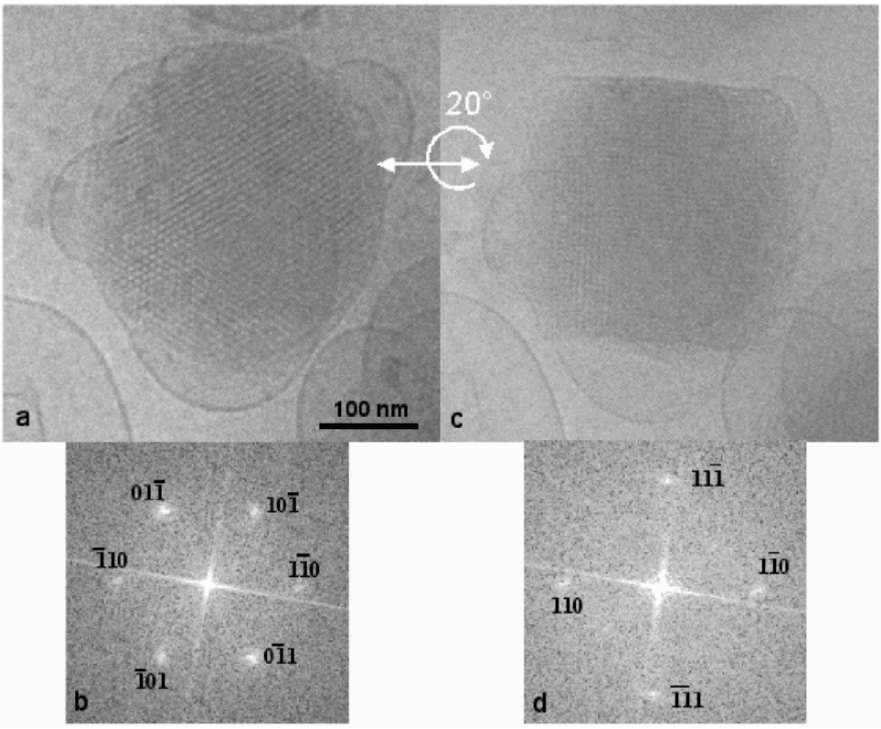

Figure 11.11. Determination of exact space groups present in a cubosome (diamond-type space group Pn3m) using cryo-TEM tilt experiments and fast Fourier transform analysis. (a) In the untilted particle a hexagonal motif is observed, as evidenced in the intensity representation of the Fourier transform shown in (b). (c) Same particle observed after 20° tilting, showing a different motif in the Fourier transform shown in (d). Adapted from Sagalowicz et al. 2006c.

of smaller size and its lipolysis was greater than that of the coarse emulsion. In the duodenum, lipolysis of the fine emulsion was on the whole higher. A surprising result was, however, that the triacylglycerol peak was delayed with the fine emulsion, which confirmed results previously obtained with rat experiments (Borel et al. 1994). These data suggest that emulsions with different particle sizes lead to different time courses of plasma lipids post-prandially. The authors mention as possible causes a difference in gastric emptying, the formation of intermediate phases such as mixed micelles and vesicles and differences in the diffusion of lipids through the unstirred water layer. This example shows that structure can play an important role in the dynamics of nutrient uptake.

Currently there is a big knowledge gap regarding the effect of food structures on nutrient uptake, and we need to establish sound relationships between food structure, the involved biotransformation processes and the final uptake of nutrients. In the past,

some attempts have been made to follow structures developing upon lipid transformation using in vitro digestion approaches of model systems (Borné et al. 2002; Gantz et al. 1999; Patton and Carey 1979; Patton et al. 1985; Rigler et al. 1986). These first approaches indicate the complexity of the subject and already give some guidance on how to close the above-mentioned gap. We are convinced that a greater effort in this area will lead to interesting strategies for controlling nutrient uptake and that the results obtained will help us in optimizing the design of adequate food structures with well-defined functionalities such as release properties of bioactives.

11.8 Conclusions and Outlook

Food structure analysis has made considerable progress in applying state-of-the-art methodologies originating from other disciplines such as physics, biology and material science. Various structure characterization methodologies are currently available that give us insight on a multitude of length scales, whereas methodologies for assessing dynamic processes need further development. The best technologies are those that are either non- or minimally invasive, such as various scattering (light, x-ray, neutron) and NMR techniques. In most cases, however, they need confirmation by other methods such as microscopy.

Food structure analysis is particularly powerful when it is applied in combination with validated physical models allowing the prediction of a food system's behavior such as the glass transition concept. Advances in computational modeling will definitely speed up structure design in food products (Limbach and Kremer 2006). Another difficulty in food materials science is the presence of a variety of food structures and the rather large particle size distribution present in many food systems. This makes it difficult to relate structural characteristics to specific functionalities. This gap may be closed with microfluidic technologies that allow precision engineering of colloidal entities such as oil droplets or air bubbles with well-defined sizes and shapes (Garstecki et al. 2004; Link et al. 2004).

Establishing structural changes occurring during biotransformation processes involved in consumption and digestion of a food will remain a further challenge in the near future. Current attempts focus on *in vitro* systems, studying specific aspects of structure breakdown, for example, during mastication or digestion. Major breakthroughs can be expected as soon as we have access to noninvasive techniques, providing high enough spatial and time resolution to perform in vivo tracking of structural changes.

Acknowledgements. We thank Martin Leser for useful discussions and feedback on the manuscript, Gilles Vuataz for his valuable input on lactose crystallization and Marie-Lise Dillmann, Martine Rouvet, Pierre Aichinger and Eric Koldziejczyk for their microscopy contributions. We also thank Fred Chavannes, Olivier Girault, Jean-Albert Stucki, Dino Tomasi, and Laurent Peissard (CRN) for having built the environmental chamber for the cryo-TEM analysis. We greatly acknowledge Kenneth Moffitt for English corrections.

11.9 References

Adrian, M., Dubochet, J., Lepault, J., and McDowall, A.W. (1984). Cryo-electron microscopy of viruses. *Nature*. 308, 3236.

Agarwal, P.K. (2006). Enzymes: an integrated view of structure, dynamics and function. *Microbial Cell Factories*. 5, 2–13.

Aguilera, J.M. (2006). Seligman lecture 2005 food product engineering: building the right structures. *J. Sci. Food. Agric.* 86, 1147–1155.

Aguilera, J.M., Stanley, D.W., and Baker, K.W. (2000). New dimensions in microstructure of food products. *Trends Food Sci. Technol.* 11, 3–9.

Aichinger, P.A. (2005). Kinetic trapping of microstructures: control of gelation in dairy products. Glasgow: Strathclyde. p. 235.

Aichinger, P.A., Dillmann, M.L., Rami-Shojaei, S., Michel, M. and Horne, D.S. (2006). Xanthan gum in skim milk: designing structure into acid milk gels. In: E. Dickinson and M.E. Leser. *Food Colloids: Self–Assembly and Material Science*, Royal Society of Chemistry, Cambridge, pp. 283–296.

Aichinger, P.A., Michel, M., Servais, C., Dillmann, M.L., Rouvet, M., D'Amico, N., Zink, R., Klostermeyer, H., and Horne, D.S. (2003). Fermentation of a skim milk concentrate with *Streptococcus thermophilus* and chymosin: structure, viscoelasticity and syneresis of gels. *Colloids Surf. B*. 31, 243–255.

Alexander, M., Corredig, M., and Dalgleish, D.G. (2006). Diffusing wave spectroscopy of gelling food systems: the importance of the photon transport mean free path (l*). *Food Hydrocolloids*. 20, 325–331.

Alexander, M., and Dalgleish, D.G. (2004). Application of transmission diffusing wave spectroscopy to the study of gelation of milk by acidification and rennet. *Colloids Surf. B.* 38, 83–90.

Alexander, M., and Dalgleish, D.G. (2005). Interactions between denatured milk serum proteins and casein micelles studied by diffusing wave spectroscopy. *Langmuir*. 21, 11380–11386.

Alexander, M., Rojas-Ochoa, L.F., Leser, M.E., and Schurtenberger, P. (2002). Structure, dynamics and optical properties of concentrated milk suspensions: an analogy to hard–sphere liquids. *J. Colloid Interf. Sci.* 253, 35–46.

Anema, S.G., Lee, S.K., Lowe, E.K., and Klostermeyer, H. (2004). Rheological properties of acid gels prepared from heated pH–adjusted skim milk. *J. Agric. Food Chem*. 52, 337–343.

Anema, S.G., Lowe, E.K., and Lee, S.K. (2004). Effect of pH at heating on the acid–induced aggregation of casein micelles in reconstituted skim milk. *Lebensmitt. Wissen. Technol.* 37, 779–787.

Arellano, M.P., Aguilera, J.M., and Bouchon, P. (2004). Development of a digital video microscopy technique to study lactose crystallisation kinetics in situ. *Carbohydr. Res.* 339, 2721–2730.

Armand, M., Borel, P., Pasquier, B., Dubois, C., Senft, M., Andre, M., Peyrot, J., Salducci, J., and Lairon, D. (1996). Physicochemical characteristics of emulsions during fat digestion in human stomach and duodenum. *Am. J. Physiol.* 271, G172–183.

Armand, M., Pasquier, B., Andre, M., Borel, P., Senft, M., Peyrot, J., Salducci, J., Portugal, H., Jaussan, V., and Lairon, D. (1999). Digestion and absorption of 2 fat emulsions with different droplet sizes in the human digestive tract. *Am. J. Clin. Nutr.* 70, 1096–1106.

Bertram, H.C., Wiking, L., Nielsen, J.H., and Andersen, H.J. (2005). Direct measurement of phase transitions in milk fat during cooling of cream: a low-field NMR approach. *Int. Dairy J.* 15, 1056–1063.

Bhat, S., Tuinier, R., and Schurtenberger, P. (2006). Spinodal decomposition in a food colloid biopolymer mixture: evidence for a linear regime. *J. Phys. Condens. Matter.* 18, L339–L346.

Boisgard, R., Chanat, E., Lavialle, F., Pauloin, A., and Ollivier-Bousquet, M. (2000). Roads taken by milk proteins in mammary epithelial cells. *Livestock Prod. Sci*. 70, 49–61.

Borel, P., Armand, M., Pasquier, B., Senft, M., Dutot, G., Melin, C., Lafont, H., and Lairon, D. (1994). Digestion and absorption of tube–feeding emulsions with different droplet sizes and compositions in the rat. *J. Parenter. Enteral. Nutr.* 18, 534–543.

Borné, J., Nylander, T., and Khan, A. (2002). Effect of lipase on different lipid liquid crystalline phases formed by oleic acid–based acylglycerols in aqueous systems. *Langmuir*. 18, 8972–8981.

Brosel, S., and Schubert, H. (1999). Investigations on the role of surfactants in mechanical emulsification using a high–pressure homogenizer with an orifice valve. *Chem. Eng. Processing.* 38, 533–540.

Caboi, F., Amico, G.S., Pitzalis, P., Monduzzi, M., Nylander, T., and Larsson, K. (2001). Addition of hydrophilic and lipophilic compounds of biological relevance to the monoolein–water system. I. Phase behavior. *Chem. Phys. Lipids*. 109, 47–62.

Caboi, F., Borne, J., Nylander, T., Khan, A., Svendsen, A., and Patkar, S. (2002). Lipase action on a monoolein–sodium oleate aqueous cubic liquid crystalline phase–a NMR and x–ray diffraction study. *Colloids Surf. B*. 26, 159–171.

Castillo, M., Lucey, J.A., and Payne, F.A. (2006). The effect of temperature and inoculum concentration on rheological and light scatter properties of milk coagulated by a combination of bacterial fermentation and chymosin: cottage cheese-type gels. *Int. Dairy J.* 16, 131–146.

Challis, R.E., Povey, M.J.W., Mather, M.L., and Holmes, A.K. (2005). Ultrasound techniques for characterizing colloidal dispersions. *Rep. Prog. Phys*. 68, 1541–1637.

Cross, K.J., Huq, N.L., Palamara, J.E., Perich, J.W., and Reynolds, E.C. (2005). Physicochemical characterization of casein phosphopeptide–amorphous calcium phosphate nanocomplexes. *J. Biol. Chem.* 280, 15362–15369.

Dalgleish, D., Alexander, M., and Corredig, M. (2004). Studies of the acid gelation of milk using ultrasonic spectroscopy and diffusing wave spectroscopy. *Food Hydrocolloids*. 18, 747–755.

Dalgleish, D.G., Spagnuolo, P.A., and Goff, D.H. (2004). A possible structure of the casein micelle based on high–resolution field-emission scanning electron microscopy. *Int. Dairy J.* 14, 1025–1031.

de Campo, L., Yaghmur, A., Sagalowicz, L., Leser, M.E., Watzke, H.J., and Glatter, O. (2004). Reversible phase transitions in emulsified nanostructured lipid systems. *Langmuir*. 20, 5254–5261.

del Angel, C.R., and Dalgleish, D.G. (2006). Structures and some properties of soluble protein complexes formed by the heating of reconstituted skim milk powder. *Food Res. Int*. 39, 472–479.

Delacroix, H., Gulik-Krzywicki, T., and Seddon, J.M. (1996). Freeze fracture electronmicroscopy of lyotropic lipid systems: quantitative analysis of the inverse micellar cubic phase of space group Fd3m (Q227). *J. Mol. Biol.* 258, 88–103.

Dickinson, E. (2000). Structure and rheology of simulated gels formed from aggregated colloidal particles. *J. Colloid Interf. Sci*. 225, 2–15.

Dickinson, E. (2001). Milk protein interfacial layers and the relationship to emulsion stability and rheology. *Colloids Surf. B*. 20, 197–210.

Dickinson, E. (2003a). Food colloids: drifting into the age of nanoscience. *Curr. Opin. Coll. Interf. Sci.* 8, 346–348.

Dickinson, E. (2003b). Hydrocolloids at interfaces and the influence on the properties of dispersed systems. *Food Hydrocolloids*. 17, 25–39.

Dickinson, E., Radford, S.J., and Golding, M. (2003). Stability and rheology of emulsions containing sodium caseinate: combined effects of ionic calcium and nonionic surfactants. *Food Hydrocolloids*. 17, 211–220.

Durrenberger, M.B., Handschin, S., Conde-Petit, B., and Escher, F. (2001). Visualization of food structure by confocal laser scanning microscopy (CLSM). *Lebensmitt. Wissen. Technol.* 34, 11–17.

Dwyer, C., Donnelly, L., and Buckin, V. (2005). Ultrasonic analysis of rennet-induced pre-gelation and gelation processes in milk. *J. Dairy Res*. 72, 303–310.

Egelhaaf, S.U., Schurtenberger, P., and Muller, M. (2000). New controlled environment vitrification system for cryo-transmission electron microscopy: design and application to surfactant solutions. *J. Microsc.* 200, 128–139.

Evers, J.M. (2004). The milkfat globule membrane–compositional and structural changes post–secretion by the mammary secretory cell. *Int. Dairy J.* 14, 661–674.

Famelart, M.H., Tomazewski, J., Piot, M., and Pezennec, S. (2004). Comprehensive study of acid gelation of heated milk with model protein systems. *Int. Dairy J.* 14, 313–321.

Farrell, H.M., Malin, E.L., Brown, E.M., and Qi, P.X. (2006). Casein micelle structure: what can be learned from milk synthesis and structural biology? *Curr. Opin. Coll. Interf. Sci*. 11, 135–147.

Fernandez, E., Schebor, C., and Chirife, J. (2003). Glass transition temperature of regular and lactose hydrolyzed milk powders. *Lebensmitt. Wissen. Technol*. 36, 547–551.

Franzen, K., Singh, R.K., and Okos, M.R. (1990). Kinetics of nonenzymatic browning in dried skim milk. *J. Food Eng*. 11, 225–239.

Gantz, D.L., Wang, D.Q., Carey, M.C., and Small, D.M. (1999). Cryoelectron microscopy of a nucleating model bile in vitreous ice: formation of primordial vesicles. *Biophys. J*. 76, 1436–1451.

Garstecki, P., Gitlin, I., DiLuzio, W., Whitesides, G.M., Kumacheva, E. and Stone, H.A. (2004). Formation of monodisperse bubbles in a microfluidic flow-focusing device. *Appl. Phys. Lett*. 85, 2649–2651.

Gebhardt, R., Doster, W., Friedrich, J., and Kulozik, U. (2006). Size distribution of pressure–decomposed casein micelles studied by dynamic light scattering and AFM. *Eur. Biophys. J.* 35, 503–509.

Golding, M., and Sein, A. (2004). Surface rheology of aqueous casein–monoglyceride dispersions. *Food Hydrocolloids.* 18, 451–461.

Granger, C., Barey, P., Combe, N., Veschambre, P., and Cansell, M. (2003). Influence of the fat characteristics on the physicochemical behavior of oil-in-water emulsions based on milk. *Colloids Surf. B*. 32, 353–363.

Graveland-Bikker, J.F., and de Kruif, C.G. (2006) Unique milk protein based nanotubes: food and nanotechnology meet. *Trends Food Sci. Technol*. 17, 196–203.

Graveland-Bikker, J.F., Fritz, G., Glatter, O., and de Kruif, C.G. (2006). Growth and structure of [α]-lactalbumin nanotubes. *J. Appl. Crystallogr*. 39, 180–184.

Grigoriev, D.O., Leser, M.E., Michel, M., and Miller, R. (2006). Component separation in spread sodium stearoyl lactylate (SSL) monolayers induced by high surface pressure. *Colloids Surf. A*. 286, 57–61.

Gulik–Krzywicki, T., and Delacroix, H. (1994). Combined use of freeze fracture electron microscopy and x-ray diffraction for the structure determination of three-dimensionally ordered specimens. *Biol. Cell.* 80, 193–201.

Haque, K., and Roos, Y.H. (2005). Crystallization and x-ray diffraction of crystals formed in water-plasticized amorphous spray-dried and freeze-dried lactose–protein mixtures. *Carbohydr. Res*. 340, 293–301.

Hardy, G. (2000). Nutraceuticals and functional foods: introduction and meaning. *Nutrition*. 16, 688–689.

Hemar, Y., Hebraud, P., Sarcia, R., and Pinder, D.N. (2004). Diffusing-wave spectroscopy of gelling dairy systems. *AIP Conf. Proc*. 708, 434–435.

Hemar, Y., Singh, H., and Horne, D.S. (2004). Determination of early stages of rennet-induced aggregation of casein micelles by diffusing wave spectroscopy and rheological measurements. *Curr. Appl. Phys.* 4, 362–365.

Hillbrick, G.C., McMahon, D.J., and McManus, W.R. (1999) Microstructure of indirectly and directly heated ultra-high-temperature (UHT) processed milk examined using transmission electron microscopy and immunogold labelling. *Lebensmitt. Wissen. Technol.* 32, 486–494.

Holt, C., de Kruif, C.G., Tuinier, R., and Timmins, P.A. (2003). Substructure of bovine casein micelles by small-angle x-ray and neutron scattering. *Colloids Surf. A*. 213, 275–284.

Horne, D.S. (1984). Determination of the size distribution of bovine casein micelles using photon correlation spectroscopy. *J. Colloid Interf. Sci*. 98, 537–548.

Horne, D.S. (1991). Dynamic light scattering from casein micelle suspensions. *Biochem. Soc. Trans.* 19, 489.

Horne, D.S. (1999). Formation and structure of acidified milk gels: vocabulary development and the relations between sensory properties. *Int. Dairy J*. 9, 261–268.

Horne, D.S. (2006). Casein micelle structure: models and muddles. *Curr. Oppin. Coll. Interf. Sci.* 11, 148–153.

J. Kim, E.H., Chen, X.D., and Pearce, D. (2005). Melting characteristics of fat present on the surface of industrial spray-dried dairy powders. *Colloids Surf. B.* 42, 1–8.

Jouppila, K., Kansikas, J., and Roos, Y.H. (1997). Glass transition, water plasticization, and lactose crystallization in skim milk powder. *J. Dairy Sci.* 80, 3152–3160.

Kakalis, L.T., Kumosinski, T.F., and Farrell, H.M. (1990). A multinuclear, high-resolution NMR study of bovine casein micelles and submicelles. *Biophys. Chem*. 38, 87–98.

Kalab, M., Allan–Wojtas, P., and Miller, S.S. (1995). Microscopy and other imaging techniques in food structure analysis. *Trends Food Sci. Technol*. 6, 177–186.

Kalnin, D., Garnaud, G., Amenitsch, H., and Ollivon, M. (2002). Monitoring fat crystallization in aerated food emulsions by combined DSC and time-resolved synchrotron x-ray diffraction. *Food Res. Int.* 35, 927–934.

Kolar, Z.I., Verburg, T.G., and van Dijk, H.J.M. (2002). Three kinetically different inorganic phosphate entities in bovine casein micelles revealed by isotopic exchange method. *J. Inorg. Biochem*. 90, 61–66.

Krog, N.J. (1997). Food emulsifiers and their chemical and physical properties. In: S.E. Friberg and K. Larson. *Food Emulsions*, Marcel Dekker, New York, pp. 141–188.

Larsson, K., and Krog, N. (1973). Structural properties of the lipid-water gel phase. *Chem. Phys. Lipids*. 10, 177–180.

Leser, M.L., Michel, M., and Watzke, H.J. (2003). Food goes nano: new horizons for food structure research. In: E. Dickinson and T. Van Vliet. *Food Colloids, Biopolymers and Materials*, The Royal Society of Chemistry, Cambridge, pp. 3–13.

Limbach, H.J., and Kremer, K. (2006) Multiscale modelling of polymers: perspectives for food materials. *Trends Food Sci. Technol*. 17, 215–219.

Link, D.R., Anna, S.L., Weitz, D.A., and Stone, H.A. (2004). Geometrically mediated breakup of drops in microfluidic devices. *Phys. Rev. Lett.* 92, 05403–05404.

Lopez, C. (2005). Focus on the supramolecular structure of milk fat in dairy products. *Reprod., Nutr., Dev.* 45, 497–511.

Lopez, C., Bourgaux, C., Lesieur, P., Bernadou, S., Keller, G., and Ollivon, M. (2002). Thermal and structural behavior of milk fat. 3. Influence of cooling rate and droplet size on cream crystallization. *J. Colloid Interf. Sci*. 254, 64–78.

Lopez, C., Lavigne, F., Lesieur, P., Bourgaux, C., and Ollivon, M. (2001). Thermal and structural behavior of milk fat. 1. Unstable species of anhydrous milk fat. *J. Dairy Sci*. 84, 756–766.

Lopez, C., Lesieur, P., Bourgaux, C., Keller, G., and Ollivon, M. (2001). Thermal and structural behavior of milk fat. 2. Crystalline forms obtained by slow cooling of cream. *J. Colloid Interf. Sci.* 240, 150–161.

Loren, N., Langton, M., and Hermansson, A.M. (1999). Confocal laser scanning microscopy and image analysis of kinetically trapped phase-separated gelatin–maltodextrin gels. *Food Hydrocolloids*. 13, 185–198.

Lucas, P.W., Prinz, J.F., Agrawal, K.R., and Bruce, I.C. (2002). Food physics and oral physiology. *Food Qual. Pref.* 13, 203–213.

Lucey, J.A., and Singh, H. (1997) Formation and physical properties of acid milk gels: a review. *Food Res. Int*. 30, 529–542.

Lucey, J.A., Tamehana, M., Singh, H., and Munro, P.A. (1998). A comparison of the formation, rheological properties and microstructure of acid skim milk gels made with a bacterial culture or glucono-D-lactone. *Food Res. Int.* 31, 147–155.

Lucey, J.A., Tamehana, M., Singh, H., and Munro, P.A. (2000). Rheological properties of milk gels formed by a combination of rennet and glucono-delta-lactone. *J. Dairy Sci*. 67, 415–427.

Lucey, J.A., Tamehana, M., Singh, H., and Munro, P.A. (2001). Effect of heat treatment on the physical properties of milk gels made with both rennet and acid. *Int. Dairy J*. 11, 559–565.

Lucic, V., Föster, F., and Baumeister, W. (2005). Structural studies by electron tomography: from cells to molecules. *Annu. Rev. Biochem.* 74, 833–865.

Man, D. (2004). *Shelf Life*, Blackwell Science, London.

Marangoni, A.G., and Narine, S.S. (2002). Identifying key structural indicators of mechanical strength in networks of fat crystals. *Food Res. Int.* 35, 957–969.

Mazzobre, M.F., Aguilera, J.M., and Buera, M.P. (2003). Microscopy and calorimetry as complementary techniques to analyze sugar crystallization from amorphous systems. *Carbohydr. Res*. 338, 541–548.

McMahon, D.J., and McManus, W.R. (1998). Rethinking casein micelle structure using electron microscopy. *J. Dairy Sci*. 81, 2985–2993.

Meyer, S., Hindle, S.A., Sandoz, J.P., Gan, T.H., and Hutchins, D.A. (2006). Noncontact evaluation of milk-based products using air-coupled ultrasound. *Meas. Sci. Technol*. 17, 1838–1846.

Mezzenga, R., Schurtenberger, P., Burbidge, A., and Michel, M. (2005). Understanding foods as soft materials. *Nat. Mater*. 4, 729–740.

Michalski, M.C., Ollivon, M., Briard, V., Leconte, N., and Lopez, C. (2004). Native fat globules of different sizes selected from raw milk: thermal and structural behavior. *Chem. Phys. Lipids.* 132, 247–261.

Miller, R., Fainerman, V.B., Aksenenko, E.V., Leser, M.E., and Michel, M. (2004). Dynamic surface tension and adsorption kinetics of β-casein at the solution–air interface. *Langmuir*. 20, 771–777.

Milner, J.A. (1999). Functional foods and health promotion. *J. Nutr*. 129, 1395–1397.

Milner, J.A. (2000). Functional foods: the US perspective. *Am. J. Clin. Nutr*. 71, 1654S–1659.

Murray, B.S. (2002). Interfacial rheology of food emulsifiers and proteins. *Curr. Oppin. Coll. Interf. Sci.* 7, 426–431.

Muse, M.R., and Hartel, R.W. (2004). Ice cream structural elements that affect melting rate and hardness. *J. Dairy Sci*. 87, 1–10.

Narine, S.S., and Marangoni, A.G. (1999a). Mechanical and structural model of fractal networks of fat crystals at low deformations. *Phys. Rev. E*. 60, 6991–7000.

Narine, S.S., and Marangoni, A.G. (1999b). Microscopic and rheological studies of fat crystal networks. *J. Cryst. Growth*. 198, 1315–1319.
Nilsson, L., and Bergenstahl, B. (2006). Adsorption of hydrophobically modified starch at oil–water interfaces during emulsification. *Langmuir*. 22, 8770–8776.
Norgaard, L., Hahn, M.T., Knudsen, L.B., Farhat, I.A., and Engelsen, S.B. (2005). Multivariate near-infrared and Raman spectroscopic quantifications of the crystallinity of lactose in whey permeate. *Int. Dairy J*. 15, 1261–1270.
Patton, J.S., and Carey, M.C. (1979). Watching fat digestion. *Science*. 204, 145–148.
Patton, J.S., Vetter, R.D., Hamosh, M., Borgström, B., Lindström, M., and Carey, M.C. (1985). The light microscopy of triglyceride digestion. *Food Microstr.* 4, 29–41.
Phadungath, C. (2005). Casein micelle structure: a concise review. *Songklanakarin J. Sci. Technol.* 27, 201–212.
Phan, C.M., Nguyen, A.V., and Evans, G.M. (2006). Dynamic adsorption of β-casein at the gas–liquid interface. *Food Hydrocolloids*. 20, 299–304.
Pisecky, J. (1997). *Handbook of Milk Powder Manufacture*, Niro A/S, Copenhagen.
Radford, S.J., and Dickinson, E. (2004). Depletion flocculation of caseinate-stabilised emulsions: what is the optimum size of the nonadsorbed protein? *Colloids Surf. A*. 238, 71–81.
Rahman, M.S. (2006). State diagram of foods: its potential use in food processing and product stability. *Trends Food Sci. Technol*. 17, 129–141.
Renard, D., van de Velde, F., and Visschers, R.W. (2006). The gap between food gel structure, texture and perception. *Food Hydrocolloids*. 20, 423–431.
Rigler, M.W., Honkanen, R.E., and Patton, J.S. (1986). Visualization by freeze fracture, in vitro and in vivo, of the products of fat digestion. *J. Lipid Res*. 27, 836–857.
Rodrguez Patino, J.M., Rodrguez Nino, M.R., Carrera Sanchez, C., and Cejudo Fernandez, M. (2001). The effect of pH on monoglyceride–caseinate mixed monolayers at the air–water interface. *J. Colloid Interf. Sci*. 240, 113–126.
Roefs, S.P.F.M., De Groot–Mostert, A.E.A., and Van Vliet, T. (1990). Structure of acid casein gels. 1. Formation and model of gel network. *Colloids Surf*. 50, 141–159.
Rollema, H.S.. and Brinkhuis, J.A. (1989). A 1H–NMR study of bovine casein micelles; influence of pH, temperature and calcium ions on micellar structure. *J. Dairy Res*. 56, 417–425.
Roos, Y. (1995). *Phase Transitions In Foods*, Academic Press, New York
Roos, Y., and Karel, M. (1991). Applying state diagrams to food processing and development. *Food Technol*. 45, 68–71.
Sagalowicz, L., Leser, M.E., Watzke, H.J., and Michel, M. (2006a). Monoglyceride self-assembly structures as delivery vehicles. *Trends Food Sci. Technol*. 17, 204–214.
Sagalowicz, L., Mezzenga, R., and Leser, M.E. (2006b). Investigating liquid crystalline mesophases. *Curr. Opp. Coll. Interf. Sci*. 11, 224–229.
Sagalowicz, L., Michel, M., Adrian, M., Frossard, P., Rouvet, M., Watzke, H.J., Yaghmur, A., de Campo, L., Glatter, O., and Leser, M.E. (2006c). Crystallography of dispersed self-assembly structures studied by cryo-TEM. *J. Microsc.* 221, 110–121.
Sagalowicz, L., Michel, M., Watzke, H.J., and Adrian, M. (2003). Advanced electron microscopy methods to characterise food colloids. *Sci. Technol. Educ. Microsc*., 557.
Sanchez, C., Zuniga-Lopez, R., Schmitt, C., Despond, S., and Hardy, J. (2000). Microstructure of acid-induced skim milk–locust bean gum–xanthan gels. *Int. Dairy J.* 10, 199–212.
Schmidt, D.G., Both, P., Van Markwijk, B.W., and Buchheim, W. (1974). The determination of size and molecular weight of casein micelles by means of light-scattering and electron microscopy. *Biochim. Biophys. Acta.* 365, 72–79.
Servais, C., Jones, R., and Roberts, I. (2002). The influence of particle size distribution on the processing of food. *J. Food Eng.* 51, 201–208.

Siegel, D.P., Burns, J.L., Chestnut, M.H., and Talmon, Y. (1989). Intermediates in membrane fusion and bilayer–nonbilayer phase transitions imaged by time-resolved cryo-transmission electron microscopy. *Biophys. J.* 56, 161–169.

Soderberg, I., and Ljusberg–Wahren, H. (1990). Phase properties and structure of a monoglyceride–sucrose–water system. *Chem. Phys. Lipids*. 55, 97–101.

Taifi, N., Bakkali, F., Faiz, B., Moudden, A., Maze, G., and Decultot, D. (2006). Characterization of the syneresis and the firmness of the milk gel using an ultrasonic technique. *Meas. Sci. Technol.* 17, 281–287.

Talmon, Y. (1996). Transmission electron microscopy of complex fluids: the state of the art. *Ber. Bunsenges. Phys. Chem*. 100, 364–372.

ter Beek, L.C., Ketelaars, M., McCain, D.C., Smulders, P.E., Walstra, P., and Hemminga, M.A. (1996). Nuclear magnetic resonance study of the conformation and dynamics of β-casein at the oil–water interface in emulsions. *Biophys. J.* 70, 2396–2402.

Thomsen, J.K., Jakobsen, H.J., Nielsen, N.C., Petersen, T.E., and Rasmussen, L.K. (1995). Solid-state magic-angle spinning ^{31}P–NMR studies of native casein micelles. *Eur. J. Biochem.* 230, 454–459.

Tuinier, R., and Kruif, C.G.d. (1999). Phase behavior of casein micelles–exocellular polysaccharide mixtures: experiment and theory. *J. Chem. Phys*. 110, 9296–9304.

Tuinier, R., and Kruif, C.G.d. (2002). Stability of casein micelles in milk. *J. Chem. Phys*. 117, 1290–1295.

Tuinier, R., Rieger, J., and de Kruif, C.G. (2003). Depletion-induced phase separation in colloid–polymer mixtures. *Adv. Colloid Interf. Sci.* 103, 1–31.

Unwin, N. (1995). Acetylcholin–receptor channel imaged in the open state. *Nature*. 37, 373.

Urban, C., and Schurtenberger, P. (1998). Characterization of turbid colloidal suspensions using light scattering techniques combined with cross-correlation methods. *J. Colloid Interf. Sci*. 207, 150–158.

Uricanu, V.I., Duits, M.H.G., and Mellema, J. (2004). Hierarchical networks of casein proteins: an elasticity study based on atomic force microscopy. *Langmuir*. 20, 5079–5090.

van der Graaf, S., Schroen, C.G.P.H., van der Sman, R.G.M., and Boom, R.M. (2004). Influence of dynamic interfacial tension on droplet formation during membrane emulsification. *J. Colloid Interf. Sci*. 277, 456–463.

Vasbinder, A.J., van Mil, P.J.J.M., Bot, A., and de Kruif, K.G. (2001). Acid-induced gelation of heat-treated milk studied by diffusing wave spectroscopy. *Colloids Surf. B*. 21, 245–250.

Vuataz, G. (2002). The phase diagram of milk: a new tool for optimising the drying process. *Lait*. 82, 485–500.

Waninge, R., Nylander, T., Paulsson, M., and Bergenstahl, B. (2003). Milk membrane lipid vesicle structures studied with cryo-TEM. *Colloids Surf. B*. 31, 257–264.

Ward, R., Watzke, H., Jiminez, F.R., and German, J. (2004). Bioguided processing: a paradigm change in food production. *Food Technol*. 58, 44–48.

Won, Y.-Y. (2004). Imaging nanostructured fluids using cryo-TEM. *Korean J. Eng*. 21, 296–302.

Yaghmur, A., de Campo, L., Sagalowicz, L., Leser, M.E., and Glatter, O. (2005). Emulsified microemulsions and oil-containing liquid crystalline phases. *Langmuir*. 21, 569–577.

Ye, A., Singh, H., Taylor, M.W., and Anema, S. (2002). Characterization of protein components of natural and heat-treated milk fat globule membranes. *Int. Dairy J*. 12, 393–402.

Zheng, Y., Lin, Z., Zakin, J.L., Talmon, Y., Davis, H.T., and Scriven, L.E. (2000). Cryo-TEM imaging the flow-induced transition from vesicles to threadlike micelles. *J. Phys. Chem.* 104, 5263–5271.

STRUCTURING OPERATIONS

Chapter 12

Structure–Property Relationships in Foods

José M. Aguilera[1] and Peter J. Lillford[2]

[1] Pontificia Universidad Católica de Chile, Department of Chemical and Bioprocess Engineering, Vicuña Mackenna 4860, Santiago, Chile, jmaguile@ing.puc.cl
[2] University of York, Department of Biology, PO Box 373, York, YO10 5YW, UK, PL8@york.ac.uk

12.1 Introduction

Structure–property relationships, the connection between the structure and the way a product behaves, is central to materials science and product engineering and design. For example, understanding the relationship between structure and specific physical properties is crucial for ultimately designing advanced materials and nanomaterials. For traditional engineering materials, finding structure–property relationships is somewhat easier than for foods because specific properties are well defined (e.g., strength, electrical conductance, etc.), measured with precise instruments and usually intrinsic to the structure of the final product. Also, the microstructures involved are those of more or less homogeneous materials (simple as it may appear, they do not contain water!) and are required not to change appreciably with time.

Even where structure–property relationships are still poorly understood from a fundamental point of view, a vast body of experience exists on how to change the structure to improve the properties. This empiricism is very common in food fabrication. Generations of cooks have produced the recipes used in kitchens throughout the world. However, modern food manufacture cannot rely on or translate much of this knowledge into high volume, efficient food manufacture.

In foods, structure matters because it is responsible for many of the desirable properties, such as appearance, texture, and even flavour release. However, unlike other composites that are designed to provide final physical and mechanical properties from the structure (e.g., load-bearing bridges, impact-resistant fibre composites, etc.), food structures must break and fail under chewing action; otherwise they are not consumable food. In a sense, physical properties of foods are opposite to those valuable to engineers. The search for relations between the structure and physical properties of foods started only in the 1980s. [See e.g., several chapters in Peleg and

Bagley (1983) and Blanshard and Lillford (1987) dealing with qualitative structure–property relationships in meats, plant foods and baked products]. Evidence is now accumulating that structure does play a key role in controlling many other attributes important in foods beyond their basic physical or engineering properties. For example, structure is critical in texture perception (Hutchings and Lillford 1988), flavor release (Taylor 2002) and the bioavailability of some nutrients (Aguilera 2005).

12.2 Properties

12.2.1 Two Axes for Food Properties

The design challenges to food fabricators have evolved and expanded through time. Until the late 1980s the main properties assessed by scientists were those associated with the physical states of products as they moved from producers to consumers along the supply chain (Figure 12.1).

In the developed world, the last 10 years have seen the direction of the producer-to-consumer axis reversed. Now consumers' expectations largely dictate how foods are produced, processed and delivered as products compete in a well-supplied market. Nowadays additional demands are present either implicitly (e.g., care of animals or fish before slaughter, environmental impact during production, traceability) or explicitly (e.g., convenience, safety, health benefits). This constitutes the new consumer-to-producer axis also described by the term "from fork-to-farm." The emerging concerns of consumers for health and well-being ("I am what I eat") has identified

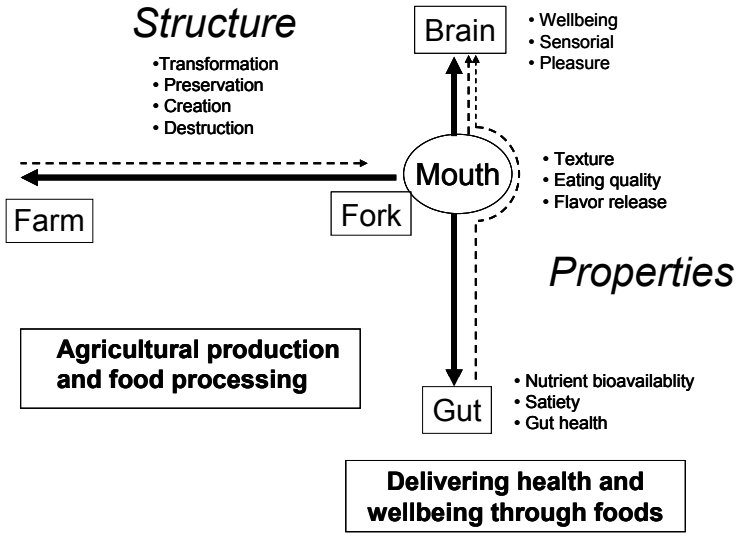

Figure 12.1. Two axes define the properties of foods: Horizontal, the *fork-to-farm* (demand) axis; vertical, the *gut–brain* axis.

new food properties targeted at the brain–gut axis (Figure 12.1) and will increasingly be the discriminating attributes that determine success in the marketplace.
Although the connection between the gut function and the health of the body and brain has been known to the medical profession for more than a century, the industry has only recently begun to exploit the positive role of factors present in food that contribute to oxidative-stress reduction, anticarcinogenicity, blood glucose regulation, body weight reduction, gastrointestinal improvement, and even long-term effects on memory and short-term effects on mood and physical performance. While most of these effects are attributable to small amounts of bioactive molecules or their precursors, it has been found that structure does play a key role in protection, delivery and targeting (see Chapter 24). For example, probiotic bacteria need to be protected in designed matrices to improve their stability during the passage to the large intestine, while the glycemic response may be lowered by limiting the accessibility of starch by enzymes in the gut through proper structuring. Some of the most important food properties that are now relevant are presented in Figure 12.2.

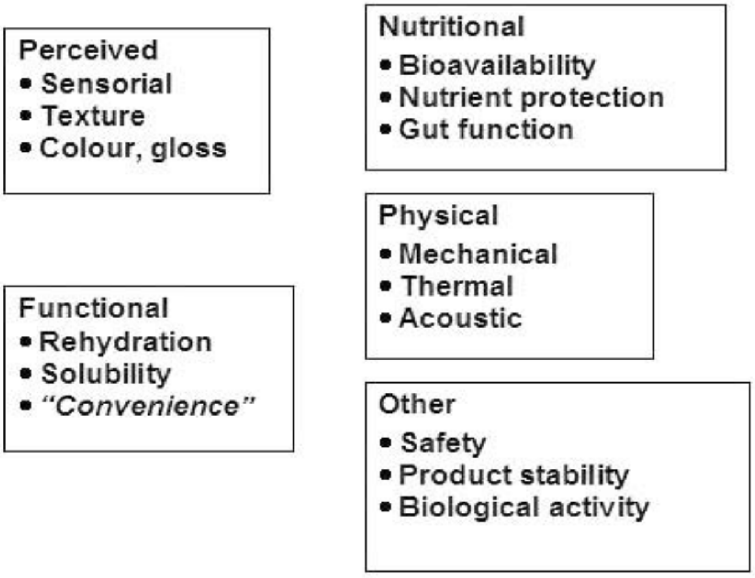

Figure 12.2. Important food properties.

12.2.2 Texture

Because texture is such an important property in foods, a brief discussion of its meaning, quantification and implications is presented. The term *texture* refers to an elusive but important quality attribute of foods that is difficult to measure or analyze. Nevertheless, it is clear that whether testing is performed in our mouth or by an engineering device, what is being measured is the manifestation of the structural

organization of the food material and its breakdown. An early definition of texture was "the sensory and functional manifestation of the structural and mechanical properties of foods, detected through the senses of vision, hearing, touch and kinesthetics" (Szczesniak 1998). Others identified that consumers perceived texture as the total sequence of structural breakdown during the entire mastication process (Hutchings and Lillford 1988).

Examination of the words required by consumers to describe their perception of texture makes it evident that attributes of foods are perceived during mastication, a process by which a solid food is torn, ripped, crushed and ground, mixed with saliva so that a bolus is formed that can be swallowed and digested. Considering that food texture is sensed through the response of nerve endings throughout the mouth and that these signals are integrated in the brain, it is easy to understand that texture can only be evaluated by humans, and whereas similar attributes are perceived by all of us, their integration into a quality judgment may result in different preferences. (e.g., levels of toughness/juiciness of meat). As occurs in any material, the mechanical properties of a food are a reflection of the structural arrangements of elements in the microstructure; hence, perception of the breakdown of structure in the mouth and the concomitant kinetics of bolus formation are directly related to the perceived texture. In addition to this direct effect on texture, structure breakdown during texture perception in the mouth modulates the amount and rate at which flavours are released from the food matrix (Taylor 2002).

Sensations perceived in the mouth during mastication may vary between subjects, but their acceptability will certainly reflect cultural as well as physiological and psychological differences. Tests for sensory assessment of texture aim at understanding "how the food feels in the mouth." They may be classified into those where consumers are constrained to record only their perception of in-mouth stimuli (e.g., trained panel assessment); in other words, they are asked to perform as an analytical instrument. Alternatively, consumers are asked to record their judgment against requirements of quality (e.g., preference testing) where perceptions are related to expectation. Sensory assessment of texture is described in many texts, for example, Kilcast (2004).

12.2.3 Quantifying Texture in Solid Foods

Notwithstanding all the limitations involved, the continuous improvement in precision and reproducibility of physical measurement equipment that relate to parameters perceived by human subjects make their use straightforward and they can provide consistent results. It is important to keep in mind that although instruments allow precise and objective measurements if applied to whole foods, they only can account for the initial structural properties contributing to texture perception. A correlative approach using sensory and instrumental techniques is often necessary. Indeed, there is no reason to determine accurately a mechanical property if it is not relevant to human sensory perception. Sensory methods become essential when calibrating instrumental equipment and are fundamental in product development, especially at early stages.

Although mechanical methods that measure texture parameters are widely used, their destructive nature is not suitable for on-line sorting of whole product, or to monitor changes through storage of a food product. For these quality assurance measures, noninvasive methods using noncontact devices have recently gained considerable interest (Figure12.3). Output data then need to be correlated with other instrumental parameters or sensorial information for validation. Juodeikiene and Basinskiene (2004) utilized acoustic spectrometry to assess the texture of porous cereal products and found good correlations between the amplitude of the penetrated acoustic signal and the mechanical strength for wafers ($r^2 = 0.92$) and crisp bread ($r^2 = 0.96$). Qiao et al. (2007) reported that indices derived from an image of products correlated well ($r^2 > 0.84$) with mechanical data such as maximum load and toughness developed by frying of chicken nuggets. MRI images also show promise in correlating with sensorial data of pork loins (Cernadas et al. 2005). Less-promising results have been obtained when using ultrasonic waves to predict the mealiness of apples, or the use of near-infrared spectroscopy to test the mealiness of peaches— probably because these sensory parameters relate to later stages of mastication and are not obviously related to the structure of the initial product.

The materials behaviour of several foods during chewing has been documented, at least qualitatively (Lillford 2000a). In each case a common process of structural breakdown and reassembly can be identified, up to the point of swallowing. It was proposed that the mechanical properties of not only the original structure but all of the transiently perceived fragments are measured and that perceived "texture" is the sum of all these attributes. Preference or quality judgments are then related to the performance of any given sample relative to previous experience of that particular named food type. A consequence of this proposal is that an instrument (or instruments) is

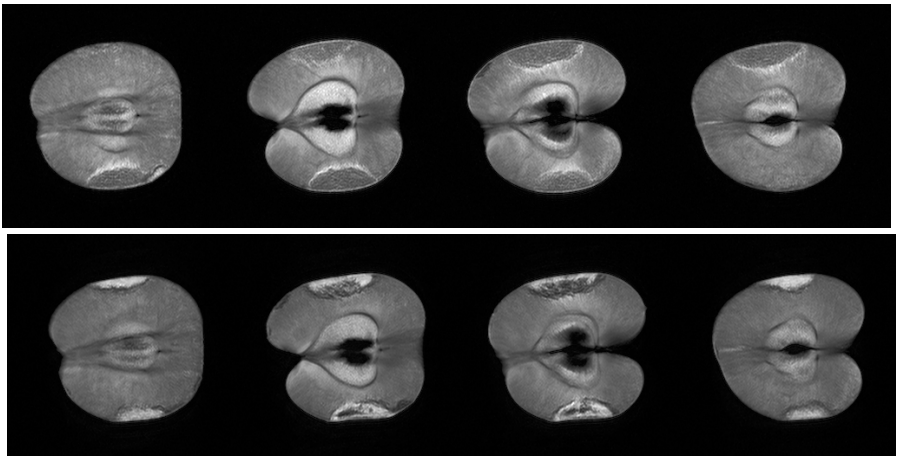

Figure 12.3. Internal bruising affects texture and acceptability of fruits but is hardly detected by inspection of the outer surface. Nondestructive visualization of internal bruising in a single apple by MRI. *Above*: Sections at time 0. *Below*: Evolution after 10 days.

necessary that similarly measures all these parameters and furthermore assembles the data in a similar weighted fashion. Otherwise, we cannot expect accuracy in prediction of either perceived or preferred texture from instrumental measures.

12.3 Food Microstructure

12.3.1 Structure

All definitions of food microstructure emphasize three key aspects: (i) the presence of identifiable discrete elements or domains, (ii) some kind of organization among these elements in space (architecture), and (iii) the presence of interactions. For example, a thin slice of raw potato under the microscope shows discrete cells bound at their cell walls and containing starch granules in their aqueous interior. This structural information is the minimal requirement to begin a study of the cooking of potatoes, since each of these elements can respond individually to the external variables. The properties of the composite potato will not be a simple sum of the contributing changes in structure and unlikely to be related simply to temperature and time.

To be rigorous, we know that food structuring starts at the molecular level and processing can modifying the "structure" of molecules that then have to be proven functional and safe. Molecular functionality may mean the absence of an allergenic response, delivery of an antimicrobial effect or a sweet taste, and so on. However, we wish to explain how molecular structure affects product microstructure and its properties. Higher levels of molecular organization depend on the interplay between intermolecular and external forces. Self-assembly processes at the mesoscale are known to occur in proteins and lipids and are dealt with in Chapters 9 and 17, respectively. On a larger scale and in the realm of polymer physics, phase separation and network formation may take place providing new microstructural elements. Dispersed phases formed by particles, bubbles, crystals, droplets, and so on, are clearly discernible with a simple light microscope. At the next structural level, these composites can be further organized and set into anisotropic structures (see Chapter 18). It is self-evident that a range of measurement techniques covering the range of relevant structural dimensions will be necessary, if we are really to understand the structural properties delivered by any complex food.

12.3.2 Formation of Food Structures

Throughout evolution humans have received nutrients in the form of palatable foods that have often been associated with the sensations experienced during mastication. All foods, whether consumed with minimal preparation or after processing, are derived from nature. The "natural" structures from which foods are created may be classified into four broad categories: (1) Fibrous structures assembled hierarchically from macromolecules into tissues for specific functionality (e.g., muscles) and held together at different levels by specific interfacial interactions; (2) fleshy materials from plants that are hierarchal composites of hydrated cells that exhibit turgor pressure and are bonded together at the cell walls (e.g., tubers, fruits and vegetables); (3) encapsulated embryos of plants that contain a dispersion of starch, protein and

lipids assembled into discrete packets (e.g., cereals, nuts and pulses); and (4) a unique complex fluid called milk, intended for nutrition of the young mammal containing several nutrients in a state of dispersion.

Some foods are eaten around the world either with no processing that modifies this structure (e.g., fresh fruit and vegetables, nuts, fluid milk), with minor processing for microbial safety and texture (e.g., meat, fish, vegetable roots and tubers), or with major processing to create new structures for the enjoyment of their textures and flavors. It is not surprising that the food industry produces, at a large scale, food textures and structures that we enjoy. The motivations for the continuous stream of structured products include: (i) expand the variety and appeal of conventional food sources (e.g., ice cream from milk, snacks from cereals); (ii) improve the stability and convenience, for example, dried foods, instant and precooked products; (iii) add value to ingredients and by-products, for example, extruded products from powders and processed meats; (iv) introduce into the food chain inedible or underutilized sources of nutrients, (e.g., cereal grains, and, more recently, fish meal from lower quality marine organisms and residues); and (v) respond to health requirements by lowering the caloric content or conveying potentially beneficial bioactive compounds.

Foods are nonequilibrium structures stabilised by relatively weak forces. As engineered structures they are "poor," because they change appreciably with time. As a consequence, properties vary in both beneficial and deleterious directions. For example, fresh cheeses with soft textures are recommended to be consumed soon after production, while ripened cheeses develop desirable aromas and more complex structures and textures after storage. The metabolic activity of fruits and vegetables continues after harvesting with concomitant changes in microstructure, flavour and taste components. The skill of the modern food distributor is to control this biological senescence so that fruit with the exact ripeness arrives on our supermarket shelf. The hygroscopic behavior of most dry foods and the ubiquitous presence of moist air, plasticizes vitreous phases, thus changing their physical properties. For example, most low-moisture baked or extruded products such as breakfast cereals, biscuits and snacks lose their crispness as they adsorb water from the atmosphere.

The hard-to-cook phenomenon (HTC) in stored dry legumes (or the inability to soften after cooking) illustrates many of the complexities of foods as materials. HTC, responsible for enormous physical losses as well as increased energy consumption for cooking in tropical countries, is favored in the natural high relative humidity and high temperature of those climates. Physiologically, it is a false senescence process as dry beans continue to respire during storage, becoming "old" at a faster rate. Tougher textures after standard cooking (e.g., 2 hr in boiling water) correlate well with instrumental hardness.

Figure 12.4 depicts the correlation between instrumental texture measured by the force required in a penetration test of cooked beans and the microstructure of hard and soft cotyledons. Individuals also discriminate between hard and soft beans as they are compressed between molars. In soft beans, individual cells, whose middle lamella have been dissolved during cooking, slide one past another during compression. Hard beans with undissolved cell walls cells feel tougher because they are fractured across the cotyledons. Think of how effortless it would be to tear down a brick wall that had no mortar binding the bricks.

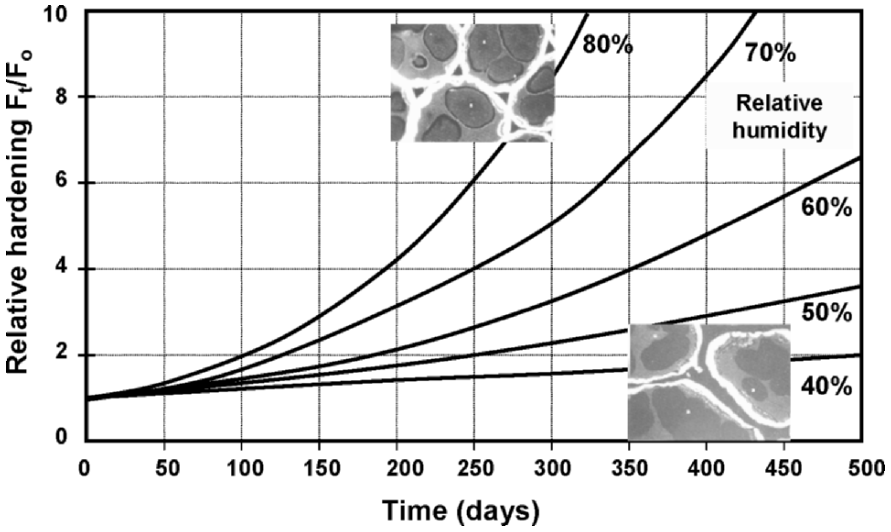

Figure 12.4. Hardening of dry beans stored at 32°C and at different relative humidity measured as the penetration force after standard cooking. Curves show relative hardness (i.e., force at time 0 divided by force at any time after storage) as a function of storage time. Inset: Light micrographs of cotyledons of hard (*upper*) and soft beans (*lower*). Notice separation of cells in soft cooked beans.

In contrast to natural structures the morphological features of structures in fabricated foods are in principle within our control. The source of the many structures of foods, even those made from a single raw material (e.g., wheat flour), lies in the ingredient mix and the fact that thermodynamic equilibrium is practically never required or achieved during processing. These metastable structures can be attained because they are favored kinetically, that is, the approach to equilibrium is slow. At any point during the development of a particular structure a process of shape stabilization sets in, usually by vitrification, partial crystallization, phase separation and/or formation of a network (Figure 12.5).

It can be concluded that the morphology or the form and structure of foods is strongly dependent on processing conditions, in particular, time, temperature and shear. Furthermore, from the evidence and arguments presented above, it is obvious that the properties of a food product are more related to the architecture (i.e., how the formed elements relate to one another) than to the composition itself.

12.3.3 Probing the Microstructure

Chapter 11 deals with methods and techniques used to examine the microstructure of foods. In trying to relate microstructure and food properties the main problem is selecting the relevant scale at which elements interact to produce a given behavior or

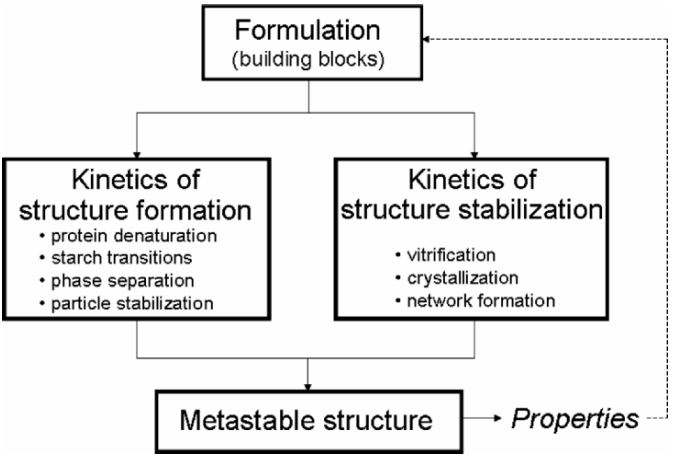

Figure 12.5. Formation of structures in processed foods is a delicate balance between the kinetics of structure formation and that of structure stabilization. Most of the time the result is a metastable structure.

effect. In complex, multicomponent systems such as foods this is a major task because interactions may occur at different length scales from molecules to the macroscale, and may extend as well many decades on the time scale. Figure 12.6 depicts important elements and phenomena associated with bubble formation and stability of food foams.

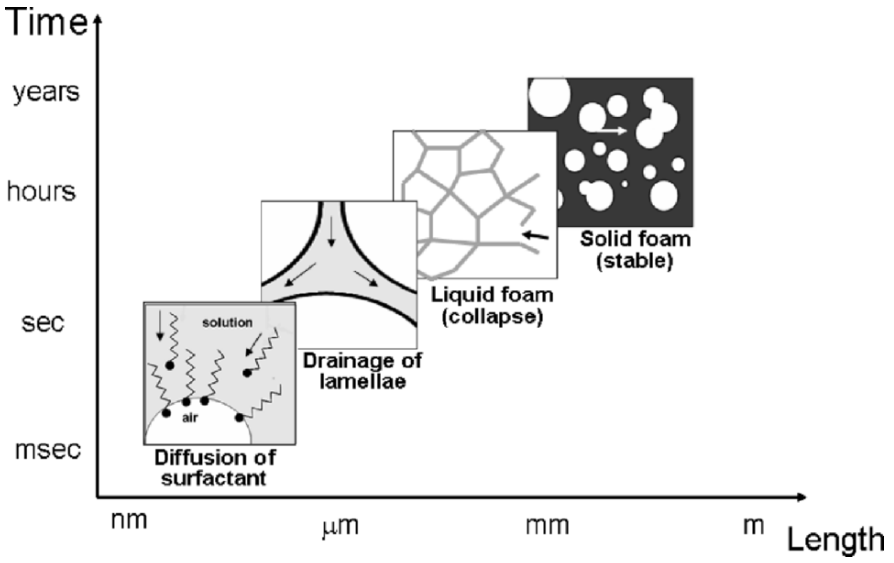

Figure 12.6. Scheme showing the approximate length and time-scales in important phenomena related to the formation of bubbles and stability of food foams.

A number of researchers have identified the value of examining structure formation and structure collapse. As a result, the trend is towards the use of non-destructive and noninvasive techniques, and coupling imaging with physical and chemical probing. For example, a hybrid instrument combining a deformation tool and the ESEM to image has been used to study the fracture of carrots (Thiel and Donald 2000). Microscope testing stages of various configurations has been developed to observe the effect of deformation modes (e.g., shearing, extension, compression, etc.), on gel particles and droplets in a fluid, simulating conditions in oral processing (Nicolas et al. 2003). Hot-stages placed under the microscope's lens provide opportunities to examine nondestructive changes in microstructure induced by thermal treatment.

12.3.4 Quantifying the Microstructure

> "*Measure what can be measured, and make measurable what cannot be measured.*"
> Galileo Galilei, as quoted by J. Gaarder in his book "Sophie's World"

It would be an oversimplification to assume that the use of more powerful and sophisticated microscopes and the ample availability of images will automatically lead to a more useful knowledge of the microstructure of foods. Although the proverb says that "an image is worth a thousand words," the human visual system is not well suited to make objective and quantitative determinations of features that we see in images.

Most foods are heterogeneous materials composed of elements or domains where the length scale of heterogeneity spans between hundreds of nanometers to several hundred microns. With the emergence of the digital image (i.e., a matrix array of pixel values ranging from 0 to 255) and the development of image processing techniques, relevant features can be identified in photomicrographs at different magnifications and quantitative data derived thereof. The diverse nature of properties that we are concerned with has led us to define a wide variety of microstructural descriptors specific for each particular food.

The subject of image processing and image analysis is too specialized to be treated in a chapter like this. The reader is referred to Russ (2004) and Aguilera and Stanley (1999) for an introduction to the subject of image analysis as applied to foods. Image analysis software is available (both commercial and free via the Internet) to extract morphological parameters (i.e., those related to the form of objects) from 2-D images, and to perform 3-D reconstructions. Through segmentation techniques, different objects or elements as they appear in the 2-D image can be isolated and their shapes identified. The extraction of quantitative information such as the number of objects, diameters, areas and distances is then quite simple. An interesting application is *sterology*, whereby inference about dimensions of 3-D objects can be made from areas of intersection from randomly positioned cutting planes (e.g., cells diameter from several 2-D sections).

Another method used for data analysis of non-Euclidean objects is fractals. A true fractal object is scale invariant (i.e., exhibits self-similarity); thus a fractal dimension is obtained from the outline of an object by varying the scale of analysis. The fractal dimension (*FD*) of an irregular geometry is a measure of the space-filling

potential. Thus, a jagged line fills more space than a straight line ($D = 1$) but less than a polygon ($D = 2$) and a rough surface occupies more volume than a plane but less than a cube ($D = 3$). It turns out that for jagged lines $1 < FD < 2$ and for rough surfaces $2 < FD < 3$. A review of fractals and their applications to foods is discussed in Peleg (1993); their use to describe microstructures is presented in Quevedo et al. (2005) and Lu and Hellawell (1995). In fact, most images for which a fractal dimension can be calculated are not true fractals, but the following power law relation can be established:

$$M_\delta \approx \delta^{FD} \tag{12.1}$$

where M_δ is a measurement performed and δ is the scale at which the measurement is made. Suppose that we want to calculate the total surface area (M_δ) of a piece of chocolate by fitting the topography data obtained by laser microscopy (i.e., resolution better than 3 μm). We can use a triangular tile to join three values of height. As the scale (or area) δ of the tile diminishes the total surface area increases, because smaller tiles can fit better the intricacies of a rough surface. The slope of the line from a plot of log M_δ versus log δ is the *FD* obtained by this method. Figure 12.7 shows that the *FD* of the surface of chocolate increases during storage meaning that it gets rougher due to recrystallization of cocoa butter that has migrated to the surface.

The Fourier transform is an important image processing tool that is used to decompose an image into its sine and cosine components. The output of the transformation represents the image in the Fourier or frequency domain, while the input image is the spatial domain equivalent. In the Fourier domain image, each point represents a particular frequency contained in the spatial domain image. Loren et al. (2006) have used Fourier analysis to describe the complex shape of aggregates, water domains and gel particles in food microstructures.

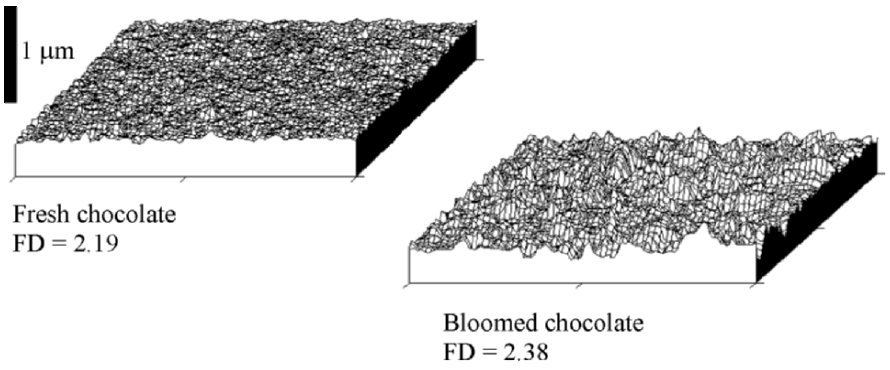

Figure 12.7. Topography of the surface of chocolate as determined by laser scanning microscopy. Fractal dimensions were calculated from a Richardson plot using SURFRAX®. A completely flat surface would have a $FD = 2.00$.

Often it is of interest to derive structure–property relationships that depend not only on geometrical features of objects but on the interrelation among them. For example, it would be interesting to know if two phases are simply interdispersed or interconnected (e.g., through pores). Correlation functions can be calculated that statistically characterize these types of microstructures (Torquato, 2002).

When it comes to demonstrating structure–property relationships for a food product data characterizing the structure (e.g., object dimensions, circularity, etc.), should be treated with the same rigor as the experimentally measured physical parameters. This means that the intrinsic heterogeneity of biological tissue and multicomponent processed foods as well as intersample variability has to be resolved first. This is one reason why nodestructive, real-time microscopy observations are preferred because at least sample variability is eliminated (although the observed sample may not be representative of the whole product!)

12.4 Structure–Property Relationships

12.4.1 Examples of Structure–Property Relationships in Foods

Food materials science is a search for basic knowledge about properties and their relation to structure. In many cases causal connections have been found between key structural features and product behavior or processing parameters (Table 12.1). Understanding the mechanisms and the science behind structure–property relationships would accelerate the prototyping stages, shorten times of product and process development, and reduce costs.

Table 12.1. Key structural features of foods and some documented properties.

Food	Key structural feature	Property
Ice cream	Ice crystal size	Sensorial “smoothness”
Meat	Intact connective tissue	Sensorial “toughness”
Freeze-dried coffee	Size of surface pores	Color
Fruits	Pore size	Impregnation with solutes
Apples	Cell turgor	Sound during biting
Tomatoes	Cell wall damage	Bioavailability of lycopene
Instant soup	Dextrinization of starch granules	Viscosity
Oilseeds	Obliteration of cellular structure	Diffusion of oil

12.4.2 Structure–Property Relationships in Casein Gels

Many desirable properties of foods, particularly texture, are experienced during mastication and derived directly from the microstructure. Crispness found in many fruits and vegetables is largely associated to the brittle fracture of prestressed cell walls containing liquid-filled vacuoles. Beans that after cooking normally exhibit incomplete solubilization of the middle lamellae cementing cells become fractured during mastication across cells (rather than along the intercellular spaces as in soft cooked beans) and feel tough.

Transgranular and intergranular fracture is common in some brittle engineering materials with a microstructure composed of multiple adjacent grains, and similar

processes occur in chocolate, giving it its "snap" properties (Narine and Marangoni 1999). Undissolved collagen linking the fibers of cooked meat is partly the cause of toughness (Lillford 2000b). The sensation of crispness in dry cellular foods such as potato chips and crackers is accompanied by sounds originating from the crack propagation velocity during fracture and vibrations of the broken cell walls (Lillford 2000a). As may be appreciated, different structural elements having dimensions spanning from nanometers to microns are responsible for specific properties. However, literature in which microstructural evidence is linked to data on physical, sensorial and nutritional properties is rare.

Gel structures are ubiquitous in foods and responsible for many of their physical properties. The space-filling network of polymers or aggregates provides solidlike properties in the presence of an enormous amount of water. They are a form of solid water at ambient temperature and in fact they are used to immobilize free water in dietetic products. Gels have been extensively used as model systems to study structure–property relationships due to their simple biphasic nature and the fact that the kinetics of structural changes can be continuously followed by oscillatory rheometry.

Casein gels are unstable structures whose properties change with time. Mellema et al. (2002) studied the increase in storage modulus G' with time during aging of rennet-induced casein gels. In another paper they reported changes in gel structure observed by confocal scanning laser microscopy (Mellema et al. 2000). Gel aging resulted in coarsening of the structure reflected by the gradual formation of larger pores and of compact aggregates in the gel matrix (Figure 12.8). The final G' values relate nicely with microstructure. Stronger gels (aged at pH 6.6) exhibited a more extended continuous matrix formed by protein strands. At pH 5.5 the protein network had been rearranged into dense aggregates (dark blobs) leaving almost no strands linking them, thus, the lower G' value.

12.4.3 Modeling

Assuming that structural data are available, and that a property has been correctly measured, the next problem is to establish a relationship. Fundamental models are preferred by engineers because they are based on basic principles of physics and the physical chemistry of the described phenomenon. Once it is realized that foods are essentially composite hierarchical structures, we can borrow models and theories developed for nonfood systems and apply them. A good example is the adaptation of mechanical principles for the description of cellular solids, (Gibson and Ashby 1988) to the properties of solid food foams (Attenburrow et al. 1989; Warburton et al. 1990). Examples are provided in Chapter 10.

Empirical models are often derived using linear, "best fit" combinations of measured parameters. For these models, no physical significance can be assigned to the parameters or their weighting terms. They can only be used for interpolation within the specific system that has been measured (Peleg 2006).

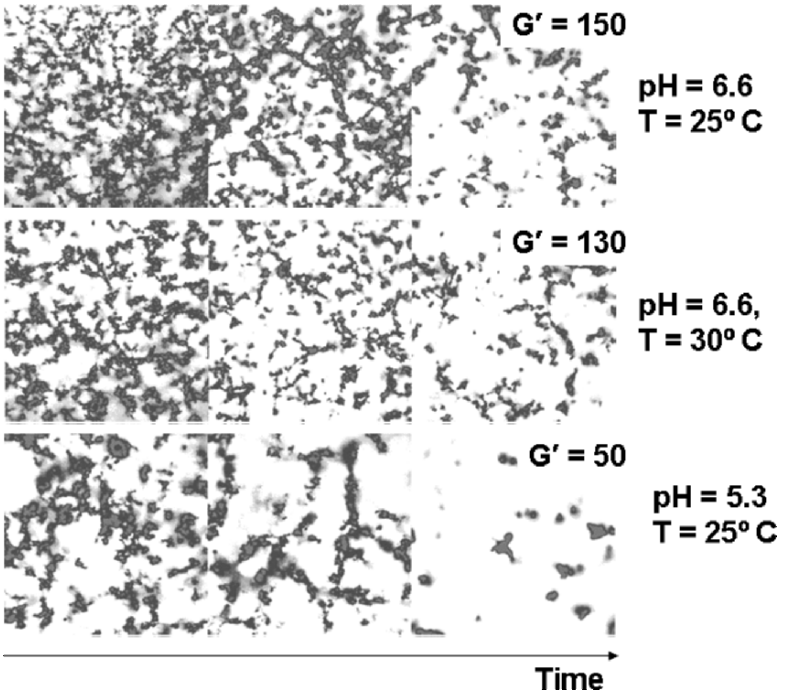

Figure 12.8. Changes is microstructure of rennet-induced casein gels aged under different conditions and the respective final G' values. Dark blobs represent aggregates of high protein concentration. Picture frames are ~90 × 90 μm. (Adapted from Mellema et al. 2000.)

12.4.4 Mechanical Models for Composite Food Gels

Several food gels include in their formulation more than one type of gel-forming material. Often a blend of gelling polymers provides superior properties (e.g., gel strength) and cost advantages. Mixed gels are formed by more than one gelling species, and composite gels are those having reinforcing elements such as membrane-modified fat globules or gelatinized starch granules.

A detailed example is taken from Aguilera and Baffico (1997) for a composite gel of whey protein isolate (WPI) and potato starch. Native starch is often added to heat-set gels (e.g., those made of egg white, WPI or washed fish protein) to improve the gel strength. This is amazing since starch gels are relatively weak. The ability to improve the mechanical properties of protein gels is related to the *in situ* hydration and swelling capacity of native starch as it undergoes gelatinization during heating.

Hydration of starch during gelatinization (ca. 65°C) removes water from the system, leaving behind a concentrated protein solution in which swollen starch granules are dispersed. As temperature increases further (e.g., 75°C for WPI) the protein solution sets into a strong continuous gel matrix around the hydrated granules (as a general rule, the compressive strength of a protein gel varies with $[\text{protein}]^2$). Provided that

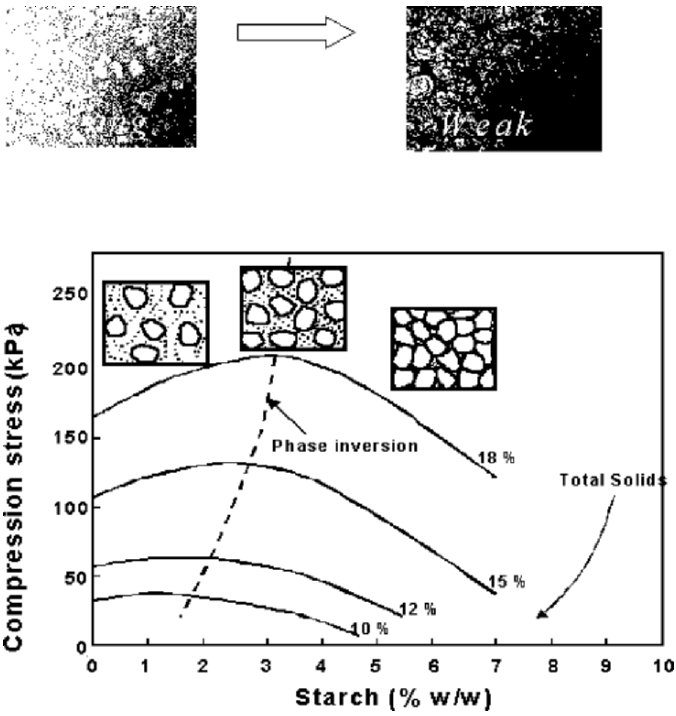

Figure 12.9. Effect of replacing protein by native potato starch on the compression strength of whey protein isolate gels prepared by heating to 85°C. Insert: Corresponding microstructures. Numbers in curves represent the total solid content of the starting dispersions. *Above*: Light photomicrographs of a strong mixed gel (protein continuous matrix) and a weak mixed gel (swollen starch is the continuous phase). Adapted from Aguilera and Baffico (1997).

the continuous gel matrix is protein, the composite gel is stronger than a pure protein gel of the same nominal concentration. If too much native starch is added then the swollen starch granules become the continuous phase and the gelled protein occupies the interstitial spaces. In this case the mechanical properties of the composite fall dramatically (Figure 12.9). The net result is that curves relating gel strength and starch concentration at different total solid contents (protein + starch) exhibit a maximum.

A mechanical model that has been successfully applied to phase-separated systems and composites is that of Takayanagi et al. (1963) which relates the overall modulus of the composite to those of the individual phases and their respective volume fractions. If the matrix is stronger than the filler, the overall modulus of the composite is given by:

$$G_c = G_x\phi_x + G_y\phi_y \tag{12.2}$$

where G represents a modulus; ϕ the volume fraction of the respective phases; and the subindices c, x and y mean composite, component 1 and component 2, respectively. When the matrix is weaker than the filler the following expression holds:

$$\frac{1}{G_c} = \frac{\phi_x}{G_x} + \frac{\phi_y}{G_y} \tag{12.3}$$

Curves in Figure 12.9 show the prediction of Takayanagi's model for the strength of the composite gel. Fitting to the actual data was good (data not shown). The advantages of having a mathematical model are quite obvious. First, the effect of adding starch to the protein solution on gel strength is clearly predicted. Second, a composite gel of any desired consistency can be formulated by adjusting the total solids content or the amount of added starch. Since the cost of starch is much lower than that of WPI, replacing protein by starch is a convenient way to lower product costs.

In the case that the composite is filled with rigid particles featuring some adhesion, the so-called Kerner equation (Kerner 1956) can be used to estimate the modulus of the composite:

$$G = G_m \left[1 + \frac{15(1-\nu)}{8-10\nu} \frac{\phi}{1-\phi} \right] \tag{12.4}$$

where G_m is the modulus of the matrix, ϕ is the volume fraction of particles and ν the Poisson ratio for the matrix. There are several models available to describe the modulus and other mechanical parameters of composites once morphological data (e.g., ϕ) becomes available. (See, e.g., Manski et al. 2006; Bliznakov et al. 2000). Interestingly, these models do not take into account the size or shape of the filler particles and their distribution within the matrix.

12.4.5 Flow Models for Complex Fluid Foods

Most liquid foods that we ingest are complex fluids. They may contain polymer molecules in solution and fibers or particles (rigid and deformable) in suspension, and exhibit non-Newtonian behaviour. This complex rheology can be related to their perceived properties (Shama and Sherman 1973). While rheometry gives quantitative data, it does not per se provide an insight into the fluid structure. Thus, microscopy and scattering methods are often used to characterize the fluid structure and flow-induced structural changes. What is relevant to this section is that several expressions are available relating viscosity data with variables that depend on the "structure" of a fluid. The subject of structured fluids is treated in detail in the book by Larson (1999).

The simplest model to predict the viscosity of liquids containing solid particles is that derived for a dilute suspension of uniform, monodisperse, noninteracting hard spheres in a solvent of viscosity η_s:

$$\eta = \eta_s \left(1 + 2.5\phi\right) \tag{12.5}$$

where ϕ is the volume fraction of spheres. Note that there is no effect of particle size and that all structural effects are assigned to ϕ. When interactions between spheres are important, higher-order terms in ϕ are added to the previous expression. A theoretical model is only available for extensional viscosity (Barnes et al. 1989):

$$\eta = \eta_s \left(1 + 2.5\phi + 6.2\phi^2\right) \tag{12.6}$$

In general, these formulas hold well for $\phi \leq 0.10$, while empirical models using higher-order polynomials in ϕ can be used to fit almost any viscosity data. An equation that is often used for emulsions and concentrated suspensions of rigid spheres is that by Krieger and Dougherty:

$$\eta = \eta_s \left(1 - \phi / \phi_m\right)^{-[\eta]\phi_m} \tag{12.7}$$

where ϕ_m is the maximum packing fraction and $[\eta]$ is the intrinsic viscosity. By inspection, this equation does provide sensible prediction for the effects of size and shape on suspension viscosities, since at a given phase volume, if the maximum packing fraction decreases (e.g., by changing shape from spheres to rods) then the viscosity will increase. Likewise, if the maximum packing fraction decreases (by a broadened size distribution of spheres) then viscosities will decrease. Some authors have proposed an analogy between the rheology of suspensions and the elasticity of composites, thus extending the use of these expressions to calculate moduli (Manski et al. 2006).

Controlling the size of a dispersed phase and its size distribution are critical in the control of rheological properties, long-term stability and palatability of many foods. Particles in foods induce texture sensations that depend on their size. Hard particles with sharp edges produce gritty sensations at smaller sizes than soft and round particles. The smallest particles in chocolate—which are not very hard and do not have sharp edges—detected by the palate are ~25 μm (Engelen et al. 2005). Particle size distribution has a significant effect on rheological properties of nondeformable particles. A 2- to 20-fold reduction in the viscosity, yield value, elastic moduli and loss moduli have been found when a system is very polydispersed compared to a monodisperse one (Luckham and Ukeje 1999).

This behaviour can be qualitatively explained by Equation (12.7) since ϕ_m increases as the width of the size distribution increases. A good example of the effects that particles and polymers have on the rheological behavior of liquids is cloudy apple juice (Genovese and Lozano, 2000). The aqueous milieu of the juice is a solution of sugar, acids and salts (i.e., the clarified juice) that contains charged particles (0.25–5 μm in size) and pectin as a colloidal dispersion. The viscosity of cloudy apple juice has been described by the expression:

$$\eta = \eta_s \left[1 + 14.5\phi + 80.4\left(\frac{\phi}{1-\phi} \right) \right] \tag{12.8}$$

This equation accounts for the effect of the solvent, presence of charged particles (second term) and pectin (third term) on viscosity (r^2 = 0.996). Summarizing, the viscosity of some complex liquids is adequately represented by empirical equations that have as a structural parameter the volume fraction of the dispersed phase. Particle deformation, specific interactions between particles and the presence of a non-Newtonian continuous phase, all which contribute to the "structure" of a complex liquid, are more difficult to model.

12.4.6 Simple Models for Viscoelastic Foods

In several chapters in this book, including this one, mention has been made to two shear moduli, G' and G'', used to characterize the rheological behavior of several foods. Some materials simultaneously exhibit viscous and elastic responses depending on the time-scale of the experiment and the relation to a characteristic time of the material itself. They are referred to as "viscoelastic." The response of viscoelastic foods ranges from solidlike at short times to liquidlike at long times. In other words, they behave as a solid or as a liquid depending on the observation time. In linear viscoelasticity the storage modulus G' represents the energy stored per cycle of deformation (solidlike contribution), and the loss modulus G'' the corresponding energy loss per cycle (liquid-like contribution). Today any well-equipped food materials laboratory has a rheometer in which oscillatory testing under shear can be performed and the two moduli obtained as a function of time or frequency.

Relevant to this chapter is that the rheological behaviour (*property*) of any "viscoelastic food" can be well approximated by an arrangement (*structure*) of two mechanical elements: springs and dashpots. In these models the Hookean elastic contribution is represented by a spring (with modulus E) and the viscous component by a dashpot (operating with a liquid of viscosity μ).

Figure 12.10 shows the mechanical response as a function of time of two structures formed by combining a spring and a dashpot in series (Maxwell model) and in parallel (Voigt model). Creep is slow deformation of a viscoelastic material under constant stress (σ), while relaxation is the time response of the stress after imposing a constant deformation (ε). Thus, a simple mathematical expression accounts for the relation between structure (combination of elements) and a property (creep or relaxation). Evidently, more complex responses can be obtained by combining several elements in series and in parallel.

12.5 Structure–Property Relationships in Nutrition and Health

Structure–property relationships as they relate to nutrition and health are drawing enormous interest in view of the mounting evidence linking diet and non-transmissible

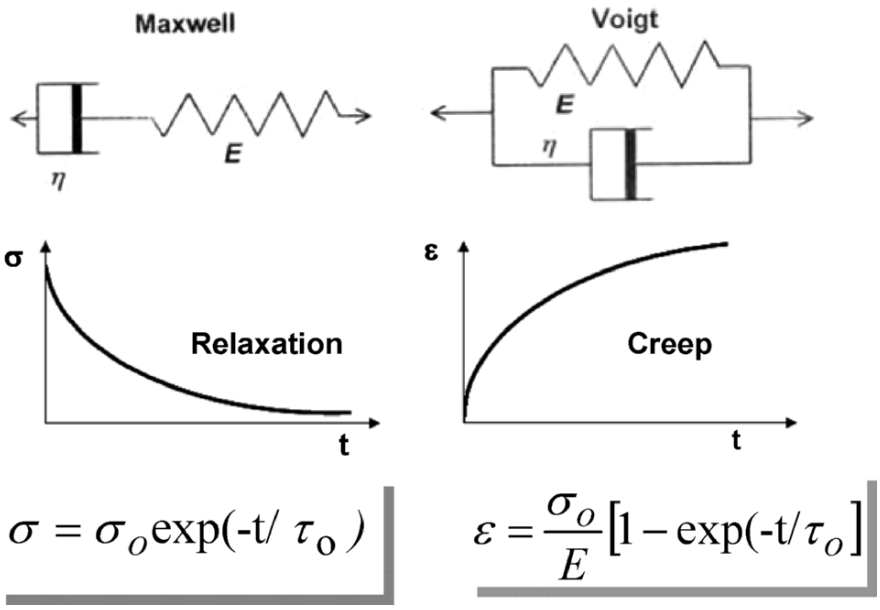

Figure 12.10. Simple mechanical models representing the structure of a viscoelastic material (*top*), their response with time (*center*) and the expression that relates structure to behavior (*bottom*). $\tau_o = \mu/E$ is a relaxation time.

diseases (e.g., some types of cancers, diabetes, obesity, etc.). This is part of the reason for the emergence of the gut–brain axis. When it comes to nutrition the first level of structure is, of course, the molecular level since nutrients perform their beneficial action in cells after absorption in the gut in their biologically usable conformation. At dimensions larger than the molecular level the microstructure or matrix containing the nutrient plays an important role in their "bioavailability" or the fraction of an ingested nutrient available for utilization and storage in normal physiologic functions, that is, that reaches the blood plasma.

Bioavailability has become a more relevant nutritional index than the nutrient content in raw and processed foods determined by analytical techniques (Table 12.2). Several factors influence bioavailability: the chemical form of the nutrient, interactions with other nutrients, the presence of suppressors or cofactors, synergistic effects among nutrient and other components in *digesta*, formation of stable compounds that are slowly metabolized, and so on. It is not surprising that some nutrients in raw plant foods exhibit lower bioavailability than their cooked or processed counterparts. Plant cell walls effectively limit the access of gastric juices and digestive enzymes to intracellular contents, thus hindering nutrient release (Fig. 12.11). Ellis et al. (2004) identified almond seed tissue in fecal material collected from healthy

subjects fed on an almond-rich diet. In particular, the cell walls were intact and hindered the release of intracellular lipid, thus increasing fecal fat excretion. Indeed many plant seeds have evolved to resist digestion, using mammalian hosts as the vector for dispersal. The problem is that recommendations of daily consumption of nutrients have been based on composition tables derived from laboratory assays that measure the nutrient content of foods. Structure frequently is the controlling factor determining the difference between composition and bioavailability of both macro and micronutrients.

Table 12.2. Effect of the food matrix (microstructure) on nutrient bioavailability.

Nutrient	Food (matrix)	Matrix state (processing effect)	Bioavailability	Reference
β-carotene	Carrot	Raw	19–34%	van het Hof et al. (2000b)
		Carrot juice	70% higher than raw	
	Spinach	Whole leaf	5.1%	Castenmiller et al. (1999), van het Hof et al. (2000b)
		Minced leaf	6.4%	Castenmiller et al. (1999)
		Liquefied leaf	9.5%	
Trans β-carotene	Carrot	Raw carrot	41.4%	Livny et al. (2003)
		Cooked carrot (puree)	65.1%	Livny et al. (2003)
Lutein	Spinach	Whole leaf	45%	Castenmiller et al. (1999), van het Hof et al. (2000b)
		Minced leaf	52%	Castenmiller et al. (1999)
		Liquefied leaf	55%	
	Tomato	Tomato paste (homogenization and heat treatment)	22%–380% greater plasma response than fresh tomato	van het Hof et al. (2000a)
α-tocopherol	Broccoli	Different cooking methods	480%–530% higher than raw	Bernhardt & Schlich (2005)
Antioxidant activity	Tomato	No homogenization,	63.9 μmol*h/l	van het Hof et al. (2000a)
		Mild homogenization	82.6 μmol*h/l	
		Severe homogenization	118 μmol*h/l	

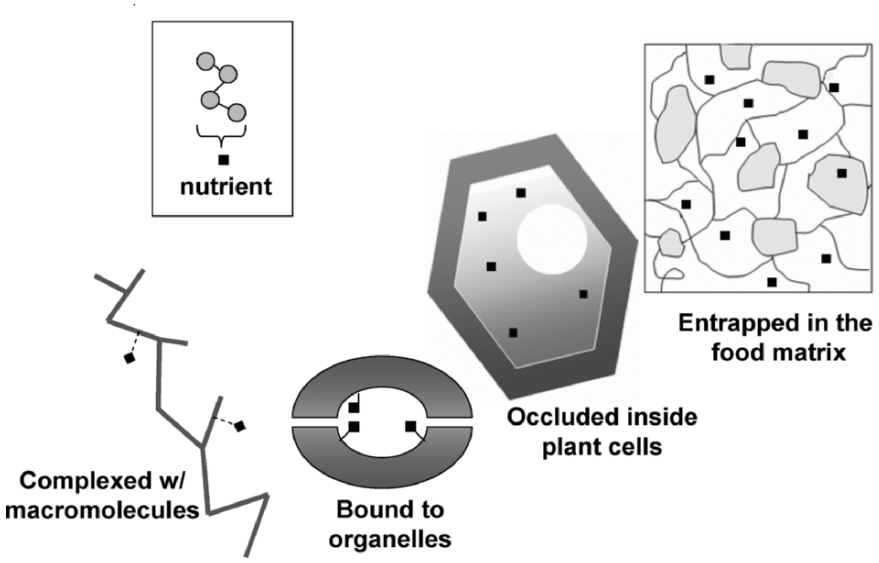

Figure 12.11. Interactions of a nutrient (■) with macromolecules and cellular organelles or entrapment within the food matrix may affect the release during digestion and absorption in the gut, thus reducing its bioavailability.

Although structure breakdown in the mouth is important in texture perception and flavor release, it is often insufficient for nutrient liberation. Moreover, structural properties of the swallowed bolus play an important role in gastric emptying and absorption of nutrients. Advances in functional brain imaging techniques such as positron emission tomography (PET), functional MRI and less invasive modalities of gastrointestinal imaging are assisting in the study of connections between the food ingest, the gut function and the human brain. Differences in cerebral blood flow in response to food intake between lean and obese individuals have been detected by PET and believed to be related to obesity (DelParigi et al. 2005). Gastric emptying has been monitored noninvasively by MRI and shown to depend on meal viscosity.

Matrix design for proper delivery of specific nutrients is an area of active research (see Chapter 24). One example is the use of β-lactoglobulin gel matrices to control the delivery of iron. It has been shown that under *in vitro* conditions of simulated digestion that filamentous gels released most of the iron in the intestinal phase, thus protecting iron during its transit through the gastric zone (Remondetto et al. 2004).

How far can the design of food structures go? Agricultural research, interested in the past mostly in production yields, now centers part of its activity on quality and the functionality of raw materials and primary products. Notwithstanding the debate about the consumer's acceptance of genetically modified foods, the potential exists

to control food microstructure and the presence of valuable components directly in raw materials using genetic engineering techniques. Tomatoes are a good example of applied plant biotechnology. Suppression of a gene related to ripening resulted in increased viscosity of tomato juice and tomato paste (Kalamaki et al. 2003). Similarly, up to a 3-fold increase of lycopene was achieved by genetic engineering (Enfissi et al. 2006). In cereals, the amylose/amylopectin ratios within starch granules have been changed, with the potential to modify not only differences in textural perception but also the amounts and rates at which glucose is released during digestion (Richardson et al. 2000). Evidently, a limit to genetic manipulation of fruits and vegetables is that it must not be a detriment to plant vigor and yield, but more importantly, to flavor and texture.

12.6 Gastronomical Engineering: Structuring Foods for Pleasure and Luxury

With the advent of gastronomy in the nineteenth century came the restaurant. Nowadays, expensive restaurants open every day in large cities all around the world. At restaurants one can experience the delights of almost any traditional or ethnic cuisine and the creativity of talented chefs. This is in contrast to the fact that "fast food" is becoming cheaper and ubiquitous, and can only be explained by the desires of people to experience the full pleasure of their senses.

Some modern chefs have broken with old culinary routines and invented their own dishes based on sophisticated techniques in their own "laboratories" guided by scientific principles. In fact, most dishes are dispersed systems where gas bubbles, oil or water droplets, gels and solid particles have to be dispersed into a continuous phase. Taking science into the chef's domain has been called molecular gastronomy (This 2005). Food science and gastronomy have merged in the kitchen to prepare artificial caviar, cryogenic desserts, and "airs" or foams, among other creations.

These structural creations are the envy of food technologists who experimented with them in the past but found no opportunity in the supermarket shelf due to the high costs involved. Food engineers in the kitchen do not have to bother about scaling up, since a few portions may be prepared almost under laboratory conditions. Chefs and food scientists/engineers together are called to expand the offer of good food and the appreciation for taste and quality. Later, knowledge can be extended to cooks at smaller restaurants, learned by students at college and schools, and applied when cooking at home. We welcome gastronomical engineering!

12.7 Conclusions

Structure–property relationships are central to food materials science and product design, since food microstructure determines to a large extent many desirable characteristics of what we eat. Our expectations have gone far beyond the basic properties of eating quality and microbiological safety. We want to know how our food was produced and where. Consumers' concerns about health and well-being demand that some nutrients are bioavailable after absorption in the gut. Last, but not least, we want to derive pleasure from gourmet quality foods.

In the last decade significant advances in elucidating the food microstructure have resulted from a myriad of imaging and physicochemical techniques that allow characterization at different length and time-scales, often nonintrusively and in real time. Areas that are likely to exhibit considerable progress in years to come are the quantification of relevant structural features from images, modeling of structure–property relationships, integration of events related to structure breakdown in the mouth and reassembly of *digesta* in the gut, the design of foods for delivery of healthy nutrients and pleasure, and the engineering of functionality using molecular biology.

12.8 References

Aguilera, J.M. (2005). Why food microstructure? *J. Food Eng*. 67, 3–11.

Aguilera, J.M., and Stanley, D.W. (1999). *Microstructural Principles of Food Processing and Engineering*, 2nd ed. Aspen Publishers Inc., Gaitherburg, MD.

Aguilera, J.M., and Baffico, P. (1997). Structure–mechanical property relationships in thermally induced whey protein–cassava starch gels. *J. Food Sci*. 62, 1048–1053.

Attenburrow, G.E., Goodband, R.M., Taylor, L.J., and Lillford, P.J. (1989). Structure, mechanics and texture of a food sponge, *J. Cereal Sci*. 9, 61–70.

Barnes, H.A., Hutton, J.F., and Walters, K. (1989). *An Introduction to Rheology*. Elsevier, Amsterdam.

Blanchard, J.M.V., and Lillford, P.J. (1988). *Food Structure and Behaviour*. Academic Press, London.

Bliznakov, E.D., White, C.C., and Shaw, M.T. (2000). Mechanical properties of blends of HDPE and recycled urea-formaldehyde resin. *J. Appl. Polym. Sci*. 77, 3220–3227.

Castenmiller, J., West, C.E., Linssen, J.P., van et Hof, K.H., and Voragen, A.G. (1999). The food matrix of spinach is a limiting factor in determining the bioavailability of β-carotene and to a lesser extent of lutein in humans. *J. Nutr.* 129, 349–355.

DelParigi, A., Chen, K., Salbe, A.D., Reiman, E.M., and Tataranni, P.A. (2005). Sensory experience of food and obesity: a postron emission tomography study of brain regions affected by tasting a liquid meal after a prolonged fast. *NeuroImage* 24, 436–443.

Cernadas, E., Carrión, P., Rodriguez, P.G., Muriel, E., and Antequera, T. (2005). Analyzing magnetic resonance images of Iberian pork loin to predict its sensorial characteristics. *Comput. Vis. Image Und*. 98, 344–360.

Ellis, P.R., Kendall, C.W., Ren, Y., Parker, C., Pacy, J.F., Waldron, K.W., and Jenkins, D.J. (2004). Role of cell walls in the bioaccessibility of lipids in almond seeds. *Am. J. Clin. Nutr.* 80, 604–613.

Enfissi, E.M.A., Fraser, P.D., and Bramley, P.M. (2006). Genetic engineering of carotenoid formation in tomato. *Phytochem. Rev*. 5, 59–65.

Engelen, L., de Wijk, R.A., van der Bilt, A., Prinz, J.F. Janssen, A.F., and Bosman, F. (2005). Relating particles and texture perception. *Physiol. Behav*. 86, 111–117.

Genovese, D.B., and Lozano, J.E. (2000). Effect of cloud particle characteristics on the viscosity of cloudy apple juice. *J. Food Sci*. 65, 641–645.

Gibson, L.J., and Ashby M.F. (1988). *Cellular Solids: Structure and Properties*, Pergamon Press, Oxford.

Gilsenan, P.M., Richardson, R.K., and Morris, E.R. (2003). Associative and segregative interactions between gelatin and low-methoxy pectin. 3. Quantitative analysis of co-gel moduli. *Food Hydrocoll*. 17, 751–761.

Gregory, J.F., Quinlivan, E.P., and Davis, S.R. (2005). Integrated the issues of folate bioavailability, intake and metabolism in the era of fortification. *Trends Food Sci. Tech*.16, 229–240.

Hutchings, J.B., and Lillford, P.J. (1988). The perception of food texture: the philosophy of the breakdown path. *J. Texture Stud*. 19, 103–115.

Juodeikiene, G., and Basinskiene, L. (2004). Nondestructive texture analysis of cereal products. *Food Res. Int.* 37, 603–610.

Kalamaki, M.S., Harpster, M.H., Palys, J.M., Labavitch, J.M., Reid, D.S., Brummell, D.A. (2003). Transgenic overexpression of expansin influences particle size distribution and improves viscosity of tomato juice and paste. *J. Agric. Food Chem*. 51, 7456–7464.

Kerner, E.H. (1956). The elastic and thermoelastic properties of composite media. *Proc. Phys. Soc.* 69B, 808–813.

Kilcast, D. (2004). Measuring consumer perceptions of texture: an overview. In: *Texture in Foods*, *Vol. 2: Solid Foods.* Woodhead, Cambridge, pp. 3–32.

Krieger, I.M., and Dougherty, T.J. (1959). A mechanism for non-Newtonian flow in suspensions of rigid spheres. *Trans. Soc. Rheology* 3, 137–152.

Larson, R.G. (1999). *The Structure and Rheology of Complex Fluids.* Oxford University Press, New York.

Lillford, P.J. (2000a). The materials science of eating and food breakdown. *MRS Bulletin* 25, 12, 38–43.

Lillford, P.J. (2000b). Food: the quality is in the structure. *2nd International Symposium on Food Rheology and Structure*, Zurich, pp. 85–90.

Livny, O., Reifen, R., Levy, I., Madar, Z., Faulks, R., Southon, S., and Schwartz, B. (2003). β-carotene bioavailability from differently processed carrot meals in human ileostomy volunteers. *Eur. J. Nutr*. 42, 338–345.

Lorén, N., Hamberg, L., and Hermansson, A.-M. (2006). Measuring shapes for application in complex food structures. *Food Hydrocoll*. 20, 712–722.

Lu, S.-Z., and Hellawell, A. (1995). Using fractal analysis to describe irregular microstructures. *J. Min. Met. Mat. Soc.* Dec 1995, 14–17.

Luckham, P.F., and Ukeje, M.A. (1999). Effect of particle size distribution on the rheology of dispersed systems. *J. Colloid Interf. Sci*. 20, 347–356.

Manski, J.M., Kretzers, I.M.J., van Brenk, S., van der Goot, A.J., and Boom, R.M. (2006). Influence of dispersed particles on small and large deformation properties of concentrated casein composites. *Food Hydrocoll*. 21, 73–84.

Mellema, M., Heesakkers, J.W.M., van Opheusden, J.H.J., and van Vliet, T. (2000). Structure and scaling behavior of aging rennet-induced casein gels examined by confocal microscopy and permeametry. *Langmuir* 16, 6847–6854.

Mellema, M., Walstra, P., van Opheusden, J.H.J., and van Vliet, T. (2002). Effects of structural rearrangements on the rheology of rennet-induced casein particle gels. *Adv. Colloid Interfac. Sci.* 98, 25–50.

Narine, S.S., and Marangoni, A.G. (1999). Relating structure of fat crystal networks to mechanical properties. *Food Res. Int.* 32, 227–248.

Nicolas, Y., Paques, M., van den Ende, D., Dhont, J.K.G., van Polanen, R.C., Knaebel, A., Steyer, A., Munch, J.-P., Blijdenstein. T.B.J., and van Aken, G.A. (2003). Microrheology: new methods to approach the functional properties of food. *Food Hydrocoll*.17, 907–913

Peleg, M. (2006). *Advanced Quantitative Microbiology for Food and Biosystems*. CRC Taylor and Francis, Boca Raton, FL.

Peleg, M. (1993). Fractals and foods. *CRC Crit. Rev. Food Sci*. 37, 491–518.

Peleg, M., and Bagley, E.B. (1983). *Physical Properties of Foods.* AVI Publishing, Westport, CT.

Qiao, J., Wang, N., Ngadi, M.O., and Kazemi, S. (2007). Predicting mechanical properties of fried chicken nuggets using image processing and neural network techniques. *J. Food Eng*. 79, 1065–1070.

Quevedo, R., Brown, C., Bouchon, P. and Aguilera, J.M. (2005). Surface roughness during storage of chocolate: fractal analysis and possible mechanisms. *J. Am. Oil Chem. Soc*. 82, 457–462.

Remondetto, G.E., Beysacc, E., and Subirade, M. (2004). Iron availability from whey hydrogels: an in vitro study. *J. Agric. Food Chem*. 52, 8137–8143.

Richardson, P. H., Jeffcoat, R. and Shi, Y. C. (2000) High amylose starches, *MRS Bulletin* 25, 12, 20–24.

Russ, J.C. (2004). *Image Analysis of Food Microstructure*. CRC Press, Boca Raton, FL.

Shama, F., and Sherman, P. (1973). Identification of stimuli controlling the sensory evaluation of viscosity, *J. Texture Stud*. 4,111–119.

Shewry1, P.R., Tatham, A.S., Fido, R., Jones, R.H, Barcelo, P., and Lazzeri, P.A. (2004). Improving the end use properties of wheat by manipulating the grain protein composition. *Euphytica* 119, 45–48.

Szczesniak, A.S. (1998). Sensory testing profiling: historical and scientific perspectives. *Food Technol*. 52(8), 54–57.

Taylor, A.J. (2002). Release and transport of flavors in vivo: physicochemical, physiological and perceptual considerations. *Compr. Rev. Food Sci. Food Safety* 1, 45–57.

Takayanagi, M., Harima, H., and Iwata, Y. (1963). Viscoelastic behavior of polymer blends and its comparison with model experiments. *Mem. Faculty Eng. Kyushu Univ.* 23, 1–13.

Thiel, B.L., and Donald, A.M. (2000). Microstructural failure mechanism in cooked and aged carrots. *J. Texture Stud.* 31, 437–455.

This, H. (2005). Molecular gastronomy. *Nat. Mater*. 4, 5–7.

Torquato, S. (2002). Statistical description of microstructures. *Ann. Rev. Mater. Res.* 32, 77–111.

van den Hof, K.H, de Boer, B.C., Tijburg, L.B., Lucius, B.R., Zijp, I., West, C.E., Hautvast, J.G., and Weststrate, J.A. (2000a). Carotenoid bioavailability in humans from tomatoes processed in different ways determined from the carotenoid response in the triglyceride-rich lipoprotein fraction of plasma after a single consumption and in plasma after four days of consumption. *J. Nutr*.130, 1189–1196.

van den Hof, K.H., West, C.E., Weststrate, J.A., and Hautvast, J.G. (2000b). Dietary factors that affect the bioavailability of carotenoids. *J. Nutr*.130, 503–506.

Warburton, S.C., Donald, A.M., and Smith, A.C. (1990). The deformations of brittle starch foams. *J. Mater. Sci*. 25, 4001–4007.

Chapter 13

Structuring Water by Gelation

Anne-Marie Hermansson

SIK, The Swedish Institute for Food and Biotechnology, PO Box 5401, 40229 Gothenburg, Sweden, amh@sik.se

13.1 Introduction

Gels are of central importance for most semisolid food products. A gel can contain more than 99% water and still retain the characteristics of a solid. The network structure will determine whether the water will be firmly held or whether the gel will behave more like a sponge, where water is easily squeezed out. The gel structure will also have a major impact on the texture as well as diffusion of water and soluble compounds. Many food matrixes are based on colloidal gels such as yoghurts, cheeses, many desserts, sausages etc (see also Chapters 19 and 20). In whole foods, there is often a combination of colloidal structures and fragments of biological tissues or gel structures in combination with particles, emulsion and foam structures. This level of complexity of composite food structures will not be dealt with here.

In this chapter, we will focus on biopolymer gels and their microstructure. It will be demonstrated that biopolymer gel structures span a wide range of length scales and that length scale provides important information for the understanding of structure-related properties. Gelation can be approached from different directions, where the molecular approach has to be combined with colloidal models based on depletion mechanisms, classical aggregation–gelation theories or, more recently, mode-coupling theories based on dynamic arrest or jamming (Mezzenga et al. 2005). Incompatibility between biopolymers and gelation can lead to segregative or associative phase separation with mixed gel structures and properties varying according to the distribution of the phases (see Chapter 3).

Since several mechanisms often come into play in a gelation process, the relative kinetics will determine the final structure and related properties. Nowadays we have tools that enable us to follow the development of the microstructure directly under the microscope giving insights of great interest to food engineering (see also Chapter 11). Here we will discuss not only structure formation but also structural breakdown.

The way a gel structure deforms and breaks under stress is crucial for properties such as flow and fracture behaviour, sensory perception of structure and release of water and flavours.

13.2 Gelation Approaches and Length Scales

13.2.1 Molecular Interactions and Gel Formation

Much work has been focused on molecular properties in relation to gelation. For proteins, denaturation and conformational changes as well as the role of special bonds such as disulphide bonds, special sequences of the polypeptide chain, and so on, have been thoroughly investigated for proteins such as soy proteins, ß-lactoglobulin, bovine serum albumin, ovalbumin, and so on (Hoffman and van Mils 1997; Verheul et al. 1998). For "molecular gels" of globular proteins conformational changes triggered by denaturation initiate the formation of a percolating network structure. Transparent fine-stranded gels will form at pHs outside the isoelectric region at a sufficiently high net charge. As will be discussed later, colloidal particulate gels can form in the isoelectric regions far below the denaturation temperature of the proteins.

As far as polysaccharide gels are concerned, our knowledge of how the molecular structures relate to gel formation is substantial. Pectin provides a good example of how different gel properties can be achieved by varying the degree of methylation or amidation as well as the distribution of the substituents (Löfgren 2005; Löfgren et al. 2005; Löfgren et al. 2006). Other well-researched commercial food polysaccharides include carrageenans, alginates, xanthans, galactomannans, amyloses, amylopectins and cellulose derivatives. Considerable efforts have been made to understand the mechanisms for conformational changes necessary for gel formation such as helix formation and the structures in the junction zones connecting two macromolecules during gel formation (Morris 1986).

However, we do not know enough about how dimers or trimers of polysaccharides align into a network strand of a much larger dimension, and we still need much more information on how to relate the network morphology to the properties of the gel. This is schematically illustrated in Figure 13.1. There is considerable experience of the relations between molecular characteristics and gel properties. The ingredient manufacturers have been fairly successful in adjusting the molecular structure to the gel performance. However, commercial samples are heterogeneous and are often blends of fractions and the blending tunes the properties. A typical example is gelatin, where fractions of varying molecular weights are blended to give a product with a characteristic gel strength expressed as Bloom number.

Substantial research efforts have been made to relate molecular properties to the structures of the junction zones and provide mechanisms for gel formation. Thus we have models for the formation and alignment of double helices for kappa-carrageenan, formation of triple helices for gelatin and egg box models for calcium induced gelation of alginate and pectin to mention a few examples (Morris 1986; Djabourov 1988). However, a gel strand of a physical biopolymer gel is of larger dimensions

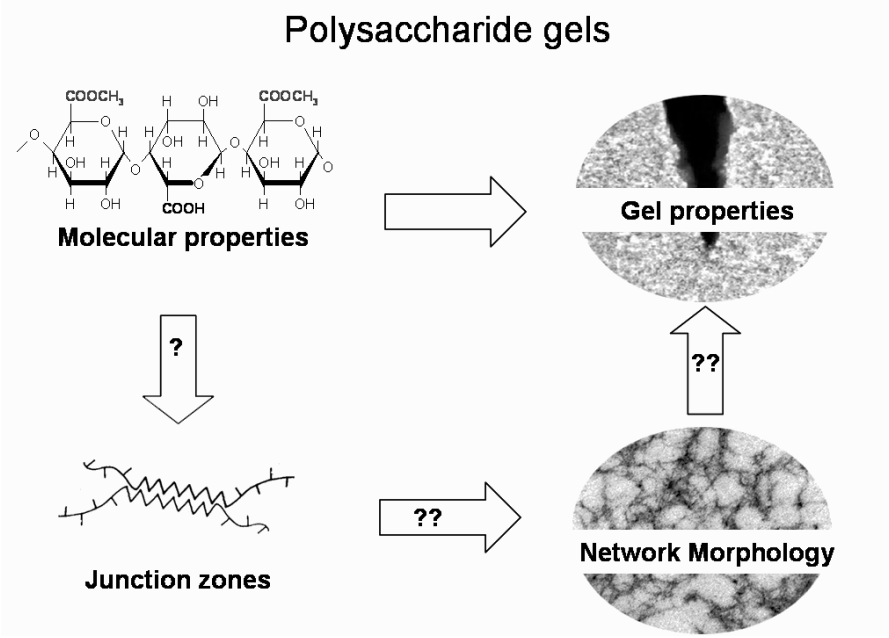

Figure 13.1. Important aspects of gels.

and more highly aggregated than the alignment of two entities. It remains a challenge to understand how the network strands form beyond the alignment of molecules initiating gel formation as well as how the interplay between network morphology and the intermolecular forces within the gel strands determine the gel properties.

13.2.2 Fine-Stranded Gels

Strand-like gel networks cover a very wide range of length scales. Proteins outside the isoelectric region and most polysaccharide gels have nanoscale networks that require electron microscopy for their visualisation. Even so, there are large variations in length scales, as illustrated in Figure 13.2. Gels such as the superabsorbent shown in Figure 13.2(a) and entanglement gel structures of gelatin, iota-carrageenan, locust bean gum, cellulose derivatives etc have a very fine network structure with pores in the range of 10 nm (Hermansson and Langton 1994). Typical of this structure is that the entities building up the strands have a low tendency to aggregate further. Gelatin, for example, has strands composed of triple helices similar to those in native collagen. The strands do not aggregate but form an entangled network with interactions between strands in the network (Djabourov 1988; Djabourov et al. 1988).

Figure 13.2(b) shows another type of network structure that is more open, typical of coarser and more aggregated and heterogeneous fine-stranded gels. The example, Sepharose is a commercially modified agarose gel, but many polysaccharides form gels in this range of length scale, for example, kappa-carrageenan, pectins, agarose and

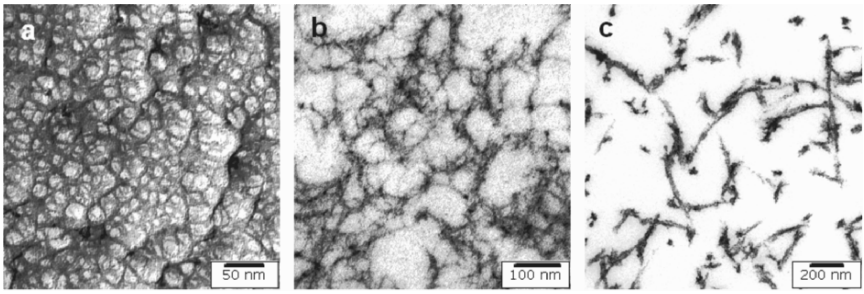

Figure 13.2. Transmission electron microscope (TEM) images of (a) freeze-etched replica of a superabsorbent; (b) thin section of a Sepharose gel; (c) thin section of an amylose gel.

alginates. For these gels, dimers or other junction forming entities align and form coarser strands composed of several aggregated entities. Often a transition from random coils to dimers is necessary for the initiation of gel formation by the formation of double helices for carrageenan or egg box dimers for alginate or low methoxyl pectin. The micrograph to the right shows an amylose gels with an even more complex mode of aggregation and a more open gel structure than the gels illustrated in Figure 13.2(c) (Hermansson et al. 1995).

Even if the networks of gels have similar length scales, the kinetics of gel formation can be quite different both with regard to the molecular composition and the conditions during gel formation. This will be demonstrated by a comparison of kappa-carrageenan and pectin. They both form transparent gels at very low polysaccharide concentrations and water can apparently be solidified yet without changing its physical properties by gel formation at a polysaccharide concentration below 1%.

Gelation of kappa-carrageenan is initiated by coil–helix transition promoted by salts and the gel strands are composed of aggregated double helices (Morris 1986). Potassium has a specific effect and will initiate the formation of double helices as well as aggregation of double helices into a gel structure. Kappa-carrageenan is sensitive to aggregation, and the gel morphology will change as a function of the salt composition as well as by the kinetics of gel formation (Hermansson 1989; Hermansson et al. 1991). At 20 mM KCl, a very fine-stranded dense gel is formed. There is enough potassium for coil–helix transition and gel formation, but not enough to drive aggregation beyond the fine-stranded dense network structure.

At 100 mM KCl, the situation is quite different and aggregation will be promoted. This is illustrated in Figure 13.3. When the gel is quenched by cooling, aggregation is suppressed and a dense network structure is formed. During slow cooling, time is allowed for aggregation, which results in a considerable coarsening

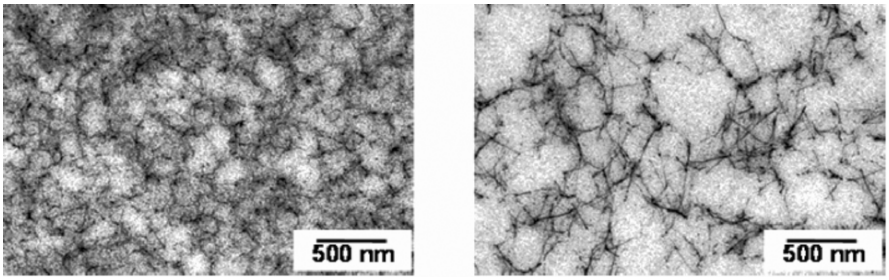

Figure 13.3. TEM images of 1% kappa-carrageenan in 100 mM KCl rapidly cooled by quenching (left) and slowly cooled (right).

of the network structure and an increase in pore size, as shown in Figure 13.3. The difference in the state of aggregation is reflected both in the rheological properties and in the diffusion rate of macromolecules in the gel structures, as will be discussed later (Walther et al. 2006).

Kappa-carrageenan has one sulphate group per disaccharide. Iota-carrageenan is more charged and has two sulphate groups per disaccharide. Gel formation of iota carrageenan is also initiated by formation of double helices, but the change in charge density leads to a change in gel structure and a more flexible dense entanglement structure similar to that of gelatin with a lower tendency towards aggregation.

Pectin is a commonly used polysaccharide, the specifications of which are related to the chemical composition. Pectin is mainly composed of galacturonic acid, where some of the carboxyl groups are present in the methyl ester form. Pectins are divided into high methoxyl (HM) and low methoxyl (LM) pectin with different requirements for gel formation (Oakenful and Scott 1984; Voragen et al. 1995, Löfgren 2005). In HM pectin more than 50% of the carboxyl groups are esterified, compared with less than 50% in LM pectin. Gelation of HM pectin requires at least 55% sugar and a pH below 3.5. Under these conditions there is enough suppression of electrostatic repulsion and polymer–water interactions. Gelation of LM pectin occurs in a wide pH range mainly by ionic interactions between unesterified galacturonic acid residues and divalent ions such as Ca^{2+}.

LM and HM pectin differ both in their gelation mechanisms and rheological behaviour (Löfgren and Hermansson 2004). Figure 13.4 shows that the storage modulus increases slowly with time for HM pectin, whereas the kinetics of gel formation is much faster for LM pectin at a comparable concentration. The measurements were made after rapid cooling and the temperature profile is shown in Figure 13.4(b). Gelation measured as the crossover between G′ and G′′ takes 50 minutes for HM pectin at a concentration of 0.4%, whereas G′ is already considerably higher than G′′ for LM pectin at the start of the measurements. G′ increases gradually with time for the HM pectin, whereas there is a rapid initial increase in G′ for LM pectin, after which it remains constant.

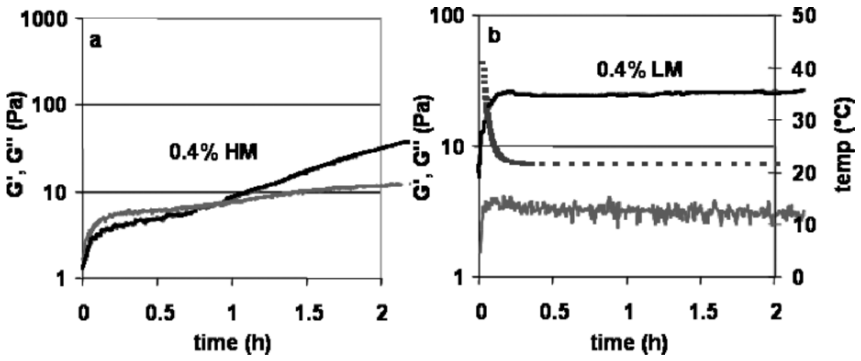

Figure 13.4. Development of the storage modulus G′ and the loss modulus G′′ at pH 3.0 for HM pectin in 60% sucrose and LM pectin in 30% sucrose and 0.08% $CaCl_2$.

Despite the differences in the rheological behaviour, the overall morphology of pectin is surprisingly similar regardless of the difference in their chemical composition. Figure 13.5 shows the microstructure of LM and HM pectin at two magnifications (Löfgren et al. 2002). Even if there are some differences in homogeneity and chain flexibility, the characteristic length scales of the network structure are similar in LM and HM pectin gels, with many pores in the range of 500 nm. It seems as if the overall morphology of the pectin network does not relate to changes in rheological behaviour. Micrographs of HM pectin taken after different gelation times show that the network morphology develops early and does not change with time, whereas the storage modulus increases progressively with time (Löfgren 2005).

The distribution of methyl groups in LM pectin has a strong impact on the rheological behaviour of gels with the same chemical composition but no significant impact on the morphology of the gel network. A blockwise distribution of ester groups will give rise to much faster gel formation than for a pectin with a random distribution of ester groups, but the overall network structure is similar with regard to the length scale and morphology (Löfgren et al. 2006).

Thus kappa-carrageenan and pectin form gel networks on similar length scales, but the relationship between their structure and rheological properties differs in character. Both the network structure and the rheological properties of kappa-carrageenan are affected by the kinetics of aggregation. Therefore the morphology of kappa-carrageenan is sensitive to factors that affect aggregation, such as the presence of salts and cooling rates. Pectin, on the other hand, has a morphology that is surprisingly consistent regardless of the chemical composition and factors that promote aggregation. However, the kinetic behaviour and the rheological properties of pectin can be considerably varied by altering the chemical composition as well as by the presence of ions such as calcium. This implies that these factors influence the molecular interaction within the network strands rather than the overall morphology of the network.

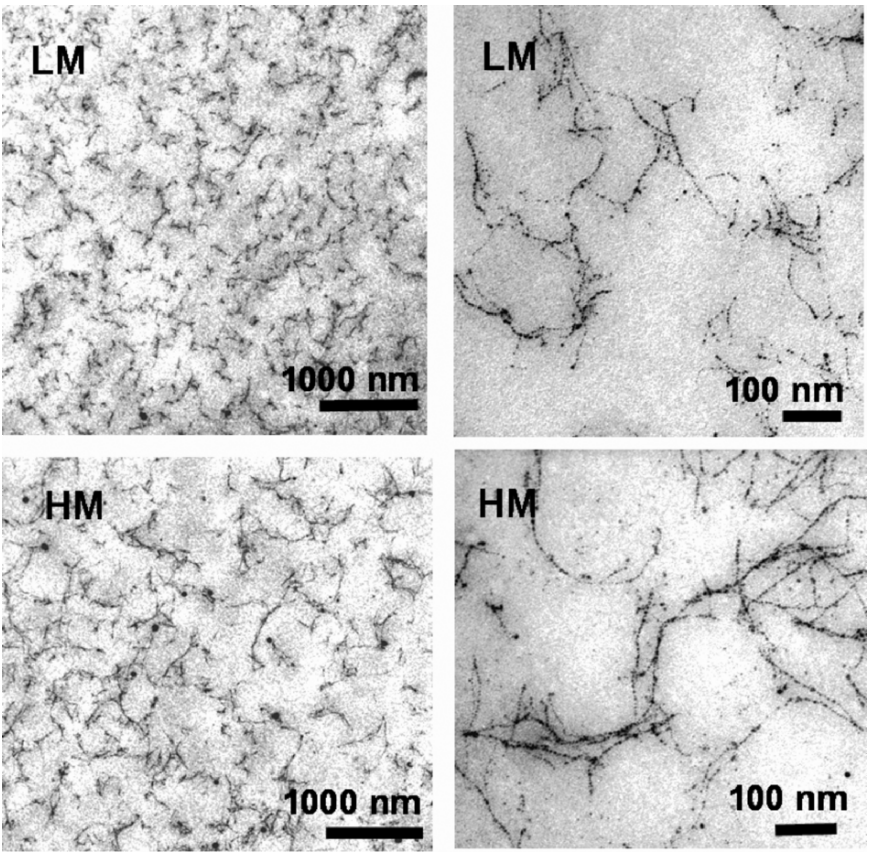

Figure 13.5. TEM images of 0.75% HM pectin in 60% sucrose and 0.75% LM pectin in 30% sucrose and 0.15% $CaCl_2x2H_2O$ at two magnifications.

13.2.3 Particulate Gels

In the isoelectric region of proteins, where the net charge is low, there is a high tendency towards aggregation. Gels formed in this region are highly aggregated particulate gels, and the kinetics of aggregation has a dramatic effect on structure formation, aggregation often being observed prior to gel formation. For many globular proteins, this region is in the pH range 4–6, which is also a common pH range for many food products such as dairy products. Whey protein gels are therefore frequently used as a model system.

Figure 13.6 shows that a change in heating rate has a pronounced effect on aggregation and the particulate network structure of whey protein gels prepared under exactly the same conditions prior to heating (Stading et al. 1993). The figure shows two-dimensional sections of gel networks formed at different heating rates.

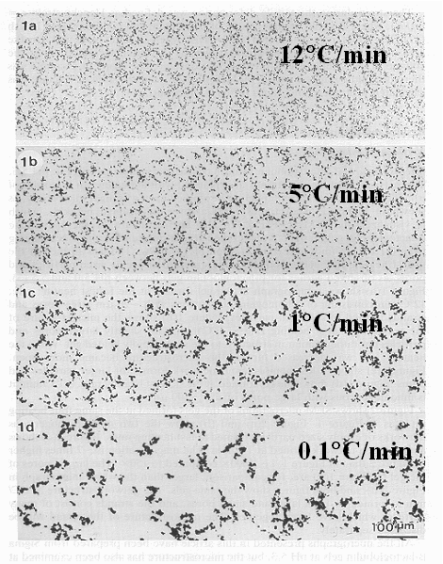

Figure 13.6. Light microscopy (LM) images of 10% gels at pH5.3.

The slower the heating rate, the more time available for aggregation and the coarser the network structure formed.

The change in heating rate affects pore size as well as the size of the protein aggregates. The pore diameter increased from ~20 to ~100 µm when the heating rate was decreased from 12 to 1°C/min. Not only the pore size but also the degree of clustering and the particle size increased as the heating rate decreased.

Dramatic changes in the state of aggregation can also be obtained by adding a second component that stimulates aggregation of the ß-lactoglobulin. When ß-lactoglobulin is mixed with non-gelling amylopectin, the whey protein network structure is changed. Both the increased concentration and molecular weight of amylopectin enhance aggregation into particle aggregates and clusters. A combination of TEM, LM and CLSM reveals the complexity of particulate ß-lactoglobulin networks over a wide range of length scales (Olsson et al. 2000; Olsson et al. 2002a,b; Olsson et al. 2003). The effects of adding high molecular-weight (HM) and low-molecular weight (LM) amylopectin on the aggregation of ß-lactoglobulin have been studied. Figure 13.7 shows an example of a 6% ß-lactoglobulin protein gel with and without added amylopectin. The LM micrographs show that the network is built up of clusters that increase in size on addition of amylopectin. The clusters themselves are composed of particle aggregates, and the TEM micrograph at the highest magnification shows that the particles are more densely packed and increase in size when mixed with amylopectin. These particles have a diameter in the range of 100 nm, and sometimes it is even possible to detect the subparticles making up these particles (Olsson et al 2002a; Langton and Hermansson 2001).

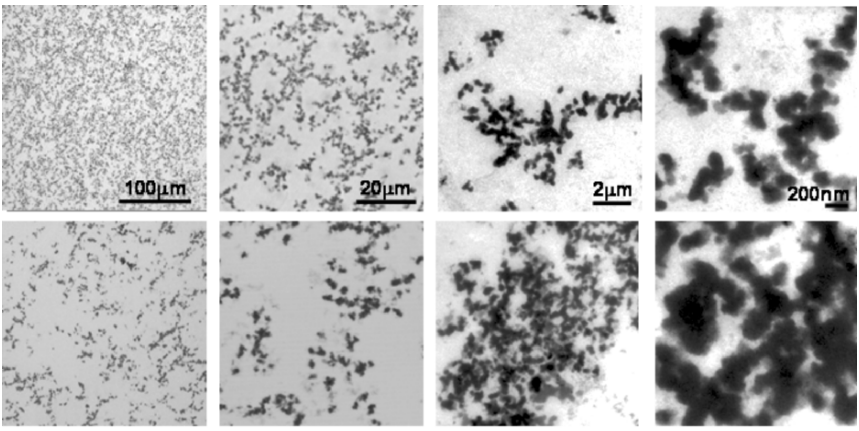

Figure 13.7. LM and TEM images of pure 6% ß-lactoglobulin gels (upper row) and mixed with 0.75% HM amylopectin (lower row) at different magnifications.

CLSM enables us to follow the protein aggregation as a function of time directly under the microscope. This improves our understanding of the gelation mechanism of particulate gels. Figure 13.8 shows images from time temperature series of a number of ß-lactoglobulin/non-gelling amylopectin mixtures (Olsson et al. 2002b). The images show the structure of a specific focal plane. We can see that the bright whey protein structures become arrested at a certain temperature depending on the composition of the mixture. The arrest of the structure coincides with gelation as measured by rheology, and this temperature is below the denaturation temperature of whey proteins for all systems studied. The temperature of arrest becomes lower the more the aggregation is promoted by amylopectin. This means that, for these systems, molecular conformational changes induced by denaturation do not cause the initial network at the gel point, even if they have a pronounced effect on the rheological properties at later stages of gelation.

The aggregation and gelation of fractal particulate gels have been explained as irreversible aggregation through classical diffusion or reaction-limited cluster-cluster aggregation. An interesting new approach for this type of gels comes from mode coupling theories (MCT) and describes dynamic arrest, local trapping of particle clusters and onset of elasticity at the transition. This has been recently reviewed by Trappe and Sandkühler (2004). They describe the fractal clusters as an elastic solid, where the motion of the particles within the clusters is constrained and can be considered to be in a glassy state. For high volume fractions, the clusters can be locally trapped into a glassy arrest, whereas for small volume fractions finite clusters are formed, where the particles are arrested within the clusters. A percolating network is formed by connecting clusters, giving rise to elasticity.

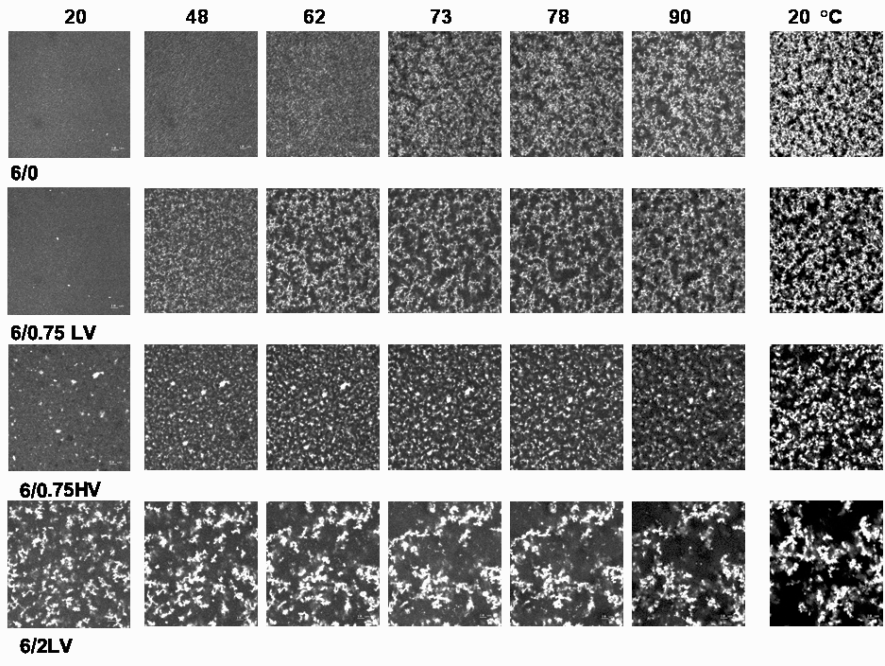

Figure 13.8. CLSM images showing the structure evolution of 6% ß-lactoglobulin structures with and without added amylopectin of low and high molecular weight.

In models that describe irreversible aggregation, the kinetics determine the mechanisms for gel formation. The results from the studies of ß-lactoglobulin/amylopectin systems coincide surprisingly well with the MCT theories. We can clearly see how particles aggregate and become immobilized in finite clusters that interconnect to form a network structure. The more we enhance aggregation by adding amylopectin to the system, the earlier we observe dynamic arrest in the system as illustrated in Figure 13.8. Additional support for this theory is given by results from rheological measurements. Figure 13.9(a) shows the viscoelastic properties developed during heating and cooling of a whey protein/amylopectin mixture (Olsson et al. 2002b). The temperature of the first increase in G´ at around 75°C corresponds fairly well to the denaturation temperature of the whey proteins. However, if we increase the sensitivity of the instrument, we will see that there is already a crossover of G´ and G´´ at below 60°C and the formation of a weak gel. The crossover temperature varied from 60°C for the pure whey protein mixture to 38°C for the most aggregating whey protein/amylopectin mixture.

The gel point is interpreted as the result of dynamic arrest of the clusters building up the network. Denaturation of the protein does not induce any visible changes in the morphology of the network structure of the aggregated clusters, but the storage modulus increases due to increased intermolecular bonds formed during the conformational changes induced by denaturation, which strengthen the network. There is an

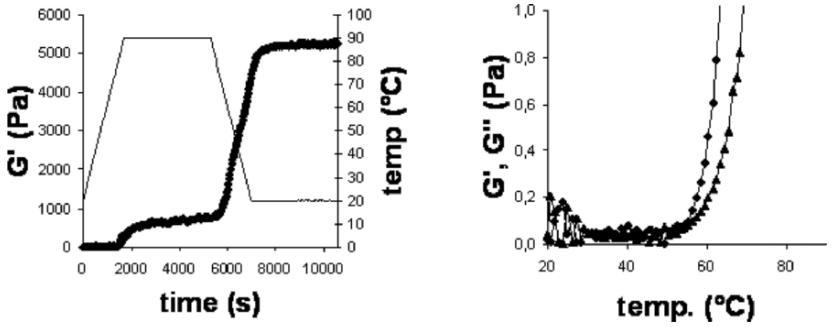

Figure 13.9. The development of G' as a function of temperature for 6% ß-lactoglobulin/ and 0.25% HM amylopectin (left) and the initial G'/G'' at the onset of gelation (right).

enormous increase in the storage modulus on cooling without any major changes in the network morphology. Sometimes shrinkage and rearrangements take place, but this is not always the case. The major reason for this increase is probably intermolecular strengthening of the bonds within the existing network. Thus, the events taking place during cooling have the biggest impact on the gel strength and more research on gels that are already set would be of interest in order to control the final gel properties.

13.3 Gelation and Phase Separation of Biopolymer Mixtures

When phase separation is coupled with gel formation, the structure of the mixed system can be trapped by gel formation, and both the distribution of phases and the properties of each phase and interfacial interactions determine the properties of the mixed gel system. Phase separation can occur due to incompatibility or due to different gel conditions of the biopolymers in the mixture.

Incompatibility between biopolymers results in phase separation, which can roughly be divided into segregative and associative phase separation. Both biopolymers are enriched in the same phase during associative phase separation, also called complex coacervation. In contrast, during segregative phase separation, each phase is enriched in one of the polymer components. A schematic illustration of a phase diagram showing associative and segregative phase separation is given in Figure 13.10 (Picullel and Lindman 1992). Phase separation in gelled systems has often length scales on the micron level and form bicontinuous structures or discontinuous so-called water-in-water emulsions. More compatible biopolymers can form interpenetrating network on the supramolecular level during gel formation. Interpenetrating networks can also be found within domains of a gelled phase-separated system. Coupled networks will form when there are specific interactions between the biopolymers (Morris 1986).

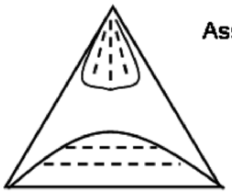

Figure 13.10. Illustration of a ternary phase phase diagram showing associative and segregative phase separation.

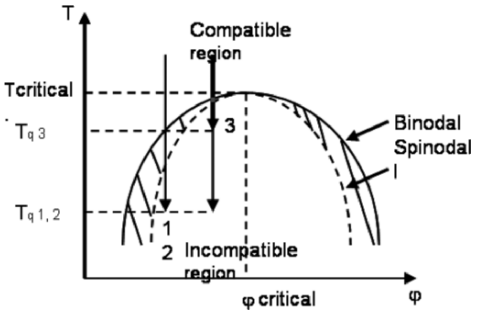

Figure 13.11. A schematic phase diagram of a binary mixture. Broken line spinodal. The metastable phase is hatched.

13.3.1 Segregative Phase Separation

There are many routes to manipulating the structure by phase separation and gel formation. Both the phase diagram and the kinetics of phase separation and gel formation determine the final morphology of the structure. One example of kinetic routes based on a phase diagram is schematically shown in Figure 13.11 (Lorén 2001). When the temperature is lowered and the mixture passes the binodal line phase separation starts. The binodal separates the compatible from the incompatible region in the phase diagram. The incompatible region can be divided into the metastable region, where the mixture separates through nucleation and growth and the unstable region inside the spinodal line, where the mixture separates through spinodal decomposition.

The temperature of the binodal and onset of phase separation is dependent on the composition. In a quench experiment, the time evolution of the phase separation is dependent on the end temperature and the composition. This means that the depth into the incompatibility region at a given position has an impact on the time evolution. Phase separation will then be trapped by gel formation, and it is the relative kinetics between phase separation and gel formation that determines the final morphology. Figure 13.12 gives an example of how the morphology of a discontinuous system depends on the composition and the relative kinetics of phase separation and gel formation (Lorén and Hermansson 2000).

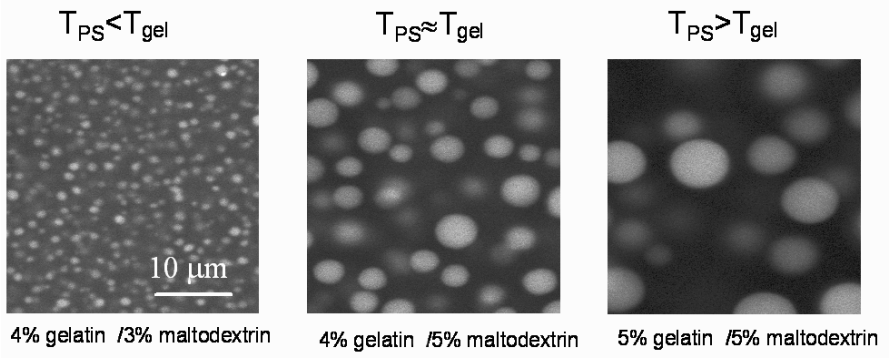

Figure 13.12. CLSM imagers of three different gelatin/maltodextrin mixtures cooled with 1°C/min.

Gelatin maltodextrin mixtures phase separate on cooling, and gelatin forms a gel that can kinetically trap the morphology. When the temperature of phase separation is below that of gel formation, the gel network traps the phase separation early. The micrograph to the left shows a gelatin continuous structure with small inclusions of maltodextrin. Bigger droplets are formed when the phase separation and gelation temperatures are similar, and the biggest droplets form when phase separation starts at a higher temperature than gel formation does. If there is no trapping by gel formation, bulk phase separation will eventually take place with time. Not only can the composition be used to tune the drop size of the phase separated inclusions, but similar results can also be achieved by increasing the cooling rate to allow less time for phase separation prior to trapping by gel formation. It should be pointed out that even if gel formation traps the overall morphology of the system, structural rearrangements can take place in the gelled system.

Spinodal decomposition into a bicontinuous structure and a slow evolution of phase separation and coarsening of the structure can be observed in the vicinity of the critical composition (Figure 13.11). The phase separation starts as a mottled structure, and the contrast increases with time, which indicates that the concentration of the fluorescent maltodextrin increases in one of the phases (Lorén et al. 2001). It can be seen in Figure 13.13 that the characteristic length scale of the bicontinuous structure increases with time. Eventually, a second phase separation can take place, as shown in the micrograph taken after 40 min in Figure 13.13. Small dark inclusions of gelatin appear in the maltodextrin phase and vice versa. Secondary phase separation is dependent on the quench depth and may be due to factors such as increased helix formation of gelatin, molecular weight distributions and rapid hydrodynamic coarsening. The regular spacing of the bicontinuous structures makes it suitable for image analysis, which makes it possible to obtain quantitative information on the mechanisms and kinetics involved in phase separation (Lorén et al. 2002).

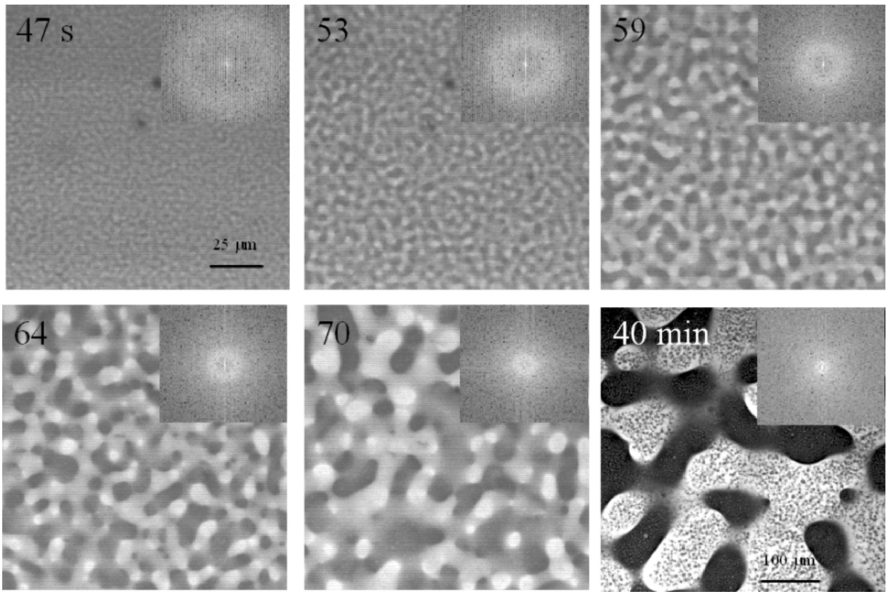

Figure 13.13. CLSM images of a 4.2 *W/W*% gelatin and 7.9% maltodextrin mixture quenched to 20°C. The bright phase is the gelatin phase. The corresponding 2D-FFT is inserted in each micrograph.

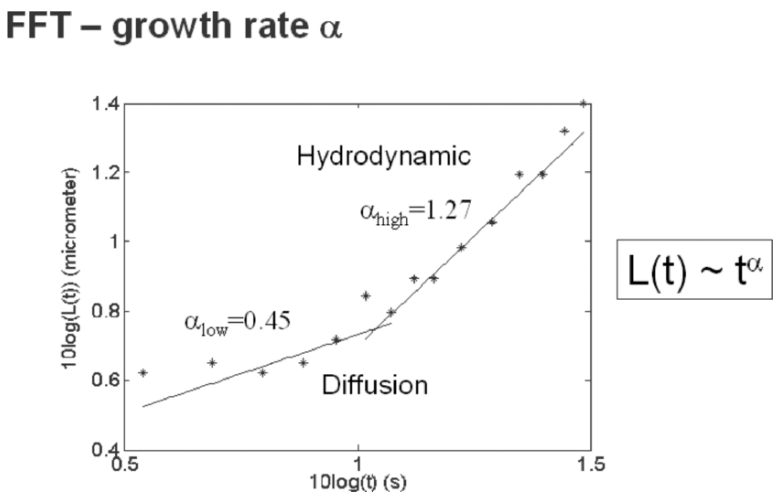

Figure 13.14. The characteristic wavelength *L(t)* as a function of time t of the phase separation.

Lorén analyzed the characteristic length scales of the bicontinuous structure using Fourier image analysis (Lorén et al. 2002). As illustrated in Figure 13.14, there is a crossover from a lower growth rate to a higher growth rate during the coarsening of the phase-separating structure. At small length scales diffusion is predominant, whereas capillary and hydrodynamic flow comes into play at later stages of coarsening during phase separation. This result is a good illustration of how the length scale of a structure determines mass transport.

The complexity of phase-separating gel systems is a challenge that paves the way for structure design of gels with unique properties. Segregative phase separation is thermodynamically driven by the incompatibility of biopolymers that are enriched in different phases. The quenching depth and the end temperature affect morphological Development and the relative kinetics between phase separation and gel formation determines the outcome of the morphology and related properties.

13.3.2 Orders of Gel Formation

Two-phase gel systems can result from the order of gel formation. This is a common situation in mixtures in which one of the biopolymer forms a gel on heating and the other biopolymer forms a gel on cooling. One example is mixtures of ß-lactoglobulin, which forms a gel network on heating and polysaccharides or gelatin, which gel on cooling. When there are no significant interactions as in mixtures of whey protein and gelatin, the whey protein forms a gel network on heating and the gelatin gel just fills the pores of the whey protein network on cooling. However, if there are some incompatibilities that enhance the kinetics of aggregation, the whey protein network will be affected by the second biopolymer as illustrated by the whey protein/amylopectin mixtures in Figure 13/8.

The order of gel formation can sometimes be changed by processing. Walkenström and Hermansson (1997a,b) studied mixed whey protein/gelatin gels induced by heating/cooling, high pressure and a combination of temperature and high pressure treatment. Some examples are outlined in Figure 13.15, which shows sections of mixed gel taken in a light microscope (LM). The three gels shown have the same composition and pH but have been processed differently.

Only the coarsely aggregated whey protein can be seen in the LM and appears black in the micrographs. The micrograph to the left shows a section of a bicontinuous gel, where whey protein forms a coarse aggregated network and the gelatin gel fills the pores of the coarse network. When conventional heating and cooling are used as the gelling technique, the whey protein gel sets first, while a combination of high pressure and heating allows the gelatin to set first or at the same time as the whey protein.

By varying the order of gel formation we can restrict the space available for the respective biopolymer gel to a greater or lesser degree. This is illustrated by the middle and right micrograph in Figure 13.15. When the gelatin gel sets prior to pressure treatment, little space is available for the whey protein, which forms small inclusions in the gelatin continuous gel structure (Figure 13.15, right). If the temperature is tuned during high-pressure treatment, the whey protein is less restricted

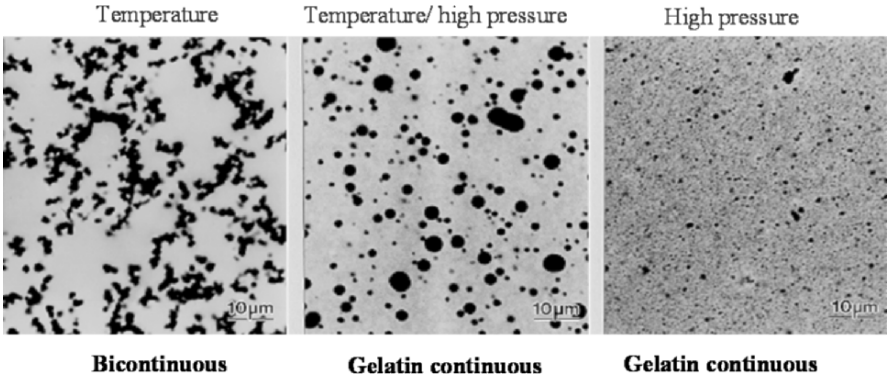

Figure 13.15. LM images of different gels types of 12% whey protein/3% gelatin at pH5.4 induced by temperature and high pressure processing.

by gelatin and bigger whey protein domains are formed in the gelatin continuous system (Figure 13.15, centre).

Figure 13.16 shows the corresponding differences in rheological behaviour due to the distribution of the phases in the mixed gels. The bicontinuous gel has a storage modulus that is more than three times higher than that of the gelatin continuous systems. It is also highly frequency-dependent which is typical of an inhomogeneous aggregated system. The gelatin continuous systems have a lower storage modulus which is more independent of frequency. One very important difference between the systems is their melting properties. The bicontinuous system will not melt on reheating, whereas the gelatin continuous systems have a melting behaviour that is very similar to that of pure gelatin (Walkenström and Hermansson 1997b). Whether a system will melt or not is a very important factor in many food applications.

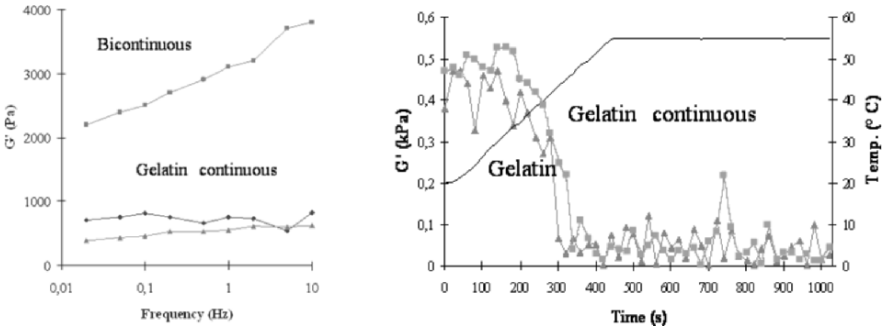

Figure 13.16. Frequency dependency of *G´* for bicontinuous and gelatin continuous gels of 12% whey protein/3% gelatin and pH 5.4 (left). Melting of 3% gelatin and 12% whey protein/3% gelatin at pH 5.4 (right).

Heating/cooling resulted in bicontinuous gel structures regardless of the pH range where particulate or fine-stranded whey protein gels form. Walkenström et al. investigated the rheological properties of whey protein mixtures with increasing concentrations of gelatin. The bicontinuous morphology remained regardless of the ratio of whey protein/gelatin. However, there was a shift in the rheological properties and a rheological "phase inversion" occurred at a certain gelatin concentration. At low gelatin concentrations, the rheological behaviour had the characteristics of the whey protein network, whereas the gelatin dominated above the transition point. Thus, in a bicontinuous gel structure, the strongest network structure dominates the rheological behaviour of the mixed gel. The results illustrate that a shift in the rheological properties does not necessarily allow conclusions to be drawn with regard to the microstructure of a complex mixture.

13.4 Structure–Fracture Properties of Gels

Substantial efforts have been made to understand the mechanisms underlying the structure formation of biopolymer mixtures, such as gel formation, aggregation and phase behaviour. We also need a more detailed understanding of how we can build structures to fracture and break down in a predictable way. This is essential in order to design structures with the desired properties. We cannot easily eat a food product if it does not fracture and break.

Materials science associated with fracture mechanics has mainly been confined to composite materials such as concrete, ceramics and metals. Much of the emphasis of the research has been on preventing fatigue and failure rather than designing for it to occur. The way a structure deforms and breaks under stress is crucial for properties such as flow and fracture behaviour, sensory perception of structure, water release and the mobility and release of active compounds. In the case of foods, the ability to break down and interact with the mouth surfaces provides texture and taste attributes. The crack propagation in a complex supramolecular structure is highly dependent on the continuous matrix, interfacial properties and defects and the heterogeneity of the structure. Previous structure-fracture work has dealt with cellular plant foods, and it has been demonstrated that the fracture path differs between fresh and boiled carrots due to cellular adhesion and cell wall strength as well as cell wall porosity and fluid transport (Thiel and Donald 1998; Stoke and Donald 2000; Lillford 2000).

Access to tensile stages that can be mounted on the CLSM make it possible to obtain simultaneous information about the mechanical properties and underlying structural changes on the macro scale and micron scale during a fracture measurement (Plucknett et al. 2000; Öhgren et al. 2004; Brink et al. 2006). The principle of the measurement is illustrated in Figure 13.17. A sample with a well-defined geometry is cut with a small notch to initiate failure at a specific location. The microscope can be focused on the area close to the notch tip, where the stress is high and the structural rearrangement prior to fracture can be observed.

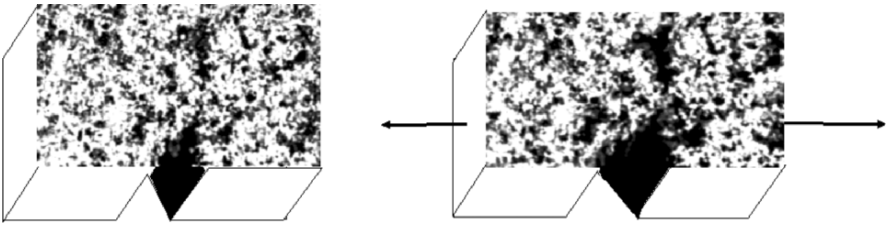

Figure 13.17. Principle of the tensile measurements.

Structure-fracture measurements have been made on the same whey protein/amylopectin mixtures previously discussed with regard to gel formation. In Figure 13.9 we follow the formation of the particulate whey protein network as a function of temperature, where addition of low viscous amylopectin enhanced protein aggregation and gave rise to a coarser and stronger particulate protein network. Figure 13.18 shows crack propagation as well as stress strain curves during initial fracture of two 6% whey protein gels, one without and one with addition of 2% LV amylopectin (Öhgren et al 2004). The maximum stress is almost twice as high in the mixed gel and the corresponding strain considerably higher when the nongelling amylopectin is added to the whey protein system and enhances aggregation and network formation. The crack propagation of the pure whey protein gel proceeds slowly until maximum stress is obtained, after which it accelerates. The more aggregated mixed gel is stronger, and the slow initial stage of the crack propagation goes on beyond maximum stress. The initial stages of crack propagation are measured on the micron scale.

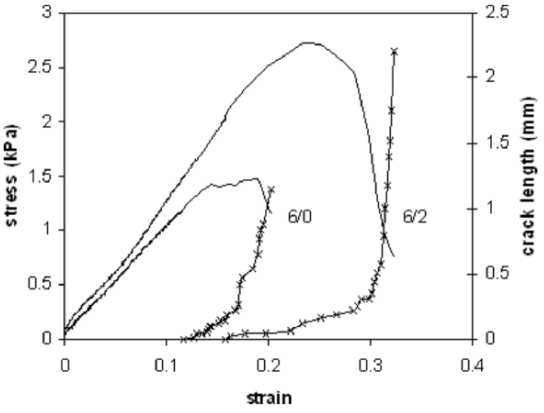

Figure 13.18. Stress–strain curves and crack propagation during initial fracture of 6% ß-lactoglobulin gels with and without 2% LV amylopectin.

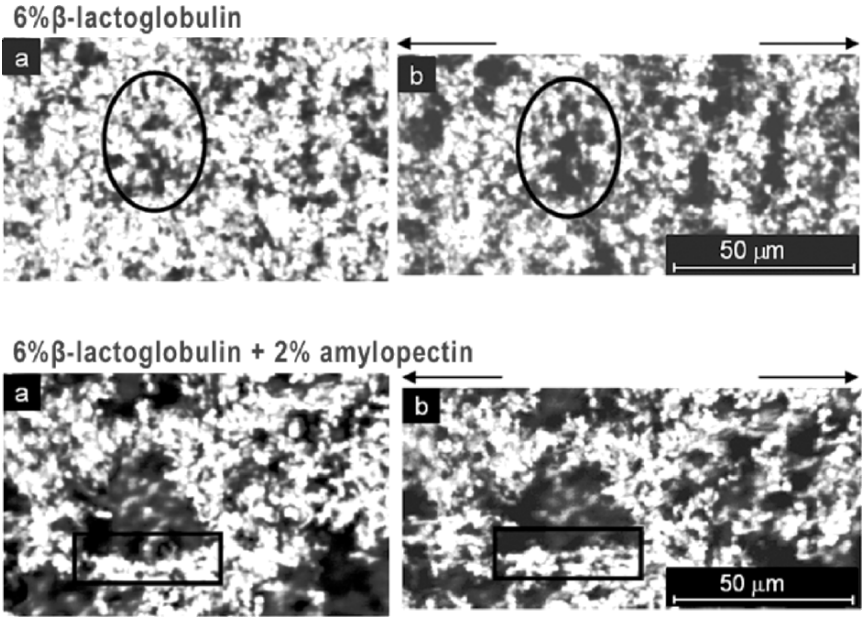

Figure 13.19. Microstructure before (a) and at maximum deformation (b) of 6% ß-lactoglobulin gels without and with addition of LV 2% amylopectin.

Corresponding microstructural changes are shown in Figure 13.19 with undeformed structures to the left and the structures in the vicinity of the crack in the deformed state to the right (Öhgren et al. 2004). The fracture is initiated in the pores of the weaker ß-lactoglobulin system, which increase in size with increasing stress concentration; see, for example, the pore in the marked region. The stronger strands in the mixed system respond differently and can be extended in the direction of the tensile test, which is illustrated in the lower part of Figure 13.19.

Figures 13.18 and 13.19 illustrate how information about the structure and fracture behaviour can be obtained simultaneously under dynamic conditions. On the micron scale, structural changes can be observed far below deformation to maximum stress and, as illustrated in Figure 13.19(b), the stronger mixed gels have stress-bearing structure far beyond the maximum stress.

Information about the initial fracture behaviour of semi-solid foods will give important new insights into food structure design. The technique is now available and new knowledge can be obtained from structure–fracture studies of complex colloidal foods. Of particular interest is the significance of initial fracture for the sensory perception of semi-solid food products such as dairy products. A number of sensory characteristics are most likely related to the initial fracture behaviour, including structural rearrangements and fluid transport.

13.5 Gel Structure and Mass Transport

A gel can contain more than 99% water and still behave like a solid that does not flow. The ability of a gel structure to hold and release water is a very important functional property. The typical length scales present in the gel structure determine water uptake, release and water-holding, diffusion and molecular mobility of soluble compounds.

In many structured products, water management includes several mass transport mechanisms such as hydrodynamic flow, capillary flow and molecular self-diffusion depending on the length scale. Hydrodynamic flow is active in large and open structures and it is driven by external forces such as gravity or by differences in the chemical potential, that is, differences in concentrations at different locations in the structure. Capillary flow also depends on surface tension and occurs in channels and pores on shorter length scales than in hydrodynamic flow. A capillary gel structure will hold water, and external pressures equivalent to the capillary pressure will be needed to remove the water.

Hydrodynamic and capillary flows are of importance for water loss and the permeability of relatively coarse gel structures such as, for example, the particulate whey protein structures. Moisture loss can be achieved by gravity or by application of a gentle centrifugation force that is stronger than the capillary pressure but not strong enough to break the gel. Moisture loss of particulate whey protein gels and blood plasma gels has been measured as a function of pH, temperature, protein and salt concentration (Hermansson 1982, 1986). Permeability measurements have been made of coarsely aggregated dairy gels such as casein gels (Mellema et al. 2000.) Roughly speaking, gels with pore sizes above 100 nm can release water on application of an external force without breaking. However, the exact relationships between the pore size distribution and the water-holding properties of heterogeneous gel structures are far from being completely described, and much more work is needed in this area.

For gels of finer dimensions, such as transparent fine-stranded gels, the capillary pressures are too high for water to be pressed out. Such gels can also release water, but this is mostly due to syneresis, which is related to aggregation of the network beyond the gel point and subsequent shrinkage. The water will be squeezed out because of the decrease in volume of the gel network and there will simply be less space available.

Diffusion is the prevailing mass transport mode for water in fine-stranded gels with small pores in the nanometer region. For such length scales, it is not the diffusion of water that is the main subject of research but rather the mass transport of active molecules and nanoparticles in the gel matrix. There is a strong focus on the design of structures for optimal release properties both with regard to the gel matrix and the probes carrying the active compounds.

Diffusion can be divided into free and restricted diffusion. A combination of NMR diffusometry and microscopy has proved useful for the study of probe diffusion in gels and emulsions (Hagslätt et al. 2003; Lorén et al. 2005; Hermansson et al. 2006; Walther et al. 2006) For such studies the probe should be much larger than water so that the obstruction can be clearly observed in NMR diffusometry. Small molecules

that diffuse in a material with small amounts of obstructing matter having an open structure network structure will not be significantly slowed down. However, the diffusion rate of a much larger molecule can be greatly affected. The degree of obstruction depends on the size of the pores in the material compared to the size of the probe molecule.

Studies have been made of probe diffusion of PEG (polyethylene glycol) of different molecular weights in kappa-carrageenan gels in D_2O, where the network structures have been varied by aggregation induced by cooling and addition of salts (Walther et al. 2006). The relation between microstructure and diffusion was qualitatively investigated by comparing the gel microstructure with the corresponding self-diffusion coefficient, D, and the diffusion quotient, D/D_0, where D_0 is the diffusion coefficient of PEG in D_2O. Figure 13.20 shows some results of the impact of strand and void properties on D and D/D_0. Without any addition of salt there is no gel formation, kappa-carrageenan is present as random coils, and the diffusion in the random coil solution is low. On addition of 20 mM KCl a very fine-stranded network is formed.

There is enough potassium for coil–helix transition and gel formation to occur but not enough potassium to drive aggregation further. Therefore, the change of cooling rate has little effect. The fine network structure obstructs diffusion and D/D_0 is low regardless of the cooling rate. At higher salt concentrations, aggregation is enhanced. Quenching in 100 mM KCl results in a fine network structure, whereas slow cooling allows aggregation into a coarser network. This has an effect on the diffusion coefficients, as shown in Figure 13.20. Addition of a combination of sodium and potassium results in a mixed aggregated and very fine structure on quenching and an even coarser aggregated structure on slow cooling. The very fine structure cannot be seen in the TEM micrograph. As can be seen in Figure 13.20, aggregation induced by cooling has an effect on the PEG diffusion. In the most aggregated system, the diffusion ratio is one, which means that there is no obstruction from the kappa-carrageenan structure.

The results illustrate that a combination of NMR diffusometry and microscopy techniques provides an important tool for mastering inherent structural properties giving rise to functionality with regard to mass transport, water management and molecular mobilities. The example shows how the diffusion of PEG molecules is obstructed by the gel structure. The character of the diffusing probe is also important. In a crowded gel, a linear polymer can always reptate or move in a wormlike manner when the pores are small compared to the size of the hydrodynamic radius of the polymer. However, a nanoparticle like a dendrimer cannot change its structure and can only diffuse with the same diffusion mechanism independent of its surroundings. Other factors that have to be taken into account are interactions between the matrix and the diffusing molecules, as well as the flexibility of the gel network.

Tools are available for tuning the network structure and thereby its properties relating to mass transport of solvents or solutes. Differences in the microstructure have been qualitatively related to water-holding properties mainly under hydrodynamic flow conditions. Studies of coarse aggregated protein gels have shown that an increase in the coarseness and pore size in the range of 0.2–2 μm resulted in pronounced loss of water-holding capacity (Hermansson 1986). For large pore sizes in the micron range, permeability studies give information on the hydrodynamic flow

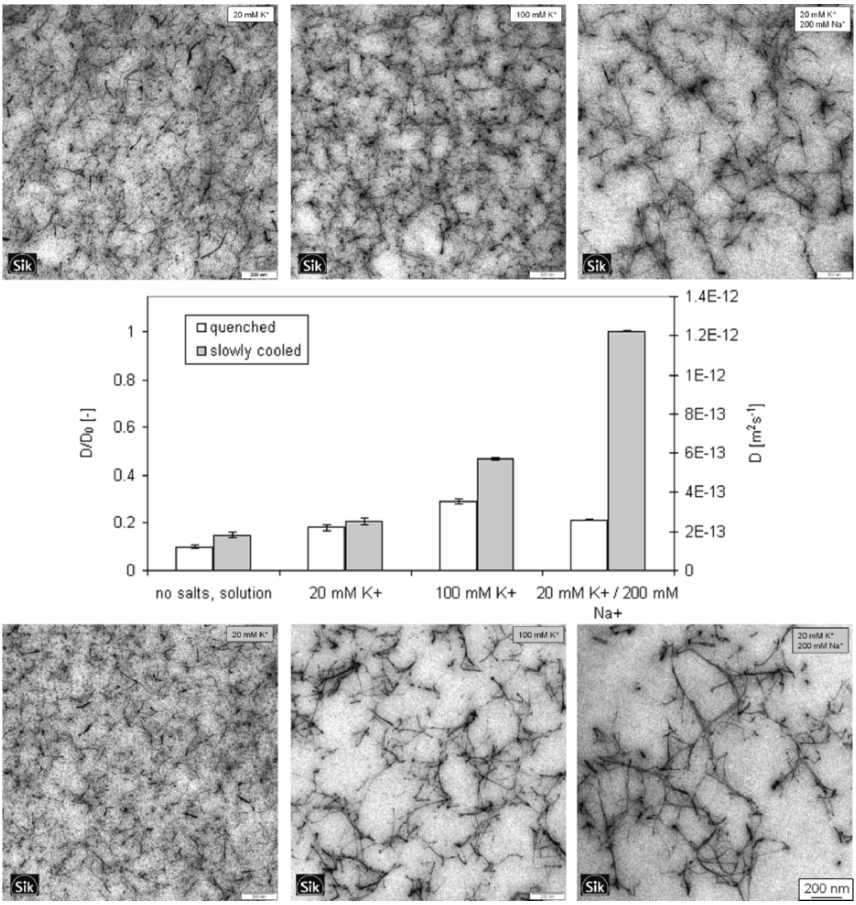

Figure 13.20. Self diffusion D and D/D_0 of a 634 kgmol-1 PEG in kappa-carrageenan gels formed under various ionic conditions. The upper row shows gels cooled by quenching and the lower row shows slowly cooled gels.

and diffusion in gel networks. However, we still lack information on how the heterogeneity over length scales from the nano- to the micrometer region comes into play in connection with mass transport of solvents or solutes. This information is necessary for a complete understanding of the relationships between the microstructure and mass transport.

13.6 Some Future Trends

Gel structures are the matrices that give many food products their characteristic properties. This chapter gives some insights into what is needed to master the architecture of gels to design products with the desired properties. Micrographs show that

a biopolymer gel network can span over a wide range of lengths scales, with pores from a few nanometers to hundreds of micrometers depending on the biopolymer and the processing conditions used. There are also variations within one biopolymer network, which demonstrate the heterogeneous nature of the gel structure. In future work, more focus is needed on the heterogeneic nature of the gel and the significance of different length scales for various gel properties. This is quite obvious for mass transport, where the length scale can be directly correlated to the types of flow and timescales. Substantial efforts have been made to purify fractions of proteins and polysaccharide to more completely understand the impact of the molecular structure on performance. Now we need to know more about the rules for strand and network formation. In future work, we also need to learn more from multifunctional hierarchical structures in biological systems.

There are now tools available for studies of dynamic events. This means that we can follow the course of structure formation and based on this knowledge, design new processing equipment to engineer structure formation on the micron scale as well as the nano scale. Again, the combination of micron and nano-technologies will give insight into the design of hierarchical structures. The importance of the kinetics of gel formation, especially where several mechanisms come into play during gel formation, has been clearly demonstrated. This opens up new possibilities but it also tells us that we may have to adjust our process technology to take full advantage of this knowledge.

One of the biggest challenges for the food industry is to make products that break down or fail in a predictive way so that they function in the way desired. The way a structure deforms melts or breaks down during consumption is critical for the sensory perception of the structure, the fracture behaviour, water release and mobility and release of active compounds. Access to new research tools opens up new avenues for structure–fracture research of pure gels, composite gel structures and networks at interfaces in complex food structures. As stated above, the way a structure breaks down determines the sensory perception, but it is also of importance for interactions with body fluids and the bioavailability of food compounds. There is an increasing demand for healthier foods, and we also have to address this issue on a microstructural level. The kinetics of structure breakdown in the body will affect the uptake of nutrients. This can be modified by structure design of a gel matrix either to enhance the availability of active nutrients or slow down the digestion and release of, for example, sugars or other compounds.

13.7 References

Brink, J., Langton, M., Stading, M., and Hermansson, A.M. (2006). Simultaneous microstructure and mechanical analysis of whey protein/gelatin gels during fracture. *Food Hydrocolloids*. 21 (2007), 409–419.

Djabourov, M. (1988). Architecture of gelatin gels. *Contemporary Phys*. 29, 273–297.

Djabourov, M., Leblond, J., and Papon, P. (1988). Gelation of aqueous gelatin solutions. I. Structural investigation. *J. Phys. (Paris)*, 49, 319–332.

Hagslätt, H., Jönsson, B., Nydén, M., and Söderman, O. (2003). Prediction of pulsed field gradient NMR echo-decays for molecules diffusing in various restrictive geometries.

Simulations of diffusion propagators based on a finite element method. *J. Magn. Res.*, 161, 138–147.

Hermansson, A.M. (1989). Rheological and microstructural evidence for transient states during gelation of kappa-carrageenan gels in the presence of potassium. *Carbohydrate Polymers,* 10, 163181.

Hermansson, A.M. (1986). *Fat and Waterholding in Functional Properties of Food Macromolecules*. J.R. Mitchell and D.A. Ledwards (eds.). Elsevier Applied Science Publishers, London and New York.

Hermansson, A.M. (1982). Gel characteristics: Structure as related to texture and water binding of blood plasma gels. *J. Food Sci.* 47, 1965–1972.

Hermansson, A.M., Eriksson, E., and Jordansson, E. (1991). Effects of potassium, sodium and calcium on the microstructure and rheological behaviour of kappa-carrageenan gels. *Carbohydrate Polymers,* 16, 297–320.

Hermansson, A.M., and Langton, M. (1994). Electron microscopy of food biopolymers. In: S.B. Ross-Murphy (ed.). *Physical Techniques for the Study of Food Biopolymers*. Blackie Academic & Professional, Glasgow.

Hermansson, A.M., Kidman, S., and Svegmark, K. (1995). Starch – A phase separated biopolymer system. In: J.R. Mitchell (Ed.), *Biopolymer mixtures*. pp. 225–246.

Hermansson, A.M., Lorén, N., and Nydén, M. (2006). The importance of microstructure for water diffusion on micro and nano length scales. In: P. Buera, J. Welti-Chanes, P. Lillford, and H. Corti (eds.). *Water Properties of Food, Pharmaceuticals and Biological Materials*, CRC Taylor and Francis, Boca Raton, FL, pp. 79–100.

Hoffman, M.A.M., and van Mil, P.J.J.M. (1997). Heat-induced aggregation of ß-lactoglobulin: Role of free thiol and disulfide bonds. *J. Agricult. Food Chem.*, 45, 2942–2948.

Langton, M., and Hermansson, A.M. (2001). Effect of emulsifiers on the aggregation of β-lactoglobulin. In: E. Dickinson and R. Miller (eds.), *Food Colloids, Fundamentals of Formulations*, Royal Society of Chemistry, Cambridge, pp. 369–372.

Lillford, P.J. (2000). The material science of eating and food breakdown. *MRS Bulletin*, 25, 38–43.

Löfgren, C. (2005). *Microstrucure and Rheological Behaviour of High Methoxyl and Low Methoxyl Pectin Gels and Their Mixtures*. Thesis, Chalmers University of Technology, Gothenburg, Sweden.

Löfgren, C., Guillotin, S., Evenbratt, H., Schols, H., and Hermansson, A.M. (2005). Effects of calcium, pH and blockiness on kinetic rheological behavior and microstructure of HM pectin gels. *Biomacromolecules*, 6, 647–652.

Löfgren, C., Walkenström, P., and Hermansson, A.M. (2002). Microstructure and rheological behaviour of pure and mixed pectin gels. *Biomacromolecules*, 6, 1144–1153.

Löfgren, C., and Hermansson, A.M. (2004). Microstructure and kinetic behaviour of pure and mixed pectin gels. In: P.A. Williams and G.O. Phillips (eds.), *Gums and Stabilisers for the Food Industry*, No. 12, The Royal Society of Chemistry, Cambridge, pp. 153–159.

Löfgren, C., Guillotin, S., and Hermansson, A.M. (2006). Microstructure and kinetic rheological behaviour of amidated and non-amidated LM pectin gels. *Biomacromolecules*, 7, 114-121.

Lorén, N. (2001). *Structure Evolution During Phase Separation and Gelation of Biopolymer Mixtures*. Thesis. Chalmers University of Technology, Gothenburg, Sweden.

Lorén, N., and Hermansson, A.M. (2000). Phase separation and gel formation in kinetically trapped gelatin/maltodextrin gels. *Int. J. Biol. Macrom*, 27, 249–262.

Lorén, N., Altskär, A., Hermansson, A.M., Lorén, N., Altskär, A., and Hermansson, A.M. (2001). Structure evolution during gelation at later stages of spinodal decomposition in gelatin/maltodextrin mixtures. *Macromolecules*, 34, 8117–8128.

Lorén, N., Langton, M., and Hermansson, A.M. (2002). Determination of temperature dependent structure evolution by FFT at late stage spinodal decomposition in bicontinuous biopolymer mixtures. *J. Chem. Phys*., 116, 10536–10546.

Lorén, N., Hagslätt, H., Nyden, M., and Hermansson, A.M. (2005). Water mobility in heterogeneous emulsions determined by a new combination of confocal laser scanning microscopy, image analysis, NMR diffusometry and finite element method simulation. *J. Chem. Phys*. 122, 024716

Mellema, M., Heesakkers, J.W.M., van Opheusden, J.H.J., and van Vliet, T. (2000). Structure and scaling behaviour of aging rennet-induced casein gels examined by confocal microscopy and permeametry. *Langmuir*, 16, 6847–6845.

Morris, V.J. (1986). Gelation of polysaccharides, In: J.R. Mitchell and D.A. Ledwards (eds.), *Functional Properties of Food Macromolecules*. Elsevier Applied Science Publishers, London and New York, pp. 121–170.

Mezzenga, R., Schurtenberge, P., Burbridge, A., and Michel, M. (2005). Understanding food as soft materials. *Nature Mater.* 4, 729–740.

Oakenful, D., and Scott, A. (1984). Hydrophobic interactions in the gelation of high methoxyl pectins. *J. Food Sci*. 49, 1093–1109.

Öhgren, C., Langton, M., and Hermansson, A.M. (2004). Structure–fracture measurements of particulate gels. *J. Mater. Sci*. 39, 6473–6482.

Olsson, C., Frigård T., Andersson, R., and Hermansson, A.M. (2003). Effects of amylopectin structure and molecular weight on microstructural and rheological properties of mixed ß-lactoglobulin gels. *Biomacromolecules*, 4, 1400–1409.

Olsson, C., Langton, M., and Hermansson, A.M. (2002a). Microstructures of β-lactoglobulin/amylopectin gels on different length scales and their significance for rheological properties. *Food Hydrocolloids*, 16, 111–116.

Olsson, C., Langton, M., and Hermansson, A.M. (2002b). Dynamic measurements of β-lactoglobulin structures during aggregation, gel formation and gel break-up in mixed biopolymer systems. *Food Hydrocolloids*, 16, 477–488.

Olsson, C., Stading, M., and Hermansson, A.M. (2000). Rheological Influence of amylopectins on mixed β-lactoglobulin gel structures. *Food Hydrocolloids*, 14, 473–483.

Piculell, L., and Linman, B. (1992). Association and segregation in aqueous polymer/polymer, polymer surfactant mixtures: similarities and differences. *Advanced Colloid Interface Science*, 41, 149–178.

Plucknett, K.P., Pomfret, S.J., Normand, V., Ferdinando, D., Veerman, C., Frith, W.J., and Norton, I.T. (2000). Dynamic experimentation on the comfocal laser scanning microscope: application on soft-solid composite food materials. *J. Microscopy*, 201, 279–290.

Stading, M., Langton, M., and Hermansson, A.M. (1993). Microstructure and rheological properties of inhomogeneous particulate β-lactoglobulin gels. *Food Hydrocolloids,* 3, 195–212.

Stokes, D.J., and Donald, A.M. (2000). In situ mechanical testing of dry and hydrated breadcrumb in the environmental scanning electron microscope. *J. Mater. Sci.* 35, 599–607.

Thiel, B.L., and Donald, A.M. (1998). In situ mechanical testing of fully hydrated carrots (*Daucus carota*) in the environmental SEM. *Ann. Botany*, 82, 727–733.

Trappe, V., and Sandkühler, P. (2004). Colloidal gels: low-density disordered solid-like states. *Curr. Opinion Colloid Interface Sci.* 8, 494–500.

Verheul, M., Roefs, S.P.F.M., and de Kruif, C.G. (1998). Kinetics of heat-induced aggregation of ß-lactoglobulin. *J. Agricul. Food Chem.* 46, 896–903.

Voragen, A.G.J., Pilnik, W., Thibault, J.F., and Axelos, M.A.V. (1995). Pectins. In: A.M. Stephen (ed.), *Food Polysaccharides and Their applications*, Marcel Dekker, New York, pp. 287–339.

Walkenström, P., and Hermansson, A.M. (1997a). High pressure treated mixed gels of gelatin and whey proteins. *Food Hydrocolloids*, 11, 195–208.

Walkenström, P., and Hermansson, A.M. (1997b). Mixed gels of gelatin and whey proteins, formed by combining temperature and high pressure. *Food Hydrocolloids*, 11, 457–470.
Walther, B., Lorén, N., Nydén, M., and Hermansson, A.M. (2006). Influence of kappa-carrageenan gel structures on diffusion of probe molecules determined by transmission electron microscopy and NMR diffusometry. *Langmuir*, 22, 8221–8228.

Chapter 14

Bubble-Containing Foods

K. Niranjan[1] and S.F.J. Silva[2]

[1] Department of Food Biosciences, University of Reading, Whiteknights, POBox 226 Reading RG6 6AP, UK, afsniran@rdg.ac.uk
[2] Department of Food Biosciences, University of Reading, Whiteknights, POBox 226 Reading RG6 6AP, UK, s.f.j.silva@rdg.ac.uk

14.1 Introduction

The presence of bubbles in a number of food products, such as bread, champagne, ice cream and beer, has dominated our perception of product quality. Novel bubble-containing products occupy a greater proportion of supermarket shelf space. The inclusion of bubbles in foods permits the creation of very novel structures while offering lighter alternatives in terms of calories. Manufacturers generally find that most products manage to gain a positive market image by highlighting bubbles. Consumers also associate such products with health and luxury. It is generally recognised that the mechanisms governing the formation and stability of such structures are very complicated, because the recipes often contain a number of ingredients that undergo very complex interactions during processing as well as storage. At the same time, there is also recognition of the fact that these complex interactions between ingredients have not been adequately researched. A significant body of published information exists on the formation of porous structures in bread and their relation to the processes adopted to mix the dough (Chiotellis and Campbell 2003; Martin et al. 2004). However, such studies in relation to the whole range of other bubble-containing food products such as cakes, creams used in biscuits, ice cream, and so on, are very sketchy. This chapter describes the formation of bubble-containing food structures, particularly focusing on products other than bread, and aims to develop the relationship between process variables and the structure characteristics, and to explore the interplay between structure and mouth-feel.

14.2 Methods for Creating Bubble-Containing Food Structures

14.2.1 Dispersion Formation by Mechanical Agitation Under Positive Pressure

Beating a material to induce air entrapment and produce a foam is a relatively common process. Beating machines, comprised of of a mixing bowl and a motor-driven whisker, are generally used for the purpose. Figure 14.1 shows the top view of a mixing bowl fitted with a whisk. The mechanical energy generated within the system by impeller rotation results in the dispersion of gas bubbles. Larger air bubbles are initially incorporated from the head space, and their sizes diminish as agitation proceeds (Prins 1988). Air can be incorporated by this process into a range of foods having different viscosities. Examples of mechanically whipped products are whipped cream, bread dough, and cake and biscuit batters.

Mixing operations in industry can be carried out batchwise or continuously. When whipping occurs in an open bowl by a rotating whisk, the amount of liquid (or continuous phase) is fixed, but air supply is unlimited. In this case, the amount of air taken up by the material is related to the apparatus geometry and the physicochemical properties of the material (Prins 1988). Air content and bubbles size distribution of the dispersion at any given moment during aeration will depend on the balance between the rates of entrainment and disengagement of gas between the headspace and continuous phase (Campbell and Mougeot 1999; Massey et al. 2001). Headspace pressure and whisk speed are important process parameters in such mechanically agitated processes. The whisk speed must be kept above the minimum speed for air entrainment and below values causing the destruction of structure. Rolling vortices of liquid formed on the surface entrain gas, and the bubbles formed are captured into the bulk by liquid circulation. Increasing headspace pressure will often reduce the time taken to achieve a set level of air incorporation (Cheng 1992).

Continuous processes are being increasingly employed by the food industry for forming bubble-containing structures in soft solids, as well as for dissolving gases such as carbon dioxide in liquids and syrups to produce beverages. In most processes, the gas dissolution occurs under pressure and the bubbly structure is formed when excess dissolved gas desorbs upon pressure release. Mass transfer principles therefore play an important role in structure formation. Carbonated beverages are produced in specific mixing equipment called carbonators. This equipment allows close contact between carbon dioxide and the liquid. The pressure of the system, gas solubility, time and area of contact, as well as the presence of other gases in the mixture, are the main factors determining the degree of carbonation. A typical carbonator is shown in Figure 14.2. It is noteworthy that the carbon dioxide gas can either be dissolved directly into concentrated sugar syrup or be dissolved in water prior to syrup addition (Mitchell 1990).

Ice cream is normally aerated during freezing, either by injecting air under pressure in a continuous freezer or by blending air pockets during freezing in a batch process. The shearing process that accompanies freezing reduces the size of the larger air bubbles just as the fat globules coalesce. The type of freezer and the operating conditions employed will ultimately influence dispersion properties: generally continuous operation generates smaller air bubbles than batch processes (Goff and Clarke 2003).

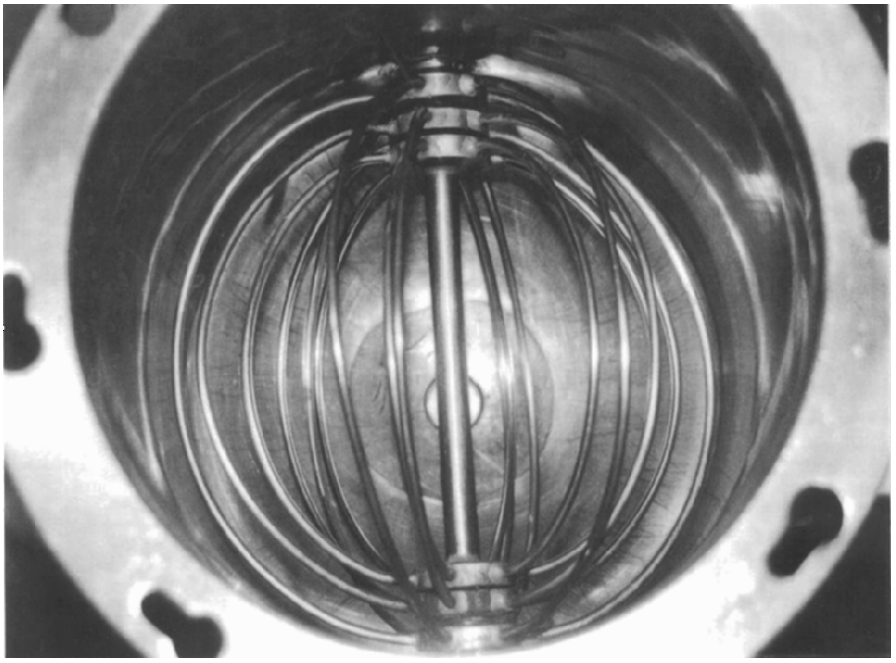

Figure 14.1. Top view of a commercial whisk.

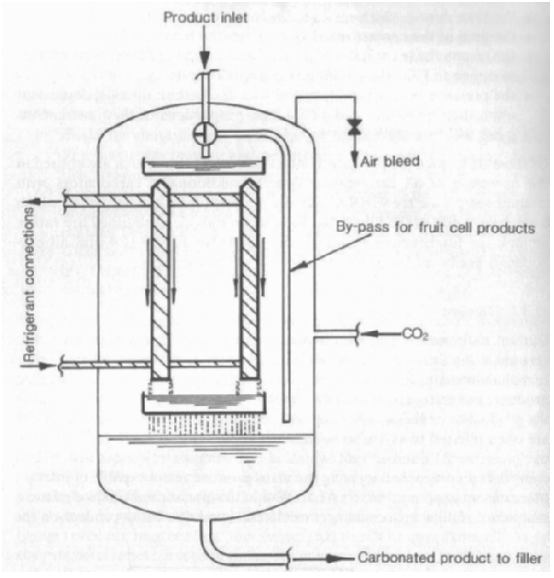

Figure 14.2. Typical carbonator (Mojonnier carbo-cooler) carbonator. Taken from Mitchell (1990).

14.2.2 Dispersion Formation Under Vacuum

This process is based on applying vacuum to a liquid or a continuous phase in order to allow dissolved gases to come out of solution (Wolfe 1995). The foam formed is normally cooled to generate a solidified structure in which the bubbles are trapped. In the case of confectionery mixes, air is injected into the mix to reduce the dispersion specific gravity. Individual pieces are then shaped and directed to the vacuum tunnel held at around 0.03 atm. Some bubbles may well be lost during shaping. The remaining bubbles expand to cause a 6–10 fold increase in the volume of the shaped product (Jones 1995).

14.2.3 Steam Induced-Formation of Dispersion

Steam-induced structure development is applied to a range of food products. An example of this is the application of dry heat inside an oven to bread dough or cake batter. A porous structure is formed that is largely influenced by steam generation, although thermal expansion of other gases and CO_2 desorption also play a critical role (Campbell and Mougeot 1999). The structure of breakfast cereals such as wheat flakes and puffed rice, and also popcorn, are also formed by this method, which consists of introducing material pellets into a toasting oven where the material stays exposed to up to 300°C temperatures for 30–90 seconds. This exposure results in the formation of steam in the pellets which escapes against a resisting pressure to cause "puffing" which is a significant volume expansion of up to 20 times the original pellet size (Kent and Evers 1994). When corn is subjected to high heat, the water inside the kernel vaporizes. This steam expands, causing the disruption of the hard pericarp, and forms a highly porous structure of what is commonly known as popcorn (Matz 1984).

As an alternative to the above method, cereal puffing can also be accomplished by a "puffing gun." The process relies on the immediate transfer of the heated cereal containing superheated steam from a high to a low pressure allowing water condensation and consequent expansion. The suddenness at which pressure transition occurs is the key parameter determining the porosity (Kent and Evers 1994).

The popular array of milk-based foamed coffee products found in every coffee shop has a common characteristic contributing to its appeal: a milky frothy head. Milk foams are traditionally generated by injecting steam through a nozzle into milk contained in a cup. Air is essentially entrained from the headspace due to high surface turbulence, and the dispersion is stabilized by biochemical changes accompanying a steep increase in milk temperature. The extent of air entrainment and the nature of the dispersion formed are critically dependent on the nozzle design. A variety of designs are commercially available, including one where the air is entrained by venturi action through a pipe having one end open to the atmosphere and the other end connected to the tip of the steam injector as shown in Figure 14.3. The exact mechanism by which the dispersions formed are stabilized is not clearly understood, and further research is needed in this area.

The direct immersion of foods in hot oil, that is, frying, also generates steam within the exposed material. An example is the commercial production of potato crisps. As the potato slices pass trough the fryer, they are exposed to temperatures

around 180–200°C. The high temperature causes the water in the slices to evaporate, leaving behind voids that play a critical role in characterizing the "crispiness" of the final product (Matz 1984).

Extrusion is used in a range of products from cereals to crisp snacks and sugar confectionery. However, its most representative application is in breakfast cereals. In extrusion cooking the raw material is conveyed through a rotating screw while being compressed, and then it is sheared at high temperatures and pressures to form a plasticized mass. As this mass passes through a die at the end of the screw, the temperature and pressure are suddenly reduced, when moisture evaporation in the channeled strips forms a honeycombed structure (Kent and Evers 1994). Extruded product properties are very dependent on an array of interrelated operational parameters (such as temperature, pressure, die diameter, screw configuration and available water), which complicates the control of the structure.

Low-temperature extrusion has been applied in the manufacture of ice cream. It involves the conveying of ice cream mix at –5°C through a refrigerated screw extruder. As the ice cream leaves the extruder at low temperature the hardening step is eliminated and the ice cream can be taken directly to the cold store. The manufacture of ice cream by this process also generates smaller air bubbles than conventional freezing as the low temperature will result in a reduction in the coarsening of air bubbles and ice crystals (Clarke 2004). Low-temperature extrusion of chocolate has also been patented though no commercially available products are known to be produced by this method (Mackley 1994).

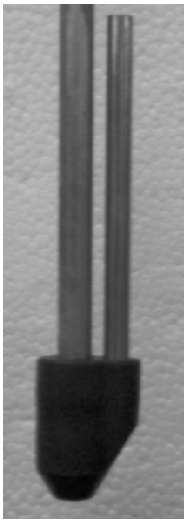

Figure 14.3. Venturi-type nozzle from a commercial espresso machine, used in the formation of frothy milk.

14.2.4 Other Aeration Methods

The dispersion formation methods discussed so far are largely reliant on physical changes occurring within the product, which may either be mechanically induced or thermally induced. However, chemical reactions leading to the evolution of CO_2, for example, yeast metabolism during fermentation or the decomposition of "baking soda," are mainly responsible for structure development in universally appreciated foods such as bread and cakes. Sodium bicarbonate and phosphates can be thermally activated at temperatures over 90°C. This decomposition results in the formation of carbon dioxide and water vapour, which in turn causes volume expansion of the product (Bennion and Bamford 1997). The unique texture of bread is achieved through gas incorporation and bubble manipulation within the dough during mixing, proving and baking. Proving is the defining operation of the whole process during which yeast metabolizes flour sugars into CO_2. This gas diffuses into bubbles previously incorporated in the mixing stage, and expands the dough (Chiotellis and Campbell 2003). In crumpet production, the batter expands due to the formation of CO_2 during fermentation; the larger bubbles then escape leaving behind a population of small nuclei. The water in the batter evaporates into the nuclei during hot plate baking at 200–230°C to form a series of vertical cones as shown in Figure 12.4 (Pyle 2005).

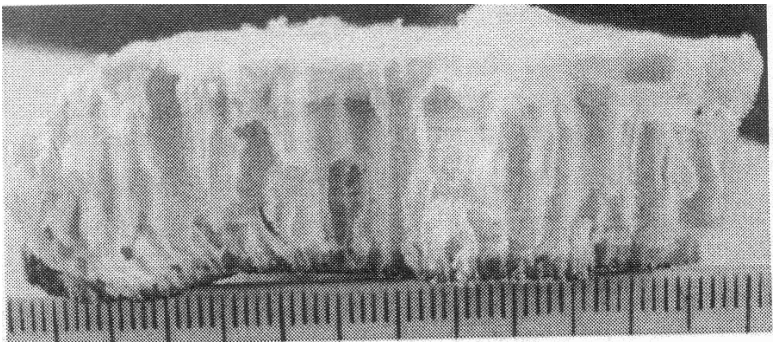

Figure 14.4. Structure of a crumpet cross-section, after 75 s baking. Taken from Pyle (2005).

14.3 Characterization of Bubble-Containing Structures

14.3.1 Gas Hold-Up

Gas hold-up (ϕ) is a common measure of the level of bubbles present in foods. It is normally defined as the volume fraction of gas based on the dispersion volume, but commonly expressed as a percentage. Gas hold-up values in bubble containing foods range from 15% to 20%, for example, in milkshakes, to over 90% in extruded products such as popcorn and rice cakes (Campbell and Mougeot 1999). Experimentally, gas hold-up can be estimated by the density difference between the bubble-containing dispersion and the material forming the continuous phase. This is most commonly achieved by completely filling, covering and weighing a cup, first with the continuous

phase (m_i), then with the bubble-containing dispersion (m_f), and using the following equation:

$$\phi = \left(1 - \frac{m_f}{m_i}\right) \times 100 \tag{14.1}$$

This standard procedure can be applied to liquids and pastes having medium to high viscosity such as ice cream, whipped cream and dough (Massey et al. 2001; Lau and Dickinson 2005; Jakubczyk and Niranjan 2006), where the dispersion is stable and air release during the measurement process is negligible. In the case of solid foams, such as aerated chocolate, where it is difficult to sample a defined volume, the flotation method is more suitable (Haedelt et al. 2005). A mass of aerated material is noted (m_f) and placed in a corked glass cylinder filled with water. The total weight is noted as m_a; and the weight of the container filled with water alone is noted as m_c. The density of the solid foam is then calculated as:

$$\rho_f = \frac{\rho_w \times m_f}{\left(m_f + m_c - m_a\right)} \tag{14.2}$$

where ρ_w is the density of water (kgm^{-3}) and m_f is the mass of solid foam (kg). Gas hold-up is then calculated by comparing the density of the aerated solid foam (ρ_f) with the gas-free density, that is, density of the continuous phase (ρ_i), as follows:

$$\phi = \left(1 - \frac{\rho_f}{\rho_i}\right) \times 100 \tag{14.3}$$

In more fragile systems, such as aqueous foams forming a head on a clear liquid (e.g., draught beer, cappuccino), where even careful foam manipulation can induce significant air release, the gas hold-up in the foam at any instant can be measured by noting the height of the foam (h_f), the height of the clear liquid taken initially (h_i) and the height of the clear liquid at the instant (h_l) (all heights being measured in a vessel of uniform cross sectional area), and calculating the hold up using the equation:

$$\phi = \frac{h_f - h_i}{h_f - h_l} \times 100 \tag{14.4}$$

A number of instrumental methods have also been developed to measure hold-up directly. Bisperink et al. (1992) observed good agreement between ϕ values read by an optical probe and those estimated by using Equation (14.4). Ultrasound-based techniques have also been applied to measure the specific gravity of food batters, which is a promising method because it avoids sampling procedures in a manufacturing

environment (Fox et al. 2004). In systems with high air content, such as egg white foam, the term "overrun" is most commonly used to characterize the level of aeration. Overrun (*OR*) represents the additional air added to the material and it is related to gas hold-up as follows (Campbell and Mougeot 1999):

$$OR = \frac{\phi}{100 - \phi} \times 100 \tag{14.5}$$

In other words, the overrun represents the fraction of gas based on the clear volume of the continuous phase.

During the process of bubble inclusion, the gas hold up varies with time. In most systems, the gas hold up increases initially, reaches a peak and drops. A maximum gas hold-up of 48% was observed after 9 minutes of whipping UHT cream in a standard device followed by a decrease for longer whipping times; see Figure 14.5 (Jakubczyk and Niranjan 2006). Similar profiles have been reported in the cases of cake batter whipping (also shown in Figure 14.5), formation of high sugar containing egg albumen foams for a range of sugar concentrations and aeration of a model maltodextrin solution (Bee and Prinz 1986; Massey et al. 2001; Lau and Dickinson 2005).

This trend in gas hold-up variation can be attributed to physical or chemical changes occurring in the continuous phase during shearing. Such changes include the irreversible fat droplet aggregation in the case of whipping cream or the irreversible denaturation of proteins adsorbed at the gas–water interface during the whipping of protein solutions (Halling 1981; Walstra 1984).These observations suggest that, for a set of operating conditions in a given aerator, there is an optimum holding time that will give the desired level of bubble inclusion in a product. It is important to note that this optimum time does not necessarily have to coincide with the time taken for the hold-up to peak. For instance, a given product may not be able to sustain such a high level of bubble fraction if, for instance, it has to be baked in an oven after bubble inclusion.

The optimum time clearly depends on the desired product quality as perceived by a consumer. Very long holding times often result in loss of quality, as do very short holding times. It is thus very important in a manufacturing environment to relate operating variables with the desired dispersion characteristics, which include texture, mouth feel and so on. The transient variation in gas hold-up in any given system can be accounted for by considering the instantaneous rate of change of hold up to be determined by a balance between the rate of hold-up formation and the rate of hold-up loss. The rate of formation of hold-up depends on the method used to form bubbles within the system, that is, whether the bubbles are whipped into the headspace or whether they are generated by chemical/biochemical reactions. (Massey et al. 2001) proposed a mechanistic model for the time dependency of gas hold-up entrapped in cake batter when the batter was aerated in a pressure whisk. This model successfully described the experimental data for a range of whisk speeds and headspace pressures. Two mechanisms were considered for the formation of bubbles which can potentially be entrapped in the batter: a primary mechanism, where entrapped bubbles are directly entrained from the headspace during whisking, and a secondary mechanism involving the break up of larger bubbles entrained from the headspace.

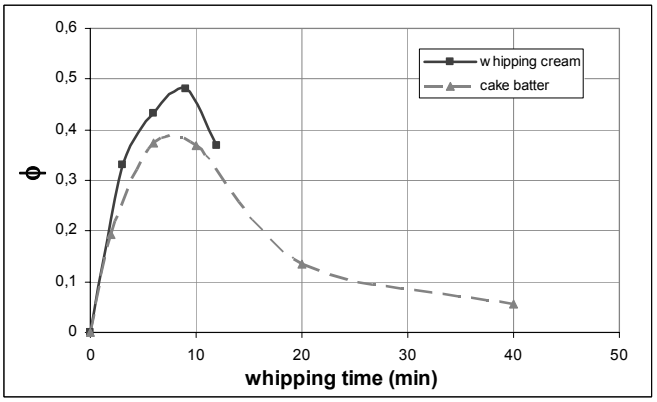

Figure 14.5. Fractional gas hold-up profile during the whipping of cream at atmospheric pressure and 380 rpm and cake batter at 3 bar, 5 rps. (From Massey et al. 2001; Jakubczyk and Niranjan 2006.)

The loss of entrapped bubbles was considered to occur mainly due to coalescence of the bubbles, which subsequently escaped from the system. On the basis of these assumptions the following correlation was derived and shown to be valid, where the empirical parameters k_1, k_2, k_3 and k_4 were determined to fit the equation to the experimental data:

$$\varphi = \left[\frac{k_1}{k_4} + \frac{k_2}{k_4 - k_3} e^{-k_3 t} - \left(\frac{k_1}{k_4} + \frac{k_2}{k_4 - k_3} \right) e^{k_4 t} \right] \times 100 \qquad (14.6)$$

Just as operating time influences the extent of bubble build-up in a system, the operating conditions, and more importantly, the method used to create the dispersion, also influences the development of gas hold-up. During the process of generating bubbles in tempered chocolate by applying vacuum, the gas hold-up was observed to increase with the application of higher vacuum levels when the vacuum application time was maintained at the same value (Haedelt et al. 2005). This was explained by considering the mechanism of gas volume build-up under vacuum: the gas solubility in the chocolate decreases proportionally to the pressure, which in turn increases the volume of gas desorbed from the chocolate. Assuming that the dissolved gases were initially at a level corresponding to the solubility of air components (mainly N_2 and O_2) at atmospheric pressure, the following model was deduced which related the gas hold-up (ϕ) with operating pressure under vacuum (P):

$$\frac{\phi}{100 - \phi} = RT(H - k)\left(\frac{1}{P} - 1 \right) \qquad (14.7)$$

In the above equation, k is a model constant, R is the ideal gas constant and H is a pseudo-Henry's constant. These examples illustrate how, once the mechanisms underlying gas incorporation are identified, it is possible to establish a relationship between operating parameters and the level of gas inclusion.

14.3.2 Bubble Size Distribution (BSD)

Bubble size distribution is one the most difficult parameters to measure and analyze. However, its evolution with time is of great importance, because it is closely linked to the product quality as perceived by a consumer (Halling 1981; Campbell and Mougeot 1999). In some systems, a uniform bubble size may be desirable (e.g., bread dough and cake batter) which improve baking characteristics, while in others, a wide spread in the distribution may be advantageous to achieve specific mouth-feel responses.

In general, the distribution observed in any dispersion depends on the operating conditions such as pressure, agitation speed, and temperature, as well as the chemical nature of gas. It may be noted that a number of gases, apart from air, are used commercially, for example, carbon dioxide, nitrogen and its oxides, helium and other inert gases. As mentioned earlier in Section 14.2, there are three mechanisms by which the bubbles can be formed: (1) by entrapping a sparged gas and dispersing it with mechanical agitation; (2) by entraining air during steam sparging; (3) by allowing bubbles to be formed by chemical and biochemical reactions; and (4) by dissolving a gas and lowering the pressure to release it. The bubble size distributions resulting from the first two methods strongly depends on the hydrodynamics prevailing in the equipment, whereas the rate of gas generation, the gas solubility and its variation with pressure, play a critical role in the latter two methods.

Methods commonly used to determine bubble sizes in dispersions include:

(i) Photographic techniques.
(ii) Measurement of bubble penetration length trough optical probes.
(iii) Measurement of bubble volume using ultrasound sampling probes.
(iv) Freezing dispersions and visualizing cross-sections.

Bubble sizes have traditionally been examined by taking conventional photographs of dispersions, often through container walls, and analyzing them using image analysis software. The accuracy of this technique can be compromised by the fact that inferences are being drawn on a three-dimensional structure based on two-dimensional images, normally assuming symmetry. Further, it can be difficult to obtain sharp images. Moreover, wall and curvature effects can also introduce errors into the measurement. Nevertheless, it is relatively cost-effective, and a number of dispersions, such as dough and batters, have been examined using ordinary photography. Recent developments in image analysis software have turned this method into a faster and more efficient technique (Hepworth et al. 2004)

Ultrasound reflective spectroscopy application in the analysis of bubbly liquids has been known for many years. This technique is based on the transmission of ultrasound waves through a dispersion, and measuring the velocity and attenuation spectra.

The interpretation of these signals yields information on bubble sizes and gas hold-up. However, the application of this technique to dispersions having bubble concentration greater than 0.1% is complex and not yet fully developed (Kulmyrzaev et al. 2000). Bisperink et al. (1992) developed a Foam Analyzer for the measurement of foam properties based on an optical fiberglass probe that is moved through the foam while emitting a signal that depends on the medium surrounding it, thus permitting highly localised measurement of bubble size distributions. However, techniques involving probes often require a dilute system and are intrusive.

More recently, x-ray tomography has emerged a valuable tool for imaging a number of cellular food products such as strawberry mousse and chocolate muffins (Lim and Barigou 2004). This technique is noninvasive and nondestructive, avoiding laborious sample treatments, and is particularly suited in the analysis fragile bubble containing foods. The contrast obtained in this technique between the continuous and gas phases is based on their density difference. When used in conjunction with a suitable image analysis software (e.g., Imagine Pro®Plus Software, The Proven Solution™), it can successfully visualize bubble-containing sections giving information on bubble numbers and size distribution in aerated chocolates; see Figure 14.6. However,with equipment currently available, the application of x-ray is limited to relatively stable structures and bubble sizes generally over 50 μm (Haedelt 2005).

Confocal scanning laser microscopy (CLSM) is a promising technique to characterize food dispersion. In a laser scanning confocal microscope, a laser beam passes through a light source aperture and is then focused by an objective lens into a small focal volume within a fluorescent specimen. A fluorescent dye added to the sample enables the visualization of the product structure. The identification of different components partitioned within the product by dye manipulation and image overlapping is also possible by this technique. Since this method is fast and does not demand laborious sample preparation, it is suitable for BSD determination and dynamic microstructural examination in complicated structures like albumen foams ((Lau and Dickinson 2004) and emulsions containing egg, sugar and milk proteins (Martinet et al. 2005). Examples of typical bubble sizes encountered in foods are given in Table 14.1.

Processing parameters will not only influence gas incorporation into the product, but also its microstructure. An understanding of the relationship between process parameters and bubble size distribution is essential to establish the operating conditions needed to obtain the desired product quality. Bread is the oldest and one of the most popular aerated foods consumed all over the world. This makes it one of the most extensively studied aerated food products. The effect of mixing bread dough under partial vacuum was studied by (Campbell et al. 1998) who observed that bubble size distributions was not significantly influenced by the vacuum level, though the number of bubbles per unit of dough volume decreased with reduced mixing pressure. (Chiotellis and Campbell 2003) modeled the evolution of bubble size distribution in bread dough during proving for different temperatures and yeast concentrations, predicting an increased growth rate for higher temperatures and increasing yeast levels.

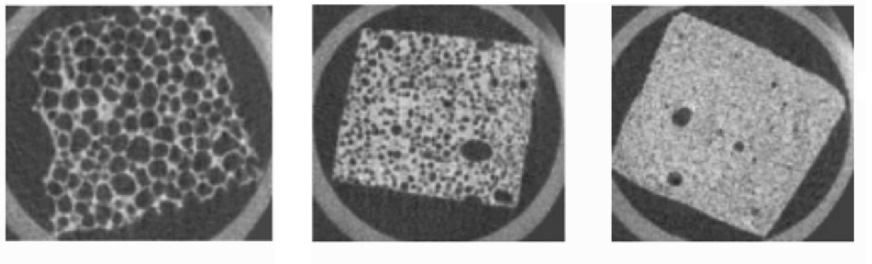

Figure 14.6. X-ray images of vacuum-induced aerated chocolate at different operating pressures (0.01, 0.05 and 0.1 bar, respectively). Taken from Haedelt et al. (2005).

Table 14.1. Typical bubble sizes and measurement methods used in the analysis of aerated foods microstructure.

Material	Technique	Bubble size (μm)	Reference
Bread dough	Freezing of sample and slicing	20–50	(Martinet al. 2004)
Whipped cream	Photography and image analysis	10–40	(Jakubczyk and Niranjan 2006)
Model cake batter	Photography and image analysis	20–50	(Massey et al. 2001)
Macro-aerated chocolate	X-ray tomography	600–1400	(Haedelt et al. 2005)
Milk Foam	CLSM	60–100	(Silva and Niranjan 2006)
Beer	Optical probe	20–120	(Bisperink et al. 1992)
Beer	Photography	137–190	(Hepworth et al. 2004)
Whey protein solution	Ultrasonic reflectance spectroscopy	10–160	(Kulmyrzaev et al. 2000)

14.3.3 Rheological characterization

The overall stability of a dispersed system is primarily affected by its rheology. The aerated lifetime of solidified structures such as chocolate and extruded cereals is up to years, while systems such as whipped cream will hold air for a few hours. The head of a beer or cappuccino, which are low-viscosity aqueous foams, will collapse in minutes. Campbell and Mougeot (1999) and before them Prins (1988) recognized that aeration is a physical process in which the rheological and interfacial properties play key roles. However, these properties, particularly the former, change during the course of aeration. Rheology can therefore be a useful tool in the assessment of structural changes occurring in a product during processing.

Dynamic oscillatory shear testing over a wide range of frequencies can provide information not easily obtained by other methods. Although this technique has traditionally been used to yield information on the fundamental structural characteristics of the food, a number of recent papers attempt to relate parameters such as the complex viscosity amplitude to sensory attributes such as perceived thickness in the mouth (Gunasekaran and Ak 2000). Dynamic oscillatory testing can also be applied to bubble-containing dispersions, its reliability depending on the dispersions remaining stable during the tests.

Dynamic oscillatory tests have been performed on whipped cream and cake batters, not only to assess their rheological properties but also to trace the way these properties change during the course of aeration (Massey 2002; Jakubczyk and Niranjan 2006). Even though a continuous phase may be purely viscous, bubble incorporation tends to make the dispersion viscoelastic. All whipped creams studied by Jakubczyk and Niranjan (2006) exhibited viscoelastic behaviour, with an increase in elastic and viscous modulii being observed during whipping, attributed to the presence of bubbles and to the clustering of fat globules; see Figure 14.7. Massey (2002) also reported on the creation of a stronger viscoelastic system while aerating cake batter by mechanical beating. The results are in agreement with those obtained for the aeration of maltodextrin solutions (Bee 1986). Although such data provide insight into the structural changes occurring in these products during bubble inclusion, there is a lack of knowledge concerning the relationship between multi-phase rheology and consumer perception (mouth-feel).

Since one of the main reasons to incorporate bubbles into foods is to impart particular textural characteristics, the rheological characterization of the dispersion is absolutely critical to the nature of the dispersion formed as well as to the product

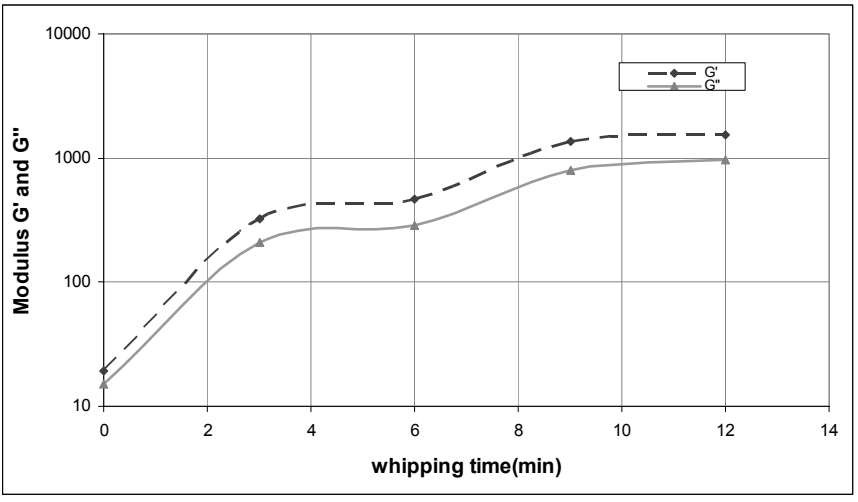

Figure 14.7. Evolution of viscous and elastic modulus with time during whipping of dairy cream (frequency: 2.2 rad s^{-1}) (Jakubczyk and Niranjan 2006).

quality (Bee 1999). For example, increasing the viscosity of the continuous phase can be detrimental to air incorporation by slowing surfactant diffusion to interface; however, it favors stability of the dispersion already formed by retarding liquid drainage (Halling 1981; Lau and Dickinson 2004). The relative viscosity—defined as the ratio of the viscosity of the dispersion to that of the continuous phase—has been reported to increase with gas hold-up (Bee 1986). However, the opposite, that is, a decrease in relative viscosity with increasing hold-up between these parameters, was observed in low-viscosity aqueous protein system by Britten and Lavoie (1992).

These discrepancies can be explained by the model proposed by Llewellin, et al. 2002) who suggested the existence of two different flow regimes, based on the extent of bubble distortion occurring under applied stress–strain conditions. The extent of distortion is characterised by the capillary number, $Ca = \eta_0 a\gamma/\Gamma$, where η_0 is the viscosity of the continuous phase; a the radius of the relaxed undeformed bubble; γ is the strain rate; and Γ the surface tension. The capillary number is a measure of the equilibrium deformation of the bubbles in a given stress field. For low values of Ca, bubbles remain more or less spherical and distort the flow around them considerably, thereby increasing the viscosity with hold-up. On the other hand, when Ca is high, bubbles get distorted and provide a high free-slip surface, so that the viscosity decreases with increasing hold-up. Llewellin et al. (2002) developed a generalized constitutive equation to describe the evolution of viscosity with gas hold-up that takes in account the two possible situations. The solution of this equation for oscillatory flow, for example, in a concentric cylinder where the imposed torque varies sinusoidally, has also been derived by Llewellin et al. (2002):

$$\eta_r = \frac{1}{3}\sqrt{9 - 30\varepsilon + 25\varepsilon^2 + \frac{(450b + 750)\varepsilon + (225b^2 - 625)\varepsilon^2}{25 + 36C_d^2}} \tag{14.8}$$

where η_0 is the viscosity of the continuous phase; ε is the fractional gas hold-up (i.e., $\phi/100$); and b is an experimentally fitted parameter found to take the value 9. C_d, known as dynamic capillary number, measures the steadiness of the flow by giving the ratio of the bubble relaxation time to the timescale over which the strain rate changes appreciably, and is defined as:

$$C_d = \lambda\omega \tag{14.9}$$

where ω is the angular frequency of the torque and λ, the relaxation time, is defined as:

$$\lambda = \frac{k\eta_0 r}{T} \tag{14.10}$$

The parameter k increases with the volume fraction of the dispersed phase (approximately one for limit of a solitary bubble in an infinite pure liquid). For $C_d >> 1$ and $C_d << 1$, Equation (14.8) reduces to:

$$\eta_r = \begin{cases} 1 + b; C_d << 1 \\ 1 - \dfrac{5\varepsilon}{3}; C_d >> 1 \end{cases} \tag{14.11}$$

Figure 14.8 compares the experimental values of η with those calculated using Equation (14.11) for $C_d << 1$, with $b = 3.8$, a value deduced for best fit between experimental data and model values (Niranjan et al. 2005). (Llewellin et al. 2002) stated a value of 9 for the parameter b, which was based on experimental data obtained using golden syrup. The difference between the values of b obtained for the two cases can be attributed to the difference between the rheology of the continuous phases: while golden syrup is essentially Newtonian, cake batter is a weakly viscoelastic system as characterized by (Massey 2002). Relating the viscosity of the continuous phase with the viscosity of the dispersed system is a sound approach to model the evolution of viscosity with gas hold-up. There is evidence that this approach works when the continuous phase is Newtonian; however, further modeling is needed to take into account more complicated continuous-phase rheological behaviour.

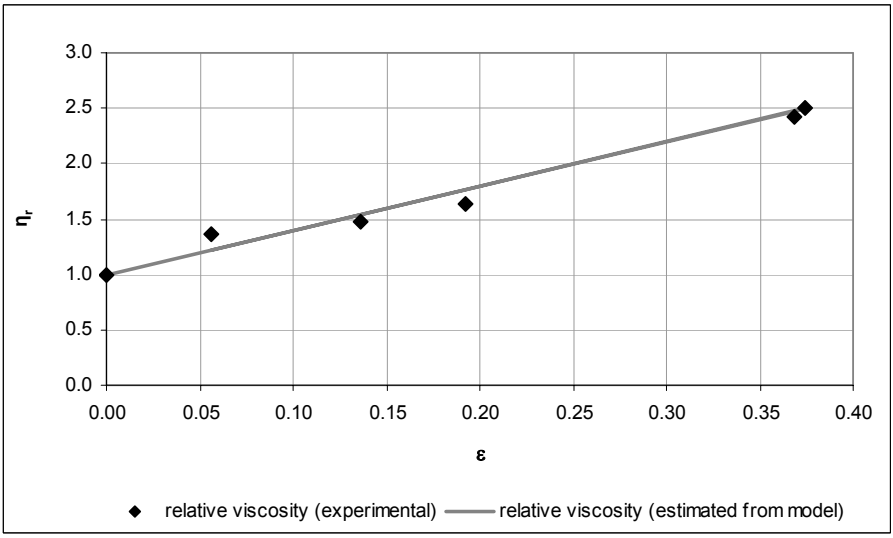

Figure 14.8. Fitting of Equation (14.11) to experimental data on cake batter (aerated at 300 rpm and atmospheric pressure) (Niranjan et al. 2005).

14.4 The Role of Gases and Specific Ingredients in Characterising Interfacial and Rheological Properties

Aerating a liquid will only result in the formation of foam if a surfactant is present. The role of the surfactant is to stabilize gas bubbles within the liquid matrix by adsorbing at the gas–liquid interface. As discussed earlier, it is well established that process or operating parameters influence hold-up development, and the stability and morphology of disperse systems. However, ingredients in the food system, their physicochemical properties and the way they interact are just as important in bubble interface stabilization. The rate of liquid drainage from a foam, for instance, will be determined by the viscosity of the serum. This can be manipulated, for example, by adding ingredients that will promote an increase in viscosity to retard drainage. Examples of this are the addition of guar gum to whipping cream, or sugar to egg albumen mixes (Smith et al. 2000; Lau and Dickinson 2004).

In protein-stabilized foams, protein flexibility is critical to the molecule functionality in stabilizing interfaces (Halling 1981; Lemeste et al. 1990). This has important consequences in the development and stability of dairy foams and emulsions, where the heat treatment received by the material can define its foamability and dispersion properties. A symbiotic effect between native and denatured proteins on the emulsifying properties of whey proteins isolate blends has been observed by (Britten et al. 1991). Though most studies on protein adsorption at interfaces have been conducted in solutions having a single well characterized protein, evidence has emerged in recent years that film properties in mixed protein systems are much more complex than in single protein systems.

Competitive adsorption to the air–serum interface has been reported even below the denaturation temperature in protein mixtures, and is dependant not only on protein properties but also on environmental factors such as pH, ionic strength and protein concentration (Dickinson 1999; Zhang et al. 2004). Fat also plays a key role in the behaviour of food foams. Depending on its physical state and size distribution in the continuous phase, the fat may act as stabilizer or destabilizer of aqueous foams, for instance, by competing with and even displacing proteins at the gas–liquid interface (Pilhofer et al. 1994). In whipped cream, the initial cream temperature is crucial to air incorporation by whipping, normally below 4°C to ensure partial crystallization of the fat droplets. The shear induced during whipping of cream can lead to droplet coalescence and bubble formation. Long-term stability in whipped cream will ultimately result from the formation of a three-dimensional network of aggregated fat droplets surrounding the air cells (Jakubczyk and Niranjan 2006).

Gas retention in bread is a function of gluten, the flour protein. The interaction between added fat and flour components also plays a key role in gas retention. Gluten must be sufficiently extensible to allow loaf rising, while sufficiently strong to prevent gas escaping and consequent loaf collapsing. Added fat interaction with flour components and quantity of sugars in the dough during fermentation will also have a significant effect on the structure of the final product (Kent and Evers 1994). Overrun and BSD in ice cream will depend not only on the type of freezer and its operating conditions but also on product formulation. Amount of fat, and type and level of emulsifier will affect the extent of destabilized fat that stabilizes the air cells (Goff and Clarke 2003).

The type of gas used to create structure in any given food will depend on the specific requirements. An example is the use of CO_2 in carbonated beverages. CO_2 is one of the few gases suitable to provide the characteristic effervescence in soft drinks. Due to its nontoxicity and lack of taste, it will not affect safety and flavour of the final product. Its availability and moderate cost makes it suitable for industrial use. Additionally, its solubility in aqueous solutions allows an acceptable retention of the gas in solution at atmospheric pressure and room temperature (Mitchell 1990). In general, the type of gas used has a significant impact on the dispersion characteristics. The use of air is avoided in a number of products, particularly those containing fat, because of the susceptibility of certain ingredients to oxidation. Often, carbon dioxide, nitrogen or one of the inert gases such as helium or argon is utilised.

Haedelt (2005) investigated the effect of the type of gas used—CO_2, N_2, N_2O and Ar—on the bubble-containing structures formed in chocolates. They reported that the solubility of the gas played a very critical role in the structure formed. When gases having higher solubility in chocolate (e.g., CO_2 and N_2O) were used, the bubbles formed tended to be larger and the dispersion, in general, tended to contain a higher fraction of bubbles. The use of relatively low solubility gases (N_2 and Ar) resulted in the formation of dispersions containing much smaller bubbles correspondingly the fractional hold-up of bubbles was also significantly lower. Based on this study, they postulated that highly soluble gases form macro-aerated structures, whereas low solubility gases form micro-aerated structures (Figure 14.9). The gas used is therefore a structure-developing aid.

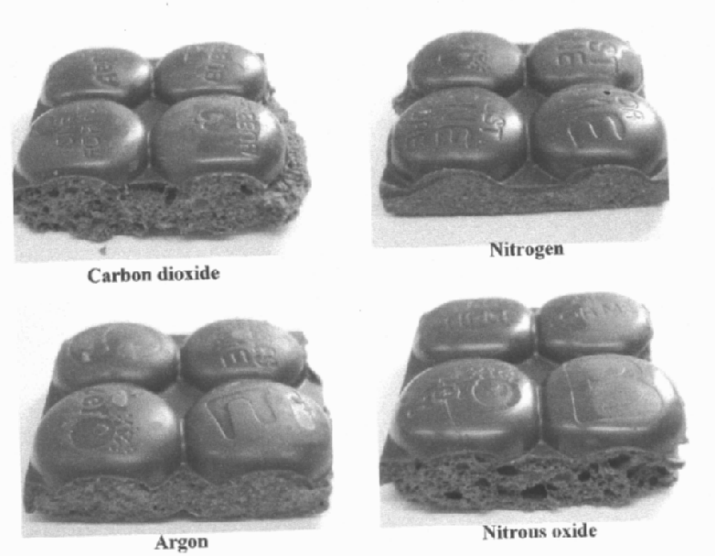

Figure 14.9. Visual appearance of aerated chocolate using different gases. Nitrous oxide and carbon dioxide give a macro-aerated structure, whereas nitrogen and argon gave a micro-aerated structure (Haedelt 2005)

14.5 Stability of Foams and Solidification of Bubbly Dispersions

Stability is the most important property of a bubble-containing product: once the desired characteristics for the product have been achieved, the structure must be kept at least until product consumption. Destabilization processes can combine in various ways and at various rates between foam formation and phase separation; thus the reference to foam "stability" must be accompanied by the specific mechanism under observation (Halling 1981). In general, the following phenomena can be distinguished when a liquid foam is allowed to stand (Prins 1986):

(i) Coalescence of gas bubbles.
(ii) Disproportionation of gas bubbles.
(iii) Liquid drainage.
(iv) Creaming of gas bubbles.

Both liquid drainage and creaming result in the loss of liquid from the foam matrix and are generally determined by the rheological properties of the foam serum and, to a certain extent, by the foam network itself (Halling 1981; Prins 1986; Lau and Dickinson 2005). These processes involve flow, that is, relative movement between gas bubbles and the serum. In foams containing spherical bubbles or low-gas fraction, the movement of bubbles is greater than the movement of liquid and individual bubbles can cream at a rate depending on the balance between buoyancy force and viscous resistance. On the other hand, when liquid movement is more pronounced than bubble movement (e.g., in polyhedral foams), drainage mechanisms predominate (Prins 1988). Bubble rise can be slowed down, though not completely stopped, by increasing the viscosity of the serum phase. Gas bubbles coalescence results in an increase in mean bubble size and a decrease on the number of bubbles, and in the case of coalescence with a decrease in air content. Coalescence is ultimately determined by the stability and attractive/repulsive forces between the thin liquid films surrounding air bubbles (Prins 1988).

Disproportionation occurs through gas diffusion between bubbles having different sizes. The excess internal pressure within any bubble, also known as the Laplace pressure (ΔP), is inversely proportional to the bubble diameter. Thus, the dissolved gas concentration at the interface of a smaller bubble will be greater than that at the interface of a larger bubble. This promotes mass transfer and therefore a net loss of gas from the small to the larger bubble. The rate of disproportionation will depend on the Laplace pressure, the solubility of the gas and other geometric factors (Halling 1981).

Foam stability is most commonly monitored by following its collapse and liquid drainage. Both are macroscopic properties and can easily be measured. These properties are not directly related to microscopic events such as drainage occurring from lamellae, but they allow a description of foam behaviour over time, and, in conjunction with the transient development of bubble size distributions (BSD), yield a complete description of foam destabilization mechanisms (Halling 1981; Bisperink et al. 1992; Patino 1995; Lau and Dickinson 2005). The common parameter characterising foam stability is half-life time for liquid drainage or foam collapse (Deeth and Smith

1983; Britten and Lavoie 1992; Patino 1995). Liquid drainage from foams has been described in the literature by empirical equations (Halling 1981; Elizalde et al. 1991; Patino 1995):

$$\frac{dV'}{dt} = K_2 V' \tag{14.12}$$

$$\frac{dV'}{dt} = K_2 V'^2 \tag{14.13}$$

where V' is the total volume of liquid in the foam at time t, and K_1 and K_2 are empirical constants. Equation (14.12) successfully described drainage in pure ovalbumin and casein foams generated by air sparging, with drainage rate constant K_2, being used as a stability parameter to compare foams generated at different temperatures and pH values (Patino 1995). Other authors, however, have suggested that such empirical equations do not describe foam behaviour completely over their life spans: drainage is slower than values predicted by either Equations (14.12) or (14.13) (Halling 1981; Elizalde et al. 1991). An empirical model proposed by Elizalde et al. (1991) fitted experimental data on liquid drainage with time for different protein solutions, and has been used in the investigation of drainage from dairy protein foams (Britten and Lavoie 1992) and egg albumen foams (Lau and Dickinson 2005) :

$$V_l(t) = \frac{V_{\max} \times t}{B + t} \tag{14.14}$$

In the above equation, V_{max} and B are empirically determined parameters representing the maximum volume of liquid drained and the time taken to drain a volume of $V_{max}/2$, respectively. B can be used as a parameters used to assess the relative stability of different foams where liquid drainage can be represented by Equation (14.14).

It is necessary to note that the measurements of the rates of foam collapse and liquid drainage yield no information on the dynamic changes occurring within the foam structure: bubbles grow and shrink by disproportionation, move and coalesce with each other, and all this is reflected on changes in foam morphology and bubble size distribution. An understanding of the destabilization mechanisms operating between formation and collapse will only be complete if an analysis of the microstructural changes is incorporated. Common techniques used for the measurement of BSD in a range of food products have already been covered previously in Section 14.3.2. Some of the techniques can also be used to monitor transient variations in bubble size distributions during destabilization.

The above description of foam destabilization mechanisms is only applicable to liquid foods. In solid dispersions, these mechanisms are significantly slowed or even eliminated. As mentioned earlier, solid matrixes such as aerated confectionery will hold air for up to years. Structure stabilization occurs for example in chocolate foams when the product is cooled to solidify and trap the bubbles formed within. The baking

of cake and bread dough is another example of how a bubble-containing structure formed during mixing and proving is stabilized when starch gelatinization is induced by the high temperatures prevailing in baking ovens.

14.6 Sensory Response and Mouth-Feel of Bubble-Containing Products

The relationship between instrumentally measured properties and consumer perception is an important and often overlooked analysis in the area of bubble-containing foods (Campbell and Mougeot 1999). It is quite possible that manufacturers may have undertaken research in this area for specific products, but such data are proprietary and not accessible in the public domain. In food products, quality depends on consumer's perception, and in the case of bubble-containing foods, this can either be related to the smooth mouth feel of whipped cream, or to the lightness and crispness of aerated chocolate. It is therefore very important to assess dispersion characteristics, and relate them to consumer perception. However, the relation between the two is not always clear, as is evident from the study on beer foams undertaken by (Yasui et al. 1998). This study simulated the pouring of beer into a glass, as in a consumer-use situation, and generated results on the visual impression of foam stability more reliably than conventional methods used to evaluate beer foam. In products such as sparkling cider or beer, foam is of utmost importance in the quality assessment by the consumer as it is the first perceived attribute. Factors such as aging time on lees and yeast strain used in the fermentation critically influence foam head persistence descriptors, and their correlation with laboratory assessed parameters such as the initial foam height and foam height after a given standing time. Some studies have found a good correlation between instrumentally assessed foam parameters and foam behaviour in a glass as evaluated by a sensory panel (Gallart et al. 2004; Picinelli-Lobo et al. 2005).

The perceived crispiness of chips and many cereal-based products is the key determinant characterising product quality. Most crispy products are characterized by a cellular, lamellar or puffed structure often described as solid foam. The crispiness of a product is closely related to its structure and the extent of porosity. However, sensory evaluation of crispiness is difficult to correlate with instrumental parameters mainly because crispiness is not a clearly defined attribute (Roudaut et al. 2002).

The importance of aeration in creaminess perception has been studied in chocolate *mousse* systems (Kilcast and Clegg 2002). Bubble size was identified as the main parameter influencing creaminess perception with air content acting as a secondary factor. This study also suggested that cocoa perception in chocolate *mousse* could be affected by bubble size and aeration extent. Support for this was evident in the study by Haedelt (2005) where bubble-containing chocolates were produced with different gases—argon, nitrogen, carbon dioxide and nitrous oxide— mentioned earlier. The chocolate made using nitrous oxide (laughing gas) had the most intense cocoa flavour. Chocolates made using argon or nitrogen, which produced micro-aerated samples, were perceived to be harder and creamier because the chocolate took longer to melt in the mouth. This study illustrates that dispersion properties can not only influence the texture and visual descriptors, but also the flavour perception.

14.7 References

Bee, R.D.C., and Prins, A. (1986.) Behaviour of an aerated food model. In: E. Dickinson (Ed.) *Food Emulsions and Foams*. Royal Society of Chemistry, London, pp. 128–143.

Bennion, A.B., and Bamford, B.S.T. (1997). *The Technology of Cake Making*, Chapman and Hall. London.

Bisperink, C.G.J., Ronteltap, A.D., and Prins, A. (1992). Bubble-size distributions in foams. *Adv. Colloid and Interface Sci.* 38, 13–32.

Britten, M., Giroux, H.J., and Rodrigue N. (1991). Emulsifying properties of whey–protein and casein composite blends. *IDF Special Issue* 9303, 368–374.

Britten, M., and Lavoie, L. (1992). Foaming properties of proteins as affected by concentration. *J. Food Sci.* 57, 1219–1222.

Campbell, G.M., and Mougeot, E. (1999). Creation and characterisation of aerated food products. *Trends Food Sci. Technol.* 10, 283–296.

Campbell, G.M., Rielly, C.D. Fryer, P.J., Sadd, P.A (1998). Aeration of bread dough during mixing: Effect of mixing dough at reduced pressure. *Cereal Food World* 43, 163–167.

Cheng, L.M. (1992). *Food Machinery for the Production of Cereal Foods, Snack Foods and Confectionery*. Ellis Horwood Ltd., Chichester.

Chiotellis, E., and Campbell, G.M. (2003). Proving of bread dough. I. Modelling the evolution of the bubble size distribution. *Food Bioprod. Proces.g* 81(C3), 194–206.

Clarke, C. (2004). *The Science of Ice Cream.* Royal Society of Chemistry, Cambridge.

Deeth, H.C., and Smith, R.A.D. (1983). Lipolysis and other factors affecting the steam frothing capacity of milk. *Austr. J. Dairy Technol*. 38(1), 14–19.

Dickinson, E. (1999). Adsorbed protein layers at fluid interfaces: interactions, structure and surface rheology. *Coll. Surf. B-Biointer.* 15(2), 161–176.

Elizalde, B.E., Giaccaglia, D., Pilosof, A.M.R., and Bartholomai, G.B. (1991). Kinetics of liquid drainage from protein-stabilized foams. J. Food Sci. 56, 24–26.

Fox, P., Smith, P.P., and Sahi, S. (2004) Ultrasound measurements to monitor the specific gravity of food batters. *J. Food Eng.* 65, 317–324.

Gallart, M., Tomas, X., et al. (2004). Relationship between foam parameters obtained by the gas-sparging method and sensory evaluation of sparkling wines. *J. Sci. Food Agric.* 84(2), 127–133.

Goff, H.D., and Clarke, C.J. (2003). Effects of structural attributes on hardness and melting rate of ice cream. Ice Cream 2: 2nd IDF Symposium on Ice Cream, Thessaloniki, Greece, International Dairy Federation, Brussels, 2004.

Gunasekaran, S., and Ak, M.M. (2000). Dynamic oscillatory shear testing of foods: selected applications. *Trends Food Sci. Technol*. 11, 115–127.

Haedelt, J. (2005). An investigation into bubble inclusion into liquid chocolate. School of Food Biosciences. Reading, University of Reading.

Haedelt, J., Pyle, D.L., Beckett, S.T., and Niranjan, K. (2005) Vacuum-induced bubble formation in liquid-tempered chocolate. *J. Food Sci.* 70, E159–E164.

Halling, P J. (1981). Protein-stabilized foams and emulsions. *CRC Crit. Rev. Food Sci. Nutrition* 15, 155–203.

Hepworth, N.J., Hammond, J.R.M., Varley, J. (2004). Novel application of computer vision to determine bubble size distributions in beer. *J. Food Eng*. 61(1), 119–124.

Jakubczyk, E., and Niranjan, K. (2006). Transient development of whipped cream properties. *J. Food Eng.* 77, 79–83.

Jones, L. (1995). Aeration of boiled sweets: a review of available methods. *The Manufacturing Confectioner* 75(10), 47–52.

Kent, N.L., and A.D. Evers (1994). *Technology of Cereals: An Introduction for Students of Food Science and Agriculture.* Elsevier Science Ltd., Kidlington, Oxford.

Kilcast, D., and S. Clegg (2002). Sensory perception of creaminess and its relationship with food structure. *Food Quality and Preference* 13, 609–623.

Kulmyrzaev, A., Cancelliere, C., et al. (2000). Characterization of aerated foods using ultrasonic reflectance spectroscopy. *J. Food Eng*. 46, 235–241.

Lau, C.K., and Dickinson, E. (2005). Instability and structural change in an aerated system containing egg albumen and invert sugar. *Food Hydrocoll*. 19(1), 111–121.

Lau, C.K., and Dickinson, E. (2004). Structural and rheological properties of aerated high sugar systems containing egg albumen. *J. Food Sci*. 69, E232–E239.

Lemeste, M., Colas, B., et al. (1990). Contribution of protein flexibility to the foaming properties of casein. *J. Food Sci*. 55, 1445–1447.

Lim, K.S., and Barigou, M. (2004). X-ray micro-computed tomography of cellular food products. *Food Res. Int*. 37, 1001–1012.

Llewellin, E.W., Mader, H.M., and Wilson, S.D.R. (2002a). The constitutive equation and flow dynamics of bubbly magmas. *Geophys. Res. Lett.* 29(24), Article no 2170, pp. 23-1–23-4.

Llewellin, E.W., Mader, H.M., and Wilson, S.D.R. (2002b). The rheology of a bubbly liquid. *Proc. Roy. Soc. London Ser. A Mat. Phys. Eng. Sci.* 458(2020), 987–1016.

Mackley, M.R. (1994). Cold extrusion of chocolate. *Patent* 9220477.

Marshall, R.T. (1986). *Ice Cream*. Chapman & Hall, London.

Martin, P.J., Chin, N.L., et al. (2004). Aeration during bread dough mixing. II. A population balance model of aeration. *Food Bioproducts Process*. 82(C4), 268–281.

Martinet, V., Valentini, C., et al. (2005). Composition of interfacial layers in complex food emulsions before and after aeration: effect of egg to milk protein ratio. *J. Dairy Sci*. 88, 30–39.

Massey, A.H. (2002). *Air Inclusion Mechanisms and Bubble Dynamics in Intermediate Viscosity Food Systems*. School of Food Biosciences. University of Reading, Reading.

Massey, A.H., Khare, A.S., et al. (2001). Air inclusion into a model cake batter using a pressure whisk: development of gas hold-up and bubble size distribution. *J. Food Sci.* 66(8), 1152–1157.

Matz, S.A. (1984). *Snack Food Technology.* AVI Publishing Co. Inc., Westport, CT.

Mitchell, A.J. (1990). *Formulation and Production of Carbonated Soft Drinks*. Blackie, Glasgow.

Niranjan, K., Khare, A.S., and Silva, S.F.J. (2005). Bubbles in foods: creating structure out of thin air! *7th World Congress of Chemical Engineering*, Glasgow.

Patino, J.M.R., Delgado, M.D.N., and Fernandez, J.A.L. (1995). Stability and mechanical strength of aqueous foams containing food proteins. *Coll. Surf. A. Physicochem. Eng. Aspects* 99(1), 65–78.

Picinelli-Lobo, A., Fernandez-Tascon, N., Madrera, R.R., and Valles, B.S. (2005). Sensory and foaming properties of sparkling cider. *J. Agric. Food Chem*. 53, 10051–10056.

Pilhofer, G.M., Lee, H.C., et al. (1994) Functionality of milk-fat in foam formation and stability. *J. Dairy Sci*. 77, 55–63.

Prins, A. (1986). Some physical aspects of aerated milk-products. *Netherlands Milk Dairy J.* 40(2–3), 203–215.

Prins, A. (1988). Principles of foam stability. In: E. Dickinson and G. Stainsby (Eds.), *Advances in Food Emulsions and Foams.* Elsevier Applied Science Publishers Ltd. Barking, UK, pp. 91–119.

Pyle, D.L. (2005). Crumpet structures experimental and modelling studies. *Food Bioprod. Process*. 83(C2), 81–88.

Roudaut, G., and Dacremont, C. (2002). Crispness: a critical review on sensory and material science approaches. *Trends Food Sci. Technol*. 13, 217–227.

Silva, S.F.J., and Niranjan, K. (2006). Unpublished data.

Smith, A K., Goff, H.D., and Kakuda, Y. (2000). Microstructure and rheological properties of whipped cream as affected by heat treatment and addition of stabilizer. *Int. Dairy J.* 10, 295–301.

Walstra, P. (1984). *Dairy Chemistry and Physics*. John Wiley, New York.
Wolfe, T.L. (1995). Vacuum aeration. *The Manufacturing Confectioner* 75(5), 97–98.
Yasui, K., Yokoi, S., Shigyo, T., Tamaki, T., Shinotsuka, K. (1998). A customer-oriented approach to the development of a visual and statistical foam analysis. *J. Am. Soc. Brewing Chem.* 56, 152–158.
Zhang, Z., Dalgleish, D.G., and Goff, H.D. (2004). Effect of pH and ionic strength on competitive protein adsorption to air/water interfaces in aqueous foams made with mixed milk proteins. *Coll. Surf. B. Biointerfaces* 34, 113–121.

Chapter 15

Emulsions: Principles and Preparation

Remko M. Boom

Wageningen University, Agrotechnology and Food Sciences Group,
Laboratory of Food Process Engineering Sciences, Wageningen, The Netherlands,
remko.boom@wur.nl

15.1 Emulsion-Based Products, Types of Emulsions and Their Uses

Emulsions are mixtures of fluids that are immiscible. Usually one fluid is present as small droplets in another phase. There are emulsions of oil in water, called oil-in-water emulsions (abbreviated as *O/W*), but also emulsions of water in oil (*W/O*). The droplet phase is called the dispersed phase, the surrounding phase the continuous phase. Emulsions are important in a great diversity of products. Some examples are:

- *Salad dressings* are made by emulsifying vegetable oil in an aqueous mixture that contains vinegar. When made at home, this emulsion is rather unstable: the droplets coalesce relatively quickly, so one has to shake it before use. Commercial variants are usually stabilized by other components.
- *Mayonnaise* is a very concentrated emulsion of oil droplets in water, stabilised by proteins from egg yolk. The emulsion is so concentrated (70–80 vol.%) that the oil droplets are squeezed together. This squeezing together causes the nice consistency of mayonnaise.
- *Egg yolk* is an emulsion of egg fat (and cholesterol) in an aqueous solution, stabilised by a mixture of phospholipids.
- *Milk* is an emulsion of milk fat in an aqueous solution containing many different proteins, lactose and salts. In raw milk the fat is present in the form of milk fat globules, which are surrounded by a membrane. When this milk is homogenized in the factory, these globules are broken, and the fat is dispersed into smaller droplets, also stabilized by proteins.
- *Margarine* is an emulsion of water droplets in fat, stabilised by a packing of needlelike crystals of fat inside the continuous fat phase.

- *Cream* is a concentrated emulsion of milk fat in an aqueous phase; the concentration depends on the type of cream.
- *Ice cream* is a very complex product; amongst others it contains droplets of milk fat, but it also contains crystals of sugar, ice crystals and bubbles of air.
- *Waterborne paints* are usually emulsions of polymer-based binder particles. They are made by making an emulsion of droplets of monomers in water, after which the monomers are polymerized to form solid particles. When applied, the water and possibly other solvents evaporate, and the binder particles fuse to form a solid layer.
- *Bitumen,* a heavy fraction produced in the refining of petroleum, is usually too viscous to be applied directly. Therefore, bitumen is emulsified in water at high temperatures. The resulting *O/W* emulsions have a much lower viscosity, and therefore are easier to apply. When applied (on the road or on a roof), the emulsion breaks, and the bitumen particles fuse into one layer.

Foams are closely related to emulsions. In foams, the dispersed phase is not an oil or water, but it is a gas. One can use similar techniques for making foam and for making emulsions, and some of the properties are comparable. Foams are ubiquitous as well: of course, the foam on beer is well known, but bread is a foam as well, as are ice cream, whipped cream, expanded polystyrene or styrofoam (which is a solid polymeric matrix with a large volume fraction of gas bubbles in it), and polyurethane foam, used, for example, for making mattresses.

In some cases, *duplex emulsions* are important. These are emulsions in emulsions. One can have water droplets in an oil phase, of which larger droplets have been made in a second aqueous phase: this is called a water-in-oil-in-water duplex emulsion (*W/O/W*). Of course, one can also have the reverse (*O/W/O* emulsion). *W/O/W* are used in some medical applications (encapsulation of drugs), and in foods, to enhance the perception of fat, for example, but also to mask taste, for example, the taste of bitter peptides. One can also imagine that an *O/W* emulsion in which the oil phase is for the most part replaced by water droplets inside the oil phase, would combine some of the properties of a concentrated *O/W* emulsion with a much lower actual oil content of the product, with obvious advantages in terms of health.

15.2 Some Important Properties

15.2.1 Interfacial Tension; Interfacial Energy

Any surface between two immiscible fluids has an interfacial tension, also called interfacial energy. This is caused by the difference in cohesion between molecules of the two phases. Creating an interface between two phases costs energy, proportional to the amount of interface generated. The amount of (Gibbs) energy that is needed to create 1 m^2 of interfacial area is called the interfacial tension or interfacial energy, with unit N/m or J/m^2 (since J = Nm, it is easily seen that these two units are the same):

$$\Delta G = \int_0^A \sigma \, dA \tag{15.1}$$

in which σ is the interfacial tension (N/m or J/m^2), A the total interfacial area created (m^2), and ΔG the Gibbs energy needed to create this interface (J). The interfacial tension is always positive, with the exception of so-called micro-emulsions. This means that ΔG is (almost) always positive: making small droplets costs energy. The system will always try to minimise the amount of interface. If we make an emulsion of oil and water, for example, we create a lot of interface: the smaller the droplets become the larger is the total interfacial area.

The existence of a positive interfacial tension implies that there is a driving force for break-up (coalescence) of an emulsion. Any system strives to reduce its Gibbs energy. A reduction in the amount of interfacial area will yield just that, according to Equation (15.1). Therefore, an emulsion has a driving force for reducing its interfacial area by coalescence: fusion of fine droplets into larger ones. Thus, we need to stabilize the emulsion against this. We can do this by creating a kinetic barrier: we take care that coalescence is too slow to have any influence in the product. This is called stabilization, and it is usually done with a surfactant or similar component. This is discussed in Section 15.3.

15.2.2 Laplace Pressure

The interfacial tension gives rise to a force in the interface, directed to reduce the interfacial area. In a spherical droplet of one immiscible fluid in another, the interface is curved. The interfacial tension exerts a force perpendicular to the interface, directed to the concave side of the interface. The size of the force is proportional to the interfacial area, and hence it can be described as a pressure. This pressure is called the *Laplace pressure*. This pressure is proportional to the curvature of the interface. If the interface is flat (zero curvature), there is no force perpendicular to the interface. A cylinder is curved in one direction (with curvature radius R_1) and straight in another, and the resulting pressure is equal to

$$\Delta P_{\text{Laplace}} = \frac{\sigma}{R_1} \tag{15.2}$$

The pressure inside such a domain is therefore always higher than in the continuous phase. An ellipsoid is curved in two directions, and therefore the curvature is stronger. The resulting Laplace pressure is found simply by adding the two curvatures:

$$\Delta P_{\text{Laplace}} = \sigma\left(\frac{1}{R_1} + \frac{1}{R_2}\right) \tag{15.3}$$

In a sphere, the two radii of curvature are identical, and the Laplace pressure is equal to:

$$\Delta P_{\text{Laplace}} = \frac{2\sigma}{R_d} \tag{15.4}$$

Therefore, inside droplets or other fluid domains surrounded by an interface, the pressure is always higher than that of the surroundings, and the smaller the domain is, the higher is the pressure difference.

15.3 Stability of Emulsions

Droplets dispersed in a continuous phase are not stable: they have a driving force to coalesce into larger droplets, and eventually the emulsion will separate into two pure liquid layers. This is avoided by stabilization of the droplets. This can be achieved in various ways:

- with surfactants or (bio)polymers that adsorb to the interface, giving rise to electrostatic or steric repulsion between the droplets;
- with polymers dissolved in continuous phase, which influence the rheology of the continuous phase;
- with particles that accumulate on the interface, giving the so-called Pickering stabilization.

15.3.1 Stabilization with Surfactants

Surfactants are molecules that have one side with greater affinity for one phase, while the other side of the molecule has more affinity for the other liquid. Thus, the molecule wants to be in both phases. This is possible if the molecule resides in the interface between the two phases. Surfactants thus tend to adsorb on the interface. Usually the hydrophobic part of the molecule (having higher affinity with oily phases) consists of an alkyl chain; the hydrophilic part (having higher affinity with an aqueous phase) can be a nonionic chain, such as an ethylene oxide chain or a chain consisting of glucose units, or a chain containing charged groups (such as a sulphonate group).

When the surfactants are adsorbed at the interface, they form a barrier for two droplets to come very close. There are a number of mechanisms by which they do this:

Steric hindrance: When a nonionic surfactant adsorbs on an interface between oil and water, the hydrophobic part of the molecule will orient itself towards the oily phase, while the hydrophilic part will stick out into the aqueous phase. One can envisage the interface, therefore, as having a coat of hydrophilic chains sticking out of the interface. When two oil droplets approach each other, the two coats would first make contact. The only way that the two droplets can coalesce is when the nonionic surfactant molecules move away from the contact point. However, they are strongly adsorbed and therefore impede the coalescence. Hence, when two droplets with such a layer approach each other, the coats will repel each other. Thus, the droplets will move apart again, and coalescence is prevented.

Electrostatic repulsion: When the surfactant is an anionic or cationic surfactant, the droplet will be coated by chains having charged groups. In effect, the surface of

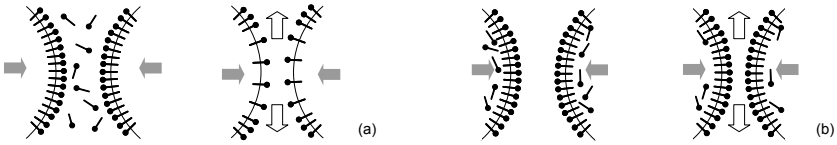

Figure 15.1. Reason for the Bancroft rule: (a) situation with surfactants in the continuous phase and (b) in the dispersed phase.

the droplet will have a net negative or positive charge. Two droplets, having the same surfactants adsorbed at their interface, will both feel an electrostatic repulsion, and thus they cannot come close enough to coalesce.

As mentioned, a surfactant typically has a hydrophobic and a hydrophilic part, and therefore it is difficult to dissolve it in just one phase. Only a small amount of the surfactant will dissolve molecularly in the liquid. When a larger concentration is applied, the surfactant will aggregate into micelles: in an aqueous phase, the hydrophobic chains of a number of the surfactant molecules cluster together, and stick out their hydrophilic parts towards the surrounding water. A surfactant that in total has more affinity with water will be much more soluble in an aqueous phase and will form micelles in that phase; a surfactant that has better interaction with an oily phase will dissolve in the oily phase and form micelles in that phase. In the latter case, one often speaks of reverse micelles.

The phase in which the surfactant is dissolved usually becomes the continuous phase. This is called the Bancroft rule. To see why this is, we first assume that the surfactant is dissolved in the continuous phase. As two droplets approach each other, a narrow slit is formed between the droplets. This is depicted in Figure 15.1(a). The continuous phase has to be removed out of this slit to enable contact between the droplets and initiate coalescence. The continuous phase, while flowing out of the slit, exerts a force on the adsorbed surfactants at the interface. The surfactant molecules flow along the surface, dragged along by the continuous phase, and are depleted from the interfaces in the slit. A concentration gradient of surfactant molecules on the surface is created, which counteracts the drag by the flow of the continuous phase. The outflow of the continuous phase is then reduced by the concentration gradient of surfactant on the interface. This is called the Marangoni effect.

The reverse situation is depicted in Figure 15.1(b). When the surfactant is dissolved in the dispersed phase, the surfactants also flow along the interface with the continuous phase flowing out of the slit, but the depletion on the interface is easily countered by diffusion and adsorption of surfactants from the bulk of the dispersed phase. Therefore, there is no Marangoni effect counteracting the outflow of continuous phase, and coalescence takes place much more easily.

15.3.2 Stabilization with Polymers and Crystals

It is also possible to stabilise an emulsion by thickening the continuous phase (see Figure 15.2). Adding a soluble polymer increases the viscosity and thereby reduces

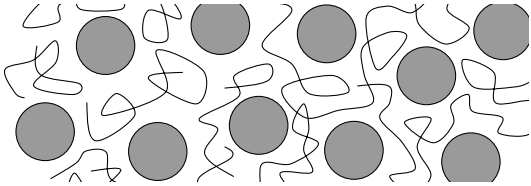

Figure 15.2. An emulsion in which the continuous phase is thickened or even gelled by a dissolved polymer.

the velocity of coalescence, especially when the polymer forms a gel: the polymer chains form a network that needs some minimum force to disrupt. In such a network, the droplets are physically captured by the network, and the emulsion will be stable. A similar method of stabilization is encountered in margarine, which is a water-in-oil emulsion. In general it is difficult to stabilize a *W/O* emulsion, since one cannot make use of charge effects. Only steric stabilization is possible. In margarine, the oil is partly crystallized in crystals that are strongly elongated. These crystals touch one another and in this way create a coherent network that gives mechanical stability. The droplets that are caught between the crystals cannot coalesce.

15.3.3 Proteins as Stabilizers/Surfactants

In most food products, proteins are used as stabilizers. Proteins are polymeric chains of amino acids. Some of the amino acids are very hydrophilic (i.e., they have a strong interaction with water), due to acidic, basic or charged groups; others are more hydrophobic (i.e., do not interact strongly with water). This means that there are always some parts of the chain of a protein that are more or less hydrophobic and some parts that are more hydrophilic. When a protein molecule dissolved in an aqueous phase comes close to oil droplet, it is possible that the more hydrophobic parts have affinity for the oily interface of the droplet. Many proteins therefore tend to adsorb at an oil/water interface.

As soon as the protein is adsorbed, its structure changes. The conformation of the molecule may change such that other hydrophobic parts of the molecules become exposed to the oil/water interface. The molecule will then be adsorbed to the interface even stronger. Typically, once a protein has become adsorbed to an oil/water interface, its adsorption will be irreversible (this is in contrast to low-molecular weight surfactants, that are at equilibrium with the phases surrounding the interface). The protein sometimes can form a more or less solid skin on the surface of the droplet.

A protein is a large molecule; therefore it diffuses slowly through the aqueous phase, towards the interface. When it arrives at the interface, the process of re-folding takes time as well. This means that the stabilization of the interface, and the lowering of the interfacial tension by the adsorbed proteins both can take a considerable amount of time. During that time, the droplets need to be stabilized in another way, or coalescence needs to be avoided in another way.

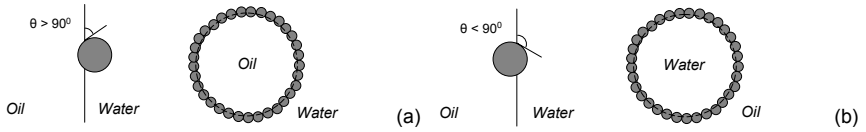

Figure 15.3. (a) Particles that are preferentially wetted by water will mostly form an oil-in-water emulsion; (b) particles that are preferentially wetted by oil will form a water-in-oil emulsion.

15.3.4 Stabilization with Particles: Pickering Emulsions

Very small particles that are not completely wetted by either the continuous or the dispersed phase have the tendency to adsorb onto the interface between the two phases. This can cause stabilisation of the interface: the particles partially stick out of the interface, giving steric hindrance for coalescence, just as non-ionic surfactants do. The stabilisation is better when the particles stick out further, that is, they act better when they are wetted better by the continuous phase. Also here a form of the Bancroft rule applies: the phase that wets the particles best will be the continuous phase (see Figure 15.3)

15.4 Characterization of Emulsions

15.4.1 Distributions: Cumulative and Frequency Distributions

The properties of an emulsion are quite dependent on the size of the droplets. When the droplets are large, gravity will cause them to cream (when they are lighter than the continuous phase) or sediment (when they are heavier). The appearance of a product is dependent on the size of the droplets as well. An emulsion with very small droplets (<50 nm) can be almost transparent. Larger droplets (50 nm–10 μm) tend to act as small lenses that scatter the incident light. Therefore, such an emulsion is milky white (in fact, that *is* the reason why milk is white). Even larger droplets scatter the light much less, which means that the actual colour of the dispersed phase becomes more prevalent (many oils are yellowish, and thus such an emulsion would be yellowish).

Unfortunately, most emulsions do not have a single droplet size. There are small, medium and large droplets present, and it is important to be able to characterise the emulsion for this. This is done by counting the number of particles that is smaller than a specific size, for many different sizes. The resulting data can then be plotted on a curve, the *cumulative distribution curve*. Alternatively, one can count all particles that have a size within an interval of sizes (e.g., 1–2 μm), and do this for all intervals. Plotting all the numbers obtained for all intervals, then results in a *frequency* distribution. The two distributions are closely related: the derivative of the cumulative curve to the particle size, will give a (continuous) curve that is similar to the discrete frequency distribution obtained earlier, and the smaller the intervals are chosen, the closer the derivative will follow the frequency distribution (see Figure 15.4).

There are different ways of counting particles to obtain the distribution. One can simply count the *number* of particles smaller than a specific size. This means that in the curve, a droplet of 0.1 μm will count for one, just as a droplet of size 10 μm. However, the amount of oil present in the 10-μm droplet is 100^3, or one million times larger. Such a distribution therefore stresses the presence of small particles. Another way is to not use the number of particles but the total *interfacial area* present on the particles. Since the interfacial area of a small droplet is much smaller than that of larger droplets, smaller droplets are counted less extremely, and the resulting distribution is more realistic. Remember that the amount of surfactant needed to stabilize the interface is proportional to the total interfacial area present on the droplets, and the total energy needed to put into the emulsion is proportional to the total interfacial area. As a third option, one can use the *volume* of the particles smaller than a specific size. In this case the distribution gives that total amount of oil that is present in small, medium or larger droplets. It depends on the application which type of distribution should be used.

15.4.2 Average Droplet Sizes

Even though it is best to use a complete size distribution for the characterization of an emulsion, it is not very convenient. Therefore, usually an average droplet size is given. And also here, it matters how this average droplet size is defined. A simple way of finding an average value is by looking at the frequency distribution and taking the size at which the distribution is maximal. This is called the *modal size.* Another simple definition of the average particle size is summing up the size of all particles and dividing this by the total number of particles. This is the *number average diameter*, or d_{10}. One can also sum up the volumes of all particles and divide this by the total number of particles. This gives the average volume per particle; taking the third-power root yields a related diameter. This is the *volume average particle diameter*, or d_{30}. A more elegant definition is that of the *Sauter diameter*, or the d_{32}: this is found by summing the volume of the particles, and dividing it by the surface area of the particles. In one equation, this is described as:

$$d_{nm} = \left(\frac{\sum_i d_i^n n_i}{\sum_i d_i^m n_i} \right)^{\frac{1}{n-m}} \tag{15.5}$$

or for continuous particle size distributions

$$d_{nm} = \left(\frac{\int_0^\infty d^n q(d) \mathrm{d}d}{\int_0^\infty d^m q(x) \mathrm{d}d} \right)^{\frac{1}{n-m}} \tag{15.6}$$

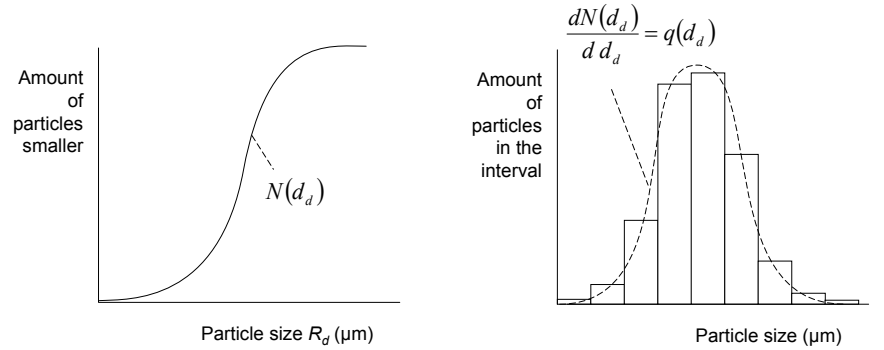

Figure 15.4. A cumulative distribution of particle sizes (left-hand graph), and a frequency distribution (right-hand graph). The dashed line in the frequency distribution is the derivative of the cumulative distribution.

where $q(d)$ is equal to the derivative of the number of particles with diameter smaller than d; see also Figure 15.4. For the three types of averages that we mentioned, the number average, the volume average and the Sauter diameter, this becomes:

$$d_{10} = \frac{\sum_i d_i n_i}{\sum_i n_i}\;;\quad d_{30} = \left(\frac{\sum_i d_i^3 n_i}{\sum_i n_i}\right)^{\frac{1}{3}}\;;\quad d_{32} = \frac{\sum_i d_i^3 n_i}{\sum_i d_i^2 n_i} \tag{15.7}$$

The values of these averages can be very different. Typically, the higher the values of n and m are, the larger is the value of the average size. Which one you should use simply depends on the application. When it relates to the surface area (think of emulsion stability, amount of surfactant needed, energy required to make the emulsion, etc.) then the Sauter diameter is probably the best one. If the application is related to the volume (e.g., amount of oil in the product, material dissolved in the particles), the volume average diameter may be more suitable.

15.4.3 Width and Span of the Distribution

Not only the average size of the droplets is important, but also the width of the distribution. The properties of two emulsions can be very different, even when the average droplet size is the same, when the two have different width of the distribution. An emulsion that is almost monodisperse (i.e., all droplets have more or less the same diameter) can, for example, be much more stable than an emulsion having very small and very large droplets present, since the large droplets will initiate creaming of the droplets. The *span* of a distribution is defined as

$$\text{Span} = \frac{d(90) - d(10)}{d(50)} \tag{15.8}$$

where $d(x)$ is the droplet size that has x% of droplets smaller than this value. It is a value for the relative width of the distribution. When the distribution function is known in detail, one can also use the standard deviation of the distribution, which is the interval around the average droplet size that contains approximately 68% of all droplets. Most equipment that yields a droplet size distribution will also generate a value for the standard deviation. One should note, however, that the standard deviation or the span can be used with the different types of distributions and averages: number-based, surface-based, and volume-based. Once more, which one to take depends on the application.

15.4.4 Measuring Droplet Size Distributions

There is a variety of methods for determining the droplet size distribution. One can directly measure the size by using microscopy. When the droplets are larger than ~1 μm, this can be done by optical microscopy; for smaller droplets this is not possible, and electron microscopy may be used.

A second possibility is the use of light scattering. A droplet in another fluid that has a different refractive index will cause scattering of light passing through the droplet. The way that a particle refracts incident light depends on its size. By studying the pattern of scattered light coming out of an emulsion that is illuminated (usually by monochromatic light), one can obtain information on the droplet size distribution. This is called static light scattering. Commercial equipment interprets the scattering pattern with the help of a model curve for the droplet size distribution; it changes the parameters of the curve until the scattering pattern expected is the same as what is observed (please note this does not necessarily mean that the fitted curve accurately represents the actual droplet size distribution).

A third possibility is to follow the dynamics of droplets. With dynamic light scattering, the Doppler shift relative to the frequency of the incident light in the scattered light is measured. This Doppler shift comes from the Brownian motion of the droplets. Since larger droplets show slower Brownian motion, one can obtain information on the droplet size distribution.

A fourth way is to count droplets individually. First, one has to dilute the emulsion strongly. Then, this diluted emulsion is pushed through a small hole. At the same time, the electrical conductivity through the hole is measured. Every time an emulsion droplet moves through the hole, the droplet will obscure part of the hole, which suddenly reduces the conductivity through the hole—the larger the droplet is, the stronger is the effect. Also in this way a droplet size distribution can be obtained. This method is usually referred to as the Coulter counter method, after an important manufacturer of this type of equipment.

15.5 Preparation of Emulsions Using Flow Fields

15.5.1 Equipment for Emulsification by Flow

By far the most often applied method to produce emulsions is by inducing very strong flow, by agitation, intense mixing or flow trough a small opening. There are

many different types of machines for this. It is outside the scope of this chapter to give an exhaustive list, but some of the types of equipment will be discussed shortly. A more extensive description can be found in, for example, Walstra (2003), Schubert and Armbruster (1992), Arbuckle (1986) and Brennan (1986).

Flow around a droplet induces a shear force onto the droplet. When this force is sufficiently large, the droplet can break up into smaller droplets. Generally, the more intense a flow field is, the smaller the droplets become. Therefore, most methods are designed to generate a flow field that is very strong at a very small volume, through which the emulsion passes.

Rotor-stator systems: These systems apply an element that rotates quickly, very close to a corrugated element that stands still (the stator). The flow field in between the two elements becomes very intense when the distance between them is very small; sometimes much less than a millimeter. There are different forms of this type of equipment. The most important ones are the stirred tank, a colloid mill, and a toothed mill.

Stirred tank. The simplest system to achieve droplet break-up is with a stirrer in a vessel. In this case, the flow field is not very intense, as the stirrer is usually not very close to the wall of the vessel, and therefore the droplets remain relatively large (>10 μm). The droplet size distribution is usually relatively wide, but will become smaller with longer treatment times. The power density that can be applied is relatively small, so if one wants to produce droplets smaller than approximately 10 μm, this equipment does not suffice.

Colloid mill. This type of mill is used extensively in the food industry. A colloid mill is a conical rotator that turns in a stator of the same shape, leaving a very narrow gap between rotor and stator. The liquid is introduced from the top, and flows through the narrow gap. Due to the high rotation rate, and the small size of the gap, the shear forces are very intense, and small droplet sizes can be realized. The regime the mill operates at depends on the viscosity of the mixture. When the mixture is highly viscous, the flow will be laminar. The transition towards turbulent flow is given by the Reynolds number, which characterizes the flow:

$$\mathrm{Re} = \frac{\rho v L}{\eta}; \quad \mathrm{Re}_{cr} \approx 370 \tag{15.9}$$

Here, L is the gap width between rotor and stator, and v is the tangential speed of the rotor (m/s); the density ρ and viscosity η are the values for the mixture. When Re < 370, the flow will be laminar; when it is larger, flow will start to become turbulent.

Toothed mill. This type of mill is used often in the chemical and pharmaceutical industry. Here, a hollow rotor having openings through the rotor wall rotates in a stator also having openings. Once more, the gap between rotor and stator is very small, giving rise to very large shear forces between the two. The mixture is pumped into the centre of the rotor, flows through the openings, and is subjected to intense mixing and shearing. It then flows out through the openings in the stator. The flow pattern is turbulent.

High-pressure homogenisers: Here, the mixture is pumped through a very small hole or gap. The extensional flow, turbulence and other phenomena give break-up of large droplets into smaller ones. The break-up is caused by the turbulence of the liquid as described above, but also by *cavitation* (see text box). Cavitation causes strong, very local turbulence, which can break up droplets further. Very intense fields can be reached, by using pressure differences of 10–50 MPa. Small, lab-scale homogenisers will operate in the laminar flow regime; industrial-scale systems will operate in the turbulent regime. The transition between these two regimes is once again given by the Reynolds number (now, L is the gap width, and v is the average liquid velocity in the gap):

$$\mathrm{Re} = \frac{\rho v L}{\eta}; \quad \mathrm{Re}_{cr} \approx 1500 - 3000 \tag{15.10}$$

Valve systems. These systems are used especially in the dairy industry. The narrow gap is created here with a valve, which is pressed shut with a disk and a strong spring. Pressing the liquid through the valve lifts the disk somewhat; the force of the spring ensures that the gap width will remain very small: for a lab-scale system the gap width will be of the order of 1 μm; for industrial-scale systems it will be 10–40 μm (Smulders 2000).

Nozzle systems. Other systems do not have a valve, but simply have a small opening through which the liquid is squeezed; in some systems two or more openings are placed in series. Sometimes the liquid is split up and then recombined through small holes, giving similar action.

Dynamic pressure and cavitation

Bernouilli's law states that velocities and pressure outside (index o) and inside the homogenizer gap (index g) are related as (neglecting frictional losses):

$$p_o + \tfrac{1}{2}\rho v_o^2 = p_g + \tfrac{1}{2}\rho v_g^2$$

The velocity of the liquid inside the nozzle (v_i) is much higher than the velocity outside it (v_o), and therefore the pressure inside the gap p_g must be much lower than the external pressure v_o. When the velocity becomes sufficiently high, p_g can become even lower than the vapor pressure of water, and bubbles of water vapor will be formed. These bubbles will collapse violently when the liquid is out of the small nozzle, creating a large amount of local turbulence. This is called cavitation. Cavitation should be kept limited, as it may form radicals, which may compromise product quality.

Using ultrasound: It is possible to induce the same phenomena as discussed before (turbulence and cavitation) with the help of sound (see Figure 15.5). Sound is a pattern of propagating pressure fluctuations. When the sound is sufficiently intense, the pressure fluctuations will become so large, that in small regions, the pressure becomes lower than the vapour pressure of water. This will induce the formation of small bubbles, which will implode almost immediately again. This implosion will, just as with high-pressure homogenisation, cause very intense, local turbulence, which

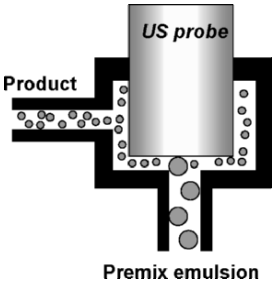

Figure 15.5. Schematic picture of an ultrasound homogenizer.

can break up the droplets according to the inertia-dominated regime. Usually, ultrasound is used (i.e., sound with frequencies higher than 20 kHz).

The ultrasound is generated by an actuator (basically a small loudspeaker), which vibrates with the specified frequency. The mixture is led around the actuator, into the volume that has the strongest field, and is then led away. The intensity of the ultrasound quickly declines away from the actuator; therefore, the treatment chamber has to be relatively small. This makes the technology not suited for very large scale production; it is used commercially for low-volume products. For systems containing unsaturated fatty acids, cavitation should be avoided (see text box). For products that allow its application, use of ultrasound is an excellent way of generating very fine emulsions, due to the high intensity of the ultrasonic field that can be generated.

15.5.2 Laminar Flow–Shear Flow and Extensional Flow

How do the techniques described above work? First, a coarse premix emulsion is made. Then, when the premix is subjected to an intense flow field, the droplets are broken apart by the forces exerted by the flow around the droplets. If one applies a force that is bigger than the forces that keep a droplet together, the droplet will be disrupted. The ratio of the externally applied stress and the internal, coherent tension is called the Weber number. For many situations this is defined as:

$$\mathrm{We} = \frac{\text{External, disruptive stress}}{\text{Internal, coherent stress}} \tag{15.11}$$

For situations where the droplets are subjected for a very short time to the disruptive stress (e.g., in turbulent flow), the viscosity of the internal phase will cause the droplet to react slowly to the external stress, and the definition into has to be extended:

$$\mathrm{We} = \frac{\text{External, disruptive stress}}{\text{Internal, coherent stress} + \text{coherent viscous forces}} \tag{15.12}$$

In general, when an external stress is applied such that the Weber number is sufficiently high, a droplet will break up into two or more smaller droplets. If flow is applied, the droplet will feel the flow around it, and this will deliver the external, disruptive force for break-up of the droplet. When the flow is laminar, we can have simple shear flow or extensional flow, or a combination of these two.

Simple shear flow is the flow of the liquid of viscosity η_c over itself along a plane; see Figure 15.6a. One encounters simple shear flow during flow through a tube, or flow over a planar surface. A droplet of size R_d subjected to simple shear flow, will be distorted due to the stress exerted on the droplet. The internal, coherent stress can be estimated with the help of the Laplace pressure in the droplets $2\sigma/R_d$, which is the pressure that the interface exerts and keeps the droplet together. The disruptive stress can be estimated through:

$$\tau_{\text{ext}} = \eta_c \left(\frac{dv}{dz} \right) = \eta_c \dot{\gamma} \tag{15.13}$$

Here, $\dot{\gamma}$ is the shear rate that is applied (s^{-1}). This yields a relation for We:

$$\text{We} = \frac{\eta_c \dot{\gamma} R_d}{2\sigma} \tag{15.14}$$

In order to achieve break-up of a droplet this We number should have a value that is higher than a certain critical value, called the critical We number:

$$\frac{\eta_c \dot{\gamma} R_d}{2\sigma} > \text{We}_{cr} \tag{15.15}$$

From this relation, the (maximum stable) droplet size follows, at a given shear rate and with a given interfacial tension. It is found that the exact value of We_{cr} is not completely constant, but is dependent on the ratio of the viscosities of the dispersed and the continuous phase. This is because the droplet will deform more when the dispersed phase viscosity is lower, which will give a higher Laplace pressure and a lower external stress. An indication of the values of We_{cr} is given in Figure 15.7.

Extensional flow takes place when the liquid is squeezed into a small opening (see Figure 15.6b). It occurs when the liquid enters (or exits) a channel or is pushed through a small hole (e.g., with high-pressure homogenization). In most practical cases, the flow pattern is a mixture of simple shear flow and extensional flow. A droplet in extensional flow will also experience a drag force exerted by the flow; only now the external force exerted on the droplet is not equal to $\eta_c(dv/dz)$ but equal to $\eta_c(dv/dy)$, where y is the coordinate in the direction of the extension. We can use the same relations as with simple shear flow, only in this case the value of We_{cr} is different. So, also here,

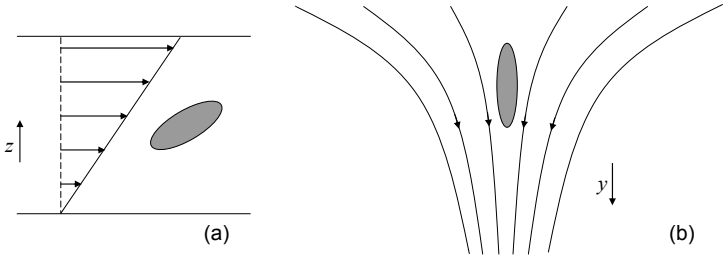

Figure 15.6. Shear flow (a) and extensional flow (b).

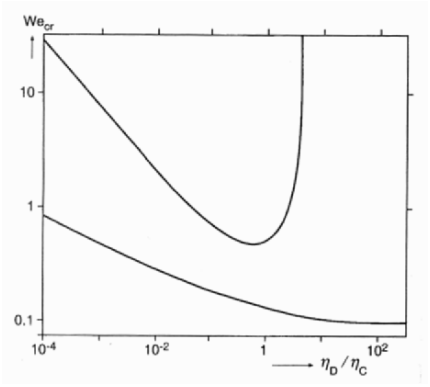

Figure 15.7. Critical We numbers for laminar flow conditions: plain shear flow (*upper curve*), and for extensional flow (*lower curve*) (Walstra 2003).

$$\frac{\eta_c \dot{\gamma} R_d}{2\sigma} > \mathrm{We}_{cr} \tag{15.16}$$

In general, extensional flow is more effective than simple shear flow in disrupting a droplet. Therefore, the We_{cr} number for extensional flow is smaller than for simple shear flow. Figure 15.7 gives an impression of the values both for simple shear flow and for extensional flow. Since in practice one will always have a mixture of the two types of flow, the critical We number will have a value in between.

15.5.3 Turbulent Flow

When flow rates are high, a liquid will not flow in a laminar fashion, but will become turbulent. The liquid will start to flow in a chaotic way, forming large and small swirls and eddies. The flow rate at which this happens depends on the geometry of the machine, on the flow rate applied, and on the overall viscosity of the mixture. The transition from laminar to turbulent flow is characterized by the Reynolds number; the critical Reynolds number depends on the geometry and the product properties (see Equations (15.9)–(15.10)).

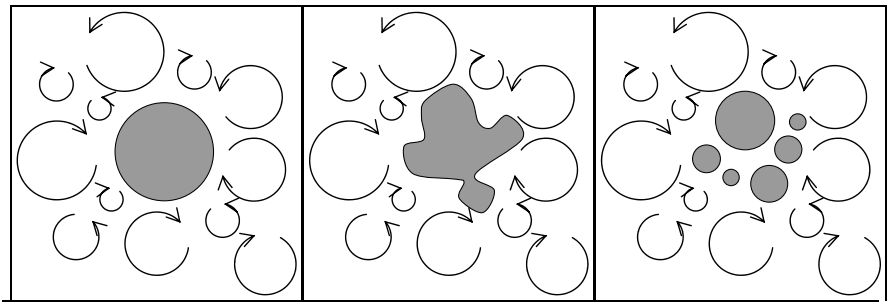

Figure 15.8. Break-up by turbulent flow: the eddies in the liquid impinge on the droplet, deforming it, which leads to break-up into smaller droplets.

Turbulent flow can be very effective in breaking up droplets into smaller ones; however, the mechanism is different compared to laminar flow. For larger droplets, many of the swirls and eddies are smaller than the droplets. They impinge on the droplets, deforming them, and when the deformation is sufficiently strong and lasts for a sufficiently long time, the droplet will break up into smaller ones (see Figure 15.8).

It is more difficult here to find a value of the critical Weber number, since the exact local flow conditions are not known. Usually, one takes the power density as a measure for the intensity of the eddies. The power density (symbol ε, with unit W/m^3) is the amount of energy per m^3 that is used to establish the flow pattern. The larger the power input, the more intense and the smaller the eddies will be.

When the turbulence is not too large, the main force on the droplets is caused by the shear imposed by the surrounding eddies. With the help of the Kolmogorov theory for turbulent flow, the external, disrupting force is can estimated as $\tau_{ext} = \sqrt{(\varepsilon \cdot \eta_c)}$. We then end up with a definition of the critical Weber number:

$$\mathrm{We}_{cr} = \frac{\tau_{\mathrm{ext}} R_d}{2\sigma} \approx \frac{\sqrt{\varepsilon \eta_c} R_d}{\sigma} \tag{15.17}$$

Assuming that the We_{cr} should be around one, the droplet size obtained can be estimated; however, this is only an order-of-magnitude estimation. When the turbulence becomes very intense, the shear forces exerted by the eddies are not the dominant force anymore; rather the inertia of the liquid impinging on the droplets become the disruptive force. With the help of the Bernouilli equation, we can estimate the external, disruptive force as:

$$\tau_{ext} \approx \varepsilon^{\frac{2}{3}} R_d^{\frac{5}{3}} \rho^{\frac{1}{3}} \tag{15.18}$$

The equation for the critical Weber number then becomes

$$\mathrm{We}_{cr} = \frac{\tau_{\mathrm{ext}} R_d}{2\sigma} \approx \frac{\varepsilon^{\frac{2}{3}} R_d^{\frac{5}{3}} \rho^{\frac{1}{3}}}{\sigma} \tag{15.19}$$

Again, by assuming that We_{cr} will be around unity, one can have an estimate of the droplet size obtained. The transition in the turbulent regime from viscous-dominated break-up to inertia-dominated break-up, takes place when the droplets are larger than (Walstra 2003):

$$R_d > \frac{\eta_c^2}{\sigma \rho_c} \tag{15.20}$$

Flow in a *stirred tank* is usually turbulent, but the turbulence is not very intense; therefore it will generally operate in the viscous-force dominated regime. Flow in a *colloid mill* can be either laminar or turbulent, depending on the viscosity of the product. For water-in-oil emulsions, the viscosity is rather large, and break-up will usually be viscous force dominated; for oil-in-water emulsions it depends on the droplet size. Flow in a *toothed mill* is often turbulent, but it depends on the droplet size and the viscosity of the continuous phase determines whether break-up is viscous or inertia dominated. Large-scale high-pressure homogenizers commonly feature turbulent flow. Here, inertial forces usually dominate. Smaller, laboratory scale high-pressure homogenizers may still operate in the laminar regime, since the throughput is smaller and the gap size is much smaller than in larger systems. Therefore, translation of results obtained on laboratory scale towards industrial scales is not always easy (Smulders 2000). Emulsification with ultrasound is always based on inertial forces, created by the cavitation of the vapour bubbles.

15.6 Membrane and Micro-channel Emulsification

An emerging class of emulsification methods is not based on imposing an overall flow field, but rather by making individual droplets on the mouths of membrane pores or micro-engineered channels. Characteristic is that the flow fields applied are much milder; energy consumption is much lower, while the droplet sizes are strongly dependent on the shape and dimensions of the pores or micro-channels. A number of processes belong to this class:

- *Cross-flow membrane emulsification* (see Section 15.6.1 and Figure 15.9)
- *Micro-channel emulsification* (see Section 15.6.2)
- *Dead-end ("pre-mix") membrane emulsification* (see Section 15.6.3)

Other mechanisms are being investigated, such as co-flow emulsification, which is potentially a very effective way to make small droplets. These methods are, however, still very far from commercialization and use for production of food products. Therefore, we will not discuss them here; one can find more information in literature

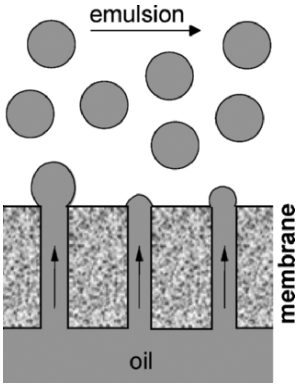

Figure 15.9. schematic representation of cross-flow membrane emulsification.

(Anna et al. 2003; Davidson et al. 2005). We will concentrate here on the three types mentioned above.

15.6.1 Crossflow Membrane Emulsification

The process and the membranes: In 1991, Nakashima developed a new type of porous membrane, made of volcanic ashes: Shirazu Porous Glass (SPG) membranes (see Figure 15.10a). When he tried to push an oil through the pores of this membrane, the oil emerged as very small droplets in the aqueous phase at the permeate side. This principle was further developed into cross-flow membrane emulsification (XME). Others have successfully used ceramic membranes for this process (see Figure15.10b; Schröder et al., 1998, 1999; Vladisavljevic and Schubert 2002). Other than with the processes described before, each droplet is formed individually on the mouth of a pore. The emulsions produced by this method can be very highly monodisperse, but the permeation rate of oil through the membrane is often relatively low. This makes it a method that is suitable for small-volume, high-value products with a lower volume fraction of dispersed phase.

Essential is that the membrane is preferentially wetted by the continuous phase: if the aim is to make an oil-in-water emulsion, the membrane should have hydrophilic surface properties; if one aims to produce a water-in-oil emulsion, the membrane should have hydrophobic surface properties. Thus, XME can be used not only to make oil-in-water emulsions, but also water-in-oil emulsions.

Process principles: As oil emerges out of a pore, it will form a small droplet on top of the pore mouth. It is retained in this position by the interfacial tension (Peng and Williams 1998). The cross-flowing continuous phase exerts a drag force on the droplet. In the droplet size ranges that XME is typically used, all other forces, such as gravity (buoyancy) and inertial lift forces, are negligible. The size of the drag force can be estimated with the help of Stokes' law:

$$F_d = -1.7\left(6\pi\eta_c R_d v_c\right) \tag{15.21}$$

in which v_c is the velocity of the continuous liquid at half-height of the droplet, η_c is the viscosity of the continuous phase, and R_d is the radius of the nascent droplet. The factor 1.7 is added, due to the nonhomogeneous velocity field around the droplet (see Figure 15.11b).

The value of v_c can be estimated with the shear stress at the wall, τ_w, since

$$\tau_w = -\eta_c \frac{dv_c}{dz} \approx -\eta_c \frac{v_c}{R_d} \tag{15.22}$$

Substituting this in Equation (15.21), gives

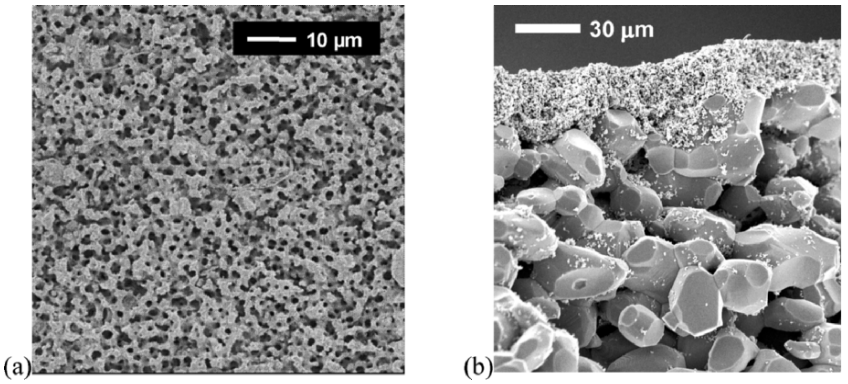

Figure 15.10. (a) Pore structure in a Shirazu Porous Glass (SPG) membrane, featuring highly tortuous pores. (b) Top-layer structure of a ceramic alumina membrane, made by sintering ceramic particles together.

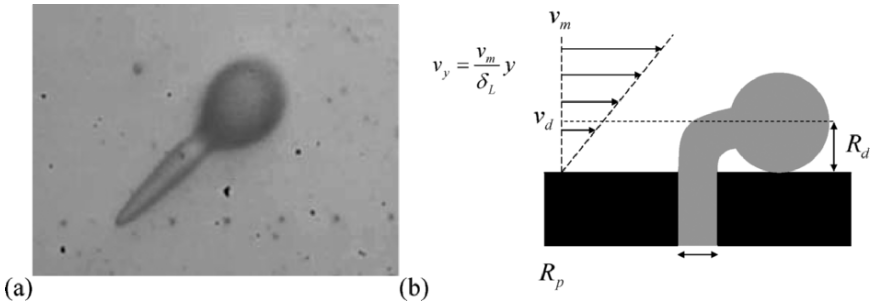

Figure 15.11. (a) Micrograph showing a droplet emerging from a pore (*lower left corner*), dragged with the cross-flow from the lower left corner to the upper right corner (courtesy C.J.M. van Rijn and C. Goeting). (b) Forces acting on a deformed droplet in cross-flow and with transversal membrane excitation.

$$F_d = -10.2\pi R_d^2 \tau_w \tag{15.23}$$

The force that retains the droplet to the pore mouth is generated by the interfacial tension, σ:

$$F_\sigma = 2\pi\sigma R_p \tag{15.24}$$

in which R_p is the radius of the pore. The neck, which retains the droplet to the pore mouth, is roughly of the same thickness as the pore, which is smaller than the droplet size. Equating these forces gives the force balance for the droplet:

$$\begin{aligned} & F_\sigma + F_d = 0 \\ \rightarrow \quad & 2\pi\sigma R_p - 10.2\pi R_d^2 \tau_w = 0 \\ \rightarrow \quad & \frac{R_d}{R_p} = \sqrt{\frac{\sigma}{5.1\tau_w R_p}} = \sqrt{\frac{1}{5.1\mathrm{Ca}}} \end{aligned} \tag{15.25}$$

Here, the capillary number, Ca, is defined as $\sigma/\tau_w R_p$; it represents the ratio between forces by interfacial tension and forces by the drag force. It is similar to the We number used earlier. As soon as the drag force exceeds the retaining force, the droplet will be detached and taken up by the continuous phase. Thus, this relation will give the size of the droplet obtained as a function of the parameters.

By reducing the pore size of the membrane R_p, droplets become smaller, just as when we increase the cross-flow velocity of the continuous phase (and therefore increase the shear stress on the wall τ_w). Addition of surfactants leads to a lower interfacial tension σ, and will therefore lead to smaller droplets. (The relation between the interfacial tension at the time of droplet snap-off and the concentration of surfactants is, however, a complex one).

In practice, this relation gives the right trends, but does not give a good quantitative prediction of the droplets obtained. One of the reasons is that droplet shape is not spherical, as was assumed, but is in fact strongly distorted. This is shown in Figure 15.12. Computational fluid dynamics calculations show that during the formation of a droplet, the shape of the droplet is very strongly distorted. The drag force exerted by the cross-flow is therefore less than would be expected on the basis of the model described above. The droplets therefore become larger than one would expect.

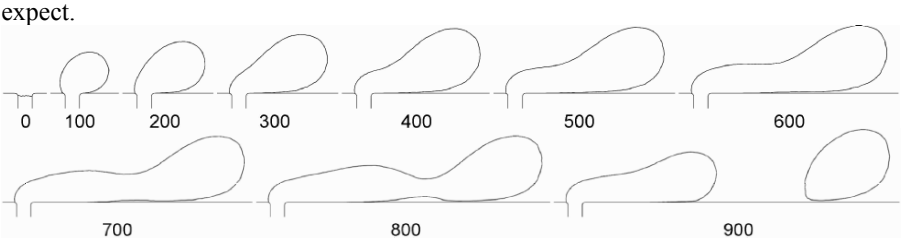

Figure 15.12. Droplet shapes as simulated with computational fluid dynamics during XME with a cross-flow velocity of 1 m/s. Numbers in the figures are the times elapsed after the start of the droplet formation in μs. After Kelder et al. (2006).

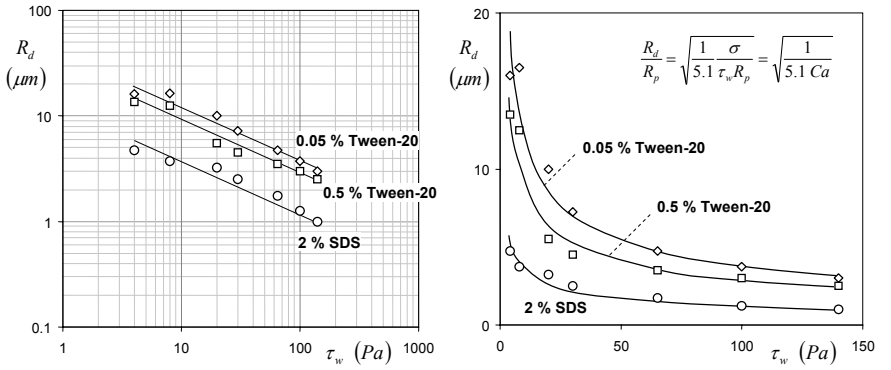

Figure 15.13. Comparison between experimentally obtained droplet sizes and descriptions by the model (data from Schröder et al. 1998, 1999). The membrane used was a ceramic membrane with average pore size of 0.4 μm, and with transmembrane pressure of 3 bar; sunflower oil was emulsified in water with different surfactants. One only obtains a good quantitative fit with the data when one assumes that the interfacial tensions are 18 mN/m with 0.05% Tween-20, 11 mN/m with 0.5% Tween-20 and 1.7 mN.m with 2% SDS. These values are not physically realistic; therefore, the model does not quantitatively describe the data.

A second complication is that the interfacial tension is not a constant (as is assumed in the model). In Section 15.3 it was mentioned that a surfactant needs time to diffuse towards a freshly created interface, and needs to adsorb and distribute over the interface. Therefore, the faster an interface is created, the higher the actual interfacial tension will be. This is shown in Figure 15.13. The dependence of the droplet size on the wall shear stress follows is qualitatively in accordance with the model (Figure 15.13, left-hand graph). When the experimental data are modelled by using the interfacial tension in the model as a fit parameter (Figure 15.13, right-hand graph), one finds values that are much smaller than could ever occur during the process. This shows that the model gives the right trends, but cannot quantitatively predict the droplet sizes obtained in this process.

The role of surfactants: Apart from the stabilizing function of surfactants to avoid coalescence of the formed droplets, Figure 15.13 shows that the dynamics of surfactants play a key role in determining the droplet sizes obtained. The force balance model shows that the lower the interfacial tension is, the smaller the droplets become. Addition of surfactants reduces the interfacial tension, and therefore the droplet size is reduced when more surfactants are added. The surfactants however need to diffuse to the interface that is continuously generated on the growing droplet. Therefore, the interfacial tension that is achieved is dependent on the rate at which the dispersed phase emerges from the membrane pore: the faster this flow, the more surfactants have to be transferred to the interface. The importance of this is illustrated in Figure 15.14. Here, the surfactant concentration was varied, and the droplet size obtained was monitored, while using a model system consisting of a single pore through a silicon chip. The more surfactant was used, the smaller the emulsion droplets became, due to the lower interfacial tension during the formation of the

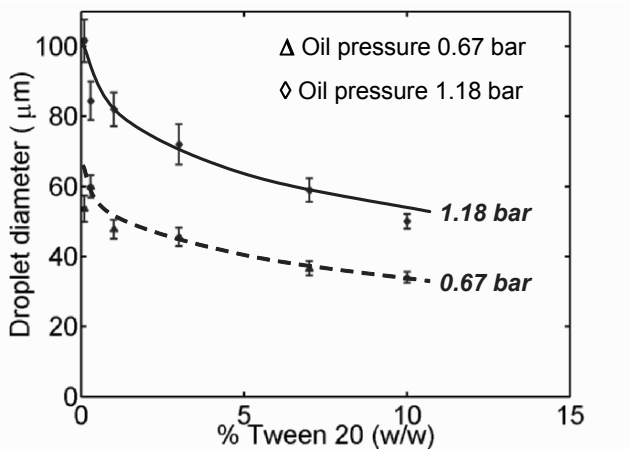

Figure 15.14. The droplet size depends on the concentration of surfactant: the more surfactant, the lower the interfacial tension will be, and therefore the smaller the droplets will become. As the pressure over the membrane is increased, the flow of the dispersed phase (in this case oil) is increased; the droplets grow faster, and the surfactant has to diffuse faster to the interface. This results in a higher dynamic interfacial tension, and larger droplets. (After van der Graaf Schoën et al. 2004.)

droplets. When the oil flux through the membrane pores was increased by increasing the trans-membrane pressure, the droplet sizes increased once more: the faster the oil emerges, the faster the droplets are created, and the faster the interface is created. The surfactants need to diffuse faster, and the interfacial tension is increased.

In industrially optimised processes, the droplet formation may be so fast, that surfactants may not have the time to diffuse towards the interface; in that case the relevant interfacial tension is that of the "empty" interface between oil and water without surfactants.

15.6.2 Systems with Droplet Snap-Off Induced by Interfacial Tension

SPG membrane emulsification: With cross-flow emulsification, the droplet size is dependent on the cross-flow velocity of the continuous phase. This is what is found at higher flows of the dispersed phase, and at high cross-flow velocities. However, when one uses SPG membranes, this is not always found. At some conditions, the droplet size is found to be independent of the cross-flow velocity (Yasuno et al. 2002). This is shown in Figure 15.15, where the force balance model predicts a strong decrease of the droplet size with the cross-flow velocity, while the experiments showed that the droplet sizes hardly changed with changing cross-flow velocity. In some cases, small droplets emerge even when there is no cross-flow at all. This is remarkable: according to the force balance model, one would expect that in that case the droplets would become infinitely large. Apparently, another droplet formation mechanism takes place.

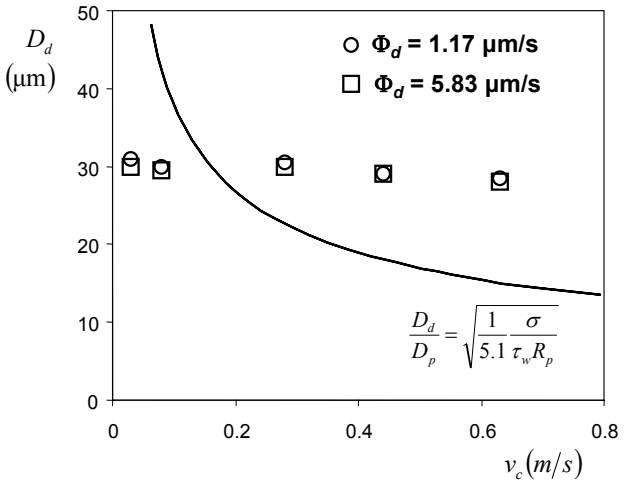

Figure 15.15. Droplet sizes obtained with an SPG membrane, as measured by Yasuno et al. (2002). One would expect that the droplet size would depend on the cross-flow velocity of the continuous phase, but it does not. Apparently, another droplet formation mechanism is active. Two flow rates through of the dispersed phases (Φ_d) are indicated.

A possible reason is shown schematically in Figure 15.16. The figure at the left shows the typical pore structure of an SPG membrane; the figures at the right-hand side show a schematized version of it. Once the oil emerges from a pore in the membrane, there is a change in Laplace pressure. When the oil is forced into the membrane, one has to overcome the Laplace pressure difference, equal to σ/R_p (note that the Laplace pressure in a cylinder is a factor two smaller than in a sphere). The same is true, but reversed, at the downstream side of the membrane. Here, the oil emerges from a pore as a droplet. There is a moment that the droplet has a Laplace pressure difference with the continuous phase that is smaller than that of the pore. At that moment there is a

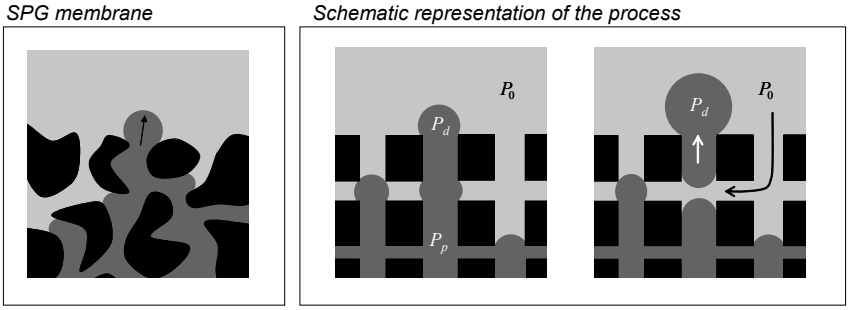

Figure 15.16. Schematic representation of the processes inside an SPG membrane. As soon as an oil droplet emerges, it will have a different Laplace pressure difference with the continuous phase. At a certain droplet size, it will be lower than the Laplace pressure inside the oil phase in the pore. When the pores are highly interconnected, the oil in the pore can be replaced by the continuous phase, leading to spontaneous snap-off.

pressure gradient from the oil in the pore, towards the droplet, and oil can flow spontaneously from the pore into the droplet, under the condition that the pore structure is such that the continuous phase can replace the oil in the pore. This is the case when the pores structure is very strongly interconnected, such as with SPG membranes. At a certain moment, the cylinder of oil in the pore snaps off, and the droplet is released in the continuous phase. The droplet snap-off is spontaneous, driven by the interfacial tension, and not by the cross-flow. Therefore, the cross-flow will not have much influence on the process, and the droplet size is (almost) independent of the cross-flow rate.

With other membranes, such as ceramic membranes, the interconnectivity can be less. In that case, the continuous phase cannot enter the pore, and the oil flowing out has to be replaced by oil, coming from other pores. The cylinder of oil in the pore remains intact, and no spontaneous snap-off takes place. This may be the reason that only some membranes show this effect.

Further, when we put a high pressure over the membrane, the flow rate of the oil through the membrane pores will be fast, and at the time when the continuous phase should replace the oil in the pore, it does not have the time. Therefore, what one sees is that the spontaneous snap-off process only takes place at low flow rates. At higher flow rates droplets will still be formed, but they will be larger, and they will be detached by the cross-flow of the continuous phase over the membrane.

When will this spontaneous snap-off take place? If the droplet has radius R_d (thus giving rise to Laplace pressure difference with the continuous phase of $2\sigma/R_d$), the point at which the oil will start to have a pressure gradient from pore to droplet is:

$$P_p + P_0 \geq P_d + P_0 \quad \rightarrow \quad \frac{\sigma}{R_p} \geq \frac{2\sigma}{R_d} \quad \rightarrow \quad R_d \geq 2R_p \tag{15.26}$$

So, as soon as the droplet (radius) is twice as large as the pore (radius), there is the possibility of spontaneous snap-off. It depends on the shape of the pore structure and on the flow rate of the oil—how large the final droplets will be—but it is usually close to this value.

Micro-channel emulsification: In a visualization cell, manufactured with micro-engineering technology, Kawakatsu et al. (2001a and b) observed oil droplets that spontaneously detached from a micro-engineered channel. The geometry is shown in Figure 15.17a. They found that the droplet size was independent of the cross-flow in the channel containing the continuous phase, and only depended on the geometry of the channel. With these micro-channels, completely monodisperse emulsion droplets could be made. They also found that this only worked for lower flow rates of the oil through the channel. At higher flow rates, the droplets became much larger. This was corroborated by others; see Figure 15.18.

The mechanism of this process is the same as was discussed in the previous section for SPG membranes, only here no interconnected pores are needed. The micro-channels that gave these effects end in a region that consists of a slit-shaped cavity in between two plates. The oil coming out of the pore has to squeeze between the two plates, and therefore will not form a droplet but a disk. The Laplace pressure

inside this disk is equal to σ/R_p, with R_p in this case half of the distance between the two plates. The disk, accumulating more and more oil, will grow and at a certain moment will reach the outer side of the slit-shaped cavity. At that moment, a spherical droplet will be formed. As soon as the pressure difference with the continuous phase in the droplet is smaller than the pressure difference in the disk (which once again happens when $R_d \geq R_p$), the droplet will snap off spontaneously. Therefore, the slit-shaped cavity has the same function as the interconnected pore structure in a SPG membrane.

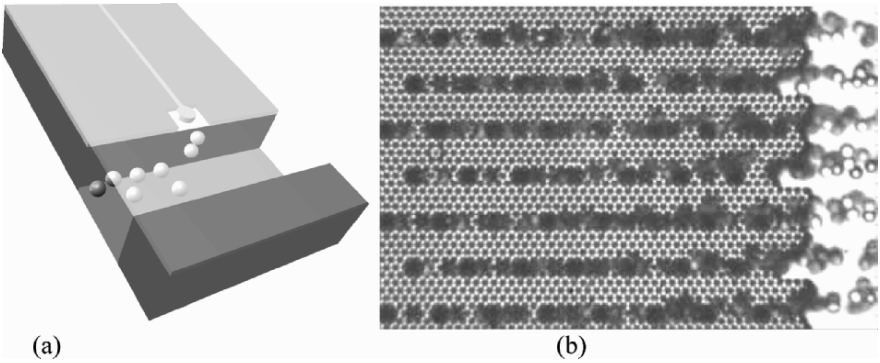

Figure 15.17. (a) Emulsification process found by Kawakatsu et al. (2001a). Oil was led through a small channel, which ended on a slit-shaped opening (Van Dijke et al. 2006). (b) A nozzle plate made by Veldhuis (2006), stacking many channels in a micro-engineered plate. (See Color Plate.)

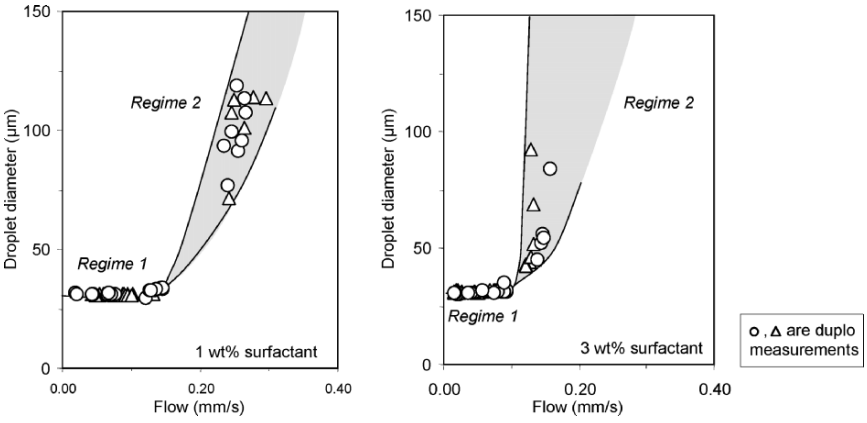

Figure 15.18. Droplet size as a function of the flow rate of oil through the micro-channel. At lower flow rates, the droplet size is independent of the flow rate (regime 1), while from a certain critical flow rate, the droplets become larger (regime 2) (Dekkers 2003).

One sees in Figure 15.18 also that this spontaneous snap-off only occurs at lower flow rates. At higher flow rates, the continuous phase does not have the time to replace the oil. The droplets now become larger, and will be dragged away by the cross-flow. Also here, one sees the transition from interfacial tension-induced spontaneous snap-off towards shear-induced snap-off by the cross-flow over the membrane.

Several researchers have been successful in the scaling up of this process. Kobayashi et al. (2001) and Sugiura (1998) have been successful by making slit-shaped pores through a layer of silicon, perpendicular to its surface. In this way one can stack many millions of channels on a single plate. Other groups have used different geometries of channels, arranged in a similar fashion to what Kobayashi and co-workers have used (e.g., Veldhuis 2006).

15.6.3 Dead-End ("Premix") Membrane Emulsification

Emulsification: In the 1990s, Suzuki found a new method to produce emulsions, once more using membranes (Suzuki et al. 1996; Suzuki et al. 1998). In this case, he did not have a to-be-dispersed phase at one side and a continuous phase at the other side, but he started with a coarse pre-emulsion, featuring large droplets. He then simply pushed this coarse emulsion through a porous membrane. At the other side, he observed a fine emulsion emerging that had a narrow droplet size distribution (see Figure 15.19).

This system proved to be very different from the systems discussed before. The throughput per m^2 membrane surface is higher than in the other systems; several m^3 product per m^2 membrane per hour operating time can be reached. It depends, however, on the pre-emulsion whether one obtains an emulsion with a narrow droplet size distribution. When the pre-emulsion is coarse, one usually obtains a mixture of small droplets plus some very large ones. Repeating the procedure a few times then helps. With every pass, the number of small droplets increases and the number of large droplets decreases, until the emulsion consists only of small ones.

The process is not yet completely understood. A number of different break-up mechanisms are responsible for the break-up of the droplets inside the pore matrix of the membrane (van der Zwan et al. 2005): snap-off due to localized shear, break-up due to interfacial tension effects, and break-up due to steric hindrance. The multiple

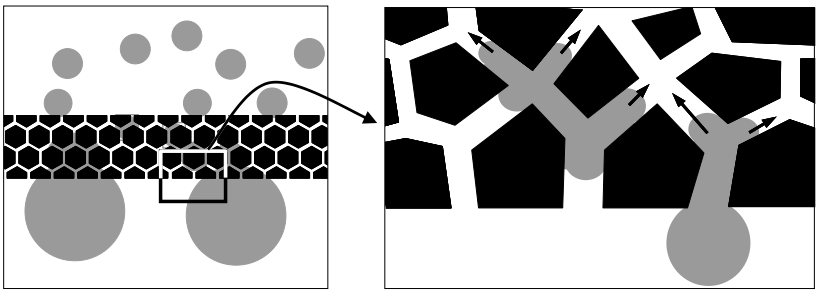

Figure 15.19. The Suzuki flow-through membrane emulsification. A coarse emulsion is pressed through a porous membrane; at the downstream side, a fine emulsion emerges.

branchings and junctions in the pore system may be important in the break-up of the droplets, but they are not essential. Also other phenomena, such as accumulation of the dispersed phase, giving rise to steric hindrance between droplets, and channelling of the flow through specific pores can induce break-up.

Droplet sizes and important process parameters: The properties of the membrane are very important in this process. The membrane should have a relatively narrow pore size distribution, just as with cross-flow membrane emulsification, and it should be wetted by the phase that should be the continuous phase.

The typical droplet size obtained is a bit larger than the average pore size of the membrane, and is hardly dependent on the flux through the membrane. The droplet size is also hardly dependent on the volume fraction of the dispersed phase (see Figure 15.20, left-hand graph). The right-hand graph in Figure 15.20 shows that the *flux* through the membrane obtained at a specific pressure drop over the membrane is strongly dependent on the amount of dispersed phase that is present in the premix. If there is hardly dispersed phase present, the flux will be very close to the clean water flux of the membrane (i.e., the flux that is obtained with only water); with more dispersed phase it can become reduced by a factor of 10.

A major disadvantage of this process is its sensitivity to internal fouling; especially where, for example, proteins are used as emulsion stabilizers. This is because the dispersed phase, the continuous phase, and also all other components need to flow through the membrane. Any particulate matter that would be present in the pre-emulsion, and that is small enough to be able to enter the pores, will be captured

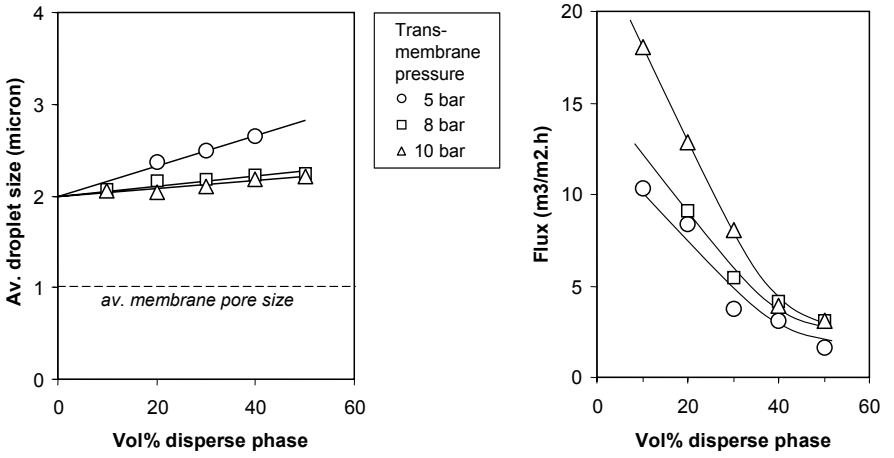

Figure 15.20. Droplet sizes obtained in premix membrane emulsification. The droplets are somewhat larger than the pore sizes, and the emulsion is relatively monodisperse. Fluxes are very high; however, internal fouling of the membrane may reduce the fluxes quickly, depending on the formulation of the product. Composition of the phases: 2% decaglycerol monolaurate in water; 2% hexaglycerol polyricinoleate in disperse oil phase. (After Altenbach-Rehm et al. 2002.)

somewhere in the pore structure. Proteins, especially those used to stabilize an emulsion, have the tendency to adsorb on interfaces, which are in abundance inside the pore matrix. Thus, they will adsorb to the wall inside the pores. Since the pores are only 100 nm to a few µm wide anyway, adsorption of a bit of protein quickly leads to a severe reduction of the effective pore size. This results in a large reduction in the flux. Unfortunately, any fouling inside a membrane is almost impossible to remove again, so the membrane has to be replaced.

It depends on the application whether this is a problem. For applications involving relatively clean streams, and not using proteins as stabilizers, the process seems to be highly effective; for others, it still poses practical problems.

Phase inversion in dead-end membrane emulsification: When one prepares an oil-in-water emulsion and presses this through a hydrophilic membrane, the resulting fine emulsion will be an oil-in-water emulsion as well. However, if you would use a *hydrophobic* membrane, the resulting emulsion will be a water-in-oil emulsion (assuming that the surfactant system would support the formation of a water-in-oil emulsion—see the *Bancroft Rule*). In this case, the emulsion is inverted from an *O/W* towards a *W/O* emulsion (see Figure 15.21). The same can be done with a water-in-oil emulsion pressed through a hydrophilic membrane, which leads to an oil-in-water emulsion.

This can be useful when one needs to prepare an emulsion with a very high volume weight of dispersed phase; for example, a water-in-oil emulsion for a sauce. Such an emulsion can be rather thick in consistency (high viscosity). By first preparing an oil-in-water emulsion (with a low volume of oil in the water phase), and then pressing it through a hydrophobic membrane, one can very easily make a thick water-in-oil emulsion.

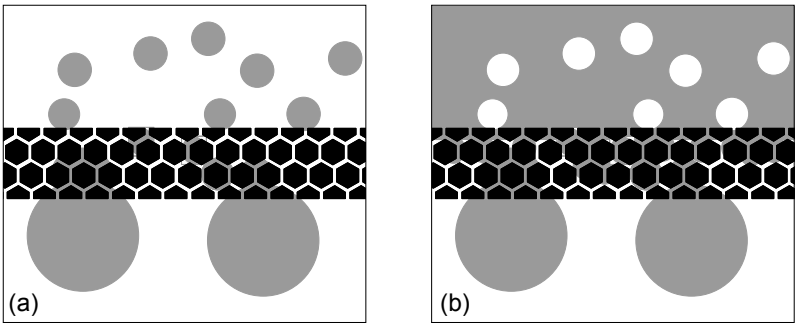

Figure 15.21. (a) When the membrane is wetted by the continuous phase of the premix emulsion, the resulting emulsion is of the same type. If we start with an oil-in-water emulsion, and we use a hydrophilic membrane, the resulting emulsion is also oil-in-water. (b) When we use a membrane that is wetted by the dispersed phase, we obtain inversion. If we start once more with an *O/W* emulsion, and we use a hydrophobic membrane, we end up with a *W/O* emulsion. (From Suzuki et al. 1996; Suzuki et al. 1998.)

15.6.4 Industrial Application of Membrane and Micro-channel Systems

As of 2006, neither of the membrane or micro-channel based methods are widely used in the food industry. The reason is that the throughputs per m^2 of membrane area are still low. Using an SPG membrane results in a throughput of around 11 $l/(m^2h \cdot bar)$ (Vladisavljevic et al. 2002); use of a ceramic membrane gives a flux of around 30.8 $l/(m^2h \cdot bar)$ (Schröder et al. 1998). An interesting development is the use of micro-engineered membranes for cross-flow membrane emulsification (Abrahamse et al. 2002), which could result in fluxes that are two to three orders of magnitude higher. However, using these membranes is still in the research phase.

A few food products have been on the market using cross-flow membrane emulsification. The method can make emulsions that have small droplets with a narrow size distribution. Thus, it is possible to make sauces with lower oil content than with conventional emulsification techniques. The technique of cross-flow emulsification is clearly the best developed process; for small-scale, high-value applications it is an attractive process.

Micro-channel emulsification is even farther away from industrial application; however, there are a few small companies offering nozzle plates that show relatively large fluxes, coming into the realm of practical feasibility. For example, fluxes of 20–100 l/m^2h for sunflower oil into water, and of 100–500 l/m^2h with low-viscous oils have been achieved by Veldhuis (2006). It will probably be some years before all aspects of using them on larger scale have been solved, but their easy geometry in combination with the possibility to make monodisperse droplets may well lead to larger-scale use in the next years. Still, it is to be expected that all methods will have their main applications in low-volume, high-value products.

Premix membrane emulsification is a powerful technique, especially where the system does not induce internal fouling of the membrane used, and where high volume fractions of the dispersed phase are required. This probably limits the applications mostly to (fine) chemicals production, but one may expect a few applications in the food industry as well.

An interesting application for any of the three processes is the preparation of double emulsions (see Figure 15.22), for example, water droplets in an oil phase, of which droplets are dispersed into a second water phase. This is called a water-in-oil-in-water (*W/O/W*) double or duplex emulsion. Even though they are currently only applied in medical and cosmetic products, they may emerge also in food production. One application is encapsulation of, for example, flavour components in a product. Another application might be the reduction of the actual amount of oil in a product, without changing the apparent volume fraction of the oil phase in the emulsion. This can lead to products that have good sensory properties and at the same time contain less fat, without having to resort to different formulations, for example, by using gelling agents.

15.7 Phase Inversion

Phase inversion (Salager 1988; Salager et al. 2000; Salager et al. 2004) is used for preparation of some food products (e.g., production of margarine and butter), but is

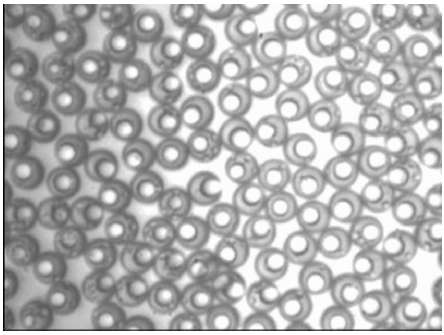

Figure 15.22. Micrograph of example of a double emulsion (*W/O/W*). Courtesy of Veldhuis (2006).

more important for the preparation of some nonfood products such as cosmetics and paints. During phase inversion, the continuous phase becomes the dispersed phase and vice versa.

One of the problems with making emulsions is that it is difficult to prepare an emulsion in which the viscosity of one of the two phases is much higher than the other. This can be seen from Figure 15.7. Only with purely extensional flow can one break-up droplets in which the viscosity of the dispersed phase is very large, but even then one needs to keep the droplets in this field for a relatively long time.

In such a situation, use of phase inversion can help: the problem of breaking up highly viscous droplets is alleviated by first making droplets of the low-viscous phase in the higher-viscous phase, and then inverting the emulsion. There are two ways of achieving phase inversion. The first is called catastrophic (sudden) inversion, achieved by adding more and more of the dispersed phase. The second is called transitional inversion, during which the properties of the emulsion (especially those of the surfactant system) are changed from favouring droplets of the low-viscous phase to droplets of the high-viscous phase.

15.7.1 Catastrophic Phase Inversion

In this process, one starts with the phase that should become the dispersed phase. We call this phase *A*. One then slowly adds the other phase (*B*) to phase *A* while the system is agitated (or rapidly flowing, or homogenized in a suitable machine). Initially, droplets of phase *B* are formed, which are broken up into small droplets by the agitation. In time, more and more of these droplets are formed. However, one ultimately wants to have an emulsion of *A* in *B*; therefore, the surfactant system is dissolved in phase *B* and not in phase *A*. Thus, at a certain time, the emulsion becomes so concentrated and the viscosity becomes so high, that the droplets of *B* are sheared apart: droplets of *B* then start to coalesce. As soon as this coalescence sets in, all droplets start to coalesce, as a snowball effect. So, suddenly the droplets of *B* combine and start to form a continuous phase, taking up droplets of phase *A*, which starts to be the dispersed phase.

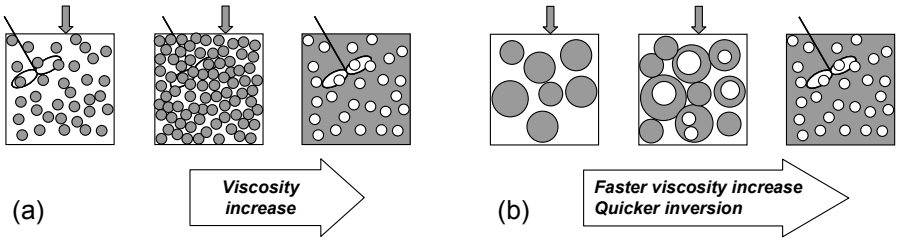

Figure 15.23. Catastrophic phase inversion. (a) If one *slowly* adds phase B to phase A, inversion takes place at a high volume fraction of B. (b) If one add phase B more quickly, inversion is faster.

Figure 15.23(a) shows that if one adds phase *B* slowly and agitates strongly, small droplets of *B* will be formed. The process of making droplets can go on for a long time, because the droplets are small, and therefore stable against deformation by flow (see Section 15.5). Therefore, it takes a long time before inversion takes place: one can go to very high volume fractions of phase *B*. The system is said to show strong hysteresis.

When one adds phase *B* quicker, or agitates the system less, the droplets of *B* will even have inclusions of phase *A*. This is shown in Figure 15.23(b). Such an emulsion is much less stable against inversion, which will take place at lower volume fractions of phase *B*. In these circumstances, the system shows much less hysteresis.

Catastrophic phase inversion is used with products that naturally occur as oil-in-water emulsions, but are to be used as water-in-oil emulsions (butter, margarine). It is also an effective way of preparing emulsions with a dispersed phase that is high-viscous. However, the final droplet size is usually not very small, and the emulsion can be rather polydisperse.

15.7.2 Transitional Phase Inversion

In transitional phase inversion the first step is to prepare an emulsion of the phase that should become the continuous phase (phase *B*) in a continuous phase (*A*). In this case, however, the surfactant system is chosen very carefully, such that at the initial conditions, it favours the formation of a *B*-in-*A* emulsion. Then, when this emulsion has been prepared, the conditions are changed such that the properties of the surfactant system changes towards favouring an *A*-in-*B* emulsion. This can be done by temperature, or by changing pH, or by other means, but the effect is of changing the affinity of the surfactants to the two phases.

Figure 15.24 schematically shows a state diagram of the system. Compositions left of the nodal curve will be a *B*-in-*A* emulsion, when more *A* is added, (catastrophic) inversion will take place at the modal line. However, in a specific area where the affinity of the surfactant system towards both phases is approximately equal, transitional inversion may take place.

Depending on the system, one can tune the properties such that the emulsion changes from a *B*-in-*A* emulsion, into a system in which there is not a clear *B*-in-*A* or

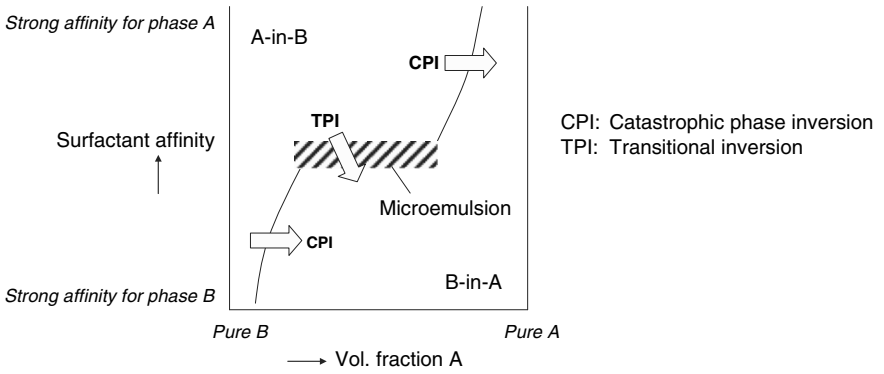

Figure 15.24. Transitional phase inversion can take place by changing the affinity of the surfactant system. There will be a region where a micro-emulsion is formed. By passing the emulsion through this area in the phase diagram, a very fine emulsion of B in A can be formed.

A-in-*B* emulsion, but in which these phases are very intimately mixed. This is called a micro-emulsion. The domains of *A* and *B* are very small now; in the range of 10–100 nm. Then, by changing the system even further, the surfactant system starts to favour an *A*-in-*B* emulsion, which is formed from this micro-emulsion. The domains in the micro-emulsion are so small, that when they combine to form the droplets of *A* in *B*, very small droplets can be formed. With this process, emulsions can be made that have droplet sizes far below 1 μm, even from systems in which the phases have very different viscosity.

Transitional phase inversion is a very effective process, but it is not used in the food industry: due to the properties of the oils commonly used in foods, finding a surfactant system that exhibits this behaviour has not yet succeeded. The process is applied widely, however, in the cosmetic and coating industries.

15.8 Summary

Emulsions are dispersions of one fluid into another. Both oil-in-water and water-in-oil emulsions are encountered. Foams are similar to emulsions, but the dispersed phase is a gas. Emulsions are everywhere: some examples of products that are based on emulsions are salad dressings, mayonnaise, egg yolk, milk, margarine, cream, ice cream, waterborne paints and bitumen. Emulsions are generally not stable, so they need to be stabilized against coalescence. One can use surfactants for that, or polymers, such as proteins and polysaccharides, or particles.

An emulsion typically consists of droplets with many different sizes. The properties of an emulsion strongly depend on the droplet sizes present. There are different average droplet sizes that one can use; the Sauter diameter is often used. Next to the average droplet size, the width of the distribution is important.

Emulsions can be made in different ways. The most common class of processes applies strong flow fields, usually a combination of simple shear flow and of extensional flow. Extensional flow is more effective than shear flow in breaking up droplets into smaller ones. Industrial equipment usually operates with turbulent flow, in which inertial forces can be important as well. In addition, for some applications ultrasound is used, which creates, through cavitation, strong local turbulence.

A second, new class of processes is that of membrane and micro-channel emulsification. A to-be-dispersed phase is here pushed through pores of a membrane or through micro-engineered micron-scale channels. At the pore or channel mouth, droplets are formed. These droplets can spontaneously detach from the pore or channel mouth (interfacial tension driven snap-off), due to the distortion of the droplet shape when it is still attached to the mouth. At higher fluxes or with channel mouths not giving a strong shape distortion, droplets are sheared off by a cross-flowing continuous phase.

A third class is phase inversion. Here, emulsions are made by starting with an emulsion in which the ultimate continuous phase is the dispersed phase and vice versa. Then by adding more and more dispersed phase, one can induce the emulsion to suddenly invert (catastrophic inversion). Alternatively, one can choose the surfactant system such that, for example, by a temperature change, the surfactant system changes from favouring the initial emulsion to favouring an inverted emulsion. This is called transitional phase inversion.

Industrial processes are at this moment predominantly based on the first class (using intense flow fields). The second class based on membranes or micro-channels seems to have large potential for making more complex products; for example, monodisperse emulsions or double emulsions. The third class is used in the production of foods, but also in other industries where emulsions need to be made in which the dispersed phase has a high viscosity compared to the continuous phase.

The future will demonstrate which processes will remain dominant and which will be replaced by new methods. It is clear that the emergence of micro-structured systems (membranes, micro-channels) opens up the route either towards products that have a very precisely defined microstructure (e.g., monodisperse droplets) or towards making products that simply cannot be made with conventional technology. Some applications can already be seen (e.g., double emulsions), some will emerge now that the production methods are available. Now that we can make these products, applications will follow quickly.

15.9 References

Abrahamse, A.J., Lierop, R. van, Sman, R.G.M., van der, Padt, A. van der, and Boom, R.M. (2002). Analysis of droplet formation and interactions during cross-flow membrane emulsification. *J. Membrane Sci.* 204(1-2), 125–137.

Altenbach-Rehm, J.P., Schubert, H., Suzuki, K. (2002). Premix membrane emulsification by hydrophilic and hydrophobic PTFE membranes for manufacture of *O/W* emulsions with a narrow drop size distribution. *Chem-Ing-Tech* 74(5), 587–588.

Anna, S.L., Bontoux, N., Stone, H.A. (2003). Formation of dispersions using “flow focusing” in microchannels. *Appl. Phys. Lett*. 82(3), 364–366.

Arbuckle, W.S. (1986). Emulsification. In: C.W. Hall, A.W. Farral and A.L. Rippen (Eds.), *Encyclopaedia of Food Engineering*. AVI Publishing Company, Westport, CT, pp. 286–288.

Brennan, J.G. (1986). Emulsification: mechanical procedures. In: C.W. Hall, A.W. Farral and A.L. Rippen (Eds.), *Encyclopaedia of Food Engineering*. AVI Publishing Company, Westport, CT, pp. 288–291.

Davidson, M.R., Harvie, D.J.E., and Cooper-White, J.J. (2005). Flow Focusing in Microchannels, ANZIAM J 46(E), C47–C58.

Dekkers, K.S. (2003). *Production of double emulsions by microchannel emulsification*, MSc thesis. Wageningen University and Technische Universität Karlsruhe.

Van Dijke, K., Schroën, C.G.P.H., van der Sman, R.G.M., and Boom, R.M. (2006), in preparation.

Van der Graaf, S., Schroën, C.G.P.H., van der Sman, R.G.M., and Boom, R.M. (2004). Influence of dynamic interfacial tension on droplet formation during membrane emulsification. *J. Colloid Interf. Sci*. 277, 456–463.

Kawakatsu, T., Trägårdh, G., and Trägårdh, C. (2001a). Production of *W/O/W* emulsions and *S/O/W* pectin microcapsules by microchannel emulsification. *Coll. Surf. A* 189(1-3), 257–264.

Kawakatsu, T., Trägårdh, G., Trägårdh, C., Nakajima, M., Oda, N., and Yonemoto, T. (2001b). The effect of the hydrophobicity of microchannels and components in water and oil phases on droplet formation in microchannel water-in-oil emulsification. *Coll. Surf. A* 179(1), 29–37.

Kelder, J.D.H., Janssen, J.J.M., and Boom, R.M. (2006). Membrane emulsification with vibrating membranes: a numerical study, submitted.

Kobayashi, I., Nakajima, M., Nabetani, H., Kikuchi, Y., Shohno, A., and Satoh, K. (2001). Preparation of micron-scale monodisperse oil-in-water microspheres by microchannel emulsification. *JAOCS* 78(8), 797–802.

Nakashima, T., Kukizaki, M. (1991). Emulsification by microporous glass. *Key Eng. Mater.* 61 & 62, 513.

Peng, S.J. and Williams, R.A. (1998). Controlled production of emulsions using a cross-flow membrane. Part I: droplet formation from a single pore. *Trans. Inst. Chem. Eng.* 76, 902–910.

Salager, J.L., Forgiarini, A., Marquez, L., Pena, A., Pizzino, A., Rodriguez, M.P., and Rondon-Gonzalez, M. (2004). Using emulsion inversion in industrial processes. *Adv. Coll. Interf. Sci*. 108–109, 259–272.

Salager, J.L., Marquez, L., Pena, A., Rondon-Gonzalez, M., Silva, F., and Tyrodem, E. (2000). Current phenomenological know-how and modelling of emulsion inversion. *Ind. Eng. Chem. Res*. 39, 2665–2676.

Salager, J.L. (1988). Phase transformation and emulsion inversion on the basis of catastrophe theory. In: P. Becher (Ed.), *Encyclopedia of Emulsion Technology*. Marcel Dekker, New York, 79–134.

Schröder, V., Behrend, O., and Schubert, H. (1998a). Effect of dynamic interfacial tension on the emulsification process using microporous, ceramic membranes. *J. Coll. Interf. Sci.* 202, 334–340.

Schröder, V. and Schubert, H. (1999a). Production of emulsions using microporous, ceramic membranes. *Coll. Surf. A* 152, 103–109.

Schröder, V, Stang, M., and Schubert, H. (1998b). Emulgieren mit microporösen Membranen. *Lebensmittel- und Verpackungstechnik* 43, 80.

Schröder, V. (1999b). *Herstellen von Öl-in-Wasser-Emulsionen mit microporösen Membranen.* PhD thesis, Technische Hochschule Karlsruhe.

Schubert, H. and Armbruster, H. (1992). Principles of formation and stability of emulsions. *Int. Chem. Eng*. 32, 14.

Smulders, P.E.A. (2000). Formation and stability of emulsions made with proteins and peptides. PhD thesis, Wageningen University.

Suzuki, K., Shuto, I., and Hagura, Y. (1996). Characteristics of the membrane emulsification method combined with preliminary emulsification for preparing corn oil-in-water emulsions. *Food Sci. Technol. Int.* 2, 43–47.

Suzuki, K., Fujiki, I., and Hagura, Y. (1998). Preparation of corn oil/water and water/corn oil emulsions using PTFE membranes. *Food Sci. Technol. Int. Tokyo* 4.

Yasuno, M., Nakajima, M., Iwamoto, S., Maruyama, T., Sugiura, S., Kobayashi, I., Shono, A. and Satoh, K. (2002). Visualization and characterization of SPG membrane emulsification. *J. Membrane Sci*. 210(1), 29–37.

Veldhuis, G. (2006). Personal communication. NanoMi BV, see www.nanomi.com.

Vladisavljevic, G.T. and Schubert, H. (2002). Preparation and analysis of oil-in-water emulsions with a narrow droplet size distribution using Shirasu-Porous-Glass (SPG) membranes. *Desalination* 144, 167–172.

Walstra, P. (2003). *Physical Chemistry of Foods.* Marcel Dekker, NY.

Van der Zwan, E., Schroën, C.G.P.H., van Dijke, K., and Boom, R.M. (2006). Visualization of droplet break-up in pre-mix membrane emulsification using microfluidic devices. *Coll. Surf. A*. 277, 223–229.

Chapter 16

Processing of Food Powders

Lilia Ahrné,[1] Alain Chamayou,[2] Koen Dewettinck,[3] Frederic Depypere,[3] Elisabeth Dumoulin,[4] John Fitzpatrick,[5] and Gabrie Meesters[6]

[1] The Swedish Institute for Food and Biotechnology, SIK, Gothenburg, Sweden; lilia.ahrne@sik.se
[2] Chemical Engineering Laboratory for Particulate Solids, Ecole des Mines d'ALBI, France; lecoq@enstimac.fr
[3] Ghent University, Faculty of Bioscience Engineering, Department of Food Safety and Food Quality, Ghent, Belgium; koen.dewettinck@UGent.be
[4] Ecole Nationale Supérieure des Industries Agricoles et Alimentaires, ENSIA, Massy, France; elisabeth.dumoulin@agroparistech.fr
[5] UCC, Dept. of Process Engineering, University College Cork, Ireland; j.fitzpatrick@ucc.ie
[6] DSM - Netherlands, Gabrie.Meesters@dsm.com

16.1 Introduction

The development of formulation engineering concepts in food manufacturing and the demand for diversity in food products has driven a substantial market increase for food ingredients. Most ingredients are supplied in powder form and therefore a better understanding of dispersed solid food systems is important both for food ingredient manufactures and food producers.

A major reason for production in powder form is simply to prolong shelf-life of the ingredient by reducing water content; otherwise the ingredient would be degraded in its natural biological environment. Another important reason is simple transport economics, because reducing water content reduces mass and costs of the ingredient to be transported. The major requirement of the powder form is to preserve the product functionality until necessary for use, which is usually in some sort of wet formulation, as not many food powders are directly consumed in their original form. The major functionalities of food ingredients in the food product to be consumed can be classified as: physical/chemical (gelation, emulsification, foaming); nutritional (vitamins, nutraceuticals); or sensorial (colour, taste, smell, texture).

Food powder processing consists of a variety of operations that will give the powder a functionality that is expected to be maintained during handling and storage. An understanding of the properties and processing characteristics of powders is an essential requirement for the design of dispersed solid food systems.

16.2 Powder Properties and Functionality

The properties of a powder can be subdivided into those related to the particle itself and those of the ensemble of particles (bulk properties). The major particle properties include: particle size and size distribution, shape, density and porosity, surface properties (van der Waals attractions, electrostatic charge), moisture content and composition. Particle properties influence the bulk properties of powders/particulates. There are a vast number of bulk properties including moisture content, bulk density, bed porosity, compressibility, flowability, permeability, sinkability, wettability and dispersibility, among others.

Design and operation of particle and powder handling and processing equipment requires knowledge of individual particle and bulk properties of the particles/powders. For example, these properties affect the separation, fluidisation and flow behaviour of particles, mixing and caking behaviour of powders and explosibility. Particle size and its distribution are very important properties in determining the degree of interaction between the particles themselves and between particles and a surrounding fluid. For example, powder particle size will affect powder flowability, fluidisability, compressibility, segregation tendency, toxicity and explosibility. Powder moisture content is another important property as it will influence powder cohesiveness, caking and stickiness and may also influence detrimental chemical reactions involving the functional ingredients.

Food ingredient powder manufacture and powder use can be broadly summarised as in Figure 16.1. Food powders are commonly produced by spray-drying, crystallisation and comminution. These particles are often further processed, for example, by separating crystals from a liquid, powder agglomeration, powder coating and powder mixing. Many operations, such as agglomeration and coating are applied to improve the functionality of the powder. Powders then need to be stored and transported. Many food powders are reconstituted or recombined into a liquid form before final application. Application liberates the food ingredient to provide its specified functionality which is usually nutritional, physical/chemical or sensory.

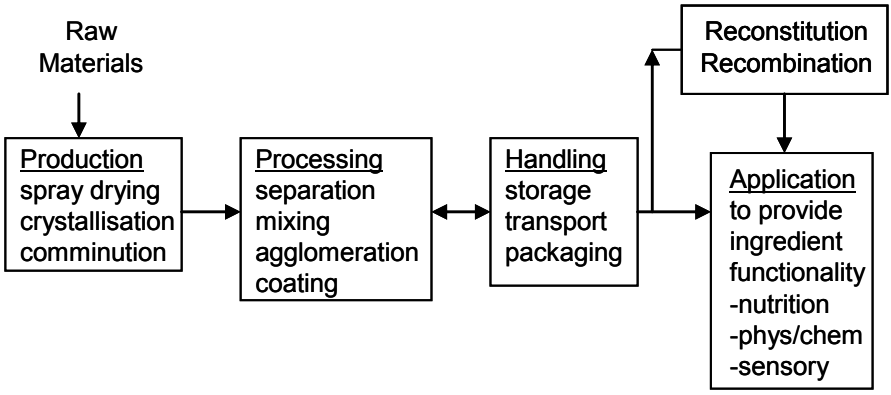

Figure 16.1. Schematic of food ingredient powder manufacture and utilisation.

Considering the above, food ingredient powders must possess a number of functionalities which can be broadly classified as: powder handling capability; reconstitution/recombination ability and ingredient functionality in the food product to be consumed. Poor handling during manufacture, storage and transport causes many problems which are quite common, such as no or irregular flow out of hoppers and silos and problems associated with stickiness and caking of powders. Reconstitution of the powder may prove problematic as it may be difficult to sink, wet, disperse or solubilise the powder. The reconstitution process may result in altering ingredient functionality.

Production and processing will determine the properties of particles and powder, such as particle size distribution, shape, surface properties and moisture content. They will also influence ingredient functionality, for example, higher temperatures may cause denaturation of proteins and coating may prevent the ingredient functionality from being destroyed by oxidation.

16.3 Production of Food Powders

16.3.1 Spray-Drying

Spray-drying is a convective drying technique used to transform a feed in the form of a formulated solution, emulsion, suspension, or slurry, into a dry free-flowing powder. The liquid phase is atomised into a spray of drops. A hot gas, usually air, is used to transfer heat, remove evaporated water (or a solvent) and to transport particles during drying (Masters 1985; Mujumdar 1995). In the food industry, high capacity plants exist for spray-drying products such as milk, whey, fruit juices, egg products, starch and derivates, aroma components, and many other food ingredients.

Spray drying proceeds through several stages:

- Formation of spray in small drops (i.e. 30 microns, with a narrow size distribution) using a rotary disc or nozzle, to enhance the product-air interface. The preparation of the feed (dry matter content, composition, temperature, mixing) must facilitate pumping and spraying with minimal modification (partition of constituents, droplet coalescence in emulsions).
- Contact between hot air and drops, with heat transfer to evaporate water, and mass transfer to remove evaporated water, facilitated by the movement of the air relative to the drops. The air is heated, filtered, sometimes dehydrated. The drying through the drop/particle surface depends on the water activity (water pressure) and temperature at the surface. As water evaporates rapidly from drop surfaces, the air temperature is rapidly decreased (i.e. 200 to 100°C).
- Separation of the spent air and particle stream (cyclone, filter), with possible post treatments (agglomeration).

The resulting positive aspects of this drying process are the elimination of solvent in a short time and the low temperature of the air close to the drop surface (wet bulb temperature) as long as water evaporates from the drop. During this period the drop/

particle temperature remains lower than the outlet air temperature. This favours drying of heat sensitive materials. The negative points include flow recirculation in the spraying chamber, non-controlled agglomeration and sticking to walls, existence of fine particles, modifying the final powder properties.

The feed and the type of atomizer are key for the formation of drops and consequently of dry particles. A homogeneous and well formulated mixture is needed to get a final determined composition of each dry particle. Due to the fast drying a minimal dry matter concentration is required in relation to the drying chamber volume. The viscosity and surface tension of the liquid affect flowing, pumping and breaking into drops (they depend on composition, dry matter content and temperature). In a fraction of seconds, the final structure in the sprayed drops is established. The size and distribution of size are also linked with the type of atomizer and spraying parameters: nozzle (pressure) or rotary disc (speed). Large drops (low specific area) with a slow drying rate will need longer residence times and bigger chambers. A large distribution of size may correspond to a non homogeneous behaviour for flowability, rehydration and density. Incorporation of air during formulating solution/emulsion to dry (e.g. with foaming capacity of milk proteins) modifies powder density and structure (porosity).

Because the influence of drying parameters is not the same for all materials, optimal drying conditions vary depending on the final objective: volatile retention, preservation of enzymatic activity and avoidance of protein denaturation, fat oxidation or crystallisation. Furthermore, some interactive influences may appear between components, an effect that is positive for protection of labile compounds by a network of polymers as polysaccharides, gums, proteins (Dumoulin and Bimbenet 1998). The phenomena may vary between centre and surface of drops, with some possible segregation by internal movement in the drop.

The outlet air temperature is very important. The cocurrent air/spray arrangement will be preferred for heat sensitive products, and mixed flow and counter current for heat stable ones. Depending on spraying conditions, the drops may behave as spheres with an external dry thin layer (rapid drying through the surface), within which transport of water from the centre is fully governed by molecular diffusion. That limits for example the losses of volatile compounds (selective diffusion) and some possible oxidation to the time when the layer is forming (Reineccius 2004). The presence of sugars in the feed has some consequences on drying behaviour of drops and powder properties, such as hygroscopicity and thermoplastic nature.

During drying the glass transition temperature of the surface material increases because the water activity decreases. The drop temperature (especially at the surface) has to be maintained lower than the glass transition temperature, to avoid sticky conditions (Truong et al. 2005). In that case, some drying aid agents with higher glass transition temperature may be added to increase the critical transition temperature of the drying mixture (at least at the drop surface). Sometimes the presence of amorphous components in powders, such as lactose in milk products, may be beneficial to improve the retention of aromas: the concentration of the feed will have an influence on the fraction of amorphous lactose in the final powder. During storage attention must be paid that environmental humidity does not promote crystallisation of amorphous components and release of aromas. A poorly soluble active component

suspended with a soluble component may be spray dried to limit the crystallisation process and improve the dissolution rate of the final amorphous powder. Polyunsaturated fatty acids susceptible to oxidation are emulsified in the presence of a mixture of wall materials like gum, gelatin, maltodextrin, caseinate, and spray dried. The wall material brings protection during processing and storage. Mixtures of low melting point fats with a carrier (carbohydrates, modified starch, cellulose, caseinate, lactose) are made more dispersible in water, with a very low percentage of fat on the surface of solid particles.

Usually, the resulting powder is made of dry particles with an average size of 30 microns and mean water activity around 0.2. The powder outlet temperature is typically less than 100°C and the residence time is of seconds. Cooling may be applied if necessary to stop further reactions. For example, a fluidized bed may be added as the final drying phase to a low temperature, for addition of specific components (by spraying) on the particles surface and/or for agglomeration, and for final cooling.

The shape of particles is normally that of more or less regular spheres, dense or hollow, with smooth surfaces and sometimes cracks. This is related to the composition and the rate of solvent evaporation, with possible existence of internal pressure inside the drops when a rigid surface layer is being formed (Walton and Mumford 1999). All these characteristics will have some effect on handling properties of powders such as: bulk and tapped densities, particle density, (mixing with other powders, storage); wettability and solubility, porosity, specific area (rehydration, instantisation); flowability (size, surface asperities), friability and creation/existence of dust, stability in specific atmosphere and medium (oxidation, humidification, active component release) (Huntington 2004).

16.3.2 Comminution

Comminution is generally understood as a size reduction operation by fragmentation phenomena. It is now widely accepted that grinding operations, at first implemented to effect size reduction, cause significant modifications of other properties such as structure, shape of the particles, surface quality, and physicochemical properties (Chamayou and Fages 2003). These transformations may be explained by the fact that the energy brought mechanically at local scale during the grinding process increases the free energy of the finished product, which may become transitorily unstable. In this case the system's energy may be dissipated by means of physicochemical transformations such as crystal polymorphism.

Modifications of user properties have various origins. First, the process of size reduction itself may change the shape of the particles. Some properties, like taste, are sometimes directly induced by the particle size at the bio-sensor's scale. For example, it is now widely known that the gustative quality of chocolate is related to particle size. Another direct consequence of size reduction is an increase of the external specific surface area, that is widely used to enhance the rate of transport phenomena, for example in the case of dissolutions or in fluid/solid extractions. For a given particle size distribution, powder properties may be a consequence of the particles' shape.

After grinding, depending on the milling process and the operating parameters, the same material, with similar size distribution, may be for example spherical and smooth, or angular and rough.

Wettability of micronized products may be affected by the grinding atmosphere: the use of wet gas or of water vapour, instead of dry air, may change completely the behaviour of some products during dispersion in water. These modifications may be explained by the effect of water adsorption on the new surfaces. Electrostatic properties of the particle surface and also cohesivity and flowability of the product may be other consequences of a comminution process. Certain types of mills induce friction between rotors and stators, or between ground powder and walls, generating electrostatic phenomena at the surface of the particles. Then, depending on the product characteristics, the electrostatic charges may be retained on the particles or liberated inducing a particular behaviour of the product.

A significant deterioration of the order of a crystalline structure may occur during a grinding operation. This deterioration on a certain thickness of the crystal lattice may confer the crushed product properties different from those of the initial product. Under the term “mechano-chemical effects” are gathered a whole range of physico-chemical phenomena, bringing into play mechanisms different from those governing the “thermochemical” transformations (phenomena observed during grindings or of prolonged co-grindings). Among these effects the occurrence of chemical reactions at low temperature is observed. The instability generated by grinding can result in an abnormal increase in the initial kinetics of dissolution and sometimes in the ion product of activity in a stationary state. This effect, called “hypersolubility” is used in pharmacy to increase the bioavailability of the active ingredients. Grinding can also generate phenomena of amorphisation of surfaces (for example, case of degradation of starch).

Another example of the influence of grinding processes on user properties through structural mass properties consist in the hydration properties and fat absorption capacity of the dietary fiber. Raghavendra et al. (2006) working on coconut fiber, concluded that the grinding operation ruptured the honeycomb physical structure of the fiber matrix and resulted in a flat ribbon type structure, thereby providing an increase in surface area for water and fat absorption. The hydration properties (water holding, water retention, swelling capacity) of the coconut residue depended on particle size.

A significant improvement in the dissolution speed of a micronized product can be obtained by co-grinding in the presence of a surfactant (Boulay 1985). This is particularly the case when the results are compared to those obtained bringing the surfactant mixed with solvent: the mixture carried out in an air jet mill allows a better covering of the elementary grains by the surfactant thus allowing a better decomposition of the aggregates formed because of smoothness of the product than one wishes to dissolve. A decomposition of this type of aggregates is obtained by co-grinding cocoa in the presence of sugar, a phenomenon classically used to avoid the formation of agglomerates during the dispersion of the cocoa. If the products co-crushed with a surfactant give in contact with water a milky suspension, those co-micronized in the presence of sugar give place to a quasi-explosion of the aggregates in contact with water.

16.4 Processing of Food Powders

16.4.1 Coating

Microencapsulation is a process in which a pure active ingredient or a mixture of ingredients is coated with or entrapped within a protecting material or system (see also Chapter 24). As a result, useful and otherwise unusual properties may be conferred to the microencapsulated ingredient(s), or unuseful properties may be eliminated from the original ingredient(s) (Shahidi and Han 1993). The particle size of "microcapsules" formed by either encapsulation or entrapment can vary between 0.2 and 5000 μm. Smaller and larger particles are denoted, respectively, as nanocapsules and macrocapsules (Jackson and Lee 1993; Schrooyen et al. 2001).

Originally developed in sectors such as those involved in the production of "carbonless carbon paper" (National Cash Register Company 1954) and the pharmaceutical industry, microencapsulation is now increasingly being applied in the food industry to tune, time or enhance the effect of functional ingredients and additives (Dewettinck and Huyghebaert 1999). In contrast to high-cost tolerating encapsulation applications in the areas of pharmacy, cosmetics or health, microencapsulation in the food industry should be considered a large-volume operation whereby production costs have to be minimised.

Whereas food ingredient microencapsulation was originally considered a rather high-priced, custom route to solving unique problems, today's increased production volumes and well-developed, cost-effective preparation techniques and materials have resulted in a significant increase in the number of microencapsulated food products (DeZarn, 1995). The growing interest by food technologists in microencapsulation can be directly derived from the exponential increase in the number of publications during the last decades (Gouin 2004). Microencapsulation can be applied for a variety of reasons, but the general underlying philosophy is always to add value to a conventional food ingredient or additive. Furthermore, it is also the source of totally new ingredients with matchless properties (Gouin 2004). A survey of the possible benefits and applications of microencapsulation include (Versic 1988; Finch 1993; Greenblatt et al. 1993; Brazel 1999; Depypere et al. 2003):

- controlled release of the core ingredient(s), e.g., enteric coating;
- protection of the core ingredient(s) from light, oxygen, moisture, etc.;
- solution to ingredient incompatibility problems;
- taste masking as well as a barrier against nutritional or flavour loss;
- increase of overall product quality, e.g., shelf-life increase, hygroscopicity reduction and dustiness reduction;
- increase of product and process convenience, e.g., free-flowing powder, easier cleaning.

So far, the term "microencapsulation" has been used in its broadest sense. However, one important differentiation in microencapsulation technology is the distinction between encapsulation leading to "true" microcapsules and entrapment resulting

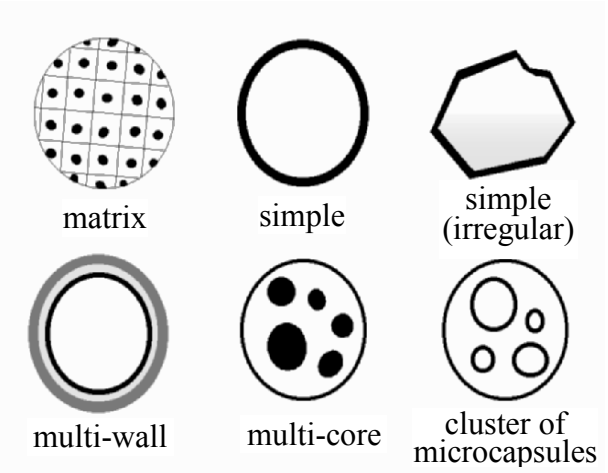

Figure 16.2. Some possible microcapsule designs: microspheres (*top left*) versus "true" microcapsules (Arshady 1993; Gibbs et al. 1999).

in microspheres (King 1995). Figure 16.2 summarises some possible microcapsule designs.

Encapsulation can be defined as the envelopment of a core by a continuous coating material. The aim of this technique, typically achieved by film coating (rotating pan, fluidised bed), is to surround the spherical or irregular core uniformly and completely by one or more, possibly different, layers of coating material (e.g., natural polymer, melt). In this way, one or several different food ingredient types can be encapsulated in single- or multi-layered microcapsules (Gibbs et al. 1999). On the other hand, entrapment involves capturing and dispersing the core material within or throughout a matrix (e.g., a gel or crystal). Entrapment is typically achieved by spray-drying, a microencapsulation technique discussed previously. The principal difference between entrapment and encapsulation lies in the fact that a small percentage of entrapped core material in a matrix is still exposed at the microsphere surface, which is to be avoided when encapsulating material. In matrix systems, the wall actually has become the continuous phase of the microparticle.

16.4.1.1 Film Coating

Film coating techniques are characterised by the deposition of a uniform film onto the surface of a core material. In the production of coated particles, the rotating pan and the fluidised bed are most frequently used. In the rotating pan, the coating solution is sprayed onto particles, set in motion by rotating the drum or pan, and dried by the supply of hot gas. This method has been in use for a long time and has been modified with several improvements, the most recent being focused on fluidisation of particles inside the drum (Litster and Sarwono 1996). However, its reproducibility is shown to be rather low, making this technology suitable only for producing particles for which no high coating uniformity is required.

Conversely, the fluidised bed is recognised for its good mixing and optimal heat and mass exchange, which are related to the bubble characteristics of the fluidising air (Senadeera et al. 2000). One of the main reasons of the success of the fluidised bed in the food industry is that this technology allows a large number of unit operations to be performed within the same piece of equipment, either separately or sequentially. Another reason is that no other encapsulation technology can apply as broad a range of coating materials. This is illustrated in Table 16.1, where some important examples of coating materials are listed. Fluidised beds can apply both water-soluble coatings and aqueous latex dispersions as well as hot melt coatings and organic solvent coatings.

Table 16.1. Some possible food coating materials in fluidised bed coating (Depypere et al. 2003).

Category	Examples
Proteins	Caseinate, albumin, gelatine, soy, gluten, zein*
Polysaccharides hydrocolloids	(Modified) starches, maltodextrins, β-cyclodextrins, alginate, gum arabic, pectin/polypectate, carrageenan, agarose
Cellulose derivatives	Methylcellulose, carboxymethylcellulose (CMC)
Fats and fatty acids	(Hydrogenated) vegetable oils*, mono-/di-/tri-glycerides*
Waxes	Shellac*, beeswax*

* Water-insoluble coatings

In contrast to the wide variety of food materials that can be coated the number of materials that can be applied in fluidised bed coating is rather limited. Encapsulating materials have to be selected from a list of FDA-approved, generally recognised as safe (GRAS) materials (Kanawjia et al. 1992). However, the FDA continuously adds new GRAS materials to the list, allowing researchers to revisit unsolved problems of the past. Furthermore, the choice of coating material depends on a number of factors such as the physical and chemical properties of both the core (e.g., porosity, solubility) and the coat (e.g., mechanical strength, viscosity, glass/melting transition, film forming ability), the compatibility of the coat with the core, the required final product performance, the release mechanism and economics (Brazel 1999).

16.4.1.2 Fluidised Bed Coating Principle

Also termed air suspension coating, fluidised bed coating is accomplished by suspending solid core particles in an upward-moving air current, which serves both as a heating or cooling medium and as a momentum carrier. The bed of particles is supported by drag forces exerted by the air flow, and acquires the characteristics of a boiling liquid—hence the term fluidisation. Suspending each particle, thereby exposing the entire particle surface area to the air stream, results in optimal convective

heat transfer. The coating, which may be dissolved in a volatile solvent or applied in a molten state, is atomised through nozzles into the coating chamber.

Owing to fast and effective evaporation of the coating liquid, the coating material is deposited as a thin layer on the surface of the suspended particles. The core particles move past the nozzle where they receive a spray of coating material and subsequently move into sections of the fluidised bed unit where the coating is solidified either by solvent evaporation (with aqueous solutions) or by cooling of a hot melt (with molten fats and waxes). The coated particles then are cycled back to the coating zone where a fresh coating is applied. This cyclic process is repeated until the desired weight of coating material has been applied. The advantage of this sequential deposition of coating material in a number of cycles is that coating defects may be covered up or healed so that relatively defect-free coatings can be obtained. In this way, also layers of different coating materials can be sequentially applied on a core particle surface.

Depending on the configuration, the solution can be sprayed from the top (top-spray configuration), from the bottom of the fluidised bed (bottom-spray) or from tangentially positioned nozzles submerged inside the particle bed (tangential- or rotary-spray). As each method influences film coating quality differently, they are further discussed individually. However, the underlying coating principle is the same for each option (see Figure 16.3).

As can be seen from Figure 16.3, droplet formation, impact, spreading, adhesion, coalescence and evaporation (with aqueous solutions), are occurring almost simultaneously in the coating zone (Guignon et al. 2002).

When dealing with porous particles, penetration of the core by water or solvents should be avoided. This can be accomplished using the evaporative efficiency of a fluidised bed, although care should be taken to avoid spray-drying of the coating solution. Other possible side-effect phenomena inside the fluidised bed (Nienow

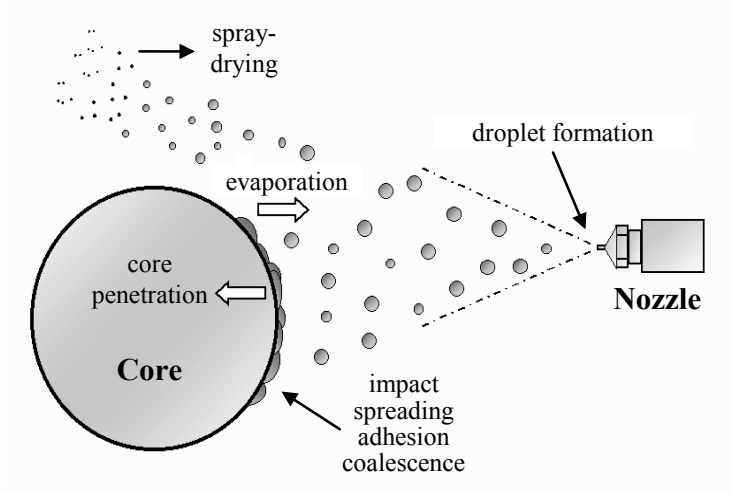

Figure 16.3. Principles of the coating process.

1995; Maronga 1998) are described below. In cases where the coating solution droplets do not manage to reach and attach to the fluidised core particle surface (e.g., when the travelling distance of the droplets towards the particles is too long), they are subject to spray-drying.

If, however, the droplets of the atomised coating solution manage to coalesce successfully with the core particles, the latter become wetted. Depending on the inlet air temperature and absolute humidity, the core particles may be individually coated and the coating layered uniformly, or, in the case of excessive wetting, liquid bridges are formed between the core particles, resulting in the formation of large, wet clumps, and eventually, collapse and defluidisation of the bed. Besides wet quenching, also dry quenching can occur with moderately wetted core particles (Maronga 1998). From the above, it is obvious that efficient process control, leading to particle coating and avoiding these possible side-effects, is of crucial importance.

16.4.1.3 Batch Fluidised Bed Coating

The principle and possible applications of the three basic processing options (top-spray, bottom-spray or tangential-spray) of the batch-fluidised bed are discussed below (Jones 1994). Both the top- and bottom-spray methods are characterised by a conical product container and expansion chamber, resulting in a more vigorous fluidisation pattern and a decrease in velocity as the particles move upward in the expansion chamber.

16.4.1.4 Bottom-Spray Fluidised Bed Coating

Bottom-spray film coating is accomplished by means of the “Wurster” system, originally developed by Dr. D.E. Wurster (Wurster 1959). A scheme of the bottom-spray fluid bed is given in Figure 16.4.

Four distinct regions, each with different controlling parameters, are recognised to describe the bottom-spray fluidised bed coating process (Christensen and Bertelsen 1997). In the bottom-spray unit, the number and the diameter of the holes of the air distribution plate are different between the inner and outer sections, so most free area is provided in the centre section, just below the partition. In this way, a high-velocity zone is created inside the partition, separating the core particles and transporting them past the nozzle, which is mounted at the bottom and sprays the coating liquid upwards. After passing the nozzle, the coated particles enter the expanded area, slow down and fall back into the outer section (annulus or downbed) of the product container, while continuously being dried by the upwardly flowing air column. The particles in the downbed region remain sufficiently fluidised to allow them to continuously move towards the distribution plate and to enter the horizontal transport region, where they are drawn back into the high-velocity air stream. The resulting coating polymer film is very uniformly applied, which makes bottom-spray fluidised bed coating an excellent tool to apply reproducible, controlled release protection barriers. It is the system of choice when enteric coating systems are envisaged (Singiser and Lowenthal 1961; Mehta et al. 1986).

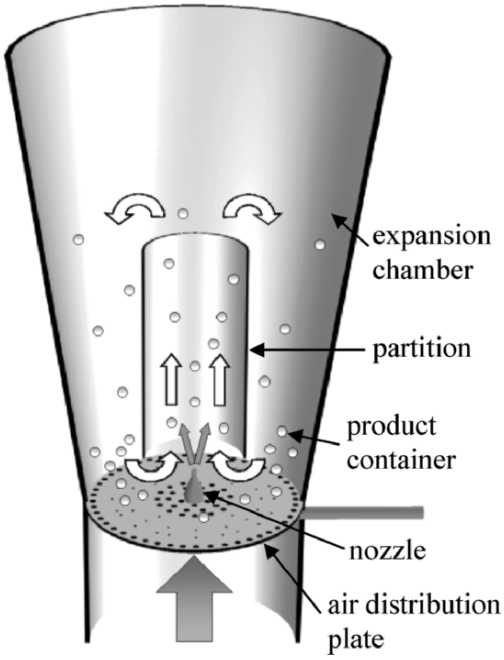

Figure 16.4. Bottom-spray ("Wurster") fluidised bed.

Particles as small as 100 μm have been coated using bottom-spray fluidised bed coating. Attempts have been made to coat smaller particles, but agglomeration was found to be almost unavoidable because of nozzle limitations and the tackiness of most coating materials. Moreover, these small particles tend to be carried away in the exhaust air (Jackson and Lee 1991). One decade ago, the Wurster high-speed processing insert, patented by Jones (Jones 1995), was introduced with the aim of offering larger batch volumes, higher throughputs and the ability to coat finer particles down to 50 μm, without the prevalence of agglomeration.

16.4.1.5 Top-Spray Fluidised Bed Coating

The top-spray system has also been used successfully to coat particles as small as 100 μm and attempts to coat smaller particles may lead to the same difficulties as encountered in the bottom-spray system. Figure 16.5 shows a schematic representation of the top-spray fluidised bed configuration.

In a top-spray fluidised bed, air is introduced through a uniform air distribution plate. Compared to the particle motion in the bottom-spray fluidised bed, the fluidisation pattern is less controlled. Particular to the top-spray method, the nozzle is positioned above the particle bed, and coating liquid is sprayed countercurrently, or down, into the fluidising core particles. Compared to a Wurster fluid bed, it is more

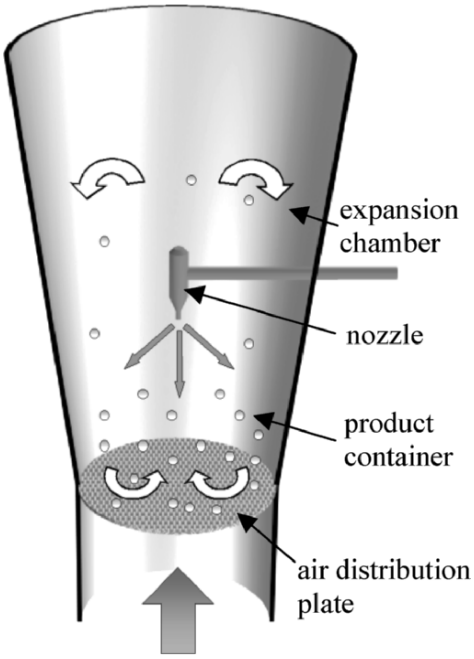

Figure 16.5. Top-spray fluidised bed.

challenging in a top-spray fluid bed to control the droplet travel distance and time before impingement on a core particle, which may possibly lead to spray-drying of the coating material.

Top-spray coating is the system of choice when lipid coating or hot-melt coating is envisaged (Rácz et al. 1997; Achanta et al. 2001). Using heated and insulated nozzles, molten materials such as hydrogenated oils and waxes are sprayed against a stream of cool air, causing the molten wall material to solidify around the core particle. The degree of protection offered by the coating, and hence the coating quality, is related to the application rate and the congealing rate. A product bed temperature that is too low results in premature congealing prior to complete spreading and, consequently, pores and defects can occur in the coating. Conversely, if the product bed temperature is too close to the melting point of the coating, the result is a significant increase in the viscous drag of the bed, favouring particle-particle agglomeration (Joszwiakowski et al. 2004). The use of cold rather than heated air and the application of 100% coating material result in short processing times and low energy consumption, making this process economically feasible for many food applications (Sinchaipanid et al. 2004).

16.4.1.6 Tangential-Spray Fluidised Bed

The latest developed configuration in fluidised bed coating is the tangential-spray or rotary-spray set-up, depicted in Figure 16.6. Unlike the two previous configurations, the product container and expansion chamber are cylindrically shaped and the air distribution plate is replaced with a rotating disk with adjustable height.

As a result, three forces determine the fluidisation pattern, best described as a spiralling helix. The combination of centrifugal forces, an upward fluidising air flow and gravity effects results in a rapidly tumbling fluidised bed. Tangentially immersed in the powder bed, a nozzle is positioned to spray the coating liquid concurrently with the particle flow. It can be expected that a rotor-applied film has at least the same quality as a Wurster-applied film. However, its use with friable substrates is discouraged, since compared with the other systems, the tangential-spray system exerts the greatest mechanical stress (Jones 1988). With respect to particle size, the tangential-spray fluidised bed has been used to coat particles of at least 250 μm. Compared with the previous configurations, this process is more susceptible to adhesion of particles on the upper container wall owing to static electricity; hence, coating of smaller and lighter particles with this system is discouraged (Jones 1994).

Table 16.2 summarises the main characteristics of the three batch-fluidised bed configurations. Evaluating the pros and cons of each type and taking into account the specific needs of the food industry, Dewettinck and Huyghebaert (1999) concluded

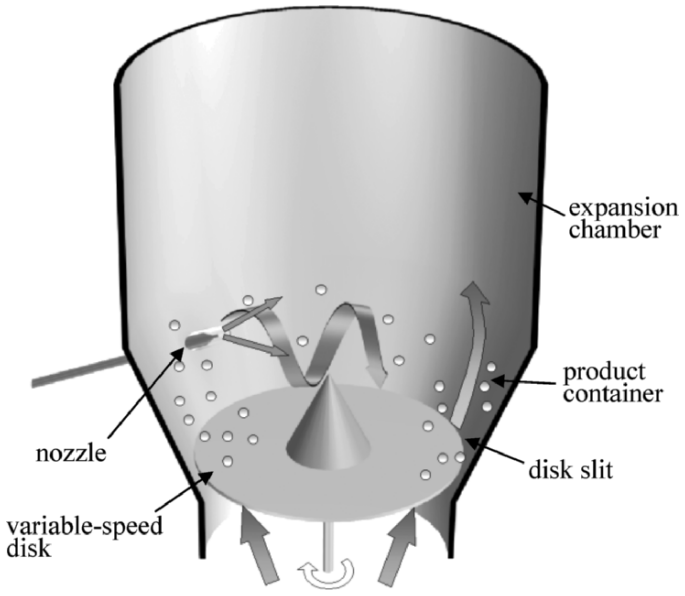

Figure 16.6. Tangential-spray (rotary-spray) fluidised bed.

Table 16.2. Comparison of batch-fluidised bed configurations (Depypere et al. 2003; Jones 1994; Eichler 1989).

Parameter	Top-spray	Bottom-spray	Tangential-spray
Air distribution plate	Homogeneous	Heterogeneous	Not applicable
Spray modus	Countercurrent	Concurrent	Concurrent
Nozzle position relative to particle bed	Above to top submerged	Bottom submerged	Tangentially submerged
Fluidisation pattern	Circulating, less controlled	Controlled, regular coating intervals	Controlled, spiralling helix
Min. particle size (μm)	100	100 (50)*	250
Max. batch size (kg)	1500	600	500
Coating quality	Porous to dense, possibly imperfect	Uniform, excellent	Dense, excellent
Advantages	Simplicity, cost efficiency	Wide application range	Spheronisation
Disadvantages	Spray-drying losses	Tedious set-up and cleaning	Unsuitable for friable substrates
Aqueous particle coating	Good	Superior	Excellent
Hot-melt coating	Superior	Good	Can be done

* High-speed Wurster

that top-spray fluidised bed coating had the greatest potential of application. Reasons for this are the high versatility, relative high batch size, relative simplicity and most importantly, the possibility to apply both water-soluble and hot-melt coatings.

16.4.1.7 Continuous Fluidised Bed Coating

A recent engineering novelty in fluidised bed technology is the development of continuous systems, with little down-time and operating times up to 8000 hr/yr. Particularly for the food industry, where large volume throughputs and lower costs are required, the introduction of a continuous coating process offers considerable advantages and opportunities (Rümpler and Jacob 1998). For example, scale-up problems, an important issue in batch systems (Jones 1985; Leuenberger 2001; Knowlton et al. 2005) are avoided.

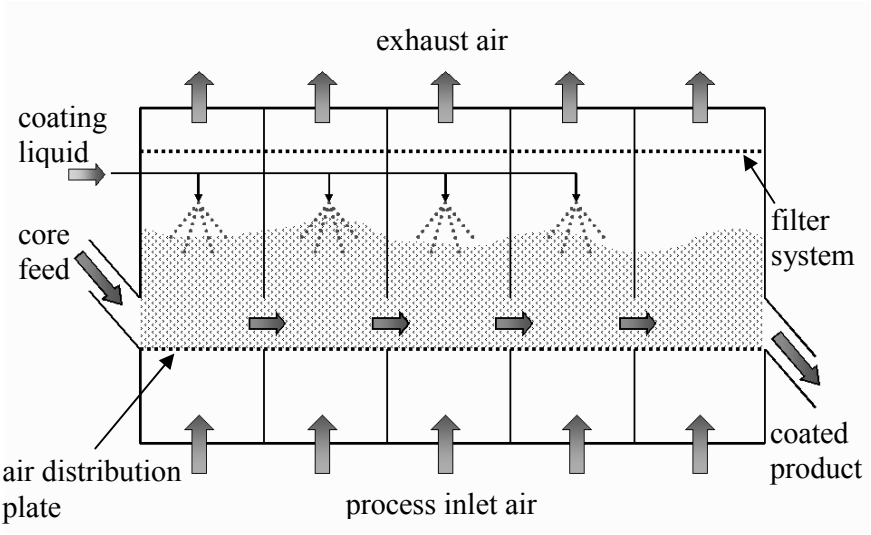

Figure 16.7. Continuous top-spray fluidised bed coating.

A more detailed overview of the development of continuous fluidised bed systems is covered in a review by Teunou and Poncelet (2002). Figure 16.7 shows a schematic diagram of a continuous top-spray fluid bed coater.

The core material is introduced at one end of the unit and the processed product is discharged continuously at the other end of the bed. The particle mixing behaviour is dependent on the product throughput and on the geometric design of the fluidised bed. Compared with a nearly ideal mixing behaviour in batch systems, the residence time distribution of the particles inside the processing unit is a very important characteristic for continuous fluid bed coating systems.

The division of the inlet air plenum into multiple chambers allows the use of different inlet air temperatures or velocities along the fluid bed. After transport of the core particles by the dosing unit, they are conveyed within the device by means of the fluidising air alone. As specially designed top-spray or bottom-spray nozzles can be positioned where appropriate for a particular application, it is possible to realise different processes within one continuous fluid bed unit, for example, coating in the first chamber, followed by drying and cooling in subsequent parts of the processing chamber. Because the process can be equipped for handling solvent or lipid coating materials and as the amount of fluid sprayed from the nozzle and the distance between the nozzles can be adjusted, the continuous system can be adapted to specific requirements, meanwhile assuring proper covering capability and maintaining the flexibility needed for large product ranges (Schrooyen et al. 2001).

16.4.2 Granulation of Food Powders

There are many reasons to granulate food powders:

- *Change the particle size distribution.* By granulation, the primary particles can be glued together forming larger particles, which may have an effect on flow and segregation behavior, wettability, density, etc.
- *Improve the flow properties.* Powders, especially some food powders, show a poor flow behavior. Often these powders are sticky, hygroscopic and may contain fats, all of which have a negative effect on the powder flow properties. By agglomeration of the powders, the flow properties usually improve substantially.
- *Enhance dosing properties*. Agglomerated powders have better flow properties, which makes the dosing of these products easier when used, for example, in vending machines (instant cacao or milk powder)
- *Improve the instant properties*. Food powders often need to be easily dispersed or dissolved in water (instant soups, sauces etc). By agglomeration, the primary particles are bound to one another, forming pores between them, which enhance the wettability by the capillary forces when put into contact with water. After they are wetted, they will easily fall apart and disperse or dissolve.
- *Reduction of lumping*. Granules show less lumping after storage compared to powders.
- *Reduction of dust*. By physically binding the particles together the formation of dust will reduce considerably, which makes handling much easier and safer.
- *Reduction of segregation*. When mixtures of powders and granules are mixed, the powder will percolate through the interstitial voids of the granules. By granulating the powder, the segregation can be reduced.

When powders are very sticky during the drying they may stick to the walls of the spray-drying chamber. Filtermat (a special type of multistage dryer) is a system that makes use of the stickiness. The powder is spray dried in a chamber, but when the powder reaches the bottom of the dryer, the product sticks to a belt. The belt is gradually moved out of the spray zone. The cake that is formed is dried in an adjacent chamber with hot air, such that the product is not sticky any more. In the last stage the product is cooled and scraped off from the belt and is milled into a finer product. The fines are recycled back into the system. Figure 16.8 shows the Filtermat system. Typical products dried with the Filtermat are high fat containing powders and hygroscopic sticky products and products with a low stickiness temperature.

There are other ways to make granulated products. Instant products such as instant cacao (a mixture of cacao powder, sugar and milk) can be made by low shear granulation like the Hosokawa Flexomix technology, as shown in Figure 16.9. For example, an instant cacao produced this way dissolves easily and disperses the cacao (very hydrophobic) quickly without lump formation.

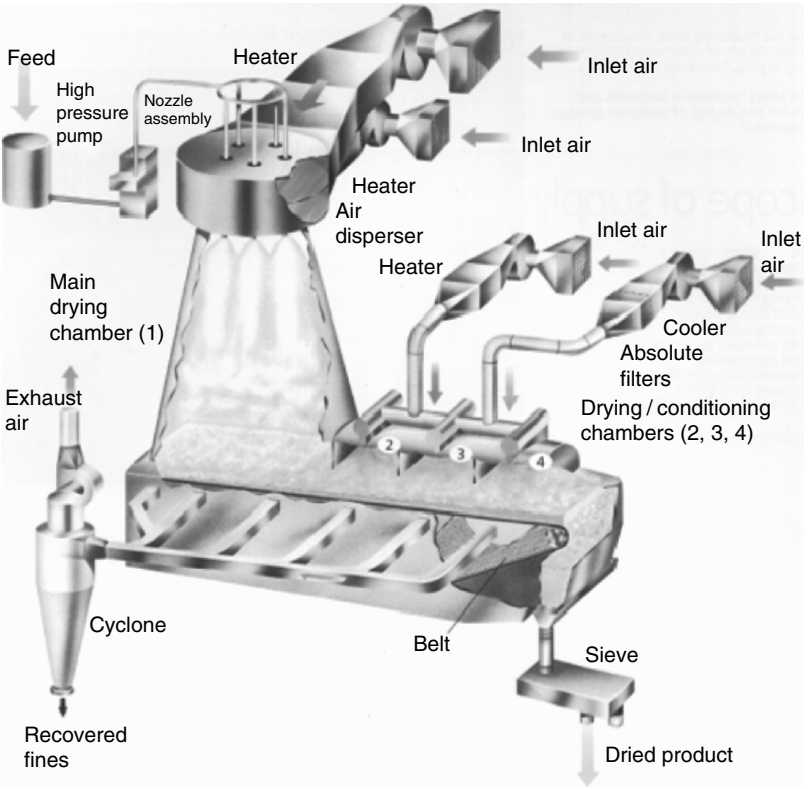

Figurre 16.8. Filtermat system used for drying sticky and fatty products. (See Color Plate.)

With the Flexomix, dry powders are fed into the mixer where the paddles mix the powder with liquid that is introduced close to the paddles, which turn at high speeds. The wet mass which exits the mixer is dried in a fluid bed system. The product from this system is an open structure granulate which exhibits instant behavior upon dissolution.

Other food powders may be produced using low-pressure extrusion technology. By wetting a powder in a mixer, for example, the wet mass can be pressed through a basket extruder (Figure 16.10), creating spaghetti-like strands. These strands may be dried and used but can be subsequently broken and rounded off in a spheroniser (Figure 16.11) as well.

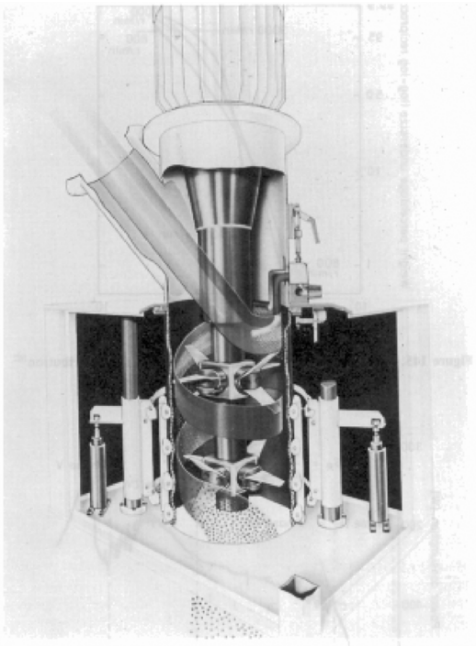

Figure 16.9. Hosokawa Flexomix, a low-shear granulator.

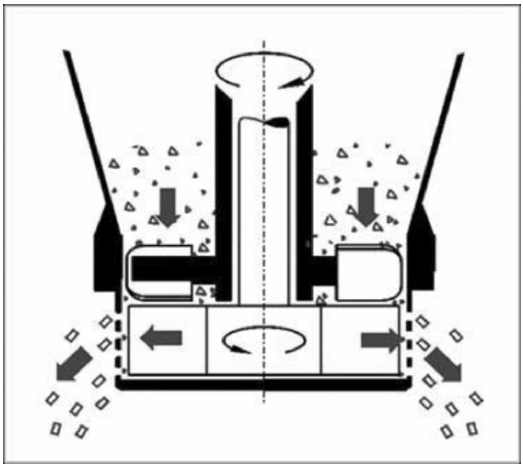

Figure 16.10. Schematic drawing of a basket extruder.

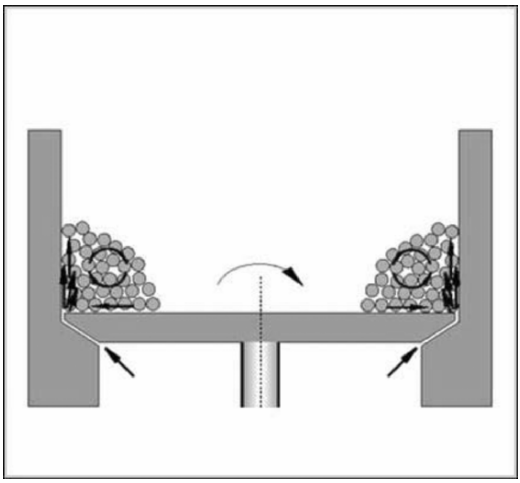

Figure 16.11. Schematic of a spheroniser. The bottom plate rotates and the strands from the extruder are broken of and become spherically shaped due to the motion of the particles.

Typical food products that are extruded include sugars and sweets which may be applied on bread and cakes, but also ingredients for soups (herbs) or cereals (fibers, vitamins, etc). Food powders may also be pressed into shapes such as cubes, which may be applied as concentrated bouillons, herbs and taste enhancers for use in soups. Here the ease of dosing and the stability (prevention of oxidation of the flavors) are the reason to make them into cubes.

16.5 Segregation

Powder storage and handling operations expose the powders to a variety of motions, atmospheric conditions and time over which the powder properties and ingredient functionality may alter. The most important property changes of a bulk powder are caused by segregation, caking and particle breakage, which are discussed below:

16.5.1 Causes and Mechanisms of Segregation

When particles to be mixed have the same physical properties, then a random mixture will be obtained if the particles are mixed for long enough. However, if the properties are different (in particular, particle size and particle density), then the particles may demix or segregate where particles with same physical property separate out and collect in one part of the mixture. The major property difference causing segregation is difference in particle size, although differences in particle density can also cause segregation.

Segregation is a real problem in industry. Some mixers may not be able to form a random mixture of some powder mixes because of powder segregation mechanisms occurring within the mixer. Some mixers may even demix a mixture due to the dominance of segregation mechanisms acting on a particular mixer, for example, a

rotating mixer will demix a mixture of dry spheres if they have a difference in particle size. Even more important are the steps that follow mixing, such as emptying the mixer, mixture transport, storage in hoppers/silos and emptying from hoppers/silos and further processing. These may introduce segregation mechanisms that can demix a mixture. For example, in filling a silo with a powder mixture containing ingredients with different size particles, the big particles have a tendency to roll to the silo wall surface, and the smaller particles tend to congregate near the centre. On emptying a silo in funnel flow discharge mode, the smaller ingredient will leave first, resulting in demixing. Segregation takes place due to the preferential motion of particles with similar properties, in particular, particle size. A summary of a number of segregation mechanisms is given below (they are mainly caused by difference in particle size):

- *The rolling heap*. This is where big particles tend to roll down the slope of the heap while smaller particles congregate more towards the centre. This is important in filling silos, containers and forming stockpiles.
- *Trajectory.* Consider a mass of particles moving around a corner. The bigger particles require a greater radius of turn than the smaller particles because of the momentum associated with their greater mass. This is important when emptying mixers or moving from one conveyor to another at right-angles. It is potentially important in any operation where there is a change in direction in the conveying of the particles and the particles are free to move.
- *Percolation of fines*. If vibration is applied to a bed of powder, the smaller particles tend to sift or percolate through the voids created between the bigger particles. This can commonly occur during transport in trucks, trains and ships due to the vibrations induced. This will lead to more fine particles in the bottom of the container and larger particles at the top.
- *Floating of coarse particles*. Consider a big steel ball placed at the bottom of a bed of finer sand particles. If the bed is vibrated, the steel ball will actually float to the top of the sand particles. As the steel ball is vibrated upwards, some sand slips into the space below it.
- *Elutriation*. Gas moving through an expanded or fluidised bed of particles tends to preferentially drag small particles upwards because they are lighter and have greater surface area per unit mass for drag forces to lift the particles. Elutriation may also occur if the particles have different densities.

16.5.2 Reducing Segregation

The main methods to reduce segregation are:

- Reducing the difference in particle size. As a difference in particle size is the main cause of segregation, reducing this difference in size should reduce segregation. It does not take much difference in particle size to get segregation of a free-flowing powder, for example, a size ratio of 1.3 (big/small) will result in significant segregation.
- Increasing the cohesion of powders: Increasing cohesion forces between powder particles will restrain individual particles from moving freely and segregating. Reducing particle size increases total particle contact area which can greatly increase surface attractive force interactions. Segregation is generally not a serious problem when all the particles are less than 20 μm. The major drawback of this

approach is that increased powder cohesion may cause other difficulties, such as flow problems.
- Change process to eliminate segregation mechanisms from taking place. Eliminate and redesign locations in the process layout where segregation can occur, for example, avoid splitting off conveying belts at right angles.
- Mix when needed. Instead of mixing followed by transport and storage, it is better to transport, store and finally mix prior to packing. This can eliminate product segregation.
- Agglomerate/granulate the mix. Once the mix is satisfactorily formed, then produce granules by getting powder particles to stick together and form larger granules. Once particles are stuck together, they cannot segregate.

16.6 Caking

During handling, storage, processing and distribution to the final consumer, the powders may experience a variety of temperatures and atmospheric humidity conditions which may alter the handling behaviour and appearance of the powders. This is especially important if powders are transported to or handled in hotter, more humid climatic conditions, where a mix may cake solidly or liquefy by adsorbing moisture. Furthermore, the consumer is usually very sensitive to any lumping, caking or difficulty in discharging the powder from its container.

Many food powders contain amorphous components, such as amorphous sugars, maltodextrins and yeast extracts. For example, many spray-dried dairy powders contain lactose in its amorphous state. These components are often responsible for caking in food powders. Amorphous components are thermodynamically unstable and there exists a driving force for them to crystallise; however, this requires that the molecules must be able to move. When an amorphous component is given sufficient conditions of temperature and moisture content, they can mobilise as a high-viscosity flow, enabling them to crystallise over time. This viscous nature renders the particle surfaces stickier, making the powder much more cohesive and susceptible to caking. In addition, many of these amorphous components are hygroscopic and crystallisation is often preceded by moisture sorption from air and the formation of liquid bridges between powder particles, which leads to an increase in the cohesiveness and caking ability of the powder.

Glass transition measurements can be used to detect the onset of this mobility. Differential scanning calorimetry (DSC) is an established thermal analytical technique that can measure glass transition properties because glass transition induces a change in the specific heat of the material due to molecular mobility (Roos 2003). The glass transition occurs over a temperature range. This is usually a relatively narrow range of 10–20°C for amorphous sugars; however, a much larger range of, for example, 50°C, may be expected for the glass transition of food polymers. Within this temperature range, the glass transition temperature is referred to the temperature initiating the onset of glass transition or the mid-point temperature within the range. The glass transition temperatures of carbohydrates and proteins are affected by water, with greater water content resulting in decreased glass transition temperatures. Water acts

as a plasticiser enabling the mobilisation of amorphous components. Consequently, a lower temperature is required to initiate the onset of the glass transition for higher water contents. Both higher temperature and water content can enable molecular mobility and the onset of the glass transition.

Crystallisation will only take place if the glass transition temperature (T_g) is below the powder temperature, whereby the molecules have sufficient mobility to initiate crystallisation (Roos 1995, 2003). T_g of amorphous components in the powder is usually well above the storage temperature for most dry powders. However, components in their amorphous state are usually very hygroscopic and will readily sorb moisture from ambient air, and this increase in moisture will cause a significant reduction in T_g. Molecular mobility will initiate if T_g is reduced below the powder temperature, and this may result in caking. Furthermore, exposure of powders to higher temperatures and humidities, such as in tropical countries, can lead to the glass transition temperature of amorphous components being exceeded, leading to powder handling and caking problems.

There is a temperature range above the glass transition temperature (for a given moisture content) where the powder particles become sticky (Kudra 2003; Boonyai et al. 2004) and this is referred to as the sticky point temperature. It is generally accepted that the sticky point temperature is about 10–20°C above the glass transition temperature, especially for low molecular weight carbohydrates (Roos and Karel 1991), as illustrated in Figure 16.12. This stickiness is due to the molecular mobility of the amorphous components as a highly viscous flow between particle surfaces, making the powder a lot more cohesive. Furthermore, contacting the powder with a wall surface when the powder is in this sticky region will lead to increased adhesion between the powder and the surface. For example, in a spray-drying process, if the surface temperature of drying droplets is greater than the T_g of an amorphous component and the particles contact the dryer wall, then the particles may stick onto the dryer wall, causing coating of the wall surface over time (Adhikari et al. 2005).

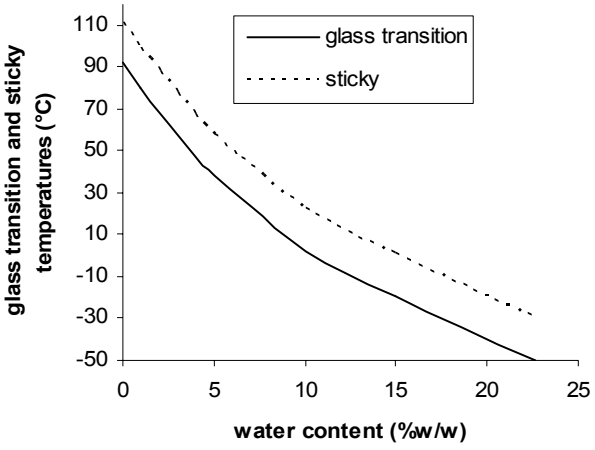

Figure 16.12. Glass transition of lactose in skim milk powder.

16.7 Particle Breakage

During handling and transport of solid food particles, particles are exposed to forces that may cause them to break. This is of most concern with granulated powders, as these granule structures tend to be much weaker than individual powder particles that construct the granule structure. The reduction in particle size may produce problems including reduced flowability, segregation of finer particles, decrease of instant properties and problems associated with dust formation. Furthermore, coated granules may suffer degradation of the coated layer due to breakage with a consequential reduction in the functionality of the coating, which is of major concern due to the cost of coating.

Particle breakage occurs in operations where the particles are moving. This can be due to normal and tangential forces acting because of interparticle motions or the relative motion between particles and the surfaces of equipment. Dilute phase pneumatic conveying is commonly used to transport solid food particles; however, the high particle speeds may lead to breakage of particles, particularly at bends where particles may collide with the pipe wall and the increased turbulence causes greater interparticle collisions leading to greater breakage.

Particle breakage mechanisms can be classified based on whether the force applied is normal or tangential to the particle surface and whether this force is low or high (van Laarhoven 2006). For example, high force in the normal direction leads to fragmentation of the particle into a small number of daughter particles of similar sizes, while low force leads to attrition and the removal of asperities on the particle surface. Low force in the tangential direction leads to abrasion or erosion of the particle surface producing many fine particles, while high force in the tangential direction leads to chipping of the particle surface producing particle chips that are larger in size and smaller in number than for abrasion. The development of testers to quantitatively measure these breakage mechanisms is an active area of research. They are being developed to evaluate the susceptibility of particles to different breakage mechanisms and to relate this to particle breakage in industrial operations so that more resistant particles can be manufactured and operations can be designed to be more “particle-friendly.”

16.8 Degradation of Ingredient Functionality

It is well known that ingredient functionality in powder form may degrade over time between manufacture and final application. This depends on the sensitivity of the individual ingredient and its exposure over time to temperature, moisture and oxygen in the air. Some ingredients are encapsulated and some powders are coated in an effort to prevent its degradation and protect its functionality. Lillford (2002) outlined some of the functional properties of food powders and particulates. Powders are important ingredients in a large variety of food formulations and they are responsible for the development important product characteristics such as texture, flavour, colour and nutritional value. Most of the powders will be used in some sort of wet formulation and therefore their functionality will depend on their interaction with water.

For example, gelatinisation properties or aroma release will be also depend on the powder ability to disperse in water without formation of lumps.

It is well known that ingredient functionality in powder form may degrade with the time between manufacture and final application. Environmental factors such as temperature, humidity, oxygen and light can activate chemical or physical mechanisms leading to quality loss. Thus, the shelf-life of a powder will be determined by a number of intrinsic and extrinsic factors such as powder composition, water activity, packaging, and storage/distribution conditions. Important chemical changes in powders are lipid oxidation, loss of vitamins, alteration of colour, degradation of proteins, and formation of off-flavours. Physical mechanisms include the diffusion of water and flavours into/from the powder matrix, rate of dispersibility, solubilisation and rehydration. Powdered foods when kept in high humidity may pick up moisture, leaving the amorphous status, which alters the handling behavior and accelerate the chemical reactions.

Changes of functionality during storage are complex and not always fully understood. Moisture uptake during storage of milk powders induces crystallisation and cementing of powder particles in large lumps (caking). Lactose crystals presented at the beginning of storage show the typical “tomahawk” shape while those formed during storage are needle-shaped. The change from amorphous lactose to crystalline lactose favours nonenzymatic browning of whey powders (Aguilera and Stanley 1990). During storage, the strength of flavours and aroma compounds decreases, leading to a perceived loss of quality in the final product (De Roos and Mansecal 2003; Yamanishi et al. 1986). Powdered dehydrated fruit juices and soups require protection against moisture and oxygen during storage to avoid degradation of volatile flavours and colour.

The development of novel and bioactive ingredients in the last years has created new challenges in production and storage of powders as many of these ingredients are highly sensitive to oxygen, humidity and light (Ubbick and Krüger 2006). Encapsulation and coating systems have been developed in an effort to prevent degradation and protect functionality of active, often sensitive ingredients. See Chapter 24.

16.9 Conclusions

Processing of food powders consists of a variety of operations that will give the powder a functionality that is expected to be maintained during handling and storage. Powders may be produced by various techniques. Spray drying is amply used to convert a liquid feed into a powder. A comminution process, affects directly the user properties at various levels. It is also important to consider the desired properties (and not only the size specifications) of the final product during the elaboration of a milling plant and in the choice of operating parameters.

Of all microencapsulation methods useful for the food industry, fluidised bed coating is among the most versatile and widely used. Microencapsulation in the food industry faces the challenge of applying an economically feasible encapsulation or entrapment technique and hereby, selecting a suitable encapsulating material from a typically short listing. Recent microencapsulation process improvements, including

the introduction of the continuous fluidised bed coating apparatus, evolved with the aim to increase production volumes and to make the process more cost efficient. Most of the food powders are produced to change the physical properties in such a way that the product flows and meters better, that the product dissolves quickly and without the formation of lumps, and that the product does not loose its flavor, taste or appearance. Most of these formulation techniques are quite cheap and relatively easy to perform.

16.10 References

Adhikari, B., Howes, T., Lecomte, D., and Bhandari, B.R. (2005). A glass transition temperature approach for the prediction of the surface stickiness of a drying droplet during spray-drying. *Powder Technol.* 149, 168–179.

Aguilera, J.M., and Stanley, D.W. (1990). *Microstructural Principles of Food Processing and Engineering*, Elsevier Applied Science, New York.

Arshady, R. (1993). Microcapsules for food. *J. Microencapsulation*, 10(4), 413–435.

Boonyai, P., Bhandari, B., and Howes, T. (2004). Stickiness measurement techniques for food powders: a review. *Powder Technol.* 145, 34–46.

Boulay, G. (1985). Microbroyage et dissolution, *S.T.P. Pharma*. 1, 296–299.

Brazel, C.S. (1999). Microencapsulation: offering solutions for the food industry. *Cereal Foods World*, 44(6), 388–393.

Chamayou, A., and Fages, J. (2003). Le broyage dans les industries agro-alimentaires. In: J.P. Melcion, and J.L. Ilari (eds.). *Technologie des pulvérulents dans les industries alimentaires et agricoles*. Lavoisier, Paris.

Christensen, F.N., and Bertelsen, P. (1997). Qualitative description of the Wurster-based fluid-bed coating process. *Drug Develop. Indus. Pharm.* 23(5), 451–463.

Depypere, F., Dewettinck, K., Ronsse, F., and Pieters, J.G. (2003). Food powder microencapsulation: principles, problems and opportunities. *Appl. Biotechnol. Food Sci. Policy*, 1(2), 75–94.

Dewettinck, K., and Huyghebaert, A. (1999). Fluidized bed coating in food technology. *Trends Food Sci. Tech*., 10, 163–168.

De Roos, K.B., and Mansencal, R. (2003). Poor performance of flavourings in heat processed products: a problem of poor flavour retention or poor flavour release? Flavour research at the dawn of the twenty-first century. *Proceedings of the Weuman Flavour Research Symposium, 10th*, Beaune, France, June 25–28, 2002.

DeZarn, T.J. (1995). Food ingredient encapsulation – an overview. In: S.J. Risch, and G.A. Reineccius (eds.). *Encapsulation and Controlled Release of Food Ingredients.* ACS Symposium Series, nr. 590. American Chemical Society, Washington, DC, pp. 74–86.

Dumoulin, E., and Bimbenet, J.J. (1998). Spray drying and quality changes. In: D.S. Reid (ed.), *The Properties of Water in Food*, Blackie Academic, London, pp. 210–232.

Eichler, K. (1989). *Principles of Fluid Bed Processing.* Glatt GmbH, Binzen.

Finch, C.A. (1993). Industrial microencapsulation: polymers for microcapsule walls. In: D.R. Karsa and R.A. Stephenson (eds.). *Encapsulation and Controlled Release.* The Royal Society of Chemistry, Cambridge, pp. 1–11.

Gibbs, B.F., Kermasha, S., Alli, I., and Mulligan, C.N. (1999). Encapsulation in the food industry: a review. *International J. Food Sci. Nutrition*, 50(3), 213–224.

Gouin, S. (2004). Microencapsulation: industrial appraisal of existing technologies and trends. *Trends Food Sci. Tech*., 15(7-8), 330–347.

Greenblatt, H.C., Dombroski, M., Klishevich, W., Kirkpatrick, J., Bajwa, I., Garrison, W., and Redding, B.K. (1993). Encapsulation and controlled release of flavours and fragrances. In: D.R. Karsa, and R.A. Stephenson (eds.). *Encapsulation and Controlled Release*. The Royal Society of Chemistry, Cambridge, pp. 148–162.

Guignon, B., Duquenoy, A., and Dumoulin, E.D. (2002). Fluid bed encapsulation of particles: principles and practice. *Drying Technol.* 20, 419–447.

Huntington, D.H. (2004). The influence of the spray-drying process on product properties. *Drying Technol.* 22, 1261–1287.

Jackson, L.S., and Lee, K. (1991). Microencapsulation and the food industry. *Lebensmittel-Wissenschaft und -Technologie*, 24(4), 289–297.

Jones, D. (1994). Air suspension coating for multiparticulates. *Drug Develop. Industrial Pharm.* 20(20), 3175–3206.

Jones, D.M. (1985). Factors to consider in fluid-bed processing. *Pharma. Technol.* 9(4), 50–62.

Jones, D.M. (1988). Controlling particle size and release properties—secondary processing techniques. In: S.J. Risch, and G.A. Reineccius (eds.). *Flavor Encapsulation*. ACS Symposium Series, nr. 370. American Chemical Society, Washington, DC, pp. 158–175.

Jones, D.M., inventor, Glatt Air Techniques, Inc., assignee (1995). Fluidized bed with spray nozzle shielding. US patent 5,437,889.

Joszwiakowski, M.J., Jones, D.M., and Franz, R.M. (1990). Characterization of a hot-melt fluid bed coating process for fine granules. *Pharma. Res.* 7(11), 1119–1126.

Kanawjia, S.K., Pathania, V., and Singh, S. (1992). Microencapsulation of enzymes, microorganisms and flavours and their applications in foods. *Indian Dairyman*, 44(6), 280–287.

King, A.H. (1995). Encapsulation of food ingredients: a review of available technology, focusing on hydrocolloids. In: S.J. Risch, and G.A. Reineccius (eds.). *Encapsulation and Controlled Release of Food Ingredients.* ACS Symposium Series, nr. 590. American Chemical Society, Washington, DC, pp. 26-39.

Knowlton, T.M., Karri, S.B.R., and Issangya, A. (2005). Scale-up of fluidized-bed hydrodynamics. *Powder Technol.* 150(2), 72–77.

Kudra, T. (2003). Sticky region in drying: definition and identification. *Drying Technol.* 21, 1457–1469.

Leuenberger, H. (2001). New trends in the production of pharmaceutical granules: batch versus continuous processing. *Eur. J. Pharma. Biopharma.* 52(3), 289–296.

Lillford, P. (2002). Functional properties of food powders and particulates. In *Proceedings of a Workshop, "Powder Research to Promote Competitive Manufacture of Added Value Food Ingredients,* SIK Report, Gothenburg.

Litster, J.D., and Sarwono, R. (1996). Fluidized drum granulation: studies of agglomerate formation. *Powder Technol.* 88(2), 165–172.

Maronga, S. (1998). On the optimization of the fluidized bed particulate coating process. PhD dissertation. Royal Institute of Technology, Stockholm, p. 70.

Masters, K. (1985). *Spray Drying Handbook*. Longman, New York.

Mujumdar, A.S. (1995). *Handbook of Industrial Drying*. Marcel Dekker, New York, Vol 1 & 2.

Mehta, A.M., Valazza, M.J., and Abele, S.E. (1986). Evaluation of fluid-bed processes for enteric coating systems. *Pharma. Technol.* 10(4), 46–56.

Nienow, A.W. (1995). Fluidised bed granulation and coating: applications to materials, agriculture and biotechnology. *Chem. Eng. Commun.* 139, 233–253.

Rácz, I., Dredán, J., Antal, I., and Gondár, E. (1997). Comparative evaluation of microcapsules prepared by fluidization atomization and melt coating process. *Drug Develop. Industrial Pharma.* 23, 583–587.

Raghavendra, S.N., Ramachandra Swamy, S.R., Rastogi, N.K., Raghavarao, K.S.M.S., Sourav Kumar, and Tharanathan, R.N. (2006). Grinding characteristics and hydration properties of coconut residue: a source of dietary fiber. *J. Food Eng.* 72, 281–286.

Reineccius, G.A. (2004). The spray-drying of food flavours. *Drying Technol*. 22, 1289–1324.
Roos, Y.H., and Karel, M. (1991). Phase transitions of mixtures of amorphous polysaccharides and sugars. *Biotech, Progr*. 7, 49–53.
Roos, Y.H. (1995). *Phase Transitions in Foods*. Academic Press, San Diego.
Roos, Y.H. (2002). Importance of glass transition and water activity to spray-drying and stability of dairy powders. *Lait*, 82*,* 475–484.
Roos, Y.H. (2003). Thermal analysis, state transitions and food quality. *J. Thermal Analysis Calorimetry* 71, 197–203.
Rümpler, K., and Jacob, M. (1998). Continuous coating in fluidized bed. *Food Market. Technol.* 12 (February), 41–43.
Schrooyen, P.M.M., van der Meer, R., and De Kruif, C.G. (2001). Microencapsulation: its application in nutrition. *Proc. Nutrition Soc.* 60, 475–479.
Senadeera, W., Bhandari, B.R., Young, G., and Wijesinghe, B. (2000). Methods for effective fluidization of particulate food material. *Drying Technol.* 18, 1537–1557.
Shahidi, F., and Han, X.Q. (1993). Encapsulation of food ingredients. *Crit. Rev. Food Sci. Nutrition* 33, 501–547.
Sinchaipanid, N., Junyaprasert, V., and Mitrevej, A. (2004). Application of hot-melt coating for controlled release of propanolol hydrochloride pellets. *Powder Technol.* 141, 203–209.
Singiser, R.E., and Lowenthal, W. (1961). Enteric filmcoats by the air-suspension coating technique. *J. Pharma. Sci.* 50, 168–170.
Teunou, E., and Poncelet, D. (2002). Batch and continuous fluid bed coating: review and state of the art. *J. Food Eng.* 53, 325–340.
Truong, V., Bhandari, B.R., and Howes, T. (2005). Optimization of cocurrent spray-drying process for sugar-rich foods. Part II. Optimization of spray-drying process based on glass transition concept. *J. Food Eng.* 71, 66–72.
Ubbick, J., and Krüger, J. (2006). Physical approaches for the delivery of active ingredients in foods. *Trends Food Sci. Tech*., 17, 244-254.
van Laarhoven, B., Wiers, S.C.A., Schaafsma, S.H., and Meesters, G.M.H. (2006). Performance of different particle coatings on particle attrition and towards abrasion testing. *5th World Congress on Particle Technology*, Orlando, FL.
Versic, R.J. (1988). Flavor encapsulationL an overview. In: S.J. Risch, and G.A. Reineccius (eds.). *Flavor Encapsulation*. ACS Symposium Series, nr. 370. American Chemical Society, Washington, DC, pp. 1–6.
Walton, D.E., and Mumford, C.J. (1999). Spray-dried products: characterization of particle morphology. *Trans IchemE*, 77A, 21–38.
Wurster, D.E. (1959). Air suspension technique of coating drug particles: a preliminary report. *J. Amer. Pharma. Assoc.* 48(8), 451–454.
Yamanishi, Y, Kobayahi, L, Kubota, K., Kihara, N., and Ikegami, A. (1986). Changes in aroma compounds of various teas during storage. In: G. Charalambous (ed.). *The Shelf-life of Foods and Beverages*, Elsevier Science Publishers, Amsterdam, pp. 563–568.

Chapter 17

Fat Crystal Networks

Michael A. Rogers, Dongming Tang, Latifeh Ahmadi, and Alejandro G. Marangoni

University of Guelph, Department of Food Science, Guelph, Canada,
amarango@uoguelph.ca

17.1 Molecular Composition

Fats and oils are comprised primarily of triacylglycerides (TAGs). TAGs consist of a glycerol (1,2,3-trihydroxypropane) backbone with three fatty acids esterified to the three alcohol groups at specific locations referred to as sn-1, sn-2, and sn-3 (Figure 17.1). Fatty acids differ based on chain length, saturation, trans- or cis-bonds, branching, as well as any combination of the aforementioned (Small 1986).

17.1.1 Fatty Acids

Fatty acids are straight-chain aliphatic carboxylic acids. A common method to name fatty acids is by using two numbers separated by a colon. The first number is the number of carbons in the fatty acid chain and the second number represents the number of double bonds. Hence, a fatty acid with one double bond and 18 carbons would be referred to as 18:1. The position of the double bond along the hydrocarbon chain is indicated as *n-x* or ω-*x*, where *x* is the number of carbons from the methyl end in the case of ω and *x* is the number of carbons from the carboxyl end in the case of *n*. Finally, denoting the *cis*- or *trans*-configuration of the double bonds is abbreviated using *c* or *t* as well as Z and E, respectively. The double bond configuration has a large effect on the packing of the triacylglycerides (Figure 17.2). Table 17.1 indicates common fatty acids and their nomenclature. For a more extensive discussion of nomenclature refer to Akoh and Min (2002). *Trans* fatty acids or nonmethylene interrupted unsaturated fatty acids do occur naturally, such as in milk fat, but are more commonly the by-products of hydrogenation reactions.

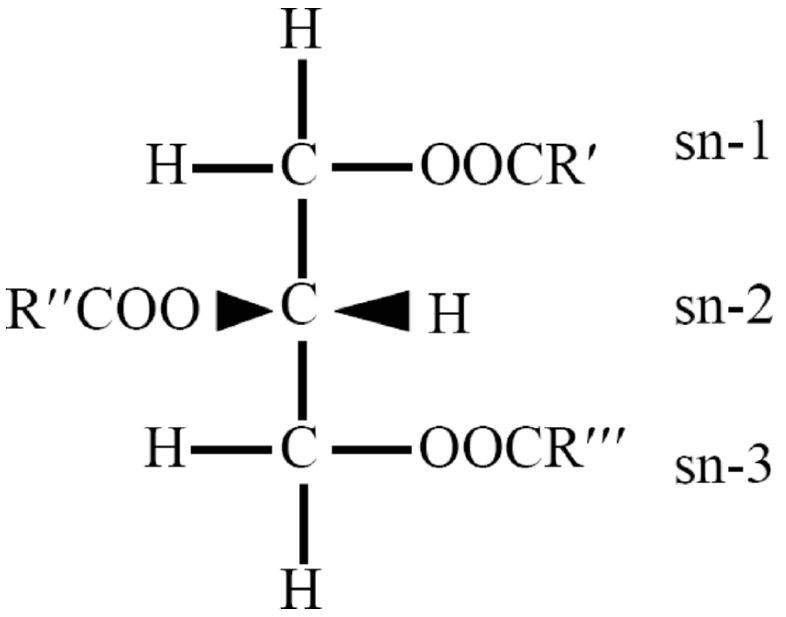

Figure 17.1. Fisher projection used in the stereospecific numbering of a triacylglyceride.

17.1.2 Triacylglycerols

There are several methods to name triacylglycerides. If a glycerol contains stearic at sn-1, palmitic at sn-2 and oleic at sn-3 the IUPAC name would be 1-steroly, 2-palmitoyl, 3-oleoyl-sn-glycerol. However, the acronym SPO is more generally used. In Fisher projections the sn-1 and sn-3 position appear to be interchangeable (Figure 17.1); yet it is important to note that since the molecule is chiral, sn-1 and sn-3 are not interchangeable and certain enzymatic reactions will occur only at sn-1 or sn-3.

17.2 Crystallization

As the temperature of a molten fat is reduced below its melting temperature it becomes supersaturated with regards to the higher-melting fraction of triacylglycerides. The process of supersaturation in fats and oils is referred to as undercooling. Typically, fats are able to undercool by approximately 5°C before crystallization occurs. When the fats exist in this region before crystallization, they are said to be in a metastable region. Molecules aggregate into tiny clusters (or embryos) and dissociate dynamically in this metastable region. The embryos form and breakdown and do not

persist to form stable nuclei. This is because the energy of interaction between the triacylglyceride molecules has to be greater than the kinetic energy of the molecules in the melt to overcome Brownian effects (Marangoni 2005).

Table 17.1. Nomenclature of common saturated and unsaturated fatty acids.

Systematic name	Trivial name	Shorthand designation
butanoic	butyric	4:0
hexanoic	caproic	6:0
octanoic	caprylic	8:0
decanoic	capric	10:0
dodecanoic	lauric	12:0
tetradecanoic	myristic	14:0
hexadecanoic	palmitic	16:0
octadecanoic	stearic	18:0
octadecenoic	oleic acid	18:1 Δ 9
octadecadienoic	linoleic	18:2 Δ 9, 12
octadecatrienoic	α-linolenic	18:3 Δ 9, 12, 15
eicosanoic	arachidic	20:0
Eicosapentaenoic	EPA	20:4ρ 5, 8, 11, 14
docosanoic	behenic	22:0
docosahexaenoic	DHA	22:6 r 4, 7, 10, 13, 16, 10
tetracosanoic	lignoceric	24:0
hexacosanoic	cerotic	26:0
octacosanoic	montanic	28:0
triacontanoic	melissic	30:0
dotriacontanoic	lacceroic	32:0
tetratriacontanoic	geddic	34:0

For stable nuclei to form, the molecules have to adopt a specific conformation. Since TAGs are flexible molecules, formation of stable nuclei is slow, thus making this meta-stable region rather large. As the level of undercooling increases, stable nuclei are formed above the critical size. The free energy (ΔG_n) associated with the formation of embryos is a combination of surface (positive) and volume changes (negative):

$$\Delta G_n = A_n \delta - V_n \frac{\Delta \mu}{V_m^s} \tag{17.1}$$

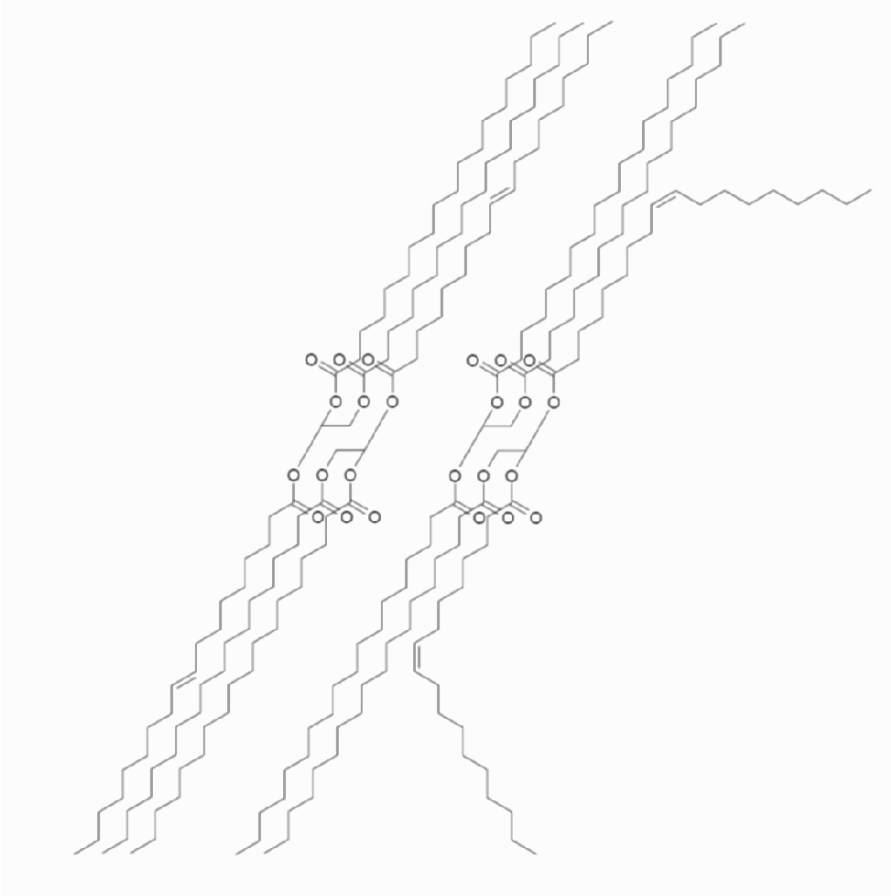

Figure 17.2. Chain packing of saturated (left), trans-unsaturated (left), cis-unsaturated fatty acids (right).

where A_n is the surface area of the nuclei, δ is the surface free energy per unit area, V_n is the volume of a nuclei, $\Delta\mu$ is the chemical potential difference between the solid and liquid and V_m^s is the molar volume of the solid.

The three most common types of nucleation include primary homogeneous nucleation, primary heterogeneous nucleation, and secondary nucleation. Primary homogeneous nucleation only occurs in pure solutions with no impurities, they require higher degrees of undercooling because no foreign surfaces are present to reduce the surface free energy. Primary heterogeneous nucleation is the most common industrial crystallization and occurs in the presence of foreign particles. Finally, secondary nucleation occurs on the surface of crystals or after primary nucleation has occurred. (See also Chapter 4 on "Crystallization")

After nucleation occurs, crystal growth is responsible for the increase in the solid fat content. Growth involves the diffusion of triacylglycerides to the surface of the crystal and then incorporation into the crystal lattice. This event depends on the degree of undercooling, rate of diffusion of molecules to the surface and time required for the molecules to assemble into the lattice. Crystal growth is usually modeled using the Avrami equation (Avrami 1939, 1940, 1941). This model quantifies the crystallization kinetics and is an indication of the nature of crystal growth. The Avrami equation as it applies to fats has the following form:

$$\frac{SFC}{SFC_{\max}} = 1 - e^{-kt^n} \tag{17.2}$$

where n is the Avrami exponent, k is the Avrami constant (t^{-n}), SFC is the solid fat content at a particular time and SFC_{max} corresponds to the maximum SFC at a particular temperature. The exponent k represents the crystallization rate constant and follows Arrhenius-type temperature dependence. The exponent k accounts for both nucleation and crystallization rates. The Avrami exponent n is a measure of the crystal growth mechanism. Nucleation is either instantaneous (nuclei appear at once) or sporadic (nuclei appear randomly) and they may grow as rods, discs or spheres in one, two or three dimensions. Table 17.2 shows the values of the Avrami exponent n and the types of nucleation and growth that occur. Half-times ($t_{1/2}$) of crystallization may be calculated using k and n,

$$t_{1/2} = \left(\frac{\ln 2}{k}\right)^{\frac{1}{n}} \tag{17.3}$$

Applying the Avrami model to the analysis of the isothermal crystallization of interesterified and noninteresterified 20%SSS/80%OOO at 30ºC, 40ºC and 50ºC, many differences can be observed (Table 17.3). At 30ºC and 40ºC growth would be described as rodlike with instantaneous nucleation for both interesterified and noninteresterified samples. Also, for the noninteresterified system at 50ºC spherulitic growth with instantaneous nucleation takes place. The half-time of nucleation

Table 17.2. Avrami exponent (n) values for different types of nucleation and dimensionality of growth.

Avrami exponent (n)	Various types of growth and nucleation
1 + 0 = 1	Rodlike growth from instantaneous nuclei
1 + 1 = 2	Rodlike growth from sporadic nuclei
2 + 0 = 2	Disclike growth from instantaneous nuclei
2 + 1 = 3	Disclike growth from sporadic nuclei
3 + 0 = 3	Spherulitic growth from instantaneous nuclei
3 + 1 = 4	Spherulitic growth from sporadic nuclei

increases as temperature increases due to the decrease in undercooling. The half-time of nucleation increases after interesterification due to decreases in high melting trisaturated TAG's (SSS) upon molecular randomization. Interesterification does not significantly affect the mechanism of growth or nucleation.

Table 17.3. Avrami parameters for chemically interesterified and non-interesterified 20%SSS/ 80%OOO blends crystallized at 30ºC, 40ºC and 50ºC. (NA) the data is not available because the system did not crystallize.

		Non-interesterified	Interesterified
	SFC_{max}	18.6	2.3
30ºC	k	0.9	0
	n	1.6	1.6
	$t_{1/2}$	0.9	184
	SFC_{max}	14.8	0.2
40ºC	k	0.01	1.90E-04
	n	2.7	1.42
	$t_{1/2}$	4.7	319
	SFC_{max}	6.4	NA
50ºC	k	0	NA
	n	3.4	NA
	$t_{1/2}$	110	NA

17.2.1 Polymorphism

Solid-state polymorphism is common in lipids, TAGs, alkanes, fatty acids, soaps or partial glycerides. Polymorphism arises because there are a number of different possible conformations for the long hydrocarbon acyl chain in a crystal lattice (Figure 17.3). With a fixed set of conditions such as temperature, pressure and composition, only one solid phase will be consistent with a minimum free energy (Aquilano and Sgualdino 2001). All other polymorphs present are considered metastable relative to the polymorph with the minimum free energy, even though these polymorphs may seem stable for extended periods of time. If the metastable crystal transforms to a stable crystal via rearrangements of the structural units without melting, it is termed a solid-state phase transformation as it is not mediated by melting and dissolution, followed by recrystallization, which is then called a melt-mediated phase transition.

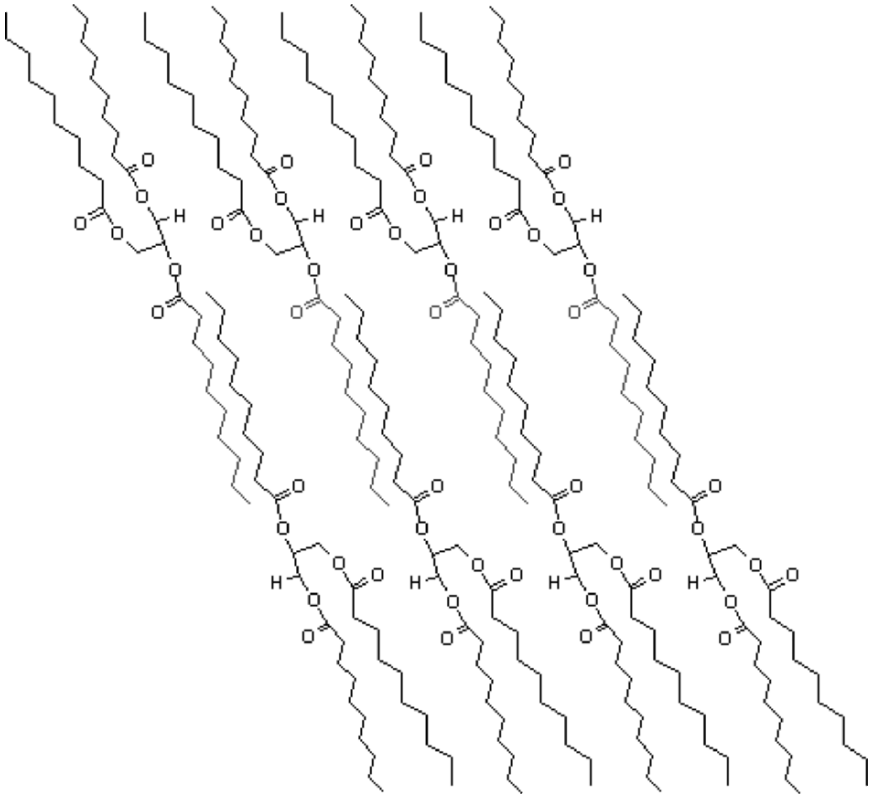

Figure 17.3. Triacylglycerol packing in a crystal lattice.

For the metastable α form, in-plane packing of the acyl chains is hexagonal, without specific orientation of the zig-zag planes of the acyl chains (Figure 17.4). For the β′ polymorph, chains pack in an orthorhombic perpendicular fashion, with an alternating straight and perpendicular arrangement of the zig-zag planes within the acyl chains (Figure 17.4). The chains themselves are tilted between 50° and 70° relative to the *c*-axis. The fatty acid chains in the stable β form pack in a triclinic fashion, with a parallel arrangement of the zig-zag planes within the acyl chains (Figure 17.4). Similarly to the β′ form, the chains are tilted between 50° and 70°.

Transformations between phases follow the Ostwald step rule, which states: "When a number of phase transformations, from a less stable state to more and more stable states are possible, usually the closest more stable modification is formed and not the most stable one corresponding to the least free energy" (Ostwald 1897). The phase transition from the metastable to the lowest free-energy polymorph is unavoidable due to the thermodynamic driving force to minimize free energy.

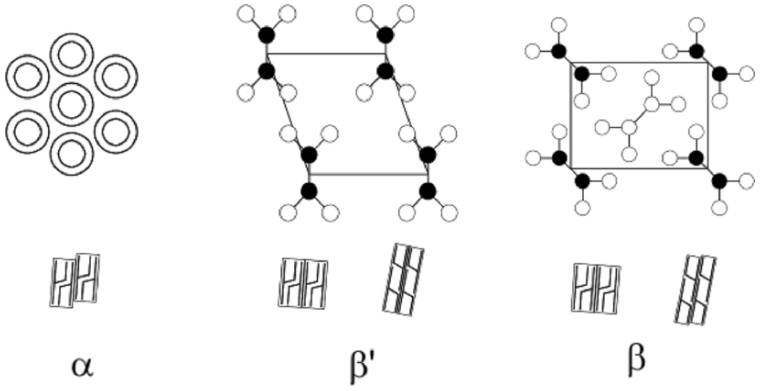

Figure 17.4. Metastable α, β′ and stable β polymorphs.

X-ray diffraction is the most common and most accurate method used to determine the polymorphic form of a sample. A change in the diffraction profile (e.g., a change in peak shape or position) indicates a change in polymorphism. The wide-angle reflections, (also called "short-spacings") are used to characterize the polymorphism of a lipid. These reflections correspond to in-plane ordering of the fatty acyl chains on the TAG molecule. Common polymorphic forms include the hexagonal, α form (d = 4.15Å), the orthorhombic perpendicular β′ form (d = 3.8 and 4.2Å) and the triclinic β form (d = 4.6Å) (Larsson 1966).

Another method commonly used to determine polymorphism is the melting point measured using differential scanning calorimetry. Polymorphic forms of coca butter have various melting points reported in the literature (Wille and Lutton 1966; Duck 1964; Chapman et al. 1971; Huyghebaert and Hendrickx 1971; Lovegren et al. 1976; Merken and Vaeck 1980). These authors report that the melting ranges for cocoa butter polymorphs are: form I (15ºC to 18ºC), form II (17ºC to 24.2ºC), form III (20.7ºC to 25.5ºC), form IV (25°C to 28°C), and form VI (33.5°C to 36.3°C). The stability of these polymorphs is in order from lowest to highest. Therefore, form I will convert to form II then to form III, and so on.

Ollivon has developed an instrument that allows for the simultaneous measurement of calorimetric and x-ray scattering properties as a function of temperature (Loisel et al. 1998). With this instrument, they can simultaneously determine short- and long-spacings (Figure 17.5) upon melting or crystallization (Figure 17.6) as a function of time. As shown in Figure 17.6, as temperature increases, form α with sharp peaks at α_{001} = 52.6Å and α_{002} = 26.3Å transforms into a β′ form with a sharp 001 reflection at 48.5Å (Loisel et al. 1998). Figsures 17.6(a) and 17.6(b) show that the evolution of the single peak at 48.5Å corresponds to the decrease observed at 52.6Å. However, Figure 17.6(c) indicates that this transition has very low energy and/or extends over a very long period. This new instrument shows the importance of coupling the x-ray and DSC data to ensure an accurate description of the phase transitions.

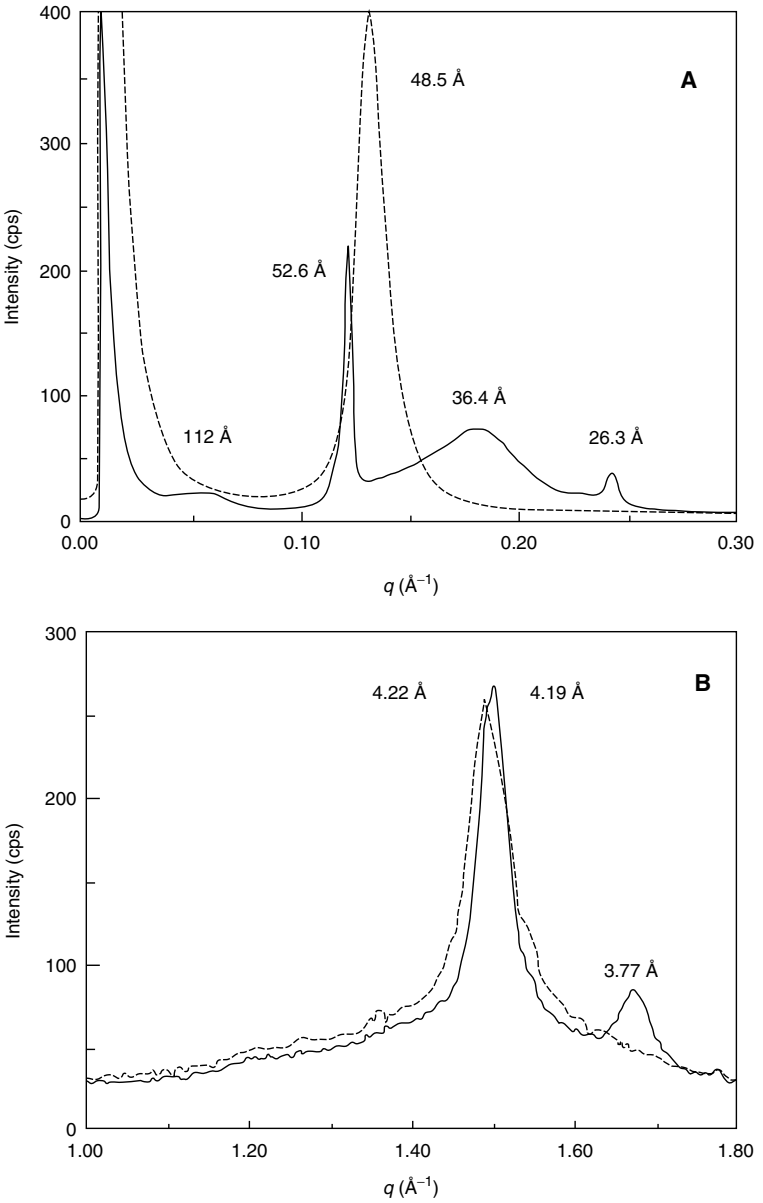

Figure 17.5. The evolution of the short- and long-spacings in cocoa butter as determined by powder XRD during heating of a sample that was quenched to –10°C at 100°C/s and then warmed from –10 to 40°C at 1°C/min. Part A shows the long spacing (small angle scattering) at 10°C, before heating, and at 20°C after the transition to the α-form. Part B shows the corresponding short spacings (wide angle scattering). ___, –10°C; ----, 20°C. (Taken from Loisel et al. 1998).

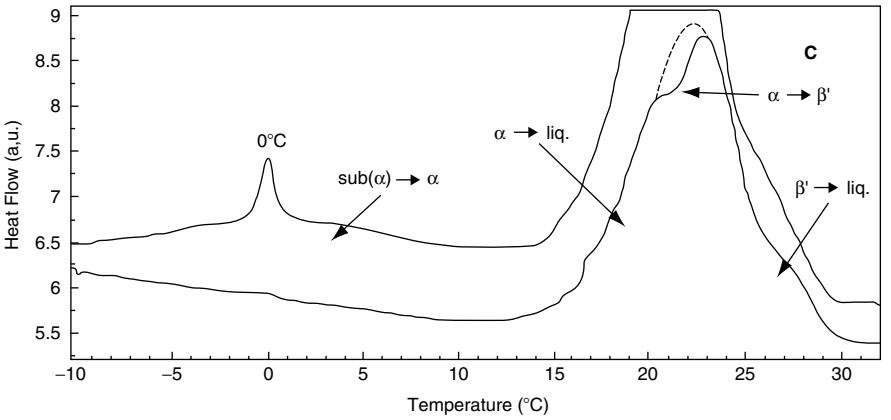

Figure 17.6. DSC thermogram obtained simultaneously with XRD during the melting of cocoa butter at 1°C/min. (Taken from Loisel et al. 1998).

17.2.2 Microstructure

This section attempts to relate the microstructural organization of fat crystals to the mechanical properties. The importance of hierarchies in structural organization will again be stressed in this section in an attempt correlate microstructure to macroscopic properties. Figure 17.7 depicts the hierarchies in a fat crystal network structure. Past work has focused on lipid composition, polymorphism and solid fat content to interpret the mechanical strength of the network (Kamphuis and Jongschapp 1985; Papenhuijzen 1971, 1972; Payne 1964).

The microstructural level of a fat crystal network will vary from 0.25 to 200 μm. It was first noted by van den Temple that this level of structure has a large effect on macroscopic rheological properties of the fat network (1961). deMan (1964) as well as deMan and Beers (1987) furthered the understanding of the effect of microstructure on macroscopic hardness when examining milk fat. Marangoni's group demonstrated the importance of microstructure on the spreadablility of chemically interesterified and enzymatically interesterified milk fat and milk fat–canola oil blends (Marangoni and Rousseau 1996, 1998). The hardness index and storage modulus (G') of chemically interesterified milk fat was lower than its non-interesterified counterpart even though the solid fat content was similar (Rousseau et al. 1996). This study indicated that there were factors other than SFC that influence the rheology of fats.

17.2.3 Imaging Methods

There are several techniques used to image the microstructure of fat crystal networks. (See Chapter 11 on "Imaging.") The most commonly used imaging method is polarized light microscopy (PLM) since fat crystals are birefringent and appear white, while the liquid oil is not and thus appears black.

Differences in microstructure between 20%SSS/80%OOO can be observed upon interesterification (Figure 17.8). Chemical interesterification caused a severe decrease in the melting point of the system as no crystals were observed above 30°C. Chemical interesterification also caused an increase in nucleation rate with a concomitant

decrease in crystal size and increase in the number of crystals in the system. For chemically interesterified mixtures, crystallization is dominated by nucleation when compared to the noninteresterified case.

A major advancement in imaging fatty products developed from the work of Heertje and others (1987). Fat crystal networks were separated from the nonvolatile vegetable oil and imaged using scanning electron microscopy (SEM). The authors found the most efficient method to separate the nonvolatile liquid oil from the fat crystal network was by de-oiling the sample with 2-butanol and methanol (90/10;v/v) between 5°C and 15°C (Heertje et al. 1987). The application of the 2-butanol and methanol mixture replaced the nonvolatile vegetable oil with the volatile mixture. This allowed surface characteristics of the fat network to be observed without interference of the liquid oil. Subsequent treatments were required to prepare the samples for SEM which included freezing, freeze drying, fracturing, coating and transfer to the SEM.

In recent years, many other techniques have been employed to elucidate the structure of fat crystal networks including: confocal laser scanning fluorescence microscopy (Heertje et al. 1987) and multiple photon microscopy (Marangoni and Hartel 1996). Another advance has been the development of three-dimensional imaging.

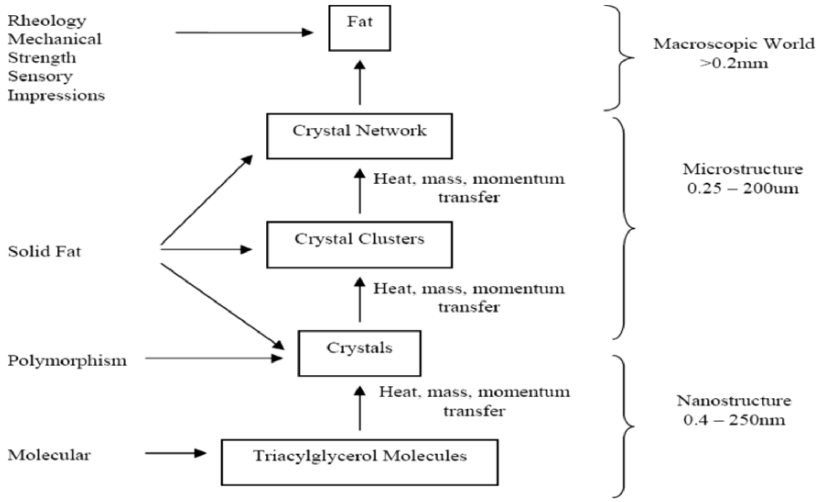

Figure 17.7. Structural hierarchy of fat crystal networks (Narine and Marangoni 2005).

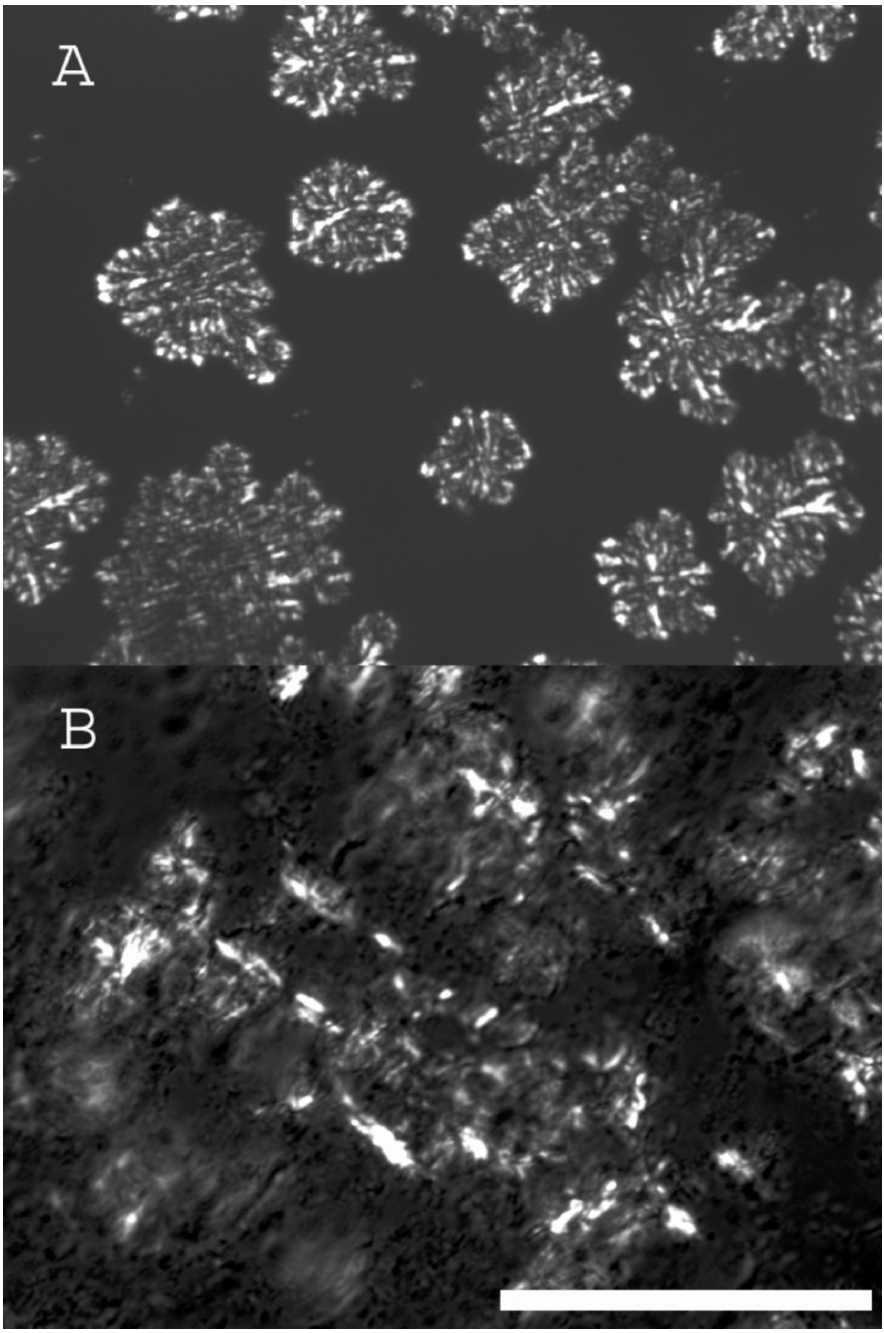

Figure 17.8. Microstructure of non-interesterified (A) and interesterified (B) 20% tristearin, 80% triolein blends stored at 20°C. Magnification bar = 100μm.

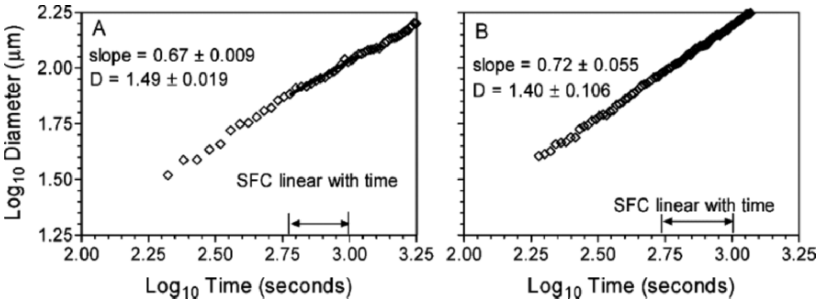

Figure 17.9. Log-log plot of diameter of the cluster versus time for 20μm and 170μm milkfat samples.

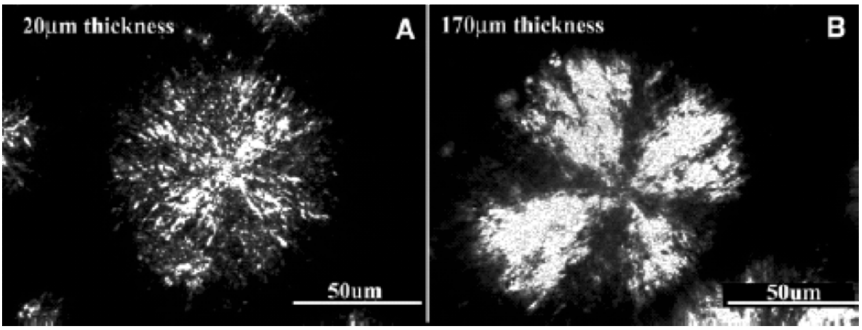

Figure 17.10. Polarized light micrograph of a milkfat spherulite grown at two different thicknesses, 20μm (A), and 170μm (B).

Recent work comparing two- and three-dimensional imaging was accomplished to determine whether the effects of two-dimensional confinement affected the dimensionality of growth (Batte and Marangoni 2005). It was determined, by calculating the fractal dimension of both systems, that two-dimensional confinement did not affect the fractal dimension for milk fat (Figure 17.9). The growth kinetics and final structure of the 20 μm and 70 μm fat films were very similar (Figure 17.10).

17.3 Lipid Phase Behavior

A strict definition of a phase is a domain with a homogenous chemical composition and physical state (Atkins 1998). Typically, phase behavior is associated with equilibrium mixtures of liquid, vapor and solid phases in a mixture of two or more substances as a function of temperature, pressure and composition. In fats, when discussing phases, it usually refers to their polymorphic form, solid/liquid states, or compositionally different fractions within a complex mixture. Therefore, when phases of fats are discussed it is important to carefully define what is being used as the definition for

the phases of interest. For instance, many different microstructures and polymorphic forms may exist in a single solid phase of fat.

During the manufacture of fat containing food products it is imperative to control the melting and solidification behavior of edible oils and fats. Understanding phase behavior allows the prediction of melting ranges and solid phase composition of a given product. It may also be used to provide a framework for understanding defects within food products such as graininess in fat spreads and bloom in chocolate. Furthermore, it can aid in the understanding of mouth-feel and hardness (Humphrey and Narine 2005).

The importance of phase equilibria is evident in every facet of foods containing triacylglycerides. Most important are the solid–liquid phase equilibria which determine melting ranges of fat containing foods such as chocolate, ice cream and cakes. Many aspects must be taken into consideration when selecting an appropriate fat; for example, a fat spread such as margarine must contain enough liquid oil at room temperature to be soft and spreadable. The importance of phase equilibria may also be demonstrated for products that are refrigerated or stored at room temperature, such as butter. For these systems, a wide melting range is desirable, so that the product may be spreadable at a wide range of temperatures. However, for chocolate, a very sharp melting profile with little melting at 20°C and complete melting at 36°C is desired.

Using a simple system of tristearin (SSS) and triolein (OOO) to illustrate the importance of lipid phase behavior, it is seen that when 30%SSS is added to 70%OOO, the melting profile is very steep because all of the solid is comprised of SSS with a specific melting temperature (Figure 17.11). However, if the system is randomized using chemical interesterification, a multiplicity of molecular species will be created. For the above mixture, for example, interesterification will change the triacylglycerol profile to 22%OOO, 32.6%SOO/OSO/OOS, 13.2%SOS/SSO/OSS and other minor components. This causes a widening of the melting profile due to the multiplicity of melting events associated with the different molecular species created upon interesterification. This trend is similar to the desired melting profile for margarine. With a good understanding of phase equilibria, different stocks of fat may be blended in industrial applications to provide the required melting profile and crystallization behavior.

17.3.1 Monotectics, Eutectics and Peritectics

Monotectic mixtures arise when the individual components have similar melting points, molecular volumes and polymorphic forms. Figure 17.12(a) represents a possible phase diagram for monotectic mixtures. A typical monotectic solution occurs when SSS is mixed with SOS. Lutton (1955) determined that the α form was present and associated with limited solid solution formation, and contrasted with the α forms of other glyceride mixtures that formed continuous solid solutions (Rossell 1967). It was found, for this system, that tristearin incorporates about 50% of the SOS into a solid solution; on the other hand, SOS incorporates very little SSS into a solid solution.

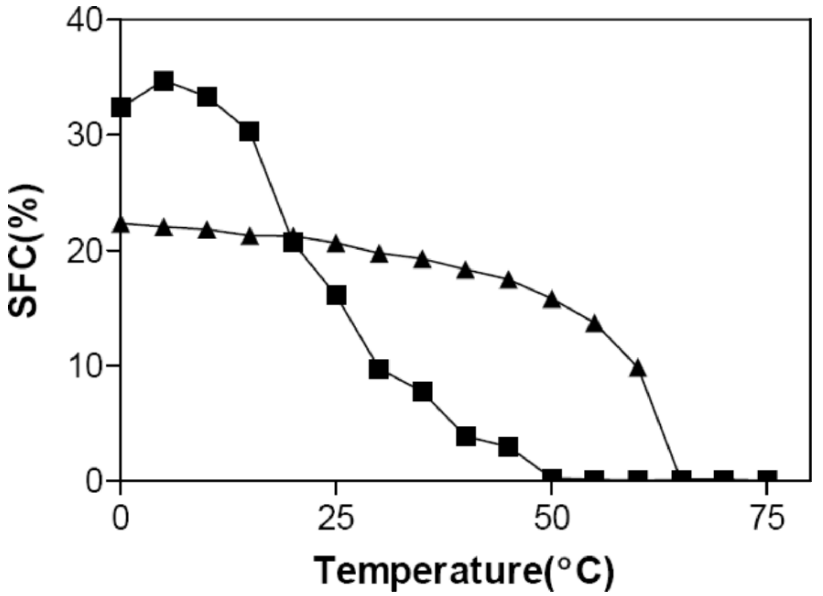

Figure 17.11. SFC-temperature profiles for interesterified (■) and non-interesterified (▲) blends of 30% tristearin and 70% triolein.

Eutectics occur when components differ with respect to molecular volume, shape and polymorphism, but do not vary with respect to melting point (Timms 1984). Figure 17.12(b) demonstrates a typical binary eutectic system. An example of a eutectic system occurs when tristearin and tripalmitin are mixed. The first phase diagram for this system was determined using the thaw–melt technique of Kerridge (1952). The phase behavior is characterized as a eutectic with partially miscible solid solutions. The eutectic point for this system occurs at 63.9°C and 25.5%SSS (Kerridge 1952). At the eutectic point, 30% Tripalmitin (PPP) and 15%SSS are soluble in the liquid phase (Rossell 1967). The tendency for the lower melting triacylglycerides to be dissolved to a greater extent in the solution and for the eutectic point to be displaced towards the composition richest in the lower melting triacylglycerides is common in triacylglyceride mixtures (Rossell 1967). Lutton (1955) constructed a similar phase diagram using melting points collected by differential scanning calorimetry, x-ray diffraction and dilatometry.

Peritectics are observed in mixed saturated-unsaturated systems. Figure 17.12(c) is a theoretical peritectic phase diagram. Several authors have reported mixtures of SOS and SOO to exhibit peritectic behavior (Rossell 1976). The peritectic mixture contained 24%SOS melted at 27.4°C, determined using differential thermal analysis. Table 17.4 list common phase behaviors of binary mixtures for different triacylglycerides adapted from Rossell (1967).

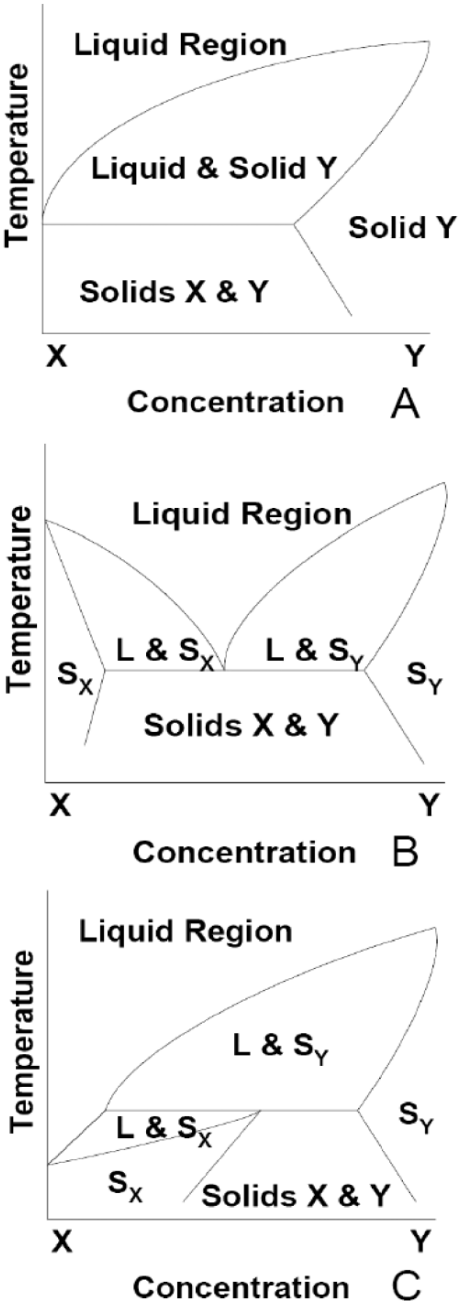

Figure 17.12. Phase diagrams for monotectic (A), eutectic (B) and peritectic (C) mixtures.

Table 17.4. Phase behavior of binary mixtures of triacylglycerides adapted from Rossell (1967). (M) represents monotectic phase behavior, (E) represents eutectic phase behavior and (P) represents peritectic phase behavior.

	SSS	PPP	LLL	OOO	EEE	LiLiLi	SOO	SBB	SEE	OSS	ESS	SBS	SOS	POP	PSP	BSB	POS	PSO	OPP	POO	OPO
SSS	--	--	--	--	--	--	--	--	--	--	--	--	--	--	--	--	--	--	--	--	--
PPP	E	--	--	--	--	--	--	--	--	--	--	--	--	--	--	--	--	--	--	--	--
LLL	E	E	--	--	--	--	--	--	--	--	--	--	--	--	--	--	--	--	--	--	--
OOO	M	M		--	--	--	--	--	--	--	--	--	--	--	--	--	--	--	--	--	--
EEE		M	E	M	--	--	--	--	--	--	--	--	--	--	--	--	--	--	--	--	--
LiLiLi	M					--	--	--	--	--	--	--	--	--	--	--	--	--	--	--	--
SOO							--	--	--	--	--	--	--	--	--	--	--	--	--	--	--
SBB								--	--	--	--	--	--	--	--	--	--	--	--	--	--
SEE									--	--	--	--	--	--	--	--	--	--	--	--	--
OSS		E								--	--	--	--	--	--	--	--	--	--	--	--
ESS	M	E									--	--	--	--	--	--	--	--	--	--	--
SBS							E	P				--	--	--	--	--	--	--	--	--	--
SOS	M	E		M	E		P	P	E	E		E	--	--	--	--	--	--	--	--	--
POP		M											E	--	--	--	--	--	--	--	--
PSP	E														--	--	--	--	--	--	--
BSB								M				M				--	--	--	--	--	--
POS													M	E			--	--	--	--	--
PSO																	E	--	--	--	--
OPP														E					--	--	--
POO														P						--	--
OPO														E					E	E	--

Industrially, milk fat is commonly added to cocoa butter to produce milk chocolate. However, there is a thermodynamic incompatibility between the milk fat and cocoa butter solids which results in eutectic phase behavior. This eutectic formation leads to a chocolate with a decreased hardness (Timms 1980; Barna et al. 1992; Bystrom and Hartel 1994; Reddy et al. 1996). Extensive work has been carried out on the addition of milk fat to cocoa butter because of its ability to reduce the incidence of bloom formation in chocolate (Hartel 1996; Kleinert 1961; Dimick et al. 1993). Chocolate bloom is evident as a white-gray layer on top of the chocolate surface and eventually the chocolate will acquire a crumbly texture.

Marangoni and Lencki (1998) used solvent fractionation to produce chemically distinct fractions of milk fat reported as high melting fraction (HMF) (12wt%), medium melting fraction (MMF) (33wt%), and low melting fraction (LMF) (55wt%). They fractionated milk fat using ethyl acetate and added anhydrous milk fat (AMF), HMF, and MMF to cocoa butter to observe the phase behavior of the milk chocolate. HMF, MMF and AMF were added in 10% increments from 0% to 100%. Isosolid SFC temperatures, as a function of blend composition, were used to construct binary phase. The isosolid diagrams for AMF-CB, MMF-CB and HMF-CB are presented in

Figure 17.13. The AMF-CB formed a slight eutectic (Figure 17.13(c)) which has been observed in industrial manufacturing of milk chocolate. More interestingly, MMF had extreme thermodynamic incompatibility with the CB, forming a strong eutectic (Figure 17.13(b)). The addition of HMF to CB did not result in a eutectic, but instead ideal monotectic formation was observed. Kaylegian et al. (1993) reported similar behavior. Therefore, higher amounts of fractionated milk fat could be added to milk chocolate without an excessive softening effect.

17.3.2 Ideal Solubility?

The premise of ideal solubility is that the system must be considered as a mixture of components that do not form mixed crystals (Wesdorp et al. 2005). If the assumption of ideality holds true, then the Hildebrand equation may predict the solubility behavior of a binary TAG mixture (Knoester et al. 1972):

$$\ln c = \frac{\Delta H}{R}\left(\frac{1}{T_{fus}} - \frac{1}{T_m}\right) \tag{17.4}$$

where c represents the mol fraction or the weight fraction for high molecular weight triaclyglycerides of the higher melting component (Timms 1984), ΔH is the enthalpy of melt for the higher melting component (J/mol), R is the universal gas constant (8.314J/mol K), T_{fus} and T_m (K) are the onset melting temperatures for the pure high melting component and the blend, respectively. Since the higher melting species may be comprised of a mixture of triacylglycerides, then the onset or peak temperature determined using DSC is often used as an approximation of both T_{fus} and T_m. Westdorp et al.'s (2005) criticisms center on solid immiscibility and the Hildebrand equation assumes that mixed crystals do not form during crystallization. He also criticizes the selection of melting points and heats of fusion.

Using an interesterified and noninteresterified SSS/OOO system, Hildebrand approximations work well for high SSS concentrations (Figure 17.14). However, as OOO concentration increases, large deviations from ideal solubility can be observed due to high solvent/solute ratios. When the SSS concentration is below 70wt% the phase behavior is not being adequately predicted by the Hildebrand equation. Furthermore, as an interesting note, the process of chemical interesterification leads to a more ideal solubility of the high and low melting components in the mixture. This is due to the creation of intermediate species between SSS and OOO, with increased structural complementarily.

Major limitations of the Hildebrand equation occur when co-crystallization occurs between the fractions of TAGs (Humphrey et al. 2003). Also, deviations from ideality occur at a high solvent/solute ratios. Inclusion of solvent in the crystal may also cause deviation from ideality as imperfect crystals have a higher solubility than perfect crystals. These major limitations, which have been observed in our SSS/OOO ideal system, have lead authors to explore other methods to quantify and predict solubility.

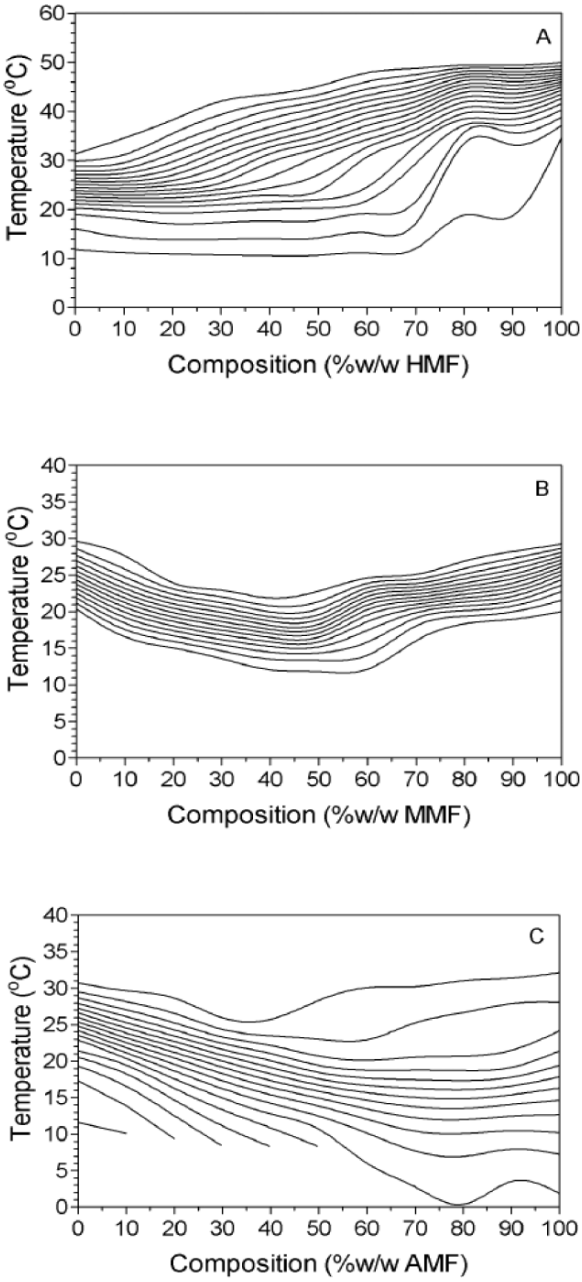

Figure 17.13. Isosolid SFC temperature phase diagrams, as a function of blend composition, for binary systems containing HMF-CB (A), MMF-CB (B) and AMF-CB (C).

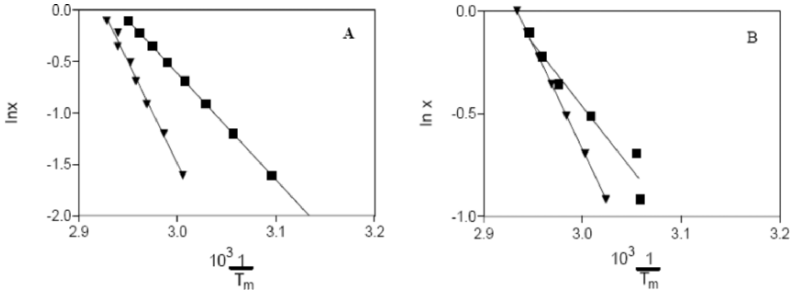

Figure 17.14. Hildebrand plots for non-interesterified (A) and interesterified (B) blends of tristearin and triolein using experimental (▼) and calculated (■) values.

17.3.3 Activity Coefficients and Predictions of Solid Phase Composition

A mixed triacylglyceride system with N components crystallizing into P phases at equilibrium (a liquid phase and P – 1 solid phases) must satisfy the equality (Prausnitz 1986):

$$\mu_i^{\text{solid}} = \mu_i^{\text{liquid}} \tag{17.5}$$

The chemical potential (μ) of each component (i) in each phase must be equal to that in any other phase. This equation can be expressed as:

$$\mu_{i,S}^{o} + RT \ln \gamma_i^S x_i^S = \mu_{i,L}^{o} + RT \ln \gamma_i^L x_i^L \tag{17.6}$$

where γ is the activity coefficient, x is the mol fraction, S represents solid phase, L represents liquid phase, and o represents the initial state of the pure liquid oil or solid. Rearranging Equation (17.6):

$$\ln\left(\frac{\gamma_i^S x_i^S}{\gamma_i^L x_i^L}\right) = \frac{1}{RT}\left(\mu_{i,L}^{o} - \mu_{i,S}^{o}\right) \tag{17.7}$$

and hence:

$$\ln\left(\frac{\gamma_i^S x_i^S}{\gamma_i^L x_i^L}\right) = \frac{\Delta H_{f,i}}{R}\left(\frac{1}{T} - \frac{1}{T_f}\right) - \frac{\Delta c_{p,i}}{R}\left(\frac{T_{f,i} - T}{T}\right) + \frac{\Delta c_{p,i}}{R} \ln \frac{T_{f,i}}{T} \tag{17.8}$$

Δc_p = 0.2kJ/mol and $T_f - T$ is never greater than 70, therefore, terms with c_p are generally very small and the following approximation becomes valid:

$$\ln\left(\frac{\gamma_i^S x_i^S}{\gamma_i^L x_i^L}\right) = \frac{\Delta H_{f,i}}{R}\left(\frac{1}{T} - \frac{1}{T_f}\right) \tag{17.9}$$

For this to be valid, the mole balance between the sum of the amount of each compound (i) in each phase (f), present in fraction ϕ_f, must be equal to the overall amount of i_t, Z_{it}: where P is the total number of Phases:

$$\sum_{f=i}^{P} x_i^f = z_{it} \tag{17.10}$$

Finally, the stoichiometric condition must show the sum of the concentrations of each component in each phase must equal to 100%:

$$\sum_{i=1}^{n} x_i^f = 1 \tag{17.11}$$

Using this set of equations, it is determined that for P phases there are $PN + P$ equations with $PN + P$ unknowns (Wesdorp et al. 2005). This set of equations may be solved to determine the number of phases, the composition of each phase and the melting temperature. To solve this series of equations, several experimental values are required. The melting point, heats of fusion for the pure compounds, the activity coefficients for the liquid phase, the activity coefficient for the solid phase and a method to solve a complex set of nonlinear equations are reported in Wesdorp et al. (2005).

17.4 Rheology of Fat Crystal Networks

17.4.1 Small Deformation

Many plastic fats exhibit a linear viscoelastic region (LVR) at low levels of stress or strain (Figure 17.15). The linear viscoelastic region occurs before point A on the graph and the strain is proportional to the stress. In fat networks the strain typically does not exceed 0.1% before the linear viscoelastic region ends (Wright et al. 2001; Rohm and Weidiner 1993). Within the LVR, fat networks behave as a Hookean solid where the strain is proportional to the stress as seen in Figure 17.15 (Rohm and Weidiner 1993). The limit of the linear viscoelastic region is referred to as the critical strain; after which point (point B) the strain no longer increases in a linear fashion. Point C represents irreversible deformation and beyond which the network fractures (point D).

When using small deformation rheology there are several useful parameters that may be obtained to describe a material: the complex modulus (G^*), storage modulus (G'), loss modulus (G'') and the tangent of the phase shift or phase angle ($\tan \delta$). These values must be taken from within the LVR, and are obtained using a dynamic oscillatory rheometer (Rao 1999). Outside the LVR, important information may be obtained such as the yield stress and yield strain.

This instrument operates by applying an oscillatory, sinusoidal stress and records the strain (Figure 17.16). The solid line corresponds to the applied stress, controlled by the instrument, and the sample's response strain appears as the dotted line. The rheometer measures the variation in strain as a function of applied stress and reports

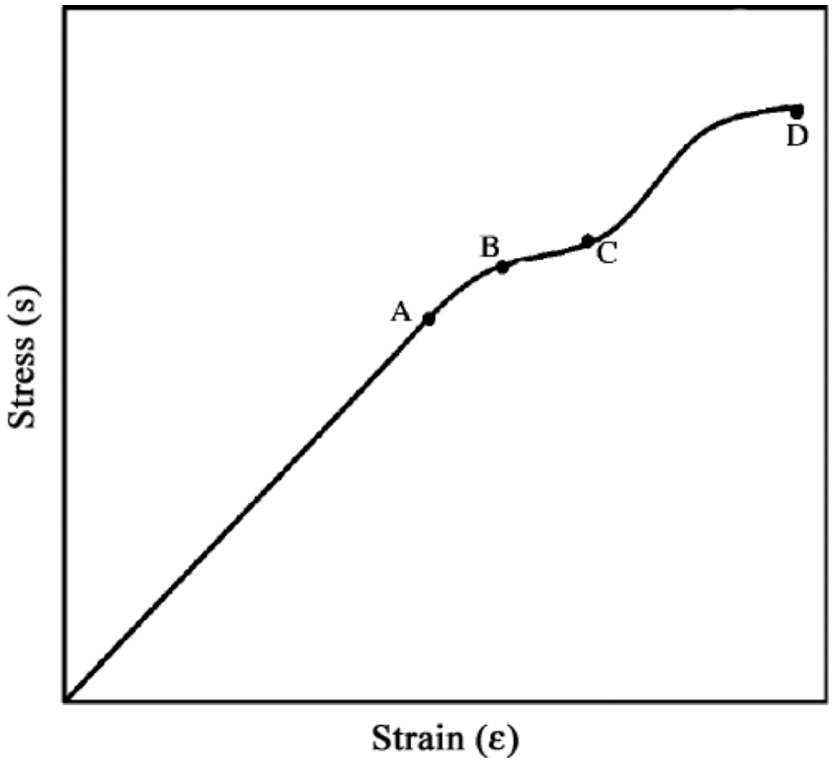

Figure 17.15. Typical stress-strain behavior for a crystallized plastic fat.

the magnitude of strain and the phase angle (δ). If the sample is in-phase (δ = 0°), meaning that the applied stress and samples response overlap (Figure 17.16), it indicates the sample is a solid and all the energy is stored in the sample. However, if they are completely out-of-phase (δ = 90°), all the energy is lost as viscous dissipation of heat during the deformation cycle. Viscoelastic materials, which fat networks are commonly referred to as, will have a δ between 0° and 90°, meaning that the samples contain a viscous and elastic component (Figure 17.16).

The storage modulus (G') is derived from the in-phase component of the stress while the loss modulus (G'') is derived from the out-of-phase component. As stated above, the moduli depend on the phase angle obtained from the following relationships:

$$G' = \left(\frac{\sigma_o}{\gamma_o}\right)\cos\delta \tag{17.12}$$

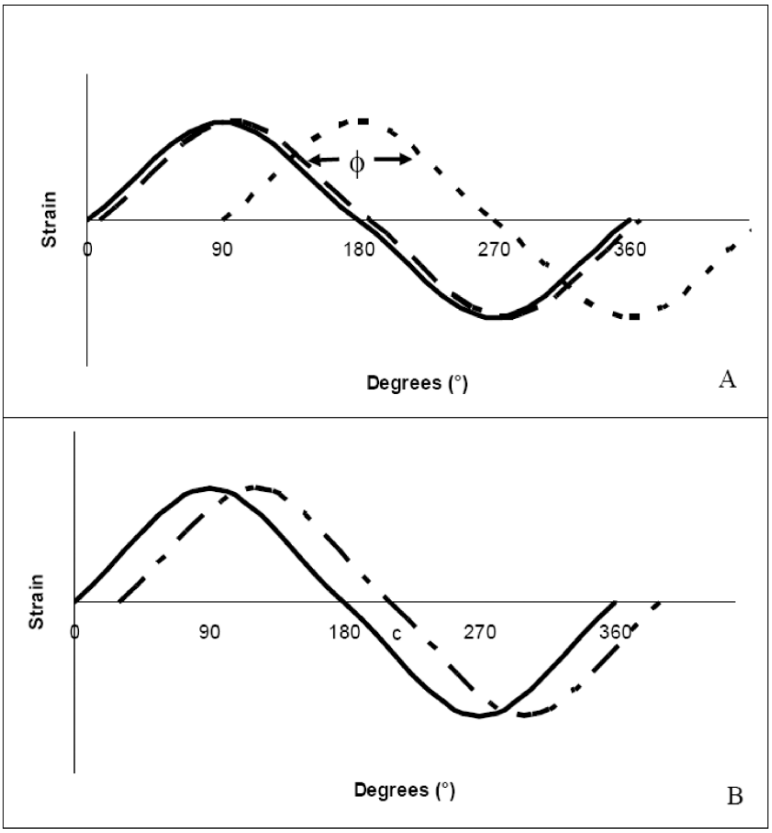

Figire 17.16. Applied oscillatory, sinusoidal stress (solid), and sample response strain for pure solid (long dash) (A), pure liquid (short dash) (B) and a viscoelastic material (long short dash). The phase angle (ϕ) is the raw single used to determine G' and G''.

$$G'' = \left(\frac{\sigma_o}{\gamma_o}\right)\sin\delta \tag{17.13}$$

where σ_o is the applies stress, γ is the resulting strain and δ is the phase angle. The complex modulus (G^*) may be calculated from using loss and storage moduli from the following equation:

$$G^* = \sqrt{G'^2 + G''^2} \tag{17.14}$$

The ratio of the loss and storage moduli may be expressed as the tangent of the phase angle ($\tan\delta$):

$$\tan\delta = \frac{G''}{G'} \tag{17.15}$$

where tanδ represents the relative balance of the elastic to viscous components of a material. Narine and Marangoni (2001) have shown these rheological measurements are associated with hardness and spreadability of fat crystal networks. Examining Equation (17.14), as the phase angle approaches 90°, G' approaches zero. All of the energy is dissipated as heat and the sample acts as a fluid (Rao 1999). The value of tanδ becomes an excellent indicator of structural integrity for intermediate values of the phase angle. This indicates the proportion of the material's structure attributable to the crystal network and to the liquid phase.

The elastic behavior of fats may be explained by the intermolecular bonding mechanism which provides coherence to the sample. The application of the oscillatory stress will cause a spatial displacement of structural elements. The mechanical properties of the material are influenced by the geometry of the network, as well as the intermolecular, internanostructural and intermicrostructural interactions. When the external force is removed, the solid component has an increased free energy stored in the inter- or intra-microstructural bonds that may then restore the sample to its original structure.

G' is higher for the interesterified at 20°C but much lower at 30°C as seen in Table 17.5. This is explained by Figure 17.11 where the SFC/temperature profile shows that the noninteresterified system has very little melting until 60°C. However, the interesterified system has a sharp melting profile at 20°C. Thus the sudden drop in SFC at approximately 20°C causes a significant decrease in the G'. At low temperatures, the interesterified SSS/OOO system has a higher SFC because the mixed triacylglycerides are able to crystallize while in the noninteresterified system only the SSS is crystallizing.

Table 17.5. Storage moduli (G', Pa) for interesterified and non-interesterified tristearin-triolein blends crystallized and stored at 20°C, 30°C and 40°C for 24 hours.

	20°C		30°C		40°C	
	Non-interesterified	Interesterified	Non-interesterified	Interesterified	Non-interesterified	Interesterified
30%SSS	$9.4\times10^5\pm2.9\times10^4$	$1.6\times10^6\pm7.2\times10^4$	$8.8\times10^5\pm2.2\times10^4$	NA	NA	NA
40%SSS	$1.5\times10^6\pm3.6\times10^4$	$4.9\times10^6\pm3.0\times10^5$	$1.7\times10^6\pm1.7\times10^5$	$2.1\times10^6\pm9.2\times10^4$	$2.2\times10^6\pm1.1\times10^5$	NA
50%SSS	$5.6\times10^6\pm3.5\times10^5$	$7.0\times10^6\pm3.9\times10^9$	$2.1\times10^6\pm1.4\times10^5$	$4.1\times10^6\pm3.2\times10^5$	$3.0\times10^6\pm2.2\times10^5$	NA

17.4.2 Large Deformation Rheology

Bulk fat products are considered to be plastic materials that are elastic when the stress and strain are below the yield stress and are viscous above the yield stress. The elastic properties of the fat are modeled using Equation (17.16) and the viscous component is modeled using Equation (17.17),

$$\tau = E\gamma \tag{17.16}$$

$$\tau - \tau_{\circ} = \eta \frac{d\gamma}{dt} \tag{17.17}$$

where τ is the stress, τ_o is the yield stress, E is the Young's modulus, γ is the strain, η is the viscosity and t is time.

In large deformation tests, the applied force is sufficient to induce permanent deformation or fracture in the sample. This measure is used to determine hardness, spreadability, cutting force and/or yield force (Wright et al. 2001). There are several different instrumental setups to carry out large deformation test. One common method is to compress a sample between two parallel plates and measure the yield force. The force required to exceed the yield stress of the network is a good indicator of hardness (Figure 17.17). Large deformation tests provide insight into the yield stress, yield strain, and compressive yield work. As well, if the compression is linear before the material yields, then the compressive modulus and onset of compression may be determined (Wight et al. 2001).

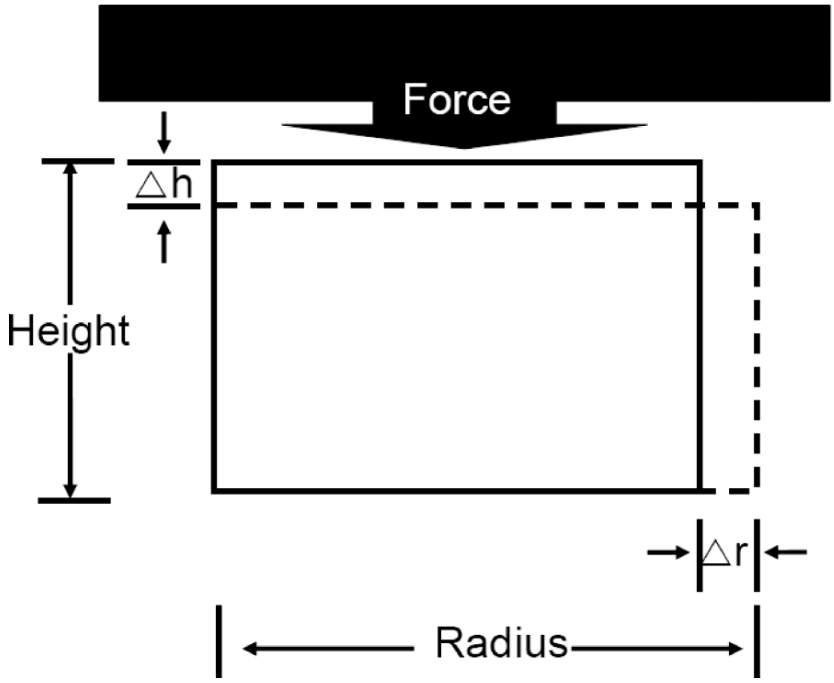

Figure 17.17. Parallel plate geometry used to measure hardness by monitoring the force required to deform the sample.

The 30%SSS/70%OOO system had the yield force measured using parallel plate compression of a thick sample. Results of the yield force for this system at 30%SSS (Table 17.6) shows similar results as seen in the SFC/temperature profile (Figure 17.11) and the small deformation rheology results (Table 17.5). At low temperatures, the SFC is higher for the interesterified blend resulting in a higher yield force required to deform the sample. At 30°C, a significant drop in SFC occurs for the interesterified system, and therefore, the sample becomes too soft to measure a yield force. However, for the noninteresterified blend, the polymorphism is β, resulting in a larger crystal size, thus less crystal–crystal interactions and a softer fat. Hence the microstructure significantly affects the rheological properties of the system.

Table 17.6. Yield force (N) for non-interesterified and interesterifiend 30% tristearin, 70% triolein blends crystallized and stored at different temperatures for 24 hours.

	20°C	30°C	40°C	50°C
Non-interesterified	1.6±0.35	Soft	Soft	Soft
Interesterified	2.7±0.04	1.1±0.01	Soft	Soft

A recent study using large deformation rheology indicated that samples with more saturated fatty acids from anhydrous milk fat will have a higher solid fat content due to the elevated melting point of the species present (Narine and Marangoni 2001). This will correspond to a higher G' which is an indicator of macroscopic hardness (Narine and Marangoni 2001). Also, as solid fat content increases, so does the yield force (Figute 17.18) (Rye et al. 2005).

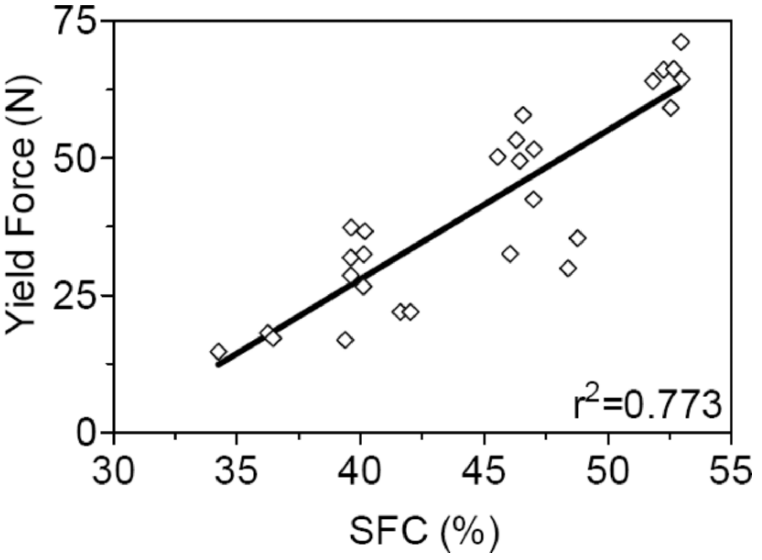

Figure 17.18. Linear correlation between solid fat content and yield force. Data represent several cooling rates and storage times for anhydrous milkfat (Rye, Litwinenko, and Marangoni 2005).

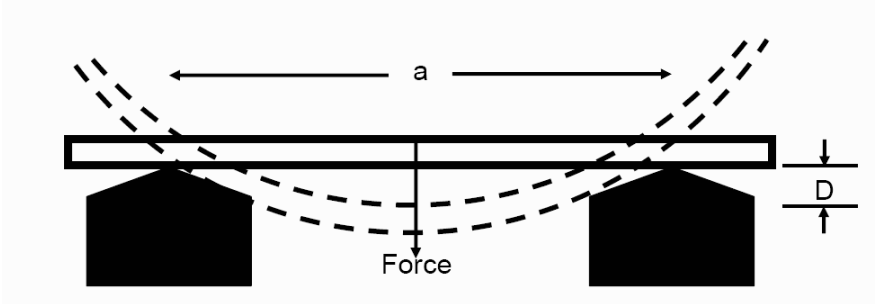

Figure 17.19. Diagram for a three-point bending geometry to determine the yield force.

Another important large deformation measurement is the three point bending test (Figure 17.19). Here a mold of the solid fat is placed on two beams and a third beam applies an external force between the other two beams. The Young's modulus (E) and yield force may be determined depending on the cross-section as (rectangular Equation (17.18) or circular Equation (17.19)):

$$E = \frac{Fa^3}{4dbh^3} \tag{17.18}$$

$$E = \frac{4Fa^3}{3d\pi D^4} \tag{17.19}$$

where F is the applied force, a is the distance between beams, d is the deformation, h is the height of the sample, b is the base length, and D is the diameter. Three point bending tests are excellent measures of chocolate snap.

Large deformation tests for fat samples are correlated to sensory tests (Rousseau and Marangoni 1998). It is, however, difficult to relate the large deformation experiments to fundamental characteristics of the microstructure of the fat crystal network due to the fact that the networks are destroyed during testing.

17.5 Fractality and Fat Crystal Networks

Upon cooling from their molten state to below their melting temperature some of the triacylglycerols in the fat undergo a liquid–solid transformation to form primary crystals. The primary crystals then aggregate to form clusters, which interact resulting in the formation of a continuous three-dimensional network. All of the levels of hierarchy previously mentioned will influence the mechanical properties of the fat.

17.5.1 Fractal Definition

1. Most simply, the object looks similar at different magnifications. Some degree of self-similarity (exact or statistical) should be displayed in the object or distributions of objects within a certain range of dilations.

In the case of fat crystal networks, fractal scaling is found between the size of a primary colloidal particle and a floc of primary particles (Marangoni 2005).

2. A specific property should scale in a power-law fashion within a length scale.

In fat crystal networks, the elastic modulus and yield stress follow a power-law relationship to the volume fraction of the solids in the network. A log–log plot of the elastic modulus or yield stress versus solids volume fraction is usually linear.

3. The "scaling factor" should be fractional and less than the dimensionality of the corresponding Euclidean embedding space (d).

If all three of these conditions are satisfied then the object or distribution of objects are said to be fractal.

17.5.2 History of the Development of the Fractal Model of Fat Crystal Networks

Modeling fat crystal networks started with Van den Tempel's work in 1961, when he proposed the linear chain model (Van den Temple 1961). It was postulated that solid fat particles form linear chains that are held together by two types of bonds—irreversible primary bonds (stronger bonds) and reversible secondary bonds (weaker bonds). In this early model, the shear modulus (G) is predicted to be directly proportional to the volume fraction Φ of solids and to particle diameter D according to the equation:

$$G = \frac{5A\Phi D^{0.5}}{24\pi H_0^{3.5}} \tag{17.20}$$

where A is Hamaker's constant, H_0 the interparticle distance, and Φ the volume fraction of solids (usually determined as SFC/100). However, G did not increase in a linear fashion with respect to the volume fraction of solids (DeMan and Beers 1987; Marangoni and Rousseau 1998; Nederveen 1963). It was found that these two parameters followed an exponential scaling relationship (Marangoni 2002; Payne 1964).

Sherman (1968) proposed a different model similar to a flocculated *O/W* emulsion. His model assumed that fat crystal networks were less densely packed and joined by localized regions of densely packed particles. Again, a linear relationship between G and Φ is predicted.

van den Tempel extended his model, in light of Sherman's work, and realized that a stronger dependence of G on Φ and D existed than was earlier predicted using the linear chain model (van den Temple 1979). The fat crystal network consisted now of linear chains, of preformed aggregates as opposed to rigid spheres. A correction factor was introduced into the calculation for G of the fat crystal networks that produce a better fitting model. However, difficulties in calculating the correction

factor and the lack of success of the previous linear chain model limited the wide spread acceptance of this work. The new model became:

$$G = G_{\text{theory}} \cdot \frac{mD_a}{nD} \tag{17.21}$$

where G is the corrected shear modulus of the fat crystal network, G_{theory} the shear modulus of the network calculated from the linear chain model, m the number of the connecting chains between two neighboring aggregates, n the average number of primary particles in an aggregate, D_a the average diameter of an aggregate, and D the average primary particle diameter.

In the field of colloidal aggregation, Brown and Ball developed an early scaling theory to explain the elastic properties of colloidal gels (1985). Brown and Ball suggested that colloidal aggregates should behave as stochastic mass fractals on a scale larger than the primary particle size, and formulated a power-law relationship of the elastic modulus to the solid volume fraction. This formulation was experimentally verified by various others, including Sonntag and Russel (1987) and Buscal et al. (1987).

Shih et al. (1990), furthered the scaling theory to explain the elastic properties of colloidal gels. The existence of two rheological regimes was proposed, depending on the relative strength of the interfloc and intrafloc links (Figure 17.20). The strong-link regime occurs when the flocs yield under an applied stress. This generally occurs at low volume fractions of solids ($\phi < 0.1$). The weak link regime occurs when the interfloc links yield under an applied stress, at higher volume fractions of solids ($\phi > 0.1$). The equations for the strong- and weak-link regimes are, respecttively:

$$G \sim \phi^{\frac{d+x}{d-D}} \tag{17.22}$$

$$G \sim \phi^{\frac{1}{d-D}} \tag{17.23}$$

The fractal dimension D is used to quantify the microstructure of the fat crystal networks, where d is the Euclidean dimension, x is the backbone fractal dimension that is estimated between 1 and 1.3. The backbone fractal dimension describes the tortuosity of the effective chain of stress transduction within a cluster of particles yielding under an externally applied stress (Shih et al. 1990; Kantor and Webman 1984).

The strong- and weak-link regimes may be determined using the strain at the limit of linearity (γ_o) of the system. According to Shih et al. (1990), γ_o increases as a function of ϕ for the weak-link regime and γ_o decreases as a function of ϕ for the strong-link regime. The equations for the strong- and weak-link regimes based on the strain at the limit of linearity are, respectively:

$$\gamma_\circ \sim \phi^{-\frac{(1+x)}{(d-D)}} \tag{17.24}$$

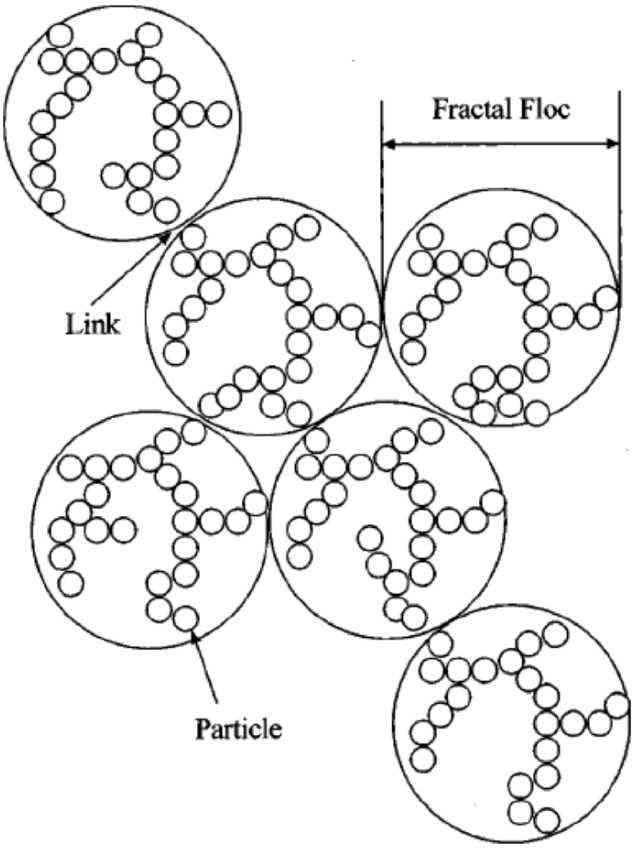

Figure 17.20. Interfloc and intrafloc links between fractal clusters of colloidal aggregates.

$$\gamma_{\circ} \sim \phi^{\frac{1}{(d-D)}} \tag{17.25}$$

Recently, the development of an intermediate regime was proposed by Wu and Morbidelli (2001) where both the inter- and intra-flocs yield under an applied stress. The transition regime is modeled via the following equation:

$$G \sim \phi^{\frac{(d-2)(2+x)(1-\alpha)}{d-D}} \tag{17.26}$$

where α is a constant between [0,1] which is dependent on the relative weighting between the strong- and weak-link regimes. $\alpha = 1$ corresponds to the weak-link regime

and $\alpha = 0$ represents the strong-link regime. The value for α and D are determined by varying the solid fat content and measuring both G and γ_o.

The strong-, weak- and intermediate regimes are all a product of the elastic constant of the basic mechanical unit (the floc, the links between the flocs, or a combination of both) and the number of these units present in the direction of the externally applied force (Shih et al. 1990). Therefore, the fractal dimension defines to the size of the clusters. A large fractal dimension represents a large cluster that translates to less cluster-cluster interactions per unit volume and a decreased elastic modulus. At high volume fractions, cluster size decreases and the number of cluster-cluster interactions increases, and thus the elastic constant also increases.

In 1992, Vreeker et al. presented rheological data for aggregated fat networks in the framework of previous fractal theories. These authors indicated that the elastic modulus varied with particle concentration according to a power law, in keeping with the proposed models for the elasticity of colloidal gels.

Marangoni's group has since advanced the fractal theory applying Shih et al.'s weak link regime with Vreeker's rheological findings to develop a fractal theory for fat crystal networks. Fat crystal networks are considered as cross-linked fractal clusters formed by aggregating fat crystals. Self-similarity is assumed to exist within the clusters, from the primary fat crystals to the clusters. If the force-constant of the links between microstructures was expressed as k_l, then the macroscopic elastic constant K (in one dimension) of the network could be modeled as:

$$K = \left[L / \xi\right]^{d-2} k_l \tag{17.27}$$

where ξ is the diameter of one microstructure, L is the macroscopic size of the system, and d is the Euclidean dimension of the sample ($d = 3$). Particles of diameter "a" are packed in a fractal fashion within flocs with size ξ. A force F acting upon the network causes the links between flocs to yield, and the original length of the system in the direction of the applied force to increase ΔL. Thus, the interfloc separation distance l also increases.

The structure within the microstructure is fractal in nature; therefore the diameter of the microstructure (or aggregates) is related to the particle volume fraction of the fat crystal networks Φ_t as:

$$\xi \sim \Phi_t^{1/(D-3)} \tag{17.28}$$

By substituting Equation (17.28) into Equation (17.27) and assuming the links between the microstructures are statistically identical, K then relates to Φ in three-dimensional space; as:

$$K \sim \Phi^{1/(3-D)} \tag{17.29}$$

The shear storage modulus of the network is proportionally related to the force constant K. Thus, G' is also related to the particle volume fraction via the fractal dimension (D) of the network.

Marangoni and Rousseau (1996) recognized that fat crystal networks at high SFCs are in the weak-link regime, so they applied Shih's weak-link theory to high SFC fat systems and used fractal dimensions to quantify the microstructure of fat crystal networks. By assuming a spherical geometry for the microstructure elements, Narine and Marangoni (1999A) obtained an expression for the elastic modulus of a fat crystal network based on fractal scaling concepts:

$$G' = \frac{mA}{6c\pi a\xi \ell_o^3}\Phi^{\frac{1}{d-D}} \tag{17.30}$$

where m is the number of neighboring microstructural elements at the interface between two microstructures, A corresponds to the Hamacker's constant, c is a constant in the expression $N = c\xi^D$ (N is the number of primary particles in a cluster of diameter, ξ), a is the diameter of a microstructural element or particle, and ℓ_o is the average equilibrium distance between microstructural elements.

Marangoni's group subsequently used a thermodynamic approach to modify the model (Marangoni 2000; Marangoni and Rogers 2003). For spherical clusters using a van der Waals forces approach or a semi-classical approach based on the bluk properties of oils, the Young modulus (E) becomes, respectively:

$$E = \frac{A}{2\pi a\varepsilon \ell_o^2}\phi^{\frac{1}{d-D}} = \frac{6\delta}{a\varepsilon}\phi^{\frac{1}{d-D}} \tag{17.31}$$

where ε corresponds to the extensional strain, and δ to the crystal-melt interfacial tension or the surface free energy.

If we assume that the shear modulus, G, is related to the Young's modulus as $G = \frac{1}{3}E$ when Poisson's ratio is $\mu = \frac{1}{2}$ (the volume does not change upon compression or extension), then Equation (17.30) may be rewritten as:

$$G = \frac{A}{6\pi\gamma a\ell_o^2}\phi^{\frac{1}{d-D}} = \frac{2\delta}{a\gamma}\phi^{\frac{1}{d-D}} \tag{17.32}$$

where γ corresponds to the shear strain. Now if the yield stress under, respectively, compression and shear are $\sigma^*_{\text{compression}} = \varepsilon \bullet E$, and $\sigma^*_{\text{shear}} = \gamma G$, then Equation (17.31) becomes:

$$\sigma^*_{\text{compression}} = \frac{6\delta}{a}\phi^{\frac{1}{d-D}} \tag{17.33}$$

$$\sigma^*_{\text{shear}} = \frac{2\delta}{a}\phi^{\frac{1}{d-D}} \tag{17.34}$$

In practice, the fractal dimensions of fat crystal networks, are measured by determining the shear storage modulus, G', of the fat crystal networks within the LVR measured by small deformation rheology. The fractal dimension of the fat crystal network may be calculated from the slope of the curve as $D = 3–1/\text{slope}$ of logarithm of G' at different SFC, Φ.

17.5.3 Physical Fractal Dimension

The fractal dimensions used to quantify the microstructure of fat crystal networks can be divided into two categories: (i) Physical fractal dimension, including the rheology fractal dimension, D_r, permeability fractal dimension, D_p, and light scattering fractal dimension, D_L, and (ii) microscopy fractal dimension, including box-counting fractal dimension, D_b, particle-counting fractal dimension, D_f, Fourier transform fractal dimension, D_{FT}, among others.

In practice, to determine the fractal dimension of a system, the elastic modulus must be measured at different volume fractions of solid fat (SFC/100). Commonly, this is accomplished by diluting the hard stock fat with an appropriate solvent in a temperature range where the solids are not significantly solubilized in the solvent. Using Equation (17.30), for anhydrous milk fat, a log–log plot of the storage modulus versus the volume fraction will produce a linear trend line that may be used to determine the fractal dimension depending on which regime is chosen (Figure 17.21).

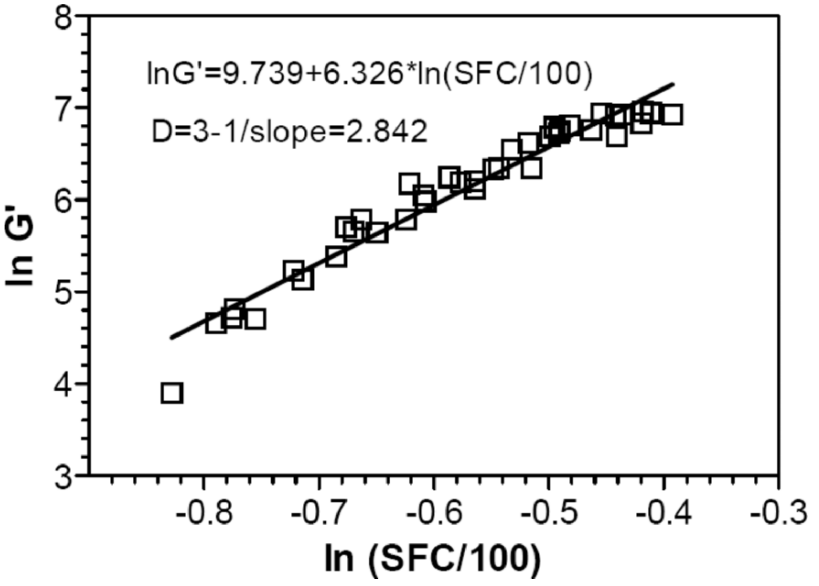

Figure 17.21. Illustration of the calculation of D from plot of lnG′ versus ln(SFC/100) for anhydrous milkfat.

The stress at the limit of linearity (σ*) of a fat containing material is defined as the point at which, when the stress is increased, the deforming solid first begins to show liquid like behavior. The yield stress is strongly correlated to sensory properties including spreadability and hardness (Wright et al. 2001). Small deformation mechanical testing is much more sensitive than large deformation techniques. In a large deformation mechanical test, the apparent yield stress is dependent on the loading rate and loading history. Figure 17.22 shows changes in the yield stress determined using small deformation rheology as a function of solids' volume fraction for blends of milk fat (Figure 17.22(a)), cocoa butter (Figure 17.22(b)) and modified palm oil (Figure 17.22(c)) in canola oil crystallized for 24 h at 5°C. The fractal dimensions of the three fats were determined from the slope of the log–log plot of σ* vs. Φ and values of milk fat, cocoa butter and modified palm oil are 2.82, 2.66, and 2.52, respectively.

A relatively new method to determine the fractal dimension is by using oil permeability measurements. In this method, the permeability coefficient, B, is measured for fat samples containing different SFC. This physical fractal dimension, the permeability fractal dimension, D_p, links the volumetric flow rate of liquid oil penetrating a colloidal fat crystal network with its SFC as (Bremer et al. 1989):

$$Q = \left(\frac{A_c}{\eta} * \frac{\Delta P}{L}\right) * \left(\frac{a^2}{K}\right) * \Phi^{2/(D-3)} \tag{17.35}$$

where Q is the volumetric flow rate of the liquid oil, A_c is the cross-sectional area through which flow takes place, η is the viscosity of the liquid oil, and ΔP is the pressure applied to the permeating oil over distance L, a is the primary particle size, K is a parameter similar to the tortuosity factor in the Kozeny–Carman equation (Bremer et al. 1989).

Bremer et al. (1989) described a detailed experimental method used to measure the permeability fractal dimension of a fat crystal network. Similarly to the rheology fractal dimension, the permeability fractal dimension, D_p, could be obtained from the nonlinear regression between Q and Φ as shown in Figure 17.23 (Tang and Marangoni 2005).

Light scattering may also be used to determine the fractal dimension of a dilute fat crystal network. This method is limited to very dilute systems. The scattering intensity is considered a function of $S(q)$, which is the structure factor corresponding to the scattering due to the spatial correlation between particles, and $P(q)$, which is a form factor corresponding to scattering arising from the properties of individual particles. At small values of the scattering vector, q, it is assumed that the form factor is constant, therefore changes in the scattering intensities are due to the spatial distribution of mass and the fractal dimension as determined from the expression:

$$I(q) \sim q^{-D} \tag{17.36}$$

The fractal dimension is determined by the slope of the log-log plot for the scattering vector versus the scattering angle.

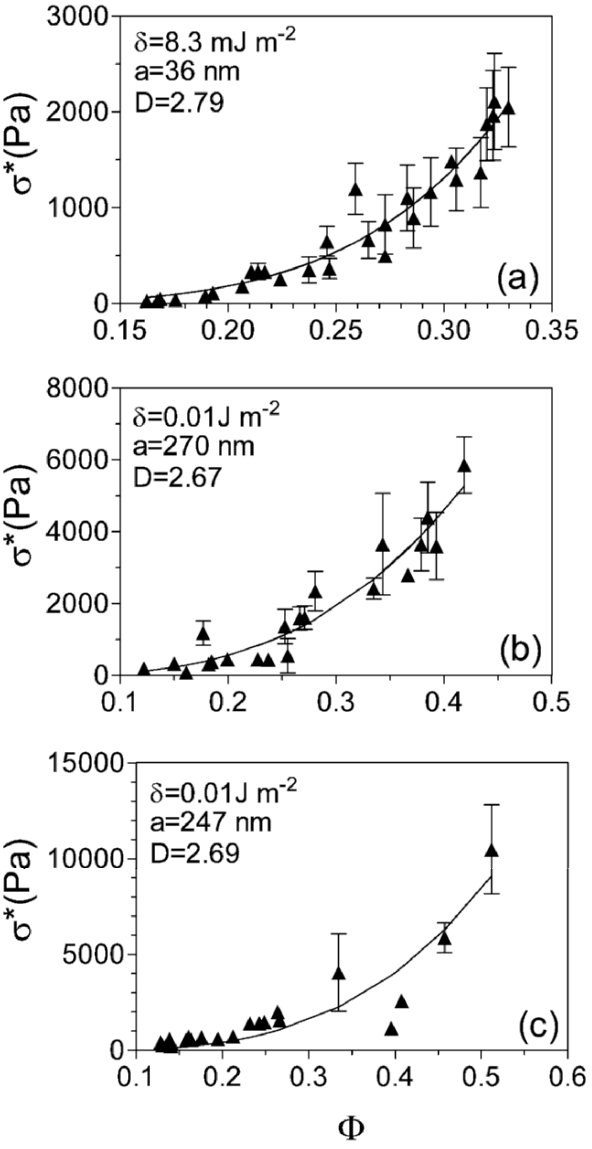

Figure 17.22. Experimentally determined changes in stress at the limit of linearity (σ*) as a function of solids volume fraction (ϕ) for blends of milkfat (A), cocoa butter (B) and modified palm oil (C) with canola oil crystallized for 24 h at 5°C. Symbols represent the average and standard deviations of 2–6 samples. The line through the data was generated by nonlinear least-squares minimization of the model to the experimental data. Indicated are the estimates of the model parameters. The surface free energy term (δ) was fixed as a constant. (Taken from Marangoni and Rogers 2003).

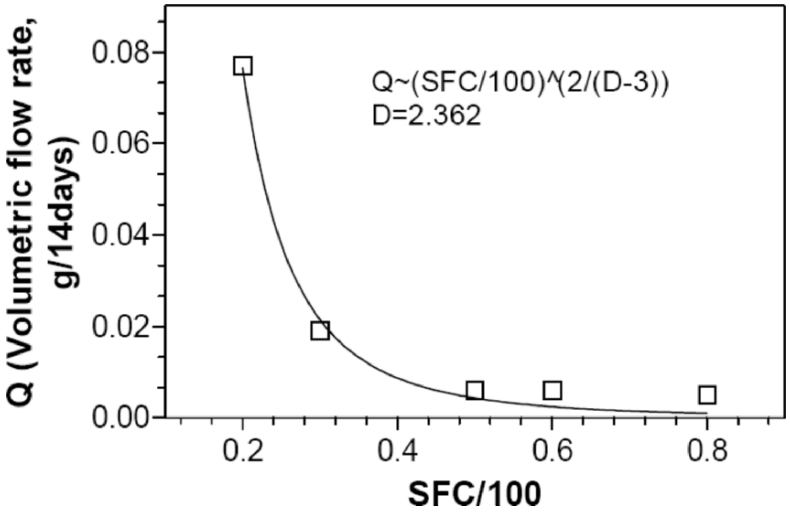

Figure 17.23. Calculation of permeability fractal dimension for mixtures of the high melting fraction of milkfat and sunflower oil fat.

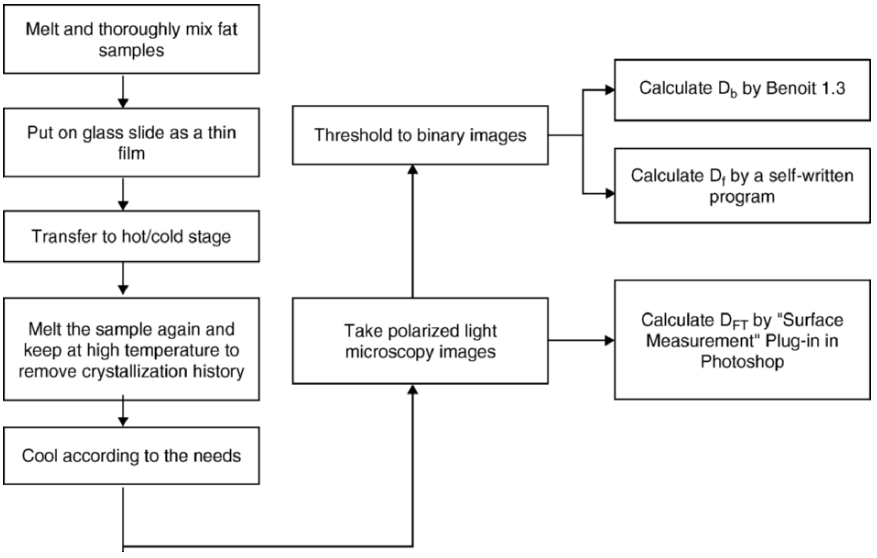

Figure 17.24. General scheme used to measure the microscopy fractal dimension of a colloidal fat crystal network.

17.5.4 Microscopy Fractal Dimension

In addition two-dimensional imaging of polarized light micrographs of fat samples may be employed to determine the fractal dimension. The general scheme to measure the microscopy fractal dimension of a colloidal fat crystal network is shown in Figure 17.24.

All the commonly available methods to calculate the microscopy fractal dimensions of a fat crystal network, such as box-counting, particle-counting, and Fourier transform method, are based on this self-similar character of the fat crystal networks. Different methods measure different properties of the fractal object, for instance, the length, area, or volume of the object at different length scales. In general, fractal dimensions, determined using microscopy, provide information on how space is occupied. For an exact self-similar fractal object, the length (or area, volume) has a power-law relationship to the length scale and the fractal dimension of the object can be derived from the exponential term of this power law relationship.

17.5.4.1 Box-Counting Fractal Dimension, D_b

The box-counting fractal dimension, D_b, is determined by placing grids with side length l_i, over a threshold binary image of a fat crystal network. The grids containing particles more than a threshold value are defined as the occupied grids. The number of occupied grids N_i is counted for a series of grid side length, l_i. Since the fat crystal network is a fractal object, the number of the occupied grids has a power law relationship with the grid side length, so the plot of the $\log(N_i)$ with $\log(l_i)$ is linear, so that:

$$D_b = -\frac{\Delta \ln(N_i)}{\Delta \ln(l_i)} \tag{17.37}$$

The box-counting fractal dimension is calculated from the log–log plot of the number of occupied boxes, N_i versus side length, l_i. The slope of this line is used to determine the fractal dimension. Both very small and very large box sizes should be exempt from the calculation to reduce surface artifacts (Awad and Marangoni 2005). This method is most sensitive to the degree of fill as well as particle size and it can be expected that if there are void volumes it will have a characteristic low fractal dimension.

17.5.4.2 Particle-Counting Fractal Dimension, D_f

The particle-counting fractal dimension relates the number of primary particles N in an object to the linear size of the fractal object R, and the linear size of one particle (σ):

$$N \sim \left(\frac{R}{\sigma}\right)^{D_f}, N>>1 \tag{17.38}$$

Here it is assumed that the average size of the microstructural element does not change with respect to mass (Narine and Marnagoni 1999A) and the equation may be rewritten as:

$$N \sim \xi^{D_f} \tag{17.39}$$

To calculate D_f, of a fat crystal network, a square shaped region of interest (ROI) with different side length, R, are drawn starting from the center of the image and the number of the microstructural elements in each ROI is counted. The logarithm of the number of microstructural elements, ln($N(R)$), is plotted against the logarithm of the side length of each ROI, ln(R), for varying values of R. The slope of the linear regression curve of this log-log plot corresponds to the fractal dimension (Litwinenko et al. 2002).

17.5.4.3 Fourier Transform Fractal Dimension

For the Fourier transform fractal dimension, D_{FT}, a two-dimensional microscopy image is considered a discrete function, $F(x,y)$, where x and y are the coordinates of the object pixels in the horizontal and vertical direction. The two-dimensional discrete Fourier transform is applied to transform the two-dimensional image to its corresponding power spectrum image $F(u,v)$ as:

$$F(u,v) = \frac{1}{MN} \sum_{x=0}^{M-1} \sum_{y=0}^{N-1} f(x,y) * e^{-j*2\pi(ux/M+vy/N)} \tag{17.40}$$

where u and v are the coordinates of the pixels in the frequency domain image. The power spectrum of $F(u,v)$,

$$P(u,v) = \left|F(u,v)\right|^2 = R^2(u,v) + I^2(u,v) \tag{17.41}$$

where $R(u,v)$ is the real part of the function $F(u,v)$ and $I(u,v)$ is the imaginary part. The power spectrum image is then transformed plotting of $P(u,v)$. The values of u and v represent the frequency with which the fractal object is repeated, and the power (or the magnitude) of the power spectrum image corresponds to the population of the microstructural elements at each repeating frequency (thus at different length scales). Thus, for a fractal object, the logarithm of the magnitude, which is the square root of the power in the power spectrum image, shows a linear relationship with the logarithm of the frequencies. The slope of this linear relationship β is used to calculate the Fourier transform fractal dimension D_{FT} by:

$$D_{FT} = \frac{4+\beta}{2} \tag{17.42}$$

D_{FT} can be used to study both self-similar and self-affine fractal objects. The data at low frequencies (u and v <10) is not to be included in the calculation of D_{FT}. Figure 17.25 from Tang and Marangoni (2006) illustrates how D_b, D_f, and D_{FT} are calculated from the double logarithmic plot of X vs. Y for polarized light microscopy images of the fat crystal networks.

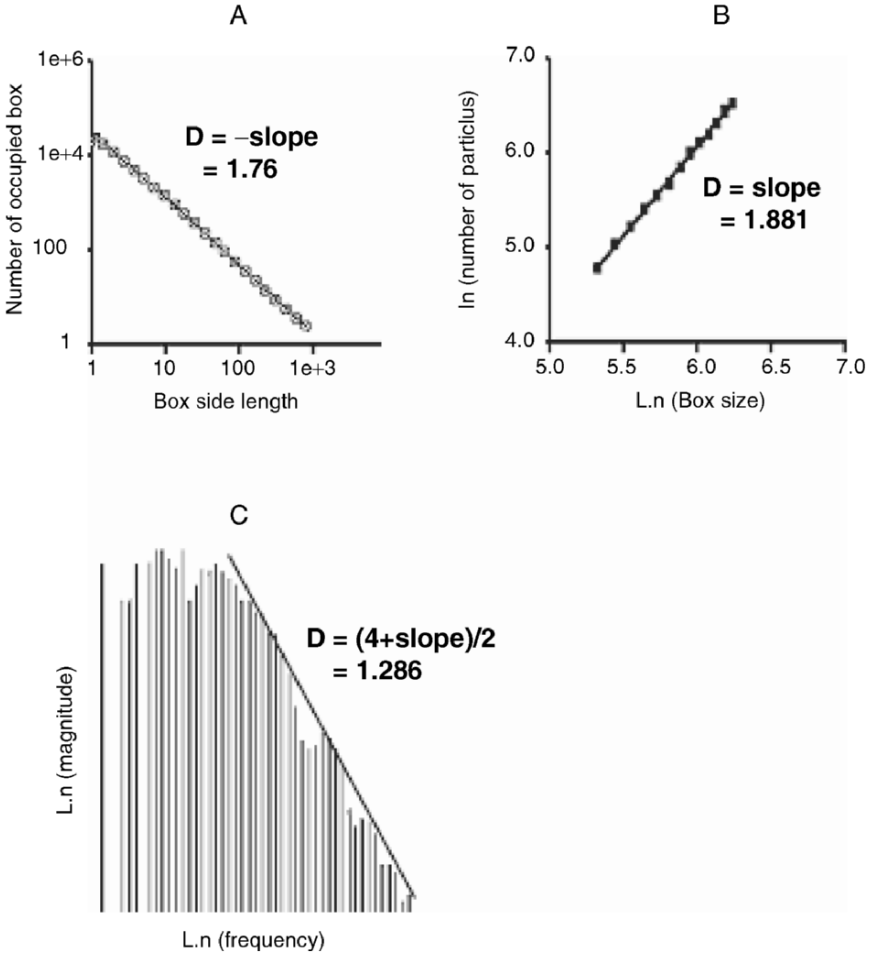

Figure 17.25. Log-log plot between (A) the number of occupied boxes with box size to calculate D_b, (B) the number of fat crystals inside each ROI (Region of Interest) with ROI size, and (C) the magnitude and the frequency of the power spectrum image obtained by 2-D Fourier-Transformation of the polarized light microscopy of fat crystal networks (Tang and Marangoni 2006).

17.5.5 Making Sense of the Fractal Dimension

In a recent study to determine the meaning of each fractal dimension measure, computer simulations of fat crystal networks with different crystal shape, size, AF (area fraction), and distribution order were generated (Tang and Marangoni 2006). By determining the D_b, D_f, and D_{FT} of these images, these authors were able to determine the effect of the different microstructural factors on the fractal dimension values. Some images generated by the computer simulation are shown in Figure 17.26.

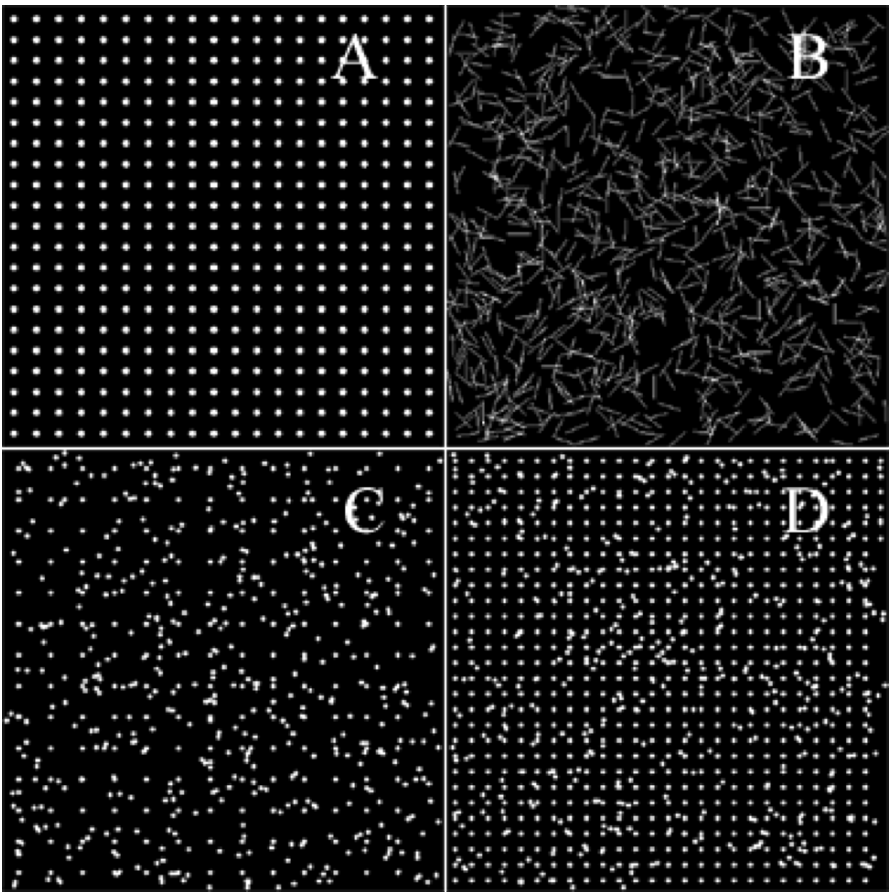

Figure 17.26. Sample images generated by computer simulation. The shape, crystal length or radius, area fraction and the distribution orderliness for the images are (A) disk, radius = 4 pixels, AF = 8%, 100% evenly distributed; (B) line, length = 26 pixels, AF = 8%, 100% randomly distributed; (C) diamond, radius = 3 pixels, AF = 6%, 30% evenly distributed; (D) diamond, radius = 3 pixels, AF = 15%, 70% evenly distributed (Tang and Marangoni 2006).

The simulation results (Tang and Marangoni 2006) showed that the box-counting fractal dimension, D_b was sensitive to crystal shape, sizes and AF. D_b increased with increasing crystal size and area fraction. It was found that the distribution of order had little effect on D_b. Complex interactions between crystal size and AF were observed (Figure 17.27). It was found that for larger AF, the effects of crystal size on D_b became less significant, while for large crystal sizes, AF had less effect on D_b as well. These findings are consistent with experimental results (Awad et al. 2002), where D_b increased with SFC, but did not vary above a critical SFC. According to these simulations, an increase in D_b at high SFC is due to the increased AF, and not from the increased number of smaller crystals. It also showed that D_b is more sensitive to structural changes at low AF (low SFC). This result explains why at high SFC some polarized light microscopy of fat samples with obviously different microstructures yield similar values of D_b (Dibildox-Alvarado et al. 2004). The simulation also showed that line-shaped crystals always had higher D_b than block-shaped crystals, such as diamond-, disk-, and square-shaped crystals.

The particle-counting fractal dimension, D_f, was not sensitive to crystal shape, size, AF or the distribution orderliness. It was found that D_f was affected by the radial distribution pattern of the fat crystals as shown in Figure 17.28. The simulation results were found to be consistent with experiments (Litwinenko et al. 2002; Tang and Marangoni 2006). D_f values close to 2 indicated more homogenously distributed fat crystals. It is important to note, the values of D_f may exceed the dimensionality of the embedding space. This is not the case for the box-counting dimension or the Fourier transform fractal dimension.

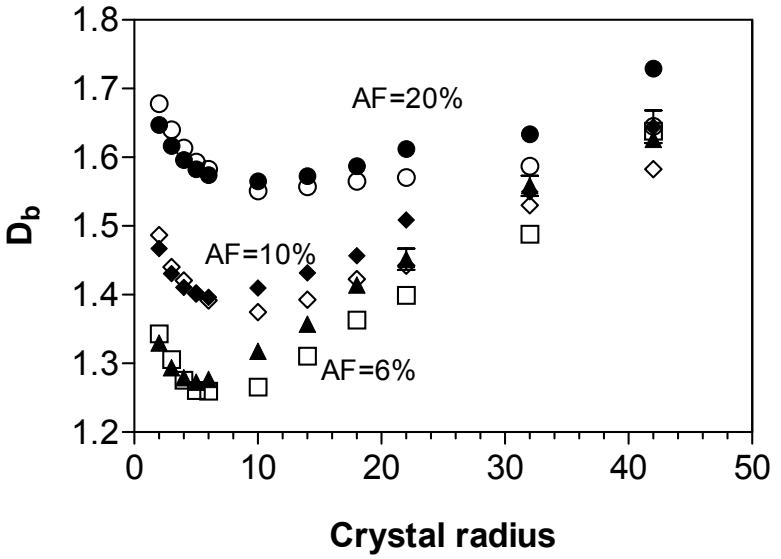

Figure 17.27. Interactions between crystal size and area fraction on D_b.

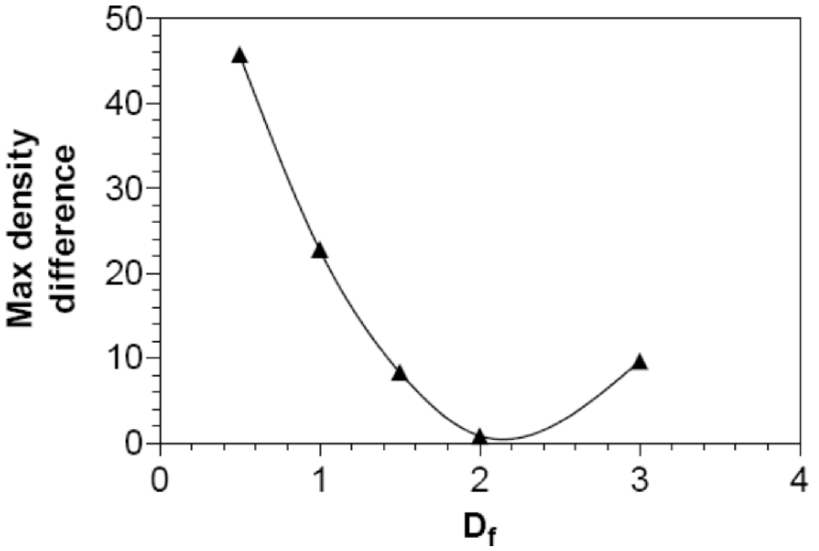

Figure 17.28. Maximum density difference of the images with different D_f values (maximum density difference = absolute value of (number of crystals per 100 pixels of the most inside box which side length is 35% of that of the original image – number of crystals per 100 pixels of the whole image)) (Tang and Marangoni 2006b).

The Fourier transform fractal dimension D_{FT} decreases almost linearly with the increasing radius of the crystals, and increases slightly when the AF increased, but no clear trend was evident among different distribution order at all AF. Relative to the effects of crystal size, the effects of the distribution order and AF of the crystals on D_{FT} were much less significant.

Table 17.7 summarizes the effects of the microstructural factors on the microscopy fractal dimensions, D_b, D_f, and D_{FT}. Different fractal dimensions reflect different aspects of the microstructure of the fat crystal networks and thus have different meanings. It is necessary to define which structural characteristic is most closely related to the macroscopic physical property of interest (mechanical strength, permeability, diffusion) and then use the fractal dimension that is most closely related to the particular structural characteristic in the modeling of that physical property.

Table 17.7. The effect of the microstructural factors on the microscopy fractal dimensions, D_b, D_f, and D_{FT}.

Affecting factors	D_b	D_f	D_{FT}
Crystal shape	√	X	√
Crystal size	√	X	√
Area fraction of crystals	√	X	X
Distribution orderliness	X	√ (radial distribution)	X

17.6 Conclusions

As consumers become more educated on the health implications of trans, saturated and polyunsaturated fatty acids, the market will be driven to produce new products with the same physical properties as current products. However, the ideal fatty acid profile desired by consumers will force industry to optimize health benefits of their products. It will become increasingly difficult to keep up with consumer trends without a greater understanding of the physical properties of fat crystal networks. In the past decade, the characterization of these trans, saturated, and polyunsaturated fats has evolved from relying on lipid phase behavior as a predictor of structure to advanced microscopy and rheology techniques as well as more accurate structural–mechanical models. Currently, powerful tools are available to determine the fractal dimensions of fat crystal networks. As our understanding of how to interpret these results increases, our ability to continue to meet the challenges of the growing market of structured fat products will also improve.

Acknowledgments. We would like to acknowledge the funding from National Science and Engineering Research Council of Canada as well as the Ontario Ministry of Agriculture and Food.

17.7 References

Akoh, C.C., and Min, D.B. (2002). *Food Lipids: Chemistry, Nutrition, and Biotechnology*, 2nd ed. C.C. Akoh and D.B. Min (eds.). Marcel Dekker, New York.

Atkins, P.W. (1998). Phase diagrams. In: *Physical Chemistry*, P.W. Atkins (ed.). Oxford University Press, Oxford.

Aquilano, D., and Sgualdino, G. (2001). Fundamental aspects of equilibrium and crystallization kinetics. In: *Crystallization in Fats and Lipid Systems*, N. Garti and K. Sato (eds.). Marcel Dekker, New York.

Avrami, M. (1939). Kinetics of phase change I. General theory. *J. Chem. Phys*. 7, 1103–1112.

Avrami, M. (1940). Kinetics of phase change I.I. Transformation–time relations for random distribution of nuclei. *J. Chem. Phys*. 8, 212–224.

Avrami, M. (1941). Kinetics of phase change. I.I.I. Granulation, phase change and microstructure. *J. Chem. Phys*. 9, 177–184.

Awad, T.S., and Marangoni, A.G. (2005). Comparison between image analysis methods for the determination of the fractal dimension of fat crystal networks. In: *Fat Crystal Networks*, A.G. Marangoni (ed.). Marcel Dekker, New York.

Awad, T.S., Rogers, M.A., and Marangoni, A.G. (2004). Scaling behavior of the elastic modulus in colloidal networks of fat crystals. *J. Phys. Chem. B*. 108, 171–179.

Barna, C.M., Hartel, R.W., and Metin, S. (1992). Incorporation of milk fat fractions into milk chocolates. *Manufact. Confectioner*. 72, 107–116.

Batte, H.D., and Marangoni, A.G. (2005). Fractal growth of milk fat crystals is unaffected by microstructural confinement. *Crystal Growth Des*. 5, 1703–1705.

Bremer, L.B.G., Vliet, T.V., and Walstra, P. (1989). Theoretical and experimental study on the fractal nature of the structure of casein gels. *J. Chem. Soc., Faraday Transforms*. 85, 359–3372.

Brown, W.D., and Ball, R.C. (1985). Computer simulation of chemically limited aggregation. *J. Phys. A*. 18, L517–L521.

Buscall, R., Mills, P.D.A., Goodwin, J.W., and Lawson, D.W. (1988). Scaling behaviour of the rheology of aggregate networks formed from colloidal particles. *J. Chem. Soc., Faraday Transactions*. 84, 4249–4260.

Bystrom, C.E., and Hartel, R.W. (1994). Evaluation of milk fat fractionation and modification techniques for creating cocoa butter replacers. *Lebens. Wissen. Technol*. 27, 142–150.

Chapman, G.M., Akehurst, E.E., and Wright, W.B. (1971). Cocoa butter and confectionery fats. Studied using programmed temperature x-ray diffraction and differential scanning calorimetry. *J. Amer. Oil Chemists Soc*. 48, 824–830.

deMan, J.M. (1964). Effect of cooling procedures on consistency, crystal structure and solid fat content of milk fat. *Dairy Industries*. 29, 244–246.

deMan, J.M., and Beers, A.M. (1987). Fat crystal networks: structure and rheological properties. *J. Texture Studies*. 18, 303–318.

Dibildox-Alvararo, E.D., Rodrigues, J.N., Gioielli, L.A., Vazquez, J.F.T., and Marnagoni, A.G. (2004). Effect of crystalline microstructure on oil migration in a semisolid fat matrix. *Crystal Growth Design*. 4, 731–736.

Dimick, P.S., Thomas, L.N., and Versteeg, C. (1993). Potential use of fractionated anhydrous milk fat as a bloom inhibitor in dark chocolate. *INFORM*. 4, 504.

Duck, W. (1964). The measurement of unstable fat in finished chocolate. *Manufac. Confectionery Fats*. 35, 67–72.

Hartel, R.W. (1996). Application of milk fat fraction in confectionery products. *J. Amer. Oil Chem. Soc*. 73, 945–953.

Heertje, I., van der Vlist, P., Blonk, J.C.G., Hendrickx, H.A.C., and Brackenhot, G.J. (1987). Confocal laser scanning microscopy in food research: some observations. *Food Microstructure*. 6, 115–120.

Humphrey, K.L., and Narine, S.S. (2005). Lipid phase behavior. In: *Fat Crystal Networks*, A.G. Marangoni (ed.). Marcel Dekker, New York.

Humphrey K.L., Moquin, P.H.L., and Narine, S.S. (2003). Phase behavior of a binary lipid shortening system: from molecules to rheology. *J. Amer. Oil Chem. Soc*. 80, 1175–1182.

Huyghebaert, A. and Hendrickx, H. (1971). Polymorphism of cocoa butter, shown by differential scanning calorimetry. *Lebens. Wissen. Technol*. 4, 59–63.

Kamphuis, H., and Jongschapp, R.J.J. (1985). The rheological behaviour of suspension of fat particles in oil interpreted in terms of a transient-network model. *Coll. Polymer Sci*. 263, 1008–1024.

Kantor, Y., and Webman, I. (1984). Elastic properties of random percolating systems. *Phys. Rev. Lett.* 52, 1891–1894.

Kaylegian, K.E., Hartel, R.W., and Lindsay, R.C. (1993). Applications of modified milk fat in food products. *J. Dairy Sci*. 76, 1782–1796.

Kleinert, J. (1961). Studies on the formation of fat bloom and methods for delaying it. *Rev. Int. Chocolate*. 16, 201–219.

Knoester, M., De Bruijne, P., and van den Tempel, M. (1972). The solid–liquid equilibrium of binary mixtures of triglycerides with palmitic and stearic chains. *Chem. Phys. Lipids*. 9, 309–319.

Larsson, K. (1966) Classification of glyceride crystal forms. Acta Chemica Scandinavica. 20: 2255–2260.

Litwinenko, J.W., Rojas, A.M., Gerschenson L.N., and Marangoni A.G. (2002). Relationship between crystallization behavior, microstructure, and mechanical properties in a palm oil–based shortening. *Journal of American Oil Chemists Society*. 79, 647–654.

Loisel, C., Keller, G., Lecq, G., Bourgaux, C., and Ollivon, M. (1998). Phase transitions and polymorphism of cocoa butter. *Journal of Amer. Oil Chem. Soc*. 75, 425–439.

Lovegren, N.V., Gline, M.S., and Feuge, R.O. (1976). Polymorphic changes in mixtures of confectionery fats. *J. Amer. Oil Chem. Soc*. 53, 83–88.

Lutton, E.S. (1955). Phase behavior of triglycerides mixtures involving primarily Tristearin, 2-Oleyldistearin and Triolein. *Journal of American Oil Chemists Society*. 32, 49–53.
Marangoni, A.G. (2000). Elasticity of high volume-fraction fractal aggregate networks: a thermodynamic approach. Physical Review B. 62: 13951–13955.
Marangoni, A.G. (2002). The nature of fractality in fat crystal networks. Trends in Food Science and Technology. 13: 37–47.
Marangoni, A.G. (2005). The nature of fractality in fat crystal networks, in Fat Crystal Networks, A.G. Marangoni (ed.). Marcel Dekker, New York, USA.
Marangoni, A.G., and Hartel, R.W. (1996). Visualization and structural analysis of fat crystal networks. Food Technology. 52: 46–52.
Marangoni, A.G., and Lenki, R.W. (1998). Ternary phase behavior of milkfat fraction. Journal of Agriculture and Food Chemistry. 46: 3879–3884.
Marangoni, A.G., and Rogers, M.A. (2003). Structural basis for the yield stress in plastic disperse systems. Applied Physics Letters. 82: 3239–3241.
Marangoni, A.G., and Rousseau, D. (1996). Is plastic fat rheology governed by the fractal geometry of the fat crystal networks. Journal of American Oil Chemists Society. 73: 993–994.
Marangoni, A.G., and Rousseau, D. (1998). The influence of chemical interesterification on the physicochemical properties of complex fat systems. 3. Rheology and fractality of the crystal network. Journal of American Oil Chemists Society. 75: 1633–1636.
Merken, G.V., and Vaeck, S.V. (1980). Etude du polymorphisme du beurre de cacao par calorimetrie DSC. Lebensmittel Wissenschaft und Technologie. 13: 314–317.
Narine, S.S., and Marangoni, A.G. (1999A). Relating structure of fat crystal networks to mechanical properties: a review. Food Research International. 12: 227–248.
Narine, S.S., and Marangoni, A.G. (1999B). Mechanical and structural model of fractal networks of fat crystals at low deformations. Physical Review E. 60: 6991–7000.
Narine, S.S., and Marangoni, A.G. (2001). Elastic modulus as an indicator of macroscopic hardness of fat crystal networks. Lebensmittel Wissenschaft und Technologie. 34: 33–40.
Narine, S.S., and Marangoni, A.G. (2005). Microstructure, in Fat Crystal Networks, A.G. Marangoni (ed.). Marcel Dekker, New York, USA.
Nederveen, C.J. (1963). Dynamic Mechanical Behavior of Suspensions of Fat Particles in Oil, Journal of Colloid Science. 18: 276–291.
Ostwald, W. (1897). Studien über die Bildung und Umwandlung fester Körper. Zeitschrift für Physikalische Chemie. 22: 289–303.
Papenhuijzen, J.M.P. (1971). Superimposed steady and oscillatory shear in dispersed systems. Rheologica Acta. 10: 493–502.
Papenhuijzen, J.M.P. (1972). The role of particle interaction in the rheology of dispersed systems. Rheologica Acta. 11: 73–88.
Payne, A.R. (1964). The elasticity of carbon black networks. Journal of Colloid Science. 19: 744–754.
Prausnitz, J.M. (1986). Molecular thermodynamics of fluid phase equilibria. Prentice Hall, New York, USA.
Reddy, S.Y., Full, N.A., Dimick, P.S., and Ziegler, G.R. (1996). Tempering method for chocolate containing milkfat fractions. Journal of American Oil Chemists Society. 73: 723–727.
Rohm, H., and Weidinger, K.H. (1993). Rheological behavior at small deformations. Journal of Texture Studies. 24: 157–172.
Rao, M.A. (1999). Rheological behavior of processed fluid and semisolid foods, in Rheology of Fluid and Semisolid Foods: Principles and Applications, M.A. Rao (ed.). Chapman & Hall, Gaithersburgh, Maryland: USA.

Rousseau, D., Hill, A.R., and Marangoni, A.G. (1996). Restructuring butterfat through blending and chemical interesterification. 2. Microstructure and polymorphism. Journal of American Oil Chemists Society. 73: 973–981.

Rousseau, D., and Marangoni, A.G. (1998). The effects of chemical and enzymatic interesterification on the physical and sensory properties of butterfat-canola oil spreads. Food Research International. 31: 381–388.

Rossell, J.B. (1967). Phase Diagrams of triglyceride systems, In, Advance in Lipid Research. Vol 5. R. Paoletti and D. Krichevsky (eds.). Academic Press, New York and London.

Sherman, P. (1968). The influence of particle size on the viscoelastic properties of flocculated Emulsions, 5th International Conference on Rheology, Kyoto, Japan, 327–338.

Rye, G.G., Litwinenko, J.W., and Marangoni, A.G. (2005). Fat crystal networks, in Bailey's Industrial Oil and Fat Products. 6th ed. F. Shahidi (ed.). Wiley-Interscience, Hoboken, New Jersey, USA.

Shih, W.H., Shih, W.Y., Kim, S.I., Liu, J., and Aksay, I.A. (1990). Scaling behavior of the elastic properties of colloidal gels. Physical Review A. 42: 4772–4779.

Small, D.M. (1986). The Physical Chemistry of Lipids, from Alkanes to Phospholipids, Vol. 4, Plenum Press, New York, USA.

Sonntag, R.C., and Russel, W.B. (1987). Elastic properties of flocculated networks. Journal of Colloid and Interface Science. 116: 485–489.

Tang, D., and Marangoni, A.G. (2005). Quantitative measurements of microstructure of fat crystal networks by microscopy and rheology methods. 96th AOCS Annual Conference Meeting, Salt Lake City. (Oral Presentation)

Tang, D., and Marangoni A.G. (2006). Computer simulation of fractal dimension of fat crystal networks. Journal of American Oil Chemists Society. 83:309–314.

Tang, D., and Marangoni, A.G. (2006). Quantitative study on the microstructure of colloid fat crystal networks and fractal dimensions. Advances in Colloid and Interface Science. 128–130: 257–265.

Timms, R. (1980). The phase behavior of mixtures of cocoa butter and milkfat. Lebensmittel Wissenschaft und Technologie. 13: 61–65.

Timms, R. (1984). Phase behavior of fats and their mixtures. Progressive Lipid Research. 23: 1–38.

van den Temple, M. (1961). Mechanical properties of plastic-disperse systems at very small deformations. Journal of Colloid Science. 16: 284–296.

van den Temple, M. (1979). Rheology of concentrated suspensions. Journal of Colloid and Interface Science. 71: 18–20.

Vreeker, R., Hoekstra, L.L., den Boer, D.C., and Agterof, W.G.M. (1992). The fractal nature of fat crystal networks. Colloids and Surfaces. 65:185–189.

Wesdorp, L.H., van Meeteren, J.A., De Jong, S., Giessen, R.V.D. Overbosch, P., Grooscholten, P.A.M., Struik, M., Royers, M., Don, A., de Loos, T.H., Peters, C., and Gandasamita, I. (2005). Phase Equilibria in Fats, in Fat Crystal Networks. A.G. Marangoni (ed.). Marcel Dekker, New York, USA.

Wille, R.L., and Lutton, E.S. (1966). Polymorphism of CB. Ibid. 43: 491–496.

Wright, A.J., Scanlon, M.G., Hartel, R.W., and Marangoni, A.G. (2001). Rheological properties of milkfat and butter. Journal of Food Science. 66: 1056–1071.

Wu, H., and Morbidelli, M. (2001). A model relating structure of colloidal gels to their elastic properties. Langmuir. 17: 1030–1036.

Chapter 18

Extrusion

Peter J. Lillford

University of York, Department of Biology, PO Box 373, York, YO10 5YW, UK,
PL8@york.ac.uk

18.1 Introduction

18.1.1 The Process: A General Description

Extrusion is a manufacturing process, common in many industries. As a unit operation it can be regarded simply as a shaping process where infinitely long fibres or semi-continuous anisotropic structures are formed, from a block or compacted dispersion. In the metals and plastics industry both "hot drawing" and "cold drawing" are performed. Both of these are known in the kitchen, where the equivalent of "hot drawing" is the formation of cheese fibres in a fondue, and "cold drawing" is the piping of icing sugar as cake decoration, or pasta production from dough. Forming into appealing shapes has also become part of the processing repertoire of ice cream, chocolate and dairy products.

It is evident that some knowledge of the properties of the extruded material must be known for these processes to work, such as the "melting temperature" of metals and plastics or the formulation of food dispersions which can be reliably formed into elongated stable structures.

Greater control and reliability of industrial processing is required, and so the science of rheology has been applied, measuring the flow and deformation characteristics of the materials in the forming process. Rheology measures the bulk properties of these materials and does not require any molecular description of the origin of forces between them, only the description of their performance. The next level of materials knowledge required is the colloidal or molecular interaction responsible for the flow behaviour. Otherwise, the interchange of components within a formulation can only be developed by costly empiricism.

18.1.2 The Process: Extrusion in Food Processing

In food extrusion, processes such as wet spinning, and even "spinneretless spinning" to form fibres need to be briefly mentioned (Tolstogusov 1988; Chapter 3 of this volume). These processes are equivalent to textile fibre spinning. They similarly operate on solutions of macromolecules and rely on gelation processes to form the continuous fibre. The molecular events taking place in the formation of fibrils are well understood because the range of temperatures, processes and moisture contents relate easily to conditions obtained in laboratory measurements, and these are reviewed elsewhere in this volume (see Chapters 3 and 13). Likewise, the spin dopes can be characterised rheologically allowing pressures, shear rates, flow rates etc to be controlled. For the engineer, these are the only characteristics required to allow predictive process control.

Fibre spinning techniques were primarily developed for the production of meat analogues. Unfortunately, their technical success did not result in cost competitive products and most of this type of extrusion processing has been shelved.

For the food processor, screw extruders present a cost competitive alternative, since they operate at high solids content, removing the requirements of soluble components and reducing the need for addition and removal of large amounts of water. Whilst the machinery was primarily developed by the plastics industry, the further advantage it offers in terms of manufacturing efficiency, by continuous or semi-continuous operation, are the same for food processing. Access to simultaneous control of heat and mass transfer within a single machine, allows great flexibility in choice of materials and the resultant product structure, so it was not long before the food industry adopted the machinery. In particular, cooker extruders are able to convert otherwise inedible cereal grains into snack products, breakfast cereals or meat like substitutes from protein flours and concentrates (see also Chapters 10, 14, 20 and 21). The extruder eliminates the former time consuming and labour-intensive batch processes of mixing, heating, forming and drying by performing them in a single piece of equipment. However, this simplicity of mechanical processing makes unravelling the details of molecular changes more difficult. The processing conditions for most products were derived empirically and it is not surprisingly, therefore, that work is still in progress to describe where and how unit operations such as mixing, melting, forming setting and cutting take place within this single engine.

Initially, the focus has been on the bulk properties of the extruded mass, such as rheology and rheological change within the processed materials. This allows predictive performance of the raw material formulation and a primary means of specifying ingredient performance and process control, and will be examined further below.

The second stage of understanding, relating these bulk properties to molecular changes in the raw materials and their role in determining product structure and properties, will be the focus of this review.

There is a further generation of extrusion products now emerging. This relates to the fact that extruders can apply an enormous variety of external variables such as pressure, shear and temperature to complex food materials. Extruders are now being used as chemical reactors, to activate or destroy enzymes (Cheftel et al. 1992). Also, their ability to transfer energy into preformed structures is being used to transform

traditional products even further from their equilibrium energy structure. For example, they can impart much reduced air cell and crystal size distribution in ice cream and chocolate products, thereby creating properties not seen before (Windhab 2002). Only by detailed understanding of how external variables influence final product properties via their effect on component molecular and microstructure will these processes become reproducible and therefore commercially viable.

18.2 Extruders and the Materials They Convert

It is almost always the case in industrial food production that its processing machinery is "borrowed" from other industries, and that our understanding of the relevant materials science of processing follows the empirical development of significant new products. Extruders and extrusion is a classic case.

The machinery has been borrowed from the plastics industry. An early single screw extruder was used in the 1940s to produce a snack product from maize grits but the operational advantage of twin screw machines was demonstrated later. It appears that they are more efficient in mass transport, less heat is dissipated, and therefore heat transfer can be better regulated by barrel heating (Lo et al. 1998).

In terms of the materials used, there is a major difference in the complexity of the feedstocks of food extrusion compared to synthetic polymers when one examines any level below that of the bulk rheology of the mix. For example:

Polyethylene is a man-made homopolymer. Its chemical synthesis is well understood. It is a random walk polymer with little secondary or tertiary structure. A batch can largely be characterised by its molecular weight distribution, and its rheology can be related to these parameters by developed rules of polymer behaviour. The action of specific chemicals as plasticisers can be used to modulate these bulk properties in a predictable way, allowing the nature and characterisation of its glass to fluid transition to be predicted.

Starch, on the other hand, is not simply a biopolymer, but a biological structure, whose composition and structure varies with botanical origin and the annual growth conditions. It is primarily comprised of two polymers, amylose and amylopectin, which have extensive secondary, tertiary and even quaternary structure. They can spontaneously phase separate on heating (Hermansson and Svegmark 1996) and amylopectin is variable in terms of degree of branching and branch lengths.

Even in its purified granule form, starch contains small amounts of lipids and proteins, some of which are active enzymes. It is highly hydrophilic so that the dominant plasticiser (water) is spontaneously absorbed and its breakdown products (small sugars) can also plasticise the total mass. Complete characterisation is almost impossible so standardisation of the source and the pre-processing steps such as milling are required. Even so, it is not surprising that molecular control of glassy and melt behaviour is only just beginning to be understood, (see Chapters 5 and 7) and the consequences of these first and second order molecular phase transitions on the subsequently rheology of any processing mix awaits a detailed examination.

Likewise, proteins are heteropolymers, having unique molecular architectures and organised structures, including casein micelles, multisubunit globular structures

(soya) and self assembling elastic networks (gluten). They denature and aggregate on heating, at critical temperatures. The existence of glass to fluid transitions present at high concentrations is only just being recognised, and the action of plasticizers, other than water and sugars, on their glass and melt behaviour has not been systematically studied. Cheaper raw materials such as flour are even more complicated, where various polysaccharides, proteins, sugars, salts and insoluble particles are also present.

Faced with all these unknowns, the food materials scientists cannot yet produce predictive and quantified models of materials behaviour in the extruder or of the post–die processes by which products are formed. Instead we concentrate here on the dominant molecular features that must be understood if even qualitative rules of behaviour and design can be stated. Fortunately, most food engineers now recognise the problem but still would like to attain the degree of predictive coupling between molecular formulation, rheology and product properties which plastics extrusion has to hand.

This need for a complete understanding, from molecules to product structure has been elegantly outlined. (Richmond and Smith 1987). This chapter will examine the status of our knowledge at each level. There are some answers, but much remains to be explained.

18.3 What Happens Inside the Extruder Barrel?

18.3.1 The Process Engineering Approach

In terms of physical form, a powder is hydrated, mixed, and transformed to a continuous liquid stream by the application of heat and shear. Residual hydrated granules and other particles may be present, depending on the starting composition and the degree of conversion. If the exit conditions just before the die are at pressures greater than atmospheric then stream driven expansion after the die is obtained. The properties of the extruding stream determine the nature and extent of expansion, making it all important to understand the conversion processes taking place within the barrel.

There have been many reviews of the mechanical operation of extruders in terms of the measured physical parameters of heat, pressure and work done (Kokini et al. 1992). This is not the first attempt to review the effects of processing on the physical chemistry of raw materials. We refer extensively to the previous reviews by Richmond and Smith (1987) and Guy and Horne (1988). Both took a forensic approach, examining bulk parameters such as temperature and pressure during extrusion in a single screw machine, then stopped the operation of the extruder and examined the effect on the processed raw material.

Richmond and Smith examined maize grits and showed extremely nonlinear increases of pressure and temperature along the barrel. Within the first two-thirds of the barrel length, the grits are hydrated, mixed and compacted, and pressures remain low. After compaction, pressures and temperature rise rapidly to ~100°C and >40 psi and result in a transformation to a starch continuum with embedded granules which

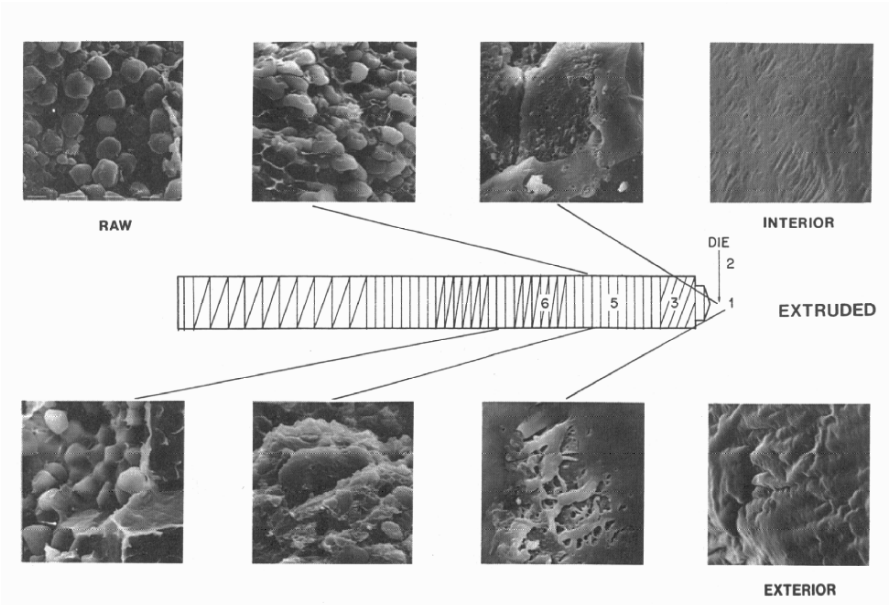

Figure 18.1. Structural change in maize grits. (From Richmond and Smith 1987, with permission.)

first develops at the high shear region of the barrel wall. The transient structures produced along the barrel length are shown below (Figure 18.1).

Clearly, mechanical work is being done on the material and the effects are "autocatalytic": the more work, the greater the structural damage, and as starch polymers are exuded into the mass, the greater the drag and disruption of remaining granules. Hence the pressure rise accelerates and energy is dissipated as heat into the mass. At the die, temperatures reached 160°C and the pressure 440 psi (approx. 3 Mpa or 31 atmospheres!).

Guy and Horne reported qualitatively similar behaviour for maize grits and wheat flour. They also identified a transition zone, where particles become deformable, so that air is excluded and a continuous mass is formed. They noted that wheat starch granules lose birefringence but remain visible at this point. Further shearing resulted in granule breakdown and the formation of a system continuous in exposed starch polymers, and entrained particles of other matter, such as protein and fibre.

Maize grits appeared to be less mechanically or thermally stable than wheat, their starch granules completely dispersing early in the transition zone. Because of the loss of birefringence and the destruction of starch granules, this transition is referred to as "melting" and allows the conditions of processing to be related to the molecular rearrangements within the components. It is also evident that the externally measured variables of pressure, temperature and flow rate are a result of the interaction between these transformations and the machine which operates at constant rotation rate. This means that the performance of an extruder is intimately linked to the raw material characteristics via the energy dissipation into an increasingly viscous con-

tinuum. The composition of the feed material is therefore vital to the entire transformation process. As a result, attempts have been made to correlate the work done on the material to the composition and resultant physical parameters (temp, pressure etc). This concept of specific mechanical energy (SME) input provides some simplification of all the geometric and local shear fields available from a variety of barrel and screw configurations. Guy and Horne showed the highly significant effect of the plasticiser content (water) on the SME applied to maize grits, and the resultant effect on bulk temperature.

Table 18.1. Extrusion cooking of maize grits showing variation in SME input and mass temperature in shear zone with moisture content.

Moisture (% wet wt basis)	SME input (kJ kg^{-1})	Mass temperature in shear zone (°C)
15	506	180
17	478	173
19	392	159
21	327	146
23	307	144
25	266	140
27	247	139

Extrusion conditions: feed rate, 800 g min^{-1}; screw speed, 300 rpm; twin dies, 4 mm diameter, barrel temperature profile, 25/55/120/150/150°C from feed port to die. From Guy and Horne (1988) with permission.

Viscous dissipation of energy clearly correlates with the primary variable of processing temperature throughout the length of the barrel, and since the structure within the flowing material is itself a function of moisture and temperature, the abrupt changes in structure along the barrel are in principle explained, by the "melting" of crystallites and the coincident disruption of starch granules. However, to provide a quantitative model, the material transformation as a function of material source, temperature, water content and shear needs to be defined, in three spatial dimensions and with time. As yet this cannot be done dynamically within the extruder, and depends on experimental simulation of the appropriate conditions in the laboratory. Simulations *in silico* are also possible and have been attempted for various configurations (e.g., Edi-Soetaredjo et al. 2003). In future, direct measurements to validate these models may be possible, by techniques such as tomographic imaging. Using MRI, shear profiles in constant temperature extrusion have already been reported (Choi et al. 2004 and references therein).

Because the performance within the extruder and the nature of the post-die extrudate will be influenced by the properties of the final viscous fluid produced, many workers have attempted to characterise the rheology of this melted mass (e.g., Jao et al. 1978; Akdogan et al. 1997). Since its structure is either that of a polymer melt or a dispersion of highly swollen particles within a polymer melt, then complex

rheology is to be expected. To measure flow properties directly, capillary or slit die rheometers have been attached to extruders. Most results have been interpreted in terms of power-law flow.

$$\eta_{app} = K\gamma^{n-1}$$

where η_{app} is the apparent viscosity, γ the shear rate, K and n are constants.

Since n is normally measured as 0.2–0.6 the liquids are referred to as shear thinning. (Note that for true shear thinning, this shear rate effect is reversible, whereas some irreversible damage may occur in most of these measurements.) Increasing temperatures also reduces K values, as does water (plasticiser) content. This form is certainly an oversimplification of the real melt rheology. Yield stresses may be exhibited at low shear rates and may be significant in low shear rate regions behind screw flights. As is the case for many polymer melts, the liquids have an elastic component, exhibiting large die swell, even when no bubble expansion occurs (Guy and Horne 1988). Therefore, whilst subsequent expansion by steam pressure correlates to a degree with the apparent viscosity, a much more careful analysis of the post-die expansion process is required and will be discussed later.

The rheology determines a distribution of residence time in the barrel, and the resultant heat transfer characteristics. Even with simple flow behaviour, finite-element modelling predicts greater shear rates and heating at the walls. This explains the observations by Richmond, that homogeneous melt structures first form at the wall, and further implies that on exit from the die, the melt stream may not be homogeneous with regard to its shear and/or temperature history.

18.3.2 The Materials Science Approach

Because direct dynamic measurements of materials state within the barrel are impossible, the structural and molecular changes relevant to extrusion must be measured "off-line" and related to real process conditions. In principle, we need to explain not only the effect of applied physical parameters of heat, shear and pressure, but also the effect of formulation. This is not yet possible, and for reasons stated above, the behaviour of carbohydrate (starch) dominated systems will be quite different from proteinaceous systems, since their heat denaturation behaviour and glass to rubber transitions are different in detail during their conversion from a moist powder to a continuous "melt."

Hydration: In most continuous processes, water is added and mixed into dry powder in the early stages of the extrusion screw. Whilst viscosities do not change significantly, there are physicochemical changes apparent which have been measured by differential scanning calorimetry (DSC). An extensive review of techniques applied to starch can be found in *Starch, Structure and Functionality* (Frazier et al. 1997). In extrusion, water is added up to 50% by weight, but more usually between 10% and 25%. Under these conditions, complete granule swelling cannot occur, but water does cause molecular rearrangement. In particular, as systems containing ~10–25% water are heated to around 50°C, on the first scan, an endothermic event is

observed. This is not present on cooling and immediate rescanning, but is recovered on storage.

This event has been named "stress relaxation" and does not involve gelatinisation or melting since it occurs not only for starch but other dried polysaccharides. Neither is a glass transition obvious in the first scan of native starches probably because of their high levels of crystallinity and low level of amorphous polymer content. Instead, the next major transition was at a much higher temperature (peak at ~150°C for maize starch containing 9.1% H_2O), and corresponds to the loss of long-range crystalline order. This is often referred to as the "melt temperature" (Gidley et al. 1993). A glass transition was observed when these samples were cooled to room temperature and rescanned. The centre of the second-order glass transition was found at ~90°C at the same moisture content. This transition is obviously relevant to the post-die cooling process, and will be discussed later.

The molecular origin of the stress relaxation endotherms is still currently unknown. They may relate to small conformational changes in any polymer as water is adsorbed. These occur very slowly at ambient, but show sharp transitions as temperature increases molecular mobility, allowing fast water mass transfer. However, the fact that they occur in many dried polysaccharide systems and have recently been observed in native and denatured soya protein (our unpublished results) is of great importance, since this first scan is equivalent to real extrusion processes. Secondly, these results indicate that for starch, even without shearing, barrel temperatures above 150°C will gelatinise (or melt) native starch, producing an amorphous material whose glass transition temperature is much below its original gelatinisation temperature. Thus, the subsequent rheological properties of the extrudate should not be related to the starting material, but to the gelatinised "amorphous" material.

Both this melt temperature and the glass transition of the resultant material are highly susceptible to the presence of plasticizers. The dominant species is water, but small sugars and salts may also have an influence (see Chapter 5). Nonetheless, it is clear that whereas the processes in the extruder barrel should be related to the effect of plasticizers on gelatinisation or melting, their effect on final product properties should be related to the glass transition of the amorphous molten extrudate.

Gelatinisation or "Melting" of Starch: Cereal grains contain a higher proportion of starch than protein, and high temperature extrudates are always continuous in starch polymer, with inclusions of protein and other particles (Hermansson 1988). The rheology in the barrel will therefore be dominated by the structural changes in starch, with the other materials acting as fillers.

The behaviour of cereal starch granules during gelatinisation in excess water has been widely studied. This process commences at around 65°C when crystalline order is lost. Solubilisation of amylose starts in the amorphous centre of the granules (Figure 18.2).

A second stage occurs at 90°C when amylopectin-rich granules swell and deform (Hermansson and Svegmark, 1996). These temperatures are altered by starch type, and the presence of small solutes; sugars elevate the gelatinisation temperature and ionic solutes exhibit varying effects related to their position in the Hoffmeister series.

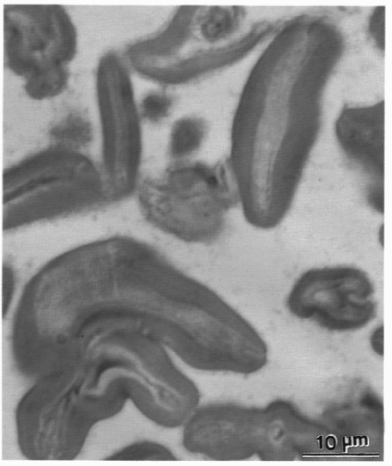

Figure 18.2. Initial solubilisation of amylose. (Fom Hermansson and Svegmark 1996, with permission.)

For example, 1.5M KCl elevates the DSC transition in pea starch, and separates the transition into a lower temperature B-type starch transition, and a higher A type. (Bogrecheva et al. 1997).

Unfortunately, there is little comparable detail on starch behaviour under extruder conditions, at low moisture. The previously cited scanning microscopy shows that at moisture contents of 25%, the SME imparted by the extruder is sufficient to form a starch continuum in most systems, and extrudates formed from maize grits extruded at 28% moisture 160°C and a die pressure of only 1 Mpa show homogenous polymeric cell walls (Donald et al. 1993).

Four further studies are of note, however:

(1) Chiang and Johnson (1977) examined wheat flour and found complex behaviour. Maximum gelatinisation occurs at high temperatures and moisture content as expected from static DSC measurements. Increasing screw speed *decreased* gelatinisation probably due to a decreased residence time and more limited heat transfer.
(2) Gomez and Aguilera (1983) showed that for maize flour, granule structure can survive, but at high levels of gelatinisation the whole extrudate appears homogeneous and significant dextrinisation (rupture of amylopectin and amylose molecules) occurs.
(3) Lai and Kokini, (1991) also measured the effect of high pressure on starch melting. The characteristic temperatures were increased—as would be expected for a process involving a net increase in polymer volume. Two separate enthalpy peaks were observed, possibly due to A- and B-type starches.
(4) In a series of recent experiments in this laboratory where flours were extruded at a moisture content of only 28%, residual ungelatinised starch, measured by DSC, was shown to be less than 10% for all barrel temperatures above 110°C.

Dextrinisation: The dominant polymers of starch (amylose and amylopectin) are very high molecular weight extended molecules subject to size reduction by shear and amylase degradation in dilute solution. Conditions in the extruder should rapidly deactivate amylase, but the very high shear conditions have been shown to reduce the average molecular weight (Colonna et al. 1984; Davidson et al. 1984).

The most degradation occurs at high SME and high temperature as expected. The size reduction only causes debranching of amylopectin, and probably some amylose fracture. Thus, high polymers remain present throughout and few oligosaccharides are formed, but this degradation has a significant effect on viscosity since, for extended linear polymers, viscosity is directly proportional to molecular weight.

18.3.3 Protein Extrusion

Using sources of materials with higher protein content, such as legume flours and concentrates, the continuous phase of the melt becomes protein, with inclusions of carbohydrate. Proteins from different sources are even more different in their molecular architecture than are starches, resulting in quite different performance during extrusion. Necessarily, we will examine them separately.

Milk Proteins: Dairy proteins and in particular caseinate-dominated mixtures spontaneously form fibres when "hot drawn" due to the temperature dependence of their rheology. This was developed into an extrusion technology, "melt spinning," in the 1970s and is described in detail elsewhere (Visser 1988). Spin dopes were formed by heating moistened caseinates to 80°C, and pumping through a multi-hole spinneret. Up to 40% of other components (gluten, soy protein, starch) could be added, and provided mechanical stability to the fibres which otherwise swelled extensively in aqueous or salt solutions. The process is not operated commercially due to the high cost of raw materials and the downstream assembly into meat analogues.

Soy, and Other Legume Proteins: Two quite different product types have been constructed by extrusion, high-density flaked structures for meat analogues, and lower density and crispy products for high-protein snacks. The latter uses conditions similar to that of starch-based cereal extrusion to obtain low bulk density in the expanded product; the former uses a higher water content in the extruder barrel and lower exit temperatures to obtain a dense material with open pores or even flaked structures. For these two types of processes, molecular changes in the extruder barrel are not dissimilar. Post-die structuring of the extrudates determines final product properties.

DSC of soy isolates show two distinct and different classes of behaviour. Where proteins are in the native state, distinct denaturation transitions from the 7S and 11S globulins are observed. For raw materials that have been denatured during their preparation by moist heat treatment or exposure to denaturing solvent conditions, no large endotherms associated with the native proteins are seen. (Morales and Kokini 1997) Glass transitions in soya proteins have been reported previously (Morales and Kokini 1997; Mizuno et al. 2000).

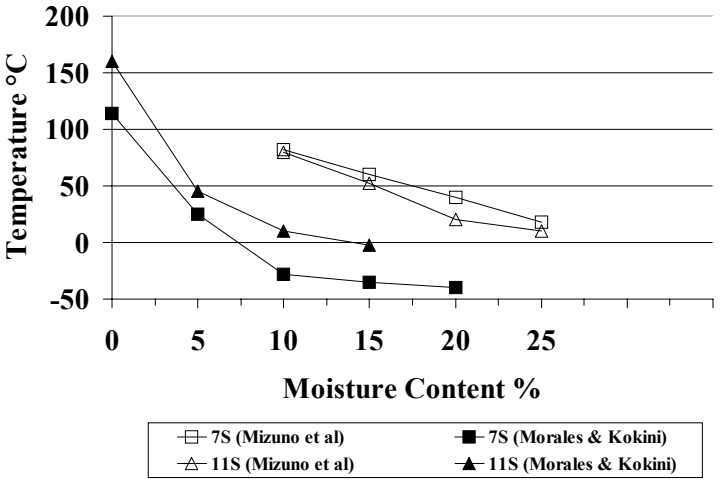

Figure 18.3. Glass transitions of soya proteins. (From Morales and Kokini 1997; Mizuno et al. 2000.)

These move up in temperature as water content decreases (Figure 18.3).

Notice that the reported data are not comparable, despite the fact that partially purified protein samples were used in both cases. It would appear that minor changes in the preparative procedure, such as addition of reducing agent, and/or the pH or buffer conditions used during drying, may have a major effect on the observed apparent glass transition. Neither do the authors report the presence of "stress relaxation" behaviour which we detected in the first scan of proteins at low moisture. This is shown below (Figure 18.4). At moisture contents within the hysteresis region of rehydration, the first scan shows an apparent exotherm, even though samples have been equilibrated for several days. On cooling and rescanning, this peak is not observed. Furthermore, its magnitude decreases and width increases as moisture content is increased. Since water is normally added to powder in the mixing stages of extrusion, this event must occur in all processing , and is not unique to soya protein.

The effect of small molecule plasticisers on glass transitions and denaturation temperatures has also been observed. Replacement of water by small sugars increases both the glass transition and denaturation temperatures (Kalichevsky et al. 1992).

The effect of ions on denaturation temperatures is well-studied for dilute solutions. Effects related to the Hoffmeister series are apparent. Unfortunately, no systematic studies of ions on protein glass transitions are available, and it cannot be assumed that these will have a negligible effect on the materials properties during extrusion.

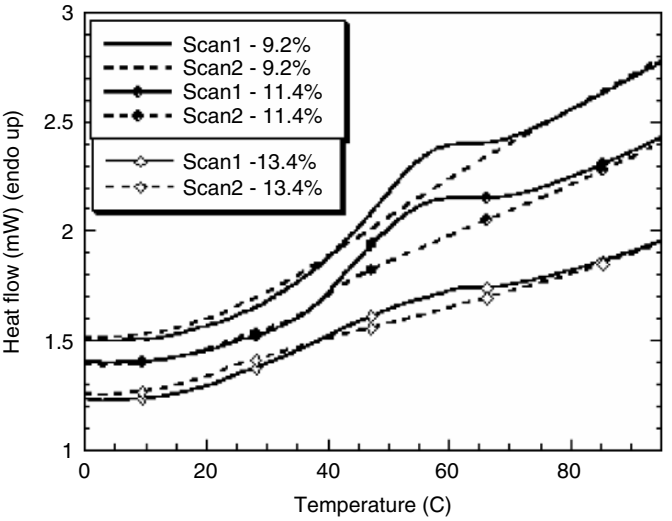

Figure 18.4. Soya 11S glass transitions at low moisture contents. The first scan was stopped at 100°C, the sample cooled and rescanned.

Unlike starch, even in their denatured state, proteins or their dissociated subunits maintain a globular structure. Size reduction by shear is very much less pronounced, so that electrophoretic analysis shows little change in subunit molecular weights between native and extruded materials.

18.3.4 Summary

We have identified the differences in molecular behaviour between proteins and starches, which must be understood if extrusion is to be systematically controlled.

Nonetheless, the extrusion of globular proteins do show some overall similarity with native starch if their molecular architecture is considered, as follows:

After hydration, a rise in temperature causes disruption of internal structure, for example crystallites in starch or folded structure in proteins. The extent to which this is achieved is determined primarily by a specific cooperative "melting" event, whose temperature is dependent upon moisture content and applied pressure. If these critical conditions are reached by any part of the flow stream, then shear can cause further fragmentation of both starch granules and the polymers released from them, whereas for proteins or their dissociated subunits, molecular weights remain largely unchanged. A polymer continuous melt is formed in both cases.

For pregelatinised starch or denatured proteins, no cooperative unfolding transitions are observed, and the systems are more similar to synthetic polymers. A similar plastic mass is formed, but in this case its formation is largely determined by the glass transition of the amorphous system and subsequent disruption of any hydrogen-bonded structures. This temperature depends primarily on moisture content, and the

width of the transition may be determined by different degrees of "randomness" present within different molecular species.

For both "melting" of native structures and glass transitions in pre-treated denatured materials, small solutes influence the transitions provided they are homogeneously and molecularly mixed into flowing mass. The influence of sugars and small polyols is known and the relative effects can be estimated by empirical relationships such as the equation of ten Brinke et al. (1983).

$$T_g = \frac{w_1 \Delta C_{p1} T_{g1} + w_2 \Delta C_{p2} T_{g2}}{w_1 \Delta C_{p1} + w_2 \Delta C_{p2}}$$

where w_1 is the weight fraction of the plasticiser, C_{p1} is the change in heat capacity at T_{g1}, its glass transition temperature, w_2 is the weight fraction of polymer and ΔC_{p2} is the change in heat capacity at the glass transition temperature, T_{g2}, for pure polymer.

The effects of ionic cosolvents are less well understood. For denaturation ("melting"), trends have been related to Hoffmeister series effects, but for glass transitions no systematic data exists.

18.4 What Happens After the Die?

It has long been the aim to relate the properties of the extruded product or half-product to the state of the extrudate as it leaves the die. We have noted that this is often attempted via the apparent viscosity of the melt but must fail if mixes are regarded as simple power law fluids. Elasticity in melts is easily demonstrated as "die swell," caused by elastic normal forces. This occurs with many cereal flours and protein/carbohydrate mixes (e.g., soya flour, grits and concentrates) and does not involve puffing, or gas expansion. It occurs immediately after the die and may relax before the structure is set. Nonetheless, die swell expansions of up to 200% have been recorded (Guy and Horne 1998).

18.4.1 Expanded Products

In most processes, some expansion by puffing of the flow stream by water vapour pressure is required to achieve low-density expanded products. Bubble expansion has been comprehensively reviewed recently by Kokini and Moraru (2003). The extent and nature of expansion of the structures so formed are critical to their subsequent use and in-mouth texture. Highly expanded structures (0.1 g/ml), when eaten dry, give crisp textures, which "melt in the mouth" as plasticisation by saliva causes their cell walls to collapse. Hardness increases as bulk density increases, but many of the denser products are designed to be eaten in a rehydrated state as meat-like analogue products. Not surprisingly, the rate of structure collapse on hydration also increases as bulk density decreases, since these materials are both hydrophilic and porous.

Capillary suction draws water into these structures, and moves their cell walls from a glassy to rubbery state as they hydrate.

Kokini et al. (1992) obtained a significant correlation between extrudate specific volume and pressure drop/viscosity ratios, particularly at moisture content below 25%.

Fan et al. (1994) proposed a simple relation between pressure, surface tension, extrudate viscosity, and bubble growth

$$dR/dt = R(\Delta P - 2\sigma)/4\eta$$

where R is bubble radius, ΔP is the pressure drop, σ is the surface tension and η the viscosity of the fluid. They attempted a mathematical model of bubble growth, which showed that pressure drop and viscosity were the dominant variables.

Guy and Horne (1998) report a detailed study of expansion as a function of barrel exit conditions. Firstly they note that even under conditions where melting of crystallites of starch should be complete, if shearing conditions are low, expansion is limited to 1–1.5 $ml.g^{-1}$ specific volume. This implies that for high expansions, the starch must not only be gelatinised but that its component polymers must be exuded into the continuous mass.

Expansion increases with increasing mechanical treatment (SME) at moisture contents between 15% and 27% and soluble starch levels also increase in the extrudate. Since SME also correlates with temperature in the shear zone, expansion is increased not only by the disruption of molten starch granules, but also by the reduced viscoelasticity of the melt, *and* the increased pressure of steam in the expanding fluid stream. Whilst this trend will be observed by varying SME on a single formulation it should be noted that SME is itself dependent on water content, declining as higher levels of plasticising water is added. Under these conditions where more steam pressure is available, expansion might be expected to increase, but this will *only* occur if the structure of the melt and its rheology are the same. However, since higher water contents *reduce* the disruption of starch granules by reducing shear in the barrel, a continuous homogeneous melt will not be formed. Therefore, there will be an optimum in expansion corresponding to a continuous melt state, high exit temperature and low resistance to vapour bubble growth in the matrix. High SMEs are indicative and in part causal for this condition, explaining why high specific volumes of extrudates often arise with low water content at coincidentally high SME (Figure 18.5).

Why do high expansions not occur when shearing of melted materials is low? The phenomenon needs to be considered in terms of the biaxial extension of the films around the expanding steam bubble. Bubbles will grow as long as the expansion does not exceed the fracture limit of the film *or* the expansion rate is not greater than any strain relaxation time of the expanding sheet. Where films comprise homogeneous starch polymer (or protein polymer) phases, this is likely to be optimal. Similar arguments have been presented by (Donald et al. 1993). The presence of particles, whether they be residual starch granules, protein inclusions or even added fibre will cause strain and stress concentrations to arise in the expanding film, and may cause premature rupture, particularly if the polymer film does not completely

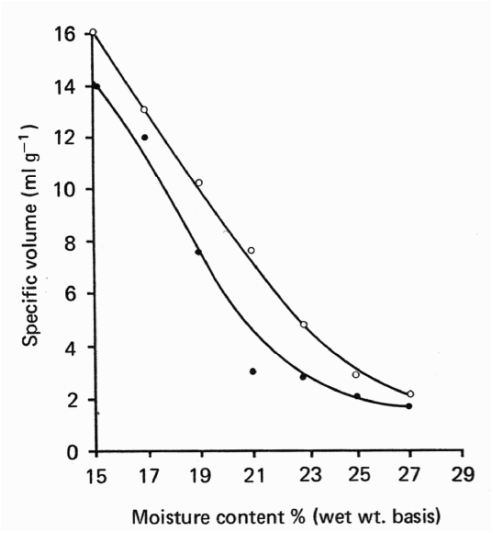

Figure 18.5. Specific volume and moisture content for maize grits extruded at 300 rpm, feed rate 800 g/min through ○, 3 or ●, 4 mm dies. (From Guy and Horne 1988, with permission.)

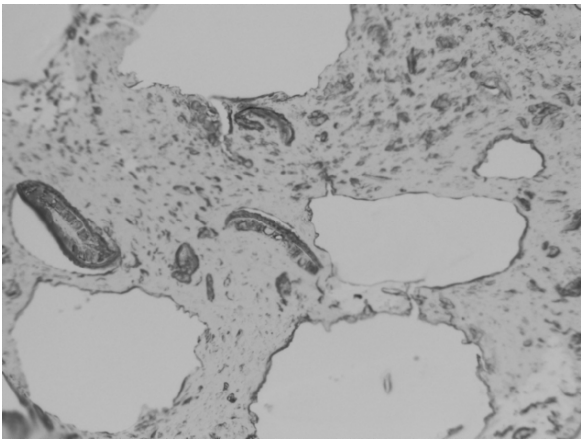

Figure 18.6. Location of particulates in expanded products. (Reprinted with permission of Dr. H. Chanvrier, *Food Science Australia* 2006.)

adhere to the included particle. Indeed bubble growth appears to be initiated at these weaker interfaces (Figure 18.6).

This may provide reasons for the observation that in the manufacture of whole bran products, the addition of 10% bran can cause between 10% and 50% decrease in expansion. (Andersson et al. 1981) Likewise, in materials subjected to lower SME where homogeneous polymer matrices are *not* formed, expansion is low and specific volumes are low. This is not only true for starch-based systems (see above) but also

for protein continuous systems. Here, if the fluid stream exiting the die consists of heavily swollen particles but a minimal continuous matrix, then extrudates are high density and consist of adhering particles rather than the expanded films produced at lower moisture contents.

The decrease in expansion seems to occur at moisture levels above ~30% moisture for both cereal (starch-based) polymer systems, and protein (soy grits). This corresponds to a point on their adsorption curves where water activity rises rapidly with added moisture; that is, at a level where the water added to a mix has little effect on primary hydration of polymers, but behaves as a diluent. In mechanical terms, this may be explained by proposing that at above levels of 25%–30% water plasticisation of the polymers is complete, and further added water acts as a lubricant, reducing the shear-induced temperature rise and particle damage necessary for the formation of homogeneous melts.

The expansion at the die is not the sole determinant of final product specific volume. Guy and Horne (1998) also report the extent of shrinkage on cooling of extruded maize grits (Figure 18.7).

Since steam is the driving force for expansion, as the products cool and steam condenses, an overpressure of up to one atmosphere is experienced by intact bubbles. It is not surprising that some collapse occurs. Rather, we need to explain why *no* collapse occurs under certain conditions. The process of bubble formation and stabilisation after the die is similar to the rise and collapse of cake batter during cooking and cooling, but at a much accelerated rate. We have shown previously, by gas per-

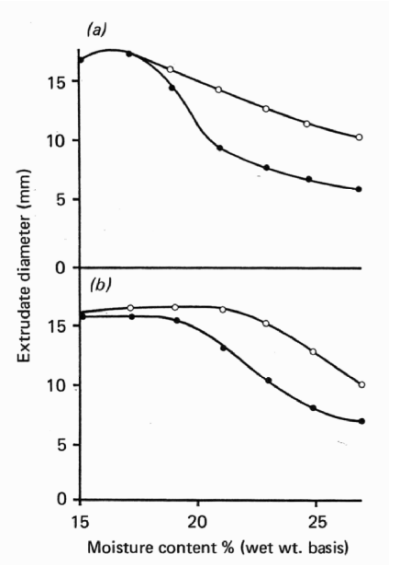

Figure 18.7. Expansion and shrinkage for products extruded as in Figure 18.5, diameters of extrudates when hot O and after cooling ●; (a) 4 mm dies; (b) 3 mm dies. (From Guy and Horne 1988 with permission.)

meametry measurements, that collapse in cakes while cooling occurs in less gas permeable regions of their structure, (author's unpublished results), that is, structures will always collapse unless the gas cells fracture and therefore become permeable to air as the steam condenses. Fracture of bubble cell walls will occur if their polymers form glasses as moisture content reduces by evaporation, and as cooling to ambient temperatures occurs, making them brittle and fractured by the atmospheric overpressure.

In extrusion, explosive expansion after the die causes rapid steam evaporation, dehydration and cooling. Those melts produced in the barrel at lower moisture content (below 15%) would be within their glassy region at room temperature, even without evaporative loss. The degree of shrinkage is most certainly related to the speed at which cell walls glass during evaporation and cooling. Thus bulk densities can be low for two reasons:

1. The gas cells leak or burst prematurely during steam driven expansion, *or*
2. The cells expand, but subsequently collapse because they do not burst during expansion, or crack during cooling.

Therefore, the water-dependent glass transition of the cell walls is a critical parameter in predicting the expanded structure, and this must be related to the material at the die exit, *not* the properties of the starting material. Similar arguments relating expansion directly to the moisture content dependence of extrudate T_g have been presented by Donald et al. (1993).

A simple attempt to correlate the two critical parameters of melt and glass transition temperatures of extruded raw materials with the structure of the final extrudate has been made. (Strahm et al. 2000). They measured glass transition temperatures (T_g) and melt temperatures (T_m) on a breakfast cereal formulation by rheometry. T_g's were observed as broad transition commencing at 67°C at 9.7% moisture and 14.6°C at 20% moisture. T_m's for the same formulations were 146° and 54.5°, respectively. While these temperatures are obviously relevant to mass flow, it is not obvious how they relate to molecular events. Comparable measurements by DSC and NMR on the same samples would be extremely illuminating.

Nonetheless, the correlations they obtained with product structure are very informative. The "melt penetration" was defined as the temperature above the T_m/moisture curve at the point of extrusion. (Note that from the arguments presented above, this parameter will correlate positively with both the steam-driving pressure for expansion and inversely with melt elasticity and viscosity, that is, conditions for rapid bubble expansion.) The second parameter measured was the moisture and temperature of the expanded product immediately after the die, and its value was compared to the midpoint of the measured T_g of the ingredient mix at the same water content.

They show an inverse correlation between "melt penetration" and bulk density for all but two of their experiments as expected, and for the two outliers, the post-die extrudate was above its glass transition even after cooling.

They report no microscopic structures of their extrudates, but from the extrusion conditions reported it is likely that homogeneous starch continuous melts were

formed in all cases, so it is reasonable to support their conclusion that the higher bulk density of the two anomalous high moisture samples is due to collapse rather than limited expansion.

These results are extremely informative, but it may well be that even simpler and more direct correlations can be made by relating the effective expansion process to the temperature above the melt temperature for any mix, since this correlates directly with the steam pressure and with thermal reduction of the "rheology" of the melt. The T_m/water content line should ideally be derived for material at the die exit rather than for the raw materials, since the effects of dextrinisation or particulate dispersion in the barrel would not be present in the raw materials. This can be done quite simply by measuring pretreated mixes. However, the fact that measurements of two state transitions (glassy and melting) of a formulation, one prior to extrusion and the second after it, are sufficient to predict raw material performance is remarkable, and deserves to be tested widely on other materials.

Furthermore if we know the effect, at least in direction, of small solutes, then design rules relating formulation and processing to product properties are beginning to emerge. No comparable experiments have been done for protein continuous systems, but there seems no reason why the same type of causal connections between formulation, state changes and product properties cannot be made.

One other parameter critical to product properties is the size distribution of the bubbles in the expanded product. Comparable bulk densities will be measured either with a few large bubbles or a large number of small ones. However, the rehydration and textural properties of the two structures will be markedly different. The distribution of bubble sizes relates to nucleation rather than growth. Frequently, the presence of insoluble particles in the melt is sufficient to cause multisite nucleation as shown in the above figure, but when this is not the case, small amounts of finely divided powder can be added to the formulation. Calcium carbonate is frequently used, acting as a weak point in the continuous melt, and also releasing gaseous carbon dioxide (personal communication, Charles Chessari, *Food Science Australia*, N. Ryde, Australia).

18.4.2 Meat Replacers

These products are usually made from formulations of high protein content (soya, meat particles, etc.), so the continuous phase at the die exit is proteinaceous, with inclusions of carbohydrate. These products are required to deliver a significant textural strength (bite) even when fully hydrated. Massive expansion and low bulk density is not required. Instead, a degree of "fibrosity" (anisotropic structure) is required to simulate meat. The early structures were extruded by processes similar to those discussed above, but with a deliberately low expansion. This was achieved by extruding with a higher moisture content and die exit temperatures below 100°C (Cheftel et al. 1992; Liu et al. 2005).

Meat-like texture relied upon the presence of a few limited bubbles within the structure providing failure sites for breakage during chewing. Not surprisingly, these products tended to have a "pasty" texture rather than exhibiting meat-like fibrosity.

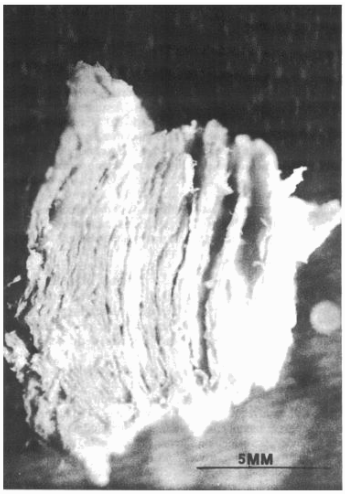

Figure 18.8. Meat analogue product from soya flour extrusion.

Later products employed "double extrusion." The viscous mass consisting of protein continuous and carbohydrate inclusions was extruded, with some air present, in long dies. The elongational shear produced layered structures with flake-like substructure (Figure 18.8).

This process is the equivalent of the water-based "spinneretless spinning" of gels referred to previously, but at high solids content, temperature and shear rates. Whereas the former method deforms phase-separated gels into anisotropic structures, the elongational flow in the extruder forms layers of protein, carbohydrate and air, which is particularly effective if elongated fibrous particles are present in the mix. A long barrel length allows relaxation of stresses in the flowing material, and the formation of a permanent anisotropic product structure.

18.5 Summary

Much of the published work on extrusion has attempted to correlate process conditions and formulation with final product properties. Correlations are almost always found, and may be systematic within the particular set of variables examined, but do not survive when further parameters are examined in other studies. This makes them of limited use in even qualitative explanation of product properties. Re-examination of published data, bearing in mind the effect of material states on the expansion process after the die, shows that there is a systematic explanation that can be related to the material properties of the extruded mass, during the dynamic formation of bubbles and cellular structures. However, because of the transformation of materials within the barrel, both at the microscopic and molecular level, it is unrealistic to expect test methods on raw materials alone to relate directly to product structures and

properties. The analysis provided here, presents a qualitative model which allows the use of offline physico-chemical measurements to evaluate the potential of any formulation to expand, form open or closed cell structures, or collapse, using laboratory physical test methods rather than extensive trial-and-error empiricism. It is hoped that future work will test this proposal extensively.

Acknowledgements. The author wishes to acknowledge a Flagship Fellowship grant from CSIRO during which this chapter was prepared. In particular, thanks for discussions and contribution are due to Jay Sellahewa, Charles Chessari, Aung Htoon, Manoj Rout and Helene Chanvrier, all of Food Science Australia, North Ryde.

18.6 References

Akdogan, H., Tomas, R.L., and Oliviera, J.C. (1997). Rheological properties of rice starch at high moisture content during twin screw extrusion. *Leben.-Wissen. Technol*, 30, 488–496.

Andersson, Y., Hedlund, B., Jonsson, L., and Svensson, S. (1987). Extrusion cooking of a high-fibre cereal product with crispbread character. *Cereal Chemistry*, 58, 370–374.

Blanshard, J.M.V., and Mitchell, J.R. (1988). *Food Structure: Its Creation and Evaluation*. Butterworths, London.

Bogrecheva, T.Y., Ring, S., Morris, V., Lloyd, J.R., Wang, T.L., and Hedley, C.L. (1997). The use of mutants to study the structural and functional properties of pea starch. In: P.J. Frazier, P. Richmond and A.M. Donald (Eds.) *Starch-Structure and Functionality*. Royal Society of Chemistry, London, pp. 230–237.

Cheftel, J.C., Kitagawa, M., and Queguiner, C. (1992). New texturisation processes by extrusion cooking at high moisture levels. *Food Rev. Int.,* 8, 235–275.

Chiang, B.Y., and Johnson, J.A. (1977). Gelatinisation of starch in extruded products. *Cereal Chemistry*, 54, 436–443.

Choi, Y.J., McCarthy, M.J., and McCarthy, K.L. (2004). MRI for process analysis: co-rotating twin screw extruder. *J. Process Anal. Chem.* 9(2), 72–84.

Colonna, P., Doublier, J.L., Melcion, J.P., de Monredon, F., and Mercier, C. (1984). Extrusion cooking and drum drying of wheat starch. *Cereal Chemisty*, 61, 538–543.

Davidson, V.J., Paton, D., Diosady, L.L., and Laroque, G. (1984). Degradation of wheat starch in a single screw extruder. *J. Food Sci.,* 49, 1154–1157.

Donald, A.M., Warburton, S. C., and Smith, A.C. (1993). Physical changes consequent on the extrusion of starch. In: J.M.V. Blanshard and P.J. Lillford (Eds.), *Glassy State in Food,* Nottingham University Press, Nottongham, UK, pp. 375–393.

Edi-Soetaredjo, F., Nashed, G., Rutgers, R.P.G., and Torley, P.J. (2003). Numerical analysis on the effect of extrusion conditions on flow in slit die rheometer. *3rd Int. Conf. On CFD in Minerals and Processing Ind.,* CSIRO, Melbourne, Australia, pp. 300–302.

Fan, J., Mitchell, J.R., and Blanshard, J.M.V. (1994). A computer simulation of the dynamics of bubble growth and shrinkage during extrudate expansion. *J. Food Eng.* 23(3), 337–356.

Frazier, P.J., Donald, A.M., and Richmond, P. (1997). Starch-structure and functionality. *Roy. Soc. Chem.* Special Pub. 205.

Gidley, M.J., Cooke, D., and Ward-Smith, S. (1993). Low-moisture polysaccharide systems: thermal and spectroscopic aspects. In: J.M.V. Blanshard and P.J. Lillford (Eds.), *The Glassy State in Foods,* Nottingham University Press*,* Nottingham, UK, pp. 303–316.

Gomez, M.H.. and Aguilera, J.M. (1983). Changes in the starch fraction during extrusion–cooking of corn. *J. Food. Sci.,* 48, 378–381.

Guy, R.C.E., and Horne, A.W. (1988). Extrusion and co-extrusion of cereals. In: J.M.V. Blanshard and J.R. Mitchell (Eds.), *Food Structure: Its Creation and Evaluation,* Butterworths, London, pp. 331–349.

Hermansson, A.-M. (1998). Gel structures in biopolymers. In: J.M.V. Blanshard and J.R. Mitchell (Eds.), *Food Structure: Its Creation and Evaluation,* Butterworths, London, pp. 25–40.

Hermansson, A.-M., Kidman, S. and Svegmark, K. (1995). Starch, a phase separated biopolymer system. In: S.E. Harding, S.E. Hill and J.R. Mitchell (Eds.), *Biopolymer Mixtures,* Nottingham University Press, Nottingham, UK, pp. 225–245.

Jao, Y.C., Chen, A.H., Lewandowski, D., and Irwin, W.E. (1978). Engineering analysis of soy dough rheology in extrusions. *J. Food Process. Eng*. 2, 97–112.

Kalichevsky, M.T., Jaroszkiewicz, E.M., and Blanshard, J.M. (1992). Glass transitions of gluten. 1: Gluten and gluten sugar mixtures. *Int. J. Biol. Macromol.,* 14, 257–266.

Kokini, J.L., Chang, C.N., Lai, S. (1992). The role of rheological properties on extrudate expansion. In: J.L. Kokini, C.-T. Ho, M.V. Karwe, (Eds.), *Food Extrusion Science and Technology*, Marcel Dekker, New York, pp. 631–653.

Kokini, J.L., and Moraru, C.I. (2003). Nucleation and expansion during extrusion and microwave heating of cereal foods. *Comp. Revs. Food Science Food Safety*, 2, 120–138.

Lai, L.S. and Kokini, J.L. (1991). Physico chemical changes and rheological properties of starch during extrusion. *Biotech. Progress* 7, 251–266.

Liu, S.X., Peng, M., Tu, S., Li, H., and Cai, L. (2005). Development of a new meat analog through twin screw extrusion of defatted soy flour–lean pork blend. *Food Sci. Technol. Int.,* 11(6), 463–470.

Morales, A., and Kokini, J.L. (1997). Glass transitions of soy globulins using differential scanning calorimetry and mechanical spectrometry. *Biotechnol. Prog.* 13, 624–629.

Mizuno, A., Mitsuiki, M., and Motoki, M. (2000). Effect of transglutaminase treatment on the glass transition of soy protein. *J. Agric. Food Chem.* 48, 3286–3291.

Richmond, P., and Smith, A.C. (1987). Rheology structure and food processing. In: J. Blanshard and P.J. Lillford (Eds.), *Food Structure and Behaviour,* Academic Press, New York, pp. 259–283.

Strahm, B., Platner, B., Huber, G., and Rokey, G. (2000). Application of food polymer science and capillary rheology in evaluating complex extruded products. *Cereal Foods World,* 45(7), 300–302.

Svegmark, K., and Hermansson, A.-M. (1991). Distribution of amylose and amylopectin in starch pastes: effects of heating and shearing. *Food Structure,* 10, 117–129.

Ten Brinke, G., Karasz, F.E., and Ellis, T.S. (1983). Depression of glass transition temperatures of polymer networks by diluents. *Macromolecules*, 16, 244–299.

Tolstogusov, V. (1988). Creation of fibrous structures by spinneretless spinning. In: J.M.V. Blanshard and J.R. Mitchell (Eds.), *Food Structure: Its Creation and Evaluation,* Butterworths, London, pp. 181–196.

Visser, J. (1988). Dry spinning of milk proteins. In: J.M.V. Blanshard and J.R. Mitchell (Eds.), *Food Structure: Its Creation and Evaluation,* Butterworths, London, pp. 197–218.

Windhab, E.J. (2002). Ultra low temperature ice cream extrusion (ULTICE): a novel technology for the manufacture of ice cream. *Abstract*, *Ann. Meeting and Food Expo*., Anaheim, California.

POLYPHASIC FOOD SYSTEMS

Chapter 19

Structuring Dairy Products by Means of Processing and Matrix Design

Ulrich Kulozik

Technische Universität München, Chair for Food Process Engineering and Dairy Technology, ulrich.kulozik@wzw.tum.de

19.1 Introduction

Dairy products can be classified in terms of their base structures as either gels (such as yoghurt and cheeses), emulsions (such as milk, cream or butter), or foams (such as whipped cream or whipped desserts). Many dairy products (such as ice cream), however, are comprised of more than one structural property, that is, they may contain features of a gel, an emulsion and a foam next to each other.

These structures are based on the technological functionalities, that is, on the molecular capabilities of ingredients, proteins or fat in particular, to create these structures. Molecular capabilities, such as interfacial activity or the capacity to aggregate and to form gels, can be influenced by processing means to enhance the functional behaviour or to avoid partial losses of functionality. This is illustrated in Figure 19.1, indicating that molecular ingredient properties and processing unit operations normally applied in structure formation reactions equally play important roles in food manufacture. The scheme is meant to demonstrate that matrix design and process design go hand in hand in the formation of structured products, that is, emulsions, gels, foams or mixtures thereof. Molecular properties can be influenced by processing means to achieve or induce structural or biological effects. The real situation, of course, is by far more complex, since interactions between ingredients and their diverse reactivity upon processing conditions are usually difficult to predict.

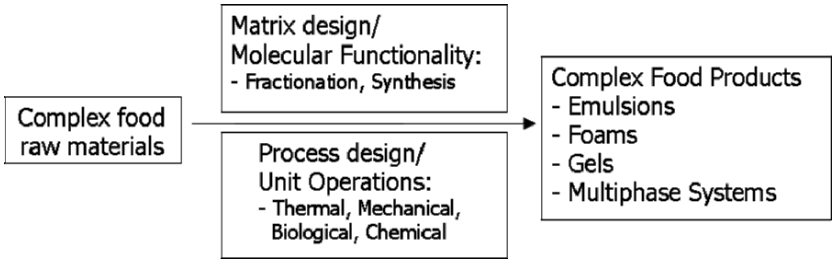

Figure 19.1. Creation of food structures by matrix and process design.

The following sections review the established knowledge related to the principal mechanisms of structure formation in protein based or fat-based systems before more recently developed options for structure formation will be described in more detail.

19.2 Protein-Based Structures

The primary structuring components in milk and dairy products are proteins. Eighty percent of the milk protein belongs to the casein fraction. Casein, in most cases, dominates the formation of product structures and is present in milk in the form of a molecular assembly called the casein micelle. The outer shell of the spherical micelle is comprised of a hydrophilic shell, the κ-casein fraction, which carries a glycosylated peptide making the casein micelle hydrophilic, whereas the inner core of the micelle contains the more hydrophobic α_s- and β-fractions. The micelle is stabilised by various factors, the most important being calcium–phosphate bridges and hydrophobic interactions. Various models exist to characterise the inner structure of the casein micelle (Phandungath 2005), so-called coat–core models, subunit models and internal structure models, the most widely accepted ones being the so-called sub-micelle model first established by Morr (1967) and the calcium–phosphate cluster model established by Holt and Horne (1996), De Kruif and Holt (2003) and Horne (1998).

Approximately 20% of the total milk protein is made up by the whey protein fraction, which is less dominating in the formation of structures, but can nevertheless play a decisive role in the optimisation of structural properties due to the capability of the globular β-lactoglobulin (β-lg) and α-lactalbumin (α-la) sub-fractions to unfold and to form aggregates amongst themselves or as co-aggregate together with the casein fraction. In terms of the physico-chemical details of milk proteins, reference is made to Fox and McSweeney (2002), who have thoroughly reviewed the state of knowledge.

Figure 19.2 summarises the most important features of the casein micelle and β-lg. Both the micellar casein and the globular β-lg depend in size and structure on pH and thermal conditions. Processing and compositional factors thus induce a considerable variability in molecule size, which needs to be taken in account when trying to establish structure–function relationships or in membrane separation, where the molecule size influences retention.

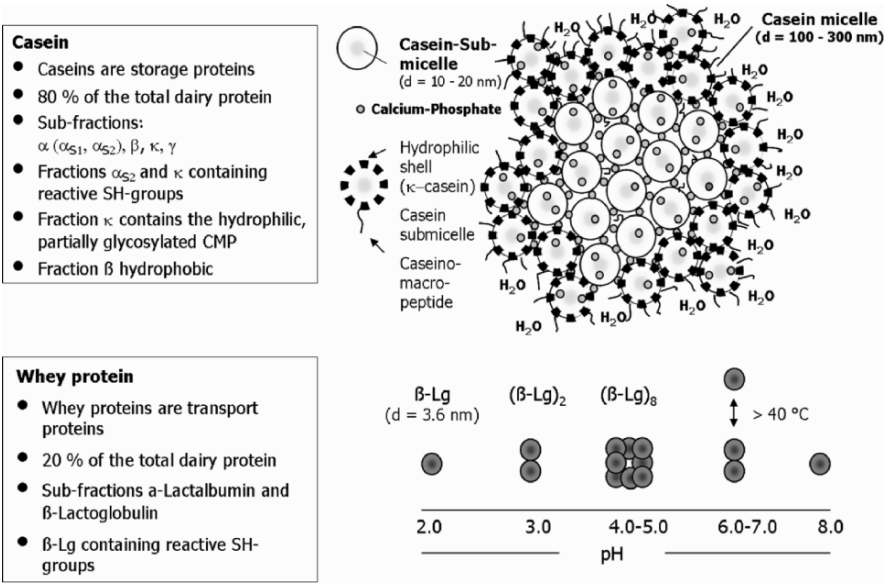

Figure 19.2. Structural properties of the casein micelle and β-lactoglobulin.

Various mechanisms are used to generate protein based dairy products:

1. Enzymatic cleavage of hydrophilic peptides from casein.
2. Isoelectric coagulation of milk proteins, mainly of caseins.
3. Thermal aggregation and thermal coagulation of milk proteins.
4. Interfacial stabilization of protein based foams.

19.2.1 Enzymatic Coagulation of Casein by Chymosin

The mechanism of enzymatic structure formation by means of chymosin is key in the manufacture of many cheese products. In milk, the casein micelle with a size of up to 300 nm is colloidally stable. The enzymatic process removes the hydrophilic shell of the casein micelle by releasing the hydrophilic caseinomacropeptide (CMP) into the aqueous outer environment, thus rendering the remaining para-casein micelle sensitive to calcium assisted aggregation and coagulation, as shown in Figure 19.3. Following aggregation, the resulting gel is cut into pieces to separate the coagulum from the aqueous phase (whey). It is then further mechanically and thermally treated to induce syneresis of the gel particles. The gel particles are thereafter transferred into forms shaping the cheese body where they are pressed to fuse and form the cheese. Depending on the intensity of mechanical and thermal treatment the gel properties of the resulting cheeses vary quite considerably, as demonstrated by the spectrum of various cheese types, that is, hard cheeses such as Emmental-type cheese, or soft cheese such as camembert. Other factors playing an important role are the gelification rate, calcium supply, thermal milk pretreatment and protein concentration. For further details see Brulé et al. (2000).

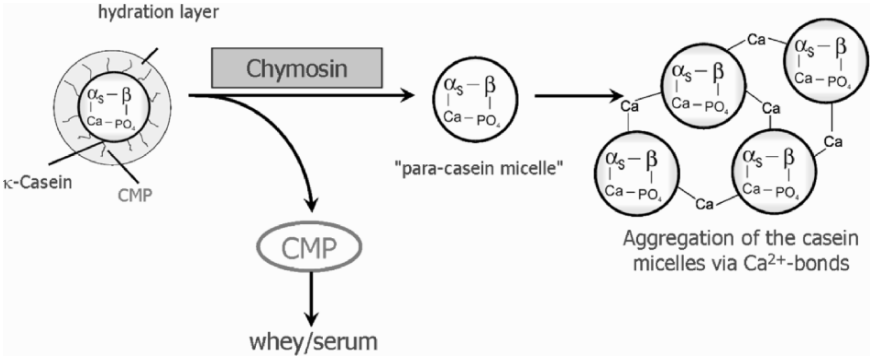

Figure 19.3. Sketch of the enzymatic coagulation of casein based on the action of chymosin.

19.2.2 Coagulation by Iso-electric Flocculation

In progressive microbial fermentation processes, milk acidification results in the formation of smooth and homogeneous gels known from products such as yoghurt or desserts based on yoghurt, but also in fresh cheeses. Upon acidification the charge distribution within the casein micelle is modified, thus reducing the surface potential of the casein micelle and lowering the repulsive forces between micelles, while at the same time molecular reorganisations take place. The micelle loses its amphiphilic character and a reduction of hydrophobic links within the core of the casein micelle contributes to structural changes resulting in the formation of a coagulum. A sponge-like insoluble protein network is formed immobilising the aqueous phase in its cavities. The molecular bonds stabilising the network are summarised as van-der-Waals forces attracting the network forming protein particles while repulsive forces are lowered. The structural behaviour in terms of gel stability, serum binding capacity and mechanical sensitivity mainly depends on acidification velocity, the protein and fat content, but also on a variety of processing factors. In particular, upstream milk treatment by means of homogenization and milk heating play decisive roles in the properties of the acidification based gel as is demonstrated in the following sections.

19.2.2.1 Effect of Milk Pre-Heat-Treatment Prior to Acidification

The iso-electric coagulation of the casein fraction is the key element in the structure formation in acidified dairy products, while the whey protein fraction is less sensitive to acidification. Nevertheless, a targeted thermal pretreatment aiming at denaturation (aggregation) of the whey proteins of 90%–99%, β-lg in particular, results in a significant improvement of the gel properties compared to yoghurt gels produced from milk with undenatured whey proteins or lower degrees of denaturation. Gel firmness and serum-binding capacity can thus be increased quite considerably, as was shown by Dannenberg and Kessler (1988).

Figure 19.4 depicts texture analyzer penetration curves of yoghurt gels obtained from milks, which were differently pretreated to produce degrees of β-lg denaturation between 10% and 99%. Whey protein denaturation follows a two-step reaction, unfolding followed by aggregation of the unfolded molecules. The reaction was found to be rate limited by either of the two steps, depending on the temperature regime. Below approximately 90°C the unfolding step is rate limiting, above 90°C it is the aggregation step as can be seen from the denaturation iso-effect lines (Figure 19.6).

As can be seen, denaturation degrees of β-lg increasing from 10% to 99% raise the resistance to penetration, that is, increase the gel firmness significantly. Figure 19.5 includes additional data for degrees of denaturation between 30% and 100% and compares skim milk (sm) yoghurt with whole (wm) milk yoghurt. As demonstrated, the gel resistance against penetration increases up to a point very close to complete β-lg denaturation. It is also of influence whether the heating was conducted at higher temperatures around 110–130°C or around 85–90°C. While the loss in gel resistance as a function of degrees of denaturation beyond 90% is pronounced at 110–130°C the effect is less obvious at 85–90°C. In summary, the gel properties are improved by

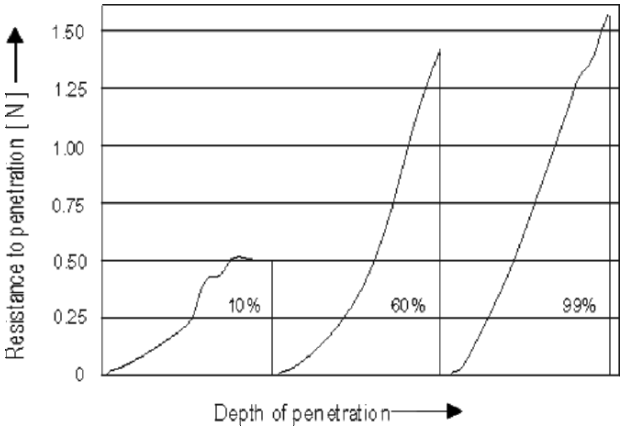

Figure 19.4. Penetration profiles for yoghurt gels produced from milks with different degrees of whey protein denaturation (related to β-lg) (Dannenberg 1986).

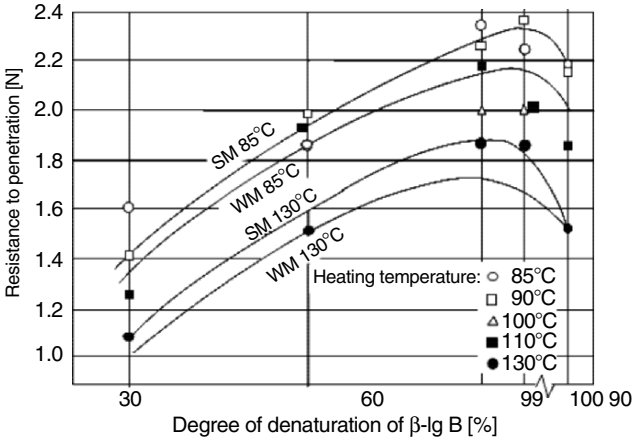

Figure 19.5. Resistance to penetration of a yoghurt gel as a function of the degree of β-lg (genetic variant B) denaturation resulting from milk heating pre-treatment; sm: skim milk, wm: whole milk (Dannenberg 1986).

the heat induced denaturation of the whey proteins, which, by way of co-aggregation together with the caseins upon acidification, become an additional constructive element of the gel network.

As a result of these data yoghurt manufacture today basically applies the conditions included by the dotted area as shown by Figure 19.6 with the milk pretreatment taking place at T/t-combinations in the range 80–100°C/2000-60 s, as was concluded by Dannenberg (1986) from his experiments on the optimisation of yoghurt structure. The linear iso-effect curves refer to the degree of denaturation of β-lg.

19.2.2.2 Effect of Yoghurt Milk Prehomogenization

Next to stabilising the fat globule to avoid creaming during fermentation homogenization also positively influences the yoghurt texture. Figure 19.7 schematically summarizes findings related to the manufacture from yoghurt from whole milks which were differently pretreated by heating and/or homogenization. The gel structure of whole milk yoghurt is thought to be a result of various combinations of heat treatment and homogenization of the yoghurt milk. The gel produced by unheated milk is thin, rough, grainy and has a low serum retention capacity.

Homogenization generates a higher number of smaller fat globules whose new membranes consist to a large extent of casein as secondary fat globule membrane material which, upon fermentation, become part of the finely meshed network as a result of pH decrease and acid coagulation in the form of a sort of support junctions, while in the case of unhomogenized milk the fat globules more or less remain unconnected. In other words, the combination of whey protein denaturation and homogenization was found to result in optimized properties of whole milk yoghurt.

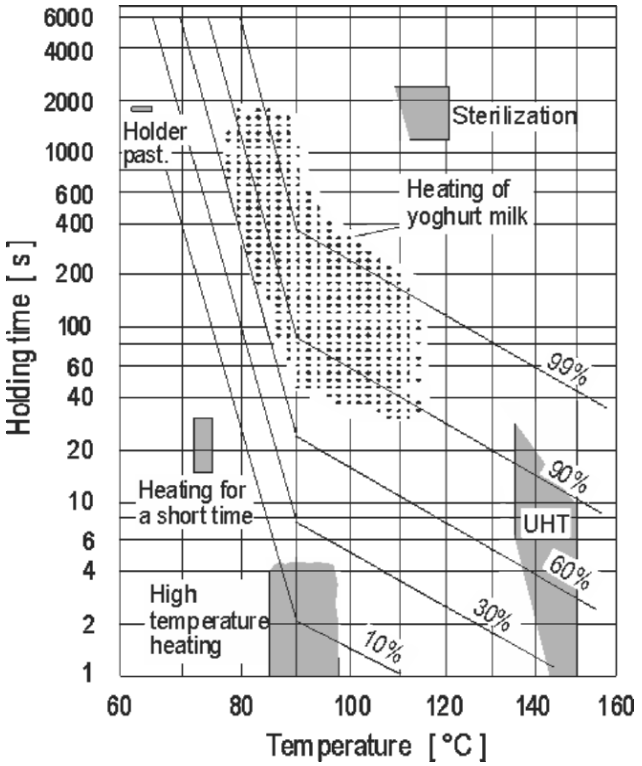

Figure 19.6. Heating temperatures and holding times for yoghurt milk pretreatment. The dotted area indicates the conditions preferable to optimise the gel structure according to Dannenberg (1986).

Established knowledge is also that the protein content is an important factor. In regular yoghurt manufacture, the dry matter or protein content is normally increased by 1%–3% to obtain the required textural attributes, the processing means presented above being options to lower the required protein addition to the minimum.

19.2.3 Heat-Induced Gel Formation by Milk Proteins

Irrespective of specific product systems to be produced, principally the same heat induced reaction between whey proteins and caseins resulting in gels from co-aggregated particles can be applied. Important factors in this respect are the calcium level and the casein/whey protein ration as was found by Kennel (1994) and Beyer (1990), key results are summarized in Kessler (2002). Figure 19.8 depicts the gel firmness as a function of the calcium content for two heat-induced gels with different casein/whey protein ratios. Whey protein solutions with a casein/whey protein ratio of 5/95 produced gels with a clearly reduced firmness as their calcium content was increased, with structures similar to a sandy cream. Solutions with a casein/whey

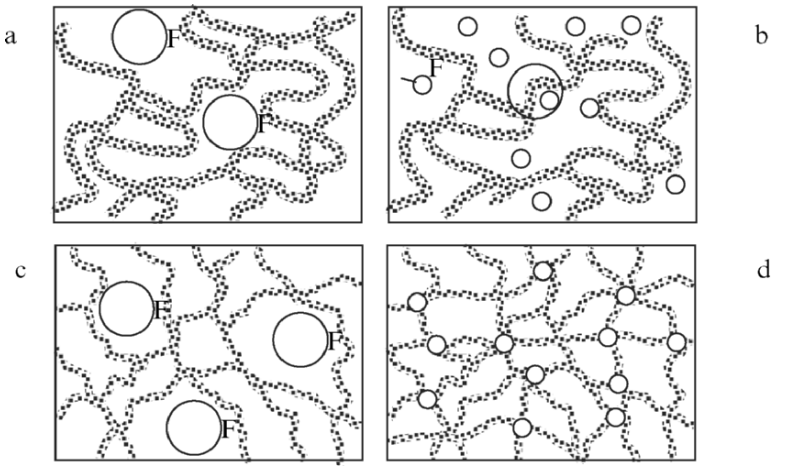

Figure 19.7. Schematic of four yoghurt milk pretreatment combinations, (a) related to not heated/not homogenized, (b) related to not heated/homogenized, (c) related to heated/not homogenized, (d) related heated/homogenized (FG: fat globule).

protein ratio of 35/65, however, produced particularly firm gels as continuous homogeneous network as the calcium content was increased.

19.2.4 Milk Protein–Based Foams

In producing dairy-based foams two principal options exist to make use of surface active components, proteins or fat, the latter one being discussed in Section 19.3. Observations comparable to pouring beer into glasses are made in filling skim milk

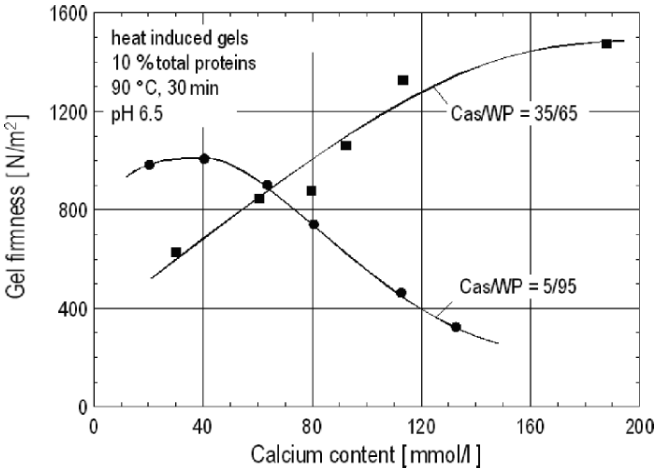

Figure 19.8. Gel firmness of heat-induced gels as a function of calcium content (Kessler 2002).

into packages, where foaming problems result in problems related to a correct high-speed filling operation. The problem is related to the fact that milk proteins are surface active agents being able to spontaneously occupy air bubble interfaces. This is being exploited in gastronomic cappuccino machines, where an in situ formation of cappuccino foams takes place.

19.3 Fat-Based Structures

19.3.1 Butter

Butter is made from sweet or cultured cream, that is, from oil-in-water (*O/W*) emulsions, which is converted into a water-in-oil (*W/O*) emulsion where fat forms the continuous phase with water droplets being finely dispersed as the discontinuous phase (Kessler 2002). Depending on the concentration of fat or water droplets different structural properties can be established. Butter is a highly concentrated fat system of about 82% fat and 18% aqueous phase. To turn the cream into butter a three-step procedure is normally applied:

Preparation of the cream in a churning process to produce fragile fat globules by crystallizing the higher fat fractions in a so-called physical "ripening" process prior to high shear treatment. The physical ripening process consists of a sequence of temperature holding steps to create a fat globule with a thin shell of crystallised fat just behind the native fat globule membrane. This procedure makes the globule fragile and mechanically sensitive to be broken up and to release the fat, which then acts as an aggregation aid to induce the entire fat phase to coalesce.

The next step is mechanical high shear treatment to break up the fat globule membrane. The fat then coalesces and the bulk aqueous phase (butter milk) are removed together with the fat globule membrane material to concentrate the fat.

The remaining water is finely distributed across the fat phase by a kneading or extrusion process. During this phase aroma compounds, for example, lactic acid fermentation extracts, can be added to modify the taste profile in case sweet cream was used to produce the butter.

19.3.2 Foam (Whipping Cream)

In contrast to protein stabilized foams the foam formation and stabilization mechanisms in whipping cream are supposed to depend on the bubble stabilization by means of fat rather than proteins. The fat content can therefore not be less than 30% butterfat, and whipping cream is expected to fulfil certain criteria, namely whipping time, foam firmness, foam volume increase (or overrun), and volume of dripping-off (or drainage).

The physicochemical models consistent with foam formation and stabilization are derived from the work on pasteurized and UHT processed milk-creams advanced by Besner (1997). Foam formation and stabilization can basically be explained as a multistage process, with some significant differences between non-homogenized (pasteurized cream) and homogenized (UHT cream) systems. These differences

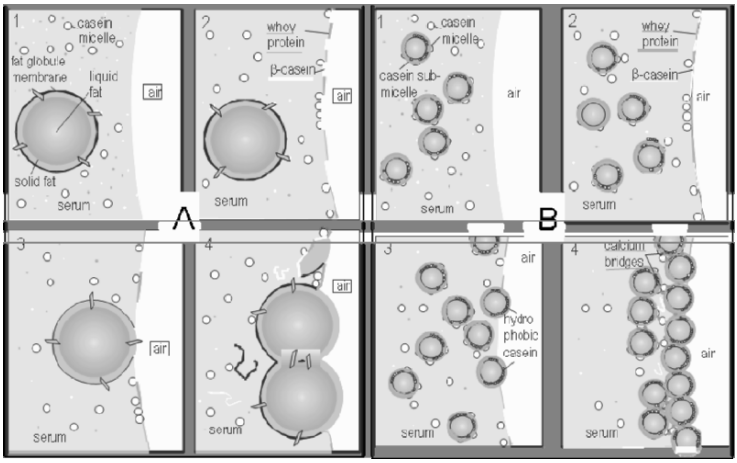

Figure 19.9. Sketch of the bubble interface stabilization (A. nonhomogenized cream; B. homogenized cream) (Besner 1997).

originate from the size and state of fat globules in each particular system prior to whipping, that is, air incorporation into cream in the form of large air-bubbles. Cream contains fat globules with a median diameter $d_{50,3} \approx 4$ µm in non-homogenized, pasteurized cream and ≈ 1 µm in homogenized UHT cream. Fat globules are either covered by the native fat globule membrane or by a modified membrane including proteins from the bulk phase as a result of the newly formed protein layer around the fat globules upon homogenization. Very rapidly, proteins adsorb at the gas–liquid interface, a diffusion-controlled process, enhanced by the mechanical action and convective transport mechanisms to obtain the maximum overrun within a few seconds.

During the whipping process, in the case of unhomogenized cream, fat globules partially lose their fairly instable protein layer. The liquid fat inside the fat globule now covers the newly formed air bubble interface to create a more stable situation at the interface. In case of homogenized UHT cream the fat globule membrane cannot be easily removed and fat globule stability against mechanical stress is favoured. According to Besner (1997) calcium bridges form aggregates of protein-covered fat globules to create a situation typical for a so-called "Pickering emulsion," where the surface of hydrophobic particles or bubbles is covered by solid particles. Figure 19.9 illustrates the different situations in whipping nonhomogenized and homogenized creams.

19.4 Complex Structures: Ice cream

Ice cream is a very heterogenic dispersed three-phase system consisting of a liquid, a solid and a gas phase. The liquid aqueous phase, originally the ice cream mix, contains the solutes including the proteins, sugars and stabilizers. Upon freezing part of the water is converted into ice crystals, which form a solid phase together with the

fat globules, which are solid at the temperature of the frozen system. Prior to freezing, gas is injected into the ice mix, which becomes dispersed as air bubbles and evenly distributed in continuous phase. Ice cream is normally produced in three steps:

1. *Preparation of the ice cream mix*: including homogenization, pasteurization and ripening at about 4°C to allow full hydration of proteins and hydrocolloids present in the mix.
2. *Partial freezing in the freezer*: Ice cream mixes are frozen in continuous freezers applying mechanical agitation and large temperature differences to achieve as small as possible ice crystals. The mix enters the freezer after the required amount of air was injected. Given that exit temperatures are normally not below –3.5 to – 7°C, only part of the water becomes frozen.
3. *Final freezing and hardening*: To obtain the typical textural properties of ice cream and to enable longer periods of storage the partially frozen, still soft ice cream is filled into the finished product containers, further cooled down, and thus hardened, down to temperatures of –15 to –25°C such that 80%–90% of its water is finally frozen.

The mouth feel of ice cream strongly depends on the size distribution of the ice crystals (Trgo et al. 1999). Therefore, the resulting size distribution achieved through rapid cooling in production should be retained throughout distribution and storage. Crystals above 50 μm in average diameter are sensorically undesired. Changes in the size of the crystals can occur, because they are thermodynamically instable. Recrystallization or the phenomenon of Ostwald-ripening result in crystal growth over storage, at the expense of smaller ones, especially if temperature fluctuations during transportation cannot be avoided. Single or multiple intermediate temperature step changes are particularly damaging since this mainly affects the outer parts of the packages and there is no way of reforming small crystals at the conditions salient in ware houses etc.

19.5 Developments in Microstructure Engineering of Dairy Products

19.5.1 Thermal Processing

Thermal processing has been long established as a key step in producing microbially stable products. Examples shown in the paragraphs above also include thermal processing as a means to influence structure formation in dairy-based products. Whey proteins, β-lg and α-la are particularly heat sensitive and can be affected by heat in a targeted manner to make use of their potential to create or optimise food structures. Lead substance, in many cases, is β-lg due to its heat sensitivity, to characterise the denaturation (aggregation) based effects.

19.5.1.1 Whey Protein Particulation and Applications in Food Matrices

The reaction of β-lg upon heat treatment, that is, the complex unfolding and aggregation reaction of the originally globular protein, can also be induced in whey. In this

case, however, it is not the casein micelle surface providing the reactive partner. In whey, the proteins react amongst themselves and form particulated whey protein aggregates. Depending on the reaction conditions, several options exist to create whey protein particles (WPP) with novel and specific functional properties which can be exploited by using WPP in food formulations as a structuring agent. Figure 19.10 schematically depicts the unfolding reaction of β-lg and the exposure of reactive SH-groups, which are the key for the formation of aggregates by means of S-S- bridges between unfolded molecules. If this thermal reaction is induced while simultaneously shear is applied, for example, in a scraped surface heat exchanger, the size of the resulting aggregates can be controlled.

Size as well as inner structure of the WPP depend on the reaction conditions in terms of the temperature regime and the medium composition. As shown by Plock et al. (1997) and by Spiegel (1999), the lactose content in the aqueous phase is of great influence. Figure 19.11 shows the resulting aggregate size of the WPP,

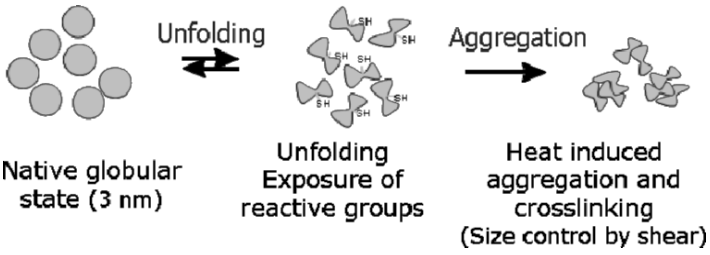

Figure 19.10. Denaturation of β-lg in whey under the influence of heat and shear.

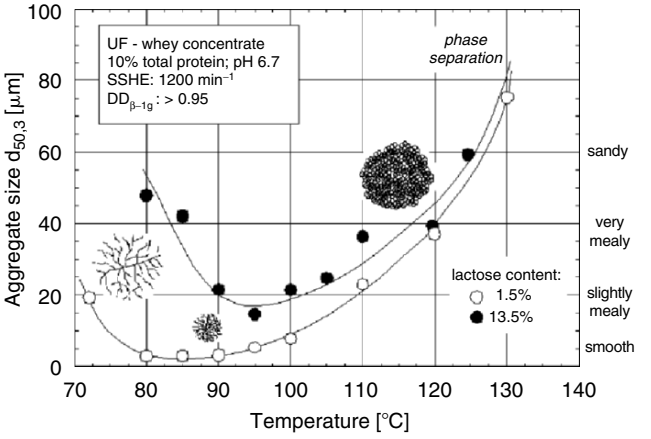

Figure 19.11. Whey protein particulation under various temperature conditions and serum compositions (SSHE: scraped surface heat exchanger; DD: degree of denaturation) (Plock et al. 1997; Spiegel 1999).

expressed as mean particle size $d_{50,3}$, as a function of temperature and lactose concentration. Lactose content and temperature both have a strong influence on the aggregate size. As was concluded from serum holding capacity data, also their internal structure varies with changing heating conditions and serum composition.

Such WPP can be used to enhance product textures by making use of the functional properties of WPP, such as serum binding capacity (Figure 19.12), as long as their size does not exceed approximately 20 μm to prevent undesired mouth feel sensations.

Figure 19.13 depicts the meltdown behaviour of ice creams with different compositions. In experimental situations, 50% of the skim milk powder was replaced by whey protein in the form of either conventional whey protein or WPP (Koxholt et al. 2001).

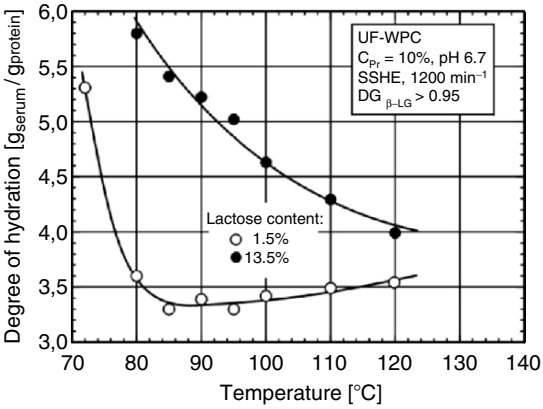

Figure 19.12. Effect of temperature and lactose content on the degree of hydration of WPP (Spiegel 1999).

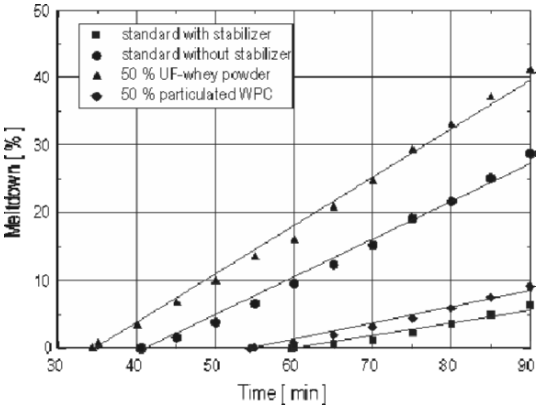

Figure 19.13. Meltdown behaviour of ice creams with different compositions (Koxholt 2000).

Some other factors play an important role in this particulation reaction, namely pH, calcium and ionic environment, protein concentration and heat exposure time so that a very complex set of variables can be used to steer the reaction towards a desired point. For instance, these circumstances can be considered to let individual whey proteins aggregate selectively as shown in the next section.

19.5.1.2 Thermal Fractionation of Whey Proteins

Specific WPP can be produced based on the individual sensitivities of α-la or β-lg to heat as was shown by Kulozik et al. (2003) and Tolkach and Kulozik (2005). Figure 19.14 shows the denaturation reaction rate constants of β-lg and α-la as a function of lactose content and protein concentration. As can be seen, β-lg and α-la react quite differently under these conditions. Depending on the medium composition either one of the proteins can be preferentially denatured, that is, aggregated, while the other one mostly remains native in solution. The aggregated protein can easily be separated from the mixture, for example, by microfiltration. The diagram also reminds of the typical compositions of whey (low protein content, high lactose), and of different whey derivatives such as whey protein concentrates (WPC: high protein, high lactose content) or isolates (WPI: high protein, very low lactose content) which differ in protein and lactose contents quite considerably and, hence, their thermal behaviour varies accordingly, as experience with supposedly similar materials shows. This also needs to be taken in account when comparing different study results on the thermal reactivity of the same molecule under various conditions.

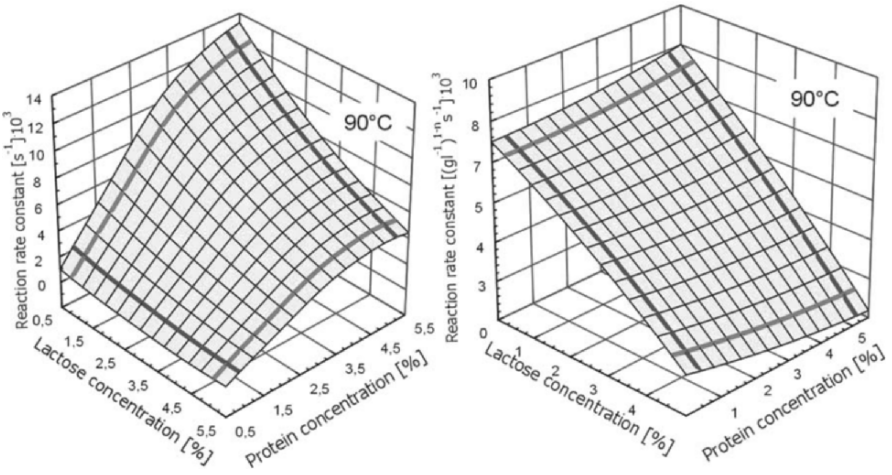

Figure 19.14. Reaction rate constants for β-lg (right) and α-la (left) under various medium conditions upon heat treatment at 90°C (Kulozik et al. 2003).

19.5.1.3 Multistage Reactions in Gel-like, Protein-Based Systems

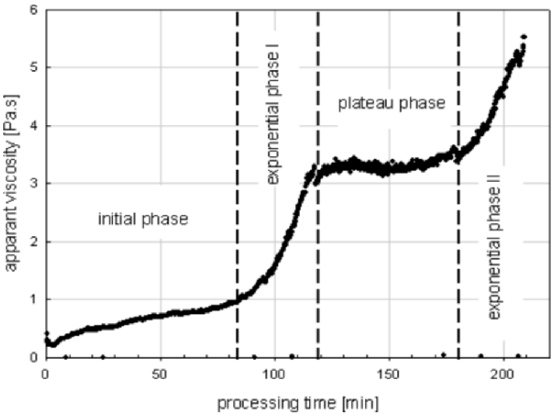

Figure 19.15. Course of structure formation in a high-protein dairy-based system.

A peculiar four-stage scheme of a structure formation course of different protein-based systems, high in protein concentration was assessed by Röck and Kulozik (2006) by an inline viscosity assessment in a small scale reaction chamber with the stirrer as a probe directly linked to the rheometer. A typical new structure formation course, not been reported until now, was obtained. The apparent viscosity is plotted as a function of the processing time. This typical progression is explained in Figure 19.15.

At present, it is unclear why the reaction in our investigation goes through stages, and it is under investigation which reactions control the individual stages and how the different factors influence the typical viscosity course. To provide an answer to some of these questions the following factors were varied and studied with regard to their impact on the structure formation. First, the influence of the fat content in the range up to 20% was examined. The dry matter differences between fat levels were balanced out with lactose. The influence of the fat content is presented in Figure 19.16. The same characteristic shape of curve was found with the absolute viscosity levels as a function of time depending on fat content. Obviously, the fat droplets in the system have an impact on the reaction, although the source of the structure build up is thought to be protein-based. Therefore, the effect of the protein content was assessed. As expected, a higher level of the protein content in the continuous phase increases the probability of networking and gel formation as also shown in Figure 19.16.

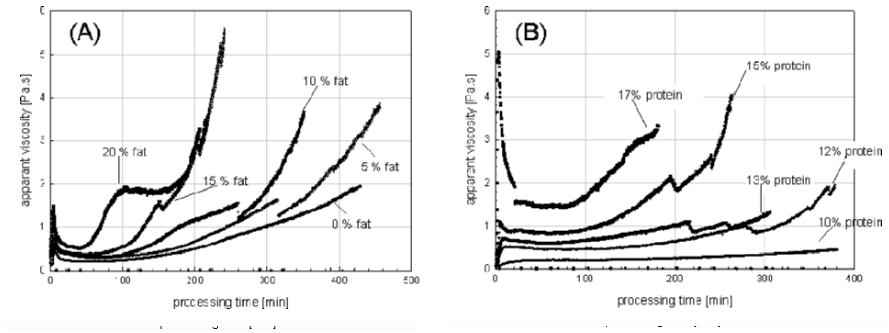

Figure 19.16. Effect of the fat (a) and protein content (b) on the multistage reaction scheme.

Efforts to visualize the structure formation reaction by means of electron micrographs delivered an interesting observation: While at the start of the reaction the protein seems to be enriched at fat droplet interfaces, a reduction in protein concentration around fat droplets seems to have taken place (Figure 19.17). The proteins seem to approach a more stable situation assembling a network within the continuous phase, rather than staying at the interface, which seems to explain the viscosity increase.

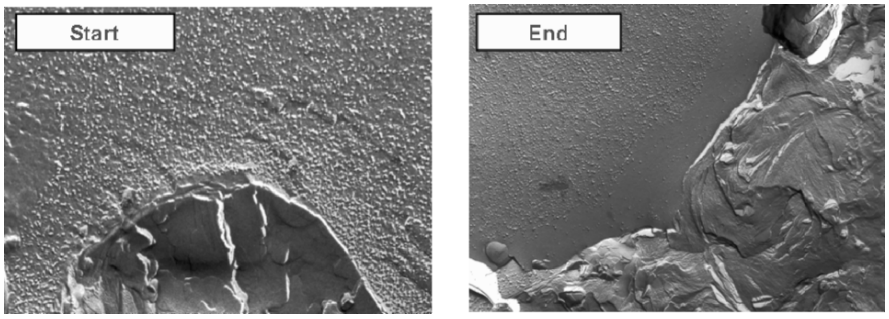

Figure 19.17. Electron micrographs taken from samples at the beginning and the end of the time course of the multistage reaction.

In total, many factors play important roles, the results so far obtained suggesting that a very complex multistage reaction is responsible for the course of reaction. Processing factors such as temperature, shear rate, prehomogenization of the fat phase and compositional factors such as pH, protein and fat content and others play important roles. Image and chemical analysis should shed more light on the mechanisms behind this multistage reaction in protein-based systems such as cream cheese or processed cheese. This kind of reaction scheme has not been described in literature so far. Understanding the basics behind it should open new ways to optimise structures and to increase formulation robustness against processing variations.

19.5.2 Ultrahigh Pressure Technology

A still emerging technology offering alternatives and new ways to influence dairy product properties is ultrahigh pressure (UHP) technology, operating at static pressure levels between 200 and 1000 MPa. Under UHP the volume compression effect in water occurs and affects intramolecular chemical bonds in and between proteins, for instance. As a result these bonds can either be weakened or enforced such that, for instance, hydrophobic bonds in biological membranes or the tertiary structure of enzymes are deteriorated (Hinrichs 2000). This effect has been investigated by Rademacher et al. (2002) and Rademacher and Hinrichs (2002) for the inactivation of micro-organisms and structural effects of biological membranes.

19.5.2.1 Pressure-Induced Texture Generation

Hinrichs (2000) and López-Fandiño (2006) studied and reviewed the effect of UHP on protein structures that result from treating milk concentrates, WPCs and individual milk protein fractions, that is, casein micelles and whey proteins separately from each other. As demonstrated by these investigations milk protein concentrates can be coagulated even without renneting or acidification. Figure 19.18 provides an impression of the impact of UHP on casein micelles (protein concentration 10%) at a maximum pressure level of 600 MPa and both at different holding times and pressure release rates. Gels with variable strengths are formed, depending on hold times and downward pressure ramps. Whey proteins were found to react differently on UHP building different structures and aggregating selectively like in thermal treatment such that, depending on conditions, the individual whey proteins can be fractionated.

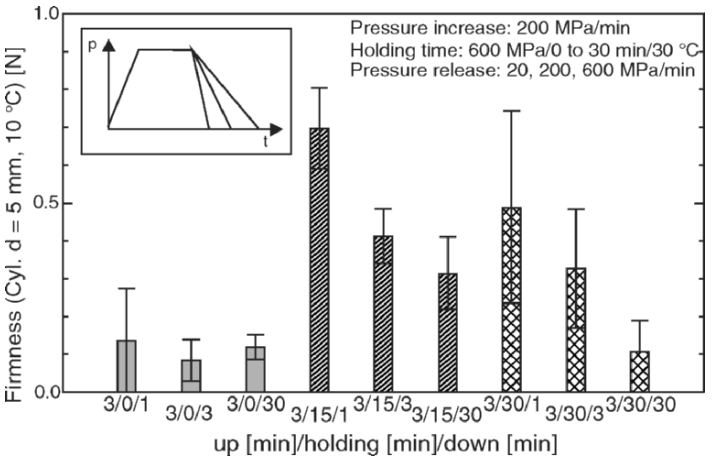

Figure 19.18. Gel strengths of casein micelle suspensions after UHP treatment (Fertsch et al. 2003).

19.5.2.2 In Situ Observation of UHP-Induced Changes in Casein Micelles

To discriminate between reversible and irreversible UHP-induced structural changes in the casein micelle size distribution in situ dynamic light scattering experiments using an optical cell were performed (Gebhardt et al. 2006). Below, further in situ light scattering experiments in combination with ex-situ atomic force microscopy in a liquid cell are presented. Figure 19.19 shows normalized particle size distributions at various pressures. The solid lines denote the *z*-averaged size distribution obtained by an "unweighted" inversion of the correlation function. The correlation function is thus biased by heavy particles $\propto n \cdot M^2$, where M denotes the molecular weight and n is the density number. The most probable diameter amounts to 220 nm, and the distribution is about 100 nm wide. Similar numbers were reported by Anema et al. (2005).

At 100 MPa the turbidity has nearly vanished, since the particle size has been reduced to 20 nm. A large fraction of the casein micelles is decomposed into smaller fragments dominating the number average up to 200 MPa suggesting the existence of stable "mini-micelles." Above 250 MPa the micelles dissociate further forming particles with d = 3 nm, most likely the casein monomers. Releasing the pressure induces limited reassociation to particles with d = 5 nm, the native micelle is not recovered.

Figure 19.20(a) depicts the time evolution of the back-scattered light intensity scattered by a turbid casein solution following different pressure steps. An increase in pressure leads to a drop in scattered intensity, indicating a particle size reduction. The intensity reaches a plateau within 300 s, depending on the pressure level. The plateau decreases with pressure, suggesting increasing dissociation into fragments. The intensity reaches a minimum value at 300 MPa, the final state of pressure-induced dissociation. Figure 19.20(b) shows the effect of pressure release: At 50 MPa the signal recovers indicating full reversibility. In the range of 120–250 MPa, the intensity curves converge to a common plateau, which is significantly lower than

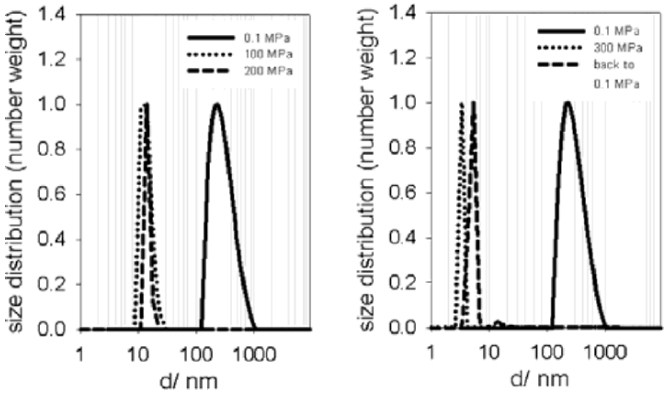

Figure 19.19. In situ particle size distribution versus pressure (Gebhardt et al. 2006).

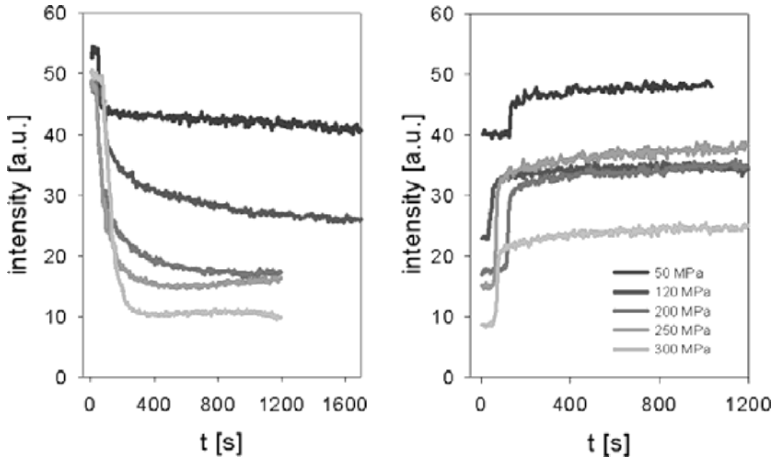

Figure 19.20. In situ pressure dissociation-association kinetics of casein-micelles after a pressure jump monitored by the average back-scattered light intensity: (a) dissociation upon pressure increase; (b) reassociation upon pressure release (Gebhardt et al. 2006).

the original value at 0.1 MPa. Above 300 MPa, where the casein micelles dissociate completely into subunits, only a small recovery of the intensity is observed.

The results of the pressure cycle experiments are summarized in Figure 19.21. The symbols represent the final states of association, which are achieved under pressure exposure and after pressure release. Increasing the pressure leads to a continuous decrease in the final degree of association and a regular transition curve. In contrast to that, pressure release leads to three discrete states: Two well-defined irreversible protein fragments and the reconstituted micelle (Gebhardt et al. 2006).

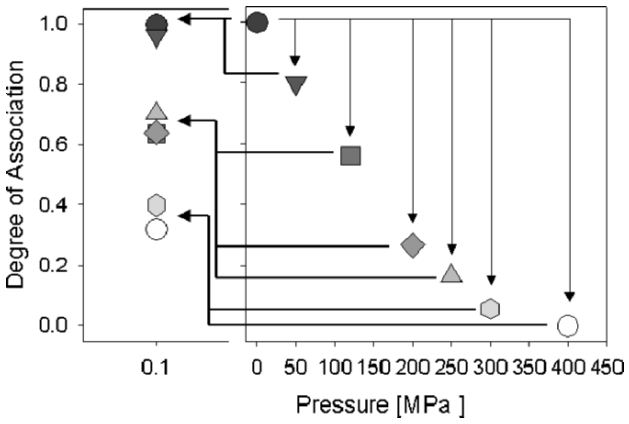

Figure 19.21. Dissociation–association cycle of casein micelles. Pressure dissociation (vertical arrows), reassociation (horizontal arrows) upon pressure release (Gebhardt et al. 2006).

To elucidate the surface morphology and size distribution of pressure treated casein micelles and their irreversible fragments, AFM experiments were performed. The samples were pressure-treated for 30 min in discrete steps (0.1–400 MPa) across the dissociation transition (Figure 19.22). Instead of a continuous evolution of the structure with pressure three characteristic morphologies can be observed: The native micelles, existent up to 50 MPa, appear to be composed of sub-elements, suggesting

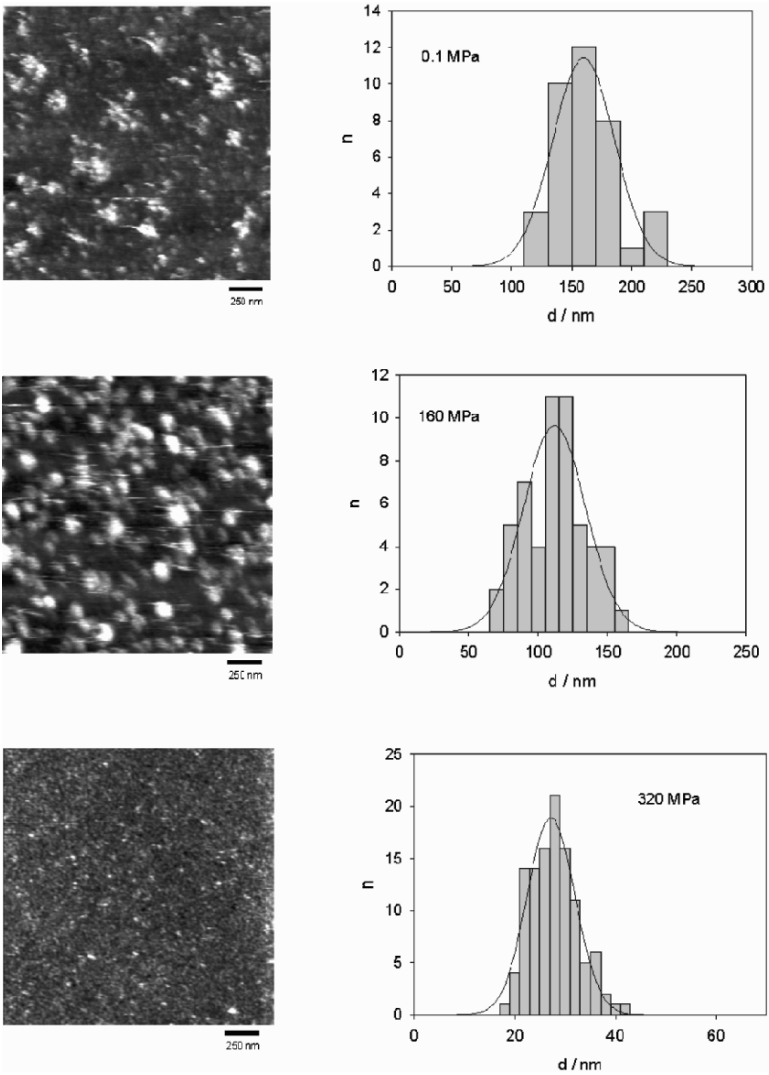

Figure 19.22. Structures of pressure-treated casein micelle (Gebhardt et al. 2006). (See Color Plate.)

a rather inhomogeneous morphology. They exhibit little sub-structure and are less easily perturbed by the AFM tip. Finally, the AFM images of samples exposed to pressure levels above 280 MPa do not show any micelles. Only particles with diameters near 20–30 nm persist. In summary, the in-situ measurement and offline AFM analysis clearly indicate that native casein micelles can be transformed into novel structures, whose value and potential benefits still remain to be fully exploited or appreciated.

19.5.3 Enzymatic Protein Cross-Linking

The generation of stability- and texture-improved product structures of proteinaceous systems can further be enhanced by enzymatic cross-linking. Functional properties of hydrocolloids could thus be replaced or extended by proteins in addition or instead of improving the native functional properties by heat or pressure induced changes. Enzymatic cross-linking of proteins by means of transglutaminase (Tg), which is widely applied in the meat industry already, is still an emerging technology in the dairy industry. Tg catalyzes the formation of covalent bonds by means of an acyl transfer reaction between proteins provided, they contain the amino-acids glutamine as an acyl-donor and lysine as an acyl-acceptor, as shown in Figure 19.23.

Among the milk proteins the casein fraction, in particular monomeric caseins such as in caseinate, is the preferred substrate for Tg due to the presence of the required amino acids Glu and Lys. In gel-like products such as yoghurt the effect of enzymatic cross-linking by Tg is an increased gel strength, which can be assessed rheologically or by measuring the degree of protein cross-linking (DP) by means of gel permeation chromatography (GPC). Tg therefore opens the possibility to achieve enhanced gel structures at lower protein levels. Figure 19.24 shows its effect on the degree of protein cross-linking as a function of reaction time and protein source. Caseinate is by far the preferred substrate due to its monomeric structure while casein micelles appear to be hardly accessible for the enzyme to create cross-links.

In set style yoghurt, the cross-linking of the caseins can be exploited to increase the firmness or, in stirred yoghurt, to raise the viscosity level (Figure 19.25). Also shown is the increase in the degree of polymerisation ΔDP as compared to untreated milk. It is notable that the viscosity level is considerably enhanced by the Tg cross-linking reaction. While for untreated milk a viscosity level of 0.07 Pas can be obtained at a protein concentration of 4.9%, the same viscosity was measured for the Tg treated milk at 3.6%, that is, a very costly increase in protein level can be avoided and a considerable raw material reduction of 1.3% protein, equivalent to about 3.6% milk dry matter, can possibly be achieved.

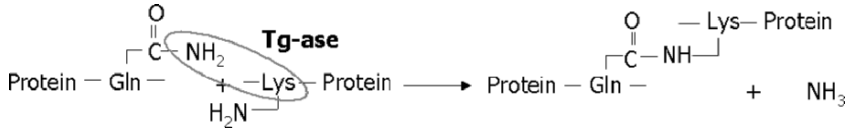

Figure 19.23. Transglutaminase (Tg)-induced cross-linking reaction between lysine and glutamine.

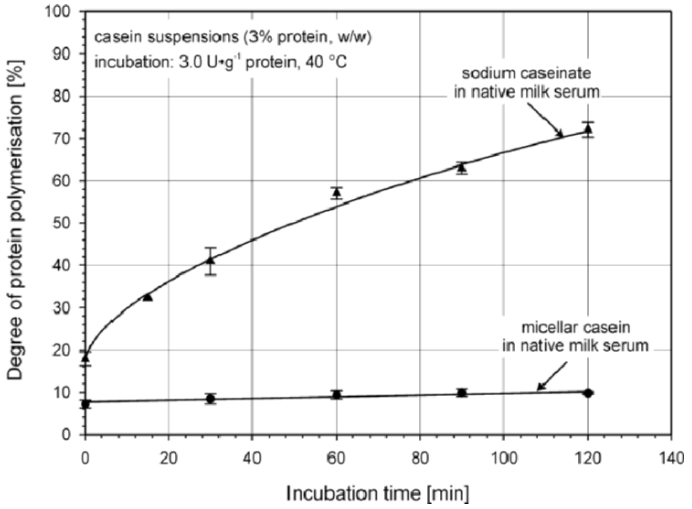

Figure 19.24. Degree of polymerisation in Tg cross-linked casein micelles and caseinate (Bönisch et al. 2007).

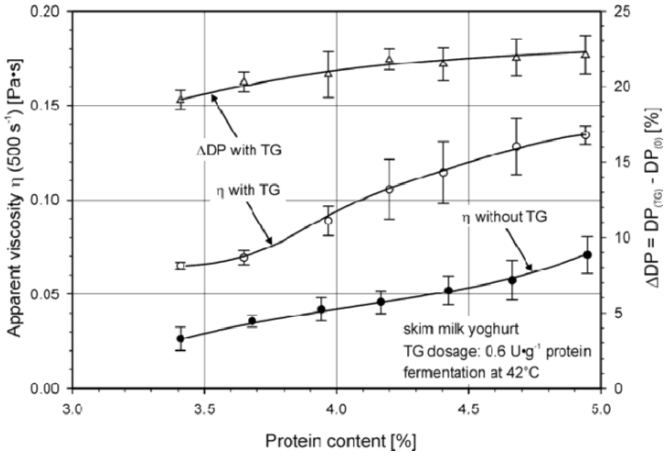

Figure 19.25. Viscosity of stirred yoghurt as a function of protein level.

It was further found that an upstream heat treatment also helps to improve the Tg effect in milk with the casein present in micellar form, in addition to integrating the whey proteins in the gel. The increased Tg effect in milk, which was heat treated at higher levels above pasteurisation level. The same applies for milk which was UHP treated, as shown by Lauber (2002). This can be explained by the heat inactivation of a so-called Tg-inhibitor substance present in milk (De Jong et al. 2003). Bönisch et al. (2006) also proved that the inhibitor substance is located in the milk serum and demonstrated the effect of heat treatment for systems, where only the milk serum

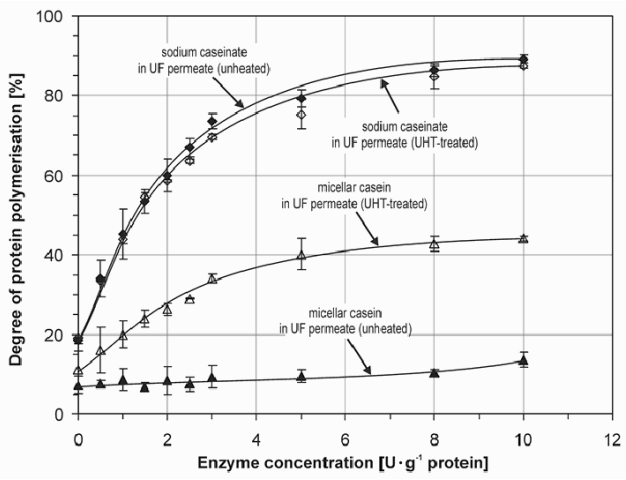

Figure 19.26. Protein polymerisation by TG of micellar casein (3% *W/W*) in unheated and UHT-treated (140°C, 40 s) milk serum (UF permeate) and sodium caseinate (3% *W/W*) in unheated and UHT-treated (140°C, 40 s) milk serum (incubation at 40°C, 120 min) (Bönisch et al. 2006).

was UHT heat treated while the casein micelles were concentrated by MF and added back to the milk serum after the heat treatment (Figure 19.26). The Tg effect in this case is much stronger. For caseinate, the heat effect is negligible, the casein monomers are already fully accessible and the effect of inhibiting the Tg inhibitor is lower in comparison.

19.5.4 Membrane Technology

The design of matrices to construct certain consumer-preferred food structures is one of the keys to competitiveness not only in the dairy industry. Exploiting the functional properties of individual dairy proteins has not yet been considered in detail in industrial manufacture. Membrane technology therefore was investigated in order to assess the processing variables and conditions required to come up with innovative possibilities for, for example, protein fractionation. Starting point was the uniform transmembrane pressure microfiltration (UTP MF) concept, originally developed in the mid-1970s and then further optimized (Osterland et al. 1995) intending to reduce the microbial count in milk. Other researchers later on made use of this concept for the fractionation of caseins and whey proteins with a nominal pore size of 0.1 µm (Maubois and Olivier 1992; Kersten 2001).

As can be seen from Figure 19.27 skim milk can be fractionated by means of UTP MF (0.1 µm), in combination with an UF diafiltration step, in its two main protein fractions, i.e. native casein micelles and native whey proteins since no heat treatment step was required to separate the proteins. The MF permeate can be considered a sort of sweet whey, however, without containing the caseinomacropeptide (CMP). This MF permeate can be further concentrated to obtain a WPC product. The

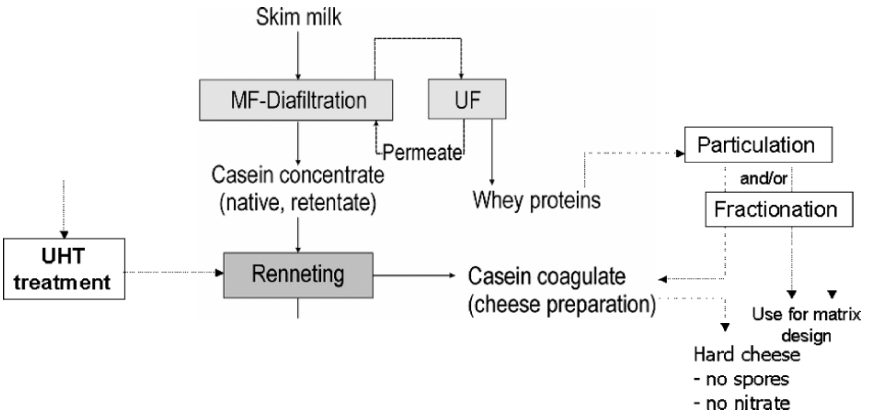

Figure 19.27. Fractionation of skim milk by UTP-MF and UF and related technical options (Bulca and Kulozik 2004).

UF permeate, in turn, is recirculated to the MF stage as a diafiltration medium to fully remove the whey proteins from the milk without changing the outer environment for the casein fraction.

The casein retentate, when used as cheese milk, can almost be fully depleted of all whey proteins through a sufficient number of diafiltration volume turnovers. In contrast to conventional cheese technology, it is then possible to UHT treat the cheese milk in order to destruct spore formers. The whey proteins can be used as a WPC or WPI product or treated further in order to fractionate the whey proteins in their main components. Alternatively the whey proteins can particulated to form WPP; see Section 19.5.1. Both approaches are options to build a platform for novel product matrices with specific properties such as gelling, foaming or emulsification.

Alternatively, to entirely depleting the milk from the whey proteins, the casein content in cheese milk can be raised to reduce the sensitivity of the renneting process to whey protein denaturation, which impairs the rennetability of conventional cheese milk (Bulca et al. 2004). Investigations were conducted at different casein and whey protein levels. The different milks were the UHT treated (140°C/10 s) and compared against standard cheese milk. The effect of these variations on the rennet coagulation was assessed by measuring the gelling time and the resulting gel firmness. Figure 19.28 shows the relative values of these two properties of the experimental rennet gels versus the standard rennet gel. The target was to identify the set of conditions required to achieve the same properties in terms of gelling time and firmness (relative values of "1"). As can be seen, the iso-effect lines crossover at two points at which the UHT treated and compositionally modified milks behave as intended.

19.6 Technologies Combining Structural and Nutritional Targets

Milk and dairy products are well recognised for their healthy composition. However, new tasks and expectations to provide products with preventive or even therapeutic

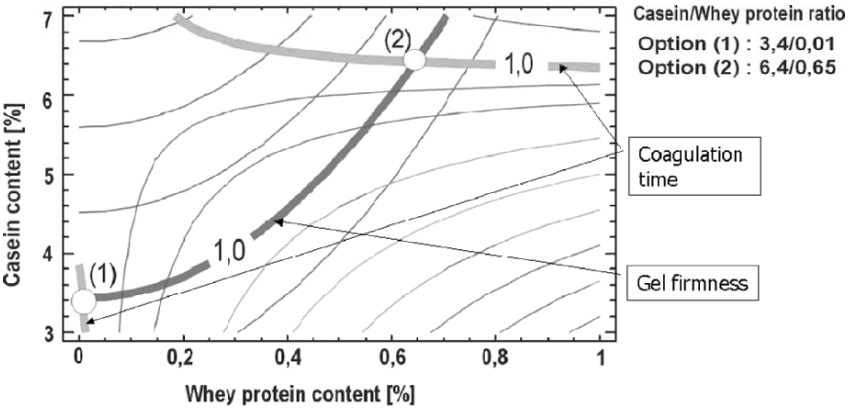

Figure 19.28. Iso-effect lines regarding relative coagulation time and gel firmness for UHT treated modified milk relative to pasteurized cheese milk. (See Color Plate.)

properties are emerging (Chatterton et al. 2006; Pihlanto 2006), for example, retention of calcium in fresh cheese or by recovery of GMP from the cheese process. Both examples include challenges on the structural level in order to ensure an active contribution to food microstructure or texture of the components, which were originally included for their nutritional function.

19.6.1 Calcium Retention in Fresh Cheese

In standard fresh cheese manufacture most of the original milk calcium is lost in the concentration step (either centrifugal separation or UF) where the desired protein and dry matter level is achieved, because the colloidal calcium, at acid pH values, is ionic and therefore leaves the casein micelle into the serum. While in the separation process the whey proteins and the calcium are lost in the serum, the UF process retains the whey proteins and, therefore, achieves a higher yield, but the calcium is still lost into the UF permeate. Fresh cheeses therefore are relatively low in calcium content. Figure 19.29 compares the conventional fresh cheese process with a new process proposal that can retain most of the milk calcium in the product.

The new process includes an upstream nanofiltration twofold pre-concentration step. Thereafter, the regular process including an UF concentration step to achieve the final dry matter value follows. In this case, however, the calcium losses into the serum are much lower as compared to the conventional process, because the final concentration step only has to remove a small amount of serum including the ionic calcium. The final UF step, that is, a partial calcium removal is still necessary to prevent the product to assume a bitter taste during shelf-life.

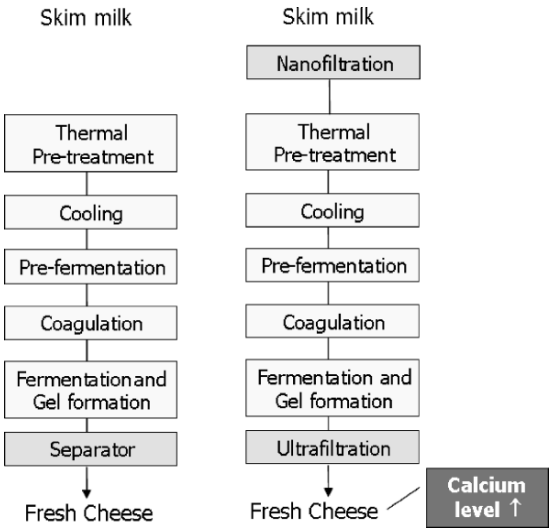

Figure 19.29. Conventional and a NF/UF based fresh cheese process (Schkoda and Kessler 1997).

19.6.2 Caseino-glycomacropeptide (GMP)

One of the biologically active ingredients that have a potential to be used more explicitly in dairy product formulations or in other areas of the food industry is GMP, which is enzymatically cut off the casein micelle during the renneting process in cheese making. GMP is a variable molecule dependent on the genetic variant and on a great variety related to glycosylation. The sugar residues attached and the glycosylation sites vary considerably. GMP offers a large variety of well-documented biological and physiological functions, such as toxin binding, suppression of pathogens, prebiotic nutrient for a healthy gut flora, osteoporosis prevention and other properties (Abd El-Salam et al. 1996; Brody 2000; Clare 1998; Neeser 2000). New nutritional concepts could make use of this potential. However, the ion exchange technology available to isolate GMP from sweet whey is neither very efficient nor overly environmentally friendly. More importantly, though, is the lack of knowledge on the functional properties of GMP and on the active, targeted integration of GMP in product matrices in conjunction with novel nutritional concepts.

The UTP MF process, depicted in Figure 19.27, is the starting point of new considerations in developing an alternative process to obtain GMP. After the casein/whey protein fractionation the casein retentate is renneted to produce cheese. The "whey" resulting from this procedure does not contain whey proteins, some casein coagulate particles and GMP. The casein particles can easily be removed by MF or centrifugation, thus obtaining a GMP solution that can be further concentrated or pre-treated to influence the functionality. Current investigations focus on its functional properties in dairy product matrices. Figure 19.30 schematically shows the process for the isolation of GMP from native casein micelles.

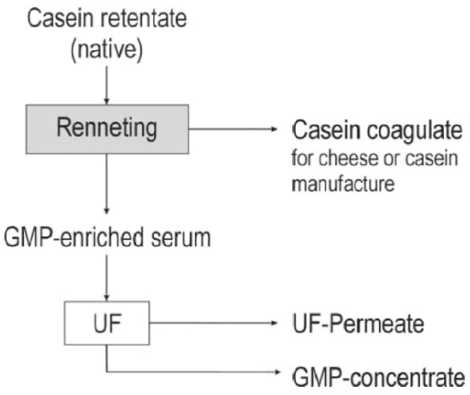

Figure 19.30. Process to obtain GMP from native casein micelles (Thomä and Kulozik 2004).

19.7 Processing Effects on Protein–Polysaccharide Interactions

Different biopolymers are used when the texture-building capacity of protein alone, for instance, is insufficiently capable to create the target structure. However, phase separation effects can occur, as described in theory and technical detail in other chapters of this publication. These phenomena are also dependent on processing factors such as heat or mechanical treatment, the latter effects being rarely investigated so far.

19.7.1 Effects of Heat Treatment and Homogenization

UHT-treated dairy systems containing carrageenan are often found to vary considerably in textural properties. The textural properties and the stability mainly depend on the interaction of the carrageenan and the casein micelle surface which was assessed by means of the hysteresis loop area between the upward and downward flow curves upon variation of the shear stress. The loop area was used as a dimension for the energy required to break down the systems' internal structure. The hysteresis loop area was found to be significantly increased the higher the heating temperature and the lower the cooling temperature was. Figure 19.31 shows flow curves of samples heated at 120°C and 139°C, respectively. It can be seen that a hysteresis loop area results from the upward and downward flow curve measurement, which varies depending on the UHT heating temperature. A distinct structure point was observed as a discontinuity within the flow curve. This point indicates a sudden rupture of a network after elongation due to the rising shear stress (Schenz 1997). In addition, the initial viscosity for a treatment temperature of 139°C is much higher than for 120°C.

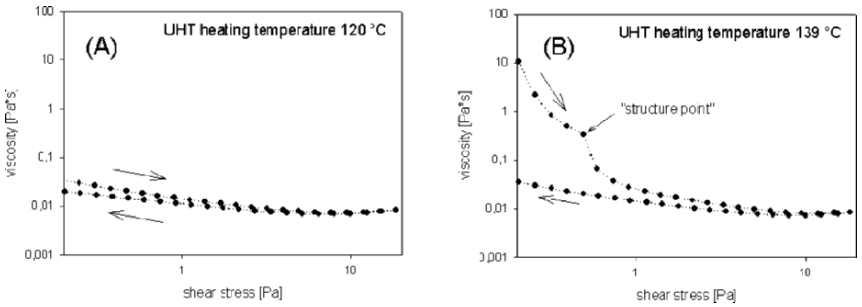

Figure 19.31. Flow curve of carrageenan–milk protein system, heated at (a) 120°C, (b) 139°C, afterwards cooled down to 4°C and stored for 24 h before measurement (Sedlmeyer and Kulozik 2006).

This kind of structure formation, assessed by means of the hysteresis loop area, depends in a nonlinear way on the UHT temperature, as can be seen in Figure 19.32. The higher is the UHT temperature, the larger is the rheological hysteresis loop area resulting from the upwards and downwards flow curves. In addition, the cooling temperature right after the heating step has an influence on the structure formation in the carrageenan–protein system.

The heating conditions significantly influence the rheological properties of milk protein–carrageenan systems. With regard to the mechanisms involved in the rheologically detectable changes, the following explanations are proposed: The mixed system entering the UHT heating section consists of hydrated carrageenan chains in coiled form, whey proteins mostly in their native state, and native casein micelles which are not sensitive to temperatures below 95°C. However, the UHT heating temperature up to 139°C was found to induce shifts in the calcium phosphate equilibria of the micelles (O'Connell and Fox 1999). Also, changes in size were reported (Singh and Latham 1993).

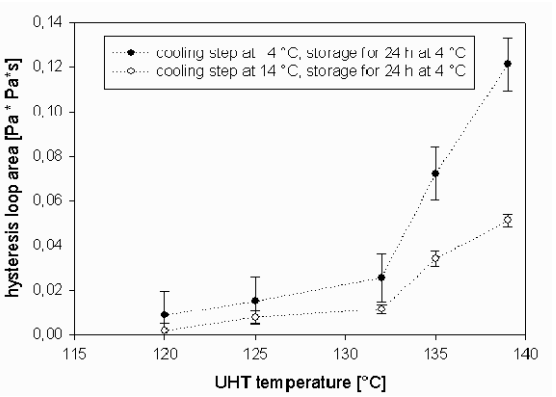

Figure 19.32. Hysteresis area depending on UHT temperature and cooling step temperature (Sedlmeyer and Kulozik 2006).

On the other hand, carrageenan is sensitive to changes in the ionic serum composition. A shift from micellar bound calcium to free ionic Ca^{2+} in the serum is known to influence the coil-helix transition of carrageenan upon cooling. The κ-/ι-hybrid-type used comprise 60% of ι-units that are known to prefer calcium ions for charge neutralization when forming helices (Sedlmeyer et al. 2003; Syrbe et al. 1998). Ca^{2+} also bridges negatively charged parts of proteins thus reinforcing the network (Vega et al. 2005).

Another example for processing effects on protein–hydrocolloid interactions is a milk-based system containing pectin, where heating and homogenization conditions were found to have an influence. Acidification of micellar casein based systems causes the milk protein system to become sensitive to heat treatment. Due to the neutralisation of the charged groups of the proteins and the respective reduction of their hydration shell, aggregation of the protein particles is observed in the form of sedimentation and phase separation. High methoxyl pectin (HMP) is a commonly used stabilizer to provide a hydrated layer on the protein particles surface at low pH, thus preventing aggregation (Syrbe et al. 1998). Electrostatic interactions are responsible for the complexation of milk proteins by a pectin layer (Dickinson 1998). In such systems, a fraction of the pectin is adsorbed to the protein particles, the rest remains freely suspended (Tromp et al. 2004). As long as the ionic strength is low, pectin is in abundance and stability achieved (Sedlmeyer et al. 2004). The shift between inorganic and organic phosphorus is temperature sensitive in acid systems (Vasiljevic and Jelen 1999).

Figure 19.33 shows the influence of temperature and homogenization pressure on the size of protein clusters. The cluster size ($d_{90,3}$) is reduced with increasing homogenization pressure when the system was afterwards heated between 73°C and 120°C, when the heating temperature was 140°C, the cluster sizes increases dramatically. Homogenization reduces the particle size, and reduces the ratio of pectin-to-surface area ratio. Obviously, a bridging phenomenon due to the loss of pectin's capability to cover the total surface of the protein particles occurs.

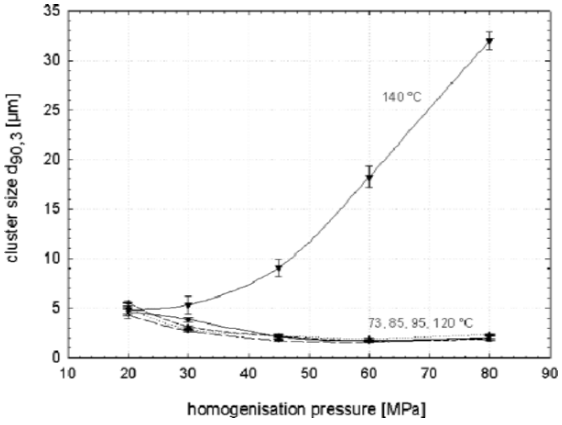

Figure 19.33. Cluster size of a milk protein–pectin system processed at 73, 85, 95, 120 or 140°C and homogenization pressure between 20 and 80 MPa (Sedlmeyer et al. 2006).

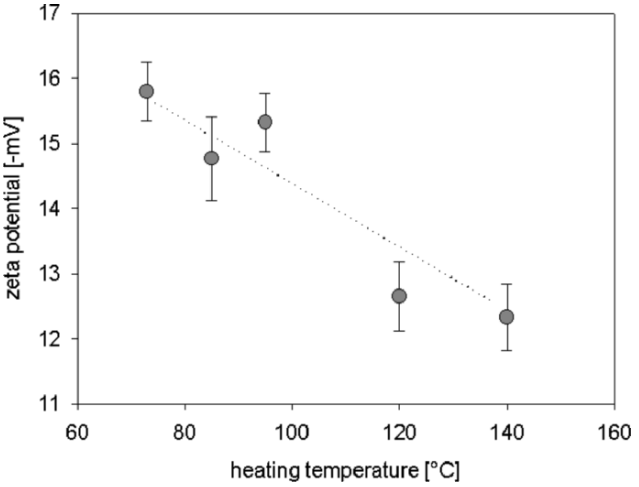

Figure 19.34. Zeta potential of a milk protein–pectin system processed at 73, 85, 95, 120 or 140°C and homogenization pressure between 20 and 80 MPa.

To explain this phenomenon the zeta-potential of the particles was measured. The zeta-potential of the particles resulting from the thermal reaction depends on the heating temperature, as can be seen in Figure 19.34. This is due to changes in the ionisation equilibrium between particles and continuous phase. To stabilize the system, adsorbed pectin has to provide the necessary surface charge to the protein particles. The zeta potential was reduced to –12.5 mV at 140°C compared to –16 mV at 73°C. This finding is consistent with the observed flocculation, that is, the reduced surface charges lead to lower repulsion forces and enable van der Waals attraction forces to gain importance for particle–particle interactions.

19.8 Conclusions and Outlook

Food microstructures result from molecules able to create networks or to occupy interfaces. The actual outcome, however, quite frequently is still based on empirical matrix and processing design. Material science in the past was not so well advanced to be able to understand texture generation or the occurrence of mal-structures well enough to prevent unexpected problems to occur. Appropriate analytical techniques were also not available. As a result, scientific knowledge was often restricted to simple test systems; complex food systems were rarely investigated and, therefore, not well understood.

Up-to-date food technology, in contrast, tries to overcome these gaps and weaknesses resulting from not being able to predict the behaviour of complex systems. Dairy science and technology, in particular, has always been at the forefront of scientifically coping with such challenges in complex products. The combination of novel processing approaches combined with new insights in material science will result in

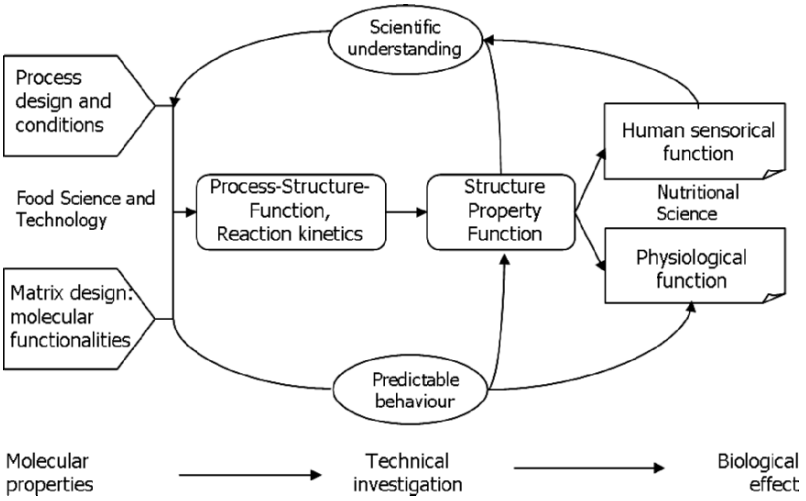

Figure 19.35. Food material and processing science and its relationship to physiology.

a deeper knowledge of the reaction kinetics even in complex dairy systems. Target functions are, however, not only related to structural sensory attributes anymore. Bio-functionality related objectives come on top and need to be considered in product design and manufacture since dairy and other products are expected to possess properties preventing diseases, supporting a healthy life style. Figure 19.35 tries to depict the relationships between the elements of product and processing design and food properties.

From the examples presented in this paper it can be concluded that for the design of new product concepts the fractionation of dairy ingredients is key to offering novel development possibilities. Both the structural properties of products as well as their nutritional value depend on the capability to enrich or deplete certain ingredients that have an influence on these functions. As demonstrated, membrane technologies can produce native single dairy proteins for product design. In combination with an improved understanding of thermal treatments on protein reactivity under certain milieu conditions these possibilities provide a whole new platform for developing innovative dairy and other food products.

Material sciences and biology are expected to have a comparable influence on food product engineering and product development like the methods of chemical engineering had in the past few decades. Novel analytical techniques are available or combinations thereof can be applied for a deeper understanding of structure formation in complex systems. Ultrasonic measurement, for instance, is a suitable additional method to quantify the denaturation degree of proteins even with a higher degree of reproducibility than DSC. The ultrasound technique additionally delivers information on structure and size of whey protein aggregates formed during heating, depending on the temperature level and rate and protein concentration. The structure

and size have an influence the ultrasonic velocity by scattering theory and compressibility (Corredig et al. 2004; Wang et al. 2006). As another example, changes in the water-mobility during fermentation can be assessed in great detail by nuclear magnetic resonance (NMR), as was demonstrated by Hinrichs et al. (2007). For instance, a significant change in the mobility of the water phases and their fractions can be observed during fermentation of native casein solutions while decreasing the pH-value.

Not understanding structure formation reactions may result in the occurrence of mal-structures such as phase separation or mealiness, which results in product systems not appreciated by the consumer or creating avoidable costs due to trial-and-error product development with variable product performance.

Considering the variety of dairy products worldwide, it is notable that these often depend on milks from other species than cow. On the other hand, the availability of other milks is limited even in the home countries of such products, for instance, mare's milk for the manufacture of koumiss in Turkey. Hence, another direction for developing new dairy products is trying to adapt the cow's milk composition to that of milks from other species. Again, membrane technologies are able to modify the contents of the key dairy ingredients including the casein/whey protein ratio, thus also helping to develop the required food textures and microstructures that are depending on the functionality of individual proteins or combinations thereof, as has been shown by Küçükcetin et al. (2003). In this context, especially because of their nutritional value, the minor substances of milk are of equal importance and will find more attention in the near term future.

19.9 References

Abd El-Salam, M.H., El-Shibiny, S., and Buchheim, W. (1996). Characteristics and potential use of the casein macropeptide. *Int. Dairy J.* 6, 327–341.

Anema, S., Lauber, S., Lee, S. K., Henle, T., and Klostermeyer, H. (2005). Rheological properties of acid gels prepared from pressure- and transglutaminase-treated skim milk. *Food Hydrocoll*. 19, 879–887.

Beyer, H.-J. (1990). Zum Einfluss der Proteinkonzentration auf das Denaturierungsverhalten der Molkenproteine sowie die damit verbundenen rheologischen Veränderungen. Dissertation, TU München.

Besner, H. (1997). Grenzflächenwechselwirkungen und Mechanismen der Schaumstabilität beim Aufschäumen von Sahne. Dissertation, TU München.

Bönisch, M.P., Tolkach, A., and Kulozik, U. (2006). Inactivation of an indigenous transglutaminase inhibitor in milk serum by means of UHT-treatment and membrane separation techniques. *Int. Dairy J.* 16 (6) 669–678.

Bönisch, M.P., Lauber, S., and Kulozik, U. (2007). Improvement of enzymatic cross-linking of casein micelles with transglutaminase by glutathion addition. *Int. Dairy J.* 17, 3–11.

Brody, E.P. (2000). Biological activities of bovine glycomacropeptide. *Brit. J. Nutr.* 84, Suppl. 1, 39–46.

Bulca, S., and Kulozik, U. (2004). Heat-induced changes in native casein micelles obtained by microfiltration. In: *Advances in Fractionation and Separation: Processes for Novel Dairy Applications.* Bull. 389, International Dairy Federation (IDF), Brussels, pp. 36–39.

Bulca, S., Leder, J., and Kulozik, U. (2004). Impact of UHT or high heat treatment on the rennet gel formation of skim milk with various whey protein contents. *Milchwissenschaft* 59, 590–593.

Chatterton, D.E.W., Smithers, G., Roupas, P., and Brodkorb, A. (2006). Bioactivity of ß-lactoglobulin and α-lactalbumin: technological implications for processing. *Int. Dairy J.* 16 (11), 1229–1240.

Clare, R. (1998). The benefits of CMP. *Dairy Industries Int.* 63, 29–31.

Corredig, M., Alexander, M., and Dalgleish, D.G. (2004). The application of ultrasonic spectroscopy to the study of the gelation of milk components. *Food Res. Int.* 37, 557–565.

Dannenberg, F. (1986). Zur Reaktionskinetik der Molkenproteine und deren technologischer Bedeutung. Dissertation, TU München.

Dannenberg, F., and Kessler, H.G. (1988). Application of reaction-kinetics to the denaturation of whey proteins in heated milk. *Milchwissenschaft* 43, 3–7.

De Jong, G.A.H., Wijngaards, G., and Koppelman, S.J. (2003). Transglutaminase inhibitor in milk. *J. Food Sci.* 68, 820–825.

De Kruif, C.G., and Holt, C. (2003). Casein micelle structure, functions and interactions. In : P.F. Fo., P.L.H. McSweeney (Eds.), *Advanced Dairy Chemistry, Vol. 1: Proteins* (3rd Ed.). NY: Kluwer Academic/Plenum, New York, pp. 233–276.

Dickinson, E. (1998), Stability and rheological implications of electrostatic milk protein–polysaccharide interactions. *Trends Food Sci Technol.* 9, 347–354.

Brulé, G., Lenoir, J., and Remeuf, F. (2000). The casein micelle and milk coagulation. In: A. Eck and J.C. Gillis (Eds.) *Cheese Making: From Science to Quality Assurance. Intercept*, Lavoisier Publishers, 2nd Ed., Paris, pp. 9–40.

Fertsch, B., Müller, M., and Hinrichs, J. (2003). Firmness of pressure-induced casein and whey protein gels modulated by holding time and rate of pressure release. *Innovative Food Sci. Emerging Technol.* 4, 143–150.

Fox, P.F., and McSweeney, P.L.H. (2002). *Advanced Dairy Chemistry*, 3rd Ed., Kluwer Academic/Plenum, New York.

Gebhard, R., Doster, W., Friedrich, J., and Kulozik, U. (2006). Size distribution of pressure decomposed casein micelles studied by dynamic light scattering and AFM. *Eur. Biophys. J.* 35, 503–509.

Hinrichs, R., Bulca, S., and Kulozik, U. (2007). Water-mobility during renneting and acid coagulation of casein solutions: a differentiated low-resolution nuclear magnetic resonance (NMR) analysis. *Int. J. Dairy Technol.* 60, 37–43.

Hinrichs, J. (2000). Ultrahochdruckbehandlung von Lebensmitteln mit Schwerpunkt Milch und Milchprodukte–Phänomene, Kinetik und Methodik. Fortschr.-Ber. 3/656, VDI, Düsseldorf.

Holt, C. (1994). The biological function of casein: research reviews. In: *Hannah Research Yearbook*, Ayr, Scotland, pp. 60–68.

Holt, C., and Horne, D.S. (1996). The dairy casein micelle: evolution of the concept and its implications for dairy technology. *Neth. Milk Dairy J.* 50, 85–111.

Horne, D.S. (1998). Casein interactions: casting light on the black boxes, the structure in dairy products. *Int. Dairy J.*, 8, 171–177

Kennel, R. (1994). Hitzeinduzierte Aggregatbildung von Molkenproteinen: Größenbestimmung und Strukuranalyse. Dissertation, TU München.

Kersten, M. (2001). Proteinfraktionierung mittels Membrantrennverfahren. Fortschr.-Ber. 3/709, VDI, Düsseldorf.

Kessler, H.G. (2002). *Food and Bioprocess Engineering.* 5th Ed., A. Kessler, München.

Koxholt, M. (2000) Untersuchungen zur Strukturierung und Strukturstabilisierung von Eiskrem: Einfluss verfahrenstechnischer Parameter und technologischer Variationen. Dissertation, TU München.

Koxholt, M., Eisenmann, B., and Hinrichs, J. (2001). Effect of the fat globule sizes on the meltdown of ice cream, *J. Dairy Sci.* 84(1), 31–37.

Küçükcetin, A., Yaygin, H., Hinrichs, J., and Kulozik, U. (2003). Adaptation of bovine milk towards mares' milk composition by means of membrane technology for Koumiss manufacture. *Int. Dairy J.* 13, 945–951.

Kulozik, U., Tolkach, A., Bulca, S., and Hinrichs, J. (2003). The role of processing and matrix design in development and control of microstructure in dairy food production: a survey. *Int. Dairy J.* 13, 621–630.

Lauber, S. (2002). Beziehungen zwischen Struktur und Geleigenschaften posttranslational quervernetzter Milchproteine. Fortschr.-Ber. 14/107, VDI, Düsseldorf.

López-Fandiño, R. (2006). High pressure-induced changes in milk proteins and possible applications in dairy technology. *Int. Dairy J.* 16(10), 1119–1131.

Maubois, J.L., and Olivier, G. (1992). Milk protein fractionation. In: *New Applications of Membrane Processes.* IDF Special Issue 9201, pp. 15–22.

Morr, C.V. (1967). Effect of oxalate and urea upon centrifugation properties of raw and heated casein micelles. *J. Dairy Sci.* 50, 1744–1751.

Neeser, J.R. (2000). Milk protein hydrolysate for addressing a bone or dental disorder. Intern. Patent No. WO 00/49885.

O'Connell, J.E., and Fox, P.F. (1999). Heat-induced changes in the calcium sensitivity of caseins. *Int. Dairy J.* 9, 839–847.

Osterland, N., Andersen, S., and Ottosen, N. (1995). Membrane filtration assembly. Int. Patent WO 95/23639.

Phandungath, C. (2005). Casein micelle structure: a concise review. Songklanakarin *J. Sci. Technol.* 27(1), 201–212.

Pihlanto, A. (2006). Antoixidative peptides derived from milk proteins. *Int. Dairy J.* 16(11), 1306–1314.

Plock, J., Spiegel, T., and Kessler, H.G. (1997). Reaction kinetics of the thermal denaturation of whey protein in sweet whey concentrated by evaporation. *Milchwissenschaft* 53, 327–331.

Rademacher, B., and Hinrichs, J. (2002). *Ultra High Pressure Technology for Dairy Products.* Bull. 374, International Dairy Federation, pp. 12–18.

Rademacher, B., Werner, F., and Pehl, M. (2002). Effect of the pressurizing ramp on the inactivation of Listeria innocua considering thermofluid–dynamical process. *Innovative Sci. Emerging Technol.* 3, 19–24.

Röck, S., and Kulozik, U. (2006). Multistage gel structure formation at elevated thermal conditions in dairy-based systems: processing and compositional effects. In: *Proc. Int. Conf. on Food Structure and Rheology* (ISFRS), Zürich, pp. 17–24.

Schenz, T.W. (1997). Using rheology of weak gels to improve fluid foods. *Food Technol.* 51(3), 83–85.

Schkoda, P., and Kessler, H.G. (1997). *Manufacture of Fresh Cheese From Ultrafiltered Milk with Reduced Amount of Acid Whey.* In: Bull. 311, International Dairy Federation, pp. 33–35.

Sedlmeyer, F., and Kulozik, U. (2006). Impact of process conditions on the rheological detectable structure of UHT treated milk protein–carrageenan systems. *J. Food Eng.* 77, 943–950.

Sedlmeyer, F., Brack, M., Rademacher, B., and Kulozik, U. (2004). Effect of protein composition and homogenization on the stability of acidified milk drinks. *Int. Dairy J.* 14, 331–336.

Sedlmeyer, F., Daimer, K., Rademacher, B., and Kulozik, U. (2003). Influence of the composition of milk–protein kappa/iota-hybrid–carrageenan gels on product properties. *Coll. Surf. B: Biointerfaces* 31(1-4), 13–20.

Singh, H., and Latham, J.M. (1993). Heat stability of milk: aggregation and dissociation of protein at ultra-high temperatures. *Int. Dairy J.* 3, 225–237.

Spiegel, T. (1999). Whey protein aggregation under shear conditions: effects of lactose and heating temperature on aggregate size and structure. *Int. J. Food Sci. Technol.* 34, 523–531.

Syrbe, A., Bauer, W.J., and Klostermeyer, H. (1998). Polymer science concepts in dairy systems: An overview of milk protein and hydrocolloid interaction. *Int. Dairy J.* 8, 179–193.

Thomä, C., and Kulozik, U. (2004). *Methods of Obtaining Isolated Casein-Macropeptide From Milk and Whey and Functional Properties.* In: Bull. 389, International Dairy Federation, Brussels, pp. 74–77.

Tolkach, A., and Kulozik, U. (2005). Optimization of thermal pretreatment conditions for the separation of native α-lactalbumin from whey protein concentrates by means of selective denaturation of β-lactoglobulin. *J. Food Sci.*, 70(9), 557–566.

Trgo, C., Koxholt, M., and Kessler, H.G. (1999). Effect of freezing point and texture regulating parameters on the initial ice crystal growth in ice cream. *J. Dairy Sci.* 82(3), 460–465.

Tromp, R. H., de Kruif, C. G., van Eijk, M., and Rolin, C. (2004). On the mechanism of stabilisation of acidified milk drinks by pectin. *Food Hydrocoll*. 18, 565–572.

Vasiljevic, T., and Jelen, P. (1999). Temperature effect on behaviour of minerals during ultrafiltration of skim milk and acid whey. *Milchwissenschaft* 54(5), 243–246.

Vega, C., Dalgleish, D.G., and Goff H.D. (2005). Effect of κ-carrageenan addition to dairy emulsions containing sodium caseinate and LBG. *Food Hydrocoll*. 19, 187–195.

Wang, Q., Tolkach, A., and Kulozik, U. (2006). Quantitative assessment of thermal denaturation of bovine α-lactalbumin by low-intensity ultrasound in comparison to HPLC and DSC. *J. Agric. Food Chem.* 54, 6501–6506.

Chapter 20

Structured Cereal Products

B.J. Dobraszczyk

Department of Food Biosciences, The University of Reading, Whiteknights, Reading RG6 6AP, UK.

20.1 Introduction

This chapter describes the importance of cereals and their products and the various structures that can be produced from them. It shows how cereals have been, and continue to be, the main source of nutrition for much of the world, and how the development of structure in foods such as bread has provided improved sensory texture, appearance and palatability to these foods.

The importance of aeration and the development of foam structures is seen as the key process in this development, and the main structuring processes used in the industry such as baking are described (see also Chapters 10, 14 and 18). Bread is discussed as an example of a typical structured product where the introduction of air bubbles through mixing, fermentation and baking has created an entirely new structure and improved sensory properties. The importance of extensional rheology in the incorporation and stabilization of bubbles is described, and the influence of gluten polymer structure and molecular weight on the development of extensional strain hardening is shown to be the key factor in the stabilisation of bubbles in bread, which in turn determine the expansion of doughs during fermentation and ultimately the final volume and texture of baked bread (see also Chapter 6).

Methods of objective measurement of cereal foam structures are reviewed, including image analysis, confocal microscopy and x-ray tomography. The analysis of foam structures and their relationship with mechanical and rheological properties is described, and also the relationships between these structures and sensory descriptors such as crispness, crunchiness and texture. The size, shape and anisotropy of bubbles and their cell walls in foams are seen as critical in determining their fracture properties and sensory perception of crispness. Techniques for measuring crispness using acoustic emission and force-deformation profiles are discussed.

20.2 The Importance of Cereals

Cereals provide a substantial amount of the world's nutritional needs, and in many countries they can provide up to 60% of total nutritional intake in the form of complex carbohydrates and protein. Historically, cereals have developed their importance because of their relatively high yields and ease of growing, storage and transport. Cereals are grown in most inhabited parts of the world, and with an annual total production of over 2 billion Tonnes, give an average intake of 0.5 kg cereals per person per day. The main cereals consumed are wheat, maize and rice, with regionally significant quantities of barley, sorghum, millet, oats and rye. Their use as foods ranges from whole grains, porridges, beer, fermented bread, flat breads, tortillas, pizzas, pasta, noodles, cakes, biscuits and snack products.

20.3 Processing Cereals into Food and the Development of Structure

Many of the processes that transform the cereal into food products involve the development of structure in the food, for example, fermentation transforming dough or batter into a foam, and baking into the light, aerated open sponge structure characteristic of bread and cakes. Some cereals are expanded or "puffed" as in rice cakes, popcorn, puffed wheat, expanded snacks, and so on, while others are extruded to give expanded foam structures. All of these processes involve the production of a foam structure by some means, with the resulting foam giving an entirely new texture or mouthfeel to the original product. The final foam structure responsible for sensory texture in cereal foods is strongly dependent on the size and distribution of the bubbles within them, due to the effect of the growth of these bubbles on the distribution of wall thicknesses between the bubbles. Hence, the presence of bubbles in foods provides improved texture, appearance and volume to many foods, which without bubbles would be unappealing.

20.4 Bread as a Structured Product

The creation of fermented (leavened) bread was one of the first "structured" foods, where the growth of bubbles by fermentation and baking created an entirely different product with considerably enhanced textural sensory properties. Historical records have been found in ancient Egyptian tomb carvings dating from 3000 B.C., which show fermented bread being made from wheat flour and baked in clay ovens. Nutritionally, the production of aerated bread is of little benefit. During fermentation, the yeast converts some of the starch sugars into CO_2 and ethanol, which escapes during baking, decreasing the nutritional benefit of the flour. The production of aerated bread is also energetically wasteful, requiring considerable effort and expertise. It is the sensory and textural benefits of the aerated structure of fermented bread that outweigh the losses which encourage us to spend the time and effort in baking bread.

The baking process can be divided into three main processes: mixing, fermentation (or proof), and baking.

20.5 Mixing

Mixing of bread dough has three main functions: (i) to blend and hydrate the dough ingredients, (ii) to develop the dough, and (iii) to incorporate air into the dough. In the production of doughs, the nature of the mixing action develops the viscoelastic properties of gluten and also incorporates air, which has a major effect on their rheology and texture. There is an intimate relationship between mixing, aeration and rheology: the design and operation of the mixer will develop texture, aeration and rheology to different extents, and conversely the rheology of the food will affect the time and energy input required to achieve optimal development. This is seen in the great variety of mixers used in the baking industry, where certain mixers are required to produce a desired final texture in the bread.

Hence modification of the conditions during the mixing process can control the structure of the final product. For example, different types of mixers have been shown to produce different levels of air incorporation and bubble size distributions (Figure 20.1).

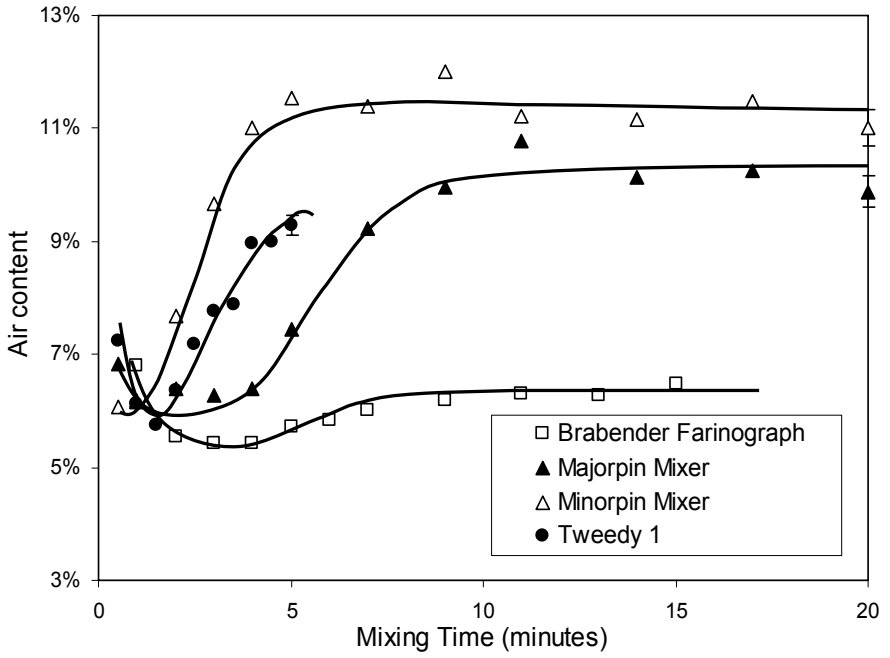

Figure 20.1. Change in air content during the course of mixing in four laboratory-scale mixers. (From Campbell, G.M. (2003). Bread aeration. In: Bread Making: Improving Quality, Cauvain, S.P., ed., Woodhead Publishing, Cambridge. Figure 17.1, p. 358.)

Control of mixer headspace atmosphere has been used to achieve a given bread cell structure and texture. Through the use of pressure and vacuum it is possible to obtain a wide range of cell structures in baked products. The use of a partial vacuum during the later stages of mixing gives a uniform, fine texture typical of U.K. sandwich bread. If the dough is mixed under pressure, more air is incorporated into the dough, which gives an uneven coarse bubble structure, typical of French baguette bread (Figure 20.2). Measurement of bubble size distributions in dough just after mixing has shown a decrease in the number and size of bubbles when mixed under partial vacuum, while an increase in pressure near the end of mixing increases the number and size of bubbles (Alava 2003) (Figure 20.3). The use of different gases

Figure 20.2. Effect of mixing at different pressures on bread texture. (Courtesy of Grant Campbell, University of Manchester.)

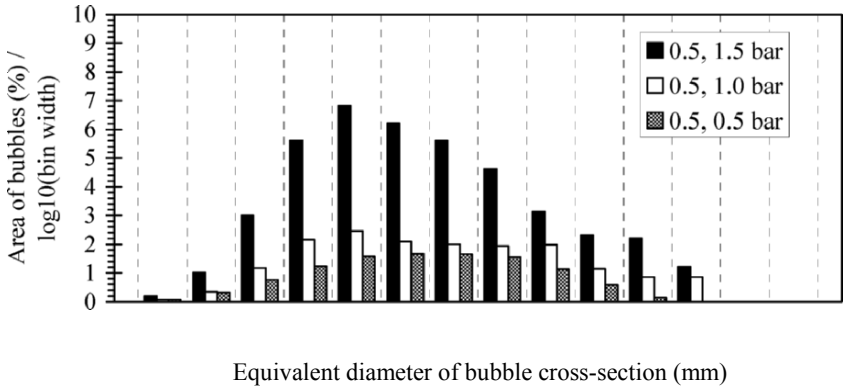

Figure 20.3. Effect of pressure and vacuum during mixing on bubble area distributions of gas bubbles in doughs. (By permission from Juan Alava PhD thesis, University of Reading 2003.)

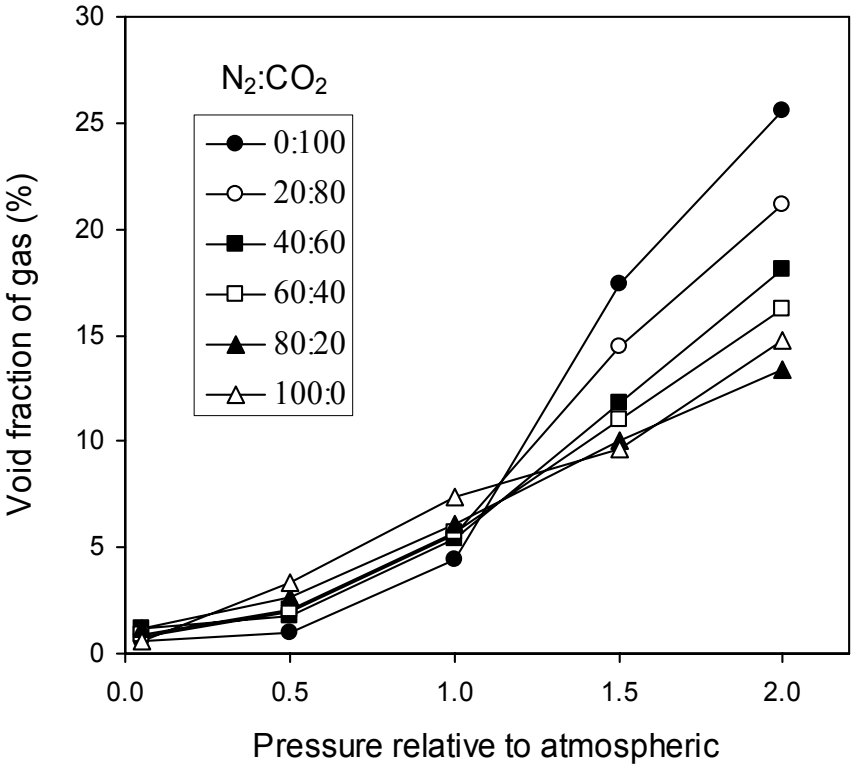

Figure 20.4. Effect of gas composition (proportions of nitrogen and carbon dioxide) in the headspace atmosphere during mixing on the aeration of the dough. (From Campbell, G.M. (2003). Bread aeration. In: *Bread Making: Improving Quality*, Cauvain, S.P., ed., Woodhead Publishing, Cambridge, Figure 17.2, p. 360.)

during mixing has been shown to have an effect on the aeration and bubble size distribution of dough: mixing under CO_2 at higher pressure significantly increased void fraction of gas trapped in bread dough (Campbell 2003) and biscuit doughs (Brijwani 2006), and mixing under nitrogen at higher pressures gave a lower void fraction of gas trapped in dough (Figure 20.4) and reduced the average diameter of bubbles in dough (Alava 2003).

The final texture of bread is also strongly influenced by the development of the dough and the mixing conditions it experiences. In the production of dough from wheat flour and water, the nature of the mixing action develops the viscoelastic properties of the gluten matrix and also incorporates air, which has a major effect on the rheology and texture of the subsequent dough. Extensive work on dough mixing has shown that mixing speed and energy (work input) must be above a certain value to develop the gluten network and to produce satisfactory breadmaking (Kilborn and Tipples 1972), and an optimum in work input or mixing time has been related to

optimum breadmaking performance, which varies depending on mixer type, flour composition and ingredients (Mani et al. 1992).

Mixing beyond the optimum (overmixing) is thought to damage the dough, causing the gluten network to break down, resulting in more fragile bubble walls and less gas retention and lower baking volume. Overmixing can also result in sticky, difficult-to-handle doughs that cause production problems. The strong relationship between mixing and handling and baking properties has resulted in a large number of commercial force-recording dough mixers, such as the Farinograph and Mixograph (Dobraszczyk 2001; Dobraszczyk and Schofield 2002), which are used to determine the optimum in mixing speed and energy. Mixing doughs by elongational flow in sheeting to achieve optimum development requires only 10–15% of the energy normally used in conventional high speed shear mixers (Kilborn and Tipples 1974), suggesting that much higher rates of work input and a more efficient dough development can be achieved due to the enhanced strain hardening of doughs under extensional deformation.

20.6 Fermentation (Proof)

Fermentation, or proof is the critical step in the breadmaking process, where the expansion of air bubbles previously incorporated during mixing provides the characteristic aerated structure of bread, which is central to its appeal. During proof, the gas content within dough increases from around 4–8% to approximately 80%. The original bubble structure, which is formed during mixing and subsequently altered during punching and moulding, is slowly expanded by the diffusion of CO_2 which is dissolved in the surrounding liquid phase within the dough (Chiotellis and Campbell 2003a). This causes the steady increase in the volume of the dough known as proof,

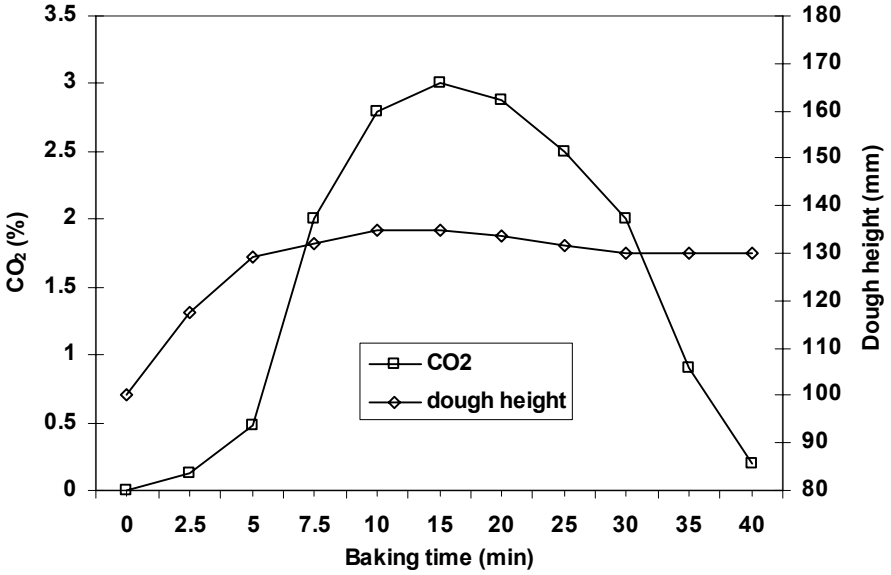

Figure 20.5. Release of CO_2 from dough during baking.

since at this stage the bubbles are discrete and no gas can escape. Eventually the bubbles start to inter-connect or coalesce, CO_2 gas begins to escape, and volume expansion ceases (Figure 20.5).

The growth and stability of gas bubbles during proofing determine the ultimate expansion of the dough and its final baked texture and volume (Chiotellis and Campbell 2003b). The coalescence of gas bubbles is the key event that determines the extent of bubble expansion and volume increase during proof, and also the final loaf texture. If coalescence is delayed, bubbles can expand for much longer, giving a larger proof volume and a finer texture (i.e., smaller gas cells). If coalescence occurs early, then gas escape occurs much earlier and proof volume is decreased and the texture is much coarser. The rheological properties of the bubble cell walls are very important in controlling coalescence in doughs, in particular the elongational strain hardening properties of the gluten polymers (Kokelaar et al. 1996; Dobraszczyk and Morgenstern 2003).

20.7 Baking

In baking the foam structure of the dough, created by the gas cells, is turned into a loaf of bread with an interconnected sponge structure supported by the starch–protein matrix. Within the first few minutes of baking in the oven the volume of the dough increases rapidly and reaches the maximum size of the loaf; this period is called oven rise or oven spring (He and Hoseney 1991). At the end of oven spring there is a sharp increase in the rate of gas lost from the loaf, which is due to the rapid coalescence or rupture of the bubble cell walls. At the temperature of starch gelatinisation (~65–70°C) there is a transfer of water from the protein to the starch, leading to a swelling of the starch granules and a rapid increase in viscosity of the dough, which sets the sponge structure. These physical changes lead to a change from a closed cell foam structure to an open cell sponge structure (Figure 20.6).

During baking there is an evaporation of water from the loaf, this is particularly marked near the surface of the loaf, and this evaporation plus the occurrence of the Maillard reaction cause a characteristic dark brown crust to be formed on the exterior of the loaf. The Maillard reaction is a complex set of chemical reactions in which the amino acids in proteins react with reducing sugars such as glucose and fructose, and which are very important to our perception of flavour in baked bread.

20.8 Gluten Polymer Structure, Rheology and Baking

Gluten is the major protein in wheat flour doughs, responsible for their unique viscoelastic behaviour during deformation. It is now widely accepted that gluten proteins are responsible for variations in baking quality, and in particular it is the insoluble fraction of the high molecular weight (HMW) glutenin polymer which is best related to differences in dough strength and baking quality amongst different wheat varieties (MacRitchie and Lafiandra 1997; Weegels et al. 1996). For example, the rheological properties of gluten are known to important in the entrainment, retention and stability of gas bubbles within dough during mixing, fermentation and baking (Dobraszczyk and Morgenstern 2003; Chin and Campbell 2005), which ultimately are responsible for the texture and volume of the final baked product.

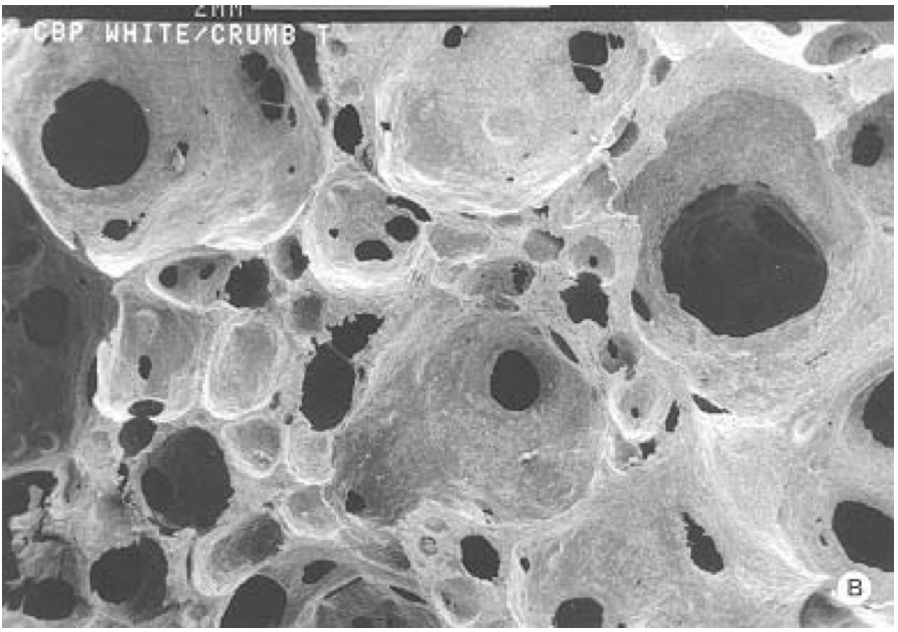

Figure 20.6. Scanning electron micrograph showing open cell foam structure of bread.

Gluten proteins comprise a highly polydisperse system of polymers, classically divided into two groups based on their extractability in alcohols: gliadins and glutenins. The gliadins are single-chain polypeptides with molecular weight (MW) ranging from 2×10^4 to 7×10^4, while the glutenins are multiple-chain polymeric proteins in which individual polypeptides are thought to be linked by interchain disulphide and hydrogen bonds to give a wide MWD ranging between 10^5 up to 10^9. Gluten has a bimodal MW distribution which roughly parallels the classical division based on solubility into gliadins and glutenins (Carceller and Aussenac 2001; Arfvidsson et al. 2004). Individual glutenin polymers have an extended rodlike structure ca. 50–60 nm in length made up of a central repetitive region, which is known to adopt a regular β-spiral structure (Figure 20.7) (Shewry et al. 2002), and terminal regions containing cysteine residues, which are associated with intermolecular crosslinking by disulphide bonds. The rheological properties of gluten are known to depend on the three-dimensional organisation of the polymer network, where individual linear HMW glutenin polymers (subunits) are linked by disulphide and hydrogen bonding and entanglements to form a network structure. Branching along the linear HMW glutenin polymers is also known to occur (Figure 20.7), possibly by chain terminating LMW subunits. The microscopic network structure of gluten protein in a developed dough is seen clearly using confocal laser scanning microscopy (Figure 20.8), where gluten strands form a three-dimensional network in which are embedded rigid starch granules and air bubbles.

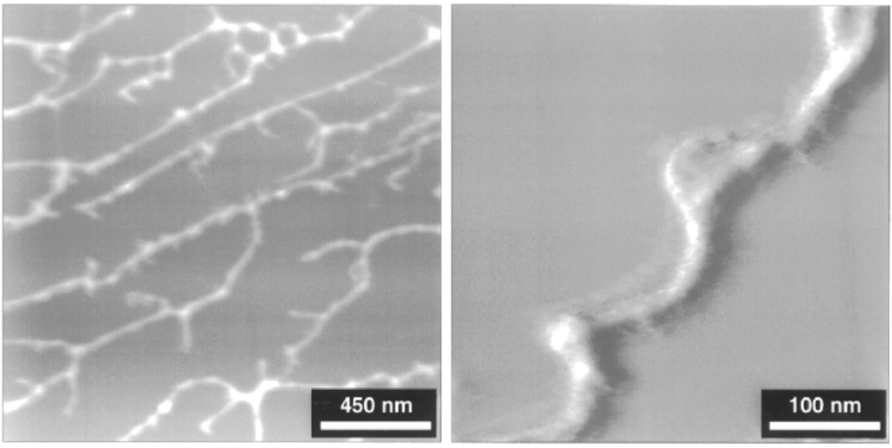

Figure 20.7. Structure of HMW glutenin subunit showing (a) branching (b) spiral structure by Atomic Force Microscopy (AFM). (From Humphries et al. (2000), *Cereal Chem.* 77, 107–110.)

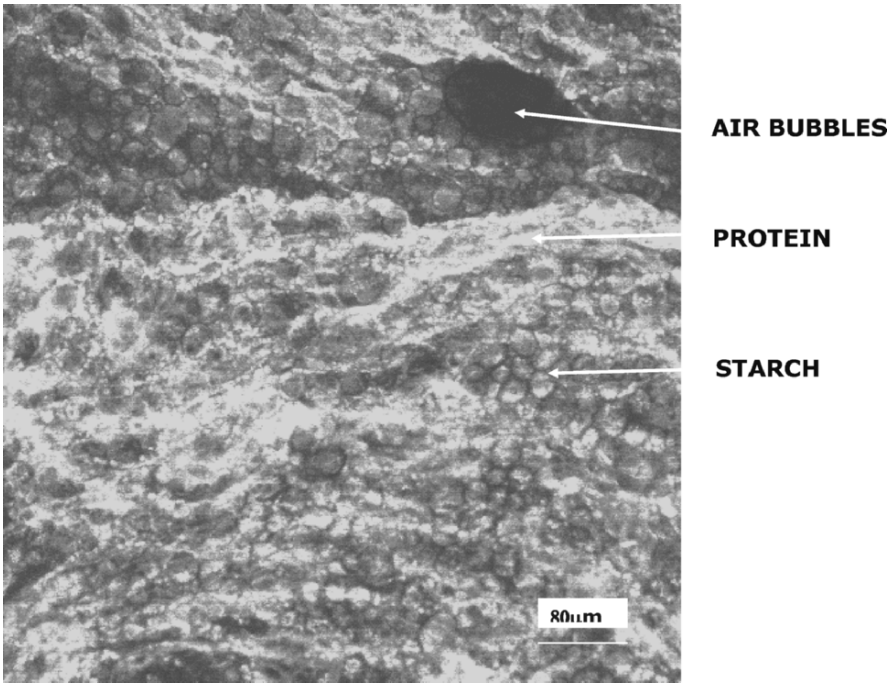

Figure 20.8. Microstructure of dough showing gluten, starch and air bubbles during the early stages of proof. (Obtained by Confocal Laser Scanning Microscopy.)

Recent studies in polymer physics have shown that molecular size, structure and molecular weight distributions of polymers are intimately linked to their rheological properties and ultimately to their performance in various end-use applications (Doi and Edwards 1986; McLeish and Larson 1998). Beyond a critical molecular weight (MW_c), characteristic for each polymer, rheological properties such as viscosity, relaxation time and strain hardening start to increase rapidly with increasing MW. Above this critical MW, the polymers start to entangle, giving rise to the observed rapid increase in viscosity with MW (Figure 20.9). Entanglements can be viewed as physical constraints between segments of the polymer chain, rather like knots. A relatively small variation in the highest end of the MWD can give rise to a large increase in viscosity and strain hardening, and is likely to have a large effect on baking performance. If the polymers are branched, viscosity rises even more rapidly. The effect of polymer chain branching on shear and extensional viscosity of polymers and doughs is shown in (Figure 20.10).

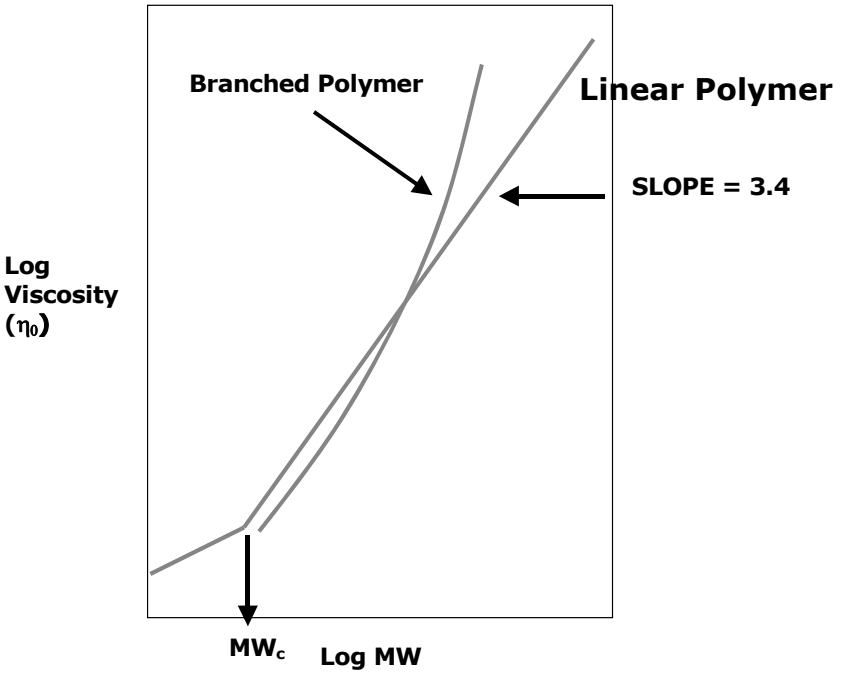

Figure 20.9. Effect of molecular weight (MW) on viscosity of linear and branched polymer melts. Beyond a critical molecular weight for entanglements (MW_c) viscosity (η_0) increases rapidly for linear polymers as $MW^{3.4}$.

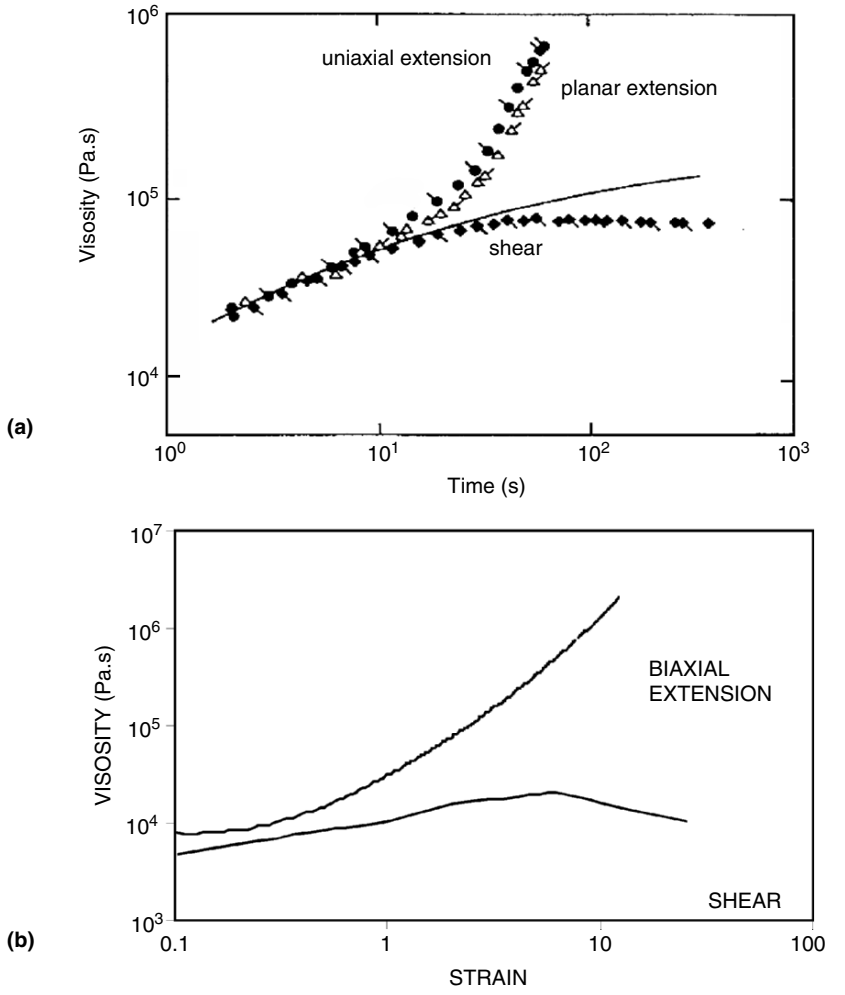

Figure 20.10. Effect of polymer chain branching on shear and extensional viscosities of (a) branched LDPE (low-density polyethylene) melts, and (b) dough.

At low strains, shear and extensional viscosities are very similar, but as deformation increases the effect of polymer branching and entanglement becomes apparent, with a steep rise in viscosity with strain (known as strain hardening) apparent for extensional deformation, and a decrease in viscosity with shear deformation (known as shear thinning). An increase in the number of branches increases strain hardening and extensional viscosity, and decreases shear viscosity. Extensional rheological properties appear to be more sensitive to changes in MW, polymer entanglements and branching than dynamic shear properties. This indicates that is more likely to be the physical interactions of the secondary molecular structure of the insoluble HMW glutenin (such as branching and entanglements) that are responsible for the rheological properties of dough and its baking performance, rather than the current hypothesis which assumes that the primary chemical structure or size of individual glutenin subunits determine the rheological properties and baking quality of dough. Recent evidence suggests that these insoluble HMW polymers form an entangled polymer network with a long relaxation time, they are branched, and form extensive intermolecular secondary structures held together by hydrogen bonding, and that differences in these secondary polymer structures and interactions are likely to be strongly related to extensional rheology of dough and its ultimate baking performance (Li et al. 2003; Humphris et al. 2000; Belton 1999).

20.9 Baking Quality and Rheology

During proof and baking the growth and stability of gas bubbles within the dough determines the expansion of the dough and therefore the ultimate volume and texture of the baked product. The limit of expansion of these bubbles is related directly to their stability, due to retardation of coalescence and loss of gas when the bubbles fail. The rheological properties of the expanding bubble walls will therefore be important in maintaining stability in the bubble wall and promote gas retention. The relevant rheological conditions around an expanding gas cell during proof and baking are biaxial extension, large extensional strain and low strain rates.

Any rheological tests that seek to relate to baking performance should be performed under conditions similar to those of baking expansion. Methods such as bubble inflation and lubricated compression offer the most appropriate method for measuring extensional rheological properties of doughs. The major advantage of these tests is that the deformation closely resembles practical conditions experienced by the cell walls around the expanding gas cells within the dough during proof and oven rise, *i.e.* large deformation biaxial extension and can be carried out at the low strain rates and elevated temperatures relevant to baking (Dobraszczyk and Morgenstern 2003).

In bread doughs the stability of the bubble walls has been shown to be directly related to the extensional strain hardening properties of the dough. These are measured using a new technique developed by Stable Micro Systems Ltd., Godalming, UK, called the D/R Dough Inflation System (Figure 20.11) which measures the extensional rheological properties of dough and gluten in biaxial extension under

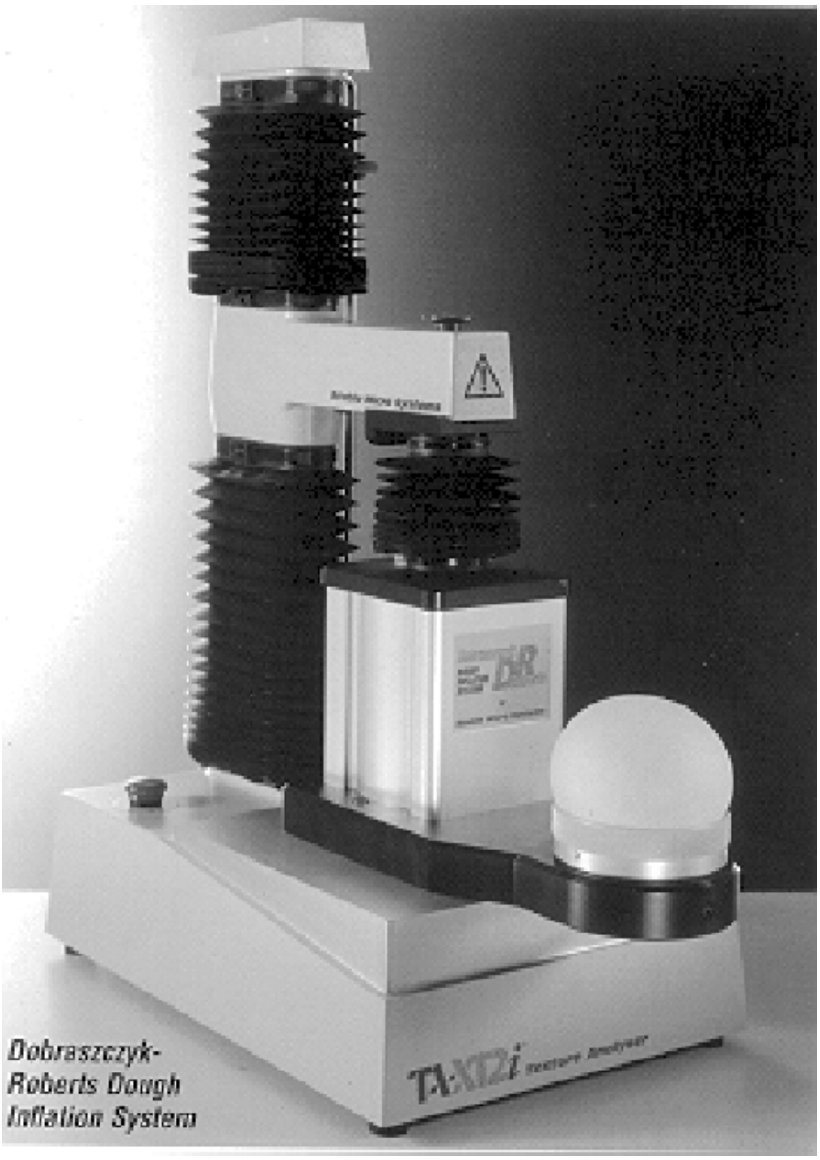

Figure 20.11. The D/R dough inflation system (Stable Microsystems Ltd. Godalming, UK).

conditions of deformation, strain rate and elevated temperatures relevant to bread-making. The latest version of the instrument (TA.XTPlus) has the option of continuously variable speed, which allows tests to be performed at constant strain rates and higher temperatures more relevant to proof and baking conditions. Strain hardening is shown as an increase in the slope of the stress–Hencky strain curve with increasing

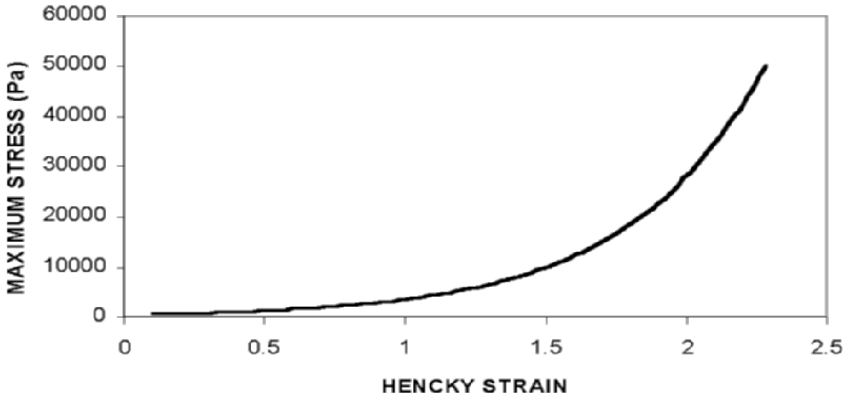

Figure 20.12. Stress–strain curve for inflating dough bubble showing strain hardening as a nonlinear increase in stiffness with increasing strain.

extension, giving rise to the typical J-shaped stress–strain curve observed for highly extensible materials (Figure 20.12). The failure of gas cell walls in doughs is related to the elongational strain hardening properties of the dough measured under large deformation biaxial extension (Dobraszczyk and Roberts 1994). Strain hardening measured at 50°C for a number of commercial flours of varying quality clearly shows that a value of around 1 discriminates well between flours of poor to moderate baking quality and those considered to be good and excellent (Dobraszczyk et al. 2003).

Strain hardening in doughs is thought to arise mainly from stretching of polymer chains between points of entanglement in the larger glutenin molecules, which gives rise to the increasing stiffness observed at large strains. Under extensional flow, entangled polymers exhibit strain hardening which is enhanced for polymers with a broad MW distribution, particularly a bimodal distribution and branching. It is therefore expected that the broad bimodal MW distribution and branched structure typical of gluten will result in enhanced strain hardening and a bimodal distribution of relaxation times. Recent work has shown that bread doughs exhibit strain hardening under large extensional deformations, and that these extensional rheological properties are important in baking performance (van Vliet et al. 1992; Kokelaar et al. 1996; Dobraszczyk and Morgenstern 2003).

Strain hardening allows the expanding gas cell walls to resist failure by locally increasing resistance to extension as the bubble walls become thinner, and provides the bubble walls greater stability against early coalescence and better gas retention. It is expected therefore that doughs with good strain hardening characteristics should result in a finer crumb texture (e.g., smaller gas cells, thinner cell walls and an even distribution of bubble sizes) and larger baked volume than doughs with poor strain hardening properties. Good bread-making doughs have been shown to have good strain-hardening properties and inflate to larger single bubble volume before rupture, while poor bread-making doughs inflate to lower volumes and have much lower

strain hardening (Figure 20.13). Loaf volume and crumb score for a number of doughs from flour varieties with varying baking performance has been related directly to the strain hardening properties of single dough bubbles measured at elevated temperatures in biaxial extension. Once strain hardening drops below a value of around 1, bubble wall stability decreases rapidly (Figure 20.14). Bubble wall

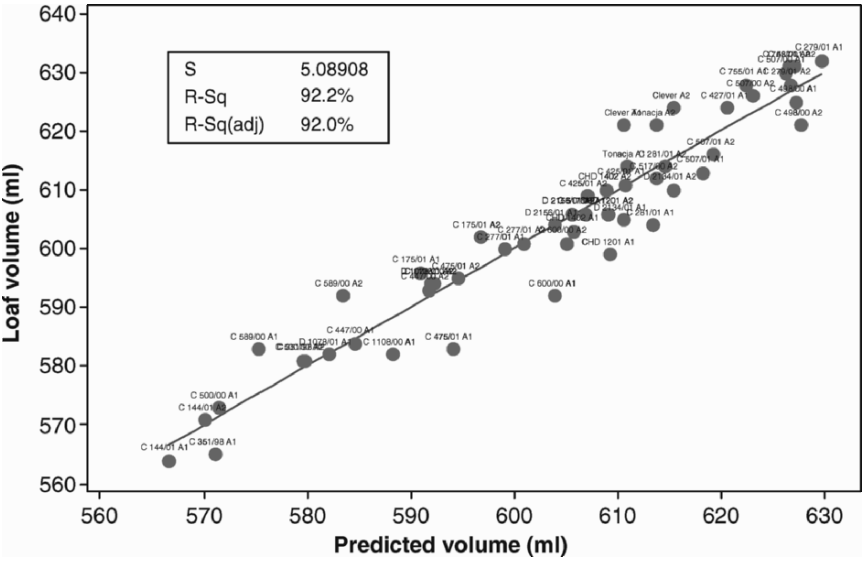

Figure 20.13. Loaf volume for a number of wheat varieties predicted from dough inflation properties (strain hardening index and failure strain).

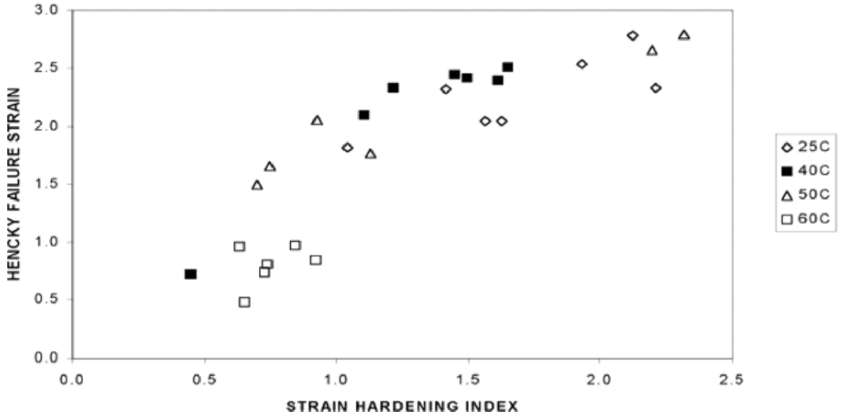

Figure 20.14. Dough bubble stability (Hencky failure strain) as a function of strain hardening measured at various temperatures, showing increasing bubble instability at strain hardening <1.

stability (as indicated by a strain hardening value of 1), is increased to progressively higher temperatures with increasing baking volume, allowing the bubbles to resist coalescence and retain gas for much longer during the baking process. Bubble wall instability in poorer breadmaking varieties occurs at much lower temperatures, giving earlier bubble coalescence and release of gas, resulting in lower loaf volumes and poorer texture (Dobraszczyk et al. 2003).

20.10 Structuring by Bubble Expansion

Bubble expansion is widely used in the food industry to develop structure within products such as expanded snacks, breakfast cereals and bread products made from cereals such as rice, maize (corn), wheat, oat and sorghum flour. Expansion can be brought about by various mechanisms, including fermentation and baking, melt extrusion, gun puffing, hot air expansion, deep frying and microwave baking. The resulting expanded foam structures are responsible for the novel textures of the food products, giving them desirable sensory attributes such as lightness, crispness, crunchiness, and so on.

The way air is incorporated as bubbles, and their subsequent growth and stability, is strongly related to the rheological properties of the surrounding matrix material, and these in turn are related to the composition, molecular size and structure of the biopolymers making up the food. Air inclusion is also dependent on the physical process conditions, such as pressure, temperature, moisture etc., especially in extrusion where variation in T, P, MC are used to control texture.

20.11 Measurement of Foam Structure

Until recently, measurement of the foam structure of foods such as bread has been carried out subjectively by visual inspection using specially trained observers, but this is prone to large variations between different observers and not capable of independent standardisation or calibration. New automated digital image analysis techniques are now available which make it possible to quantify the foam structure by taking digital images of the food and use software which automatically measures dimensions of all the individual bubbles and cell walls in the foam (Figure 20.15). The spread of sizes and shapes of the bubbles and their cell walls can then be related directly to our perception of the appearance and texture of the food.

Many imaging techniques have been used to measure and quantify foam structures in foods: Electron Microscopy (Gan et al. 1995; Bache and Donald 1998; Keetels et al. 1996; van Duynhoven et al. 2003; Elmehdi et al. 2003). Many of the microscopic techniques suffer from the optically opaque nature of dough and bread, their invasive nature and from preparation artefacts. More recently, noninvasive techniques have been used which allow three-dimensional imaging of foam structures in cereal foams: confocal laser scanning microscopy (CLSM) and computerised microtomography (CMT), which also have the possibility of following the growth of bubbles directly in real time during their expansion.

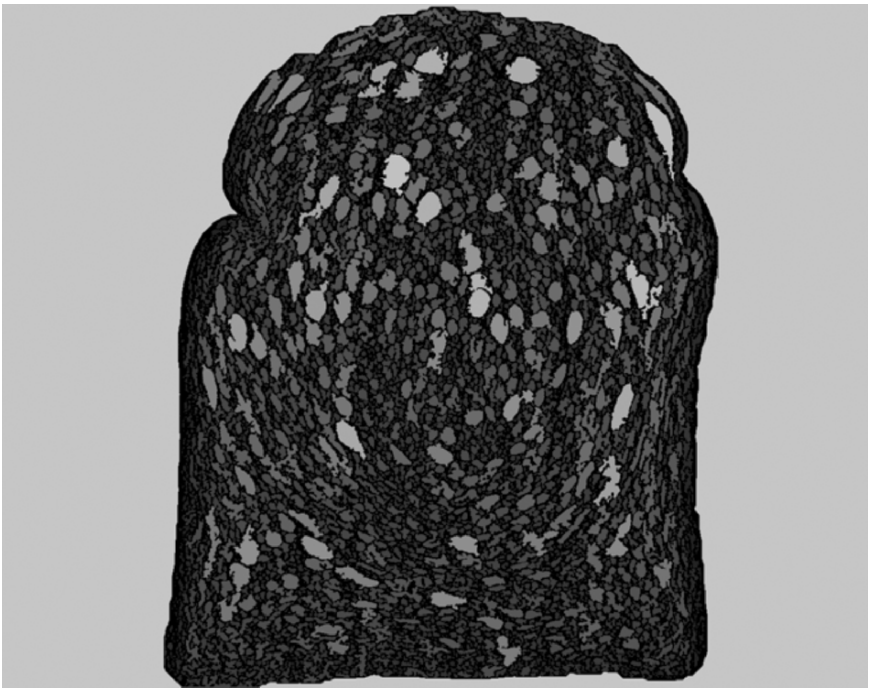

Figure 20.15. Digital image of bread obtained by automated image analysis (C-Cell, Calibre Controls).

CLSM is rapidly becoming established as a tool for the noninvasive imaging of structural components of fragile multi-component food systems, where it is possible to image the separate phases of complex food systems using fluorochrome phase staining techniques. Conventional microscopic imaging methods often cause artefacts and damage to the structure, while CLSM can penetrate noninvasively into opaque food systems such as dough to obtain a three-dimensional image of the structure at resolution of a few microns, and monitor time-dependent changes such as bubble expansion in doughs during proof and baking in real time. Wheat flour doughs have been studied using the confocal laser scanning microscope with a heating stage to quantify the structural changes that occur within dough during proof and baking (Li et al. 2004).

Computerised microtomography (CMT) has recently been used to analyse the cellular structure of food foams (Lim and Barigou 2004; Whitworth and Alava 2004; Falcone et al. 2005; Trater et al. 2005; Babin et al. 2006) (Figure 20.16). Babin et al. have followed the growth of bubbles and foam setting during the baking process using fast x-ray computerised microtomography with the aid of high energy x-ray beams from a synchrotron source, which enable a scan time of 20 ms and a resolution of 15 μm (Figure 20.17). They found that the void volume fraction of the bubbles

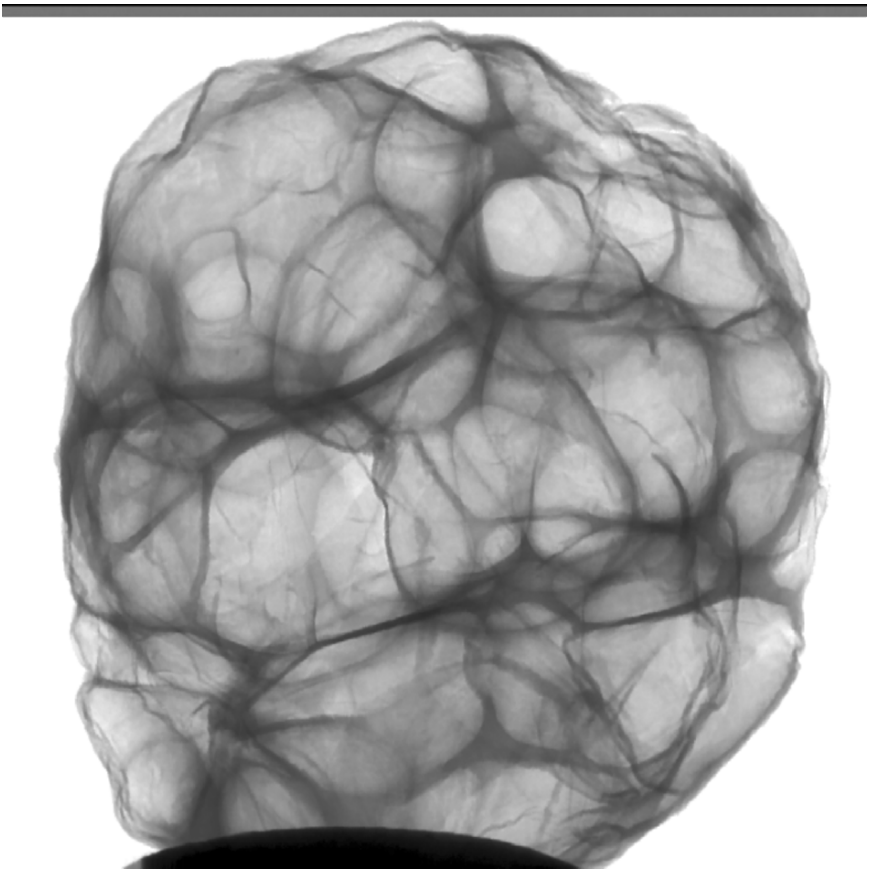

Figure 20.16. Three-dimensional image of an expanded maize foam using x-ray microtomography. (From Trater and Alavi 2005.)

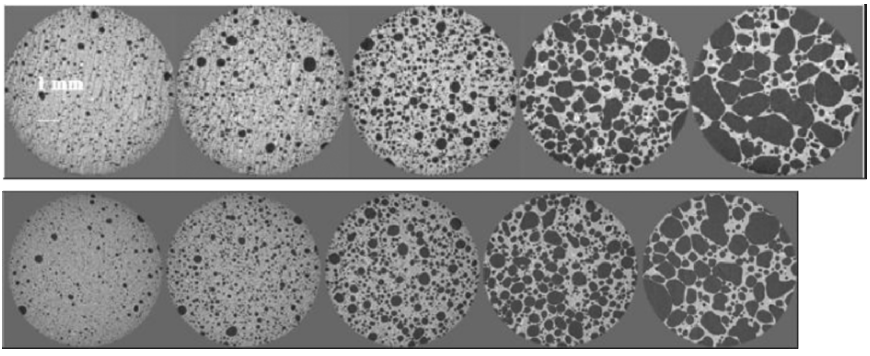

Figure 20.17. Bubble growth in dough during fermentation observed using computerized x-ray microtomography. (From Babin et al. 2006.)

increased linearly until an inflection point around 20–25 minutes, beyond which bubble growth slowed. The average cell wall thickness initially decreases linearly during proof, indicating free growth of bubbles, until a plateau was reached beyond which cell wall thickness increased, which was related to disappearance of thinner cell walls by coalescence.

20.12 Mechanics of Solid Cereal Foams

A clearer understanding of the relationship between foam structure and mechanical properties of solid foams has been developed by Gibson and Ashby (1988). They related the mechanical properties (e.g., strength, modulus, yield stress, fracture toughness) of idealised cellular solids to their relative density. This work considered the cell walls of solid foams as a three-dimensional network of beams (Figure 20.18) and treated their deformation in terms of classical solid mechanics, with strength and modulus related to beam thickness and length by the equations:

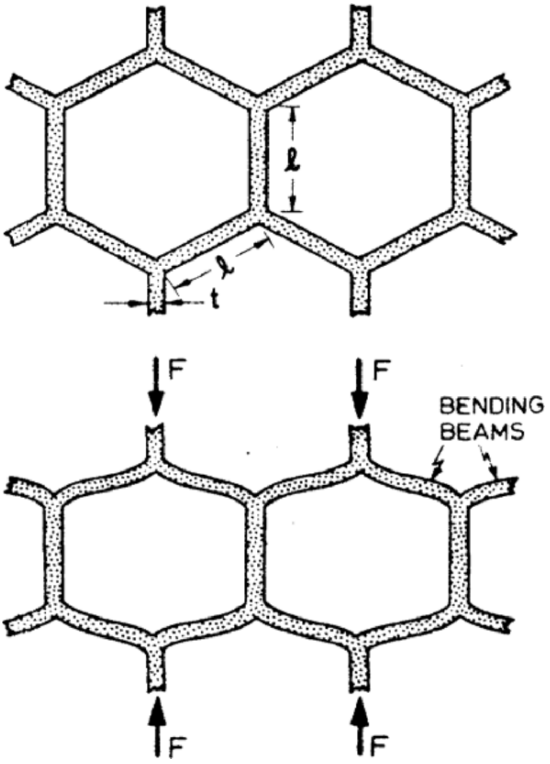

Figure 20.18. Generalised model for deformation of a foam material. (From Gibson and Ashby 1988.)

Modulus (stiffness): $$E = \frac{FL^3}{4t^4 d}$$

Maximum stress: $$\sigma_{\max} = \frac{3FL}{2t^3}$$

where F = applied force, L = length of beam, t = thickness, and d = deflection**.** The relative density of the foam is then related directly to the geometry of the beams:

$$\rho_f / \rho_S = (t / L)^2$$

where ρ_f = density of the foam, ρ_s = density of the solid foam wall material

From these relationships it is then possible to obtain a theoretical relationship between the mechanical properties of the beams and the density of the material

$$E_f / E_S = C(\rho_f / \rho_S)^n$$

where the slope n indicates the type of deformation.

The theory indicates that the mechanical properties of the foam are dependent on the properties of the cell wall materials and their size and shape. By relating the density of the foam to its bulk mechanical properties, the slope of the fitted line (n) can give us information about the type of failure mechanism (Figure 20.19). This also indicates that the size and shape of the bubbles in a foam will have a predictable effect on the strength and fracture of the foam. Bread and extruded cereal foams have been considered as cellular solids using the Gibson and Ashby analysis, and have been shown to follow the Gibson and Ashby prediction (Keetels et al. 1996; Hayter et al. 1986).

Bread consists mainly of an open cell structure (interconnected pores) with solid starch and protein material forming the cell walls. Keetels et al. found very good agreement between measured mechanical props such as Young's modulus of bread and the theoretical values predicted by the Gibson and Ashby analysis, but not such good agreements with critical fracture stress. Departure from the theoretical values were explained by large variations in cell wall thickness and anistropy due to large variations in pore sizes in bread. Hayter et al. (1986) also found relationships for maize and wheat starch extruded foams deviated from theoretical predictions, based on nonuniform distribution of pores and the presence of a much stronger extrudate outer wall.

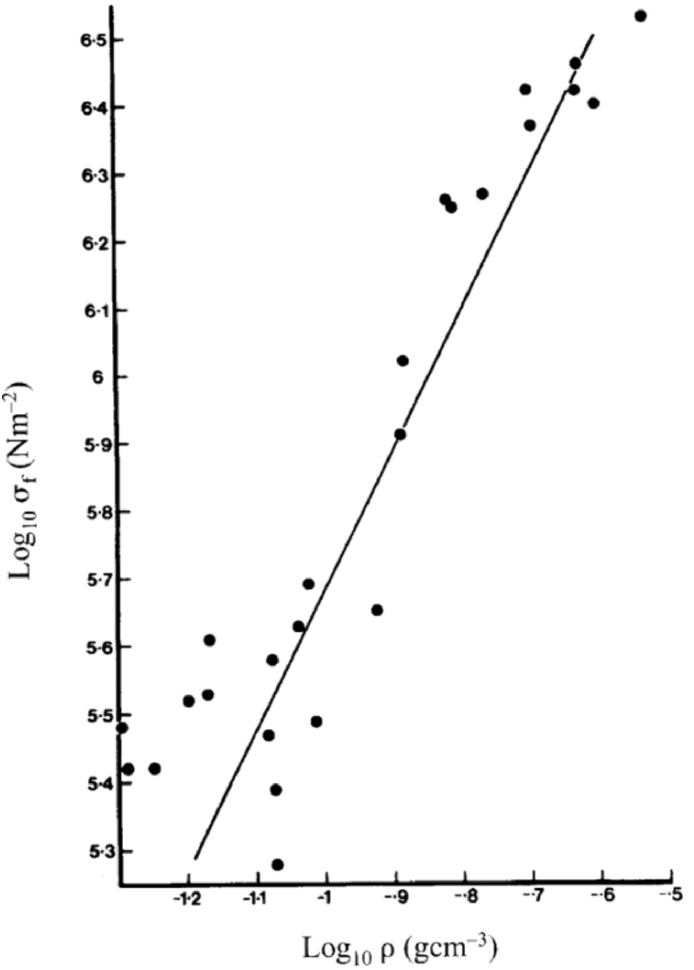

Figure 20.19. Flexural strength of extruded maize foam as a function of bulk density. (From Hutchinson 1987.)

20.13 Crispness, Structure and Mechanics of Foams

Crispness is a desirable sensory property in many cereal foods such as toast, the crust of bread, crispbreads, crisps, biscuits, extruded snacks and breakfast cereals. Since it is a subjective sensory assessment crispness is difficult to define unambiguously and its perception varies greatly between individuals and also between countries (Bourne 2002). In general it is known that crisp foods are at low moisture, in the brittle or glassy state well above T_g and fracture rapidly (see also Chapters 5 and 7). We can

all detect when crisp foods lose their crispness, using terms such as soggy, soft, stale and so on, but it is difficult to correlate these with single mechanical and thermal transitions because of the complex nature of our sensory assessment of crispness.

Extensive work has attempted to correlate crispness with mechanical properties of food, many of them not very successfully because the deformation conditions of the mechanical test were far removed from the conditions known to operate during biting and mastication (Dobraszczyk and Vincent 1999; see also Chapter 2 of this volume). A more fundamentally based materials approach has been to investigate the fracture behaviour of crisp foods, on the basis that crispness is judged to be a series of fracture events that are sensed in the mouth (Vincent 1998, 2004; Christensen and Vickers 1981; Vickers 1985, 1988). Crisp foods give sequential, jagged force-displacement curves that indicate a large number of small fractures (Figure 20.20). Each force drop is thought to correspond to an individual failure event in the material, and because of the structural inhomogeniety of foams, it is thought that the failure events are related to the structural features of the foam material such as pore size and wall thickness.

The sensation of crispness is related to the detection of numerous small fracture events within the mouth, either by direct detection by the muscles around the jaw (Muller et al. 1990), or by the sound generated (acoustic emission) as the food is broken down (Luyten and van Vliet 2006; Duizer 2001).

Luyten and van Vliet (2006) and Chen et al. (2005) have measured the acoustic properties and fracture behaviour of crisp foods and found that acoustic emission showed good relationship with sudden drops in force and the rate of energy release on fracture.

Vincent found that the critical stress intensity factor (K_c), defined as the product of stiffness (E) and the work of fracture (G_c) in the form:

$$K_c = EG_c^{0.5}$$

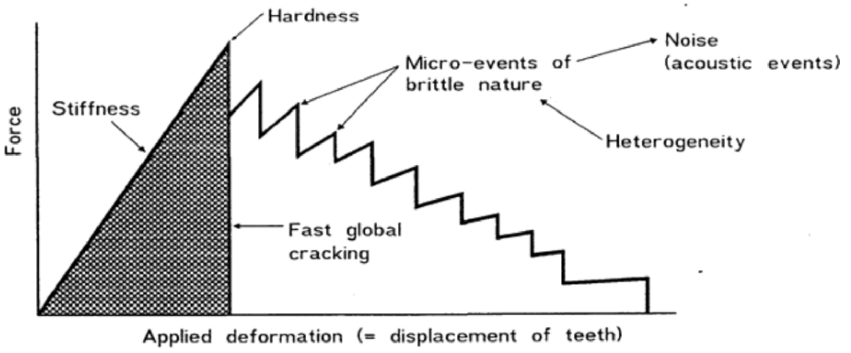

Figure 20.20. Generalised force-displacement trace for a crisp food material. (From Vincent 1998.)

where K_c correlated well with the sensory perception of hardness or crunchiness in fruits and vegetables ($R^2 = 0.996$), but that the relationship between sensory crispness and stress intensity factor was not as good ($R^2 = 0.448$).

Fracture mechanics relates the critical stress σ or energy to fracture G_c to the size (a) and geometry of a crack via the relationship:

$$G_C = \pi\sigma^2 a / E$$

The critical stress at which a material fails (σf) is therefore related to the stiffness of the material, its fracture energy or toughness G_c and a critical flaw size (a_c). In a foam structure, Gibson and Ashby have related failure stress of the cell wall to the foam geometry via the equation:

$$\sigma f = \frac{L^3}{t^3}\sqrt{a / L\sigma} = \sqrt{EG_C / a}$$

Using the previous equation for beam bending it is then possible to relate force values to cell wall geometry in foams. Vincent (2004) has measured the distribution/spectrum of force drops/events from crisp and crunchy cereal foam products, and has found that crisp materials typically showed fracture drops between 0.05 N to 5 N, whereas foams classified as crunchy gave larger force drops in the region of 5–50 N. Substituting these values into the above equations Luyten and van Vliet (2006) have defined the upper and lower values of wall thickness and pore sizes for crisp cereal foams:

Table 20.1. Wall thickness and pore sizes for crips cereal foams.

	Minimum	**Maximum**
Wall thickness	50–100 mm	300–400 mm
Pore size	120–200 mm	270–350 mm

By substituting values for the typical material and foam geometry properties E, beam length L and strain ε, and typical force drops for crispy and crunchy foams, the critical beam thickness at fracture can be obtained, calculated as being between 130 and 380 μm. Muller et al. have shown that the smallest load drop that can be detected in the mouth is ~0.05 N , which if substituted into the equation above provides a minimum foam cell wall thickness of 70 μm for sensory detection of fracture, and a maximum cell wall thickness of 300–400 μm, with pore sizes in the range 120–350 μm. This indicates the influence of the pore and wall geometry on the fracture behaviour and sensory perception of crispness in food foam materials. In principle it is then possible to design foam materials to produce a given sensory property by adjusting the pore sizes and density of the material through knowledge of the mechanics of bubble expansion in polymer melts.

20.14 References

Alava, J.M. (2003). *Formation and Development of Bread Structure in High-Speed Bread-making Process*, Ph.D. thesis, University of Reading.

Arfvidsson, C., Wahlund, K.G., and Eliasson, A.C. (2004). Direct molecular weight determination in the evaluation of dissolution methods for unreduced glutenin, *J. Cereal Sci.* 39, 1–8.

Babin, P., Della Valle, G., Chiron, H., Cloetens, P., Hoszowska, J., Pernot, P., Réguerre, A.L., Salvo, L., and Dendievel, R. (2006). Fast x-ray tomography analysis of bubble growth and foam setting during breadmaking, *J. Cereal Sci.* 43, 393–387.

Bache, I.C., and Donald, A.M. (1998). The structure of the gluten network in dough: a study using environmental scanning electron microscopy. *J. Cereal Sci.* 28, 127–133.

Belton, P.S. (1999). On the elasticity of wheat gluten, *J. Cereal Sci.* 29, 103–107.

Bourne, M. (2002). *Food Texture and Viscosity, Concept and Measurement*, 2nd ed., Academic Press, San Diego.

Brijwani, K. (2006). *Aeration of Biscuit Doughs During Mixing*, M.Sc. thesis, UMIST, UK.

Campbell, G.M. (2003). Bread aeration. In: S.P. Cauvain (ed.), *Bread Making: Improving Quality*, Woodhead Publishing, Cambridge, pp. 352–374.

Carceller, J.L., and Aussenac, T. (2001). Size characterisation of glutenin polymers by HPSEC-MALLS, *J. Cereal Sci.* 33, 131–142.

Chen, J, Karlsson, C., and Povey, M. (2005). Acoustic envelope detector for crispness assessment of biscuits, *J. Texture Studies* 36, 139–156.

Chin, N.L., and Campbell, G.M. (2005). Dough aeration and rheology. II. Effects of flour type, mixing speed and total work input on aeration and rheology of bread dough, *J. Sci. Food Agriculture* 85 2194–2202.

Chiotellis, E., and Campbell, G.M. (2003a). Proving of bread dough. I. Modelling the evolution of the bubble size distribution, *Trans IChemE*, 81, 194-206.

Chiotellis, E. and Campbell, G.M. (2003b) Proving of bread dough II. Measurement of gas production and retention, *Trans. IChemE*, 81, 207–216.

Christensen, C.M., and Vickers, Z.M. (1981). Relationships of chewing sounds to judgments of food crispness. *J. Food Sci*. 46, 574–578.

Dobraszczyk, B.J., and Morgenstern, M.P. (2003). Review: Rheology and the breadmaking process, *J. Cereal Sci.* 38, 229–245.

Dobraszczyk, B.J., and Schofield, J.D. (2002). Rapid assessment and prediction of wheat and gluten baking quality with the two-gram direct-drive Mixograph using multivariate statistical analysis, *Cereal Chem.* 79, 607–612.

Dobraszczyk, B.J., and Roberts, C.A. (1994). Strain hardening and dough gas cell-wall failure in biaxial extension, *J. Cereal Sci.* 20, 265–274.

Dobraszczyk, B.J. (2001). Wheat and Flour. In: D.A.V. Dendy, and B.J. Dobraszczyk (eds.), *Cereals and Cereal Products: Chemistry and Technology*, Aspen Publishers, Inc., Gaithersburg, MD, pp. 100–139.

Dobraszczyk, B.J., Smewing, J., Albertini, M., Maesmans, G., and Schofield, J.D. (2003). Extensional rheology and stability of gas cell walls in bread doughs at elevated temperatures in relation to breadmaking performance. *Cereal Chem.* 80, 218–224.

Dobraszczyk, B.J., and Vincent, J.F.V. (1999). Measurement of mechanical properties of food materials in relation to texture: the materials approach. In: A.J. Rosenthal (ed.), *Food Texture: Measurement and Perception,* Aspen Publishers, Gaithersburg, MD, pp. 99–151.

Doi, M., and Edwards, S.F. (1986) *The Theory of Polymer Dynamics*, Oxford University Press, Oxford.

Duizer, L. (2001). A review of acoustic research for studying the sensory perception of crisp, crunchy and crackly textures. *Trends Food Sci. Technol*. 12, 17–24.

Elmehdi, H.M., Page, J.H., and Scanlon, M.G. (2003). Monitoring dough fermentation using acoustic waves. *Trans. Institute Chem. Eng.* 81, 217–223.

Falcone, P.M., Baiano, A., Zanini, F., Mancini, L., Tromba, G., Dreossi, D., Montanari, F., Scour, N., and Del Nobile, M. (2005). 3D quantitative analysis of bread crumb by x-ray tomography, *J. Food Sci.* 70, 265–272.

Gan, Z., Ellis, P.R., and Schofield, J.D. (1995). Mini review: gas cell stabilisation and gas retention in wheat bread dough. *J. Cereal Sci.* 21, 215–230.

Gibson, L.J., and Ashby, M.F. (1988). *Cellular Solids: Structure and Properties*, Pergamon, Oxford.

Hayter, A.L., Smith, A.C., and Richmond, P. (1986). The physical properties of extruded food foams. *J. Mat. Sci.* 21, 3729–3736.

He, H., and Hoseney, R.C. (1991). Gas retention of different cereal flours, *Cereal Chem.* 68, 334–336.

Humphris, A.D.L., McMaster, T.J., Miles, M., Gilbert, S.M., Shewry, P.R., and Tatham, A.S. (2000). Atomic force microscopy (AFM) study of interactions of HMW subunits of wheat glutenin, *Cereal Chem.* 77, 107–110.

Hutchinson, R.J. (1987). Influence of processing variables on the mechanical properties of extruded maize, *J. Materials Sci.* 22, 3956–3962.

Keetels, C.J.A.M., Visser, K.A., van Vliet, T, Jurgens, A., and Walstra, P. (1996). Structure and mechanics of starch bread, *J. Cereal Sci.* 21, 215–230.

Kilborn, R.H., and Tipples, K.H. (1974), Implications of the mechanical development of bread dough by means of sheeting rolls. *Cereal Chem.* 51, 648–657.

Kilborn, R.H., and Tipples, K.H. (1972). Factors affecting mechanical dough development. I. Effect of mixing intensity and work input, *Cereal Chem.* 49, 4–47.

Kokelaar, J.J., van Vliet, T., and Prins, A., (1996). Strain hardening and extensibility of flour and gluten doughs in relation to breadmaking performance, *J. Cereal Sci.* 24, 199–214.

Li, W., Dobraszczyk, B.J., and Schofield, J.D. (2003). Stress relaxation behaviour of wheat dough and gluten protein fractions, *Cereal Chem.* 80, 333–338.

Li, W., Dobraszczyk, B.J., and Wilde, P.J. (2004). Surface properties and locations of gluten proteins and lipids revealed using confocal scanning laser microscopy in bread dough, *J. Cereal Sci.* 39, 403–411.

Lim, K.S., and Barigou, M. (2004). X-ray micro-computed tomography of cellular food products, *Food Res. Int.* 37, 1001–1012.

Luyten, H., and van Vliet, T. (2006). Acoustic emission, fracture behaviour and morphology of dry crispy foods: a discussion article, *J. Texture Studies* 37, 221–240.

Luyten, H., Plijter, J.J., and van Vliet, T. (2004). Crispy/crunchy crusts of cellular solid foods: a literature review with discussion. *J. Texture Studies* 35, 445–492.

MacRitchie, F., and Lafiandra, D. (1997). Structure–function relationships of wheat proteins. In: S. Damodaran and A. Paraf (eds.), *Food Proteins and Their Applications*, Marcel Dekker, New York, pp. 293–323.

Mani, K., Eliasson, A.-C., Lindahl, L., and Trägårdh, C. (1992). Rheological properties and bread-making quality of wheat flour doughs made with different dough mixers, *Cereal Chem.* 69, 222–225.

McLeish, T.C.B., and Larson, R.G. (1998). Molecular constitutive equations for a class of branched polymers: the pom-pom model, *J. Rheology* 42, 81–110.

Müller, F., Heath, M.R., Kazazoglu, E., and Hector, M.P. (1990). Muscle inhibition with food fracture in man. *J. Oral Rehabilitation*, 17, 193–194.

Shewry, P.R., Halford, N.G., Belton, P.S., and Tatham, A.S. (2002). The structure and properties of gluten: an elastic protein from wheat grain, *Phil. Trans. R. Soc. Lond. B*. 357. 133–142.

Trater, A.M., Alavi, S., and Rizvi, S.S.H. (2005). Use of noninvasive x-ray microtomography for characterizing microstructure of extruded biopolymer foams, *Food Res. Int.* 38, 709–719.

van Duynhoven, J., Van Kempen, G., Van Sluis, R., Rieger, B, Weegels, P., van Vliet, L., and Nicolay, K. (2003). Quantitative assessment of gas cell development during the proofing of dough by MRI and image analysis. *Cereal Chem.* 80, 390–395.

van Vliet,T., Janssen, A.M., Bloksma, A.H., and Walstra, P. (1992). Strain hardening of dough as a requirement for gas retention, *J. Texture Stud.* 23, 439–460.

Vickers, Z.M. (1985). The relationships of pitch, loudness and eating technique to judgments of the crispness and crunchiness of food sounds. *J. Texture Stud.* 16, 85–95.

Vickers, Z.M. (1988). Evaluation of crispness. In: J.M.V. Blanshard and J.R. Mitchell (eds.), *Food Structure: Its Creation and Evaluation.* pp. 433–448, Butterworths, London.

Vincent, J.F.V. (1998). The quantification of crispness. *Journal of the Science of Food and Agriculture* 78 2 162-168.

Vincent, J.F.V. (2004). Application of fracture mechanics to the texture of foods, *Eng. Failure Analysis* 11, 695–704.

Weegels, P.L., Hamer, R.J., and Schofield, J.D. (1996). Critical review: functional properties of wheat glutenin, *J. Cereal Sci.* 23, 1–18.

Whitworth, M., and Alava, J.M. (2004). Nondestructive imaging of bread and cake structure during baking. In: S.P. Cauvain, S.S. Salmon and L.S.Young (eds.), *Using Cereal Science and Technology for the Benefit of Consumers*; Woodhead Publishing, Cambridge, UK, pp. 221–231.

Chapter 21

Structured Meat Products

Milagro Reig,[1] Peter Lillford,[2] and Fidel Toldrá[3]

[1]Instituto de Ingeniería de Alimentos para el Desarrollo (UPV), Camino de Vera s/n, 46022 Valencia, Spain; mareirie@doctor.upv.es.
[2] CNAP, University of York, Heslington, York, YO10 5YV, UK; pl8@york.ac.uk.
[3]Instituto de Agroquímica y Tecnología de Alimentos (CSIC), PO Box 73, 46100 Burjassot (Valencia), Spain; ftoldra@iata.csic.es.

21.1 Introduction

After an animal has been slaughtered, the objective is to maximise the conversion of the carcass to safe edible foodstuff. As a result, mankind has experimented empirically and created a host of meat products. Their classification depends on the initial raw materials, type of processing and characteristics of the final product. So, a first classification is between entire pieces (i.e., cooked meat pieces, hams, etc.); coarse comminuted meats (burgers and reformed or restructured meat); and minced meats (i.e., sausages). Types of processing include cooking, salting (curing), drying, fermentation, and almost any combination of these that provides protection against microbial spoilage and yet offers an edible texture and flavour (Flores and Toldrá 1993). As a result, a wide variety of products are obtained.

Whole meat joints remain a major part of the sales volume of muscle food, most of which are simply cooked before use and provide a well-recognised, high-value protein food. Fresh burgers and many sausages have high moisture content, greater than 50–60%. Because of the high water activity, they can be stored for only a few days under refrigeration and need to be cooked before eating (Toldrá and Reig 2007). Raw fermented sausages are fermented by lactic acid bacteria, causing a drop in pH toward acid values. Semidry sausages have an intermediate moisture content, between 35% and 50%, as a result of a mild drying and short ripening. Dry sausages experience a more intense drying and longer ripening, and reach moisture contents below 35%. In addition, the denominations may vary according to the geographical area where they are produced, or depending on physical (shape, diameter, size of fat particles) or chemical characteristics (smoking, addition of specific spices, presence of molds on the external surface, etc.) of the sausages. Cooked sausages are subject

to a heat treatment (Toldrá and Reig 2007) and include well-known products such as garlic sausages, frankfurters, mortadella, and so on. Dry-cured ham like Iberian, Parma or Serrano are subject to mild drying and long ripening times, while cooked ham is subject to a heat treatment (Toldrá 2007). A more detailed description of main processes and products and the effects on their structure as well as the relevance to the final quality is given in this chapter.

21.2 Muscle Structure and Muscle Composition

The structure of a muscle is very complex and hierarchically constructed. The outer cover is the epimysium, a sheath of connective tissue. Thin connective tissue layers, the perimysium, cover several bundles of fibers inside the muscle and the endomysium, a thin collagenous sheath wraps each individual fiber. About 1,000 myofibrils are contained in each muscle fiber that may have an approximate diameter of around 50 μm and a length up to several centimeters (Honikel 1992). These myofibrils are arranged in a parallel way and are responsible for the contraction of the muscle (Cassens 1987). They are composed of thick and thin filaments arranged in an array. These filaments are responsible for muscle contraction and relaxation and when observed under the microscope and appear as visible alternate dark (A) and light (I) bands. The Z and M lines bisect each I and A band, respectively (Bechtel 1986). The Z line joins sarcomeres and is resistant to physical forces although is highly susceptible to postmortem degradation by muscle endoproteases action (Okitani et al. 1980). Myofibrils are composed of several myofibrillar proteins (see Table 21.1).

Table 21.1. Relative Amounts of Major Myofibrillar Proteins (adapted from Pearson and Young, 1989).

Protein	Main function	Amount (% of total)
Myosin	Contractile	43
Actin	″	22
Titin	Major cytoskeletal	8
Nebulin	″	3
Tropomyosin	Regulatory	5
Troponins C, T and I	″	5
α-actinin	″	2
C protein	Minor cytoskeletal	1.5
B-actinin	″	1.1
X protein		0.2
H protein	″	0.18
Desmin	″	0.18
M protein	″	0.15
Paratropomyosin	″	0.15

Thin filaments, mainly actin, depart from Z lines and extend between thick filaments (Yamaguchi et al. 1986). Thick filaments are mainly composed of myosin. There is a liquid in the fibers, known as cytoplasm or sarcoplasm, where several organelles such as mitochondria and lysosomes as well as soluble compounds such as enzymes, lipids, glycogen, myoglobin, ATP and creatine are immersed (Toldrá and Reig 2006).

The main constituents of skeletal muscle are water, protein, fat, carbohydrate and other soluble compounds present in minor amounts. The amount of water is usually found in the range 70–80%, and is distributed throughout the structure. Its location depends on the condition of the tissue, whether prerigor, postrigor or processed (Lillford et al. 1980) and has an important influence on juiciness, color, texture and surface appearance of the muscle. The rest of muscle is composed by proteins (myofibrillar, sarcoplasmic and connective), peptides (carnosine, anserine and balenine), free amino acids, nucleotides/nucleosides (ATP-derived compounds), lipids (triacylglycerols, phospholipids and cholesterol), water-soluble vitamins (group B vitamins) and a few fat-soluble vitamins (vitamins A, D, E and K), carbohydrates (glycogen, glucose, etc.), minerals (iron, phosphorus, sodium, potassium, etc.) and trace elements (zinc, selenium, etc.).

21.3 Postmortem Changes in Muscle

Postmortem changes in muscle have a very strong influence on many factors related to quality, for instance, water binding and drip loss. Main reactions are briefly summarised in Figure 21.1. An important change in living muscle just after death is its inability to synthesise or remove certain metabolites. Blood circulation is stopped and the main consequence is a rapid decrease in oxygen concentration in the muscle cell. The lack of available oxygen produces a progressive reduction of cell respiration in mitochondria. Then, there is a progressive reduction in the redox potential toward anaerobic values. The differences between living and dead muscle are shown in Figure 21.2. The living muscle, in aerobic conditions, produces twelve moles of ATP per mole of glucose. Additionally, ATP might also be formed from ADP and creatine phosphate through the action of the enzyme phosphocreatin kinase. However, in postmortem muscle where anaerobic conditions are prevalent, lactic acid is produced from glucose (or glycogen) through glycolysis but only 2 moles of ATP are produced per mole of glucose. ATP is produced in the muscle because of its importance function to supply the energy necessary to drive the Na/K pump of the membranes, to drive the calcium pump in the sarcoplasmic reticulum and to provide energy for muscle contraction. Once ATP is exhausted, the muscle remains contracted (Toldrá 2006a).

The generation of lactic acid through glycolysis produces a pH drop due to its accumulation in the muscle. The rate of drop may be faster or slower depending on the metabolic status of the muscle. In general, acid pH values (5.6–5.9) may be reached in just a few hours postmortem. Water binding decreases rapidly as pH approaches the isoelectric point of muscle proteins (pI values around 5.0). There is also a tightening of the structure and partial denaturation of myofibrillar proteins.

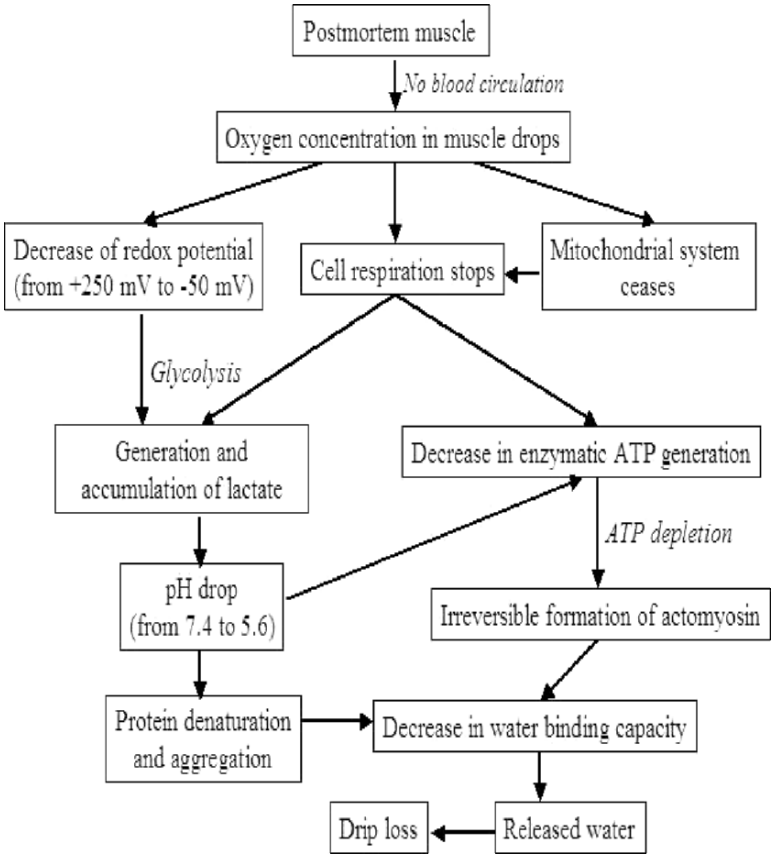

Figure 21.1. Scheme summarising early postmortem changes in muscle and its influence on water binding. Reproduced with permission from Toldrá (2002).

The main consequence is an increased amount of water (liquid) released as drip loss. Important muscle nutrients such as free amino acids, vitamins and minerals are solubilised in the water released from muscle and partly lost in the drip. This has an important effect on the final quality (Toldrá and Reig, 2006).

21.4 Structured Muscle Foods

21.4.1 Heat Treatment

The majority of meat is cooked before eating, not only to destroy contaminant microorganisms but also to change the structure. Since we do not possess the dental apparatus of a true carnivore which cuts raw meat with specially developed slicing

molars, we use a process of grinding and chewing that is more appropriate to cooked meat. (See Chapter 1.)

We now know that cooking involves separate denaturation of the different protein components. A differential scanning calorimeter (DSC) scan shows distinctly different thermal processes, which are relevant to the thermal processing of all meat products (Figure 21.3). Though these characteristic temperatures are sensitive to

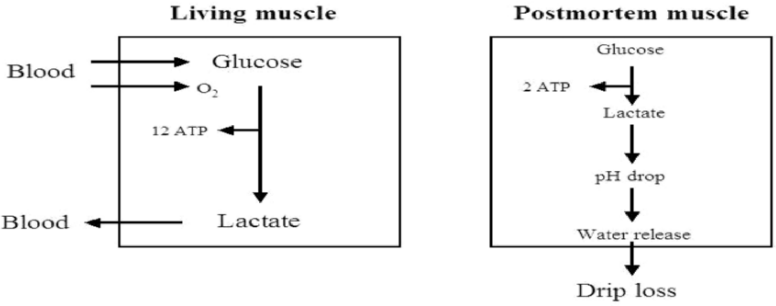

Figure 21.2. Mean differences between living and postmortem muscles. Reproduced with permission from Toldrá (2002).

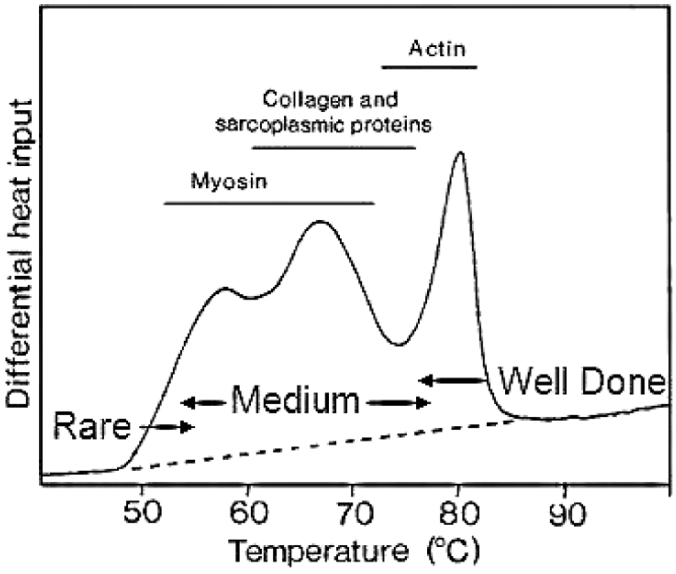

Figure 21.3. Scanning calorimetry of post rigor meat.

changes in ionic strength and pH induced by other process treatments (Wright et al. 1977; Wright and Wilding 1984). In the figure 21.3, we show temperature ranges associated with the culinary condition of "rare," "medium," and "well-done" meat. In the first, only myosin is denatured; in the second, myosin, sarcoplasmic and some connective tissue; and only in the third are all skeletal proteins denatured. Notice that in a "pot roast," where temperatures are around boiling for several hours, the process provides maximal solubilisation of the cross-linked connective tissues present in older animals.

21.4.2 Pressure Treatment

Recently, processes using extreme pressures (e.g., 400 MPa) have been applied to meat in all its product forms (Hayashi and Balny 1996). Just as in heat processing, vegetative cells of microorganisms are destroyed, so the process is equivalent to pasteurisation. However, the sensitivity of muscle proteins to pressure denaturation is different from in heat treatment so, while the same safety status is achieved, a product whose appearance, colour and texture is more like that of an uncooked meat is obtained.

21.4.3 Enzymatic Protein Cross-Linking

Different textures can be obtained through enzymatic cross-linking of meat proteins by means of enzymes such as transglutaminase and thrombin. Details of the action and uses of both enzymes are given below.

21.4.3.1 Transglutaminase

Transglutaminase (EC 2.3.2.13) catalyzes the formation of covalent bonds by means of an acyl transfer reaction between proteins (Nonaka et al. 1989). The catalyzed reaction is between the γ-carboxiamide group in glutamine, acting as acyl donor, and certain amino acids such as lysine, acting as an acyl-acceptor (Motoki and Seguro 1998). So, peptide bonds are formed intra- and intermolecularly between glutamine and lysine residues, ε-(γ-glu)-lys. A good number of applications were developed in the 1990s for better functional properties of proteins (Zhu et al. 1995), especially textural properties of meat (Sakamoto et al. 1995; Kuraishi et al. 2001).

Optimal activity of transglutaminase is achieved within the pH range 5–8 and at temperatures near 50°C even though it can work at refrigeration temperatures (Motoki and Seguro 1998). The stability is relatively good below 50°C but is rapidly lost above 60°C. The enzyme has high activity with myosin as substrate and mild against collagen but does not react with actin. Some substances such as caseinate, potassium chloride or fiber, can increase the enzyme efficiency by improving the emulsion stability and reducing the cooking losses (Jiménez-Colmenero et al. 2005). A recent report suggests that 0.15% of transglutaminase can be used to produce sensory acceptable cooked forelegs with no added phosphates and low salt content (Dimitrakopoulou et al. 2005).

Transglutaminase can modify gel formation properties. The meat gels have improved thermal stability in their firmness and water holding capacity (Motoki and Seguro 1998; Kuraishi et al. 2001; Pietrasik and Jarmoluk 2003). Texture parameters are improved in meat protein gels obtained with transglutaminase in comparison to those prepared without the enzyme (Pietrasik and Li-Chan 2002; Pietrasik 2003). Transglutaminase does not affect meat color.

21.4.3.2 Thrombin and Fibrinogen

Thrombin and fibrinogen are usually obtained from blood plasma. Thrombin (EC 3.4.21.5.) is a serine proteinase consisting of two chains and with an apparent molecular mass of about 36.5 kDa. It is most active at pH 8 in the presence of at least 0.1 M NaCl and is involved in the final step of blood coagulation (Barrett et al. 2004). This enzyme cleaves only certain arginine–glycine peptide bonds such as those found in fibrinogen which is its most abundant natural substrate (Stryer 1995). Fibrin monomers having a different surface-charge pattern are released. These monomers aggregate forming an insoluble fibrin network (Stryer 1995).

The thrombin: fibrinogen preparation is applied to meat where thrombin transforms fibrinogen to fibrin that interacts with collagen, enabling the binding of meat pieces of any desirable size and/or form in reconstituted meat. The strength of the binding depends on several additional factors such as pH, temperature, moisture content, the size of meat cuts and the direction of meat fibres (Nielsen et al. 1995). The optimum pH is 7.0 and the binding strengthens as particle size increases. Better results are obtained when the fibrin gel runs parallel to the available collagen in meat (Boles and Shand 1998; Chen and Lin 2002). Enzyme activity is rapidly lost when heating the meat Frozen/thawed meats can be used with no effect on the binding process (Boles and Shand 1999).

21.5 Processing Technologies and Protein Structure

A different effect may be observed in the protein structure depending on the type of processing (see Figure 21.4). These effects are briefly described.

21.5.1 Comminution

Not all the muscle from a carcass is suitable for whole joints, and the remainders are “restructured” by various processes. The first stage is to cut the piece to regular shapes by “dicing” “flaking.” “chopping” or “grinding.” A host of mechanical cutters have been developed to perform these operations, and while the mean particle size can be varied from centimeters to less than a millimeter, a range of particle sizes is always produced. This may have a major influence on the subsequent reassembly processes, particularly where salt is added and mass transfer rates are directly influenced by available surface area of all the meat pieces, and their size. Recently,

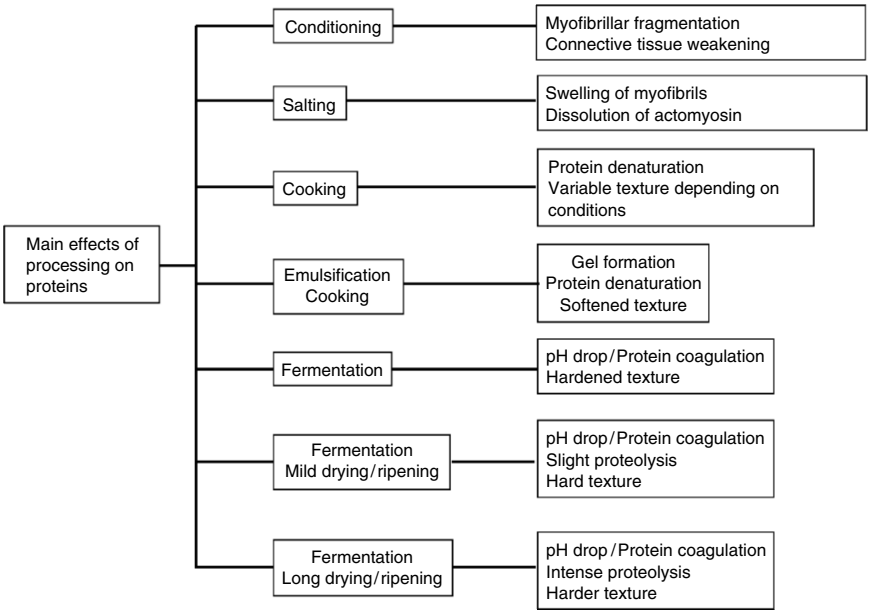

Figure 21.4. Main effects of meat processing on muscle proteins.

with a growing international commodity trade in frozen meat, size reduction can be carried out in the frozen state, where the fracture properties of muscle are obviously very different. The impact of this on subsequent eating texture will be mentioned later. Particularly significant is the degree of postmortem conditioning to which the meat has been exposed. Conditioning allows enzymic degradation of both the myofibrillar proteins and the endo and perimysium. The endomysium becomes much more shear sensitive, and once disrupted allows much greater swelling and easier solubilisation of actomyosin in subsequent process steps. (Wilding et al. 1986). The best processes therefore specify, not only the setting of the machine, but also the temperature and pretreatment conditions of the meat to be comminuted.

Comminution is a basic stage in the processing of sausages. A cutter machine is typically used to produce a fine comminute, and the batter may be stuffed into either natural or synthetic (collagen or synthetic) casings by using vacuum filling machines. Natural casings are only used for traditional products. Synthetic casings are made with co-extruded collagen, alginate or plastic (Rust 2004).

21.5.2 Adhesion

Large pieces are reassembled into whole products, ranging from joints, tp aligned flake products, to the ubiquitous burger. All these processes require that the particles adhere to one another. Adhesives, such as egg white or other soluble proteins and gelling polysaccharides can be added, but most frequently, muscle proteins themselves

are solubilised, by salt addition, both sodium chloride and various combinations of phosphates and polyphosphates. These are frequently chosen to achieve a pH increase, away from the isoelectric point of actomyosin, thereby causing further solubilisation. To complete the adhesion, pressure is applied, usually by static moulding, but also by low-pressure extrusion and cutting. Since meat is a viscoelastic material, the acceleration of process lines is not simply a matter of making the machinery run faster. Pressure cycling in moulds at rates greater than the relaxation rate of the pressed material can produce quite different end product properties, from an over-adhered rubbery block, to a porous fragile structure (Figure 21.5).

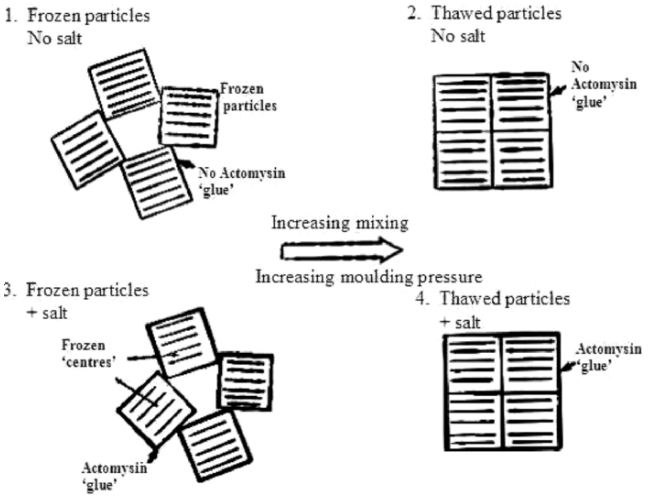

Figure 21.5. Possible structures of coarse comminute meats, showing the influence of process and temperature.

Recently, the simultaneous application of pressure and elongational shear by extrusion, allows the production of elongated particles, lightly adhered to their neighbours. This produces a remarkably meatlike aligned flake structure (Cheftel et al. 1992). For fine comminutes, the adhesion occurs in the batter itself, and casings are used to form the final product shape.

21.5.3 Thermal Processing

Thermal treatment of meat products ensures microbial destruction of microorganisms but also the denaturation of structural proteins, forming a gelled structure, and the inactivation of many endogenous enzymes (see Figure 21.3 above). In precooked products, characteristic color and flavor of the product are also developed during heating. Thermal treatment can be performed in forced convection ovens, both in

batch or continuous operation, and with the possibility of simultaneous smoking. The processing is designed to achieve inactivation of pathogen and spoilage micro-organisms for extended shelf-life of the product and, at the same time, affect sensory characteristics as little as possible (Guerrero-Legarreta 2006). This treatment is a kind of pasteurization where the internal temperature reaches 72°C for 30–60 minutes. Color changes from red to pink due to the transformation of nitrosylmyoglobin into nitrosylhemocrome during the processing, especially when temperatures approach 65°C. Upon heating, globin denatures and detaches itself from the iron atom, and surrounds the heme moiety. This typical light pink cured meat color is also known as cooked cured-meat pigment (Pegg and Shahidi 2000). The texture depends on many factors such as the extent of heating, the moisture content in the product, the extent of proteolysis, the content of intramuscular fat and the content of connective tissue.

21.5.4 Emulsification

Emulsification procedures must be followed when producing emulsified cooked sausages. This process consists of a mixing step and an emulsifying step. Preblended lean meat and fat mixtures including spices, binders, and so on, are combined in a mixer that operates below a temperature of 5–7°C, ensuring that fats are partially crystalline and thereby limiting smearing over the meat matrix. This mixture is then passed several times through an emulsifier or homogenizer (Knipe 2004). Comparable rheological characteristics of fats and the aqueous meat matrix are required. Since the viscosity of the aqueous meat matrix is high, the presence of a low viscosity liquid oil is a disadvantage, making emulsification difficult. After the emulsion has formed, they are stabilized not only by the surface activity of the soluble protein, but also by the viscosity of the continuous meat matrix.

21.5.5 Fermentation

Both physical and chemical changes occur during fermentation. Lactic acid produced during the fermentation stage induces a pH drop, thus protein coagulation and some water release. The acidulation also reduces the solubility of sarcoplasmic and myofibrillar proteins and the development of certain consistency. The drying process is a delicate operation that must achieve equilibrium between two different mass transfer processes: diffusion and evaporation (Toldrá 2006b). Rates must be similar because a very fast reduction in the relative humidity in the environment would cause an excessive evaporation at the surface of the sausage that would reduce the water content on the outer parts, causing hardening. This problem is usual in sausages of large diameter because of the long mass transfer times to bring moisture from the centre to the surface. The cross section of these sausages shows a darker, dry and hard outer ring. On the other hand, when the water transfer rate is driven by shrinkage of the meat mass, and is much higher than the evaporation rate, water accumulates on the surface of the sausage causing wrinkled casings. This problem usually happens in sausages of small diameter where there is high relative humidity in the environment. The progress in drying reduces the water content, up to 20% weight loss in semi-dry

sausages and 30% in dry sausages. Water activity decreases as drying proceeds, reaching values below 0.90 for long ripened sausages (Toldrá 2006c).

Many enzymes, of both muscle and microbial origin, are involved in reactions related to color, texture and flavor generation. The reactions, especially proteolysis and lipolysis, are very important for the final sensory quality of the product (Toldrá 1998, 2004a). An intense proteolysis during fermentation and ripening is mainly carried out by endogenous cathepsin D, an acid muscle proteinase very active at acid pH. Myosin and actin are easily hydrolyzed by this enzyme, producing an accumulation of polypeptides that are further hydrolyzed to small peptides by muscle and microbial peptidylpeptidases and to free amino acids by muscle and microbial aminopeptidases. The generation of small peptides and free amino acids increases as the process proceeds. However, the generation rate is reduced when sausages are fermented to very acid pH values because the enzyme activity is far from its optimal conditions. Free amino acids may be further transformed into other products like volatile compounds through Strecker degradations and Maillard reactions, ammonia through deamination and/or deamidation reactions by deaminases and deamidases, respectively (present in yeasts and molds) and amines by microbial decarboxylases (Toldrá et al. 2001).

Another important group of enzymatic reactions, affecting muscle and adipose tissue lipids, is known as lipolysis (Toldrá and Flores 1998). Lipolysis is important in fermented meats. A large amount of free fatty acids (between 0.5% and 7%) is generated in fermented sausages through the enzymatic hydrolysis of triacylglycerols and phospholipids. Most of the observed lipolysis is attributed to endogenous lipases present in muscle and adipose tissue such as the lysosomal acid lipase, present in the lysosomes and very active at acid pH (Toldrá 1992; Hierro et al. 1997; Molly et al. 1997).

Catalases are mainly present in microorganisms such as *Kocuria* and *Staphylococcus* and are responsible for peroxide reduction. This reaction contributes to color and flavor stabilization. Nitrate reductase, also present in those microorganisms, is a very important enzyme for the reduction of nitrate to nitrite in slow ripened sausages where there is initial addition of nitrate. Recently, two strains of *Lactobacillus fermentum* have proved to be able to generate nitric oxide and give an acceptable color in sausages without nitrate/nitrite. This may be important in the case of cured meats with no addition of either nitrate or nitrite (Moller et al. 2003).

21.5.6 Dry Curing

This is a typical process that has been performed in Mediterranean countries for many centuries (Toldrá 2002). Hams are salted by rubbing salt on their surface and then leaving for a few days, depending on the ham weight. Once the salt has penetrated, hams are hung in drying chambers (the postsalting stage) in order to get the salt diffused throughout the entire piece of ham. This stage takes about two months. Then, the ripening and drying processes may be more or less intense depending on the desired final quality. Temperature, relative humidity and air flow have to be carefully controlled during ripening and drying to allow correct enzyme action and adequate

drying. The air velocity is kept at around 0.1 m/s which is enough for a good homogenization of the environment. Ripening and drying are important for enzymatic reactions related with flavor development and to get the required water loss and thus reduction in water activity (Toldrá 2004b). The length of the ripening/drying period for hams may take from 3 to 24 months or even longer depending on many factors such as the type and size of ham, fat content, desired quality, etc. In general, dry-cured meat products ripened for long time tend to be drier and more flavorful (Toldrá 2006d). This is important to allow the activity of endogenous muscle enzymes. The amount of muscle enzymes depends on the original crossbreeds (Parolari et al. 1996) and the age of the pigs (Rosell and Toldrá 1996). Other important factors are related to the processing technology: for instance, the temperature and time of ripening will determine the major or minor action of the enzymes, and the amount of added salt, which is a known inhibitor of cathepsins and other proteases, will also regulate the enzyme action (Toldrá 1992; Toldrá Rico and Flores 1992).

There is a progressive degradation and intense breakdown of major meat proteins (sarcoplasmic and myofibrillar proteins) during dry curing. This creates a weakening of the myofibrillar network and an increase in tenderness. An example of muscle structure in 8 months dry-cured ham is shown in Figure 21.6. The activity of endogenous muscle enzymes, mainly cathepsins B, D and L, play an important role in this protein breakdown (Toldrá et al. 1993). These enzymes are quite stable and operate for several months at a good rate depending on the drying/ripening temperature and

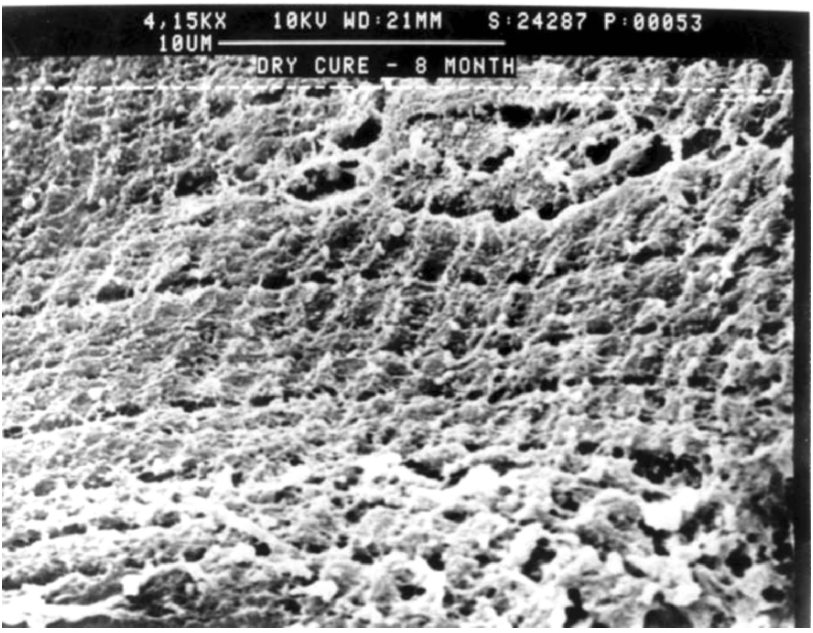

Figure 21.6. Scanning electron micrograph showing the structure of 8 month dry-cured ham. Maginification: 4150x. Voyle and Toldrá. (1987, unpublished).

salt content into the hams. The added salt is an important factor because salt is a known inhibitor of cathepsins and other proteases and thus regulates the enzyme action (Rico et al. 1990, 1991; Toldrá et al. 1992). In fact, an excessive softness of ham has been correlated with high cathepsin B activity and low salt content (García-Garrido et al. 2000) Simultaneously, there is an important generation of small peptides and free amino acids.

21.6 Effects of Proteolysis

Microbial and endogenous muscle proteases are the main factors responsible for proteolysis during meat fermentation and dry-curing processes. A good knowledge of the properties and mode of action of these proteases is essential in order to control proteolysis (Toldrá 2006e). Different enzymes are involved in the generation routes of these compounds: Endo-peptidases, also known as proteinases, are responsible for protein breakdown. Calpains and cathepsins B, D, H and L are the most important muscle proteinases. Several groups of enzymes are involved in further proteolysis of polypeptides and peptides. Tri- and di-peptidylpeptidases are involved in the generation of small tri- and di-peptides, respectively, and tri- and di-peptidases may act on these peptides, respectively, and generate free amino acids.

Aminopeptidases and carboxypeptidases constitute the last stage of the proteolysis chain and release free amino acids from the amino and carboxy termini of peptides and polypeptides, respectively (Toldrá 2006e). Peptides and free amino acids usually get accumulated in meat and meat products. The generation of small peptides, especially within the range 2,700 to 4,500 Da, or even below 2,700 Da increases as processing progresses (Aristoy and Toldrá 1995). This generation rate may be increased or decreased depending on the amount of added salt that inhibits muscle peptidases (Toldrá et al. 2002). Some of these peptides give characteristics tastes (Toldrá 1998). The amount of released free amino acids by the action of endogenous muscle aminopeptidases may reach several hundreds of mg per 100g of ham (Toldrá and Flores 1998).

Free amino acids may be subject of a number of enzymatic transformations such as decarboxylation, deamination and/or transamination, by microorganisms present in the product (Toldrá 2004a). In addition, there are non-enzymatic pathways for amino acid conversion such as the Strecker degradation of amino acids that is an oxidative deamination–decarboxylation producing branched aldehydes. The generation of 3-methylbutanal, 2-methylbutanal and phenylacetaldehyde from leucine, isoleucine and phenylalanine, respectively, has been found in dry-fermented sausages. It is also remarkable for Strecker degradation of sulfur-containing amino acids such as methionine, cisteine and cystine which leads to the production of sulfur compounds characterized by low threshold values and therefore a high aromatic impact in meat products (Toldrá 2006d).

An excess of proteolysis must be avoided as it can impair the sensory characteristics for the following reasons (Toldrá 2002): (i) Development of a bitter and metallic taste as a consequence of the accumulation of an excess of peptides and free amino acids; (ii) formation and random distribution of white crystals of tyrosine

throughout the product, which is the case in long ripening meat products; and (iii) an excessive softness of the meat product as a consequence of the excessive myofibrillar proteins breakdown.

21.7 Meat Protein Structure and Its Effects on Sensory Quality

As described above, meat has a complex hierarchical structure, so the sensory properties relate to the extent to which this remains in the final product. For whole meat products and coarse comminutes, the entire hierarchy remains. The fibrosity of these products relates to the higher order structure of muscle bundles (see below). For finer comminutes, such as sausages of various forms, muscle myofibrillar proteins, and residual disorganised myofibrils are dominant. These experience an intense proteolysis during meat aging and especially during further processing such as fermentation or dry-curing. The result, as discussed below, is an extensive protein breakdown that affects tenderness but also flavour, by influencing the interaction of proteins with flavour volatile compounds.

21.7.1 Flavor: Interactions of Proteins with Volatile Compounds

The effect of meat structure on the binding of volatile compounds has not been elucidated until recently where some studies have been performed based on the solid phase microextraction (SPME) technique (Gianelli et al. 2002). The ability of skeletal dipeptides (carnosine and anserine) and a sarcoplasmic protein (myoglobin) to interact with key flavor compounds was investigated. The results obtained showed carnosine as the peptide with the higher affinity for volatile compounds. However, myoglobin, which is the major sarcoplasmic protein, showed a higher number of binding sites than the dipeptides. These results indicate different aroma retentions by skeletal dipeptides and myoglobin that can result in different sensory perceptions of muscle foods depending on its processing (Gianelli et al. 2003) not only the effect of structure of peptides is important in binding but also the volatile compound structure.

According to Kinsella (1990), pH may produce alterations on the binding sites of proteins induced by conformational changes such as in the case of the interaction of BSA with 2-nonanone. For instance, the variation of interaction of β-lactoglobulin according to the medium pH is related to structural variations of the protein (Jouenne and Crouzet 2000). In the case of meat peptides and proteins, the effect of pH was only significant for some volatile compounds like hexanal. So, the hexanal–myoglobin binding was observed to be significantly lower ($p < 0.05$) at pH 6.0 and 6.5 than at pH 5.0 and 5.5. The location of chemical compounds present in different sections of dry-cured ham have been reported to exert some effects on the retention of volatile compounds (Flores et al. 2006). The curing agents also exert some effects on the interaction with proteins. So, nitrite, nitrate and ascorbic acid appeared to favour the release of volatile compounds (Flores et al. 2007).

The binding of sarcoplasmic and myofibrillar proteins extracted from post-rigor pork muscle, and from 7- and 12-months dry-cured hams with volatile compounds such as 3-methyl-butanal, 2-methyl-butanal, 2-pentanone, hexanal, methional and

octanal was also compared. The results showed that binding ability of sarcoplasmic proteins from pork muscle was higher than the ability shown by 7- and 12-months dry-cured ham sarcoplasmic homogenates and also higher than the binding ability of myofibrillar homogenates. The binding by myofibrillar proteins was affected by the ionic strength due to changes in protein conformation that affect their binding ability. However, the sarcoplasmic protein binding ability was more related to the small components contained in the homogenate than with the aqueous phase ionic strength (Pérez-Juan et al. 2006). Two specific myofibrillar proteins, actomyosin and actin in its globular and polymerized form, were isolated from post-rigor porcine muscle and used to study their binding ability to selected volatile aroma compounds. Actomyosin was able to bind all the assayed volatile compounds although the binding was dependent on protein concentration and conformation, and highly affected by frozen storage. The polymerized form (F-actin) was the isolated myofibrillar protein that was able to bind higher quantities of the assayed volatile compounds. However, G-actin was unable to bind any of the assayed volatile compounds and furthermore, it produced the release of several of them (especially aldehydes like 3-methyl-butanal, hexanal, methional and octanal) at the highest protein concentration (Pérez-Juan et al. 2007).

The curing agents exert some effects on the interaction with proteins. So, nitrite, nitrate and ascorbic acid appeared to favour the release of volatile compounds (Flores et al. 2007). According to Kinsella (1990), pH may produce alterations on the binding sites of proteins induced by conformational changes such as in the case of the interaction of BSA with 2-nonanone. For instance, the variation of interaction of β-lactoglobulin according to the medium pH is related to structural variations of the protein (Jouenne and Crouzet 2000). In the case of meat peptides and proteins, the effect of pH was only significant for some volatile compounds such as hexanal. So, the hexanal–myoglobin binding was observed to be significantly lower ($p < 0.05$) at pH 6.0 and 6.5 than at pH 5.0 and 5.5.

21.7.2 Texture

Many pieces of equipment have been developed to measure the mechanical properties of meat and its various products (Purslow 1991). While the need for quality control devices is not disputed, the ultimate arbiter of texture and its quality is the human consumer. The problem for the materials scientist is to link the events in the mechanical device called the mouth, (and the subsequent sensations of eating quality) to the material properties of the product being eaten. We probably have more detailed knowledge of the biochemistry and hierarchical structure of meat, than any other foodstuff, thanks to the efforts of medicine, biomechanics and food science. The problem is to relate all this information to the perception of texture, identifying the stimuli that give rise to the required response.

As well as understanding meat itself, in the recent past the ability to copy or synthesise meatlike structure has had an economic benefit, because of the high cost of meat as a protein source. Most recently, pressure from animal welfare concerns, vegetarianism, and the need to reduce saturated fat intake has led to a proliferation of products which provide some kind of meat-like textures by processing. What are the structural elements, and how should they be assembled? Much of the story can be pieced together from the published literature.

Most studies identify three critical properties in the quality of meat and its products. These "dimensions" are toughness/tenderness, juiciness/dryness, and of course flavour. The first two of these are obviously materials properties related to the architecture of the product, and its subsequent fracture and failure modes. Attempts to match these attributes to simple physical tests proves successful provided that the range of specimens have similar architecture.

To understand further what sensations make up these general descriptors, Horsfield and Taylor (1976) used human subjects and free choice profiling to develop a comprehensive list of descriptors needed to discriminate between whole meats and analogues, after various process treatments. After panelling such a set, principle Component analysis showed that indeed these three primary dimensions were still identified, but that each dimension consisted of groups of attributes, all of which were necessary for product discrimination. This shows immediately, that the average meat eater is sensitive to many different mechanical and particulate stimuli, in obtaining a view about whether the product is tough or tender, juicy or dry.

21.7.2.1 The Toughness Dimension

This dimension was dominated by terms such as resistance, resilience, chewiness and breakdown. In a later study, this last parameter was broken down into terms describing the type of breakdown, e.g., flakiness, flakesize and fibresize (Taylor L.J. personal communication). Not surprisingly, all these parameters were influenced by the raw material source (cow, sheep, pig, chicken); the extent of cooking; and the effect of postmortem aging.

Willems and Purslow (1997) studied the effects of cooking and aging on the tensile properties of meat fibre bundles by extending them in the fibre alignment direction. They also found significant effects, but whereas aging reduced both the stress and strain-to-break of cooked fibres, cooking itself increased the same parameters relative to raw meat, not what is described by panellists. However, in our study, where tensile and compression studies were performed at right angles to the fibre alignment, good correlation with panel scores were obtained for resistance, resilience and chewiness; see, for example, Figures 21.7 and 21.8. A negative correlation with flakiness was also seen (Lillford 2000, 2001). Therefore, the toughness parameter is primarily determined by the separation of fibre bundles and fibres from each other., This was confirmed by examining microscopically the damage done to meat during chewing. Even immediately before swallowing, few fibres are broken, but fibre bundles and fibres are separated (Lillford 2000). The best meatlike analogue products should show the same behaviour.

21.7.2.2 The Juiciness Dimension

What also follows from the above microscopic examination is that most of the liquid inside fibres is not released during chewing, and therefore is unlikely to contribute to the perceived juiciness. Horsfield and Taylor's results indicate that this sensory dimension contains elements of liquid identifiable during the first chew, together

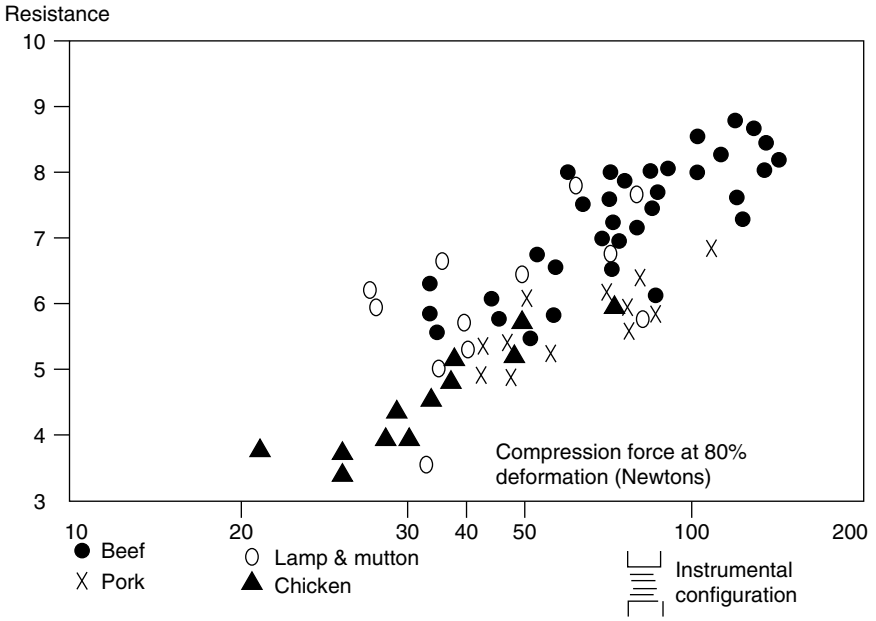

Figure 21.7. Correlation of sensorically perceived resistance and compression forces.

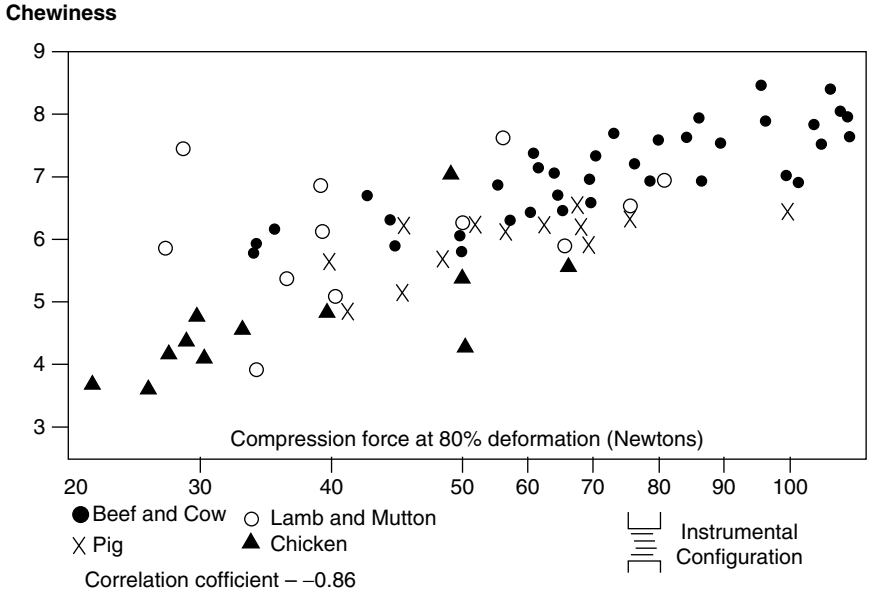

Figure 21.8. Correlation of sensorically perceived resilience and compression forces.

with the juiciness immediately prior to swallowing, and the ease of forming a swallowable bolus. It is most likely that this liquid is weakly retained in the capillary structures between fibres and bundles. The use of NMR relaxometry allows us to explore this further.

Lillford et al. (1980) showed that the nonlinear relaxation properties of the water in porous structures and fibre assemblies can be transformed into a measure of the relative pore size distribution. Tornberg and co-workers (1984, 1986) have used the technique to study the migration of water during muscle processing. Can the same measurement be correlated with juiciness perception during chewing? Using the complete set of samples already scored for their juiciness, we have measured NMR relaxation time distributions, and examined the correlation between these and the sensory property. The results are shown schematically in the following Figure 21.9. Notice that the correlation coefficient increases as water with long relaxation

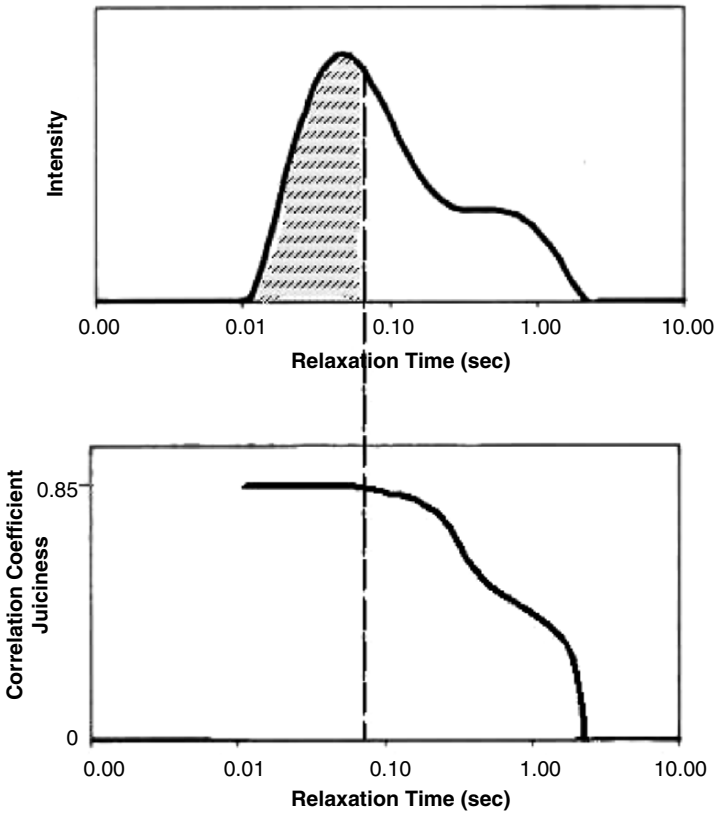

Figure 21.9. Correlation between distribution of water relaxation times (NMR) and perceived juiciness.

times (within larger pores) is included, but only down to a relaxation time of approximately 50 ms. This corresponds almost exactly to the relaxation time of water retained within cooked fibres, ratifying the conclusions drawn from the microscopic examination of chewed meat. A good meat analogue should exhibit a similar relaxation spectral width.

This result also explains why meat products designed to have maximal water content can at the same time appear texturally dry. The protein gel formed, by solubilising actomyosin, or adding polysaccharide "water binders," retains water during chewing so successfully that little or none is released.

In many meat products there is a second lubricant, namely fats and oils. This result also implies that if emulsion or other fat inclusions are not fractured during chewing, then these too will have the effect of softening the structure, reducing the toughness, but will have little effect on juiciness or lubrication. Rather than aim for small droplets in highly stable emulsions, some larger droplets or even partial breakdown should be beneficial.

21.8 Conclusions

In aiming to maximise the use of animal protein from any carcass, technologies have been developed that use the molecular, nano-, meso- and microstructures of muscle. An enormous array of structured products can be fabricated, all of which are recognised individually as desirable foodstuffs. Each have a range of eating quality attributes which we can begin to relate to the control of their processes of manufacture, their raw material selection and their resultant architecture. This depth of understanding does allow more systematic product design and innovation..

21.9 References

Aristoy, M.-C., and Toldrá, F. (1995). Isolation of flavor peptides from raw pork meat and dry-cured ham. In: G. Charalambous, (ed), *Food Flavors: Generation, Analysis and Process Influence*, Elsevier, Amsterdam, pp. 1323–1344.

Barrett, A.J, Rawlings, N.D., and Woessner, J.F. (2004). Thrombin. In: *Handbook of Proteolytic Enzymes*. 2nd edition, vol. 2, Elsevier, Amsterdam, pp. 1667–1672.

Bechtel, P.J. (1986). Muscle development and contractile proteins. In P.J. Bechtel (ed.), *Muscle as Food*. Academic Press, Orlando, pp. 1–35.

Boles, J.A., and Shand, P.J. (1998). Effects of comminution method and raw binder system in restructured beef. *Meat Science* 49, 297–307.

Boles, J.A., and Shand, P.J. (1999). Effects of raw binder system, meat cut and prior freezing on restructured beef. *Meat Science* 53, 233–239.

Cassens, R.G. (1987). Structure of muscle. In: J.F. Price and B.S. Schweigert (eds.), *The Science of Meat and Meat Products*. Food & Nutrition Press, Westport, CT, pp. 11–59.

Cheftel, J.C., Kitagawa, M., and Queguiner, C. (1992). New texturisation processes by extrusion cooking at high moisture levels. *Food Reviews Int*., 8, 235–275.

Chen, M.J., and Lin C.W. (2002). Factors affecting the water-holding capacity of fibrinogen/plasma protein gels optimized by response surface methodology. *J. Food Sci.* 67, 2579–2582.

Dimitrakopoulou, M.A., Ambrosiadis, J.A., Zetou, F.K., and Bloukas, J.G. (2005). Effect of salt and transglutaminase (TG) level and processing conditions on quality characteristics of phosphate-free, cooked, restructured pork shoulder. *Meat Science*, 70, 743–749.

Flores, M., Pérez-Juan, M., and Toldrá, F. (2006). Generation of volatile flavour compounds as affected by the chemical compounds present in different sections of dry-cured ham. *Eur. Food Res. Technol.* 222, 658–666.

Flores, M., Gianelli, M.P., Pérez-Juan, M., and Toldrá, F. (2007). Headspace concentration of selected dry-cured aroma compounds in model systems as affected by curing agents. *Food Chem.* 101, 1588–1593.

Flores, J., and Toldrá, F. (1993). Curing: processes and applications. In: R. Macrae, R. Robinson, M. Sadle, G. Fullerlove, (eds.), *Encyclopedia of Food Science, Food Technology and Nutrition*, Academic Press, London, pp. 1277–1282.

García-Garrido, J.A., Quiles, R., Tapiador, J., and Luque, M.D. (2000). Activity of cathepsin B, D, H and L in Spanish dry-cured ham of normal and defective texture. *Meat Science* 56, 1–6.

Gianelli, M.P., Flores, M., and Toldrá, F. (2005). Interactions of soluble peptides and proteins from skeletel muscle with volatile compounds as affected by curing agents, *J. Agric. Food Chem.* 53, 1670–1677.

Gianelli, M.P., Flores, M., and Toldrá, F. (2003). Interactions of soluble peptides and proteins from skeletel muscle on the release of volatile compounds. *J. Agric. Food Chem.* 51, 6828–6834.

Gianelli, M.P., Flores, M., and Toldrá, F. (2002). Analysis of volatile compounds of dry-cured ham using different solid-phase microextraction (SPME) fiber coatings. *J. Sci. Food Agric.* 82, 1703–1709.

Guerrero-Legarreta I. (2006). Thermal processing of meats. In: Y.H. Hui, E. Castell-Perez, L.M. Cunha, I. Guerrero-Legarreta, H.H. Liang, Y.M. Lo, D.L. Marshall, W.K. Nip, F. Shahidi, F. Sherkat, R.J. Winger, K.L. Yam (eds.), *Handbook of Food Science, Technology and Engineering*, volume 4, CRC Press, Boca Raton, FL, pp. 162–1 to 162–9.

Hayashi, R., and Balny, C. (1996). *High-Pressure Bioscience and Biotechnology*, Progress in Biotechnology, 13, Elsevier, Amsterdam.

Hierro, E., De la Hoz, L., and Ordoñez, J.A. (1997). Contribution of microbial and meat endogenous enzymes to the lipolysis of dry fermented sausages. *J. Agric. Food Chem.* 45, 2989–2995.

Horsfield, S., and Taylor L.J. (1976). Exploring the relationship between sensory data and the acceptability of meat. *J. Sci. Food Agric*. 27, 1044–1056.

Honikel, K.O. (1992). The biochemical basis of meat conditioning. In: J.M. Smulders, F. Toldrá, J. Flores, M. Prieto (eds.), *New Technologies for Meat and Meat Products*. Audet, Nijmegen, The Netherlands, pp. 135–161.

Jiménez-Colmenero, F., Ayo, M.J., and Carballo, J. (2005). Physicochemical properties of low sodium frankfurter with added walnut: effect of transglutaminase combined with caseinate, KCl and dietary fibre as salt replacers. *Meat Science*, 69, 781–788.

Jouenne, R., and Crouzet, J. (2000). Effect of pH on retention of aroma compounds by β-lactoglobulin. *J. Agric. Food Chem*. 48, 1273–1277.

Kinsella, J.E. (1990). Flavor perception and binding. *Inform*, 1, 215–226.

Knipe, C.L. (2004). Sausages: types of emulsion. In: W. Jensen, C. Devine and M. Dikemann (eds.), *Encyclopedia of Meat Sciences*. Elsevier, London, pp. 1216–1220.

Kuraishi, C., Yamazaki, K., and Susa, Y. (2001). Transglutaminase: its utilization in the food industry. *Food Rev. Int.*, 17, 221–246.

Lillford, P.J. (2000). *The Materials Science of Eating and Food Breakdown*, MRS Bulletin, 25, 12, 38–43.

Lillford, P.J., (2001). Mechanisms of fracture in foods, *J. Texture Studies* 32, 5/6 , 397–417.

Lillford, P.J., Clark, A.H., and Jones, D.V. (1980). Distribution of water in heterogeneous food and model systems, ACS Symposium Series 127, In: S.P. Rowland (ed.) *Water in Polymers.* American Chemical Society, Washington DC, pp. 177–195.

Molly, K., Demeyer, D.I., Johansson, G., Raemaekers, M., Ghistelinck, M., and Geenen, I. (1997). The importance of meat enzymes in ripening and flavor generation in dry fermented sausages. First results of a European project. *Food Chem.* 54, 539–545.

Moller, J.K.S., Jensen, J.S., and Skibsted LH. (2003). Microbial formation of nitrite-cured pigment, nitrosylmyoglobin, from metmyoglobin in model systems and smoked fermented sausages by *Lactobacillus fermentum* strains and a commercial starter culture. *Eur. Food Res. Tech.* 216, 6, 463–469.

Motoki, M., and Seguro, K. (1998). Transglutaminase and its use for food processing. *Trends Food Sci. Technol.* 9, 204–210.

Nielsen, G.S., Petersen B.R., and Moller A.J. (1995). Impact of salt, phosphate and temperature on the effect of a transglutaminase (FXIIIa) on the texture of restructured meat. *Meat Sci.* 41, 293–299.

Nonaka, M., Tanaka, H., Okiyama, A., Motoki, M., Ando, H., Umeda, K., and Matsuura A. (1989). Polymerization of several proteins by Ca^{2+}-independent transglutaminase derived from microorganism. *Agric. Biolog. Chem.* 53, 2619–2623.

Okitani, A., Matsukura, U., Kato, H., and Fujimaki, M. (1980). Purification and some properties of a myofibrilar protein-degrading protease, cathepsin L from rabbit skeletal muscle. *J. Biochem.* 87, 1133–1143.

Parolari, G., Virgili, R., and Schivazzappa, C. (1994). Relationship between cathepsin B activity and compositional parameters in dry-cured hams of normal and defective texture. *Meat Sci.* 38, 117–122.

Pearson, A.M., and Young, R.B. (1989). *Muscle and Meat Biochemistry*. San Diego, CA, Academic Press, pp. 1–261.

Pegg, R.B., and Shahidi, F. (2000). *Nitrite Curing of Meat*. Food & Nutrition Press, Trumbull, CT, pp. 23–66.

Pérez-Juan, M., Flores, M., and Toldrá, F. (2007). Simultaneous process to isolate actomyosin and actin from post-rigor porcine skeletal muscle. *Food Chem.* 101, 1005–1011.

Pérez-Juan, M., Flores, M., and Toldrá, F. (2006). Model studies on the efficacy of protein homogenates from raw pork muscle and dry-cured ham in binding selected flavor compounds. *J. Agric. Food Chem.* 54, 4802–4808.

Pietrasik, Z., and Li-Chan, E.C.Y. (2002). Response surface methodology study on the effects of salt, microbial transglutaminase and heating temperature on pork batter gel properties. *Food Res. Int.* 35, 387–396.

Pietrasik, Z. (2003). Binding and textural properties of beef gels processed with κ-carrageenan, egg albumin and microbial transglutaminase. *Meat Sci.* 63, 317–324.

Pietrasik, Z., and Jarmoluk, A. (2003). Effect of sodium caseinate and κ-carrageenan on binding and textural properties of pork muscle gels enhanced by microbial transglutaminase addition. *Food Res. Int.* 36, 285–294.

Purslow, P.P. (1991). Measuring meat texture and understanding its structural basis. In: Vincent, J.F.V., and Lillford, P.J. (eds.), Feeding and the Texture of Food, Cambridge University Press, Cambridge, pp. 35–56.

Rico, E., Toldrá, F., and Flores, J. (1990). Activity of cathepsin D as affected by chemical and physical dry-curing parameters. *Z. Lebensm. Unters. Forsch.* 191, 20–23.

Rico, E., Toldrá, F., and Flores, J. (1991). Effect of dry-curing process parameters on pork muscle cathepsins B, H and L activities. *Z. Lebensm. Unters. Forsch.* 193, 541–544.

Rust, R.E. (2004). Sausage casings. In: W. Jensen, C. Devine and M. Dikemann (eds.), *Encyclopedia of Meat Sciences*. Elsevier, London, pp. 1203–1207.

Sakamoto, H., Kumazawa, Y, Kawajiri, H., and Motoki, M. (1995). ε-(γ-glutamyl)-lysine cross-link distribution in foods as determined by improved method. *J. Food Sci.* 60, 416–419.

Stryer, L. (1995). *Biochemistry*. 4th edition. WH Freeman Company, New York, pp. 252–258.

Toldrá, F. (1992). The enzymology of dry-curing of meat products. In: F. Smulders, F. Toldrá, J. Flores, and M. Prieto (eds.), *New Technologies for Meat and Meat Products*, Audet, Nijmegen, pp. 209–231.

Toldrá, F. (1998). Proteolysis and lipolysis in flavour development of dry-cured meat products. *Meat Sci.* 49, S101–S110.

Toldrá, F., Flores, M., and Sanz, Y. (2001). Meat fermentation technology. In: Y.H. Hui, W.K. Nip, R.W. Rogers, and O.A. Young (eds.), Meat Science and Applications. Marcel Dekker, New York, pp. 537–561.

Toldrá, F., Rico, E., and Flores, J. (1993). Cathepsin B, D, H and L activity in the processing of dry-cured-ham. *J. Sci. Food Agric.* 62, 157–161.

Toldrá, F., Rico, E., and Flores, J. (1992). Activities of pork muscle proteases in cured meats. *Biochimie* 74, 291–296.

Toldrá, F., and Flores, M. (1998). The role of muscle proteases and lipases in flavor development during the processing of dry-cured ham. *CRC Crit. Rev. Food Sci. Nutr.* 38, 331–352.

Toldrá, F. (2002). *Dry-Cured Meat Products*, Food & Nutrition Press, Trumbull, CT.

Toldrá, F. (2004a). Fermented meats. In: Y.H. Hui and J.S. Smith (eds.), *Food Processing: Principles and Applications*, Blackwell Publishing, Ames, IA, pp. 399–415.

Toldrá F. (2004b). Dry curing. In: W. Jensen, C. Devine, and M. Dikemann (eds.), *Encyclopedia of Meat Sciences*. Elsevier, London, pp. 360–365.

Toldrá, F., and Reig, M. (2006). Biochemistry of raw meat and poultry. In: Y.H. Hui, W.K. Nip, M.L. Nollet, G. Paliyath and B.K Simpson (Eds.), Food Biochemistry and Food *Processing*, Blackwell Publishing, Ames, IA, pp. 293–314.

Toldrá, F. (2006a). Meat: chemistry and biochemistry In: Y.H. Hui (ed.), *Handbook of Food* Science, Technology and Engineering vol. 4, CRC Press, Boca Raton, FL, pp. 28–1 to 28–18.

Toldrá, F. (2006b). Meat fermentation. In: Y.H. Hui (ed.), *Handbook of Food Science, Technology and Engineering* vol. 4, CRC Press, Boca Raton, FL, pp. 181–1a 181–12.

Toldrá, F. (2006c). Biochemistry of fermented meat. In: Y.H. Hui, W.K. Nip, M.L. Nollet, G. Paliyath, and B.K. Simpson (eds.), *Food Biochemistry and Food Processing,* Blackwell Publishing, Ames, IA, pp. 641–658.

Toldrá F. (2006d). Dry-cured ham. In: Y.H. Hui (ed.), *Handbook of Food Science, Technology and Engineering*, vol. 4, CRC Press, Boca Raton, FL, pp. 164–1 to 164–11.

Toldrá F. (2006e). Biochemical proteolysis basis for improved processing of dry-cured meats. In: L.M.L. Nollet and F. Toldrá (eds.), *Advanced Technologies for Meat Processing*, CRC Press, Boca Raton, FL, pp. 329–351.

Toldrá, F. (2007). Ham. In: Y-H. Hui, R. Chandan, S. Clark, N. Cross, J. Dobbs, W.J. Hurst, L.M.L. Nollet, E. Shimoni, N. Sinha, E.B. Smith, S. Surapat, A. Titchenal, and F. Toldrá (eds.), *Handbook of Food Product Manufacturing*, vol. 2, John Wiley Interscience, New York, pp. 231–247.

Toldrá, F., and Reig M. (2007). Sausages. In: Y.-H. Hui, R. Chandan, S. Clark, N. Cross, J. Dobbs, W.J. Hurst, L.M.L. Nollet, E. Shimoni, N. Sinha, E.B. Smith, S. Surapat, A. Titchenal, and F. Toldrá (eds.), *Handbook of Food Product Manufacturing*. Vol. 2, John Wiley Interscience, New York, pp. 249–262.

Tornberg E., and Nerbrink, O. (1984). Swelling of whole meat and myofibrils, *Proc. 30th European Meeting of Meat Research Workers*, Bristol, 3: 10, 112,

Tornberg, E., and Larsson, G. (1986). Changes in water distribution in meat during cooking, *32nd European Meeting of Meat Research Workers*, Ghent, 2: 4, 85.

Wilding, P., Hedges, N., and Lillford, P.J. (1986). Salt-induced swelling of meat: The effect of storage time, pH, ion-type and concentration. *Meat Sci.* 18: 55–75.

Wright, D.J., Leach, I.B., and Wilding, P. (1977). Differential scanning calorimetric studies of muscle and its constituent proteins. *J. Sci. Food Agric.* 28 (6), 557–564.

Wright, D.J., and Wilding, P. (1984). Differential scanning calorimetric study of muscle and its proteins: myosin and its subfragments. *J. Sci. Food Agric.* 35 (3), 357–372.

Yamaguchi, M., Kamisoyama, H., Nada, S., Yamano, S., Izumimoto, M., Hirai, Y., Cassens, R.G., Nasu, H., Mugurama, M., and Fukuzawa, T. (1986). Current concepts of muscle ultrastructure with emphasis on Z-line architecture. *Food Microstruct.* 5, 197–205.

Zhu, Y., Rinzema, A., Tramper, J., and Bol, J. (1995). Microbial transglutaminase: A review of its production and application of food processing. *Appl. Microbiol. Biotechnol*. 44, 277–282.

Chapter 22

Structured Chocolate Products

B.J.D. Le Révérend,[1] S. Bakalis, and P.J. Fryer[2]

Centre for Formulation Engineering, s.bakalis@bham.ac.uk, Department of Chemical Engineering, University of Birmingham.
[1] bjl545@bham.ac.uk
[2] fryerpj@bham.ac.uk

22.1 Introduction: Chocolate Manufacture

It is believed that Mayas, 2600 years ago, were already drinking chocolate. At this time, chocolate was consumed in America as a sweet and spicy beverage, seasoned with chilli pepper, vanilla and pimiento. The beverage was expensive and thus reserved to elites, and cocoa was even often used as a currency. The story of chocolate begins in Europe with the discovery of America and Christopher Colombus brought some chocolate back to Spain for Queen Isabella, but Hernando de Soto introduced it much more broadly.

In the 18th century, a serial of inventions led to the chocolate as we know it today:

- Van Houten developed two processes, one in 1928 in order to separate physically, cocoa butter and cocoa solids (which were then transformed to make the famous cocoa powder); the other is the alkali treatment of chocolate to remove bitterness;
- Daniel Peter proposed in 1875, after 8 years of research, his newly developed milk chocolate assisted by his baby food manufacturer neighbour Henri Nestlé;
- Rudolph Lindt invented the conching process, and additional step to decrease the average size of particles in the blend.

Chocolate manufacture is a complicated engineering process with the aim of producing a material which is attractive to the consumer. Critical to the success of processes is the control of the crystalline state of the fats used and the networks that they form (see also Chapters 4 and 17). The engineering challenge is to develop a manufacturing route that produces the required product as efficiently as possible.

The different tastes and types of chocolate reflect the histories of the industry in different parts of the world, and the tastes of different peoples. A typical composition of chocolate is shown in Table 22.1 and a typical manufacturing process shown in (Beckett 1989), which is the best single reference on chocolate manufacture. The process involves the following steps:

- Cocoa pods are harvested, dried to give flavour and the cocoa beans are extracted from the pods;
- Cocoa beans are roasted, ground and pressed. From this step two principal materials are obtained for the manufacture of cocoa based products; cocoa butter and cocoa liquor (the press-cake, which is used to make cocoa powder);
- Ingredients, such as sugar, cocoa butter, cocoa liquor, emulsifiers, vanilla, are blended;
- Conching is performed, where the blend is smoothed so that the maximum diameter in the solid phase is inferior to the tongue detection (usually 40 μm);
- Tempering, controlled crystallisation using a combination of temperature, shear and time;
- Moulding and crystallisation using different methods;
- Finally, chocolate is packaged.

Commonly chocolate comes in different forms, each of which requires slightly different manufacturing routes:

- Block chocolate in which molten chocolate is cast into moulds and solidified in cooling tunnels;
- Enrobed sweets in which centres are covered in molten chocolate before cooling;
- Filled sweets in which a sequence of steps of filling and cooling are carried out.

The taste of chocolate is partially determined by its chemistry, but also depends on the microstructure of the material, which consists of crystals and particles between

Table 22.1. Typical chocolate formulations (Jackson 1999).

Component	Typical percentage in		
	milk chocolate	dark chocolate	bittersweet chocolate
cocoa mass (cocoa solids and cocoa butter)	11.8	39.6	60.7
added cocoa butter	20.0	11.8	2.6
sugar	48.7	48.1	36.3
lecithin	0.4	0.4	0.3
flavour compounds (e.g. salt and vanillin)	0.1	0.1	0.2
whole milk powder	19.1		
total fats	31.5	36.4	35.4

10 to 120 μm in diameter, depending on the product (Narine and Marangoni 1999a; Narine and Marangoni 1999b). The non-fat solids have mean sizes in the region of 25 microns.

The complexity of chocolate manufacture arises from the polymorphic nature of its constituent fats, which can come in at least five crystal forms, each with an individual melting point. Cocoa butter is chemically a multicomponent mixture of triglycerides and trace compounds (Davis and Dimick 1986). Approximately 85% of the composition consists of just three triglycerides: POP (~20%), POS (~40%) and SOS (~25%), where palmitic (P), oleic (O) and stearic (S) are the fatty acids attached to the glycerol base. The precise composition depends on factors such as growing conditions and therefore can vary between batches, especially from different geographic regions (Chaiseri and Dimick 1989).

Examples of the conditions under which the various polymorphs arise are given in Table 22.2. The melting points are those given by Wille and Lutton (1966) who also defined the polymorph numbering system (I – VI), which label the forms in order of increasing melting point. This has now become a standard. However, in chocolate the melting points also depend on composition, for example, the addition of milk solids lowers the temperatures by up to 10°C. Different chocolate types and blends will thus have different behaviour.

Table 22.2 Overview of cocoa butter polymorphs (Aronhime and Garti 1988).

Polymorph	Conditions under which polymorphs arise	Melting point/ºC
I	Rapid cooling of melt. [Successive polymorphs are then obtained sequentially by heating at 0.5ºC.min-1].	17.3
II	Cooling of melt at 2ºC/min. Rapid cooling of melt followed by storing from several minutes up to 1 hour at 0ºC. The form is stable at 0ºC for up to 5 hours.	23.3
III	Solidification of melt at 5–10ºC. Transformation of form II by storing at 5–10ºC.	25.5
IV	Solidification of melt at 16 – 21ºC. Transformation of form III by storing at 16–21ºC.	27.3
V	Solidification of melt.Transformation of form IV.Solvent crystallisation.	33.8
VI	Transformation of form V (4 months at room temperature).	36.3

The key practical problems for the chocolate maker and for the process engineer are that the thermodynamically stable form (Form VI) is not the one that the consumer finds attractive, and that the lower forms will not effectively demould, causing problems in manufacture. Making commercial chocolate thus involves ensuring that the final product is in form V, the right form to be sold and eaten. Figure 22.1 shows

Figure 22.1. Good and bad chocolate: The well tempered chocolate on top is glossy and has come away easily from the mould. The untempered chocolate sticks in the mould and shows a spotted and marked surface.

the practical problem that can result. Two bars are shown, of tempered and untempered material; whilst the tempered form is glossy to the eye, and demoulds efficiently, making it easy to manipulate in the factory, the untempered product is spotted and marked, showing fat 'bloom' which is a surface crystallization of the fat crystal network. Figure 22.2 shows a microstructure of bloomed chocolate in which the separation of fats and sugar is clearly evident.

In addition, untempered chocolate tastes gritty on the tongue:

- this is because Form VI has a high melting temperature, so that the melting point of some of the crystals is above the temperature of the mouth. The mouth feel is thus less pleasant than the tempered form which melts at mouth temperatures;
- is softer than tempered chocolate; excessive local heating (for example around the join between the two layers in a filled sweet) can cause recrystallisation into low crystal forms, giving regions in the final product that are not as strong as the rest. Chocolate can then suffer from a process analogous to weld decay in metals, with fracture of the sweet within the region that has become untempered.

The process of tempering – by which the conditions are created for the correct crystal form to be produced – and solidification are thus crucial to successful chocolate-making. The aim of this chapter is to review work in this area and describe current understanding of the processes and their kinetics.

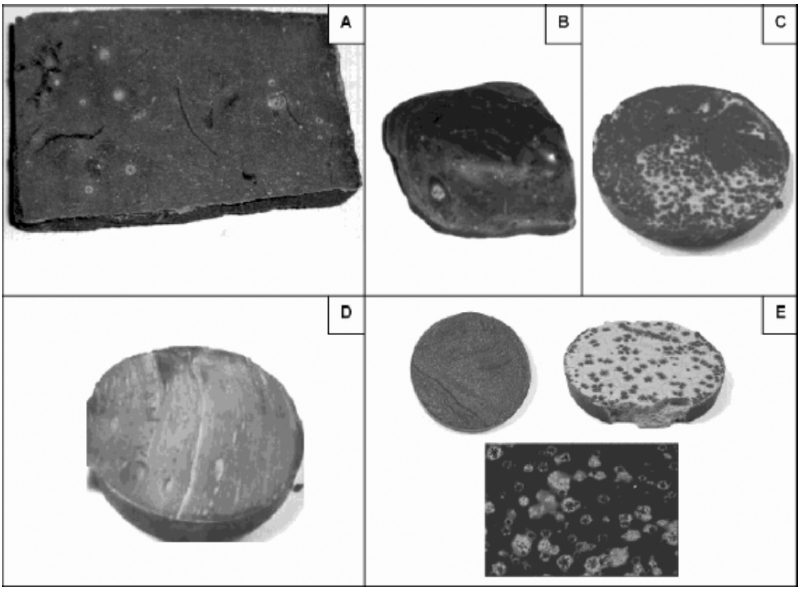

Figure 22.2. Pictures of bloomed chocolate due to (A) storage, (B) fat migration, (C) heat hit, (D) over-tempering, (E) non-tempering (Lonchampt and Hartel 2004).

22.2 Polymorphism and Its Consequences

Extensive work has been carried out to quantify the physical behaviour of the triglycerides. Five or six crystalline forms have been identified using experimental techniques such as observing crystals melting under a microscope, and more recently, differential scanning calorimetry (DSC) and X-ray diffraction (or a combination of those).

Six forms were identified (Wille and Lutton 1966) using X-ray diffraction. They found it difficult to assign X-ray nomenclature to data based on crystal spacing of a multicomponent mixture; nevertheless they identified forms II, IV, V and VI with crystallographic forms $\alpha 2$, $\beta 2'$, $\beta 3$ of POS. The precise number of polymorphs has been the subject of debate; Wille and Lutton considered that V and VI represented distinct but very closely related crystalline structures, and that Form I was a fleeting and not readily characterised sub-α state which might be a phase mixture. Form III has also been thought to be a phase mixture; Merken and Vaeck (1980) supported by others researchers (Aronhime, Sarig, and Garti, 1988) believed form III to be a mixture of form II and IV. Hernqvist (1988) similarly, on the basis of X-ray data, maintains that only five forms exist and these correspond to the X-ray classifications: sub-α, α, $\beta 2'$, $\beta 1'$ and β. Other authors confirmed the existence of only five different polymorphs (Schenk and Peschar

2004) and XRPD patterns are presented in Figure 22.3. Six polymorphic forms of cocoa butter were identified (Loisel, Keller, Lecq, Bourgaux, and Ollivon 1998) who used DSC and X-ray diffraction as a function of temperature (XRDT) at different scanning rates. Form I showed liquid-crystal form, with some β' organisation and some unordered material. This form transformed to more stable form II on heating. Form III was the most difficult to identify. The lower melting polymorphs generally form by cooling to a lower temperature and at a faster rate. The lower melting forms then transform to higher melting forms with time. Form VI is generally associated with fat bloom, the unpleasant appearance of the chocolate surface (illustrated in Figure 22.1 and Figure 22.2. Bricknell and Hartel (1998) used X-ray diffraction to study bloom. Walter and Cornillon (2001) used magnetic resonance imaging as well as DSC, and found that addition of sucrose or milk powder gave different types of bloom.

More recent studies have shown that bloom (or dull) can occur for both tempered and untempered chocolate (Lonchampt and Hartel 2004; Lonchampt and Hartel 2006). For untempered chocolate, the blooming essentially comes from the transition from low melting point polymorphs (thermally unstable crystals) to high melting point polymorphs (usually VI). During this transition, the material mobility is increased and the migration of fat crystals to the surface is facilitated. For tempered chocolate the different causes of blooming are:

- high fluctuations of temperature;
- storage to a temperature which is higher than the melting point of form V (31 C);
- migration of some liquid fat components from the filling in the centre of the product;
- formulation problems such as the blending of fats which are incompatible (fatty acids with very different lengths).

Narine and Marangoni (1999a; 1999b) have studied the microstructure of cocoa butter and other fats, and identified fractal dimensions from both rheological data and image analysis taken using polarised light microscopy. The fractal dimension obtained from microscopy is taken as a measure of the spatial distribution of crystals. The fractal dimension of the crystal network is considered to be an indicator of hardness, since the normalised elastic modulus for a number of fats lay on the same curve. The authors suggest that the fractal dimension is related to conditions of nucleation: systems with a sharp nucleation step in heat flow as the sample crystallises from the melt will have higher fractal dimensions and a more ordered system.

If the chocolate is raised to too high a temperature, and not cooled in the correct way, it will set in an unwanted form. To generate material in the right microstructure complex engineering procedures have been developed; these operate in a fixed and sometimes empirical way.

Controlled crystallisation (tempering) is a vital step in chocolate production. The aim of tempering is to generate sufficient seed crystals of form V to act as points on which the fats can crystallise. Tempering normally involves a complicated temperature-shear-time process. Such a process involves:

- complete melting of the chocolate to about 50ºC, which removes most or all of the crystal material;
- cooling to the point of crystallisation;
- maintaining a holding temperature for crystallisation for about a minute;
- reheating to melt out unstable crystals.

The tempering time varies with recipes, equipment and the purpose of the final product (Hernqvist 1988).

In industry this is done in a range of different ways. An automatic tempering machine usually consists of multi-stage heat exchangers through which the chocolate passes as described in the literature (Beckett 1989; Bolliger, Breitschuh, Stranzinger, Wagner, and Windhab 1998; Beckett 2002). The industrial process of tempering is also often checked using a tempermeter which measures the level of temper. A tempermeter mainly consists in a Peltier stage and a temperature probe. The Peltier stage cools the chocolate from the sides and the probe measures the evolution of the temperature in the product. If chocolate is properly tempered, then the crystallization plateau occurs around 21-22°C, and the slope of this plateau has to be close to 0°C/min (flat). The process is difficult to reproduce at a lab or pilot plant scale due to the complex thermal and continuous aspect of the process (in situ crystallization) but two studies (Bolliger, Breitschuh, Stranzinger, Wagner, and Windhab 1998; Stapley, Tewkesbury, and Fryer 1999) have reported some working devices sharing the common principle of shearing the product and applying a known temperature profile during the tempering process.

These researchers (Bolliger, Breitschuh, Stranzinger, Wagner and Windhab 1998) worked with a high shear crystallizer (Figure 22.4) in which the chocolate crystals are scraped from the cooled surface into the bulk to act as nuclei for further crystallization.

The correctly tempered chocolate is then subjected to the optimal conditions for cooling, usually in a series of cooling tunnels using a combination of conduction, convection and radiation heating. The cooling rate depends on temper, type, and thickness of the chocolates, and largely determines the final product quality. Too rapid a cooling rate gives a material that is kinetically trapped into the wrong form. Cooling is a special problem in the casting of block or bar chocolate, where significant conduction limitation within the chocolate is found.

The conventional cooling process involves a long and slow cooling of the product via cooling tunnels. Some experimental work has shown an average heat transfer coefficient around 20 W/m^2/K and an ambient temperature around 11°C. A rough estimation of the Biot number ($Bi = \frac{h \cdot e}{k} \approx 0.1$) where h is the external heat transfer coefficient, k the internal thermal conduction and e some characteristic length scale, shows that even for a thin layer of chocolate (an small Easter egg, for example) conduction is the controlling mechanism, as the thermal conductivity of chocolate is relatively low, (k = 0.15 W/m/K) the cooling rate will be relatively low resulting in the desirable crystal structure after processing. The problem of this method is that due to the slow cooling, the chocolate does not set immediately in the mould and thus the shape of the product cannot be reproduced very accurately.

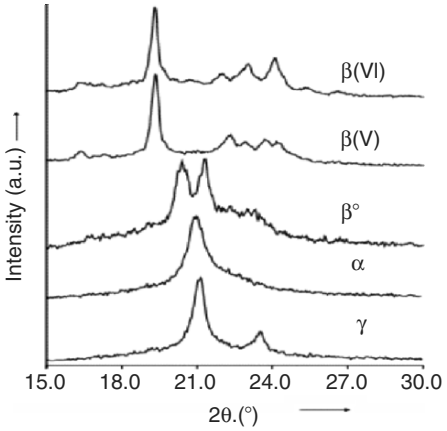

Figure 22.3. XRPD diffraction pattern of the fingerprint region (λ=1.5418 Å; d-spacing values 3.0–6.0 Å) of various cocoa-butter phases. The γ, α and β′ phases were data from Cameroon cocoa-butter after isothermal crystallization at −10.0°C, 0.0°C and 20.0°C, respectively. The β(V) and β(VI) phases were data from Bahia (Brazil) cocoa-butter, after isothermal crystallization at 22.0°C and from bulk material, respectively (Schenk and Peschar 2004).

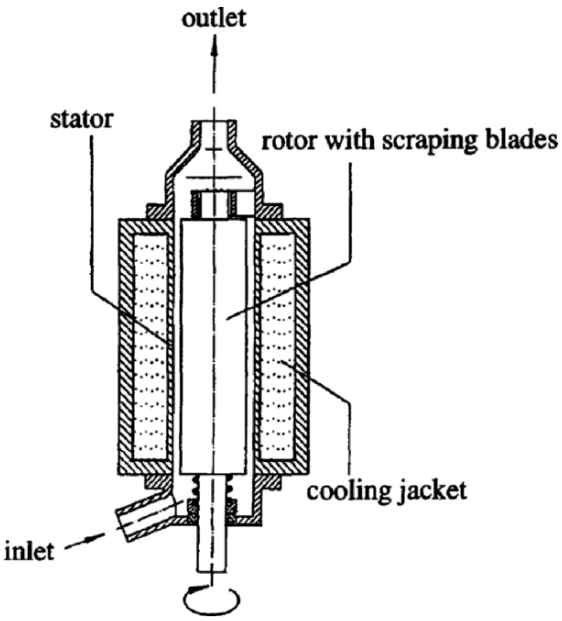

Figure 22.4. General view of a pilot scale high shear temperer (Bolliger, Breitschuh, Stranzinger, Wagner and Windhab 1998).

One other method for manufacture is to use a fast cooling device, such as the Frozen Cone system (Aasted 1992) in which the shape of the sweet is stamped out by a cold die prior to filling and cooling.

22.3 Modelling Temper and Solidification

22.3.1 Shear and Temperature Effects in Tempering

The heat evolved from a material on cooling reflects the changes that take place. Thermodynamically, phase change involves the release of latent heats, whilst in a single-phase material the specific heat capacity determines the heat evolution. Differential scanning calorimetry (DSC) can quantify the heat evolution from a material during a phase change. The heat measured by DSC is a function of both the thermodynamics and the kinetics of the process; slow cooling allows the material to approach a thermodynamic equilibrium, whilst fast cooling will produce a kinetically trapped material. When chocolate is studied in the DSC therefore an 'apparent specific heat' is measured, a complex mixture of the heats associated with phase change and temperature change effects.

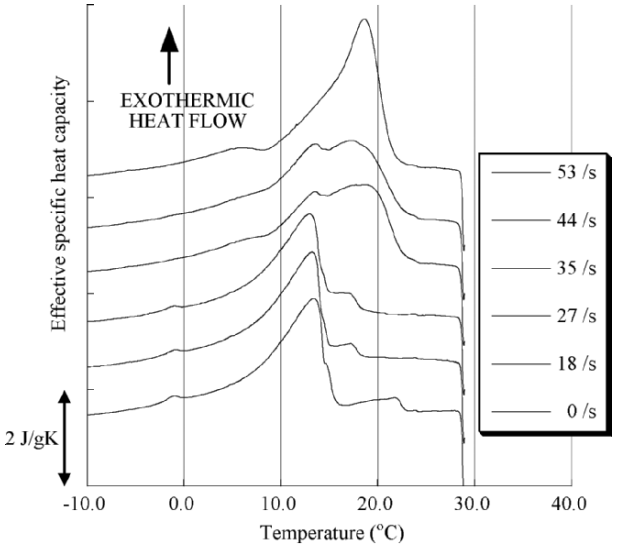

Figure 22.5. Specific heat for chocolate sheared at different rates: all the chocolates are held at 22ºC for 400s and the rewarmed to 32ºC prior to cooling and shear (Stapley, Tewkesbury and Fryer 1999).

Using a Couette device, which consists of a pair of concentric cylinders, with the inner one rotating, it is possible to generate approximately uniform shear on chocolate. The temperature of the device can be controlled and varied; this allows a controlled temperature-time-shear pattern to be provided. Figure 22.5 shows the DSC trace for milk chocolates processed at different shear rates (Stapley, Tewkesbury and Fryer 1999). The phase change temperatures are lower than those shown in Table 22.2 because the effect of adding milk fat to the cocoa butter is to lower the melting point. The higher-melting peak represents stable tempered chocolate, whilst the lower-melting peak indicates unstable untempered material. The effect of shear on temper can thus be clearly visualized.

Similar results can be produced by holding chocolate at different temperatures for different length of time. For the chocolate held at 22°C for 600 seconds (before warming to melt unstable crystals) to ensure the temper, times below 500 seconds result in badly tempered and below 300 seconds untempered material. The process is very temperature sensitive, subsequent reheating to a temperature of 30.5°C instead of 29.5°C is enough to result in a material that is not properly tempered. The data suggests that the processes of tempering can be quite well defined in terms of the treatment required. Results have been used to develop process models.

22.3.2 A model for chocolate cooling

Figure 22.6 (Stapley, Tewkesbury, and Fryer, 1999) shows the apparent specific heat for tempered milk chocolate cooled at different rates obtained using DSC. Different cooling rates shifts the main peak by about 15ºC, showing the difference between the tempered material produced at low cooling rates and the untempered material generated at the faster rates. This type of behaviour will occur throughout a cooling chocolate, and must be considered in any model. Outside of the phase change region, the specific heat capacity shows no dependence with cooling rate.

In the classical Stefan formulation of phase change problems, solidification occurs at a well defined front which moves though the material (Aziz 2003). This is appropriate for simple materials, but not for chocolate which is a multi-component mixture of triglycerides which displays a spread of melting points. A front is therefore difficult to define. Instead a “mushy” zone exists instead where solid and liquid co-exist; the process is described as continuous solidification (Voller, Swaminathan and Thomas 1990).

Franke (1998) proposed a one-dimensional model for the crystallisation of chocolate coatings of enrobed products using a heat source term (Q) to account for latent heat evolution:

$$\rho \cdot Cp \cdot \frac{\partial T}{\partial t} = \nabla(k \cdot \nabla T) + \dot{Q}$$

where ρ is the density, Cp the specific heat and k the thermal conductivity of the material. The crystallisation rate was modelled as the product of two functions with five experimentally determined parameters. One was a function of temperature, where the rate is proportional to the degree of super-cooling. The other was a function of latent heat already released (i.e. the fraction solidified). Crystallisation is

rapid initially, but then slows as crystallisable material is "consumed". The functions employed five parameters that were determined from prior experiments. Although the model showed an adequate fit to data, the approach has some drawbacks. First, the model assumes a single melting point, whereas chocolate displays a range of melting temperatures. Second, the real functional form of the kinetic equations is more complex and may depend on other factors additional to the five parameters used. Finally, a constant total enthalpy change for chocolate solidification was assumed regardless of cooling conditions, but the cooling rate affects the total enthalpy change (Stapley, Tewkesbury and Fryer 1999).

An alternative approach was used that incorporated the apparent specific heat capacity (i.e. the latent heat is included in the specific heat term) as:

$$\rho \cdot Cp_{eff} \cdot \frac{\partial T}{\partial t} = \nabla(k \cdot \nabla T)$$

where Cp_{eff} (J/g/K) is a function of temperature and thermal history, found from Figure 22.6. Tewkesbury and others (Tewkesbury, Stapley and Fryer 2000) describe the experimental tests of the model developed using the data set of Figure 22.6. Analytical solution of the thermal conduction equation is obviously not possible in this case because of the complexity of the physical properties, so the computational fluid dynamics program FIDAP was used to solve the equation. The program was first validated by comparison with simple situations, as described by Jung and Fryer

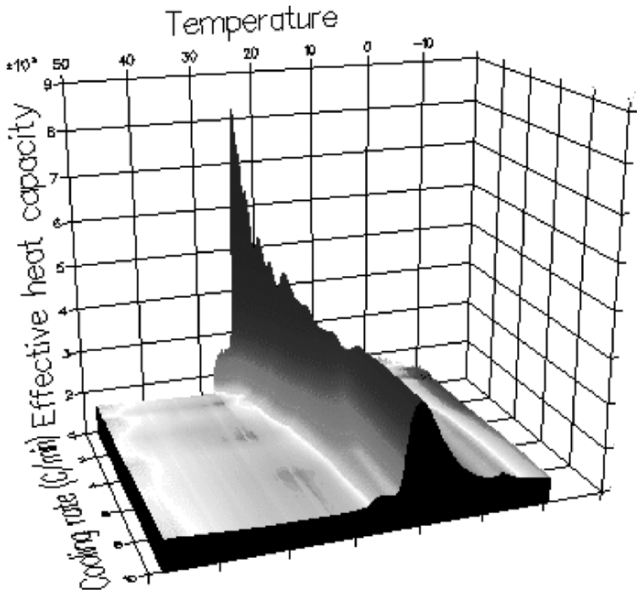

Figure 22.6. Effective heat capacity of chocolate as a function of temperature and cooling rate (Stapley, Tewkesbury and Fryer 1999).

(1999). As little movement occurs on cooling (see later) the fluid mechanics elements of the program were unnecessary, but the advantages of using a commercial program are that mesh specification, input and output are straightforward.

In commercial practice, a defined cooling rate is delivered to the chocolate by the air in the cooling tunnel. Two sorts of approach were used. First, experiments used the Cp_{eff}, values appropriate to the external cooling rate. As shown in Figure 22.7, this type of simulation, although it fits the temperature data outside the crystallisation region, totally fails to predict the temperature changes which occur on solidification. The reason for this is shown by Figure 22.8, which plots the locus of the cooling rate of the chocolate over the cooling period. The result of the heat evolution due to phase change is to cause local changes in the cooling rate, for which the apparent specific heat capacity is significantly different from that which is followed by assuming the same cooling rate as that supplied externally. The solution to this problem is to allow the program to use the apparent specific heat appropriate to the local temperature and cooling rate, i.e. to have the whole of Figure 22.6 available. The success of this technique is shown in Figure 22.9; the match between theory and experiment is good across the whole range of the experiment, and the rate and extent of crystallisation is well-predicted.

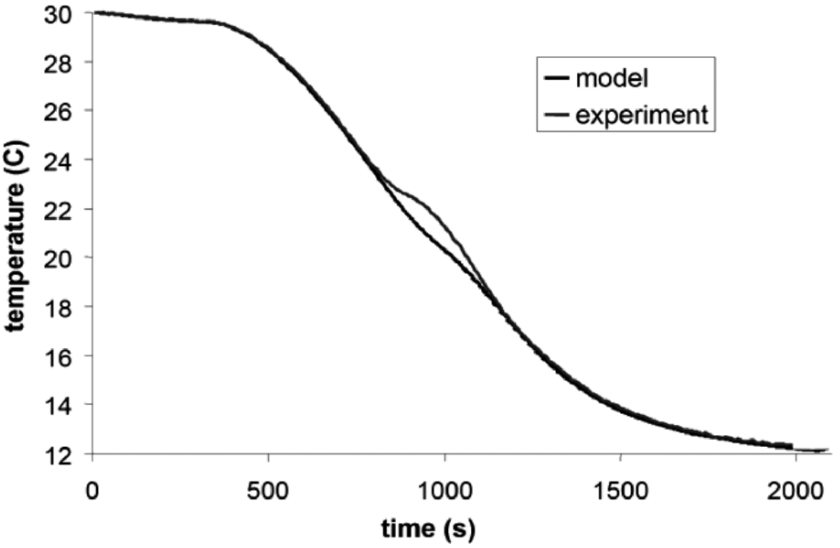

Figure 22.7. Comparison of model (thin line) and experimental (thick line) temperatures for the cooling of tempered chocolate at a nominal rate of 2 C/min. The model uses apparent specific heat capacity data taken from DSC measurements at a cooling rate of 2 C/min (Tewkesbury, Stapley and Fryer 2000).

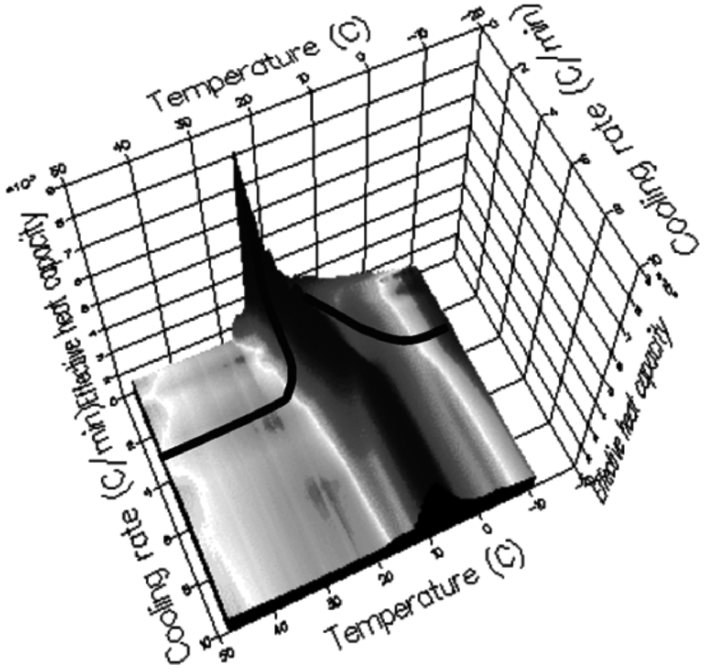

Figure 22.8. Plot of the apparent specific heat as a function of temperature and cooling rate, with the locus of cooling rates and temperatures for a real cooling situation marked. (Tewkesbury, Stapley and Fryer 2000).

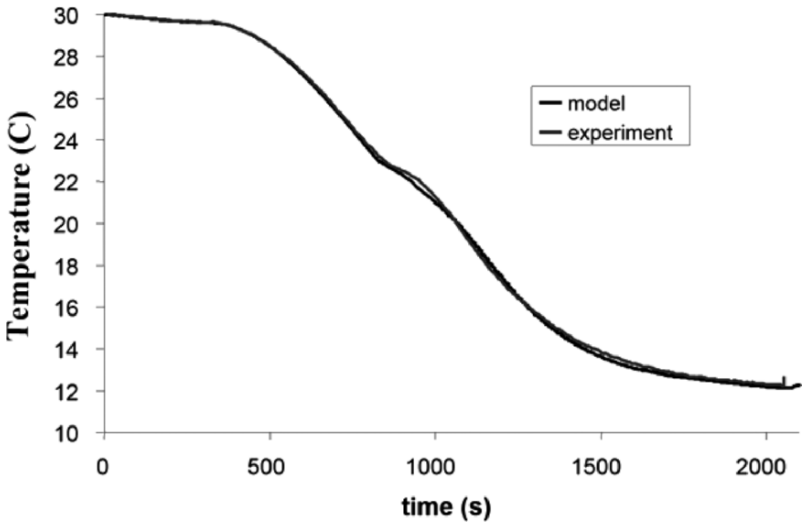

Figure 22.9. Comparison of model (thin line) and experimental (thick line) temperatures for the cooling of tempered chocolate at a nominal rate of 2 C/min. The model uses apparent specific heat capacity data obtained by first calculating the local cooling rate and temperature (Tewkesbury, Stapley and Fryer 2000).

The above method gives a good fit to experiment over the range of commonly used cooling rates: however, the approach is formally incorrect, in that it assumes that the apparent specific heats are not a function of the process history. However, rapid cooling gives a lower degree of crystallisation at low temperatures than the lower cooling rates. The model is thus not able to accommodate rapid shifts in cooling rate.

22.4 More Advanced Approaches

22.4.1 Kinetic Models

The processes of solidification and crystallisation are complex, as shown above. Some approaches to a kinetic model have been made, and it has been shown that changes occur over a wide range of time scales. Rousset et al. (Rousset, Rappaz and Minner 1998) studied the kinetics of POS-SOS crystallisation in terms of nucleation and growth kinetics, and showed transformations on time-scales of both seconds and hours. Van Malssen et al. (Van Malssen, Van Langevelde, Peschar and Schenk 1999) used x-ray powder diffraction to identify kinetic effects at all timescales between seconds and weeks: the solidification takes much longer than the few minutes in the factory process.

Other models have been developed recently to evaluate the crystallization kinetics of cocoa butter. Foubert and co-workers (Foubert, Vanrolleghem, Vanhoutte and Dewettinck 2002; Foubert 2003; Foubert, Dewettinck and Vanrolleghem 2003; Foubert, Vanrolleghem and Dewettinck 2003; Foubert, Dewettinck, Janssen and Vanrolleghem 2006), worked on a differential equation derived from the original theory of crystallization described by Avrami (1939; 1940; 1941). The main hypothesis of this work is that crystallization could be interpreted as an nth order reaction and melting as a first order reaction,

$$Melt \underset{K_n}{\overset{K}{\Leftrightarrow}} Crystals$$

leading to the partial differential equation,

$$\frac{\partial h}{\partial t} = K(h^n - h)$$

where h is the remaining melted fat (as it was found experimentally that $K \cong K_n$).

It was found that K is a function of temperature but the model was found to give a better fit than analytical expressions like the Avrami model or the modified Gompertz model (Kloek, Walstra and Van Vliet 2000). The main advantage of this model is that as it is formulated as a differential equation, it can be used to predict isothermal as well as dynamic crystallization. However, this model does not consider the polymorphism of the material which is a critical point in the crystallization of cocoa butter. Another contribution is the model of Fessas et al. (Fessas, Signorelli and Schiraldi 2005) which considers all the transitions possible between each

polymorphs and the melt phase as well as the possible solid-solid transformations using first orders kinetics. The data used to identify the reaction rates for the model were based on signal deconvolution of a DSC signal constrained by the melting or crystallization temperatures and the reaction enthalpies found in the literature (Loisel, Keller, Lecq, Bourgaux and Ollivon 1998). Unfortunately, this paper does not present any numbers and even if the method is very attractive, its application to a larger scale in terms of simulation still requires significant work.

22.4.2 Kinetics of Shape Change

As noted above solidification is critical in manufacture as it determines whether the chocolate will demould successfully. During solidification, the material changes shape. It is not possible to follow the shape of the surface of chocolate using conventional tribological techniques, which involve physical contact between the surface and a stylus of some sort. One technique which can be used to follow the surface morphology of chocolate is to use an infrared laser to measure the sample height.

A Rodenstock RM600 has been used to follow the shape change of chocolate and obtain an understanding of the nature of the kinetics of crystallisation of chocolates of different temper (Fryer and Pinschower 2000). The equipment consists of an optical distance sensor, with sub-micron vertical resolution, together with a traverse table which holds the sample and allows the sensor to be tracked across it.

The optimum horizontal tracking speed was found to be 40 mm/min acquiring 1100 data points, i.e. a horizontal spacing of 36 microns/data point. For measurement, a sample of liquid chocolate which has received a known temperature-time-shear profile is placed within a solidification rig that consists of a mould with known coefficient of expansion, contained in a temperature-controlled holder.

An example of the treatment of the data is given in Figure 22.10, the top line is that at the start of the process and the bottom line is that at the end. Raw data is shown in Figure 22.10(a); the slope of the chocolate surface is due both to any slope on the holder, and to the difficulty of producing a fully flat surface (compare the length scales of the vertical and horizontal axes).

The data can be treated by expressing the height data as a ratio in Figure 22.10(b). This both flattens the data and enables it to be seen more clearly; the effect of the cooling of the tempered chocolate is to cause the characteristic ‘cracking’ at the side of the mould. A comparison of tempered and untempered material is shown in Figure 22.11. The shapes of the two are very different, showing the different profiles of the material.

The profiles of Figure 22.11 and Figure 22.12 can be integrated as a function of of time to get some idea of the kinetics of crystallisation. Figure 22.12 shows the change in the volume of chocolate as a function of time. Details of the calculations are given in Pinschower (2003). For tempered and untempered materials, cooled more slowly than would be typical of an industrial process, at a series of step changes of 2 C every 20 minutes. The temper values for the chocolates have been inferred from a Sollich temper meter, described above. A range of effects can be seen: there is a significant difference between the rate of shape change for tempered

and untempered chocolate; the majority of the change in shape for the tempered chocolate is complete after about 30 minutes, whilst for untempered chocolate the shape change (and thus crystallisation) is still taking place after a couple of hours. This emphasises how difficult it would be to remove such material from the mould: irrespective of the other physical properties of the two types of chocolate, the untempered material shrinks much less than the tempered in the early stages of cooling.

The total volume change in the process is however similar: shape change in untempered chocolate will be similar to or even greater than tempered chocolate, although it takes significantly longer.

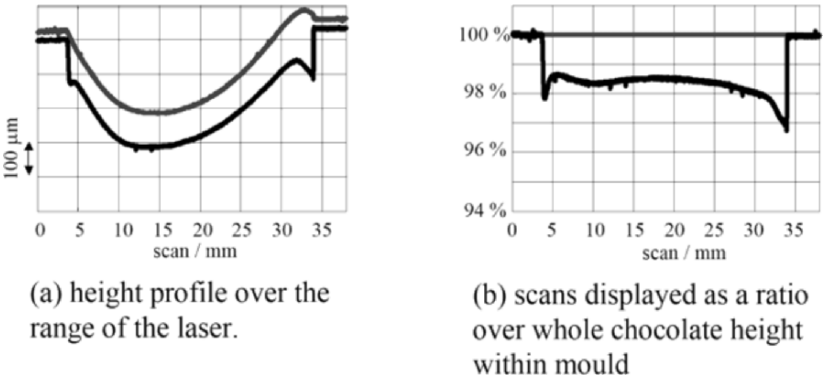

Figure 22.10. Typical scanning result for chocolate; first scan at ca. 29 C and second scan after cooling to 12 C (Pinschower 2003).

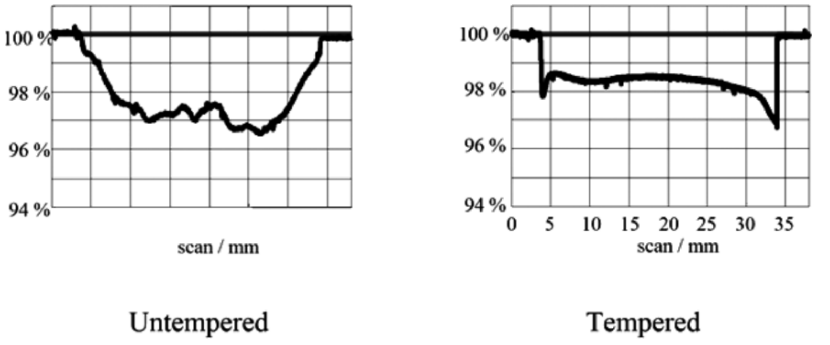

Figure 22.11. Scanning results for tempered and untempered chocolate; first scan at ca. 29 C and second scan after cooling to 12 C (Pinschower 2003).

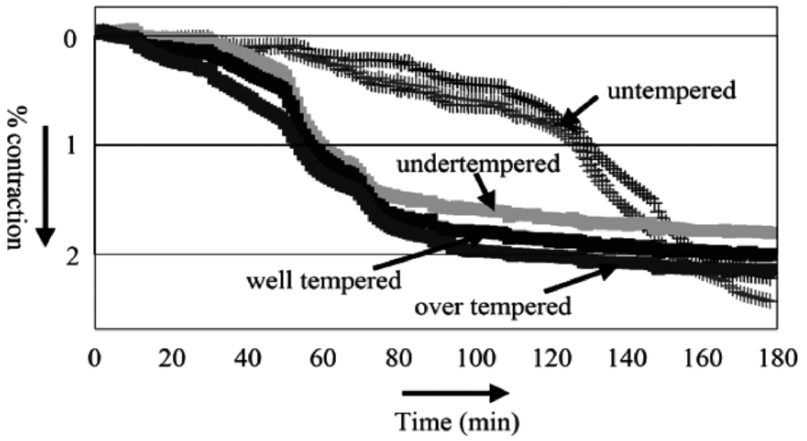

Figure 22.12. Volume changes for chocolates of different tempers. Cooling at 2 C/min for 20 mins (Pinschower 2003).

The difference between untempered and tempered samples is much more significant than that between samples with different temper values (in practice this may reflect the somewhat empirical nature of the measurement of the temper meter).

Undertempered samples start to crystallise at lower temperatures and have less volume change overall. They do however reach effectively constant volume, unlike the untempered sample. Well and over tempered samples contract further than under-tempered, but it is not possible to tell the two sets apart to any significant extent (Pinschower 2003).

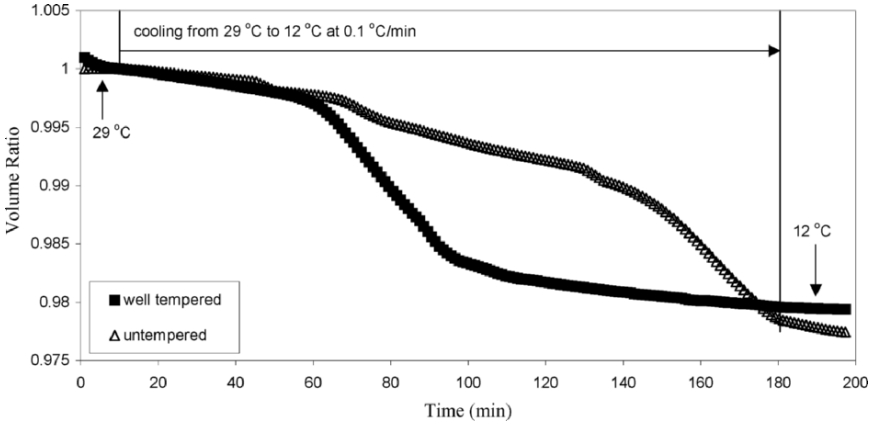

Figure 22.13. Contraction of tempered and untempered chocolate cooled at 0.1 C/min (Pinschower 2003).

Figure 22.13 compares the kinetics of crystallisation of tempered and untempered material in more detail, here for a continuous cooling rate of 0.1 C/min. The difference in the rate and extent of the shape change is clear. No experiments were done to identify the final crystal form in these experiments; the final shrinkage in untempered chocolate is however less than for tempered material.

As with the measurements of the heat changes on cooling described in (Stapley, Tewkesbury and Fryer 1999; Tewkesbury, Stapley and Fryer 2000), the amount of shape change will be a function of both the temperature and the cooling rate, because the curves reflect both the thermodynamics and kinetics of the process. Pinschower (2003) shows data for a large number of cooling rates, and details how to extract the expansion coefficients from the raw data. The volume $V(T)$ at each time or temperature during the cooling is calculated by integrating (numerically) the surface profile of the chocolate rings (X axis on Figure 22.11) with a space definition dr and the thickness (Y axis on Figure 22.11) assuming the profile is radially symmetrical (by averaging the reading $\overline{h_i}$ taken at the same radius)

$$V(T) = \sum_i \pi \cdot \overline{h_i} \cdot (2 \cdot i + 1) \cdot dr^2$$

and the contraction coefficient $\beta(T)$ is calculated by numerical differentiation of $V(T)$ divided by the initial volume $V(T_0)$.

$$\beta(T) = \frac{1}{V(T_0)} \cdot \frac{\partial V(T)}{\partial T}$$

Figure 22.14 summarises the results obtained for different cooling rates. At the slowest cooling rate, comparatively large coefficients are seen for the temperature at which phase change occurs: at lower temperatures, where no phase change is taking place, the coefficient is much less. However, as the cooling rate increases the coefficient decreases, demonstrating that solidification is a kinetic effect. At 3 C/min no peak in the coefficient is seen, showing that the material is still contracting at the lowest temperature. These results emphasise how the solidification of chocolate is dependent on the cooling rate. The structure of the material is such that a material which is apparently solid is in fact still undergoing phase change and solidification.

Figure 22.15 presents coefficients of expansion for a range of materials of different temper, all taken at a cooling rate of 0.1 C/min. As would be expected from the cooling curve data, there is little difference between samples with different temper level, whilst those of untempered material are significantly different from tempered samples. The peak for the tempered material is at about 23 C, whilst that of untempered material is at about 14 C. The data for untempered material does however show a small peak in the coefficient of expansion at 23 C, indicating that some (albeit not very much) material has been tempered. This was unexpected, and illustrates the sensitivity of the method.

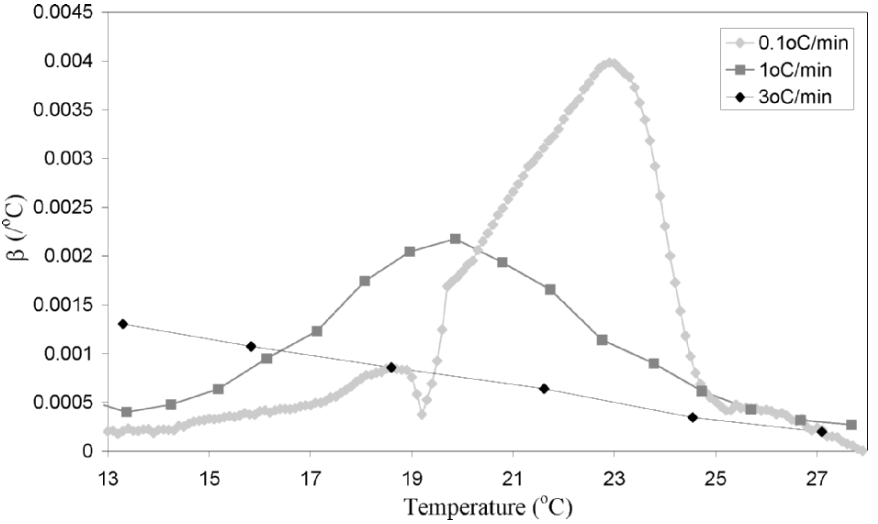

Figure 22.14. Coefficient of expansion vs temperature for well tempered chocolate cooled at different rates (Pinschower 2003).

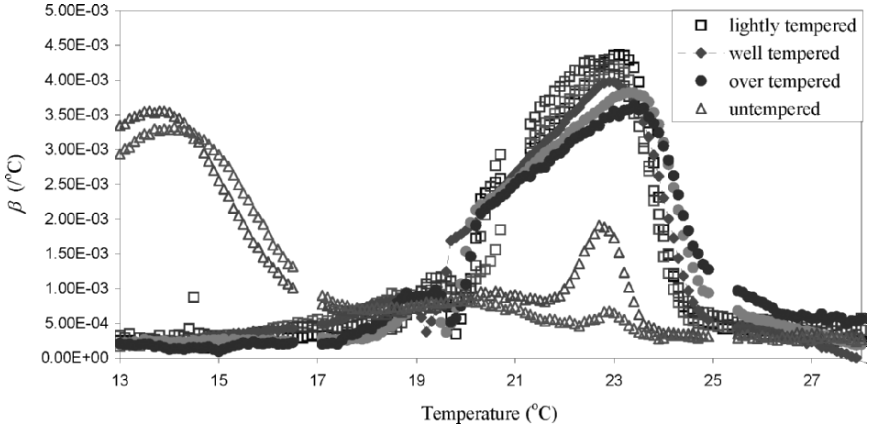

Figure 22.15. Coefficient of expansion of chocolate cooled at 0.1 C/min (Pinschower 2003).

22.5 Conclusions

The processes of chocolate formation are complex, reflected in the thermal and physical changes in chocolate during processing and cooling. A range of modelling and experimental techniques have been used to study the problem of chocolate solidification. It is possible to model conventional processes using the ideas of

apparent specific heat capacity, but the concept is limited as it relies on assuming that a kinetic variable is a thermodynamic one. The extent of solidification can be followed to show the rate and extent of crystallisation.

Due to the polymorphism of the fats, tempering has a critical role. The need to temper limits the types of chocolate process that can be designed. Better understanding of the material science of chocolate, leading to ways of rapidly generating the right crystal forms would be useful. Experiments have been carried out to study the rate at which crystallisation affects the shape of the final material; both the rate and extent of crystallisation vary with the temper of chocolate.

22.6 References

Aasted, L. (1992). Method and apparatus for the production of shells of fat-containing, chocolate-like masses under pressure build-up, *Aasted-Mikroverk APS*: 14

Aronhime, J.S. and Garti, N. (1988). Solidification and polymorphism in cocoa butter and the blooming problems. In N. Garti and K. Sato (Eds.), *Crystallization and polymorphism of fats and fatty acids*. Marcel Dekker, pp. 363–394.

Aronhime, J.S., Sarig, S. and Garti, N. (1988). Reconsideration of polymorphic transformations in cocoa butter using the dsc. *Journal of the American Oil Chemists Society,* **65**(7): 1140–1143.

Avrami, M. (1939). Kinetics of phase change. 1 general theory. *Journal of Chem.,* **7**: 1103–1112.

Avrami, M. (1940). Kinetics of phase change. 2 transformation - time relations for random distributions of nuclei. *Journal of Chemical Physics,* **8**: 212–224.

Avrami, M. (1941). Kinetics of phase change. 3 granulation, phase change, and microstructure. *Journal of Chemical Physics,* **9**: 177–184.

Aziz, A. (2003). Conduction heat transfer. In A. Bejan and A.D. Kraus (Eds.) *Heat transfer handbook*., John Wiley and Sons, pp. 161–260.

Beckett, S. T. (1989). *Industrial chocolate: Manufacture and use*, Royal Society of Chemistry publishing, p. 473.

Beckett, S. T. (2002). *The science of chocolate*, Royal Society of Chemistry publishing, p. 176.

Bolliger, S., Breitschuh, B., Stranzinger, M., Wagner, B. and Windhab, E. J. (1998). Comparison of precrystallization of chocolate. *Journal of Food Engineering,* **35**: 281–297.

Bricknell, J. and Hartel, R. W. (1998). Relation of fat bloom in chocolate to polymorphic transition of cocoa butter. *Journal of the American Oil Chemists Society,* **75**(11): 1609–1615.

Chaiseri, S. and Dimick, P. S. (1989). Lipid and hardness characteristics of cocoa butters from different geographic regions. *Journal of the American Oil Chemists Society,* **66**(12): 1771–1776.

Davis, T. R. and Dimick, P. S. (1986). Solidification of cocoa butter. *Proc. PMCA Prod. Conf.,* **40**: 104–108.

Fessas, D., Signorelli, M. and Schiraldi, A. (2005). Polymorphous transitions in cocoa butter - a quantitative dsc study. *Journal Of Thermal Analysis And Calorimetry,* **82**(3): 691–702.

Foubert, I. (2003). *Modelling isothermal cocoa butter crystallization: Influence of temperature and chemical composition*, University of Ghent, PhD, p. 263.

Foubert, I., Dewettinck, K., Janssen, G. and Vanrolleghem, P.A. (2006). Modelling two-step isothermal fat crystallization. *Journal of Food Engineering,* **75** (4): 551–551.

Foubert, I., Dewettinck, K. and Vanrolleghem, P.A. (2003). Modelling the crystallization kinetics of fats. *Trends In Food Science And Technology*, **14:** 79–92.

Foubert, I., Vanrolleghem, P.A. and Dewettinck, K. (2003). A differential scanning calorimetry method to determine the isothermal crystallization kinetics of cocoa butter. *Thermochemica Acta,* **400**: 131–142.

Foubert, I., Vanrolleghem, P.A., Vanhoutte, B. and Dewettinck, K. (2002). Dynamic mathematical model of the crystallization kinetics of fats. *Food Research International,* **35**: 945–956.

Franke, K. (1998). Modelling the cooling kinetics of chocolate coatings with respect to final product quality. *Journal of Food Engineering,* **36**: 371–384.

Fryer, P.J. and Pinschower, K. (2000). The materials science of chocolate. *MRS Bulletin*: 25–29.

Hernqvist, J.W. (1988). Crystal structures of fats and fatty acids. In N. Garti & K. Sato (Eds.), *Crystallization and polymorphism of fats & fatty acids*. Marcel Dekker, pp. 97–138.

Jung, A. and Fryer, P.J. (1999). Optimising the quality of safe food: Computational modelling of a continuous sterilisation process. *Chemical Engineering Science,* **54**: 717–730.

Kloek, W., Walstra, P. and Van Vliet, T. (2000). Crystallization kinetics of fully hydrogenated palm oil in sunflower oil mixtures. *Journal of American Oil Chemists Society,* **77**(4): 389–398.

Loisel, C., Keller, G., Lecq, G., Bourgaux, C. and Ollivon, M. (1998). Phase transitions and polymorphism of cocoa butter. *Journal of the American Oil Chemists Society,* **75**(4): 425–439.

Lonchampt, P. and Hartel, R.W. (2004). Fat bloom in chocolate and compound coatings. *European Journal of Lipid Science and Technology,* **106**(4): 241–274.

Lonchampt, P. and Hartel, R.W. (2006). Surface bloom on improperly tempered chocolate. *European Journal of Lipid Science and Technology,* **108**(2): 159–168.

Merken, G.V. and Vaeck, S.V. (1980). Etude du polymorphisme du beurre de cacao par calorimetrie dsc. *Lebensmittel Wissenshaft und Technology,* **13**: 314–317.

Narine, S.S. and Marangoni, A.G. (1999a). Microscopic and rheological studies of fat crystal networks. *Journal of Crystal Growth,* **198/199**: 1315–1319.

Narine, S.S. and Marangoni, A.G. (1999b). Relating structure of fat crystals networks to mechanical properties : A review. *Food Research International,* **32**: 227–248.

Pinschower, K. (2003). *Measurement of the contraction of chocolate during solidification*. Chemical Engineering. Birmigham, University of Birmingham. PhD.

Rousset, P., Rappaz, M. and Minner, E. (1998). Polymorphism and solidification kinetics of the binary system pos-sos. *Journal of the American Oil Chemists Society,* **75**(7): 857–864.

Schenk, H. and Peschar, R. (2004). Understanding the structure of chocolate. *Radiation Physics and Chemistry,* **71**(3-4): 829–835.

Stapley, A.G.F., Tewkesbury, H. and Fryer, P.J. (1999). The effects of shear and temperature history on the crystallization of chocolate. *Journal of the American Oil Chemists Society,* **76**(6): 677–685.

Tewkesbury, H., Stapley, A.G.F. and Fryer, P.J. (2000). Modelling temperature distributions in cooling chocolate moulds. *Chemical Engineering Science,* **55**(16): 3123–3132.

Van Malssen, K., Van Langevelde, A., Peschar, R. and Schenk, H. (1999). Phase behavior and extended phase scheme of static cocoa butter investigated with real-time x-ray powder diffraction. *Journal of the American Oil Chemists Society,* **76**(6): 669–676.

Voller, V.R., Swaminathan, C.R. and Thomas, B.G. (1990). Fixed grid techniques for phase-change problems - a review. *International Journal for Numerical Methods in Engineering,* **30**(4): 875–898.

Walter, P. and Cornillon, P. (2001). Influence of thermal conditions and presence of additives on fat bloom in chocolate. *Journal of the American Oil Chemists Society,* **78**(9): 927–932.

Wille, R.L. and Lutton, E.S. (1966). Polymorphism of cocoa butter. *Journal of American Oil Chemists Society,* **41**: 491–496.

Chapter 23

Edible Moisture Barriers for Food Product Stabilization

C. Bourlieu,[1] V. Guillard,[2] B. Vallès-Pamiès,[3] and N. Gontard[2]

[1] ENSAM-INRA Montpellier, Joint Research Unit Agropolymers Engineering and Emerging Technologies, Montpellier, France, claire.bourlieu@univ-montp2.fr
[2]University of Montpellier II, Joint Research Unit Agropolymers Engineering and Emerging Technologies, Montpellier, France, valerie.guillard@univ-montp2.fr and nathalie.gontard@univ-montp2.fr
[3] Nestlé Research Center Lausanne, Food Biopolymers, Lausanne, Switzerland, baltasar.valles-pamies@rdls.nestle.com

23.1 Introduction

The reduction of mass transfer between a food product and its surrounding atmosphere by coating the entire product with an edible material is an extremely old practice, already used in the twelfth century in China (fruit waxing), and in England during the sixteenth century (meat larding) (Kester and Fennema 1986). Today, controlling mass, and more specifically moisture transfer, still remains an important challenge to maintain the quality of fresh or processed products, such as fruits, meats and seafood products. In ready-to-eat composite foods, the limitation of internal moisture transfer between components is also of major concern. It has gained in importance as consumers' demand for this kind of convenient product has increased. Moisture transfer from the "wet" to the "dry" component of these products affect the physical properties, especially texture, and chemical composition of the food system, and consequently its quality and shelf-life (Katz and Labuza 1981).

The application of edible films and coatings can help to reduce internal and external water transfer in slightly modified and processed food products (Debeaufort, Quezada-Gallo and Voilley 2000; Guilbert et al. 1996; Guillard et al. 2003; Koelsch 1994). Edible protective films or coatings can be defined as thin layers of material that are eaten by the consumer and provide a barrier to moisture, oxygen and/or solute movement in the food itself or between the food and its environment. Films are distinguished from coatings, since they are formed as stand-alone sheets of material, whereas coatings are directly formed on the product. Edible films must have good barrier properties, but also acceptable sensory characteristics (mouth feel, taste and aftertaste), a flexible and stretchable structure for an easy application onto the food and a composition conforming to the regulations (Guilbert 1986).

This chapter will point out the promises of edible moisture barriers in the protection of fresh or slightly modified products and in the design of ready-to-eat composite food products. After a review of the film-forming materials and shaping techniques, the discussion will focus on the barrier techniques of applications. The critical factors of these application techniques will be discussed.

23.2 Edible Film-Forming Materials and Principles of Formation

23.2.1 Film-Forming Materials

Materials, properties and technologies of application of edible films have been extensively reviewed over the last 30 years (Anonymous 1997; Anonymous 2004a; Cuq et al. 1995; Daniels 1973; Debeaufor et al. 1998; Gontard and Guilbert 1994; Guilbert and Gontard 1995; Guilbert and Cuq 1998; Guilbert et al. 1996; Kester and Fennema 1986; Kroger and Igoe 1971; Morgan 1971; Nussinovitch 1998; Wu et al. 2002). Materials that can be used to form edible films or coatings can classically be divided into three groups, which are presented in Table 23.1: (i) proteins, (ii) polysaccharides and (iii) lipids and derivatives (Guilbert 1986; Kester and Fennema 1986).

Edible moisture barriers usually include lipids. Because of their apolar nature, these hydrophobic substances are capable of forming a water-impervious structure and reduce efficiently the water transfer. However, lipid-based materials are most of the time brittle so they are frequently combined with proteins and/or polysaccharides to improve their mechanical and structural properties (Wu et al. 2002). Several reviews focussing specifically on edible moisture barriers (Debeaufort et al. 2000; Koelsch 1994) and/or lipid-based edible films have been published (Baldwin et al. 1997; Callegarin et al. 1997; Greener and Fennema 1992; Hernandez 1994; Quezada-Gallo et al. 2000). The most recent review on lipid-based moisture barriers is that of Morillon et al. (2002).

An investigation of international patent databases (Anonymous 2006c) for deposited patents dealing with “edible moisture barriers” over the last 25 years gave more than 50 answers. Of the total, 18% of the patents dealt with the development of pure fat barriers, 58% with the development of a composite barriers including fat and other components (polysaccharides and protein derivatives or inorganic fillers), 13% with barriers based on pure hydrocolloids (protein or polysaccharides), 4% with sugar coatings, 4% with edible moisture barriers that can be based on any of the three kinds of components, and eventually 2% based on pure thin inorganic coatings. It is interesting to note that 25% of the patents directly describe the development of a composite food in which the edible film is supposed to be used.

A new class of barrier materials based on pure, thin (0.05 micron or less) amorphous inorganic coatings has been reported (Beyer et al. 1996). Such thin coatings overcome the textural problems associated with the use of organic coatings, which have to be applied as a thick layer to be effective. The inorganic substance must be approved to be used in foods. In the United States, according to the section 21 of the Code of Federal Regulations for edible products (Anonymous 1977), authorized inorganic compounds are silicon dioxide; single silicates, such as sodium silicate, calcium silicate and magnesium silicate; aluminium silicate; magnesium trisilicate; composite silicates such as sodium aluminium silicate, potassium aluminium silicate

and calcium aluminium silicate; talc; clay materials such as bentonite; carbon; insoluble carbonates; and phosphates. Even though the use of pure thin inorganic coatings as a moisture barrier is still marginal, the possibility of using these materials as inorganic fillers in a barrier is also suggested in 8% of the patents. Edible inorganic compounds can thus be considered as a new category of edible coating materials.

Table 23.1. Polysaccharides, proteins, lipids and derivatives potentially used as film-former or barrier compound and their origin.

Origin	Polysaccharides	Proteins	Lipids
Botanical	Cellulose and derivatives (CMC, MC, HPC, HPMC) Starch and derivatives (fractionated: amylose, amylopectin, modified: propylated, acetylated…, hydrolysed starch: dextrins, maltodextrins, glucose syrups, pregelatinized starch) Pectin and pectinates; alginate, agar, carrageenan, furcellaran Gums (arabic, guar, locust bean, carob, karaya, adragant, tara, sterculia, tamarind, ghatti)	Corn zein Wheat gluten and derivatives (gliadins, glutenin) Soya proteins and derivatives (globulin 7s, globulin 11s) Rice and manioc proteins Pea proteins Peanut (conarachin), pistachio, cotton, sunflower, and rapeseed proteins	Native or hydrogenated palm, palm kernel, rapeseed, soya, peanut, coconut, castor, cotton oils, cocoa butter and their derivatives (obtained by fractionation, esterification, concentration and/or reconstitution: fatty acids and alcohols, mono-, di- and triglycerides, cocoa butter substitutes, margarine, shortenings, acetylated glycerides, lecithins, etc) Carnauba, candelilla, rice bran, and fruit (apple, bamboo, sugar, cane, citrus) waxes, jojoba oil; Wood rosin, tree lacs, citrus terpenes, gum lacs Camphor, mint and citrus fruit essential oils Liquorice
Animal	Chitin, chitosan.	Collagen, gelatin, meat proteins Keratin Fish proteins (myofibrillar proteins and elastin) Casein, caseinates Whey proteins Ovalbumin	Native or fractionated milk , lard, tallow fats and their derivatives (obtained by fractionation, esterification, concentration and/or reconstitution: fatty acids and alcohols, mono-, di- and triglycerides, cocoa butter substitutes, margarine, shortenings, acetylated glycerides, lecithins etc) Beeswax, spermaceti*, chinese wax, shellac
Microbial	Xanthan, dextran, pullulan, gellan	Chitosan	–
Mineral, fossil or synthetic	–	–	Paraffin, polyethylene wax, microcrystalline wax Lignite, peat, montan waxes

*Formerly extracted from whale adipose tissue. No longer produced and sold in accordance with international regulations concerning whale capture. Now replaced by synthetic spermaceti made of pure cetyl palmitate or mixtures based on jojoba oil.

23.2.2 Methods of Formation of Edible Barriers

Edible films and coatings are classically made following two main methods (Guilbert and Cuq 1998):

(a) The "thermoplastic method" based on the thermoplastic properties of the film-forming material.
(b) The "solvent method" based on a coacervation from a solution or a dispersion of the film-forming material in a solvent phase, followed by the evaporation of the solvent.

An example of these methods illustrated for lipids is shown in Figure 23.1.

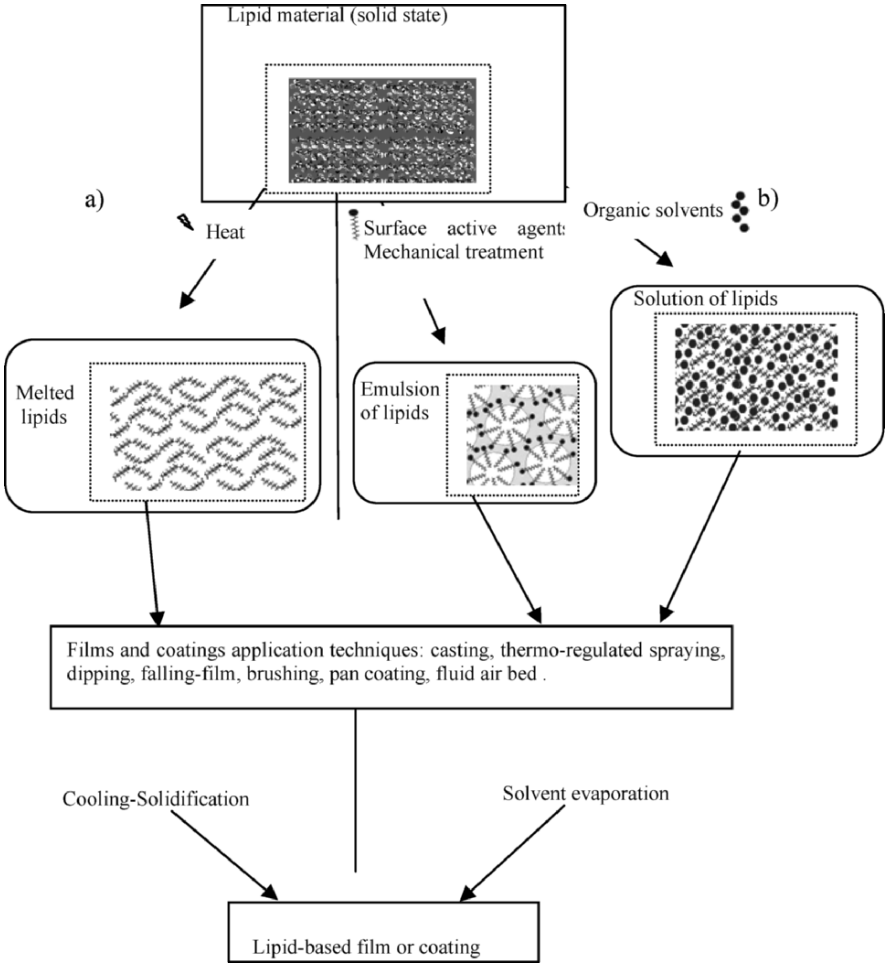

Figure 23.1. Methods of formation of edible lipid-based films by (a) the "thermoplastic" method, and (b) the "solvent method."

The thermoplastic method consists in shaping film-forming materials using thermal or thermomechanical processes in conditions of low hydration and induces structural transitions in the material such as melting of lipids and crystalline parts of polymers or a transition from the glassy metastable state to the rubbery state in the amorphous parts of the polymers (Guilbert and Cuq 1998). It is the most common procedure of forming lipid films and coatings. However, this method is less commonly used to shape hydrocolloids than the solvent method. The material is melted at an appropriate temperature or following a tempering schedule, and then it is solidified on a surface. Melting-solidification results in a dense crystalline network arrangement of the lipid material. High melting point lipids, such as waxes, require specific care since they solidify quickly. Therefore, they are often applied as emulsions or dispersions, using the solvent method to overcome this issue.

In the solvent method the separation of the solubilised or dispersed material from the solvent phase can be explained by precipitation or phase change induced by solvent evaporation, addition of electrolyte, pH modification or heat treatment (Krochta and McHugh 1997). Such treatments can be adjusted to enhance film formation or specific properties. For composite emulsion-based films or coatings a lipid material and most likely a surfactant, is added to the solution, which is then heated above the lipid melting point and homogenised. The prepared solution is then applied on an appropriate support and the solvent evaporates.

23.2.3 Hydrophilic Materials

Due to their hydrophilic nature, pure polysaccharide and protein films exhibit limited water vapour barrier ability. These coatings are thus favoured when other barrier properties are desired. Most of these films present interesting oil and gas (oxygen, carbon dioxide) barrier properties at low relative humidity (Albert and Mittal 2002). They are also characterized by good mechanical properties, specially those based on proteins which present a high intermolecular binding potential (Cuq et al. 1998). Hydrocolloid coatings can be applied in the form of high moisture gelatinous coatings, which delay moisture loss from coated foods by functioning as “sacrificing” agents rather than moisture barriers (Kester and Fennema 1986). They can also be chemically, enzymatically and/or physically treated to improve their moisture resistance (Ou et al. 2005; Tang et al. 2005).

The properties of various film-forming polysaccharides, such as alginates, pectins, starches, dextrins, cellulose, carrageenan, gums, chitosans and their derivatives have been investigated for a long time and reviewed by Nisperos-Carriedo (1994). Their wide uses in the food industry have been favoured by their abundance, variability and low-cost, and are summarized in Tables 23.2(a) and (b).

Several studies reviewed formulations, barrier properties and possible application of edible protein-based films (Table 23.3) (Gennadios et al. 1994; Krochta and Mc Hugh 1997; Torres 1994). Overall, similarly to polysaccharide films, proteins exhibit relatively low moisture barrier properties, two to four times lower than conventional polymeric packaging materials (McHugh and Krochta 1994d). The limited resistance of protein films to water vapour transmission is attributed to their substantial hydrophilicity and to the amounts of plasticizers, such as glycerol and sorbitol, incorpo-

rated into films to impart adequate flexibility. The potential occurrence of adverse reactions to native proteins constitutes a huge limitation in the potential applications of various protein-based films (e.g., allergies to milk, egg white, peanut and soybean proteins, gluten, etc.). Native proteins include two types of molecules: fibrous proteins, with structural water-insoluble groups, and biologically active globular proteins. Generally, these globular proteins have to be modified, either by heat treatment, pH modification or solvent addition, to obtain extended structures more susceptible to form a film.

Table 23.2(a). Origin, film-characteristics and uses of polysaccharide-based edible films.

Compound/ origin	Functional molecules	Film characteristics	Uses
Starch (native or modified) Various ubiquitous natural sources: tubers and cereals	Amylose: linear chain of D-glucose with α-1-4 links; Amylopectin: ramified chain with α-1-4 and α-1-6 links	Native starch: high susceptibility to hydration and low mechanical resistance Amylose-based films: coherent, relatively strong, free-standing films Amylopectin-based films: brittle and non-continuous (Zobel 1988)	Few applications of native starch High amylose starch film widely used: extruded wraps, deep fried potato products, meat products (Gennadios et al. 1997), refrigerated strawberries (Garcia et al. 1998a; Garcia et al. 1998b) Current tendency: alternative sources of starch with better physico-chemical and functional properties (Mali et al. 2004; Mali 2005)
Cellulose (modified) Structural polysaccharide of plants	D-glucose units β-1-4 glycosidic linkage Native cellulose: crystalline water insoluble Ethers: anionic (carboxymethyl cellulose or non-ionic (methyl, hydroxypropyl and hydroxypropyl methylcellulose). Relative hydrophilicity: HPC < MC < HPMC < CMC. Water insoluble derivative: microcrystalline cellulose.	Cellulose ether-based films: flexible and transparent, moderately strong, resistant to oil and fat migration and moderately barriers to moisture and oxygen (Arvanitoyannis and Yamamoto 1996; Arvanitoyannis and Biliaderis 1999; Park and Chinnan 1995)	Cellulose ethers–based films widely used: on pharmaceutical tablets, confectionery (Porter and Woznicki 1989; Woznicki and Grillo 1989), starchy fried products (Mallikarjunan et al. 1997; Williams and Mittal 1999); Microcrystalline cellulose: filler in some coatings
Sodium alginate Brown seaweeds	Linear (1 → 4) linked polyuronic acid with three types of polymer segments: poly-β-D-mannuronic acid, poly-α-L-guluronic acid, blocks consisting of alternating D-mannuronic and L-guluronic acid residues (King 1983)	Reaction with several polyvalent cations to form gel Films of increased water resistance obtained by immersion in $CaCl_2$ solutions after formation (Rhim 2004)	Patented gelatinous coatings limiting moisture loss and oxidation (Earle 1968; Earle and McKee 1976); application to various meats (Allen et al. 1963a; Earle and McKee 1987; Lazarus et al. 1976) Carriers of antimicrobial agents: potassium sorbate and ascorbate or sorbic acid (Wong et al. 1996)

Table 23.2(b). Origin, film-characteristics and uses of polysaccharide-based edible films.

Compound/ origin	Functional molecules	Film characteristics	Uses
Pectin By-product of citrus and apple productions	D-galacturonic acid polymers (α-1,4) with varying degrees of methyl esterification	Low-methoxyl pectins (esterification degree < 50 %) capable of forming gel with calcium ions Films with low moisture resistance obtained after drying	Few uses, reduction of stickiness and improved appearance of dry fruits and dates (Schultz et al. 1948; Schult et al. 1949; Swenson 1953);
Carrageenan Red seaweeds	Sulphated polysaccharides of D-galactose and 3,6-anhydro-D-galactose. Number and position of sulphate groups on the disaccharide repeating unit determine classification in three major types: κ, ι, and λ (Yuguchi et al. 2002)	Thermoreversible gels produced from heated aqueous solutions; gelation promoted by the presence of cations (potassium, calcium and sodium)	Widely used: on fresh and frozen meat and fish to prevent superficial dehydration (Shaw et al. 1980), sausage casing (Macquarrie 2002), granulation-coated powder, dry solids foods, oily foods (Ninomiya et al. 1997), soft nongelatine capsules (Bartkowiak and Hunkeler 2001; Fonkwe et al. 2003; Tanner et al. 2002)
Gums Botanical (arabic, guar) or microbial (xanthan, gellan, etc.)	Arabic gum most used: complex mixture composed of arabinogalactan oligosaccharides and polysaccharides with a proteic part.	Arabic gum solutions present good adherence properties and form film upon drying.	Arabic gum: limitation of flavour evaporation (Nisperos-Carriedo 1994)

23.2.4 Hydrophobic Materials

The most commonly used hydrophobic film-forming barrier materials include (by decreasing order of efficiency):

- waxes;
- lacs;
- fatty acids and alcohols;
- acetylated glycerides;
- cocoa-based compounds and their derivatives.

The classification of lipids by increasing efficiency can be explained by the chemical composition of the molecules (presence of polar components, hydrocarbon chain length, number of unsaturation or acetylation). For components having the same chemical nature, increasing chain length modifies the barrier properties because the polar part of the molecule decreases and does not favour water solubility in the film (McHugh and Krochta 1994d).

Table 23.3. Origin, film-characteristics and uses of the main kinds of protein-based edible films.

Compound/ origin	Functional-molecules	Film characteristics	Uses
Collagen and derivatives (gelatin) Skin, tendon, and animal connective tissues	Fibrous proteins constituted of fibril sub-units	Collagen films formed by reticulations of amine and carboxyl groups; gelatin-based films: flexible, clear, with good oxygen barrier properties, but poor moisture resistance; classical formulations: 20–30% gelatin, 10–30% plasticizer and water.	Traditionally used in the meat industry: sausage casing and meat preservation early proposed in patents disclosures (Harvard and Harmony 1869); various pharmaceutical and other food industry applications: ingredients micro-encapsulation, tablets and capsules (Gennadios et al. 1994)
Milk proteins By-product of the milk and cheese manufacture	Casein (80% of the total of milk proteins) Whey protein (20% remaining of milk protein, solubility at pH 4.5)	Casein films formed from aqueous solution without further treatment Casein/glycerol (1:2) films: transparent, flavourless, flexible, highly permeable to moisture and very water soluble (Avena-Bustillos and Krochta 1993; Chen 1995; McHugh and Krochta 1994)	Sodium caseinates films tested as wrapping on bread: preservation of bread texture for 6 hours compared to control (Schou et al. 2005) Whey protein-based coatings widely used: breakfast cereals, raisins, frozen peas cheese pieces, micro-encapsulation of food additives…
	Total milk proteins	Whey protein films: similar properties to casein films, but water insoluble; eating required for their formation (disulfide bonds)	Reduction of the textural perceptibility of whey protein film by mixing with sodium caseinate (Longares et al. 2005)
Cereal proteins Corn, wheat, sorghum, …	Nonwater (gluten) and alcohol-soluble (prolamin) fractions from cereal proteins	Films based on corn zein and wheat gluten extensively studied; homogeneous, yellowish, relatively strong and water resistant wheat gluten film (ethanol dispersions/partial denaturation) Other film-forming cereal proteins studied (sorghum kafirin, rice bran)	Corn zein-based edible coatings widely used to extend the shelf-life of nuts by retarding, rancidity, staling and sogginess Commercial uses for confectionery glaze and pharmaceutical tablets
Oilseed proteins Oilseed producing plants	Soy proteins most studied: globulin protein fractions (2S, 7S, 11S and 15S)	Flexible yellowish films with low moisture resistance properties formed from soy protein aqueous dispersions upon heating Alkaline conditions reinforce film functional properties	Protection of various food products (nuts, aroma and flavours encapsulation, fresh meat, battered meat, etc.) (Gennadios and Weller 1991)

The barrier efficiency of lipids also depends on their physical state (solid fat content at the temperature of use, crystalline form, etc.). Indeed, many lipids exist in a crystalline form and each individual crystal is impervious to water vapour. Water flow permeates mainly between crystals and the intercrystalline packing arrangement has major consequences on the barrier properties of the material (Martini et al. 2006).

Consequently, the migration rate can be slowed down to a certain extent by a proper tempering, which induces a more efficient structure against moisture migration. In the same way, in a continuous lipid phase, vapour migrates more easily in the liquid fat portion of the product. The solid fat content of the product at the temperature of application clearly influences the migration rate (Ghosh et al. 2002; Kester and Fennema 1989c; Kester and Fennema 1989d).

Paraffin followed by candelilla wax and microcrystalline waxes, and eventually by beeswax, are considered as the most effective moisture barriers derived from edible waxes (Morillon et al. 2002). There is no satisfactory chemical definition for the term "wax" which is used for a variety of products of mineral, botanical and animal origin that contain various kinds of fatty materials (Table 23.4). The term "resins" or "lacs" can also be used for plant or insect secretions that take place along resins ducts, often in response to injury or infection, and result in more acidic substances (Hernandez 1994). However, all waxes tend to contain wax esters as major components, that is, esters of long-chain fatty alcohols with long chain fatty acids. Depending on their source, they may additionally include hydrocarbons, sterol esters, aliphatic aldehydes, primary and secondary alcohols, diols, ketones, triacylglycerols, and so on.

Table 23.4. Waxes and lacs: Class, sources and prevalent molecular species in their composition. (Anonymous 2006a; Anonymous 2006b; Hamilton 1995; Spencer et al. 1977).

Class	Source	Type of waxes	Molecular species prevalent in the composition
Mineral/ fossil	Petroleum	Paraffin	Mixtures of straight-chain alkanes
	Lignite/brown coal	Polyethylene wax	Variable. Long chain (C24–C30) esters/long chain acids
		Microcrystalline wax	
		Lignite/peat/montan	
Animal	Bees secretion	Beeswax	Wax esters (C40–C46 molecular species)
	Insect secretion	Shellac	Wax esters (C28–C34)
	Insect secretion	Chinese wax	Wax esters (C46–C60)
	Whale tissues	Spermaceti	Wax esters (mainly cetyl palmitate-C32 and myristate-C30)
	Collected on sheep wool	Lanolin (wool wax)	Sterols and triterpene alcohol esters
Botanical	Brazilian palm tree	Carnauba	Wax esters (C18–C22 fatty acids linked to C20–C24 fatty alcohols)
	Mexican shrub	Candelilla	Hydrocarbons (C29–C33), fatty esters
	Jojoba seeds	Jojoba oil	Fatty esters (C38–C44)
	Rice	Rice bran oil	Unsaponifiable, long chain alcohols (C26–C30)
	Berries kernel and skin	Japan wax	Palmitic acid triacylglycerols
	Wood pulp	Wood rosin	Variable (hydrocarbons, wax esters)
	Multiple others	Apple, bamboo, sugar cane, citrus fruit, etc.	

Waxes usually present an orthorhombic system of crystallization, favoured by a slow cooling rate and possibly a small fraction of hexagonal crystals. They possess variable mechanical properties depending of their composition. Carnauba waxes are harder than all the other waxes to which they are added to improve strength and

gloss. Candelilla waxes solidify slowly and reach an intermediate hardness between carnauba and beeswax. Beeswax is relatively flexible and presents a viscoelastic behaviour (Shellhammer et al. 1997).

Wax coatings have been used since the 1930s to control desiccation and ripening of fresh fruits and vegetables by limiting gas diffusion (Callegarin et al. 1997; Hernandez 1994; Kester and Fennema 1986). Such coatings also reduce the surface abrasion of the fruit surface during handling, improve appearance by enhancing surface gloss, and were used as carrier for other active components such as fungicides. However, if the gas permeability of the coating is not adequate, waxing can result in the creation of a modified internal anaerobic atmosphere inducing off-flavours and deterioration of the product (Baldwin et al. 1997).

Many wax coatings are applied as emulsions (macro-emulsions particles size range 2,000–100,000 Å or micro-emulsions particles size range 1,000–2,000 Å) or as wax suspensions. Though most natural waxes have emulsifying properties, the stability of the wax emulsion is reinforced by the use of surface active agents such as fatty acids (palmitic, oleic, stearic, etc.), glycerol and fatty acids derivatives or lecithins (Hernandez 1994). Numerous applications of wax coatings on whole citrus fruits have been reported in the scientific literature: emulsion candelilla wax/water on limes (Paredes et al. 1974), carnauba wax on lemons (Hagenmaier and Baker 1994; Hagenmaier and Baker 1995). Wax coatings have also been applied on slightly processed fruits: carnauba wax on grapefruit pieces (Hagenmaier and Baker 1997), beeswax on orange fruits (Baldwin et al. 1997), other wax coatings on apples and pears (Drake and Nelson 1990; Drake and Nelson 1991), peaches (Kraght 1966), tropical fruits and vegetables (Baldwin 1994; Baldwin et al. 1999; Hoa et al. 2002; McGuire 1997). A limited number of processed food products have also been coated with waxes and lacs, such as shellac: waxing of candies and breakfast cereal mixes (Lowe et al. 1963; Bolin 1976; Seaborne and Egberg 1989), application of commercial glazing and antisticking blends (waxes/lacs alcoholic dispersions or suspensions) on confectionery and dry fruits (Capol®, Kaul GmbH, Germany). The restricted use of waxes and lacs as edible coatings for processed food products can be explained first by regulatory concerns and secondly because of their high melting point responsible for unappealing sensorial properties (hardness and waxy residues).

In the classification of moisture barriers efficiency established by Kester and Fennema, waxes are followed by stearyl alcohol, acetyl acyl glycerols, hexatriacontane, tristearin and stearic acid (Kester and Fennema 1989a). These authors observed that stearic alcohol was seven times more impervious to water transfer (0–100% RH gradient) than stearic acid. This result can be explained by the lower polarity of the hydroxyl function compared to the carbonyl function, but also to the specific sheet structure developed by the stearyl alcohols. Fatty alcohols and fatty acids lack structural integrity to form strong continuous coatings and are used mainly as emulsifying or dispersing agents in combination with other biopolymers. The formulation of multicomponent films can affect their properties.

McHugh and Krochta (Gennadios et al. 1994) observed that composite films based on fatty alcohols/whey proteins were less effective as moisture barriers than fatty acids/whey proteins. This discrepancy with Kester and Fennema's study can be

explained by the influence of the polar support of the fatty alcohol composite film on moisture transfer.

Roth and Longin (1984) showed that C16 or C18 fatty alcohols were the most effective to limit water evaporation from the surface of hydrated products. Similarly, Hagenmaier and Baker (1997) reported that micro-wax emulsions including stearic and palmitic acids were more effective to limit fruit desiccation than those using lauric and oleic acids as emulsifiers. Koelsch and Labuza (1992) showed that the moisture barrier properties of composite films (emulsions: methylcelulose/fatty acids, 70:30) increased with the degree of saturation and fatty acid chain length up to 18 carbons. The higher efficiency of stearic and palmitic fatty acids and alcohols compared to component of similar chemical nature but of different chain length was reported in various other studies (Hagenmaier and Shaw 1990; McHugh and Krochta 1994c; Park et al. 1994). The positive effect of long aliphatic chain up to 18 carbons can be explained by an increased apolar part in the molecule which does not favour water solubility in the film. Above this threshold, the aliphatic long chains induce a more heterogeneous structure.

Similarly to fatty acids and fatty alcohols, acyl glycerols (esters of glycerol and fatty acids) are often used as emulsifying and dispersing agents because of their poor mechanical properties (Table 23.5). Higuchi and Aguiar (1959) could not investigate the moisture barrier properties of pure self-supported films of di- and tri-glyceryl stearates because of the development of structural defects. However they studied pure glyceryl-monostearate film and blends of glyceryl-stearate with beeswax. The resistance to water transfer of glyceryl-monostearate appeared highly dependent on the relative humidity gradient the film was subjected to. This conclusion was in agreement with another study dealing with a monostearyl-glycerol film formed on a cellophane support (Martin-Polo and Voilley 1990). The film showed moisture barrier properties ten times higher than cellulose triacetate and cellulose acetate propionate films but much lower than synthetic plastic films. Mono-stearyl glycerol has been reported as a very effective emulsifier to improve the adherence of an alcane layer on a hydrophile suppport (Quezada Gallo et al. 2000). In the classification of lipid materials established by Kester and Fennema (1989a), tristearyl-glycerols were reported as 1.5 times more resistant to water transfer than stearic acid but half as resistant as hexatriacontane (alcane).

Acetyl-acyl-glycerols (acyl glycerols with one or two acetyl groups on the glycerol molecule) commonly called acetylated glycerides, can be prepared through a reaction between glycerides and acetic anhydride or through a catalysed interesterification of edible fats with triacetin. A highly noticeable property of these compounds compared to other lipids is a good flexibility in their α-polymorphic form. The acetylated glycerides are also characterized by a high resistance to oxidative degradation, a nongreasy touch and a low melting point resulting from the presence of acetyl groups in the glyceride molecule. Used at concentration from 2% to 10% (w.b.), they make excellent plasticizers and significantly improve the mechanical properties of high melting point fats or of other fats at low temperature (Alfinslater et al. 1958). Their properties depend on the nature of the acyl-glycerols they are based on, and on their acetylation degree. For example, aceto-stearin films have oxidative stability,

Table 23.5. Summary of the U.S Code of Federal Regulations (Title 21, Food and Drug Administration) and directive 95/2/EC concerning the use of the main kinds lipid film-forming materials different from waxes, lacs and their derivatives, as coating or components of coatings in food products (Anonymous 1977; Anonymous 2004b).

Substances	Authorized applications in the U.S. Code of Federal Regulations [CFR section]	Authorized applications in the consolidated directive 95/2/EC [E No]
Fatty acids	Lubricant, binder, and defoaming agent; limit: GMP*; [172.860] Stearic acid: GRAS*** substance; limit: GMP; [184.109]	#; limit: *quantum satis***; [E 570]
Mono- and diglycerides	GRAS substance; Limit: GMP; [184.1505]	#; Limit: *quantum satis*; [E 471]
Acetylated glycerides	Monoglycerides, multipurpose additive; limit: *quantum satis*; [172.828]	#; Acetic acid ester of mono and diglycerides; limit: *quantum satis*; [E 472 a]
Lactic acid esters of mono- and diglycerides	Emulsifiers, plasticizers, or surface-active agents for bakery products, desserts and shortenings; limit: *quantum satis*; [172.848]	#; limit: *quantum satis*; [E 472 b]
Acetylated or none tartaric acid esters of mono- and diglycerides (DATEM)	DATEM, GRAS substance; lLimit: GMP; [184.1101] Tartaric acid, GRAS substance; limit: GMP; [184.1099]	#; Mono and diacetylated DATEM [472 e]; DATEM [472 d]; mixed acetic and tartaric acid esters of mono and diglycerides [E 472 f]; Limit: quantum satis
Sucrose fatty esters	Emulsifiers or stabilizers in various goods; texturizers in various goods; components of protective coatings applied to a restricted number of fruits to retard ripening and spoiling; limit: GMP; [172.859]	Colours and fat-soluble antioxidant; [E 473]
Polyglycerol esters of fatty acids	Cloud inhibitor in vegetable and salad oils, emulsifiers in dry or whipped topping base; [172.854]	Fine bakery, granola breakfast (10 g/kg), emulsified liqueur (5 g/l), egg products (1g/kg), beverage whiteners (0.5g /kg), chewing gum, fat emulsions, milk and cream analogues (5 g/kg); sugar confectionery, desserts (2 g/kg); [E 475]
Salts of fatty acids	Binder, emulsifier, and anticaking agent in food; limit: GMP; [172.863]	#; Sodium, potassium and calcium salts of fatty acids; [E 470 a]; magnesium salts of fatty acids; [E 470 b]; limit: quantum satis
Lecithins	GRAS substance; limit: GMP; [184.1400].	#; limit: quantum satis; [E 322]

* GMP: Good Manufacturing Practices;
** *quantum satis*: Amount not to exceed that required to produce the intended effect;
***GRAS: Generally Recognized As Safe for human consumption;
#: Additives that may be added to all foodstuffs except for those referred to in the Article 2 (3) of the consolidated directive 95/2/EC.

especially if derived from hydrogenated vegetable oils, while aceto-olein films are less resistant to oxidation. Tailored functional properties of blends can thus be achieved by combining various molecules (Alfin-Slater 1958; Feuge et al. 1953). Distilled acetylated monoglycerides coatings produced under the trade name Myvacet (Eastman Chemical Product, Kingsport, TN) were first used in edible packaging application on

fresh products in the late 1950s (Woodmansee and Abbott 1958). Scientific and patent literature disclose numerous examples of application on meats (Dawson et al. 1962; Schneide 1972; Stemmler and Stemmler 1974; Zabik and Dawson 1963), frozen fish (Hirasa 1991; Stuchell and Krochta 1995), fresh or dry fruits, and vegetables (AvenaBustillos et al. 1997; Mate and Krochta 1997).

More recently water-related properties and water barrier properties of acetylated monoglycerides and diglycerides presenting variable chain length and acetylation degrees were evaluated by Guillard et al. (2003). The extension of shelf-life enabled by such films in a two-component composite bakery food product (sponge-cake/barrier film/agar gel) was estimated. Films with the highest acetylation degree (70%) presented significantly lower moisture sorption on the high a_w range (0.70–1.00) than other compounds and enabled the best extension of the baked product shelf-life. This observation was in accordance with the decrease in HLB (hydrophilic-lipophilic balance) observed between not acetylated (glycerol monostearate, H.L.B. of 3.8) and acetylated monoglycerides (H.L.B. of 1.5) (Hernandez 1994). According to model predictions, the most effective barrier (100 μm thick) delayed for more than 20 days the increase of the sponge-cake moisture content from 23% to 40% (w.b.) which was reached in less than two days in the product without barrier. Few applications and sensory problems associated with acetylated glycerides edible coatings have been reported, including the tendency of coatings from highly saturated acetylated compounds to crack and flake during refrigerated storage (Hirasa 1991), to pick up foreign flavours (Zabik and Dawson 1963), and to exhibit acidic or bitter aftertaste attributed to acetylated compounds (Morgan 1971).

Because of their fluidity, oils exhibit poor moisture barrier properties that can nevertheless be improved by hydrogenation. They are widely used in refrigerated or frozen product, possibly after a winterization (removal of crystalline triacylglycerols).

Among the list of the numerous materials that can be used as moisture barriers, cocoa butters and cocoa-based films are the most widely used in the confectionery (chocolate) and bakery industries (Biquet and Labuza 1988; Morillon et al. 2002). The good sensorial properties of chocolate permit using thick perceptible coatings that will both resist moisture migration and increase the commercial value of the product. The first comprehensive study on chocolate barrier property was done by Biquet and Labuza (1988). These authors determined the moisture sorption isotherms, effective diffusion coefficient and water vapour permeability of a dark chocolate film (0.6–1.2 mm thick). They reported that a 0.6 mm coating of semisweet dark chocolate used as barrier coating on a monocomponent system (agar gel) was a more effective moisture barrier than a 0.025 mm low density polyethylene coating. However, Guillard et al. (2003) pointed out the poor water barrier properties of dark chocolate film used at the interface between two components in the high a_w range ($a_w > 0.8$) which could be explained by sugar dissolution phenomena. A comprehensive review and several publications on the barrier properties of chocolate were recently published by Gosh (Ghosh et al. 2002; Ghosh 2003; Ghosh et al. 2004; Ghosh et al. 2005).

23.3 Formulation and Structuring of Moisture Barrier Films

Plasticizer addition and combination of materials (lipids, hydrocolloids or blends of lipids and hydrocolloids) are usually used to formulate moisture barriers and overcome the problems associated with the use of a single film-forming material.

23.3.1 Addition of Plasticizer

The cohesiveness and flexibility of edible films are determined by the molecular weight, branching and polarity of their constituents. Molecules with low polarity and high linearity tend to produce films with high degree of cohesiveness and rigidity (Morillon et al. 2002). Plasticizers, by weakening intermolecular forces between adjacent polymer chains, reduce brittleness, increase flexibility and tear resistance of edible films. This is particularly important when the product is stored at a low RH and/or temperature. The plasticizer must be compatible (miscible) with the polymer and if possible with its solvent. Plasticizers having food applications include: (a) mono-, di-, oligo-saccharides (mainly glucose and fructose–glucose syrups, honey), (b) polyols (mainly sorbitol, glycerol, glyceryl derivatives and polyethylene glycols), (c) lipids and derivatives (mainly fatty acids, monoglycerides and ester derivatives, phospholipids, surfactants). The formulation of films including plasticizers (usually added from 10% to 30% d.b.) must be conducted carefully, since they tend to migrate, diluting and softening the structure of the film, resulting in lower water resistance (Guilbert 1986).

23.3.2 Combination of Different Fat Materials

Multilayered pure fat structures have been advocated in several patents (Nielsen et al. 2001; Van Gastel 2006). Recently, a bilayered barrier which combined a soft spreadable fat (oil continuous spread, solid fat content of 5%–20 % at 20°C) and a high (> 35°C) melting point fat has been patented (Van Gastel 2006). The soft spread fills up the pores and homogenises the product surface whereas the second layers confers the moisture resistance. Another multilayered lipid-based barrier has been recently patented too (Gaonkar and Herbst 2004; Gaonkar and Chen 2005; Loh and Hansen 2002; Smith and Almendarez 2004). It includes a flexible layer (50 μm to 1 mm thick) containing short chain fatty acids crystallized in the α-form and a moisture resistant hydrophobic layer composed of a low melting fat (< 35°C) in which have been dispersed micro-particulated high-melting point fat (MP > 70°C). The microparticules can be added up to 35% (w.b.) of the hydrophobic layer and are responsible for fat crystals control and stabilization.

23.3.3 Combination of Hydrocolloids

Numerous examples of polysaccharide–protein, polysaccharide–polysaccharide, protein–protein multicomponent films have been available since the 1990s. Synergic effects between components, which result from interactions between the macromolecules, such as charge–charge electrostatic linkage, hydrogen bonding and covalent cross-linking have been researched. The resulting multicomponent edible barriers

can show improved water transfer resistance. For example, film barrier properties are improved by substituting 30% of gluten by keratin (Gennadios et al. 1993), by incorporating nonfat dry milk to acidic polysaccharide films such as alginate and pectin films (Parris et al. 1995) and in microcrystalline cellulose–corn starch–methylcellulose films (Psomiadou et al. 1996). Multi-components films may additionally present improved flexibility (Garcia et al. 2004; Lazaridou and Biliaderis 2002; Park et al. 2001) and sensorial properties (Longares et al. 2005).

23.3.4 Composite Films

Pure lipids can be combined with hydrocolloids such as proteins, starches or celluloses and their derivatives, either by incorporating the lipids in the hydrocolloid film-forming solution (emulsion technique) or by depositing the lipid layer onto the surface of the preformed hydrocolloid film to obtain a bilayer (Fennema and Kamper 1986; Krochta and De Mulder Johnston 1997). Multicomponent films have been extensively reviewed by Wu et al. (2002). The addition of nonlipid compounds (hydrocolloids, sugar solids, etc.) as dispersed components in fat materials permits forming fat dispersions (e.g., chocolate, Figure 23.2).

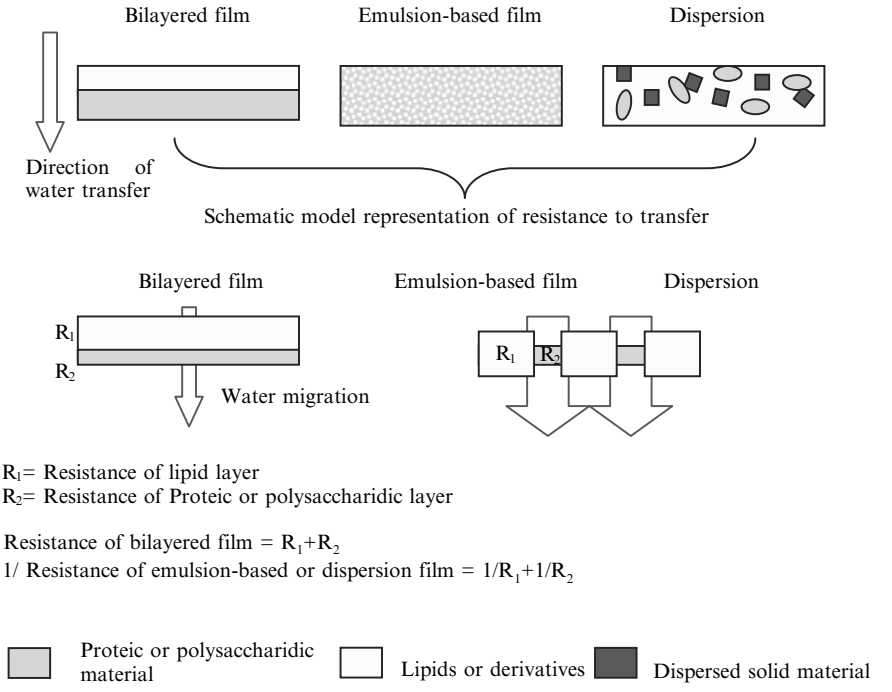

Figure 23.2. Schematic representation of the different types of composite edible films and their mechanism of resistance to transfer. (Adapted from Debeaufort et al. 1993; Debeaufort et al. 2002).

These composite films take advantage of the distinct functional properties of each class of film-formers: the moisture barrier properties of lipids and the ability to form a resistant matrix of the hydrocolloids. The resulting water barrier efficiency of bilayered films is often of the same order of magnitude than that of pure lipid (Debeaufort et al. 2000c) and is much higher than that of emulsion-based films (Debeaufort and Voilley 1995; Debeaufort et al. 1993; Martin-Polo et al. 1992; McHugh and Krochta 1994a; McHugh and Krochta 1994b). There are, however, a number of drawbacks associated with bilayered moisture barriers. The hydrocolloid layer is hydrophilic and tends to absorb water especially when the film is in direct contact with high water activity foods (> 0.75). Furthermore, the additional processing steps (casting and drying) required to form these films, make them difficult to use in high-speed commercial production.

With regard to polysaccharide–lipid films, the most cited in literature are cellulose ether–based, mainly MC- and HPMC-based films, though other trials with pectinate, chitosan, starch, and alginate have also been done. The interest towards cellulose derivatives can be explained by their excellent film-forming properties. Composite emulsified films based on HPMC/MC, stearic acid or palmitic/stearic acids blend, and possibly covered by a beeswax layer (Kamper and Fennema 1984a; Kamper and Fennema 1984b; Kamper and Fennema 1985; Rico-Pena and Torres 1990), but also bilayers of methylcellulose/waxes (Greener and Fennema 1989a; Greener and Fennema 1989b), presented really good moisture barrier properties and were early patented (Fennema and Kamper 1986). Starch/alginate/lecithin/stearic acid emulsified film, tested by Wu et al. (2001) on a 50%–100% RH difference also presented high water barrier resistance.

The possible associations of proteins and lipids in edible films have also been explored but less intensively than for polysaccharides (Wu et al. 2002). Their moisture barrier performance is generally lower than that of composite polysaccharide/lipid-based films. Among all the combinations tested and reported in scientific literature, the best moisture barrier properties were attributed to wheat gluten/lipid films (more precisely beeswax/wheat gluten/glycerol/diacetyl tartaric ester of monoglycerides; Gontard et al. 1994) and soy protein isolate/lipid films (more precisely soy protein isolate/glycerol/lecithin/stearic acid; Rhum et al. 1999). A moisture barrier based on a prolamin (10%–90%), in combination with a lipid (oil preferably: 0.1%–50%) and the salt of a fatty acid has been recently patented (Plijter-schuddemat et al. 2003). The resulting coating combines high mechanical strength, improved moisture barrier property and heat stability. Combination of shellac with prolamins presents similar properties (Glasser 1983).

23.3.5 Addition of Nonlipid Compounds as Dispersed Components

The addition of nonlipid fillers or bulking agents to improve the functional properties of edible moisture barrier (viscosity, adherence on substrate) is more frequent in commercial and patented coatings/films than in scientific literature. Indeed, in commercial references the barriers are often tested on the product to protect. Formulations are thus developed to try to adjust the viscosity of the coating and its mechanical properties in order to obtain a good adherence and protection to the coated product.

Conversely, in scientific articles, barriers have been most of the time evaluated as independent self-supported films.

The addition of dispersed saccharides/polysaccharides to enhance the adherence of composite or fat coatings on a bakery product has been suggested in various patents (Anonymous 1979; Haynes et al. 2004; Heuvel et al. 1997; Youcheff et al. 1996). The effect of sugars, cocoa powder, emulsifier and fat type on the WVP (3.5%–100% RH, 20°C) of chocolate coatings was investigated by Gosh et al. (2005) and underlined the favourable effect of sucrose on the WVP of the barrier.

The addition of inert filler material in a fat coating or a modified fat coating have been proposed in several patents (Bastiaans and Tap 2005; Rubenstein and Bank 1982; Rubenstein and Pelaez 1986). Inert fillers increase the viscosity of the fat in the molten state and evidently change its physical properties and enhance the water-occluding action, possibly by improving the coating flexibility and its resistance to external stresses. Inert filler materials must not be chemically reactive, therewith, not too hygroscopic, mechanically dispersible and possess a particle size such that they do not adversely affect the smoothness and sensorial properties of the coating. Typical filler materials include starches, chemically modified starches, dextrins, microcrystalline cellulose and insoluble cellulose derivatives but also inorganic compounds such as food grade talc, titanium dioxide, silicon dioxide, single silicates, clay materials, insoluble carbonates and phosphates. The amount of the filler material (10%–25% *W/W* of the coating) also depends on the particular type of filler utilized. If the use of inert fillers such as starch or dextrin in a fat layers improves its mechanical property and facilitate the coating application (application on ice cream cone; Rubenstein and Pelaez 1986), inorganic fillers, such as silicates, improve the moisture resistance of the barrier. Such coating permits protecting moisture sensitive food ingredients such as crispy cereals to retain their crispness even in a chilled but not frozen environment for a prolonged period, that is, four weeks or more (Bastiaans and Tap 2005).

23.4 Coatings Application Techniques and Critical Points

23.4.1 Selection of the Techniques of Application

Thermoplastic processes used to form edible films and coatings are adapted from techniques developed for synthetic polymers but take into account the specificities of natural polymers (sensibility to heat, chemical or mechanic treatment, high viscosity). These processes include: extrusion (Naga et al. 1996), injection-moulding, extrusion-blowing (Fishman et al. 2000; Liu et al. 2006; Psomiadou et al. 1996; Sothornvit et al. 2007) and compression-moulding (Cunningham et al. 2000).

Thermoplastic processes are attractive since they avoid the need to add and remove solvent but have not been as much explored as the applications from a solution or dispersion of the film forming material. The trials of extrusion, injection-moulding, compression-moulding with biopolymers and more specifically with oilseed proteins—soya (Choi et al. 2006; Foulk and Bunn 2001), sunflower (Orliac et al. 2002; Orliac et al. 2003)—and starches (Arvanitoyannis et al. 1998; Fang et al. 2005; Fishman

et al. 2000; Psomiadou et al. 1997; Suknark et al. 1997) targeted biodegradable plastics packaging. They offered strong tensile strength and included non–food-grade products in their composition.

The solutions or dispersions obtained by the "solvent" method can be cast and dry on a flat surface from which they are removed as sheets of material. This technique is the most widely used in laboratories to test the properties of the films. It can also be used by industries (MonoSol Rx®, Indiana, USA) and preformed moisture barrier films obtained by casting were early patented by Kamper and Fennema (1986). The coating-forming solutions or dispersions are nevertheless more frequently applied directly on the product surface. The techniques of application have been reviewed by Grants and Burns (1994) and include: spraying and spray-coating (drying, cooling and chilling), dipping and draining, falling film, fluidized bed processing, turbines (Table 23.6).

The dipping method is well adapted to multiple steps applications and to food products that present an irregular surface. After dipping, excess coating is allowed to drain from the product and is then dried or let solidify (Greener Donhowe and Fennema 1994). The thickness of the layer is determined by the viscosity of the coating material and/or by the rate at which the viscosity changes after application. It is widely used in the confectionery industry along with pan coating. This alternative is carried out with the aid of a sugar-coating mill. A smooth, regular and closed surface of coating material is obtained by mutual rotation of centres, on which several layers of coating have been applied. Spraying, unlike dipping, is more suitable for applying a film to only one side of the food to be covered. This is desirable when protection is needed on only one surface, for instance, when a pizza crust is exposed to a moist sauce. Air-atomization, which is a common method of micro-encapsulation, can also be considered as a coating technique. It consists in dividing an emulsion of the film-forming material and the material to coat into small drops and dry them in a warm air flow.

The coating systems that can be used to coat an inorganic material on the surface of edible products have been adapted from the biomedical and electronics fields. They include: (a) sputtering or analogous thermal sublimation, (b) electron beam, and (c) plasma deposition but their application in the food industry is still marginal.

23.4.2 Critical Factors to Consider in Barrier Coating Development

Many known barrier coatings suffer from the disadvantage that they are difficult to apply. Furthermore, to be effective, they are often applied in a thick layer, which reinforces their detrimental effect on taste and texture. The difficulty in their application can arise from the product itself: very irregular or porous surfaces make the control of the barrier thickness difficult resulting in poor ineffective coatings with defects. When lipids are used, they can impart a waxy or gummy mouth feel. Hence, the sensorial properties of the barrier have to be taken into account since they may interfere with the product characteristics. Surprisingly however, research on the sensory properties of edible film has been limited (Kim and Ustunol 2001; Longares et al. 2004).

Table 23.6. Techniques of application of edible moisture barriers films depending on the systems characteristics (shape of product to be coated and targeted thickness of the barrier) and their critical points.

		Substrate shape/characteristics		
		Flat or with flat surfaces	Irregular	Spherical
Barrier targeted thickness	Thin	Brushing: substrate with flat and smooth surfaces, brush rigidity, continuous process, drying stage following application	Fluidized thermoregulated air bed: low density small size particle/heat resistant, batch process, limited weight of centres, sensibility to heat. Screw coating: flexibility on substrate shape/quite resistant, continuous process	
	Thin to thick	Spraying: flat system unless associated to other technologies, continuous process viscosity the barrier at the temperature of spraying, tempering of the barrier, pressurization and nozzle pattern, target thickness	Dipping: Flexibility on substrate shape/ smooth surface of substrate, viscosity of the barrier, adhesion, cooling rate	Pan and drum coating: spherical substrate/quite resistant, hard shelf on soft product (sugars coatings on jelly beans/candied fruit), batch process, heat balance control, adhesion, avoid cluster formation
	Thick	Casing: large samples (e.g., confectionery bars), contraction of the barrier, cooling rate and temperature control	Enrobing: Flexibility on substrate shape/ maximal temperature of the falling film, viscosity, temperature balance substrate/barrier Coextrusion: cold flow of the filling, minimal thickness of barrier wall (1 mm), barrier formulation, splitting of the rope	

The compatibility and resulting adherence between the food surface and the coating can be critical. It is generally the case when a hydrophobic material is used to protect a hydrophilic product. A surface active agent or other kind of material (starch or cocoa powder) compatible with the two products can help improving the coating adherence (Nussinovitch 1998). Most application techniques involve a drying or a solidifying stage of the coating after its application. This stage is critical in the process since it influences the adherence of the coating to the product and its thickness. On the other hand, for economic reasons this stage has to be as short as possible. The parameters of the drying or solidification stage (temperature, air flow, etc.), but also the temperature and the state of the receiving surface have to be strictly controlled to avoid irregular coating formation.

In addition, the coating has to resist to the conditions of storage and of preparation of the food product, for example, storage temperature, oven or microwave heating. Many ready-to-eat composite food products to which edible moisture barriers are

applied are intended to be heated before consumption. Common lipid-based coatings tend to melt and flow under normal baking conditions and, thus, lose film integrity and barrier effectiveness. On the other hand, composite coatings can include temperature-sensitive compounds, such as proteins that may be denaturated by heat, and result in drastic modifications of the barrier properties.

Edible moisture coatings specifically formulated to resist elevated temperatures or specific processes, such as microwave heating, have been developed and are disclosed in the patent literature. Regarding microwave heating, complex coatings have been proposed: a bilayer comprising first an hydrophilic layer (dough layer, methylcellulose, carrageenan) which includes a susceptor (glycerine, sucrose ester, and chloride salt) and then a moisture resistant layer (Simon et al. 1995). This coating allows producing and stabilizing a food with a crisp exterior and a soft, tender interior. Davis and Gibbs (1991) proposed using a barrier coating (comprising fats and a milk protein) in chilled composite products that are to be eaten hot. The coating softens on heating without phase separation, is compatible with the product both visually and organoleptically, and results in an extended shelf-life.

23.5 Conclusions and Future Trends

An extremely wide range of edible moisture barriers has been explored in the scientific and patent literature since the 1950s. The use of such barriers on fresh and slightly modified fruits and vegetables, meats, fish and seafood, mimicking or complementing naturally present protective layers, is now generalized.

The combination of various types of film-forming agents (polysaccharides, proteins, lipids) along with the improvement in the film-forming methods, the possible modifications of the film-forming materials (denaturation, cross-linking, acetylation, grafting, etc.) has allowed the improvement and tailoring of the water vapour resistance of some barrier films. The necessity of adopting an integrated approach in the development of edible moisture barriers to combine regulatory, nutritional, organoleptic and technical requirements (Figure 23.3) is well illustrated in the recent patent literature. Indeed, most of the patents not only disclose the barrier composition but also the food product in which it has to be applied and the technique of application of the barrier. This integrative approach should also be adopted in the scientific papers dealing with the determination of moisture barriers efficiency, to determine accurately the promises of a specific barrier in a given food product.

The field of multidomain ready-to-eat food products is still developing and remains nowadays the more challenging in terms of moisture transfer control. Edible moisture barriers appear as an interesting answer to consumers' demand for composite product with good nutritional value and stable organoleptic properties. However, the development of coatings including inorganic compounds seems to be a new trend, interesting to reinforce the barrier property of the film but which may not be well accepted by consumers. Hence, the necessity of developing and characterizing, simply formulated, flexible, easy-to-apply moisture-resistant barriers is still of prime importance. These edible moisture barriers are all the more attractive as they can limit the use of highly water-resistant multilayered synthetic packaging film, generally nonrecyclable.

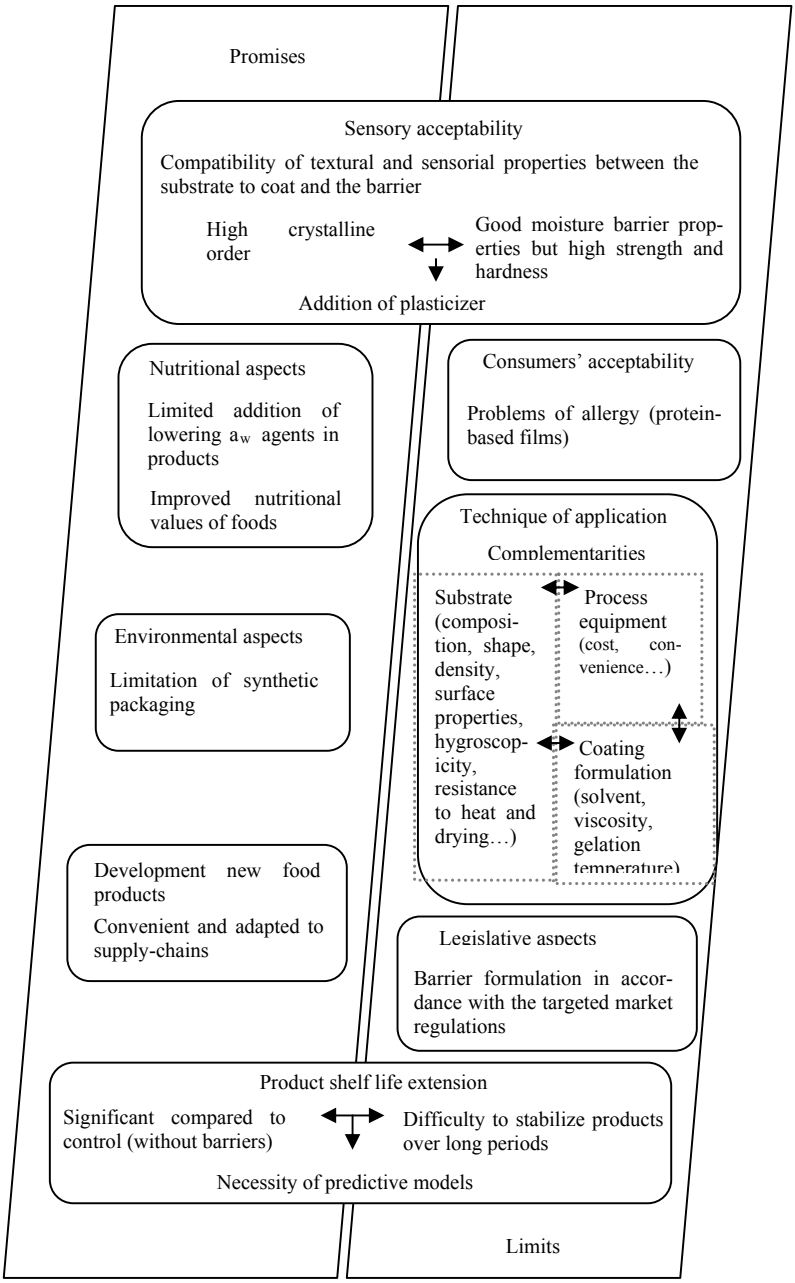

Figure 23.3. Promises and limits of edible moisture barriers.

23.6 References

Anonymous. (1977). Title 21. Food and Drug Administration. [Online] http://www. Access-data.fda.gov/scripts/cdrh/cfdocs/cfcfr/CFRSearch.cfm?CFRPart=172 (Posted 01-04-2005; verified 28-02-2006).

Anonymous. (1979). Edible moisture barrier compositions. Date issued: 1979-09-12.

Anonymous. (1997). Edible films solve problems. *Food Technol*. 51(2), 60-60.

Anonymous. (2004a). Edible films and coatings. *Food Australia*. 56, 577-577.

Anonymous. (2004b). European Parliament and council directive No 95/2/EC of February 1995. Consolidated text. On food additives other than colours and sweeteners CONSLEG system of the office for official publications of the European Communities.

Anonymous. (2006a). Waxes. [Online] http://www.cyberlipid.org/wax/wax0001.htm (verified 27-02-2006).

Anonymous. (2006b). Waxes: Structure, composition, occurrence and analysis [Online] http:/www.lipidlibrary.co.uk/Lipids/waxes/ (posted 20-02-2006; verified 27-02-2006).

Anonymous. (2006c) European Patent Office. Advanced search. [Online] http://ep.espacenet. com/search97cgi/s97_cgi.exe?Action=FormGen andTemplate=ep/en/advanced.hts (verified 10-02-2006).

Albert, S., and Mittal, G.S. (2002). Comparative evaluation of edible coatings to reduce fat uptake in a deep-fried cereal product. *Food Res. Int*. 35(5), 445–458.

Alfinslater, R.B., Coleman, R.D., Feuge, R.O., and Altschul, A.M. (1958). The Present Status of Acetoglycerides. *J. American Oil Chem. Soc*. 35(3), 122–127.

Allen, L., Nelson, A.I., Steinberg, M.P., and McGill, J.N. (1963a). Edible corn-carbohydrate food coatings. I. Development and physical testing of a starch-algin coating. *Food Technol.* 17, 1437.

Arvanitoyannis, I., Biliaderis, C.G., Ogawa, H., and Kawasaki, N. (1998). Biodegradable films made from low-density polyethylene (LDPE), rice starch and potato starch for food packaging applications: Part 1. *Carbohydrate Polymers*. 36(2–3), 89–104.

Arvanitoyannis, I., and Biliaderis, C.G. (1999). Physical properties of polyol-plasticized edible blends made of methyl cellulose and soluble starch. *Carbohydrate Polymers*. 38(1), 47–58.

AvenaBustillos, R.D., Krochta, J.M., and Saltveit, M.E. (1997). Water vapor resistance of red delicious apples and celery sticks coated with edible caseinate-acetylated monoglyceride films. *J. Food Sci*. 62(2), 351–354.

Avena-Bustillos, R.J., and Krochta, J.M. (1993). Water–vapor permeability of caseinate-based edible films as affected by pH, calcium cross-linking and lipid-content. *J. Food Sci*. 58(4), 904–907.

Baldwin, E.A. (1994). Edible coatings for fruits and vegetables: past, present, and future. In: J.M. Krochta, E.A. Baldwin, M.O. Nisperos-Carriedo (eds.), *Edible Coatings and Films to Improve Food Quality*. Technomic Publishing Company, Lancaster, PA, pp. 25–64.

Baldwin, E.A., Nisperos, M.O., Hagenmaier, R.D., and Baker, R.A. (1997). Use of lipids in coatings for food products. *Food Technol*. 51(6), 56–63.

Baldwin, E.A., Burns, J.K., Kazokas, W., Brecht, J.K., Hagenmaier, R.D., Bender, R.J., and Pesis, E. (1999). Effect of two edible coatings with different permeability characteristics on mango (*Mangifera indica L*.) ripening during storage. *Postharvest Biology and Technolog*y. 17(3), 215–226.

Bartkowiak, A., and Hunkeler, D. (2001). Carrageenanoligochitosan microcapsules: optimization of the formation process. *Colloids Surf. B* 21, 285–298.

Bastiaans, J.A.H., and Tap, W.H.J. (2005). Moisture barrier in foods. Patent NZ530643.

Beyer, D.L., Jach, T.E., Zak, D.L., Jerome, R.A., and Debrincat, F.P. (1996). Edible products having inorganic coatings. US Patent WO9622030. Date Issued: 1996-07-25.

Biquet, B., and Labuza, T.P. (1988). Evaluation of the moisture permeability characteristics of chocolate films as an edible moisture barrier. *J. Food Sci*. 53(4), 989–998.

Bolin, H.R. (1976). Texture and crystallization control in raisins. *J. Food Sci*. 41, 1316–1319.

Callegarin, F., Gallo, J.A.Q., Debeaufort, F., and Voilley, A. (1997). Lipids and biopackaging. *J. American Oil Chem. Soc*. 74, 1183–1192.

Chen, H. (1995). Functional properties and applications of edible films made of milk proteins. *J. Dairy Sci*. 78, 2563–2583.

Choi, W.Y., Lee, C.M., and Park, H.J. (2006). Development of biodegradable hot-melt adhesive based on poly-[epsilon]-caprolactone and soy protein isolate for food packaging system. *LWT Food Sci. Technol*. 39(6), 591–597.

Cunningham, P., Ogale, A.A., Dawson, P.L., and Acton, J.C. (2000). Tensile properties of soy protein isolate films produced by a thermal compaction technique. *J. Food Sci*. 65, 668–671.

Cuq, B., Gontard, N., and Guilbert, S. (1995). Edible films and coatings as active layers. In: M. Rooney (ed.), *Active Food Packaging*. Blackie Academic and Professional, London, pp. 111–142.

Cuq, B., Gontard, N., and Guilbert, S. (1998). Proteins as agricultural polymers for packaging production. *Cereal Chem*. 9, 751.

Daniels, R. (1973). *Edible Coatings and Soluble Packaging.* Noyes Data Corporation, Park Ridge, NJ.

Davis, D.J.L., and Gibbs, V. (1991). Edible moisture barrier coating. Patent GB2242815.

Dawson, L.E., Zabik, M., and Sobel, N. (1962). An edible coating for poultry meat preservation. *Poultry Sci*. 41, 1640.

Debeaufort, F., Martinpolo, M., and Voilley, A. (1993). Polarity Homogeneity and Structure Affect Water-Vapor Permeability of Model Edible Films. *J. Food Sci.* 58(2), 426.

Debeaufort, F., and Voilley, A. (1995). Effect of surfactants and drying rate on barrier properties of emulsified edible films. *Int. J. Food Sci. Technol*. 30(2), 183–190.

Debeaufort, F., Quezada-Gallo, J.A., and Voilley, A. (1998). Edible films and coatings: Tomorrow's packagings: A review. *Critical Rev. Food Sci. Nutrition*. 38(4), 299–313.

Debeaufort, F., Quezada-Gallo, J.A., Delporte, B., and Voilley, A. (2000). Lipid hydrophobicity and physical state effects on the properties of bilayer edible films. *J. Membrane Sci*. 180(1), 47–55.

Debeaufort, F., Quezada-Gallo, J.A., and Voilley, A. (2000). Edible barriers: A solution to control water migration in foods. In: *Food Packaging: Testing Methods and Applications*. American Chemical Society, Washington, DC, pp. 9–16.

Debeaufort, F., Voilley, A., and Guilbert, S. (2002). Procédés de stabilisation des produits alimentaires par les films barrières. In: M. Le Meste, D. Simatos, D. Lorient (eds.), *L'eau dans les aliments*. TEC and DOC, Paris, pp. 549–600.

Drake, S.R., and Nelson, J.W. (1990). Storage quality of waxed and nonwaxed "Delicious" and "Golden Delicious" apples. *J. Food Quality*. 13, 331–341.

Drake, S.R., and Nelson, J.W. (1991). Quality attributes of d'Anjou pears after different drying temperatures and refrigerated storage. *J. Food Quality*. 14, 455–465.

Earle, R.D. (1968). Method of preserving food by coating same. US Patent 3395024.

Earle, R.D., and McKee, D.H. (1976). Process for treating fresh meats. US Patent 3991218.

Earle, R.D., and McKee, D.H. (1987). Coated food product and method of making the same Patent CA1224354.

Fang, J.M., Fowler, P.A., Escrig, C., Gonzalez, R., Costa, J.A., and Chamudis, L. (2005). Development of biodegradable laminate films derived from naturally occurring carbohydrate polymers. *Carbohydrate Polymers*. 60(1), 39–42.

Fennema, O., and Kamper, S.L. (1986). Edible preformed film barrier materials. US Patent WO8600501.

Fishman, M.L., Coffin, D.R., Konstance, R.P., and Onwulata, C.I. (2000). Extrusion of pectin/starch blends plasticized with glycerol. *Carbohydrate Polymers*. 41(4), 317–325.

Fonkwe, L., Archibald, D., and Gennadios, A. (2003). Nongelatin capsule shell formulation. US Patent US2003138482.

Foulk, J.A., and Bunn, J.M. (2001). Properties of compression-molded, acetylated soy protein films. *Industrial Crops and Products*. 14(1), 11–22.

Gaonkar, A.G., and Herbst, L. (2004). Edible moisture barrier for food products. Patent AU2003264460.

Gaonkar, A.G., and Chen, W. (2005). Multilayer edible moisture barrier for food products. US Patent ZA200502674 2005.

Garcia, M.A., Martino, M.N., and Zaritzky, N.E. (1998a). Plasticizer effect on starch-based coatings applied to strawberry (*Fragaria x Ananassa*). *J. Agricul. Food Chem*. 46, 3758–3767.

Garcia, M.A., Martino, M.N., and Zaritzky, N.E. (1998b). Starch-based coatings: effect on refrigerated strawberry (*Fragaria x Ananassa*) quality. *J. Agricult. Food Chem*. 76, 411–420.

Garcia, M.A., Pinotti, A., Martino, M.N., and Zaritzky, N.E. (2004). Characterization of composite hydrocolloid films. *Carbohydrate Polymers*. 56(3), 339–345.

Gennadios, A., and Weller, C.L. (1991). Edible films and coatings from soymilk and soy protein. *Cereal Food World*. 36, 1004–1009.

Gennadios, A., Weller, C.L., and Testing, R.F. (1993). Modification of physical and barrier properties of edible wheat gluten-based films. *Cereal Chem.*, 70: 426–429.

Gennadios, A., McHugh, T.H., Weller, C.L., and Krochta, J.M. (1994). Edible coatings and films based on proteins. In: J.M. Krochta, E.A. Baldwin, M.O. Nisperos-Carriedo (eds.), *Edible Coatings and Films to Improve Food Quality*. Technomic Publishing Company, Lancaster, pp. 201–277.

Gennadios, A., Hanna, M.A., and Kurth, L.B. (1997). Application of edible coatings on meats, poultry and seafoods: A review. *Food Sci. Technol.-Lebensm.-Wiss. Technol.* 30(4), 337–350.

Ghosh, V., Ziegler, G.R., and Anantheswaran, R.C. (2002). Fat, moisture, and ethanol migration through chocolates and confectionary coatings. *Critical Rev. Food Sci. Nutrition*. 42, 583–626.

Ghosh, V. (2003). Ph.D. Thesis, Pennsylvania State University.

Ghosh, V., Duda, J.L., Ziegler, G.R., and Anantheswaran, R.C. (2004). Diffusion of moisture through chocolate-flavoured confectionery coatings. *Food Bioprod. Process*. 82(C1), 35–43.

Ghosh, V., Ziegler, G.R., and Anantheswaran, R.C. (2005). Moisture migration through chocolate-flavored confectionery coatings. *J. Food Eng*. 66, 177–186.

Glasser, G.M. (1983). Moisture-resistant coating for food products. Patent EP0090559.

Gontard, N., Duchez, C., Cuq, J.L., and Guilbert, S. (1994). Edible composite films of wheat gluten and lipids: Water–vapor permeability and other physical properties. *Int. J. Food Sci. Technol*. 29, 39–50.

Gontard, N., and Guilbert, S. (1994). Bio-packaging: technology and properties of edible-and/or biodegradable material of agricultural origin. In: M. Mathlouti (ed.), *Food Packaging and Preservation*. Blackie-Academic & Professional, Glasgow, pp. 159–181.

Grant, L.A., and Burns, J. (1994). Application of coatings. In: J.M. Krochta, E.A. Baldwin, M. O. Nisperos-Carriedo (Eds.), *Edible Coatings and Films to Improve Food Quality*. Technomic Publishing Company, Lancaster, pp. 189–200.

Greener Donhowe, I.K., and Fennema, O. (1994). Edible films and coatings: characteristics, formation, definitions, and testing methods. In: J.M. Krochta, E.A. Baldwin, M.O. Nisperos-Carriedo (eds.), *Edible Coatings and Films to Improve Food Quality*. Technomic Publishing Company, Lancaster, pp. 1–24.

Greener, I.K., and Fennema, O. (1989a). Barrier properties and surface characteristics of edible, bilayer films. *J. Food Sci*. 54(6), 1393–1399.

Greener, I.K., and Fennema, O. (1989b). Evaluation of edible, bilayer films for use as moisture barriers for food. *J. Food Sci*. 54(6), 1400–1406.

Greener, I.K., and Fennema, O. (1992). Lipid-based edible films and coatings. *Lipid Technology*. March–April, 34–38.

Guilbert, S. (1986). Technology and application of edible protective films. In: M. Mathlouti (ed.), *Food Packaging and Preservation*. Elsevier Applied Science, New York, pp. 371–394.

Guilbert, S., and Gontard, N. (1995). Edible and biodegradable food packaging. In: P. Ackerman, M. Jägerstad, and T. Ohlsson (eds.), *Foods and Packaging Materials-Chemical Interactions.* The Royal Society of Chemistry, Cambridge, pp 159–168.

Guilbert, S., Gontard, N., and Gorris, L.G.M. (1996). Prolongation of the shelf-life of perishable food products using biodegradable films and coatings. *Lebensmittel-Wissenschaft und-Technologie.* 29, 10–17.

Guilbert, S., and Cuq, B. (1998). Les films et enrobages comestibles. In: G. Bureau, and J. Multon (eds.), *L'emballage des Denrées Alimentaires de Grande Consommation* Lavoisier-TEC & DOC, Paris, pp. 2–66.

Guillard, V., Broyart, B., Bonazzi, C., Guilbert, S., and Gontard, N. (2003). Preventing moisture transfer in a cokmposite food using edible films: Experimental and mathematical study. *J. Food Sci*. 68, 2267–2277.

Guillard, V., Guillbert, S., Bonazzi, C., and Gontard, N. (2004a). Edible acetylated monoglyceride films: Effect of film-forming technique on moisture barrier properties. *J. American Oil Chem. Soc*. 81, 1053–1058.

Guillard, V., Broyart, B., Bonazzi, C., Guilbert, S., and Gontard, N. (2004b). Effect of temperature on moisture barrier efficiency of monoglyceride edible films in cereal-based composite foods. *Cereal Chem*. 81, 767-771.

Hagenmaier, R.D., and Shaw, P.E. (1990). Moisture permeability of edible films made with fatty-acid and (hydroxypropyl)methylcellulose. *J. Agricult. Food Chem*. 38, 1799–1803.

Hagenmaier, R.D., and Baker, R.A. (1994). Wax microemulsions and emulsions as citrus coatings. *J. Agricult. Food Chem*. 42(4), 899–902.

Hagenmaier, R.D., and Baker, R.A. (1995). Layered coatings to control weight-loss and preserve gloss of citrus fruit. *Hortscience*. 30(2), 296–298.

Hagenmaier, R.D., and Baker, R.A. (1997). Edible coatings from morpholine-free wax microemulsions. *J. Appl. Polym. Sci*. 45, 349–352.

Hamilton, R.J. (1995). *Waxes: Chemistry, Molecular Biology and Functions*. The Oily Press, Dundee.

Harvard, C., and Harmony, M.X. (1869). Improved process of preserving meat, fowls, fish, etc. US Patent 90944.

Haynes, L., Zhou, N., Slade, L., Levine, H., and Chan, W. (2004). Edible moisture barrier for food products. Patent EP1472934.

Hernandez, E. (1994). Edible coatings from lipids and resins. In: J.M. Krochta, E.A. Baldwin, M.O. Nisperos-Carriedo (eds.), *Edible Coatings and Films to Improve Food Quality*. Technomic Publishing Company, Lancaster, PA, pp. 279–304.

Heuvel, W.M., Lewis, S.D., and Povey, K.J. (1997). Composite food product with moisture barrier. Patent WO9715198.

Higuchi, T., and Aguiar, A. (1959). A study of permeability to water vapor of fats, waxes and other enteric coating material. *J. American Pharmaceutical Assoc*. 48(10), 574-583.

Hirasa, K. (1991). Ph.D. Thesis, University of California-Davis, USA.

Hoa, T. T., Ducamp, M. N., Lebrun, M., and Baldwin, E. A. (2002). Effect of different coating treatments on the quality of mango fruit. *J. Food Quality*. 25(6), 471–486.

Kamper, S.L., and Fennema, O. (1984a). Water vapor permeability of edible bilayer films. *J. Food Sci*. 49, 1478–1481.
Kamper, S.L. and Fennema, O. (1984b). Water vapor permeability of an edible, fatty acid, bilayer film. *J. Food Sci.* 49(6), 1482–1485.
Kamper, S.L., and Fennema, O. (1985). Use of an edible film to maintain water-vapor gradients in foods. *J. Food Sci*. 50(2), 382–384.
Katz, E.E., and Labuza, T.P. (1981). Effect of water activity on the sensory crispness and mechanical deformation of snack food-products. *J. Food Sci*. 46, 403–409.
Kester, J.J., and Fennema, O. (1986). Edible films and coatings: a review. *Food Technol.* 40(12), 47–49.
Kester, J.J., and Fennema, O. (1989a). An edible film of lipids and cellulose ethers: barrier properties to moisture vapor transmission and structural evaluation. *J. Food Sci*. 54, 1383–1389.
Kester, J.J., and Fennema, O. (1989b). Resistance of lipid films to water-vapor transmission. *J. American Oil Chemists Soc*. 66, 1139–1146.
Kester, J.J., and Fennema, O. (1989c). The influence of polymorphic form on oxygen and water-vapor transmission through lipid films. *J. American Oil Chem. Soc*. 66, 1147–1153.
Kim, S.J., and Ustunol, Z. (2001). Sensory attributes of whey protein isolate and candelilla wax emulsion edible films. *J. Food Sci*. 66, 901–911.
King, A.H. (1983). Brown seaweeds extracts (alginates). In: M. Glicksman (ed), *Food Hydrocolloids*. Boca Raton, FL, pp. 115–188.
Koelsch, C. (1994). Edible water vapor barriers: properties and promises. *Trends Food Sci. Technol*. 5, 76–81.
Koelsch, C.M., and Labuza, T.P. (1992). Functional physical and morphological properties of methyl cellulose and fatty acids–based edible barriers. *Lebensmittel Wissenschaft und Technologie*. 25, 401–411.
Kraght, A.J. (1966). Waxing peaches with the consumer in mind. *Produce Marketing*. 9, 20–21.
Krochta, J.M., and DeMulder Johnston, C. (1997). Edible and biodegradable polymer films: Challenges and opportunities. *Food Technol*. 51(2), 61–74.
Krochta, J.M., and McHugh, T.H. (1997). Protein-based edible films. *Trends Food Sci. Technol*. 8, 208–208.
Kroger, M., and Igoe, R.S. (1971). Edible containers. *Food Product Development*. 11, 74–79.
Lazaridou, A., and Biliaderis, C.G. (2002). Thermophysical properties of chitosan, chitosan-starch and chitosan–pullulan films near the glass transition. *Carbohydrate Polymers*. 48, 179–190.
Lazarus, C.R., West, R.L., Oblinger, J.L., and Palmer, A.Z. (1976). Evaluation of a calcium alginate coating and a protective plastic wrapping for the control of lamb carcass shrinkage. *J. Food Sci*. 4, 16–39.
Liu, L., Kerry, J.F., and Kerry, J.P. (2006). Effect of food ingredients and selected lipids on the physical properties of extruded edible films/casings. *Int. J. Food Sci. Technol*. 41, 295–302.
Loh, J.P., and Hansen, T. (2002). Oven-stable edible moisture barrier. Patent EP1247460.
Longares, A., Monahan, F.J., O'Riordan, E.D., and O'Sullivan, M. (2004). Physical properties and sensory evaluation of WPI films of varying thickness. *Lebensmittel-Wissenschaft und-Technologie*. 37, 545–550.
Longares, A., Monahan, F.J., O'Riordan, E.D., and O'Sullivan, M. (2005). Physical properties of edible films made from mixtures of sodium caseinate and WPI. *Int. Dairy J*. 15, 1255–1260.
Lowe, E., Durkee, E.L., Hamilton, W.E., and Morgan, A.I. (1963). Continuous raisin coater. *Food Technol.* 17(11), 109–111.
Macquarrie, R. (2002). Sausage casing. US Patent 01552000A1.

Mali, S., Grossmann, M.V.E., Garcia, M.A., Martino, M.N., and Zaritzky, N.E. (2004). Barrier, mechanical and optical properties of plasticized yam starch films. *Carbohydrate Polymers*. 56, 129–135.

Mali, S., Grossmann, M.V.E., Garcia, M.A., Martino, M.N., and Zaritzky, N.E. (2005). Mechanical and thermal properties of yam starch films. *Food Hydrocolloids*. 19, 157–164.

Mallikarjunan, P., Chinnan, M.S., Balasubramaniam, V.M., and Phillips, R.D. (1997). Edible coatings for deep-fat frying of starchy products. *Lebensmittel-Wissenschaft und-Technologie.* 30, 709–714.

Martini, S., Kim, D.A., Ollivon, M., and Marangoni, A.G. (2006). The water vapor permeability of polycrystalline fat barrier films. *J. Agricult. Food Chem.* 54, 1880–1886.

Martin-Polo, M., and Voilley, A. (1990). Comparative study of the water permeability of edible film composed of arabic gum and of glycerolmonostearate. *Sci. Aliments*. 10, 473–483.

Martin-Polo, M., Mauguin, C., and Voilley, A. (1992). Hydrophobic films and their efficiency against moisture transfer. 1. Influence of the film preparation technique. *J. Agricult. Food Chem*. 40, 407–412.

Mate, J.I., and Krochta, J.M. (1997). Whey protein and acetylated monoglyceride edible coatings: Effect on the rancidity process of walnuts. *J. Agricult. Food Chem.* 45, 2509–2513.

McGuire, R.G. (1997). Market quality of guavas after hot-water quarantine treatment and application of carnauba wax coating. *Hortscience*. 32, 271–274.

McHugh, T.H., and Krochta, J.M. (1994a). Water-vapor permeability properties of edible whey protein-lipid emulsion films. *J. American Oil Chem. Soc*. 71, 307–312.

McHugh, T.H., and Krochta, J.M. (1994b). Dispersed phase particle size effects on water-vapor permeability of whey protein beeswax edible emulsion films. *J. Food Processing Preservation*. 18, 173–188.

McHugh, T.H., and Krochta, J.M. (1994c). Milk-protein-based edible films and coatings. *Food Technology*. 48(1), 97–103.

McHugh, T.H., and Krochta, J.M. (1994d). Permeability properties of edible films. In: J.M. Krochta, E.A. Baldwin, M.O. Nisperos-Carriedo (eds.), *Edible Coatings and Films to Improve Food Quality*. Technomic Publishing Company, Lancaster, PA, pp. 139–187.

Morgan, B.H. (1971). Edible packaging update. *Food Product Development*, June–July, 75–78.

Morillon, V., Debeaufort, F., Blond, G., Capelle, M., and Voilley, A. (2002). Factors affecting the moisture permeability of lipid-based edible films: A review. *Critical Rev. Food Sci. Nutrition*. 42(1), 67–89.

Naga, M., Kirihara, S., Tokugawa, Y., Tsuda, F., and Hirotsuka, M. (1996). Process for producing edible proteinaceous film. US Patent US5569482.

Nielsen, B., Sparso, F.V., and Kristiansen, J.K. (2001). Composition. Patent WO0114466.

Ninomiya, H., Suzuki, S., and Ishii, K. (1997). Edible film and method of making same. US Patent 5620757.

Nisperos-Carriedo, M.O. (1994). Edible coatings and films based on polysaccharides. In: J.M. Krochta, E.A. Baldwin, and M.O. Nisperos-Carriedo (eds.), *Edible Coatings and Films to Improve Food Quality*. Technomic Publishing Company, Lancaster, PA, pp. 303–335.

Nussinovitch, A. (1998). Hydrocolloid coating of food: A review. Leatherhead Food RA, *Food Industry J.* 1, 174–188.

Orliac, O., Rouilly, A., Silvestre, F., and Rigal, L. (2002). Effects of additives on the mechanical properties, hydrophobicity and water uptake of thermo-moulded films produced from sunflower protein isolate. *Polymer*. 43, 5417–5425.

Orliac, O., Rouilly, A., Silvestre, F., and Rigal, L. (2003). Effects of various plasticizers on the mechanical properties, water resistance and aging of thermo-moulded films made from sunflower proteins. *Industrial Crops and Products*. 18(2), 91–100.

Ou, S., Wang, Y., Tang, S., Huang, C., and Jackson, M.G. (2005). Role of ferulic acid in preparing edible films from soy protein isolate. *J. Food Eng*. 70, 205–210.

Paredes-Lopez, O., Camargo, E., and Gallardo, Y. (1974). Use of coatings of candelilla wax for preservation of limes. *J. Sci. Food Agricult*. 25, 1207–1210.

Park, H.J., and Chinnan, M.S. (1995). Gas and water vapor barrier properties of edible films from protein and cellulosic materials. *J. Food Eng*. 25, 497–507.

Park, J.W., Testin, R.F., Park, H.J., Vergano, P.J., and Weller, C.L. (1994). Fatty-acid concentration-effect on tensile-strength, elongation, and water vapor permeability of laminated edible films. *J. Food Sci*. 59, 916–919.

Park, S.Y., Lee, B.I., Jung, S.T., and Park, H.J. (2001). Biopolymer composite films based on kappa-carrageenan and chitosan. *Mater. Res. Bull*. 36(3-4), 511–519.

Parris, N., Coffin, D.R., Joubran, R.F., and Ressen, H. (1995). Composition factors affecting the water vapor permeability and tensile properties of hydrophilic films. *J. Agricult. Food Chem*. 43: 1432–1435.

Plijter-Schuddemat, J., Plijter, J.J., Van Son, M.W., Ilhelmus, L., Don, J.A.C., and Noort, M.W. (2003). Moisture-barrier edible coating layer for foods. NL Patent WO 03024253.

Porter, S.C., and Woznicki, E.J. (1989). Dry edible film coating composition, method and coating form. US Patent DE3043914.

Psomiadou, E., Arvanitoyannis, I., and Yamamoto, N. (1996). Edible films made from natural resources; microcrystalline cellulose (MCC), methylcellulose (MC) and corn starch and polyols. Part 2. *Carbohydrate Polymers*. 31, 193–204.

Psomiadou, E., Arvanitoyannis, I., Biliaderis, C.G., Ogawa, H., and Kawasaki, N. (1997). Biodegradable films made from low density polyethylene (LDPE), wheat starch and soluble starch for food packaging applications. Part 2. *Carbohydrate Polymers.* 33, 227–242.

Quezada Gallo, J.-A., Debeaufort, F., Callegarin, F., and Voilley, A. (2000). Lipid hydrophobicity, physical state and distribution effects on the properties of emulsion-based edible films. *J. Membrane Sci*. 180, 37-46.

Rhim, J.W. (2004). Physical and mechanical properties of water-resistant sodium alginate films. *Lebensmittel Wissenschaft und Technologie*. 37, 323–330.

Rico-Pena, D.C., and Torres, J.A. (1990). Edible methylcellulose-based films as moisture impermeable barriers in sundae ice cream cones. *J. Food Sci*. 55, 1468–1469.

Roth, T., and Loncin, M. (1984). Evaluation of water evaporation inhibitors. *J. Colloid Interface Sci*. 100, 216–219.

Rubenstein, I.H., and Bank, H.M. (1982). Edible food containers and the method and apparatus for coating said containers. Patent EP0045522.

Rubenstein, I.H., and Pelaez, C.A. (1986). Edible food containers and method of coating said containers. Patent US4603051.

Schneide, J. (1972). Process for preserving meat. US 3667970.

Schou, M., Longares, A., Montesinos-Herrero, C., Monahan, F.J., O'Riordan, D., and O'Sullivan, M. (2005). Properties of edible sodium caseinate films and their application as food wrapping. *LWT-Food Sci. Technol.* 38, 605–610.

Schultz, T.H., Owens, H.S., and Maclay, W.D. (1948). Pectinate films. J. Colloid Sci. 3, 53–62.

Schultz, T.H., Miers, J.C., Owens, H.S., and Maclay, W. (1949). Permeability of pectinate films to water vapor. *J. Phys. Colloid Chem*. 53, 13–20.

Seaborne, J., and Egberg, D.C. (1989). Method for preparing a low water permeability edible film. US Patent US4810534.

Shaw, C., Secrist, J., and Tuomy, J. (1980). Method of extending the storage life in the frozen state of precooked foods and product produced. US Patent 4196219.

Shellhammer, T.H., Rumsey, T.R., and Krochta, J.M. (1997). Viscoelastic properties of edible lipids. *J. Food Eng*. 33, 305–320.

Simon, G, Sheen, S., and Moyer, J. (1995). Microwavable fry-like cooking process. Patent AU5646094.

Smith, G.F., and Almendarez, M.E. (2004). Microweable grilled cheese and meat sandwiches. US Patent EP1449439.

Sothornvit, R., Olsen, C.W., McHugh, T.H., and Krochta, J.M. (2007). Tensile properties of compression-molded whey protein sheets: Determination of molding condition and glycerol-content effects and comparison with solution-cast films. *J. Food Eng*. 78, 855–860.

Spencer, G.F., Plattner, R.D., and Miwa, T. (1977). Jojoba oil analysis by high-pressure liquid chromatography and gas chromatography mass spectrometry. *J. American Oil Chem. Soc*. 54(5), 187–189.

Stemmler, M., and Stemmler, H. (1974). Method for preserving freshly slaughtered meat. Patent US 3851077.

Stuchell, Y.M., and Krochta, J.M. (1995). Edible coating on frozen king salmon; effect of whey protein isolate and acetylated monoglycerides on moisture loss and lipid oxidation. *J. Food Sci*. 60, 28–31.

Suknark, K., Phillips, R.D., and Chinnan, M.S. (1997). Physical properties of directly expanded extrudates formulated from partially defatted peanut flour and different types of starch. *Food Res. Int*. 30, 575–583.

Swenson, H.A., Miers, J.C., Schultz, T.H., and Owens, H.S. (1953). Pectinate and pectate coatings. II. Applications to nuts and fruit products. *Food Technol*. 7(6), 232–235.

Tang, C.-H., Jiang, Y., Wen, Q.-B., and Yang, X.-Q. (2005). Effect of transglutaminase treatment on the properties of cast films of soy protein isolates. *J. Biotechnol.*, 120, 296–307.

Tanner, K., Getz, J., Burnett, S., Youngblood, E., and Draper, P. (2002). US Patent 0081331A1.

Torres, J.A. (1994). Edible films and coatings from proteins. In: N.S. Hettiarachchy, and G. Ziegleder (eds.), *Protein Functionality in Food Systems*. Marcel Dekker, New York, pp. 467–507.

Van Gastel, H. (2006). Moisture barriers. NL Patent WO 002734.

Williams, R., and Mittal, G.S. (1999). Water and fat transfer properties of polysaccharide films on fried pastry mix. *Lebensmittel-Wissenschaft und-Technologie*. 32, 440–445.

Wong, D.W.S., Gregorski, K.S., Hudson, J.S., and Pavlath, A.E. (1996). Calcium alginate films: Thermal properties and permeability to sorbate and ascorbate. *J. Food Sci*. 61, 337–341.

Woodmansee, C.W., and Abbott, O.J. (1958). Coating subscalded broiler parts in order to afford protection against dehydration and skin darkening in fresh storage. *Poultry Sci*. 37, 1367–1373.

Woznicki, E.J., and Grillo, S.M. (1989). Coatings based on polydextrose for aqueous film coating of pharmaceutical food and confectionary products. Patent US4802924.

Wu, Y., Weller, C.L., Hamouz, F., Cuppett, S.L., and Schnepf, M. (2002). Development and application of multicomponent edible coatings and films: A review. *Adv. Food Nutrition Res*. 44, 347–394.

Youcheff, G.G., Wodke, S.M., and Perkins, D.W. (1996). Composition for improving adherence of fat-based coatings to frozen fat-based confections. Patent US5500233.

Yuguchi, Y., Thuy, T., Urakawa, H., and Kajiwara, K. (2002). Structural characteristics of carrageenan gels: temperature and concentration dependence. *Food Hydrocolloids*. 16(6), 515–522.

Zabik, M., and Dawson, L.E. (1963). The acceptability of cooked poultry protected by an edible acetylated monoglyceride coating during fresh and frozen storage. *Food Technol.* 17, 87–91.

Zobel, H.F. (1988). Molecules to granules: a comprehensive starch review. *Starch*. 40, 44–50.

Chapter 24

Encapsulation of Bioactives

M.A. Augustin[1,2] and L. Sanguansri[2]

[1]School of Chemistry, Monash University, Clayton, Victoria 3800, Australia,
maryann.augustin@csiro.au

[2]Food Science Australia, 671 Sneydes Road, Werribee, Victoria 3030, Australia,
luz.sanguansri@csiro.au

24.1 Introduction

Food bioactives are physiologically active components in food or dietary supplements of plant or animal origin that have a role in health beyond basic nutrition. The addition of bioactive components to foods, particularly those foods that are consumed as part of the normal diet of target populations, offers opportunities for improving the health and well-being of consumers. The interest of the food industry in these functional foods has resulted in the development of a new generation of food products with enhanced levels of food components that have potential health benefits (Schmidl and Labuza 2000; Hilliam 2000; Heasman and Mellentin 2001; Augustin and Clarke 2004).

The delivery of bioactives through food is a major challenge. Many bioactives are prone to degradation, and thus there is a need to protect them throughout their shelf-life as both an ingredient and in fortified food products, without compromising the sensory properties of the food. In addition, the bioactivity needs to be maintained so it is available when consumed in order to have a physiological function when delivered to its particular target site within the body. All these requirements place stringent demands on using food to deliver bioactives. Often, these demands cannot be met by direct addition of a bioactive to food, as it needs to be protected prior to its release.

Microencapsulation has been used for protection and delivery of bioactives in food applications. In encapsulation, components (referred to as the core or active) are packaged within a secondary material (referred to as the wall material or the encapsulant) and delivered in small particles.

This chapter considers the issues relating to the delivery of bioactives through foods. The choice of materials for encapsulation of bioactives, the formulation of the encapsulated delivery system and the processes used for their manufacture are discussed. Examples of materials and processes used for the manufacture of encapsulated fat-soluble and water-soluble bioactives and encapsulated probiotics are given. The effectiveness of various encapsulated delivery systems for protection of bioactive ingredients and new trends in encapsulation technology are covered. The

requirements for effective encapsulation and the material states that may be used are very wide. Obvious connections can be drawn between the processes described in this chapter and the principles outlined in others (in particular Chapters 3, 5, 9, 15 and 23).

24.2 Issues Relating to Addition of Bioactives to Food

The range of food components now considered as bioactives include vitamins, minerals, functional lipids, probiotics, amino acids, peptides and proteins, phytosterols, phytochemicals and antioxidants (Wildman 2001). Their structure and function vary widely and are important considerations when adding them to food. The health aspects of bioactive ingredients and functional foods are not covered here as they are beyond the scope of this chapter.

Many bioactives are unstable. Irrespective of the form they are added to food, it is essential that they be stabilized prior to addition to food, during the food manufacturing process and throughout the food product's shelf-life. When choosing the food vehicle for addition of a chosen bioactive, it is important to consider its solubility in the food matrix and its interactions with other ingredients in the food formulation. The incorporation of bioactives can alter flavour, odour and texture of foods. As consumers only accept food products with good sensory appeal, the successful addition of bioactives into a range of functional food products must not compromise food quality. Furthermore, as the bioactive food component is selected for its specific physiological function, it is important that it is bioavailable when the food is consumed.

24.2.1 Solubility of Bioactives

When considering the addition of a bioactive to food, it is useful to classify them as oil-soluble (e.g., polyunsaturated fatty acids, carotenes, lycopene), water-soluble (e.g., anthocyanins, proteins and peptides), or water/oil dispersible components (e.g., probiotics). Bioactives may be added directly to food if they are in a compatible format with the food matrix and provided their direct addition does not impact negatively on food quality or the bioavailability of the bioactive. When the solubility in a food matrix is limiting, its hydrophilicity/lipophilicity may be modified to enable improved incorporation. An example is the conversion of free plant sterols to fatty acid esters in order to make them more oil-soluble and readily incorporated into spreads (Deckere de and Verschuren 2000).

24.2.2 Stability of Bioactives

Bioactive ingredients are extracted from plant and animal sources and are provided to food manufacturers as liquid extracts, concentrates or powders. Generally, once the bioactive is extracted from its natural source, it is more susceptible to degradation.

It is well-known that vitamins A and D are sensitive to oxygen, light, and the presence of oxidizing agents. Long-chain polyunsaturated oils are susceptible to

oxidation if not protected against light, oxygen and/or trace metal ions such as iron or copper (Frankel et al. 2002). Anthocyanins and polyphenols are not stable to heat during juice processing (Fang et al. 2006). The stability of anthocyanins varies depending on the processing conditions, and the presence of other components in their new environment (Kirca et al. 2006).

Food manufacturers have generally added higher levels of bioactives than required to compensate for losses during processing and storage. To ensure that the level of addition claimed is maintained throughout the shelf-life of the food, overages of 5%–50% of beta-carotene and vitamins C and E have been added to dairy products (Elliot 2001).

24.2.3 Interactions of Bioactives with Other Food Components

When a bioactive is added to food, it may react with other food components causing degradation and loss of bioactivity. Even when the bioactive is not sensitive to degradation (e.g., minerals), the addition of the component at a level higher than that normally found in the target food vehicle alters its properties. Reformulation and/or modified processing conditions may be necessary. For example, the addition of calcium into foods containing proteins can cause precipitation. Reformulation approaches, which have been used to overcome some of the heat stability problems with mineral fortified dairy products, have included the use of phosphates in Ca-fortified milks (Williams et al. 2005) and caseins to Fe-fortified products (Sher et al. 2006). Phosphates and caseins bind divalent metal ions, thus reducing the levels of the free calcium or iron, which are primarily responsible for the protein precipitation problems.

24.2.4 Taste and Odour

Many bioactives have an undesirable taste and odour. Peptides are known for their bitter taste, mineral salts for their metallic tastes and marine oils rich in omega-3 fatty acids for fishy taste and odour. Further, the addition of soluble iron salts to foods catalyses the oxidation of fats and amino acids and imparts undesirable metallic tastes to foods (Zimmermann 2004; Yang and Lawless 2006). A variety of added ingredients (e.g., sugar, flavours) have been used to mask these tastes, but with limited success.

24.2.5 Bioavailability

The bioactive needs to be in a bioavailable form when consumed. Its addition must also not affect the bioavailability of other desirable food components, and interaction with other food components can decrease bioavailability. It is important to select the appropriate form of the bioactive and the formulation for delivery in order to maintain bioavailability.

24.3 Encapsulation of Bioactives

The requirements discussed above have led to the delivery of bioactives in microencapsulated forms. Encapsulation technology alleviates many of the problems encountered with direct addition of bioactives (Pszczola 1998; Augustin 2001; Zimmermann 2004) because the components are entrapped within the matrix of a coating material (e.g., entrapment of oils within a glassy carbohydrate matrix) or encased within a protective coating (e.g., oil droplets surrounded by an interfacial layer of protein). A schematic representation of encapsulated bioactives is given in Figure 24.1. Encapsulation has the potential to isolate the bioactive until its release is triggered.

Microencapsulation technology is well developed and commercialized in the chemical, pharmaceutical, cosmetic and printing industries. In the food industry, it is used to mask unpleasant tastes and protect sensitive ingredients from degradation through reactions with its environment during storage, and from other components when it is introduced into a food matrix (Gibbs et al. 1999; Augustin et al. 2001; Pszczola 2003). The ability to control the release of the encapsulated ingredient enables suppliers to increase the effectiveness of their ingredients whilst lessening the need for over addition, and to widen their range of applications (Gouin 2004).

Microencapsulation technology has been traditionally used in the food industry for flavour encapsulation where flavours are stabilized and their release controlled (Madene et al. 2006). Microencapsulation has also been used to enable the incorporation of sensitive bioactive component in fortified foods, while ensuring that the taste, aroma, or texture of food is not adversely affected (Pszczola 1998; Brazel 1999; Augustin et al. 2001). Microencapsulation can reduce off-flavours contributed by certain vitamins and minerals, permit time-release of the nutrients, enhance stability to extremes in temperature and moisture, and reduce undesirable chemical interactions with other ingredients.

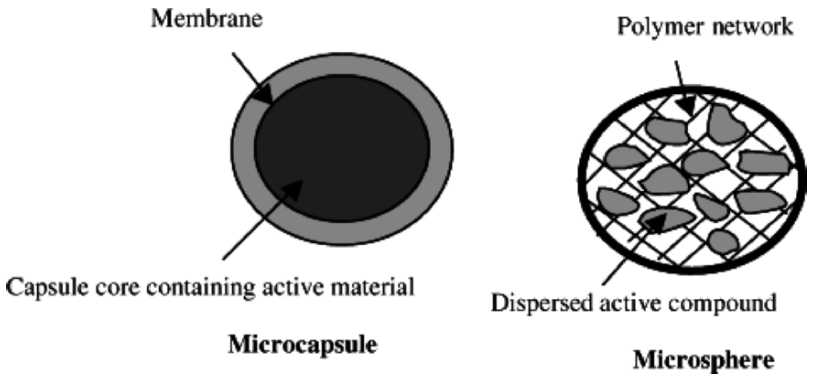

Figure 24.1. A schematic representation of encapsulated bioactives. (Reprinted with permission from Madene et al. 2006.)

24.3.1 Considerations for Design of the Delivery System

The specific requirements of the encapsulant material and the delivery system have to be considered. This includes protecting the bioactive throughout its storage as an ingredient, through the food manufacturing process, and during the shelf-life of the food product. In order for the bioactive to survive food processing conditions, it is important to ensure that the core is protected from harsh processing environments and that the release of the core is not triggered prematurely. The conditions during gastrointestinal transit of the food should also to be taken into account to deliver the bioactive to the desired site of the body to achieve its potential health benefits (Bell 2001).

The development of a successful encapsulation system for a target application requires knowledge about the stability of the chosen bioactive (core); the properties of the materials used for encapsulation (encapsulant) and the suitability of the delivery system (microcapsule) for its final application. Table 24.1 gives a summary of important considerations.

Table 24.1. Properties of the core, encapsulant material and microcapsule of importance in the design of encapsulated bioactives.

Component	Properties
Core	Bioactivity of the material
	Solubility (hydrophilicity/lipophilicity)
	Stability to environmental conditions (e.g., moisture, heat, pH, salts, light, enzymes)
	Taste
	Propensity to interact with other food components
Encapsulant material	Solubility
	Viscosity
	Stability to pH, salts, temperature, shear, enzyme degradation
	Film forming and emulsification properties
	Regulatory status for food application
Microcapsule	Format for delivery (i.e., liquid or powder)
	Storage stability
	Stability to different process conditions
	Release properties
	Particle size
	Payload (bioactive core loading)
	Cost of production

24.3.2 Encapsulant Materials

Encapsulant materials can be selected from a wide range of natural or synthetic materials depending on the properties desired in the final microcapsule (Table 24.2). The encapsulant materials in food are more restricted to natural food components (e.g. proteins, sugars, starches, gums, lipids, cellulosic material) and other ingredients

that have Generally Regarded As Safe (GRAS) status (e.g., cyclodextrin, chitosan, low-molecular weight emulsifiers such as Tweens, mineral salts, etc.). They can be used alone or in combination to achieve the desired functionality. The composition can significantly influence the functional properties of the final microcapsule as can the choice of processing technologies used. Cost also needs to be considered.

Neutral taste and odour, low viscosity, good film forming, gelling and barrier properties are some of the desired characteristics of encapsulant materials. The functional properties of food biopolymers (water binding, gelling, emulsifying) lend themselves to the development of a wide range of microstructures that can be used for delivery of bioactives. A good encapsulant protects the core from degradation during processing and storage and also masks any undesirable taste and odour associated with the bioactive core when added into a food product. Identification of the storage requirements and processing needs, as well as the mechanisms required for release of the core material (e.g., pressure-based, dissolution-based or melting-based triggers) are important. These are influenced by the mechanical strength of the capsule wall and its compatibility with the target food product. Nutritional value, sensory properties and aesthetic properties are also important considerations (Brazel 1999; Gibbs et al. 1999). Thus, the material properties of the capsule such as the permeability of the encapsulant, its resistance to conditions encountered (e.g., shear, heat, pH shift, light, enzyme, other ingredients) during processing and gastrointestinal tract transit have to be designed to enable the desired control over the release of the bioactive.

Table 24.2. Materials used for encapsulation of bioactives for food applications.

Material class	Types of materials
Proteins	Milk proteins—caseins and whey proteins,
	Soy proteins
	Wheat proteins
	Egg proteins
	Zein
	Hydrolyzed proteins
Carbohydrates	Sugars—fructose, galactose, glucose, maltose, sucrose, oligosaccharide, corn syrup solids, dried glucose syrup
	Starch and starch products—maltodextrins, dextrins, starches, resistant starch, modified starches
	Gums—agar, alginates, carrageenan, gum acacia, gum arabic, pectin,
	Carboxymethyl cellulose
	Chitosan
	Cyclodextrins
Lipids	Natural fats and oils
	Fractionated fats
	Mono- and diglycerides
	Phospholipids
	Glycolipids
	Waxes—beeswax, carnauba wax

The limited range of suitable encapsulant materials allowed for food use still remains the biggest challenge in material selection, especially when more sophisticated properties are required by food manufacturers and consumers. Modification of existing food grade materials to achieve differentiated encapsulant functionality may be required to achieve new properties in microcapsules and improved performance of microencapsulated ingredients. A new generation of encapsulant systems has emerged for food applications. Some of the new developments in materials for microencapsulation involve capitalizing on the interactions between biopolymers or modification of the native food ingredient either chemically or physically to achieve new functional properties not present in the native food ingredients. Examples are the development of protein–polysaccharide complexes (Schmitt et al. 1998) and Maillard reaction conjugates (Augustin et al. 2006).

24.3.3 Processing of Microcapsules

The selection of the method or microencapsulation process depends on the properties of the core and the coating materials, the release mechanism desired, process type, capsule morphology and particle size. Most of the processes have been adapted from the pharmaceutical and chemical industries. The use of low-cost materials and manufacturing processes for encapsulation has been a significant challenge as food products generally have lower profit margins compared to pharmaceutical and chemical products. Both physical and chemical processes are available to encapsulate a range of bioactive ingredients (Table 24.3). The selection of the method depends on the required format and inherent properties of the bioactive core and the encapsulant materials used. Selected processes used in the food industry are discussed below.

Table 24.3. Methods used for microencapsulation.

Physical processes	Chemical processes
Spray-drying	Simple coacervation
Spray-chilling	Complex coacervation
Fluidized bed coating	Solvent evaporation
Centrifugal extrusion	Liposomes
Spinning disk coating	Chemical adsorbents
Pressure extrusion	Inclusion complexation
Hot melt extrusion	
Use of supercritical fluids	

24.3.3.1 Spray Drying

Spray drying is the most commonly used method in the food industry. Bioactive ingredients microencapsulated by this method include fats and oils, flavours, essential oils and other oil-soluble bioactives. Water-soluble bioactives can also be encapsulated by spray drying, where the encapsulant forms a matrix structure rather than a film surrounding the core. This process typically involves the dispersion of the core material into a solution of the encapsulant (e.g., protein, carbohydrate) and atomization of the mixture into the drying chamber. This leads to evaporation of the solvent

(water) and the formation of powder microcapsules. For the encapsulation of oils and oil-soluble bioactives, an emulsion is prepared prior to spray drying. The advantage of the spray-drying process is that it is cheap and it can be operated on a continuous basis. Proper adjustment and control of the processing conditions enables the tailoring of desirable powder properties such as particle size, moisture content, bulk density, flowability, dispersibility, appearance and structural strength (Reineccius 2001).

24.3.3.2 Spray Chilling

Spray chilling is a process that involves dispersing the core into a warm, liquefied coating material and spraying through a heated nozzle into a controlled environment, where the encapsulant solidifies to form the microcapsule particles (Lamb 1987). The process is performed in equipment similar to that used in spray drying except that the process air is not heated. Encapsulant materials commonly used in this process are vegetable oils and waxes or their derivatives (e.g., hydrogenated or fractionated vegetable oils with high melting points). This technique is commonly used for microencapsulation of water-soluble bioactive core materials such as vitamins and minerals to minimize their solubility in the water environment, or for encapsulation of bioactives for temperature release applications (Anon 1981).

24.3.3.3 Fluidized Bed Coating

Fluidized bed coating is accomplished by suspending, or fluidizing, particles of a core material in an upward stream of air and applying an atomized coating material to the fluidized particles (Figure 24.2). The core and the encapsulant material must be stable under the processing conditions applied during the application and drying

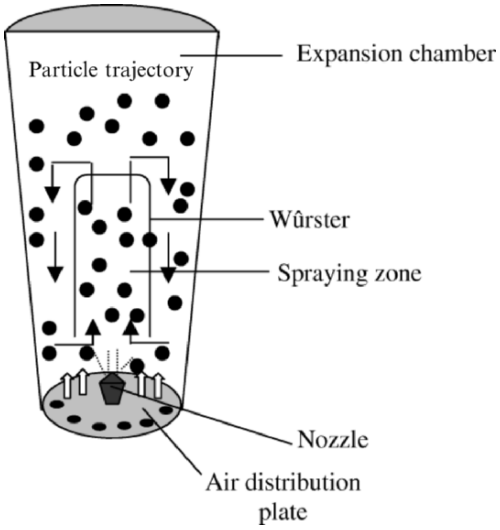

Figure 24.2. Fluidized bed coating process. (Reprinted with permission from Madene et al. 2006.)

of the coat. The coating may be a solution, dispersion, emulsion, fat or other film forming material. Fluidized bed coating has been used to enhance or tune the properties of bioactive ingredients, to increase shelf-life, mask undesirable taste, improve handling, control release, and improve aesthetics, taste and color (Dewettinck and Huyghebaert 1999). It is used for production of nutritional supplements such as vitamins B and C, ferrous sulfate, ferrous fumarate, sodium ascorbate, potassium chloride and a variety of vitamin and mineral premixes. Spray-dried oil-in-water emulsions can be given a secondary coating to improve core stability with a fluid bed coating process (Turchiuli et al. 2005).

24.3.3.4 Extrusion

Extrusion processes involve the application of pressure to a mass to make it flow through an orifice or die under controlled conditions. An extrusion device for encapsulation consists of a droplet generator and a droplet hardening bath (Rabiskova 2001). Microencapsulation by extrusion takes place at very high temperatures, and involves projecting an emulsion of the core and coating material through a die at high pressure. This method has been traditionally used in flavour encapsulation. Its potential for use in bioactive delivery was demonstrated by work on encapsulation of sunflower oil (as a model lipophilic bioactive) in a potato starch matrix by extrusion (Yilmaz et al. 2001).

24.3.3.5 Centrifugal Extrusion Encapsulation

Centrifugal extrusion encapsulation, or coaxial extrusion processing, is a liquid co-extrusion process that uses an assembly of cylindrical nozzles consisting of concentric orifices located at the outer circumference of a rotating cylinder (Figure 24.3).

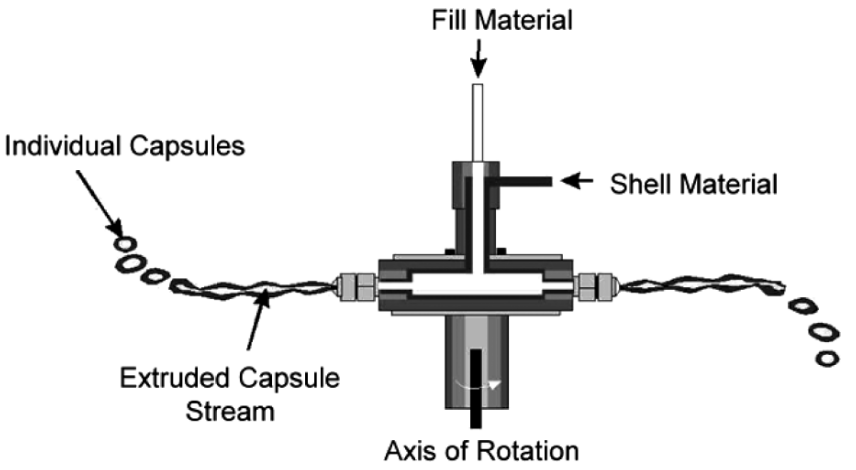

Figure 24.3. Centrifugal extrusion encapsulation. (Reprinted with permission from Southwest Research Institute, USA.)

The process involves a liquid bioactive core being pumped through the inner orifice, and the liquid encapsulant material pumped through the outer orifice, which are both located in the cylindrical head. When co-extruded simultaneously, a co-extruded liquid jet of the bioactive core material is surrounded by the encapsulant. As the cylindrical head rotates the extruded liquid jet breaks into droplets and forms the microcapsule. The microcapsules are hardened by drying, cooling, chelation, gelation, chemical reaction, or cross-linking, depending on the nature of the encapsulant material (Vasishtha and Schlameus 2001). Centrifugal extrusion encapsulation requires the bioactive core to be in a liquid form at the time of production.

24.3.3.6 Spinning-Disk Coating

Spinning-disk coating or centrifugal suspension-separation coating is a physical coating process that involves the suspension of solid core particles in a liquid encapsulating material (Sparks et al. 1995) (Figure 24.4). The encapsulant formulation can be a solution, suspension or melt directly applied without solvents. The bioactive core suspension is then passed over a rotating disk under very controlled process condition to form a thin film around the core particles. Excess film material is separated from the coated particles and recycled. This process can coat particles from about 20 microns to several millimeters in diameter (Labell 2002).

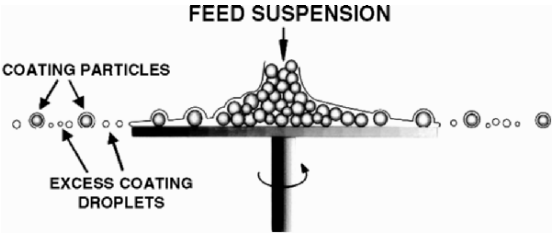

Figure 24.4. Spinning-disk coating. (Reprinted with permission from Particle Coating Technologies, USA.)

24.3.3.7 Use of Supercritical Fluids

Supercritical fluids can be used for the encapsulation of heat-sensitive cores. This solvent free-method can be used for the production of bioactive loaded microparticles as the encapsulant material is plasticized in the supercritical carbon dioxide, which is mixed with the core. In microencapsulation by rapid expansion of supercritical solutions, the pressurized supercritical fluid containing the encapsulant and core is sprayed through a nozzle. This leaves a particulate material containing the core and has been used for encapsulation of food grade ingredients such as vitamin C and xylitol (Gouin 2004). Supercritical fluid mixing has been used for the production of a protein encapsulated in poly(DL-lactic acid) microparticles in which the activity of the protein is retained, demonstrating the potential use of supercritical fluids for the controlled release of proteins and peptides (Whitaker et al. 2005). By altering depressurization conditions, particles with different morphologies may be obtained.

24.3.3.8 Complex Coacervation

Coacervation is the separation of two liquid phases in colloidal systems, where the more concentrated phase is known as the coacervate. Complex coacervates are formed by combining two oppositely charged biopolymers under controlled conditions. This causes associative phase separation (Kruif et al. 2004). Typically, protein and polysaccharide mixtures are used and the capsule is hardened by using a cross-linker (Figure 24.5). It is the hardening of the shell that remains the greatest challenge, especially for food applications. Glutaraldehyde is usually added for cross-linking in pharmaceutical applications but not in food applications. Alternative cross-linking systems are now being examined and the use of plant phenolics as cross-linking agents has been demonstrated for cross-linking gelatin gels and gelatin-pectin coacervate microparticles (Strauss and Gibson 2004).

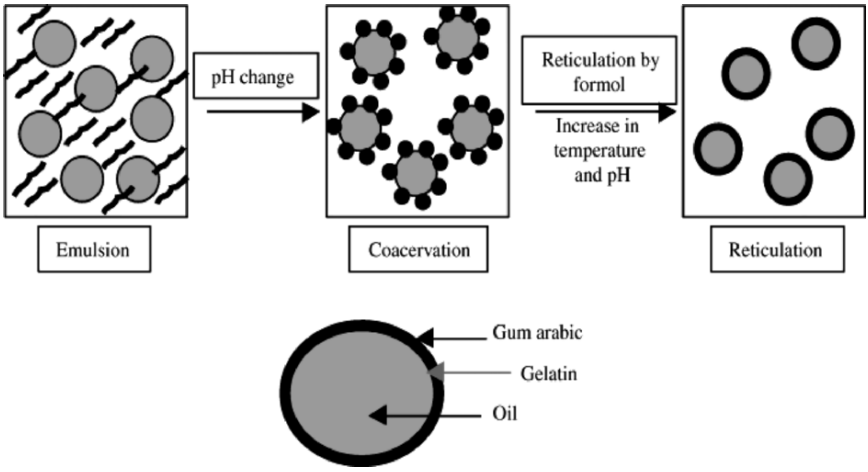

Figure 24.5. Principle of complex coacervation method. (Reprinted with permission from Madene et al. 2006.)

The advantage of complex coacervates is that high payloads can be obtained. Chitosan/alginate coacervates have been reported to encapsulate up to 87% shark liver oil, which is rich in omega-3 fatty acids (Peniche et al. 2004). Microspheres of carboxymethyl chitosan/alginate hardened with calcium chloride have been used for encapsulation of up to 80% bovine serum albumin (Zhang et al. 2004).

24.3.3.9 Inclusion Complexation

In inclusion complexation, a core is encapsulated by complexation (e.g., cyclodextrin). A supramolecular assembly is formed because of the noncovalent inclusion of an apolar core (e.g., oil) of suitable size within the hydrophobic cavity of the cyclodextrin. An example of inclusion complexation is the interaction between cyclodextrin and lycopene (Mele et al. 2002). The inclusion complex increases the water

dispersibility of the lipophilic molecules, controls their release and protects them from the environment.

24.3.3.10 Liposomes

Liposomes are spherical layered vesicles consisting of one or more concentric layers of lipids formed from dispersion of polar lipids in aqueous solvents. Liposomes have been used for the delivery of drugs in the pharmaceutical industry and also have widespread applications in the agriculture and food industry (Taylor et al. 2005). Liposomes are usually prepared with phospholipids, but glycolipids also possess liposome-forming properties (Herslof 2000). Depending on the conditions of their preparation, unilamellar or multilamellar liposomes can be formed. The entrapment of sensitive oil and water-soluble bioactives in liposomes protects them prior to their release, and the size, composition and stability of the liposomes can be tailored to meet the functional requirements of the system. Liposomes can offer a versatile approach, for encapsulation of both oil-soluble and water-soluble bioactives, with opportunities to induce controlled release of the bioactive core. It has been used in the food industry for protection of enzymes, vitamins, minerals, bacteriocins and antimicrobials, but still remains an expensive process (Zeisig and Cammerer 2001).

24.3.3.11 Multiple Emulsions

Multiple emulsions are compartmentalized liquid dispersions in which the inner dispersed phase is separate from the outer liquid phase by a middle layer of another phase. Water-in-oil in water (*W/O/W*) or oil-in-water in oil (*O/W/O*) may be prepared. Double emulsions can be used to deliver both oil and water-soluble bioactives, and are suited for controlled and sustained release of the active core encapsulated in the internal phase of the double emulsion. Conventionally, double emulsions are made with low-molecular-weight surfactants which can limit their long-term stability. This has been improved with the use of natural biopolymers to stabilize the system (Benichou et al. 2004). Alternatively, the oil phase of double emulsions may be modified to provide control of the release of an encapsulated hydrophilic bioactive. Fats with different melting points used in *W/O/W* emulsions containing L-tryptophan as a marker compound, have different capacities to perform as hydrophobic barriers. The release of L-tryptophan was slowed with increasing melting point of the lipid phase (Weiss et al. 2005). The structure of the double emulsions can be preserved after spray drying, as demonstrated with a double emulsion containing orange oil (Edris and Bergenståhl 2001). This allows double emulsions to be produced in both liquid and powder formats.

Multiple emulsions can also be formed by mixing an oil-in-water emulsion with a thermodynamically incompatible biopolymer mixture. Depending on the formulation and conditions of preparation, oil-in-water-in-water or mixed oil in water/water-in-water multiple emulsions may be formed. These have potential for the controlled delivery of a range of bioactives (Kim et al. 2006).

24.4 Encapsulated Bioactive Delivery Systems

Encapsulated delivery systems are developed with a specific purpose for each target application. To date, most research has been directed at stabilizing extracted bioactives and delivering the required levels in food. Their ultimate delivery to a target site depends on the core, the material and the methods used for encapsulation as well as the food vehicle used for delivery. Although there have been many technological advances there are still limitations to the use of microencapsulated ingredients in some applications.

24.4.1 Encapsulated Delivery Systems for Lipids

Many functional lipids including polyunsaturated lipids such as omega-3 fatty acids, conjugated linoleic acids and lipid-soluble bioactives such as carotenoids, coenzyme Q10, tocopherols and some vitamins are sensitive to oxidation. If not adequately protected from the environment, they can degrade very rapidly. This results in the development of off-flavours and reduced bioactivity. Many types of materials have been used to encapsulate sensitive lipids to isolate them from oxygen and minimize their interactions with trace metal ions (e.g., Fe) that catalyze their oxidation. Lipids may be trapped in glassy matrices, stabilised in emulsion systems with low molecular weight surfactants or film forming biopolymers, or encapsulated in liposomes or cyclodextrin.

24.4.1.1 Glassy Matrices

The ability of glassy matrices to encapsulate lipophilic bioactive molecules makes them useful for the delivery of oils and oil-soluble bioactives. However, the efficiency of encapsulation and the degree of protection offered varies with the formulation. Some authors suggest that increased molecular mobility as the temperature is raised above the glass transition temperature, leads to an increase in oxidation of encapsulated lipid components (Gejl-Hansen and Flink 1977). Shimada et al. (1991) found that above the glass transition temperature, encapsulated methyl linoleate was released from a lactose-gelatin matrix, resulting in its rapid oxidation. Labrousse et al. (1992) demonstrated that oxidation of methyl linoleate was arrested in sugar-gelatin glassy matrices but that when the matrix collapsed, rapid oxidation occurred. However, others have found that molecular mobility did not influence oxidation rates of flaxseed oil (Grattard et al. 2002). Others have shown that there was only partial protection of the oils as oxygen can permeate a glassy food matrix (25% sucrose, 45% maltodextrin, 5% gelatin and 25% rapeseed oil), where the limiting factors were oxidation at low temperature and oxygen diffusion at higher temperatures (Orlien et al. 2006).

24.4.1.2 Gels and Beadlets

Gelatin beadlets have been used for delivery of β-carotene (Pszczola 2003). Recently, multicore carotenoid beadlets have been prepared by spray drying a dispersion of

carotenoids in gelatin, pectin and medium chain fatty acid glycerides (Sadano and Sonoda 2002), and are protected against degradation when encapsulated in these matrices.

24.4.1.3 Emulsion Systems

Oil-in-water emulsions lend themselves readily to the delivery of oils and oil-soluble bioactives. The surfactant or biopolymer provides a means of isolating and protecting the lipophilic cores. Many types of materials with emulsifying capacity have been used to encapsulate oils and oil-soluble bioactives in single and multiple emulsion systems. Multilayered interfaces have also been used to improve the robustness of microcapsules.

Primary Emulsions

Proteins (e.g., milk proteins, gelatin, soy proteins) stabilize oil-in-water emulsions. Protein encapsulants have been successfully used for protecting sensitive oils against oxidation (Hu et al. 2003). Caseins are effective for stabilizing spray-dried emulsions of fish oil, with more aggregated forms of the caseins providing more protection to the oil against oxidation (Keogh et al. 2001). The proteins can inhibit oxidation either at the interface of the emulsion droplet or in the aqueous phase (McClements and Decker 2000; Faraji et al. 2004).

Although the protein component is needed for emulsification, sugars are often added to the mix. The oxidative stability of spray-dried fish oil emulsions was found to increase with increasing dextrose equivalence (DE) of the carbohydrate used in combination with caseinate (Hogan et al. 2003; Kagami et al. 2003). This may be due to the increased microencapsulation efficiencies with increasing DE of the carbohydrate as observed in soy oil powders stabilized by blends of caseinate and carbohydrates (Hogan et al. 2001) or the antioxidant properties of small sugars in fish oils (Faraji and Lindsay 2005). Higher microencapsulation efficiencies might be expected to impart improved oxidative stability of sensitive lipids. However, this does not always appear to be the case. The stability of freeze-dried fish oil emulsions containing sodium caseinate and lactose was not related to microencapsulation efficiency (Heinzelmann et al. 2000).

The encapsulating properties of a protein may be improved by conjugation of sugars to proteins. The Maillard reaction between a reducing sugar and a free amino group has been utilized to increase the emulsifying capacity of proteins. In addition, Maillard reaction products have antioxidant qualities and have been found to be superior encapsulants compared to the original protein for protecting fish oils and spray dried emulsions from oxidation (Augustin et al. 2006).

Other protein systems have been successfully used for encapsulation. For example, conjugated linoleic acid has been microencapsulated using whey proteins (Jimenez et al. 2004). A whey protein bead delivery system was prepared by emulsification of soybean oil containing retinol with pre-denatured whey protein followed by the addition of calcium ions to induce gelation. The encapsulant system protected

the retinol from enzymatic degradation at stomach pH and could be released on pancreatic digestion (Beaulieu et al. 2002).

The use of a modified starch, corn starch sodium octenyl succinate derivative, for encapsulation of sea buckthorn kernel oil (containing polyunsaturated fatty acids, tocopherols, tocotrienols, plant sterols and carotenoids) by spray-drying was found to improve oil stability. Better protection was afforded when the starch encapsulant was stored in its glassy state (Partanen et al. 2002). Methylcellulose and hydroxymethycellulose in combination with soy lecithin enabled the production of 40% (*W/W*) fish oil powders with improved stability (Kolanowski et al. 2004).

Double Emulsions

Water-dispersible microcapsules have also been prepared by spray-drying *W/O/W* emulsions containing carotenoids. These emulsions were formulated with combinations of low molecular weight emulsifiers and biopolymer blends of various gums. Microencapsulation efficiency and protection of carotenoids against degradation was significantly influenced by the formulation used (Rodríguez-Huezo et al. 2004). A double emulsification process, followed by heat gelation of protein microcapsules, holds promise for controlled core-release in food systems (Lee and Rosenberg 2000). Oil-in-water-in-oil emulsions containing fish oils that were subsequently gelled by heat or treated with transglutaminase to cross-link the proteins in the capsules exhibited improved oxidative stability and provided greater resistance to pepsin attack compared to nonencapsulated oils (Cho et al. 2003).

An alternative to the traditional *O/W/O* or *W/O/W* emulsions is the *O/W/W* format. The addition of a whey–protein oil-in-water stabilized emulsion to an aqueous two-phase system (comprising heat denatured whey protein and high methoxy pectin) resulted in the formation of such an emulsion. This was subsequently gelled with calcium ions. It has been suggested that these novel structures can provide both encapsulation and controlled release (Kim et al. 2006).

Multilayered Oil-in-Water Emulsions

Improved stability of lipophilic bioactives may be obtained by tailoring the interfacial membranes of oil droplets. Rosenberg and Lee (2004) coated a primary whey protein–based oil-in-water emulsion containing paprika oleoresin (as the model core) with calcium alginate to enhance the stability and control the core release.

Stabilization of oil droplets may also be achieved by engineering multilayered interfacial membranes by adsorption of oppositely charged biopolymers, using a layer-by-layer deposition process. Secondary emulsions, formed by the dilution of a primary anionic oil-in-water emulsion made with a low molecular weight surfactant (lecithin), with an aqueous chitosan solution. The secondary emulsions containing oil droplets stabilized by lecithin-chitosan coated membranes had increased oxidative stability and were more resistant to aggregation when exposed to heat, freeze–thaw cycling and high calcium concentration compared to the primary emulsions (Ogawa et al. 2003). Tertiary emulsions may also be formed by deposition of biopolymers of opposite charge as in the formation of lecithin–chitosan–pectin

oil-in-water emulsion droplets (Ogawa et al. 2004). By the addition of multilayers, the interfacial membranes of the primary emulsion droplet may be modified to provide the desired protection—that is, increase stability of the core or control its release.

The structure of the multilayered emulsions may be preserved during spray-drying, enabling the delivery of emulsions with multilayered interfaces in a powder format. Spray-dried tuna oil powders made from emulsions containing oil droplets with lecithin–chitosan membranes, with added corn syrup showed good oil retention and water dispersibility (Klinkesorn et al. 2006).

24.4.1.4 Liposomes

Liposomes have been successfully used to deliver a range of oil-soluble bioactives. Banville et al. (2000) showed that incorporation of Vitamin D in cheese was improved with liposomal delivery compared to the use of a water-soluble preparation, but after long term storage (3–5 months) the stability of the liposome-encapsulated vitamin decreased. Multilamellar liposomes made from soy lecithin will incorporate β-carotene. Using a lecithin to β-carotene ratio of 1:0.05, efficiencies of up to 99.7% were obtained (Rhim et al. 2000).

24.4.1.5 Inclusion Complexes

Cyclodextrin has been used to encapsulate conjugated linoleic acid. Encapsulation of conjugated linoleic acid stabilized it against oxidation for 80 h at 35°C (Park et al. 2002). The formation of an inclusion complex between bixin (a carotenoid) and α-cyclodextrin improved the solubility of the carotenoid in water and protected it against degradation in the presence of oxygen and light (Lyng et al. 2005).

24.4.2 Encapsulated Delivery Systems for Water-Soluble Bioactives

Water-soluble bioactives may also be protected from their environment by entrapment within a matrix (e.g., gel) or the use of lipid coats. Most research on delivery of water-soluble bioactives has been on systems for enriching foods with water-soluble vitamins and minerals and more recently on the use of bioactive peptides in food. The delivery of bioavailable iron has been of particular interest because of the widespread problem of iron deficiency.

24.4.2.1 Lipid Coats

Hard fats are used to coat water-soluble bioactives. Release occurs by heating above the melting point of the fat or by mechanical rupture. Fat coatings have been used for protecting many water-soluble materials, which may otherwise be volatilized or damaged during thermal processing and to deliver materials such as ferrous sulfate, vitamins and other minerals. The peptides of casein hydrolysates encapsulated in lipospheres were shown to have reduced bitterness (Barbosa et al. 2004).

24.4.2.2 Liposomes

Ferrous sulphate encapsulated in soy lecithin liposomes has been used to deliver iron. These preparations have improved bioavailability compared to ferrous sulphate directly added in milk and dairy products (Boccio et al. 1997; Uicich et al. 1999). Albaldawi et al. (2005) reported that the addition of encapsulated haem iron in lecithin/cholesterol liposomes resulted in improved rheological properties of bread dough and the sensory properties of baked bread.

Liposomes, like single lipid coats, have been examined for their ability to deliver peptides and proteins. Encapsulation of casein peptides in liposomes (0.5–1 μm in size at a rate of 50%–60%) significantly reduced bitterness and increased stability (Morais et al. 2005). Hsieh et al. (2002) showed that α-amylase can be protected against the action of pepsin at low pH, demonstrating the protection that may be offered during transit through the stomach.

24.4.2.3 Protein Gels

Cold-set whey protein gels obtained by addition of calcium ions to preheated whey proteins have been used to deliver iron (Remondetto et al. 2002). By modulating the conditions of formation, gels with different microstructures (particulate or filamentous) were formed with different encapsulating properties. Filamentous whey protein gels were more efficient than particulate gels in delivering bioavailable iron to the intestine, as less iron was released at acidic but more at alkaline pH (Remondetto et al. 2004).

24.4.2.4 Multiple Emulsions

Vitamin B_1 was entrapped in an inner aqueous phase of a double emulsion stabilized by a mixture of whey protein isolate and xanthan as the external gum. The release of the vitamin was modulated by altering the pH or the ratio of the two biopolymers. The increased rate of release of the vitamin as pH was increased from 2 to 7 has been attributed to the decreased electrostatic interaction between whey protein isolate and xanthan. Increasing the rigidity of the external interface by increasing the amount of xanthan also decreased the rate of release of the vitamin (Benichou et al. 2004).

Immunoglobulins are prone to loss of their bioactivity through proteolysis and heating. The encapsulation of immunoglobulin Y obtained from egg yolk in a multiple oil-in water-in-oil emulsion was shown to be stable to pepsin and acid and more stable to heat treatment (95°C for 10 min) than the nonencapsulated form (Cho et al. 2005).

24.4.3 Encapsulated Delivery Systems for Probiotics

Probiotics have attracted interest because they have a role in the health status of individuals, particularly in improving gut health (Saarela et al. 2002). There are many strains of probiotic bacteria, with varying susceptibilities to acid, heat and oxygen.

There is much interest in ensuring that live bacteria, which are delivered through foods, survive during storage and through stomach acids.

24.4.3.1 Polysaccharide Gels

Probiotics have been entrapped in gels or beads made with various carbohydrates. Adhikari et al. (2000) examined the use of kappa-carrageeenan for encapsulating bifidobacteria for yoghurt applications. Microencapsualtion of *Bifidobacterium longum* B6 and *Bifidobacterium longum* ATCC 15708 improved the viability of the cells, but the taste of the yoghurt was different. Alginates have been used alone or in combination with other carbohydrates as encapsulating agents to improve survival of probiotics. A range of carbohydrate-based systems containing *Lactobacillus reuteri* was prepared using either phase separation or extrusion. Alginate and alginate/starch were found to provide superior protection to the bacteria in gastric fluid compared to those prepared from kappa-carrageenan with locust bean gum or xanthan with gellan (Muthukumarasamy et al. 2006).

Coating of alginate particles containing *Lactobacillus bulgaricus* KFRI 673 with chitosan improved their survival in simulated gastric and intestinal fluids as well as during storage (Lee et al. 2004). Co-encapsulation of prebiotics (e.g., HiMaize) with *Lactobacillus acidophilus* CSCC 2400 or CSCC 2409 in alginate improved the viability of the bacteria on exposure to low pH, bile salts and in yoghurt, although the improvement was dependent on the level and type of prebiotics used (Iyer and Kailasapathy 2005). However, encapsulation of *Bifidobacterium* spp. and *Lactobacillus acidophilus* in an alginate–starch matrix did not protect the bacteria against acid and bile conditions (Sultana et al. 2000). The different degree of protection afforded to microorganisms may be due to the different conditions used, the nature of the ingredients used or the different susceptibilities of different strains to environmental conditions.

24.4.3.2 Two-Phase Aqueous Delivery Systems

A novel all-aqueous-based system that relies on the thermodynamic incompatibility of biopolymers has been described for the encapsulation of probiotics. A two-phase system comprising of polyvinyl pyrolidone and dextran was used as the carrier material for a probiotic bacterium in the preparation of spray dried preparations of probiotics. The survival of the bacteria (*Enterococcus faecium* E74) was dependent on the composition of the system. Although the survival rate during drying was better when only dextran was used, there were better survival rates of the bacteria during storage with the two-phase carrier system (Millqvist-Fureby et al. 2000).

24.4.3.3 Emulsion Systems

Probiotics may be encapsulated in protein-based emulsions. Picot and Lacroix (2003) prepared microcapsules by emulsifying milkfat containing micronized skim milk powder (as a surrogate for freeze-dried bacteria) with heat denatured whey proteins and then spray drying. Incorporation rates of up to 58% milk fat and 29% skim milk

powder were obtained. Encapsulation of the bacteria (*Bifidobacterium infantis*) into a protein-resistant starch–oil emulsion with prebiotics prior to spray-drying improved the storage stability of the resultant probiotic powder during nonrefrigerated storage and protected the bacteria at gastric pH. The bacteria were released from the system on exposure of the microcapsule to simulated intestinal fluid (Crittenden et al. 2006).

24.5 Food as a Delivery System for Bioactives

Key trends influencing the development of the functional food and drinks markets include the increase in healthy eating, increased demand for natural and organic foods, snacking and convenience foods. Many more foods are now being used as delivery systems for bioactives including fruit juices and other beverages, dairy foods, cereal-based products, sports bars, confectionery, baked goods and spreads.

The demand for healthy foods has led to the development of several entirely new healthy ingredient and additive categories (Heasman and Mellentin 2001; Sloan 2004). An entirely new sector of functional food ingredients has developed, including products such as omega-3 fatty acids and phytosterols for cardiovascular health, prebiotics and probiotics for gut health, antioxidants, polyphenols and phytochemicals, and bioactive peptides. The established vitamins and minerals sector has also benefited from this functional food trend, with more and more products being fortified with beneficial vitamins and minerals.

Successful delivery of bioactives into foods requires that the bioactive is stable during food processing and throughout the food product's shelf-life and is in a bioavailable form when the food is consumed. The bioactive must be protected from possible interaction with other ingredients. The food matrix used as the delivery vehicle has to be considered. For incorporation of bioactives into dry powder food applications, the properties of the microencapsulated bioactive powder properties must match those of the final powder mix (e.g., the particle size, water activity, bulk density) to ensure homogeneity. When a bioactive is added to a processed food product, the stage of processing at which the bioactive is added can influence whether it is successfully incorporated (Augustin 2003; Sanguansri and Augustin 2006a) as can the formulation of the bioactive ingredient and its format. This means that the supplier of the bioactive (in both its raw or encapsulated form) has to work in conjunction with the food manufacturer as the formulation of the final food and the manufacturing processes influence the stability and bioavailability of the added bioactive.

There also needs to be evidence for the delivery of the bioactive to the desired site in the body to obtain the desired health outcome. This is important as the long-term success of functional foods depends on scientific evidence to substantiate valid health claims. As the knowledge about the physiological function of bioactives, the mechanism of their action, the effective doses and the desired site for release of bioactives grows, encapsulation will be increasingly used for targeted release of bioactives for improving the health of consumers (Chen et al. 2006).

24.6 Emerging Trends

The availability of a very limited range of suitable encapsulant materials allowed for food applications still remains the biggest challenge in material selection, especially when more sophisticated microcapsule properties are increasingly being required by the food manufacturers to deliver the types of fortified foods with the health benefits demanded by consumers. Not only are consumers interested in the effective delivery of traditionally recognized bioactives, but there is also increasing demand to maximize their health benefits by combining a number of bioactives into a single food. As this interest in the delivery of cocktails of bioactives for specific health outcomes grows, there will be increasing demands on the properties of encapsulated ingredients and the encapsulation technologies used to produce them.

The use of emerging food technologies such as ultrasound, static high-pressure processing and microfluidisation may provide the platform for the creation of novel microstructured assemblies to meet future needs and provide new processing or preprocessing capabilities for encapsulation systems.

Developments in nanotechnology and control over the self-assembly behavior of components is expected to provide new insights into delivery of bioactives (Mezzenga et al. 2005; Chen et al., 2006; Sanguansri and Augustin 2006b). The development of nanoparticles with different size and structure is expected to provide a new generation of encapsulated bioactives, (Moraru et al. 2003).

Real-time monitoring during consumption of foods, to ascertain the site and the rate of release of bioactives using nondestructive methods will be needed to help develop models to link structure to breakdown during gastrointestinal tract transit. The substantiation of health claims is central to the provision of evidence-based interventions based on food. Human-based trials will be needed to provide unequivocal evidence of bioactive performance.

Acknowledgements. The authors would like to thank Christine Margetts for contributing to the sourcing of literature and useful comments.

24.7 References

Adhikari, K., Mustapha, A., Grün, I.U., and Fernando, L. (2000). Viability of microencapsulated Bifidobacteria in set yogurt during refrigerated storage. *J Dairy Sci*. 83, 1946–1951.

Albaldawi, A., Brennan, C.S., Alobaidy, K., Alammar,W., and Aljumaily, D. (2005). Effect of flour fortification with haem liposome on bread and bread doughs. *Int. J. Food Sci. Technol*. 40, 825–828.

Anon, (1981). Protected ascorbic acid. Research Disclosure, 208, 308.

Augustin, M.A. (2001). Functional foods: an adventure in food formulation. *Food Aust*. 53, 428–432.

Augustin, M.A., Sanguansri, L., Margetts, C., and Young, B. (2001). Microencapsulation of food ingredients. *Food Aust*. 53, 220–223.

Augustin, M.A. (2003). The role of microencapsulation in the development of functional dairy foods. *Aust. J. Dairy Technol*. 58, 156–160.

Augustin, M.A., and Clarke, P.T. (2004). Introducing nutritional ingredients/products into the recombined milk products market using microencapsulation. In: *Proceedings of the 4th International Symposium on Recombined Milk and Milk Products: New Challenges, New Ideas,* (9–12th May 2004: Cancun, Mexico). U.S. Dairy Export Council, Arlington, VA, pp. 194–199.

Augustin, M.A., Sanguansri, L., and Bode, O. (2006). Maillard reaction products as encapsulants for fish oil powders. *J. Food Sci*. 71, E25–E32.

Banville, C., Vuillemard, J.C., and Lacroix, C. (2000). Comparison of different methods for fortifying cheddar cheese with vitamin D. *Int. Dairy J.* 10, 375–382.

Barbosa, C.M.S., Morais, H.A., Delvivo, F.M., Mansur, H.S., De Oliveira, M.C., and Silvestre, M.P.C. (2004). Papain hydrolysates of casein: molecular weight profile and encapsulation in lipospheres. *J. Sci. Food Agric*. 84, 1891–1900.

Beaulieu. L., Savoie, L., Paquin, P., and Subirade, M. (2002). Elaboration and characterization of whey protein beads by an emulsification/cold gelation process: application for the protection of retinol. *Biomacromolecules*, 3, 239–248.

Bell, L.N. (2001). Stability testing of nutraceuticals and functional foods. In: R.E.C. Wildman (ed.), *Handbook of Nutraceuticals and Functional Foods*, CRC Press, New York, pp. 501–506.

Benichou, A., Aserin, A., and Garti, N. (2004). Double emulsions stabilized with hybrids of natural polymers for entrapment and slow release of active matters. *Adv. Colloid Interface Sci*. 108–109, 29–41.

Boccio, J.R., Zubillaga, M.B., Caro, R.A., Gotelli, C.A., Gotelli, M.J., and Weill, R. (1997). A new procedure to fortify fluid milk and dairy products with high-bioavailable ferrous sulfate. *Nutr. Rev*. 55, 240–246.

Brazel, C.S. (1999). Microencapsulation: offering solutions for the food industry. *Cereal Foods World* 44, 388–393.

Chen, H., Weiss, J., and Shahidi, F. (2006). Nanotechnology in nutraceuticals and functional foods. *Food Technol*. 60(3), 30–36.

Cho, Y.H., Shim, H.K., and Park, J. (2003). Encapsulation of fish oil by an enzymatic gelation process using transglutaminase cross-linked proteins. *J. Food Sci*. 68, 2717–2723.

Cho, Y.H., Lee, J.J., Park, I.B. Huh, C.S., Baek, Y.J., and Park, J. (2005). Protective effect of microencapsulation consisting of multiple emulsification and heat gelation processes on immunoglobulin in yolk. *J. Food Sci.* 70, E148–E151.

Crittenden, R., Weerakkody, R., Sanguansri, L., and Augustin, M.A. (2006). Synbiotic microcapsules that enhance microbial viability during nonrefrigerated storage and gastrointestinal transit. *Appl. Environ. Microbiol.* 72, 2280–2282.

Deckere, de, E.A.M., and Verschuren, P.M. (2000). Functional fats and spreads. In: G.R. Gibson and C.M. Williams (eds.), *Functional Foods, Concept to Product*. Woodhead Publishing, Cambridge, UK, pp. 233–257.

Dewettinck, K., and Huyghebaert, A. (1999). Fluidized bed coating in food technology. *Trends Food Sci. Technol*. 10, 163–168.

Edris, A., and Bergenståhl, B. (2001). Encapsulation of orange oil in a spray dried double emulsion. *Nahrung* 45, 133–137.

Elliot. J. (2001). Antioxidant vitamin application. *Food Technology in New Zealand*, 36 (8), 10–13, 36.

Fang, Z., Zhang, M., Sun Y., and Sun, J. (2006). How to improve bayberry (Myrica rubra Sieb. et Zucc.) juice color quality: Effect of juice processing on bayberry anthocyanins and polyphenolics. *J. Agric. Food Chem*. 54, 99–106.

Faraji H, McClements D.J., and Decker E.A. (2004). Role of continuous phase protein on the oxidative stability of fish oil-in-water emulsions. *J. Agric. Food Chem*. 52, 4558–4564.

Faraji, H., and Lindsay, R.C. (2005). Antioxidant protection of bulk fish oils by dispersed sugars and polyhydric alcohols. *J. Agric. Food Chem*. 53, 736–744.

Frankel, E.N., Satue-Gracia, T., Meyer, A.S., and German, J.B. (2002). Oxidative stability of fish and algae oils containing long-chain polyunsaturated fatty acids in bulk and in oil-in-water emulsions. *J. Agric. Food Chem*. 50, 2094–2099.

Gejl-Hansen, F., and Flink, J.M. (1977). Freeze-dried carbohydrate containing oil-in-water emulsions: microstructure and fat distribution. *J. Food Sci*. 42, 1049–1055.

Gibbs, B.F., Kermasha, S., Alli, I., and Mulligan, C.N. (1999). Encapsulation in the food industry: a review. *Int. J. Food Sci. Nutr*. 50, 213–224.

Gouin, S. (2004). Microencapsulation: industrial appraisal of existing technologies and trends. *Trends Food Sci. Technol*. 15, 330–347.

Grattard, N., Salaün, F., Champion, D., Roudaut, G., and Le Meste, M. (2002). Influence of physical state and molecular mobility of freeze-dried maltodextrin matrices on the oxidation rate of encapsulated lipids. *J. Food Sci*. 67, 3002–3010.

Heasman, M., and Mellentin, J. (2001). *The Functional Foods Revolution: Healthy People, Healthy Profits?* Earthscan Publications, London, UK.

Heinzelmann, K., Franke, K., Velasco, J., and Márquez-Ruiz, G. (2000). Micro-encapsulation of fish oil by freeze-drying techniques and influence of process parameters on oxidative stability during storage. *Eur. Food Res. Technol*. 211, 234–239.

Herslof, B.G. (2000). Glycolipids herald a new era for food and drug products. *Lipid Technol*. 12, 125–128.

Hilliam, M. (2000). Functional food. *The World of Ingredients*. December, 50–52.

Hogan S.A., McNamee B.F., O'Riordan, E.D., and O'Sullivan, M. (2001). Emulsification and microencapsulation properties of sodium caseinate/carbohydrate blends. *Int. Dairy J*. 11, 137–144.

Hogan S.A, O'Riordan, E.D., and O'Sullivan, M. (2003). Microencapsulation and oxidative stability of spray-dried fish oil emulsions. *J. Microencapsulation* 20, 675–688.

Hsieh, Y.F., Chen, T.L., Wang, Y.T., Chang, J.H., and Chang, H.M. (2002). Properties of liposomes prepared with various lipids. *J. Food Sci.* 67, 2808–2813.

Hu, M., McClements, D.J., and Decker, E.A. (2003). Lipid oxidation in corn oil-in-water emulsions stabilized by casein, whey protein isolate, and soy protein isolate. *J. Agric. Food Chem*. 51, 1696–1700.

Iyer, C., and Kailasapathy, K. (2005). Effect of co-encapsulation of probiotics with prebiotics on increasing the viability of encapsulated bacteria under in vitro acidic and bile salt conditions and in yogurt. *J. Food Sci*. 70, M18–M23.

Jimenez, M., García, H.S., and Beristain, C.I. (2004). Spray-drying microencapsulation and oxidative stability of conjugated linoleic acid. *Eur. Food Res. Technol*. 219, 588–592.

Kagami Y., Sugimura S., Fujishima N., Matsuda K., Kometani T., and Matsumura Y. (2003). Oxidative stability, structure, and physical characteristics of microcapsules formed by spray-drying of fish oil with protein and dextrin wall materials. *J. Food Sci*. 68, 2248–2255.

Keogh M.K., O'Kennedy, B.T., Kelly J., Auty, M.A., Kelly, P.M., Fureby, A., and Haahr, A.M. (2001). Stability to oxidation of spray-dried fish oil powder microencapsulated using milk ingredients. *J. Food Sci*. 66, 217–224.

Kim, H.-J., Decker, E.A., and McClements, D.J. (2006). Preparation of multiple emulsions based on thermodynamic incompatibility of heat-denatured whey protein and pectin solutions. *Food Hydrocolloids* 20, 586–595.

Kirca, A., Ozkan, M., and Cemeroglu, B. (2006). Stability of black carrot anthocyanins in various fruit juices and nectars. *Food Chem*. 97, 598–605.

Klinkesorn, U., Sophanodora, P., Chinachoti, P., Decker, E.A., and McClements, D.J. (2006). Characterization of spray-dried tuna oil emulsified in two-layered interfacial membranes prepared using electrostatic layer-by-layer deposition. *Food Res. Int*. 39, 449–457.

Kolanowski W., Laufenberg, G., and Kunz, B. (2004). Fish oil stabilisation by microencapsulation with modified cellulose. *Int. J. Food Sci. Nutr*. 55, 333–343.

Kruif, C.G. de., Weinbreck, F., and Vries, R. de (2004). Complex coacervation of proteins and anionic polysaccharides. *Curr. Opin. Colloid Interface Sci*. 9, 340–349.

Labell, F. (2002). New, precise methods for encapsulation. *Prepared Foods* 171(1), 55.

Labrousse, S., Roos, Y., and Karel, M. (1992). Collapse and crystallization in amorphous matrices with encapsulated compounds. *Sci. Aliments* 12, 757–769.

Lamb, R. (1987). Spray chilling. Food, Flavourings, Ingredients, Packaging and Processing 9(12), 39, 41, 43.

Lee, J.S., Cha, D.S., and Park, H.J. (2004). Survival of freeze-dried *Lactobacillus bulgaricus* KFRI 673 in chitosan-coated calcium alginate microparticles. *J. Agric. Food Chem*. 52, 7300–7305.

Lee, S.J., and Rosenberg, M. (2000). Whey protein-based microcapsules prepared by double emulsification and heat gelation. *Lebensm. Wiss. Technol*. 33, 80–88.

Lyng, S.M.O., Passos, M., and Fontana, J.D. (2005). Bixin and alpha-cyclodextrin inclusion complex and stability tests. *Process Biochem*. 40, 865–872.

Madene, A., Jacquot, M., Scher, J., and Desobry, S. (2006). Flavour encapsulation and controlled release: a review. *Int. J. Food Sci. Technol.* 41, 1–21.

McClements D.J., and Decker E.A. (2000). Lipid oxidation in oil-in-water emulsions: impact of molecular environment on chemical reactions in heterogeneous food systems. *J. Food Sci*. 65, 1270–1282.

Mele, A., Mendichi, R., Selva, A., Molnar, P., and Toth, G. (2002). Noncovalent associations of cyclomaltooligosaccharides (cyclodextrins) with carotenoids in water. A study on the alpha- and beta-cyclodextrin/psi, psi-carotene (lycopene) systems by light scattering, ion-spray ionization and tandem mass spectrometry. *Carbohydr. Res*. 337, 1129–1136.

Mezzenga, R., Schurtenberger, P., Burbidge, A., and Michel, M. (2005). Understanding foods as soft materials. *Nat. Mater*. 4, 729–740.

Millqvist-Fureby, A., Malmsten, M., and Bergenståhl, B. (2000). An aqueous polymer two-phase system as carrier in the spray-drying of biological material. *J. Colloid Interface Sci*. 225, 54–61.

Morais, H.A., de Marco, L.M., Oliveira, M.C., and Silvestre, M.P.C. (2005). Casein hydrolysates using papain: peptide profile and encapsulation in liposomes. *Acta Aliment.* 34, 56–69.

Moraru, C.I., Panchapakesan, C.P., Huang, Q., Takhistov, P., Liu, S., and Kokini, J.L. (2003). Nanotechnology: a new frontier in food science. *Food Technol*. 57(12), 24-29.

Muthukumarasamy, P., Allan-Wojtas, P., and Holley, R.A. (2006). Stability of *Lactobacillus reuteri* in different types of microcapsules. *J. Food Sci*. 71, M20–M24.

Ogawa, S., Decker, E.A., and McClements, D.J. (2003). Influence of environmental conditions on the stability of oil in water emulsions containing droplets stabilized by lecithin–chitosan membranes. *J. Agric. Food Chem*. 51, 5522–5527.

Ogawa, S., Decker, E.A., and McClements, D.J. (2004). Production and characterization of *O/W* emulsions containing droplets stabilized by lecithin–chitosan–pectin multilayered membranes. *J. Agric. Food Chem*. 52, 3595–3600.

Orlien, V., Risbo, J., Rantanen, H., and Skibsted, L.H. (2006). Temperature-dependence of rate of oxidation of rapeseed oil encapsulated in a glassy food matrix. *Food Chem*. 94, 37–46.

Park, C.W., Kim, S.J., Park, S.J, Kim, J.H., Kim, J.K., Park G. B., Kim, J.O., and Ha, Y.L. (2002). Inclusion complex of conjugated linoleic acid (CLA) with cyclodextrins. *J. Agric. Food Chem*. 50, 2977–2983.

Partanen, R., Yoshii., H., Kallio, H., Yang, B., and Forssell, P. (2002). Encapsulation of sea buckthorn kernel oil in modified starches. *J. Am. Oil Chem*. Soc. 79, 219–223.

Peniche C., Howland I., Carrillo O., Zaldívar C., and Argüelles-Monal W. (2004). Formation and stability of shark liver oil loaded chitosan/calcium alginate capsules. *Food Hydrocolloids* 18, 865–871.

Picot, A., and Lacroix, C. (2003). Production of multiphase water-insoluble microcapsules for cell encapsulation using an emulsification/spray-drying technology. *J. Food Sci*. 68, 2693–2700.

Pszczola, D.E. (1998). Encapsulated ingredients: providing the right fit. *Food Technol*. 52(12), 70–77.

Pszczola, D.E. (2003). Delivery systems help send the right message. *Food Technol*. 57(4), 68–85.

Rabiskova, M. (2001). Extrusion technology. In: P. Vilstrup (ed.), *Microencapsulation of Food Ingredients*. Leatherhead Publishing, Surrey, UK, pp. 224–248.

Reineccius, G.A. (2001). The spray drying of food ingredients. In: P. Vilstrup (ed.), *Microencapsulation of Food Ingredients*. Leatherhead Publishing, Surrey, UK, pp. 151–179.

Remondetto, G.E., Beyssac, E., and Subirade, M. (2004). Iron availability from whey protein hydrogels: an in-vitro study. *J. Agric. Food Chem*. 52, 8137–8143.

Remondetto, G.E., Paquin, P., and Subirade, M. (2002). Cold gelation of beta-lactoglobulin in the presence of iron. *J. Food Sci*. 67, 586–595.

Rhim, C.H., Lee, KE., Yuk, H.G., Lee, S.C., and Lee, C.C. (2000). Investigation of the incorporation efficiency of beta-carotene into liposomes. *J. Food Sci*. Nutr. 5, 177–178.

Rodríguez-Huezo, M.E., Pedroza-Islas, R., Prado-Barragán, L.A., Beristain, C.I., and Vernon-Cater, E.J. (2004). Microencapsulation by spray drying of multiple emulsions containing carotenoids. *J. Food Sci*. 69, E351–359.

Rosenberg, M., and Lee, S.-J. (2004). Water-insoluble, whey protein-based microspheres prepared by an all-aqueous process. *J. Food Sci*. 69, FEP 50–58.

Saarela, M., Lahteenmaki, L., Crittenden, R., Salminen, S., and Mattila-Sandholm, T. (2002). Gut bacteria and health foods: the European perspective. *Int. J. Food Microbiol*. 78, 99–117.

Sadano, S., and Sonoda, T. (2002). Multicore type caroetnoid beads. US Patent Application 2002/0052421-A1.

Sanguansri, L., and Augustin, M.A. (2006a). Microencapsulation and delivery of omega-3 fatty acids. In: J. Shi and J. King (eds.), *Functional Food Engineering Technologies and Processing*, CRC Press, Boca Raton, FL, pp. 297–327.

Sanguansri, P., and Augustin, M.A. (2006b). A nanoscience approach to material development for the food industry. *Trends Food Sci. Technol*. 17, 547–556.

Schmidl, M.K., and Labuza, T.P. (2000). *Essentials of Functional Foods.* Aspen Publishers, Gaithersburg, MD.

Schmitt, C., Sanchez, C., Desobry-Banon, S., and Hardy, J. (1998). Structure and technofunctional properties of protein–polysaccharide complexes: a review. *Crit. Rev. Food Sci. Nutr*. 38, 698–753.

Sher, A., Jacobson, M.R., Vadehra, B., and Vadehra, D.V. (2006). Ferric fortification system. US Patent 6998143-B1.

Shimada, Y., Roos, Y., and Karel, M. (1991). Oxidation of methyl linoleate encapsulated in amorphous lactose-based food model. *J. Agric. Food Chem*. 39, 637–641.

Sloan, A.E. (2004). Fortified foods get functional. *Functional Foods and Nutraceuticals*, November, 18–22.

Sparks, R.E., Jacobs, I.C., and Mason, N.S. (1995). Centrifugal suspension-separation for coating food ingredients. In: S.J. Risch and G.A. Reineccius (eds.), *Encapsulation and Controlled Release of Food Ingredients*. American Chemical Society Washington, DC, pp. 87–95.

Strauss G., and Gibson S.M. (2004). Plant phenolics as cross-linkers of gelatin gels and gelatin-based coacervates for use as food ingredients. *Food Hydrocolloids* 18, 81–89.

Sultana, K., Godward, G., Reynolds, N., Arumugaswamy, R., Peiris, P., and Kailasapathy, K. (2000). Encapsulation of probiotic bacteria with alginate–starch and evaluation of survival in simulated gastrointestinal conditions and in yoghurt. *Int. J. Food Microbiol.* 62, 47–55.

Taylor, T.M., Davidson, P.M., Bruce, B.D., and Weiss, J. (2005). Liposomal nanocapsules in food science and agriculture. *Crit. Rev. Food Sci. Nutr*. 45, 587–605.

Turchiuli, C., Fuchs, M., Bohin, M., Cuvelier, M.E., Ordonnaud, C., Peyrat-Maillard M.N., and Dumoulin, E. (2005). Oil encapsulation by spray drying and fluidised bed agglomeration. *Innov. Food Sci. Emerg. Technol.* 6, 29–35.

Uicich, R., Pizarro, F., Almeida, C., Diaz, M., Boccio, J., Zubillaga, M., Carmuega, E., and O'Donnell, A. (1999). Bioavailability of microencapsulated ferrous sulfate in fluid cow's milk: studies in human beings. *Nutr. Res.,* 19, 893–897.

Vasishtha, N., and Schlameus, H.W. (2001). Centrifugal coextrusion encapsulation. In: P. Vilstrup (ed.), *Microencapsulation of Food Ingredients* Leatherhead Publishing, Surrey, UK, pp. 120–132.

Weiss, J., Scherze, I., and Muschiolik, G. (2005). Polysaccharide gel with multiple emulsion. *Food Hydrocolloids* 19, 605–615.

Whitaker, M.J., Hao, J., Davies, O.R., Serhatkulu, G., Stolnik-Trenkic, S., Howdle, S.M., and Shakesheff, K.M. (2005). The production of protein-loaded microparticles by supercritical fluid enhanced mixing and spraying. *J. Controlled Release* 101, 85–92.

Wildman, R.E.C. (2001). *Handbook of Nutraceuticals and Functional Foods*. CRC Press, Boca Raton, FL.

Williams, R.P.W., D'Ath, L., and Augustin, M.A. (2005). Production of calcium-fortified milk powders using soluble calcium salts. *Lait,* 85, 369–381.

Yang, H. H.-L., and Lawless, H.T. (2006). Time-intensity characteristics of iron compounds. *Food Qual. Prefer*. 17, 337–343.

Yilmaz, G., Jongboom, R.O.J., Feil, H., and Hennink, W.E. (2001). Encapsulation of sunflower oil in starch matrices via extrusion: effect of the interfacial properties and processing conditions on the formation of dispersed phase morphologies. *Carbohydr. Polym.* 45, 403–410.

Zeisig, R., and Cammerer, B. (2001). Liposomes in the food industry. In: P. Vilstrup (ed.), *Microencapsulation of Food Ingredients*. Leatherhead Publishing, Surrey, UK, pp. 101–119.

Zhang L., Guo J., Peng X., and Jin, Y. (2004). Preparation and release behavior of carboxymethylated chitosan/alginate microspheres encapsulating bovine serum albumin. *J. Appl. Polym. Sci*. 92, 878–882.

Zimmermann, M.B. (2004). The potential of encapsulated iron compounds in food fortification: a review. *Int. J. Vitam. Nutr. Res*. 74, 453–461.

INDEX